UTM
UNIVERSITI TEKNOLOGI MALAYSIA
Faculty of Electrical Engineering

Proceedings of 2017 Electrical Engineering Symposium (EES2017) - Vol. 3

PROCEEDINGS OF 2017 ELECTRICAL ENGINEERING SYMPOSIUM (EES2017)

VOLUME 3

First Edition 2017

Diterbitkan oleh: Fakulti Kejuruteraan Elektrik, Universiti Teknologi Malaysia, 81310 Johor Bahru Johor, Malaysia

PREFACE

This book introduces several research works from final year undergraduate project till the level of master project by taught course. The projects have been evaluated by industries as well as academician to ensure that its fulfill the standard of each level before it can be published. The text emphasizes the combination of the research material in different field of engineering generally in power, electronic, communication, control and mechatronic which hampered by three main program offered by Faculty of Electrical Engineering.

This book is generally suitable as an accompaniment to students and researchers that generally involved with different field of study including modeling and control design for various example of application. There are also research on hardware design implementation which integrate both for simulation and experimental study as well as laboratory sessions available at a particular institution.

Mohamad Kamal A. Rahim
Md. Pauzi Abdullah
Faculty of Electrical Engineering
Universiti Teknologi Malaysia

2017 ELECTRICAL ENGINEERING SYMPOSIUM COMMITTEE

GENERAL CHAIR

PROFESSOR DR. MOHAMAD KAMAL A. RAHIM

CO-CHAIR

IR. DR. MD. PAUZI ABDULLAH

2017 ELECTRICAL ENGINEERING SYMPOSIUM MEMBERS

DR. KAMALUDIN MOHD. YUSOF

DR. SHAHARIN FADZLI ABD. RAHMAN

DR. YUSMEERAZ YUSOF

DR. MOHD. HAFIZI AHMAD

DR. NURUL EZAILA ALIAS

DR. ZULKARNAIN AHMAD NOORDEN

DR. MOHD. AFZAN OTHMAN

DR. MOHD. AMRI MD. YUNUS

DR. MOHD. RASHIDI SALIM

2017 ELECTRICAL ENGINEERING SYMPOSIUM SECRETARIAT STAFF

SABRINA ZAINAL ABIDIN

AZLINA MOHD. LAZIM

Embedded data acquisition for optical tomography system based on CMOS linear image sensor

Mohamad Fitri Bin Mohd Amir
Faculty of Electrical Engineering,
University Teknologi Malaysia,
Johor, Malaysia.
mohamadfitria94@gmail.com

Norhafizah Bt Ramli
Department of Electrical Electronic and Computer Engineering,
Faculty of Electrical Engineering,
University Teknologi Malaysia,
Johor, Malaysia.
e-hafizah@utm.my

***Abstract*—This paper propose an improved the system of optical tomography system based on CMOS linear image sensor. An optical tomography system are widely useful technique to characterizing the any particle inside the closed pipe in industry without the requirement of physical contact. Thus, the objective of this project is to make a system are friendly use by implement the embedded system on that system so that the hardware system can handle on wireless for monitoring the data acquisition on CMOS linear image sensor. Particle Characterize experiment based on size, shape, number of conducted, and sensitivity of sensor after complete setup for hardware and software part. Then, the verification of the experiment will be analysis with the actual result.**

Keywords—Tomography; pipeline; CMOS image sensor; paricle; characterizing

I. INTRODUCTION

Nowadays, particle characterization for various particle sample such as powders, liquids suspension and unwanted particle has become basic requirement for many industrial and academic research that flow through the closed pipeline. The study of particle characterization becomes crucial in industrial processes as it provides a better control of product quality [1]. Thus, it grants economic benefits such as the ability to charge a higher premium for the product and reduce the probability of customer rejection rates [2]. The study of particle characterization also aids companies to have a better understanding of their products, ingredients and processes [3]. There are many technique and technology that can analysis the particle information using instrument. Optical tomography system are one of technique that can used to characterize the particle inside the any pipeline as possible.

Process tomography is a measurement ways that use tomographic imaging method to get data from image sensor. This system are involve projecting light source beam (e.g laser, LED, or fiber-optic) through the closed pipe boundary and the sensor will detect the light intensity at opposite boundary of pipeline [4]. It not consider interrupt inside a pipe flow during analysis characteristic of particle inside it.

This project is entitled **'Embedded data acquisition for optical tomography system based on CMOS linear image sensor'.** The primary objective is to build hardware that can characterize the particle inside the pipeline with the right output possible in data sampling by using Data Acquisition System (DAQ). However, there are very limited of equipment in the market which can perform data acquisition system unit for an optical tomography because it becomes expensive. From that scenario, it will be avoided by replacing with a low cost embedded system design its call 'Embedded data acquisition' (EDA). The aim of this project is to develop a simple, cheap, easy interface and portable data acquisition system for optical tomography system. Integrated as kind of thing of a perfect system often including hardware and automated parts. Embedded systems behave many devices in common act about today [5]. Ninety-eight percent of all chip are fabricated as segments of implanted frameworks [6]. Integrated data acquisition represent a solution to remote all that data acquisition simultaneously and no need to control one by one the projection of the CMOS linear image sensor. The secondary goal of building an embedded data acquisition system is to create a DAQ which would have the capacity to gain the valuable information from CMOS linear image sensor that can calibration the system at no error and upload and record the data accurately. To make it online, Arduino Nano microcontroller is used to control the operation of optical tomography framework furthermore for clock generation of CMOS S10077 collection data.

II. HARDWARE IMPLEMENTATION

The topology is illustrated in Fig. 1. The first module is Main control unit of a CMOS image sensor based optical tomography system. The complete system consist of a laser diode, CMOS image sensor, Arduino Nano Microcontroller, Wi-Fi module, data acquisition system, and PC for data displays at a second module. The Arduino Nano and PC display are communicated by using Wi-Fi module that read data at virtual COM port.

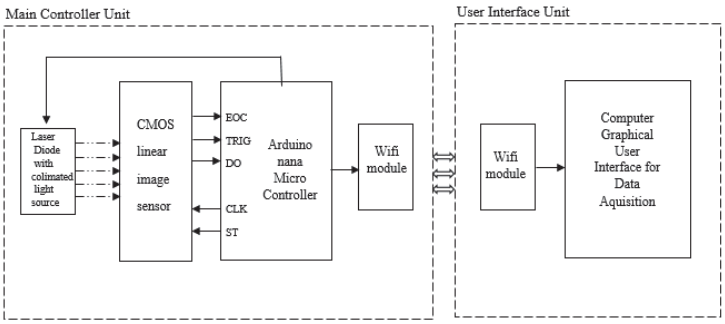

Fig.2.1. Overall concept of the project

This project mainly involve both parts of hardware and software. The work flow and several procedure are used to realize the project would be discussed in detail based on hardware component consist. The initial phase of project implementation require more understanding on working principle of CMOS linear sensor.

An octagonal-shape measurement rig was designed between the laser diode and the CMOS image sensor, with the transparent glass pipe that mounted in the middle.

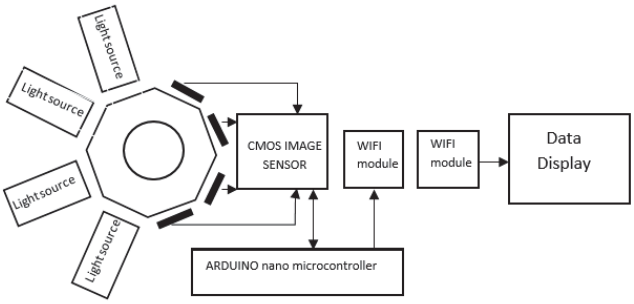

Fig.2.2. Block diagram of Optical Tomography System

Fig.2 illustrate the concept of system by four projection. A laser diode will projected through the pipeline and direct to the CMOS sensor. Arduino will read a data from sensor and sent a serial data through Wi-Fi module to the PC for data display. A laser diode that implemented are already collimated lighting system and produce 600nm wavelength of red light.

A. Laser Diode

A laser diode that implemented are already collimated lighting system and produce 600nm wavelength of red light. That laser are direct projected to each CMOS sensor through the pipeline inside the octagon box. One projection was set to calibration setting corresponding to image sensor. That calibration setting are functioning for examine condition of image sensor in stable or in control. Figure 2.3 shows the configuration and how it work inside the laser module which can produce light in line already.

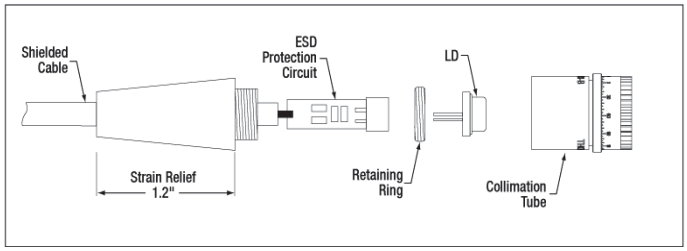

Fig.2.3. Laser line

B. CMOS image sensor

Four CMOS image sensor are implemented in this system correspond to the laser projection. That CMOS comprises of 1024 pixels which react with the laser. Each of the pixels is put in an exhibit up to 1024 numbers, along these lines framing a window of the picture sensor. The sensor works somewhere around 3.3V and 5V, making it as a low power utilization gadget. Since it includes an implicit planning generator, the sensor can work with just beginning and clock activating signals. Figure 2.7 shows the pin configuration of the CMOS sensor and the optical sensing window in the middle.

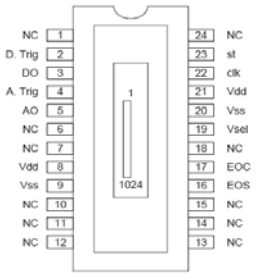

Fig.2.4.The pin configuration of CMOS S10077 Linear Image Sensor.

CMOS linear image sensor S10077 provide both type output, digital and analog. It is simultaneous all pixel integration and variable integration time function. Its optical characteristic is spectral response range in between 400 to 1000nm, and the peak sensitivity wavelength is about 700nm.

Center CMOS sensor is the dynamic zone which is the physical part of the sensor chip optical window where 1024 pixels area found. Figure 2.5 shows the dimension outline for S10077 CMOS linear image sensor which is called as an active area that performs the actual computing and the storage operation.

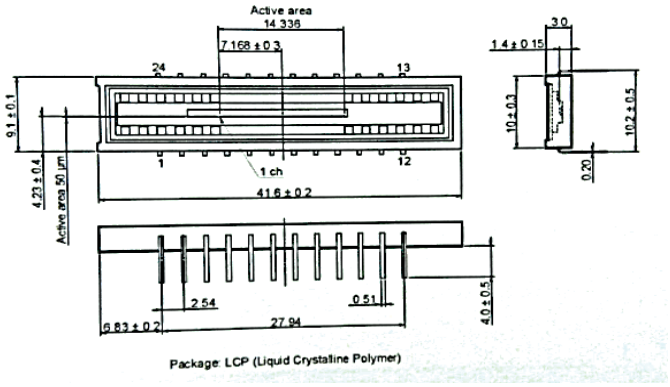

Fig.2.5.The size shape for S10077 CMOS linear image.

C. Arduino Nano Microcontroller Board

In this optical tomography system, Arduino Nano are the main controller for operation in this system. Pulse signal and clock are generate to trigger the CMOS image sensor and laser. That image sensor requirement clock frequency are in

range 1MHz to 12MHz in order to operate in 8-bit mode by Arduino Nano.

Besides that, microcontroller also functioning to retrieve the digital output from the CMOS sensor. The output serial data are sent to the computer for data acquisition process through the Wi-Fi module. The Arduino Nano can store up to 2000 bytes of Random Access Memory (RAM), which is sufficient for 1024 bytes of digital output data storage. Figure 6 shows the schematic circuit diagram of the microcontroller.

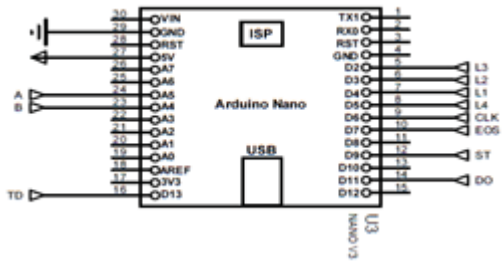

Fig 2.6: Schematic Circuit of Arduino Nano

Arduino Nano microcontroller was used to generate the clock signal and pulse signal to synchronizing with the image sensor as well. Below is the figure of flowchart for the complete system that controlled by Arduino Nano microcontroller.

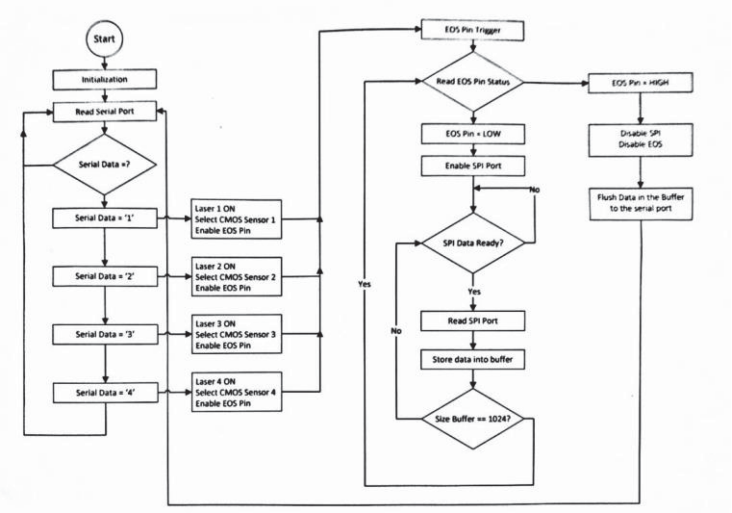

Fig. 2.7: Flow chart of the complete system controlled by Arduino Nano

D. Dual 4x1 Multiplexer, GD74LS153

A multiplexer (MUX) is described as a selector of inputs and forwards the selected input into a single line. Since four CMOS image sensors were implemented in the system, only one of them can be operated at a time. In addition, each sensor needs to deliver three signals which are D0, D.Trig and EOS to the microcontroller for data acquisition system. Thus, two units of dual 4x1 mux, IC GD74LS153 were used to select these signals from one of the image sensors. Figure 2.9 below shows the schematic diagram of the multiplexer circuit.

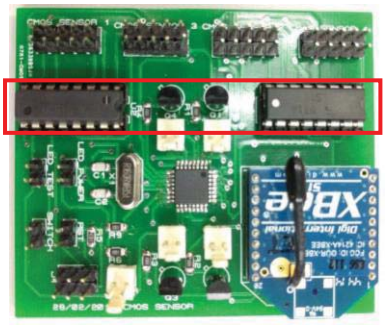

Fig. 2.8: Configuration of two IC GD74LS153 on the microcontroller board.

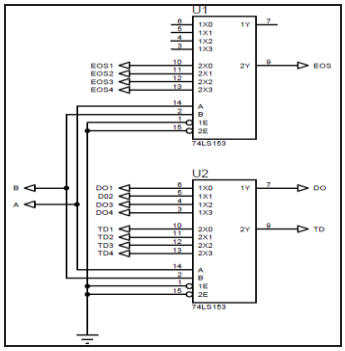

Fig. 2.9: Schematic diagram of multiplexer circuit of two IC GD74LS153.

III. SOFTWARE IMPLEMENTED

After the hardware part has been completed, the paper is ready for the Software part on the Graphic User Interface (GUI). In the software part the serial data from image sensor will be display. At end-level user, to controlling the optical tomography system Display Data Serial Port application will be used. There has selection for each sensor and combo button for operate once at a time or operate all continuously for all sensor. The CMOS pixel output are in digital output and it will be display in numeric array form. The numerical data can save in txt format for analysis in constructing or plotting graphing. Figure below shows the Graphical User Interface (GUI) of application.

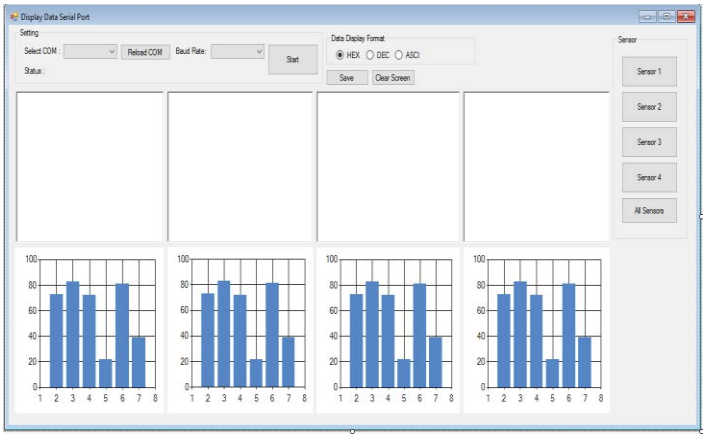

Fig.3.1: The GUI of the display data serial port application

On the GUI application, there has four text box and graph box to represent serial data for each sensor accordingly.

IV. EXPERIMENTAL RESULT

All five boards, the Arduino Nano microcontroller board and the four CMOSS10077 linear image sensors are connected together using rainbow wires. The USB cable was connected between the microcontroller board and the computer. The AC-DC adapter 9V was used to supply the voltage to the microcontroller board and the laser source.

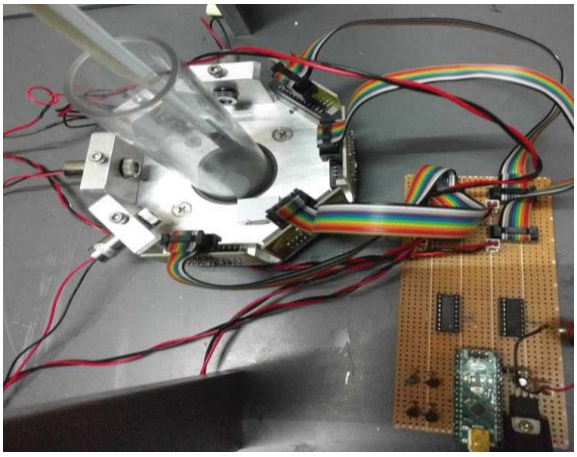

Fig. 4.1 Experimental setup of Tomography system

Using this application, the sensor button is virtually connected to the microcontroller. Each sensor button initiates the corresponding switching transistor for laser diode transmission, CMOS sensor operation and also the MUX to deliver the three corresponding signals to the microcontroller for data storage. The system takes all of the output data from the CMOS image sensors. Figure 4.2 shows the flowchart of the optical tomography system operation based on the Arduino Nano microcontroller.

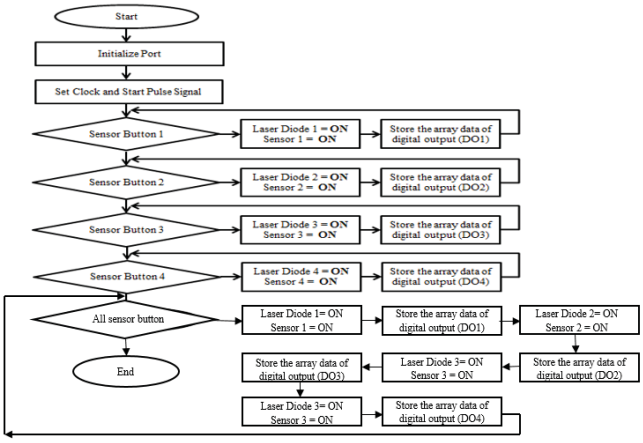

Fig. 4.2: Flowchart of the optical tomography system operation

Before starting the experiment, calibration must be done to ensure the consistency of the readings from the CMOS sensor. This can be done by testing two conditions of the CMOS sensor. The first condition is when the CMOS sensor is fully exposed to the ambient light. Maximum output data should be obtained in all 1024 pixels. The next condition is to block the light transmission on the CMOS sensor by covering it with a black paper as well as the absence of the ambient light. With very low detection of light intensity by the image sensor, the output data generated should be low across the pixels.

A. Tested Cases of Particle Characterization

This section discusses experiments based on two cases of particle characterization which are particle size and particle counts. For the particle size, a black-colored cylindrical 3D printing object was used as the subject of the experiment. Different diameters of the cone were placed and tested in the pipeline for the data acquisition process. The second experiment was based on particle counts where small sized cylindrical 3D printing object were used as the subject. Figure 4.3 below shows the illustration of the black cylinder in different type for both experiments. Both experiments were made for four projections of the CMOS sensor. The results from all cases were shown and discussed in the following section.

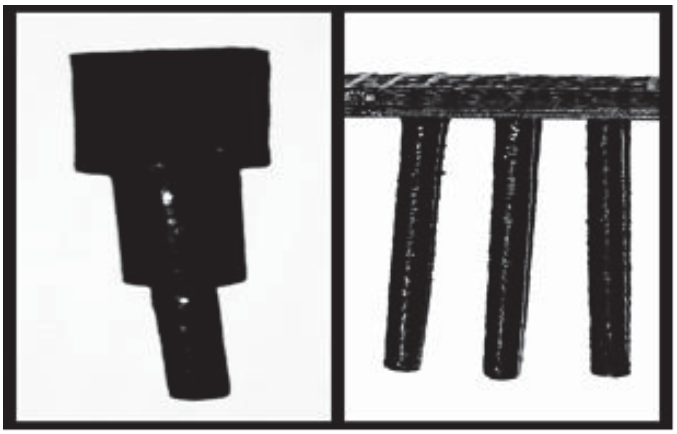

Fig. 4.3: Illustration of black cylinder in different type

a) Data Measurement of Cone Diameter

The particle size experiment was made based on three diameters of the cylinders, which were 3mm, 6mm and 9mm. The cylinder was lowered down by a diameter to allow different measurement in the pipeline. In each case, 10 trials of data acquisition were made for every projection of light. Calculation of the diameter based on these acquired data was shown in the equation 4.1.

$$\text{Cone Diameter} = [\text{Right Edged Pixel} - \text{Left Edge Pixel}] \times 14\mu m$$

The equation is based on the photosensitive area or window length of the CMOS image sensor. The diameter of the black cylinders must be in range within the area length in order to produce an accurate result. However, due to light scattering of the cone, the output data generated by the CMOS sensor may cause deviation from the actual value of the diameter. Therefore, the calculation was made based on three different percentage threshold of maximum 8-bit data which were 100%, 75% and 50%. Figure 4.4 below shows the pixel differences of the diameter based on the percentage threshold of the data.

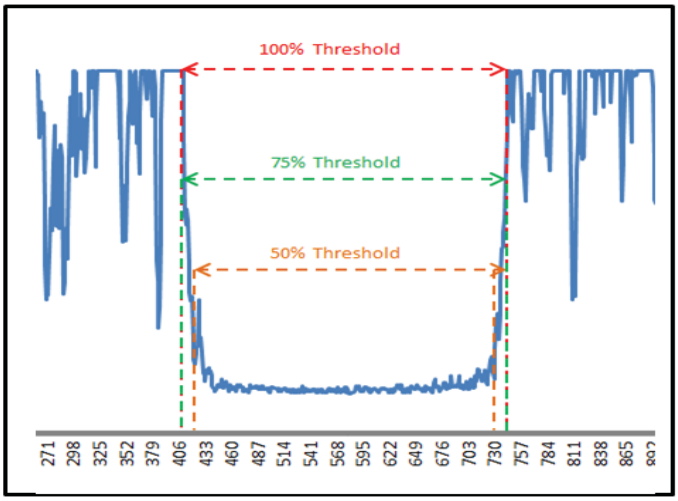

Figure 4.4: Percentage threshold of 100%, 75% and 50% of a sample output data.

In this experiment, the accuracy of diameter size is determined based on percentage error of the actual and experimental measurement. To evaluate this, the value of absolute error from all projections must be obtained from all projections. Table 4.1 show the average experimental results of the diameters.

Table 4.1: Value of experimental diameters for the three different size for actual diameter of cylinder.

	100% Threshold of Data	75% Threshold of Data	50 %Threshold of Data
3 (mm)	4.620	4.417	4.363
6 (mm)	7.360	7.103	7.012
9 (mm)	11.081	10.710	10.623

b) Data Particle Count Experiment

The particle characterization based on particle counting was made by using 3mm cylinder as the experimental subjects. In this experiment, three cylinder object were tested for counting. The objects were placed in the pipeline for image capturing by the CMOS S1077 image sensor. To identify the number of beads inside, reconstruction of the images from four projections must be made so that the visualization of beads in three-dimensional (3D) view can be seen. However, reconstructing the image requires the digital output of the CMOS sensor. Thus, observation of the diffracted cylinder object from all projections must be valid in order to allow a better 3D image generation.

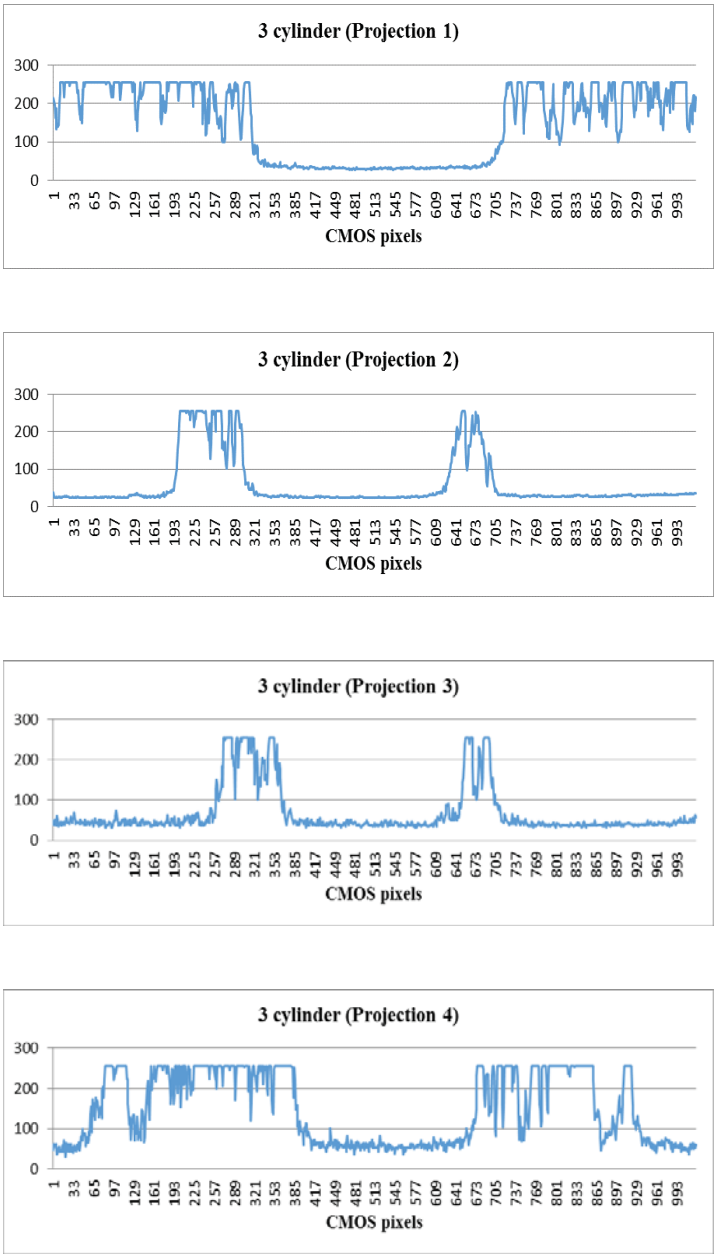

Figure 4.5: Diffraction patterns of three beads from four different projections.

V. CONCLUSION

The developed optical tomography system based on CMOS linear image sensor can detect particles in a pipe. The system has the capability to monitor particle concentration and other particle characterization elements such as particle size and concentration profile.

VI. ACKNOWLEDGMENT

I would like to acknowledge the Universiti Teknologi Malaysia for the research funding and my supervisor for the support given.

VII. REFFERENCE

[1] Gore, R.A & Crowe, C.T.,1989. Effect of particle size on modulating turbulent intensity. International Journal of Multiphase Flow, 15(2), pp. 279-285.27

[2] Hauptmann, P. Hoppe, N. & Puttmer, A., 2002. Application of ultrasonic sensors in the process industry. Measurement Science and Technology, 13(8), pp.R73-R83..

[3] Instruments, M., 2012. A Basic Guide to Particle Characterization.R.Abdul Rahim(1996). A tomography imaging system for pneumatic conveyors using optical fibers. Sheffield Hallam University.PhD.Thesis.

[4] R. Nicole, “Title of paper with only first word capitalized,” J. Name Stand. Abbrev., in press.

[5] Michael Barr; Anthony J. Massa "Introduction". Programming embedded systems: with C and GNU development tools. O'Reilly.2006.

[6] Barr, Michael "Real men program in C". Embedded Systems Design. TechInsights (United Business Media).2009

On Chip Re-configurable RF Multifunctional Filter

Lee San Kong
Faculty of Electrical Engineering
Universiti Teknologi Malaysia
Johor Bahru, Malaysia.
leesankong93@gmail.com

Prof . Dr. Abu Khari bin A'ain
Department of Electronic and Computer Engineering
Faculty of Electrical Engineering
Universiti Teknologi Malaysia
Johor Bahru, Malaysia.
abu@fke.utm.my

***Abstract*— In this paper, an improved tuning method using Digitally-Controlled Differential Voltage Current Conveyor (DC-DVCC) method implemented for the re-configurable front-end RF multifunctional filter is presented. The circuit has been designed for a frequency of 2.4GHz in 0.18µm CMOS process, high enough to cover the main wireless standards, has small die area and power consumption. Low pass and high pass filter frequency response can be obtained simultaneously from this filter and they can be tuned with the implementation of Current Summing Networks into the circuit. The filter circuit consumes 10.6mW from a 1.8 V supply at 2.4GHz frequency. The simulation results show that the filter centered at 2.45GHz with about 42MHz bandwidth is tunable from 1.13GHz to 2.45GHz and it occupies the die area of 3.97 mm^2.**

Keywords—Digitally Controlled Differential Voltage Current Conveyor (DC-DVCC); multifunctional filter; Current Suming Network (CSN); tunable active capacitor

I. INTRODUCTION

The technology advancement has led to the explosive growing market in wireless communications. Nowadays, modern devices are designed to operate at different and multiple communication standards and frequency bands [1]. This creates a strong demand on a need for a highly integrated, smaller in size and small power consumption of RF receivers. Fig. 1 shows the block diagram of a common RF receiver that is implemented in current multi standard devices.

Front end receiver components such as analog RF filter, IF amplifiers, mixers, band pass filters, modulators and demodulators are designed to be smaller, tunable and consumes less power in order to be more flexible to be integrated into multiple standard devices. Integrating or adding in more customize RF front-end components would result in power consumption issue at the same time increases the complexity of

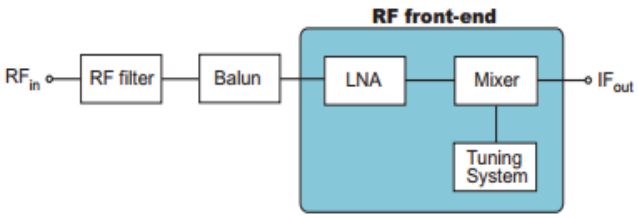

Fig. 1. Block diagram of RF front end of the receiver.

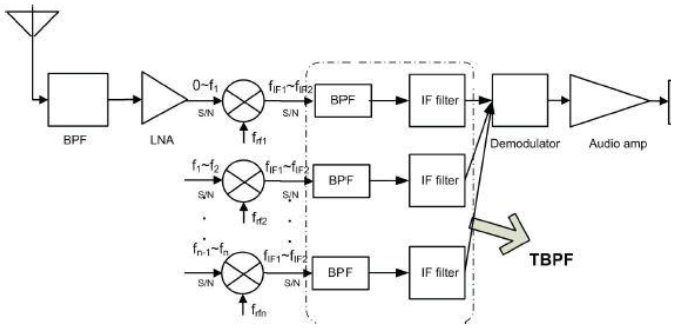

Fig. 2. Example of tunable front-end analog filter in receiver architecture[3].

the circuit when the devices are upgraded to support new standards[2]. The high power consumption issue will limit the users from switching freely among different networks of frequency if there is no efficient precaution measures are taken when designing the RF front end module.

On the other hand, if front end components are made tunable and reconfigurable, it will minimize the amount of front-end components needed and therefore reduce the power, size and cost of the products. Tunable band pass filter (TBPF) is introduced into multiple standards device as it can be pre-tuned to desired signal frequencies at the same time eliminating out-of-band signals[3]. Moreover, it will eliminate the use of off-chip mixers and passive IF amplifier as shown in Fig. 2 which in return reduce the size and power consumption of the RF front end module.

This paper proposed an improved tuning method using Digitally-Controlled Differential Voltage Current Conveyor (DC-DVCC) method implemented for the front-end RF multifunctional filter, designed for frequencies up to 2.4GHz which is high enough to cover most current wireless standards.

This paper is organized as follows. Section II presents the literature reviews of this project. Section III describes the proposed digitally re-configurable RF multifunctional filter based on the DC-DVCC design method while Section IV demonstrates the simulation results of the multifunctional filter. Finally, the conclusion is given in Section V.

II. LITERATURE REVIEW

This chapter includes the literature reviews of this project. All of the theories, equations and information from the

literature reviews read will be used as the backbone and fundamental to develop this project.

A. Multi-standard Specifications

Over the years, new standards for wireless communication systems have been introduced to boost the data rates at the same time developing new services. Advancement in communication technology enabled an improvement in the design of receiver which is capable to adjust to more challenging specifications following the generations of cellular systems. For instance, 1G, the first generation of wireless phone technology was introduced in the 1980s. It was based on analog direct voice modulation and being replaced by 2G digital telecommunications at 1990s. During this time, there are different standards being used especially GSM (Global System for Mobile Communications), which are spread widely over the world and eventually becoming one of the major mobile phone standard. The development of GSM in 2G leads to the new standards, GPRS (General Packet Radio Service) and EDGE (Enhanced Data rate for GSM evolution), effectively increasing the data rates up to 385kbps. Later, 3G was introduced to provide more services at a data transfer rate of about 5Mbps using the access scheme WCDMA (Wideband Code Division Multiple Access). In addition to high speed voice and other services by 3G, 4G provides mobile an ultra-broadband (gigabit speed) access up to 100Mbps data rates[4]. Nowadays, 4G is the kind of standard which can integrate multi-mode of wireless communication, from wireless LAN, GPS and Bluetooth to radio, mobile phone, digital TV and satellite communication. In order to allow user to switch freely among different standards, obtaining both data applications and voice, all these standards have to be supported by a high integration front-end circuit in multi-standard receiver as shown in Fig. 3. The availability of many wireless standards that can be implemented in 4G are shown in Table I.

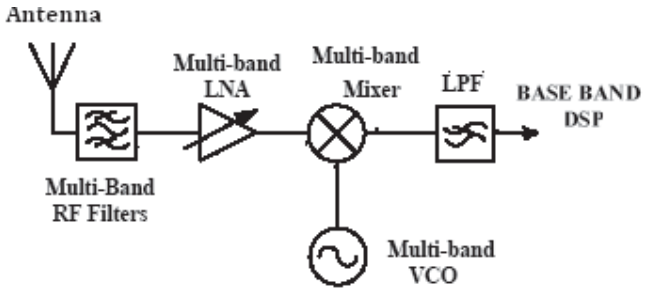

Fig. 3. Block diagram of RF front end circuit in multi-standard receiver.

B. Receiver Architectures

There are several types of receiver architectures that are widely used nowadays. Therefore, the architecture of the multi-standard receiver is carefully selected based on their multi-standard and integration capabilities. Figure 4(a) shows the architecture of a superheterodyne receiver. Superheterodyne receiver is the most common used receiver as it provides excellent selectivity and sensitivity and it reduces baseband

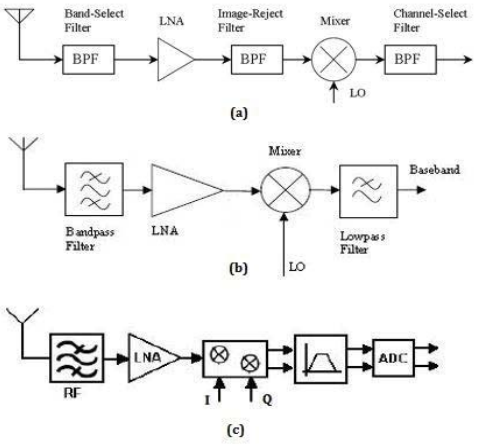

Fig. 4. Receiver architecture. (a) Superheterodyne, (b) Zero-IF (c) Low-IF.[5]

filtering needs[5]. However, it cannot be fully integrated as the design requires many off-chip components such as off-chip image-reject filter and channel-select pass filter. Figure 4(b) shows the simplified block diagram of homodyne receiver. The homodyne receiver which is also known as direct-conversion or Zero-IF receiver downconverts the RF signals to baseband frequencies in a single step using only a discrete RF filter which as a result, suppressing the others off-chip filters. The integration capability into multi-standard receiver is improved since the channel selection is performed by programmable low pass filter to support different standards. On the other hand, the Low-IF receiver as shown in Figure 4(c) downconverts the RF signal to an intermediate frequency (IF) which is closer to the baseband frequency. This Low-IF receiver is not suitable to be implemented into multi-standard receiver as the constraint of its band pass filter and ADC for wide channel bandwidth will consume large power during the down conversion process. Therefore, the Zero-IF architecture presents more advantages for the multi-standard implementation which is also proposed on [6], strengthening the use of this topology for multi-standard wireless applications.

TABLE I. TABLE STYLES

Standards	Frequency Band (MHz)	Channel Bandwidth (MHz)
WCDMA	1920-1980 2110-2170	3.84
802.11b	2400-2483.5	22
802.11g	2400-2483.5	22
GPS	1575.42	-
Bluetooth	2400-2483.5	1

C. Surface Acoustic Wave (SAW) Filter

SAW filters are electromechanical devices in which their performance is based on the piezoelectric characteristics of a substrate. SAW filters are widely used in frequency applications such as frequency controlling, frequency selection and signal processing. At first, the electrical signal is converted to the mechanical one and then reconverted back again to the electrical signal at the output as shown in Fig. 5. There are two Interdigital transducer (IDT) in SAW filter, input and output IDT. These IDTs are used to converting electromagnetic signals waves to

acoustic signals waves or the other way round, performing the filtering function.

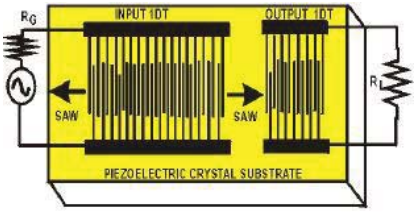

Fig. 5. Basic SAW IDT Structure on Piezoelectric substrate.

There are some wireless systems that introduces frequency division duplex (FDD), separating uplink (signals from terminal to base-station) and downlink (signals from base-station to terminal) signals in frequency domain[7]. Therefore, the transmit signal generated by the transmitter circuit will become the strongest jammer for the receiver. Fig. 6 shows the general block diagram of the FDD mode transceiver. The circuit of the transceiver consists of an antenna, an antenna duplexer (DPX), LNA and power amplifier (PA). The antenna duplexer composes of two SAW filters and two lines, which is the important parts for RF SAW devices. The strip lines acts to reduce electrical interferences between two filters and they are suitable to be embedded into DPX package. This RF SAW DPXs exhibit excellent filtering performances and are usually used in base stations. However, they are very bulky and at least 10 of them are needed in the current transceivers which make their implementation in an all chip multi standard system become more complex and hard[9].

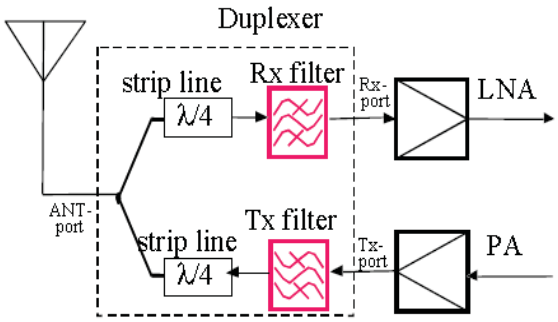

Fig. 6. RF front end module of FDD –mode transceiver.

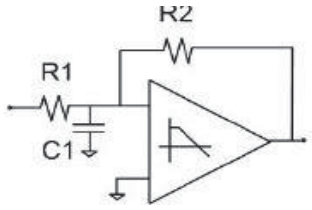

Fig. 7. Active gm-RC biquadratic cell.

D. Active-gm-RC topology filter

Active RC filters are widely used in designing RF analog filter due to its good linearity performance and frequency response accuracy. However, an Active-RC integrator will reduce the frequency response accuracy as an additional pole is introduced at its opamp unity gain bandwidth (UGB). The op amp unity gain bandwidth needs to be at least 100 times higher than the filter pole frequency which results in high power consumption and it is difficult to maintain a large dc gain. Thus, a reconfigurable Active gm-RC topology is introduced to overcome the frequency response inaccuracy[10]. In [11], the Active gm-RC biquadratic cell will reduce the noise and power consumption while constantly maintain the linearity of the system. The configuration of Active gm-RC biquadratic cell is shown in Fig. 7. Biquad complex poles pair is synthesized by exploiting the op amp frequency response. The op amp acts as open-loop integrator and the frequency of integrator UGBW is comparable with the filter poles frequency. Therefore, the power consumption can be reduced with respect to the closed-loop topologies. Since there are only two resistors and one capacitor are used in this circuit, smaller area of filter can be realized. However, this Active gm-RC topology filters can hardly operate at frequencies higher than 2GHz and thus they are not suitable to be implemented in reconfigurable filters for wireless system such as Bluetooth, WLAN, and so on.

E. SAR ADC Approach Analog Filter

The old technology of narrowband front-end and continuous time (CT) analog filters has faced the difficulty to adapt to multiple standards even though they did perform well in filtering the standards that they target. The explosive and rapid changing of communication standards make such rigid and inconvenient design approach undesirable. The invention of filtering analog to digital converter (ADC) which replaces the separate filters and ADC of the system making the highly-flexible system possible. Later, Software Defined Radio (SDR) is introduced to overcome the inconvenience and inflexibility problem of configuring the analog filter hardware every time a new communication standards come out[11]. With SDR, the frequency band can be tuned and it has the ability to receive any modulation by using only software instead of hardware. Although SDR approach introduces a way to tune to any frequency band by just controlling using software, the huge amount of the external passive components such as capacitor used to realize the baseband anti-aliasing will definitely consume lots of silicon area in which will directly increase the size of the system. After that, David T. Lin, Li Li, Shahin Farahani and Michael P. Flynn proposed that replacing the existing filtering stages by embedding the analog filter directly within a Successive Approximate Register (SAR) ADC to enable a flexible and reconfigurable system that can adapt easily to varieties of standards and its operating environment[12].

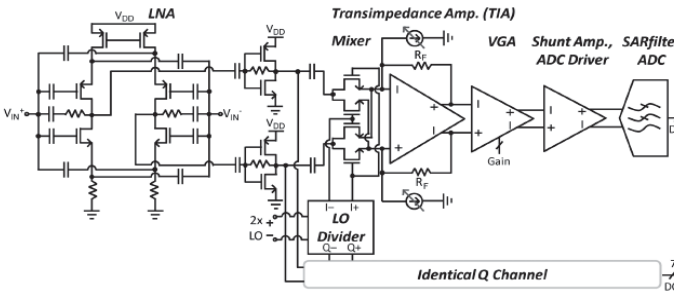

Fig. 8. SARfilter ADC applied in wireless receiver[12].

Fig. 8 shows one of the examples in which SAR ADC filter is applied in the configuration of wireless receiver. The realization

of embedded SAR ADC filter smartly reuses the capacitor of the capacitive DAC (CDAC) to make it flexible, scalable and reconfigurable which directly eliminates the use of CT filter. Thus, this reconfigurable wireless receiver can operate in the frequency range of 500 MHz to 3.6 GHz under multiple communication standards by adjusting the sampling rate and SAR ADC filter. However, the huge amount of capacitors used for this filter are space-consuming which will increase the size of the system. Not only these, due to its complexity, the design of this embedded filter is time-consuming.

F. Differential Voltage Current Conveyor (DVCC)

In the past, the discovery of current mode circuits has introduced a new and more efficient approach in developing analog building blocks. In general, the current mode circuits exhibits several advantages compared to the conventional voltage mode circuits such as simpler circuit, better linearity, higher slew rate, wider bandwidth, greater dynamic range and lower power consumption. The CCII (Second Generation Current Conveyor) which was designed and introduced by Sedra and Smith[13] has found to be the most successful, but it is unable to provide differential or floating inputs which are common inputs for several applications such as impedance converter circuits. To overcome these drawbacks, the differential difference current conveyor (DDCC)[14] and the differential voltage current conveyor (DVCC)[15] was introduced in 1996 and 1997 respectively. In fact, DVCC is a modified block of DDCC with its Y3 connected to ground. The five-terminals-DVCC is an active building block and their characteristics are described by the matrix equation as shown in (1):

$$\begin{pmatrix} I_{Y1} \\ I_{Y2} \\ V_X \\ I_{Z+} \\ I_{Z-} \end{pmatrix} = \begin{pmatrix} 0 & 0 & 0 & 0 & 0 \\ 0 & 0 & 0 & 0 & 0 \\ 1 & -1 & 0 & 0 & 0 \\ 0 & 0 & 1 & 0 & 0 \\ 0 & 0 & -1 & 0 & 0 \end{pmatrix} \begin{pmatrix} V_{Y1} \\ V_{Y2} \\ I_X \\ V_{Z+} \\ V_{Z-} \end{pmatrix} \quad (1)$$

The voltage at X terminal, V_x is the voltage difference between terminal Y_1 and Y_2 (V_{Y1}-V_{Y2}) while the output current of DVCC, I_{z+} and I_{z-} is the same with input current, I_x which is injected at X terminal. Note that the magnitude of I_{z+} and I_{z-} are the same but different direction. Figure 9 shows the block of DVCC where X terminal has zero input resistance while Y terminal and Z terminal have high resistance. The CMOS implementation of DVCC is shown as in Fig. 10.

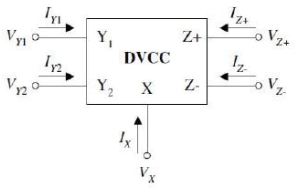

Fig. 9. Symbolic representation of the DVCC.[15]

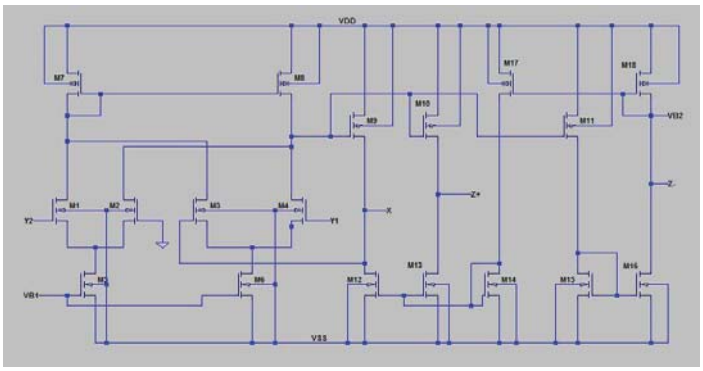

Fig. 10. The CMOS implementation of DVCC.

In this paper, the DVCC approach is adopted and modified to design an on chip reconfigurable RF filter which can be integrated into multi-standard devices.

III. CIRCUIT PRINCIPLE

To make the DVCC re-configurable, a digitally controlled DVCC (DC-DVCC) is introduced by adding in the Current Summing Networks (CSNs)[16]. The terminal characteristics of the DC-DVCC are modified as shown in (2).

$$\begin{pmatrix} I_{Y1} \\ I_{Y2} \\ V_X \\ I_{Z+} \\ I_{Z-} \end{pmatrix} = \begin{pmatrix} 0 & 0 & 0 & 0 & 0 \\ 0 & 0 & 0 & 0 & 0 \\ 1 & -1 & 0 & 0 & 0 \\ 0 & 0 & k & 0 & 0 \\ 0 & 0 & -k & 0 & 0 \end{pmatrix} \begin{pmatrix} V_{Y1} \\ V_{Y2} \\ I_X \\ V_{Z+} \\ V_{Z-} \end{pmatrix} \quad (2)$$

A. Current Summing Network (CSN)

Current summing networks (CSNs) are implemented into Z (Z+ and Z-) terminals of DVCC circuit to realize the digital control in DVCC. The current transfer gain parameter, k can be varied from 1 to 2n -1 where n represents the number of transistor arrays employed in the circuit. Fig. 11 shows the modified circuit of DVCC with the implementation of CSNs in which it consists of number of NMOS and PMOS transistor where their size ratio are given by:

$$\left(\frac{W}{L}\right)_i = 2^i \left(\frac{W}{L}\right)_9 \quad (3)$$

$$\left(\frac{W}{L}\right)_i = 2^i \left(\frac{W}{L}\right)_{12} \quad (4)$$

B. Tunable Active Capacitor

A tunable active capacitor is realized to replace the traditional passive capacitor which consumes large die area. The tunable active capacitor[17, 18, 19] and its equivalent circuit is shown in Fig. 12. All the CMOS transistor must operate in saturation mode in order to make the circuit tunable.

M_1 acts as resistive load while M_2 and M_3 are cross-coupled in active capacitor design. There are two bias voltages in the circuit, V_G and V_D. V_D controls the current I_{M2} and V_{CC} controls the current I_{M3}. On top of that, V_{CC} is determined by I_{M2} and V_G. To make M_2 in saturation, $V_D - V_t < V_{CC}$ and keep $V_{CC} - V_t < V_D$ to make M_3 in saturation. M_1 will always in saturation as its gate terminal is connected to drain terminal of the transistor.

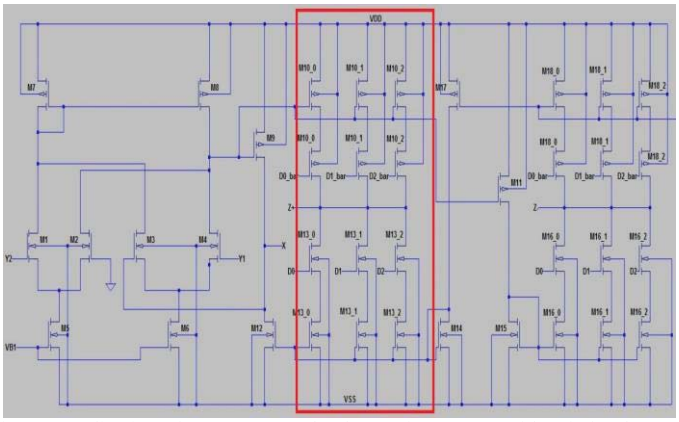

Fig. 11. Realization of DC-DVCC technology using CMOS with gain k. The red box represents the current summing network (CSN).

The active capacitor small signal equivalent circuit is demonstrated in Fig. 13. From the circuit, I_{M1} is equal to I_{M2}. In this small signal model, $V_{CC} = \rho V_{in}$ to simplify the analysis of the circuit later. ρ is controlled by transistor parameter. Based on Fig. 13, the admittance from the input port, Y is determined by I_{in} / V_{in}. I_{in} is the summation of I_{in1} and I_{in2} as follows:

$$I_{in1} = (V_{in}\text{-}V_{cc})sC_{gd2} + (V_{in}\text{-}V_{cc}) \quad (5)$$

$$I_{in2} = V_{in}sC_{gs2} + g_{m3}V_{in} \quad (6)$$

$$I_{in} = I_{in1} + I_{in2} = (V_{in}\text{-}V_{CC})s(C_{gd2}+C_{gd3}) + V_{in}(sC_{gs2} + g_{m3}) \quad (7)$$

$$I_{o1} = V_{cc}\, sC_{gs1} + gm1V_{cc} \quad (8)$$

$$I_{o2} = V_{cc}\, sC_{gs3} + gm2V_{cc} \quad (9)$$

$$I_{out} = I_{o1} + I_{o2} = V_{cc}\,(g_{m1} + g_{m2} + sC_{gs1} + sC_{gs3}) \quad (10)$$

$$(V_{in}\text{-}V_{CC})s(C_{gd2}+C_{gd3}) = V_{cc}\,(g_{m1} + g_{m2} + sC_{gs1} + sC_{gs3}) \quad (11)$$

$$Y_{in} = \frac{I_{in}}{V_{in}} = (\rho g_{m1} + \rho g_{m2} + g_{m3}) + s(\rho C_{gs1} + C_{gs2} + \rho C_{gs3})$$

$$= G_{ac} + sC_{ac} = 1/R_{neg} + sC_{ac} \quad (12)$$

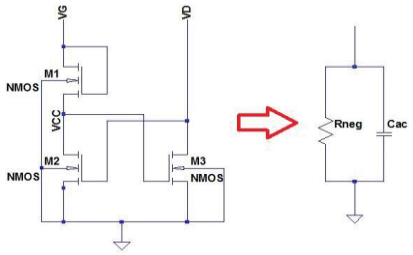

Fig. 12. The tunable active capacitor and its equivalent circuit.

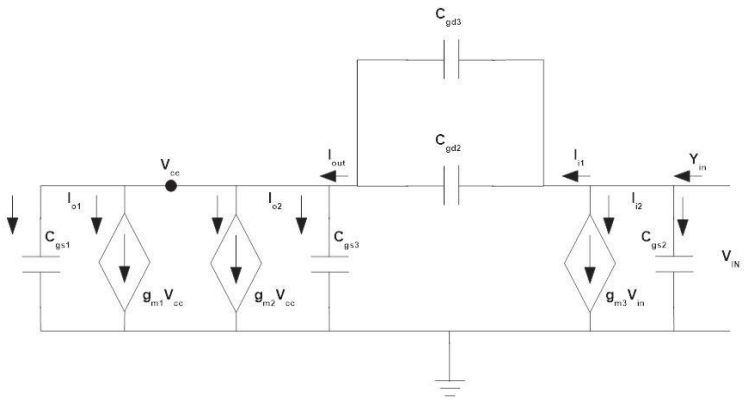

Fig. 13. Small signal equivalent circuit of active capacitor.

For the tunable active capacitor, the width and length of each transistor is set as 15um and 0.18um respectively. To ensure each capacitor is in saturation region, V_D is set as 1 V, while V_G is tunable from 1.6 V to 2 V to vary the capacitance value.

C. *Digitally Re-configurable Multifunctional Filter*

The proposed digitally re-configurable RF multifunctional filter is presented in Fig. 14. Two DVCC blocks, two DC-DVCC blocks, five grounded resistors and one tunable active capacitor are used to design and implement this re-configurable multifunctional filter. The frequency response of this multifunctional filter can be controlled using the 3-bit control word, k. The expressions for the digitally re-configurable filter responses can be expressed as:

$$\frac{V_{LP}}{V_{in}} = \frac{\frac{k^2R(R_3+R_4)}{R_1R_2R_3R_4C_1C_2}}{s^2+sk\frac{R}{R_1R_4C_1}+k^2\frac{R}{R_1R_2R_3C_1C_2}} \quad (13)$$

$$\frac{V_{BP}}{V_{in}} = \frac{\frac{skR(R_3+R_4)}{R_1R_3R_4C_1}}{s^2+sk\frac{R}{R_1R_4C_1}+k^2\frac{R}{R_1R_2R_3C_1C_2}} \quad (14)$$

The resonant angular frequency, w_0 can be defined as:

$$w_0 = k\sqrt{\frac{R}{R_1R_2R_3C_1C_2}} \quad (15)$$

The bandpass and low pass functions can be realized simultaneously at different terminals without changing the circuit configuration. In simulations, using Cadence design platform, the digitally re-configurable multifunctional filter was realized by CMOS implementation using 0.18µm CMOS process parameter. The aspect ratios of the CMOS transistors of DVCC and DC-DVCC are shown in Table II.

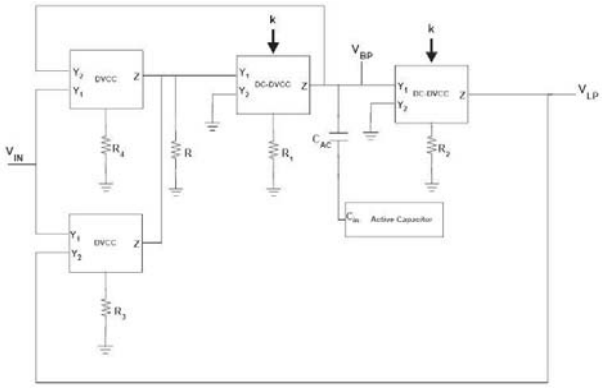

Fig. 14. The proposed digitally re-configurable RF multifunctional filter.

TABLE II.

ASPECT RATIOS OF THE CMOS TRANSISTORS OF DVCC AND DC-DVCC

Transistor	W (um)	L (um)
M1-M4	0.18	0.18
M5-M6	0.9	0.18
M7-M8	0.5	0.18
M9, M11	0.9	0.18
M10 (DVCC)	0.9	0.18
M10(0)	0.9	0.18
M10(1)	1.8	0.18
M10(2)	3.6	0.18
M12,M14	0.72	0.18
M13(DVCC)	0.72	0.18
M13(0)	0.72	0.18
M13(1)	1.44	0.18
M13(2)	2.88	0.18
M15	0.55	0.18
M16(DVCC)	0.55	0.18
M16(0)	0.72	0.18
M16(1)	1.44	0.18
M16(2)	2.88	0.18
M17	0.55	0.18
M18(DVCC)	0.6	0.18
M18(0)	0.55	0.18
M18(1)	1.1	0.18
M18(2)	2.2	0.18

V_{DD} is equal to $-V_{ss}$ which equals to 1.8 V are the supply voltages and V_{B1} =−1.2V and V_{B2}= +1V are the biasing voltages for the circuit. The resistors R_1 and R_2 are set to 50Ω, R_3 is set to 60Ω, R_4 is set to 20kΩ while R is set to 100kΩ.

IV. SIMULATION RESULTS

The proposed digitally re-configurable RF multifunctional filter as shown in Fig. 14 is simulated using Cadence. Fig. 15 and 16 shows two simulation examples of low pass and band pass frequency response of re-configurable multifunctional filter when the digital word, k is set as [d2 d1 d0] = [1 1 1] and [d2 d1 d0] = [1 1 0] respectively. The 3 bit control word is varied from [0 0 1] to [1 1 1] to obtain the cut off frequencies of low pass and band pass filter and all of the results are tabulated in Table III. The variation of cut off frequencies of the proposed filter is only by digital word while the other components in the filter remain the same throughout the simulation. A graph of cut off frequency versus control word of low pass and band pass filter is shown in Fig. 17 and Fig. 18. The maximum total power consumption of the proposed filter is 10.59mW when all the Current Summing Networks in both DC-DVCC blocks are enabled by setting [d2 d1 d0] = [1 1 1]. Fig. 19 shows the linear relationship between total power consumption of the filter and control word enabled in CSNs. The layout design for the proposed filter is shown in Fig. 20. The filter occupies a die area of 3.97mm^2. Based on Table III, the proposed digitally reconfigurable RF multifunctional filter can be tuned from 1.3GHz to 2.5GHz. The simulations and measurements have shown that this approach is feasible and can be applied to cover several targeted wireless standards such as WCDMA, 802.11b, 802.11g, GPS and Bluetooth devices.

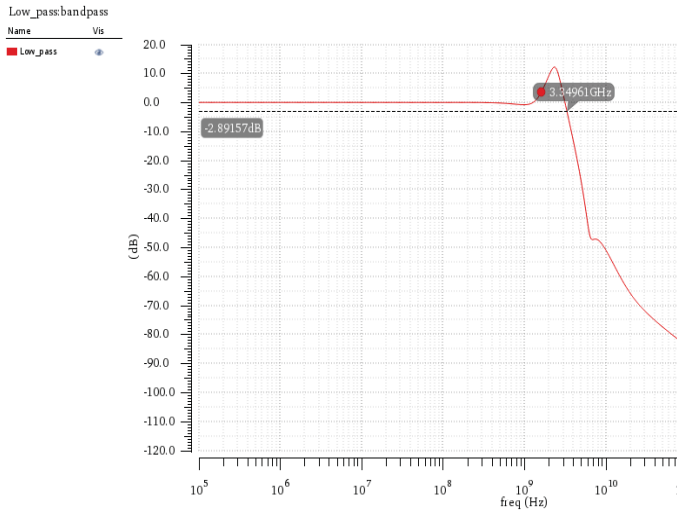

Fig. 15(a). The frequency response for low pass filter with [d_2 d_1 d_0] = [1 1 1] selected.

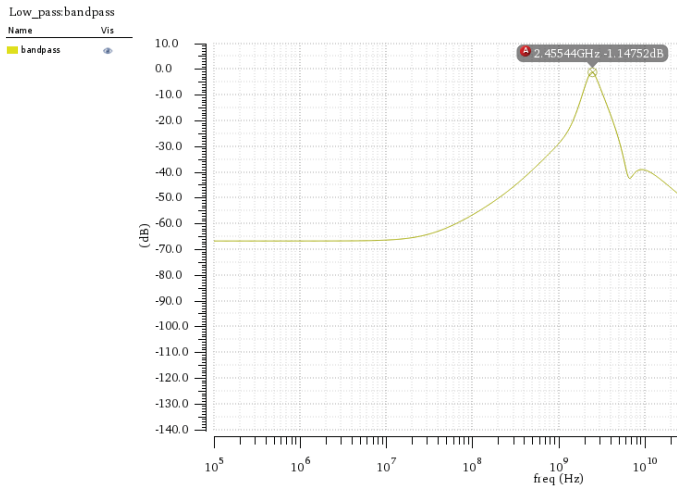

Fig. 15(b). The frequency response for band pass filter with [d_2 d_1 d_0] = [1 1 1] selected.

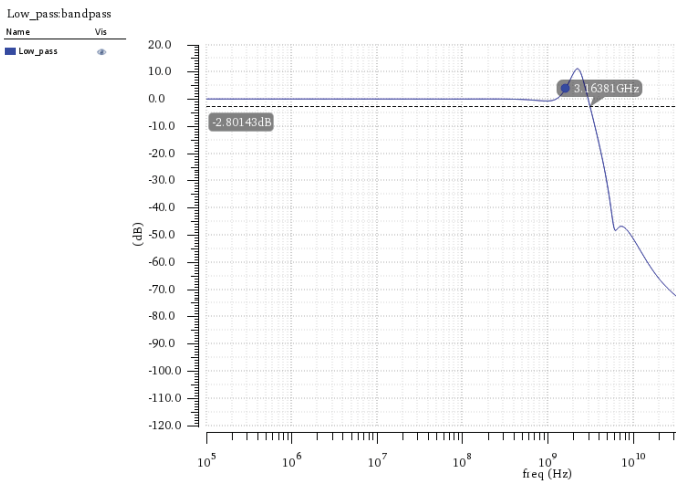

Fig. 16(a). The frequency response for low pass filter with [d_2 d_1 d_0] = [1 1 0] selected.

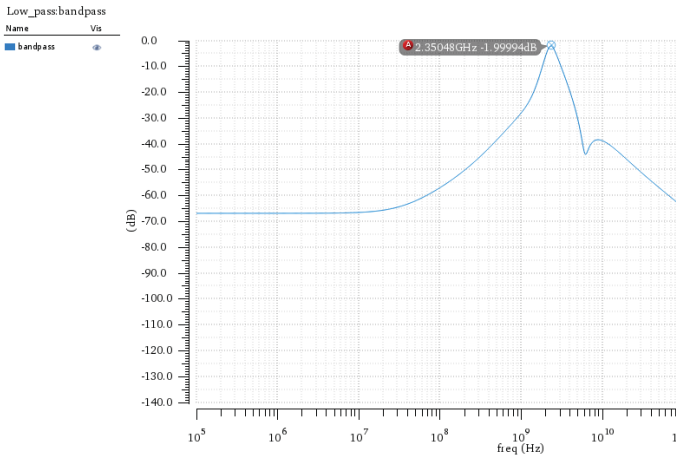

Fig. 16(b). The frequency response for band pass filter with [d_2 d_1 d_0] = [1 1 0] selected.

TABLE III.

VARIATION IN CUT OFF FREQUENCIES WITH CONTROL WORD

Control word, k	Cut off frequency of LPF (GHz)	Resonant frequency of BPF (GHz))
1	1.596	1.234
2	2.115	1.629
3	2.468	1.905
4	2.728	2.089
5	2.9618	2.239
6	3.164	2.35
7	3.35	2.455

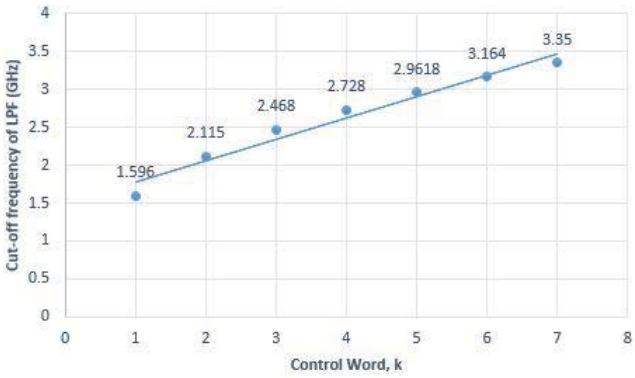

Fig. 17. Variation of cut-off frequency of LPF with control word.

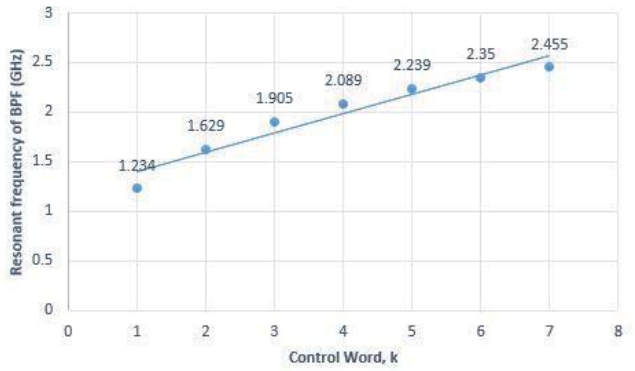

Fig. 18. Variation of cut-off frequency of BPF with control word.

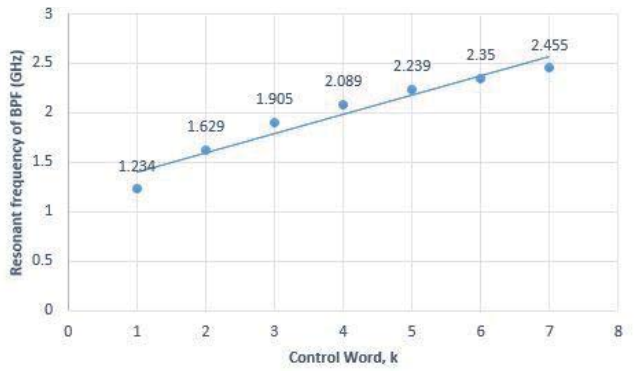

Fig. 19. Power dissipation of proposed reconfigurable filter with control word.

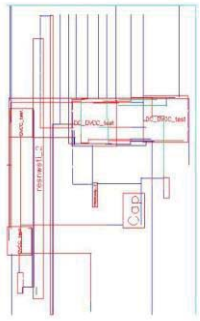

Fig. 20. The final layout of the proposed filter.

V. CONCLUSION

In this paper, a digitally re-configurable RF multifunctional filter was presented. The frequency response of the multifunctional filter can be varied by controlling the 3-bit digital control word using Current Summing Networks (CSNs). As a result, the multifunctional filter can provide low pass and band pass filter responses with different cut-off frequencies at different terminals without changing the circuit configuration. Therefore, the proposed filter can cover several main wireless standards such as WCDMA, WLAN, GPS and Bluetooth at the same time consumes less die area and small power consumption.

REFERENCES

[1] G. Miller, Modern electronic communication (9th Edition), 1st ed. Englewoo Cliffs, N.J.: Prentice-Hall, 2008.

[2] Hussaini, A.S. ; Abd-Alhameed, R. ; Rodriguez, J., " Tunable RF filters: Survey and beyond,"in IEEE international conference on electronics,circuits and systems (ICECS), 2011, pp. 512-515.

[3] J. Chen, "RF CMOS Band Pass Filters with Wide Tuning Frequency, Controllable Pass Band and High Stopband Rejection: Using Passive and Active Inductors", 2016.

[4] S. Tondare, S. Panchal and D. Kushnure, "Evolutionary steps from 1G to 4.5G", International Journal of Advanced Research in Computer and Communication Engineering, vol. 3, no. 4, 2014.

[5] J. C. Rudell et al., "Recent developments in high integration multi-standard CMOS transceivers for personal communication systems," Proceedings. 1998 International Symposium on Low Power Electronics and Design (IEEE Cat. No.98TH8379), Monterey, CA, USA, 1998, pp. 149-154.

[6] X. Li, M. Ismail, " A single-chip cmos front-end receiver architecture for multi-standard wireless applications", ISCAS'01, Sydney,Australia, May 2001, pp. 374–377.

[7] K. Hashimoto, S. Tanaka and M. Esashi, "Tunable RF SAW/BAW Filters: Dream or Reality?", 2011.

[8] C. Andriesei, L. Goras, F. Temcamani and B. Delacressoniere, "Wide Tuning Range Active RF Bandpass Filter with MOS Varactors", vol. 12, no. 4, pp. 485-495, 2009.

[9] M. De Matteis, S. D'Amico, A. Costantini, A. Pezzotta and A. Baschirotto, "A 1.25mW 3rd-Order Active-Gm-RC 250MHz-Bandwidth Analog Filter", 2012.

[10] M. DeMatteis and S. D'Amico, "Advanced Analog Filters for Telecommunications", 2008.

[11] R. Bagheri, A. Mirzaei, and S. Chehrazi et al., "An 800-MHz–6-GHz software-defined wireless receiver in 90-nm CMOS," IEEE J. Solid-State Circuits, vol. 41, no. 12, pp. 2860–2876, Dec. 2006.

[12] D. Lin, Li Li, S. Farahani and M. Flynn, "A Flexible 500 MHz to 3.6 GHzWireless Receiver with Configurable DT FIR and IIR Filter Embedded in a 7b 21MS/s SAR ADC", IEEE Transactions on Circuits and Systems I: Regular Papers, vol. 59, no. 12, pp. 2846-2857, 2012.

[13] A.S. Sedra, K.C. Smith. "A second generation current conveyor and its applications". IEEE Transactions on circuit theory, vol. 17, pp.132-134, Feb. 1970.

[14] W. Chiu, S. I. Liu, H. W. Tsao, J. J. Chen. "CMOS differential difference current conveyors and their applications." IEE Proceedings-Circuits, Devices and Systems, vol. 143, issue. 2, pp. 91-96, Apr. 1996.

[15] H.O. Elwan, A. M. Soliman. "Novel CMOS differential voltage current conveyor and its applications." IEE Proceedings-Circuits, Devices and Systems, vol. 144, issue. 3, pp. 195-200, Jun. 1997.

[16] M. Usama Ismail and B. Arif, "Single Input Multi Output Digitally Reconfigurable Biquadratic Analog Filter", 2014.

[17] Wu, C.Y., Lai, K.N, "Integrated Λ-Type differential negative resistance MOSFET device," IEEE J. Solid-State Circuits, 14, (6), pp. 1094–1101, 1979.

[18] S. Wang and W.-J. Lin, "C-band complementary metaloxide semiconductor bandpass filter using active capacitance circuit," IET Microw. Antennas Propag., Vol. 8, Iss. 15, pp. 1416–1422, 2014.

[19] Y. Wang, J. Chen and C. Henry Chen, "Chebyshev Bandpass Filter Using Resonator of Tunable Active Capacitor and Inductor", 2016.

A Wearable Asthma Monitoring Device for Children

Nur Syazwani binti Noor Azman
Faculty of Electrical Engineering
Universiti Teknologi Malaysia
Johor Bahru, Malaysia.
waniazman2211@gmail.com

Mitra binti Mohd Addi
Department of Electronic and Computer Engineering
Faculty of Electrical Engineering
Universiti Teknologi Malaysia
Johor Bahru, Malaysia.
mtira@fke.utm.my

***Abstract*—Vibration of lung of an asthmatic person is different when the asthma attack occurs. This paper proposed a wearable asthma monitoring device that can be used for children and for parents. With the existence of this proposed device, the parenting becomes much easier for them to handle their children who suffer from asthma disease. Heart rate of asthmatic children is taken to ensure the asthma attack condition. The vibration of lung is processed using Fast Fourier Transform (FFT) through MATLAB and from that, the condition for asthma has been varied according to their severity. Therefore, the performance of proposed device showed that this device can be used as an alternative for parents to keep track of their children.**

Keywords—asthma monitoring, heart rate, lung vibration, fast fourier transform

I. INTRODUCTION

Asthma is one of the chronic diseases in children. It is also the top reason for missed school days [1]. Without proper care and prevention of asthma, this disease can be lead to death. According to recent national statistics [2], current asthma was reported by over 7 million children (9.6%) ages 17 and younger in the United States, of which, 39% (2.8 million) were adolescents (12-17 years old). Nearly 12% of high school students in the United States reported a current asthma diagnosis in 2011[3].

Asthma happens due to the narrowing of airways especially bronchi and bronchioles in the lungs. During normal breathing, the air is able to flow freely into and out of the lungs. Yet, due to inflamed and swollen airways, the asthma becomes out of control making the airways too sensitive to environment changes and eventually will contribute to asthma attack.

Commonly, asthma is caused by genetic and allergies. Asthma can be triggered by many factors such as physical activities, allergic reactions from pollen, dust mites and animals, respiratory colds and infections, air pollutants, smoke from cigarettes. These triggers cause asthmatic children to experience wheezy breath where they are not able to breathe properly due to constriction of airways which produce a wheezing sound. Other than that, children may experience tightness in their chest and rapid in breathing. Currently, there is no cure for this disease which makes the management of asthma patients very important. They have to always be prepared with medication prescribed by the doctor whenever an asthma attack occurs.

In this paper, a wearable asthma monitoring device is proposed to monitor the health of asthmatic children continuously. When asthma attack is sensed to be occurred, the alarm of the monitoring device will alert the parents and give their children an immediate medication or to make sure to keep their children in safe mode. From that, we can reduce any bad consequences that might happen whenever late medication is given to the children. Even worse, the parents might not know that their child is in danger so by having this asthma monitoring device, the parents can be more alert and cautious of their child.

Children who suffer from asthma are always found to have trouble getting medication during asthma attack. In most cases, the children get panicked and had difficulties informing their parents/guardians about their condition. Without immediate treatment, asthma attack can be life-threatening.

Currently, there are two types of asthma monitoring device which are the peak flow meter and the spirometer. The asthma patients use the device for daily or weekly check-up purposes only. The peak flow meter is a simplified device of spirometer. This small handy device is typically used by asthma patients at home. Peak flow meter measures how fast air comes out from lungs when exhaled forcefully. The result of forced exhaled breath is indicated by three coloured zones. Usually, the peak expiratory flow (PEF) value is taken into account by asthmatic patient to know whether their asthma condition is in control or getting worse. For spirometer, it measures the total volume of air that is exhaled and inhaled. Both measurements are taken in order to know how well the lung is functioned. It usually comes with larger device and costs more that peak flow meter. However, these available asthma monitoring device are non-wearable. Moreover, the peak flow meter only measures PEF which is not quite effective in detecting asthma attack.

The proposed asthma monitoring device is able to monitor the condition of asthmatic children continuously and will alert the guardians when the child is about to have an asthma attack. This will allow parents provide immediate medication to the child to ensure that the asthma attack is in control. In addition, the device is proposed to be wearable for easy monitoring as it

will be able to detect early signs of wheezy breath and increased in heartbeat and alert surrounding people from the sound of the alarm. The design of the wearable monitoring device is proposed to improve the management of asthma attack and therefore reduce the probability of death caused by asthma in children.

II. BACKGROUND OF STUDY

A. Introduction

Asthma is one of the pulmonary diseases that commonly happened among people worldwide. According to Global Initiatives of Asthma (GINA) guidelines, there are four stages of severity in asthma which are intermittent, mild persistent, moderate persistent and severe persistent. The asthma stages are classified according to the frequency of attacks which determine the severity of asthma of a person [4].

B. Asthma Management Approaches

The management of asthma is important as to help maintain and improve the condition of asthmatic patients. It is also to prevent the disease from turning into worse if the asthma is not taken seriously by the patient. The asthma management plan is also required to ensure the long-term adherence of the patient to frequently take their prescribed medication.

Traditionally, most doctors propose the asthma patients to have a paper written asthma diary of types and records the times of occurrence of the symptoms. The patients are also required to record their daily medication for the doctor's monitoring purpose. It is an inconvenient approach as sometimes, the patients tend to forget recording in the diary. Thus, it is difficult for the doctors to monitor the condition of asthma patients accurately every appointment.

Besides that, a peak flow meter device (PFM) is commonly used for patients to manage asthma at home. It measures the rate of exhaled air which is expelled from the lungs. Due to its small size, it is easy to use because it fits comfortably in the palm. It is a simplified version of a spirometer as shown in Figure 2.2 that is used in clinics and hospital [5]. Many patients prefer to use this device because it is cheaper compared to a spirometer. A PFM is able to estimate several spirometric parameters which are peak expiratory flow (PEF) and forced expiratory volume of exhaled air in 1 second (FEV-1) [6]. PFM measurements are usually taken in the morning and evening to show the significance between measurements. The results are divided into 3 coloured zones for e.g. red, yellow and green which indicate 80-100%, 60-79% and <60% of full scale respectively [7].

C. Home Telemonitoring for Asthma

Transmission of data by SMS approach was conducted in a design developed by Ostojic, V., et al [8] where the PFM result is sent to the parents/guardian. They have also conducted a research regarding the practicability and adherence of such system. It was found that the system was reliable as the data was sent in real-time. When the technology of personal computers (PC-s) is widely accessible, the PFM results were uploaded to asthma web portals for the doctor to easily access the current management plan of the patient. Instead of PFM result, the diary of symptoms and medication were also regularly updated by the patient [9].

A study by Chen, I.-J. and H.-W. Chiu [10] suggested a smartphone with an asthma management plan which simplifies the interaction between patients and doctors. The research proposed an easy touch-screen user interface, PEF and some questionnaire about asthma symptoms, information on asthma triggers such as humidity or air pollution level in that area which is streamed from public sources based on GPS location. In another design by Chu, H.-T., et al [11], GPS device is used to prevent any possible of asthma attack during patient's outdoor activities. The device constantly will consult with a remote server and decides whether current ambient air quality is health threatening or not. The device collects real-time data from network of air quality monitoring stations.

Several reviews of automated peakflowmetry were made by Cobern, W.R. [12] where the PFM data is uploaded via Bluetooth connectivity to a PC or mobile phone. An extensive study is conducted to know the feasibility of electronic peak flow meter when connected to other devices such as mobile phones. As a conclusion, an automated peak flow meter shows a great achievement among asthmatic patients.

Meanwhile, there are several drawbacks of home peak flow meter as a monitoring device. Despite of the lower precision of FEV-1 value compared to spirometer, this device needs the effort of patient to fully give her/his best to exhale at maximum level as the results may vary according to the efforts given. Lastly, the home peak flow meter only monitors the condition of the patient when in relax mode, but not in the worst airflow obstructions moment [13]. Thus, continuous monitoring is highly demanded to overcome possible asthma attacks.

D. Hardware and Sensor

There are several common hardware and sensors used for monitoring of respiratory function, each depends on the design of the overall system.

(i) Sensors

Microphone: It is used to capture the sound signal. It converts the sound waves into electrical signal. It is contact-less sensing where the air cavity is formed between skin and the sensor. Majority of researchers choses to use the microphone as microphones are less susceptible to noise which are produced by body movement. Furthermore, it does not feature resonance and has a cheaper price. This type of sensor is used in paper [14-15]. A proposed wearable asthma monitoring system used microphone with model number Panasonic WM-64PN and Panasonic WM-61B to capture the breath sound [14] [15].

Accelerometer: It is used to record the mechanical vibrations. It is placed in direct contact with skin surface. The vibrations

produced by the air stream are conducted through the lung wall to surface of skin. In order for this type of sensor to work, a firm contact and no movement of sensor with respect to skin must be ensured. Researchers used this kind of sensor in paper to acquire the respiratory sound signal [16][17].

(ii) Microcontroller

Arduino UNO: This type of microcontroller is used to control the sensors and send the signal to the smart device [18].

E. Signal Processing

Asthmatic wheeze is a continuous adventitious sound which occurs during a part of the respiratory phase. It typically happens at the frequency between the ranges of 100-1500Hz. There are several algorithms that are commonly used in asthma monitoring devices to detect wheeze:

1) Short-time Fourier Transform (STFT)
This is a classical approach for wheeze detection which involves time-frequency decomposition of the sound. The weakness of the algorithm is the uncertainty of its time-frequency resolution. When the frequency resolution increases, it will reduce the time resolution and vice-versa. Example of wheeze detection using STFT is presented in [14] and [18]. A comparison of STFT time-frequency decompositions of normal respiratory sounds and wheezy sounds were made in another research by Oletic, D., B. Arsenali, and V. Bilas [18]. The peaks of wheezing are donated as local peaks along the frequency axis and spread in the direction of time axis.

III. METHODOLOGY

In this project, there are two main parts involved. The first part consists of the hardware system while the second part consists of the software system. The final project will be completed by programming the coding into the hardware system by using Arduino.

A. Hardware and Software

The hardware used in this project are Arduino UNO, WiFi Module ESP 8266, SEN-11754 Pulse Sensor and ADXL335 Accelerometer. While, the software used are:

- Arduino software: C++ programming language of pulse sensor and accelerometer are compiled in this software.
- Virtuino 2.8.2: An Android application which used to control Arduino over WiFi module ESP 8266. It can create visual interfaces with widgets like buttons, LEDs, value displays and others. From the application, the alarm will be triggered if the value of each sensor exceeds the certain threshold.
- MATLAB: The output from accelerometer is sent to MATLAB to convert the output from time domain to frequency domain. After that, each condition of asthma is determined according to the amplitude values and that data will be sent back to Arduino for the next process.

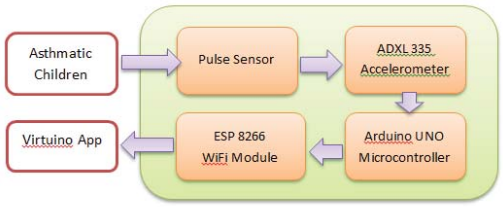

Fig. 1. Schematic overview of the proposed asthma monitoring device and its components.

B. Flowchart

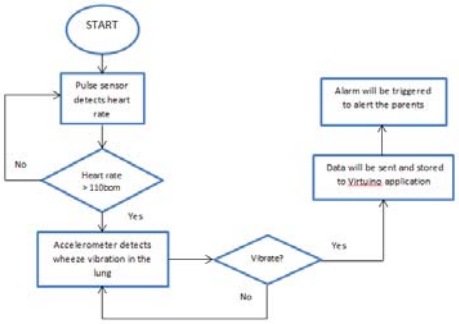

Fig. 1. Flowchart of the proposed asthma monitoring device.

Fig. 2. shows a flowchart on how the proposed device works. Firstly, the pulse sensor will detect the patient's heart rate by wrapping the Velcro around the point finger of patient. If the heart rate is exceeding 110 beats per minute, then accelerometer will play its part by detecting the vibration of lung. The accelerometer is attached on the lung of patient. When asthma attack occurs, the lung will vibrate abnormally as the patient tries to inhale and exhale oxygen vigorously. If the vibration is not detected by accelerometer, it will wait until it detects vibration.

Meanwhile, if the lung vibrates, the data from both sensors which are pulse sensor and accelerometer will be sent and stored in Virtuino application in the Android phone. The alarm will go off to alert the parents when both of the sensors exceed the fixed threshold which is set in the application.

C. Fast Fourier Transform (FFT)

Fast Fourier Transform is a simpler and faster method of implementing Discrete Fourier Transform (DFT) and it is very useful when the value of N samples is large. FFT function in MATLAB is used to convert the signal that comes from accelerometer from time domain to frequency domain. In this project, the vibration of lung during wheezing is observed between the frequency range of 350 Hz and 600Hz [19]. Hence, the need of FFT is important.

IV. RESULT AND DISCUSSION

The proposed device is tested on a normal person since it is difficult and impossible to record data from an asthmatic children and waits for them to have an asthma attack. The data of heart rate detected from pulse sensor is taken before and after a subject exercising. The heart rate data might be deviated a little bit as there is a movement of subject. In average of 15 seconds, the data from pulse sensor is quite reliable and consistent.

```
Heart rate: 80
Heart rate: 80
Heart rate: 79
Heart rate: 80
Heart rate: 81
Heart rate: 81
Heart rate: 81
Heart rate: 81
Heart rate: 80
Heart rate: 80
Heart rate: 79
Heart rate: 80
Heart rate: 80
Heart rate: 79
Heart rate: 79
```

Fig. 3. Ardu sensor before a subject exercising.

```
Heart rate: 90
Heart rate: 90
Heart rate: 89
Heart rate: 89
Heart rate: 89
Heart rate: 88
Heart rate: 87
Heart rate: 87
Heart rate: 87
Heart rate: 86
Heart rate: 86
Heart rate: 86
Heart rate: 86
Heart rate: 85
Heart rate: 85
```

Fig. 4. Arduino serial monitor shows data of heart rate captured by pulse sensor after a subject exercising.

From the Fig. 3. and Fig. 4., the difference of heart rate can be seen before and after the subject exercising. After exercising, the heart rate becomes slightly faster compared to previous ones. Logically, when a person does some exercises or any physical training, the heart rate is above the normal. So, the pulse sensor stays in loop until it detects when the heart rate exceeds 110 beats per minute.

The next process is about accelerometer. Eventhough the accelerometer can be measured in tri-axial, only the y-axis data is taken due to vibration which occurs in that axis. After running the coding in Arduino, the data is plotted using MATLAB to observe the signal of amplitude in unit gravity against time in seconds (time domain). Then, the FFT takes place where the vibration signal in time domain is converted into frequency domain to observe the amplitude values that occur during a fixed frequency range.

When the accelerometer is at rest, the amplitude is not equal to zero as it measures the acceleration in G-forces (g). A single G-force is equivalent to 9.8 m/s^2 on Earth. Fig. 5. shows the acceleration reading when the accelerometer is at rest in 100 seconds.

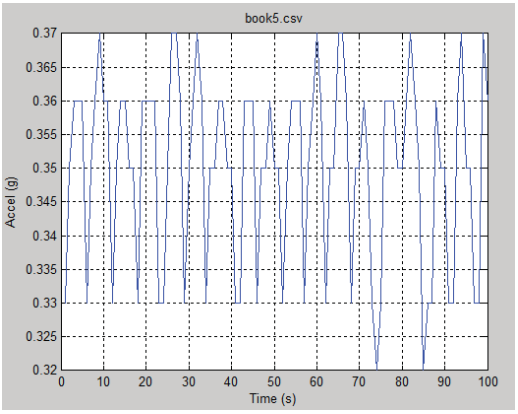

Fig. 5. Accelerometer reading when at rest in time domain

In this project, accelerometer is tested on the vibration of phone instead of lung. To know at which frequency does the phone vibrates, the amplitude of phone vibration is recorded and then, it is plotted in time domain using MATLAB as shown in Fig. 6. After FFT is applied, the signal of phone vibration is plotted in frequency domain in Fig. 7. From Fig. 7., it can be concluded that the vibration of phone is occurs around 250 Hz.

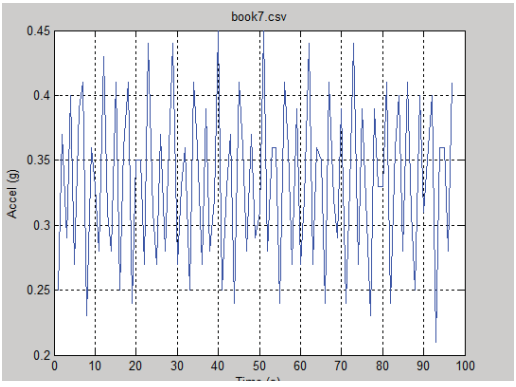

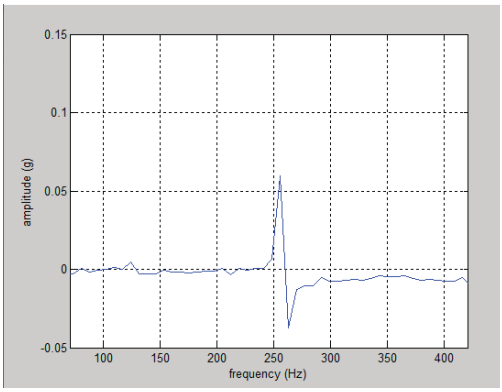

Fig. 6. Vibration of phone in frequency domain

According to [19], the threshold of amplitude vibration is fixed at 0.2 g and above. If the amplitude vibration is below 0.2 g, it is considered as normal vibration condition. So, when the accelerometer gives value of 0.2 g and above, the signal will be sent to the Virtuino application in Android phone for it to ring off the alarm. For better understanding, Table 1 shows the action to be taken next when the amplitude of vibration is detected at certain value.

Table 1. Action taken at a certain range of amplitude

Range of amplitude of accelerometer (g)	Action
≥ 0.2	Alarm will be rang to indicate the asthma attack is going to happen
< 0.2	No action

In the Virtuino application installed in Android phone, the widgets for pulse sensor and accelerometer can be self-customized on the interface. For the pulse sensor, LCD display has been chosen to show the value of pulse sensor in real time while for the accelerometer, statistics chart display has been chosen to monitor the acceleration reading.

V. CONCLUSION AND FUTURE WORK

The overall purpose of this project is to design a simple asthma monitoring system using Internet of Things (IoT) as a platform for data acquisition and analysis in real-time monitoring. However, to make the proposed device works as a wearable device, the noise produced when the body moves is still in research. Thus far, the results show that a significance chance that this proposed device can work in the future. Also, in the future work, this project can focus more on how to get data from the children who has asthma. Medical knowledge should be implemented in order to evaluate the ability of sensors' to determine the severity of patient's asthma.

REFERENCES

[1] *National Surveillance of Asthma: 2001-2010*. 2015, Center for Disease Control and Prevention: United States.

[2] *National Health Interview Survey (NHIS)*. 2009, Center for Disease and Prevention.

[3] *Youth Online: High School Youth Risk Behavior Survey*. 2011, Center for Disease Control and Prevention.

[4] *Global Strategy for Asthma Management and Prevention*. 2015.

[5] *Peak Flow Meter*. Mayo Foundation for Medical Education and Research; Available from: http://www.mayoclinic.com/health/peak-flow-meter.

[6] *Spirometry*. Mayo Foundation for Medical Education and Research; Available from: http://www.mayoclinic.com/health/spirometry.

[7] Glykas, M. and P. Chytas, *Technological innovations in asthma patient monitoring and care.* Expert Systems with Applications, 2004. **27**(1): p. 121-131.

[8] Ostojic, V., et al., *Improving asthma control through telemedicine: a study of short-message service.* Telemedicine Journal & E-Health, 2005. **11**(1): p. 28-35.

[9] Finkelstein, J., M.R. Cabrera, and G. Hripcsak, *Internet-based home asthma telemonitoring: can patients handle the technology?* Chest Journal, 2000. **117**(1): p. 148-155.

[10] Chen, I.-J. and H.-W. Chiu, *A review for information systems to support outpatient asthma health management.* 2009.

[11] Chu, H.-T., et al. *A ubiquitous warning system for asthma-inducement*. in *IEEE International Conference on Sensor Networks, Ubiquitous, and Trustworthy Computing (SUTC'06)*. 2006. IEEE.

[12] Cobern, W.R., *Asthma self-management using mobile telephone technology*. 2006, Department of Engineering Science, University of Oxford.

[13] Gavriely, N. *Acoustic asthma management, presentation.* KarmelSonix 2009; Available from: http://www.karmelsonix.com.

[14] Zhang, J., et al. *A novel wheeze detection method for wearable monitoring systems*. in *Intelligent Ubiquitous Computing and Education, 2009 International Symposium on*. 2009. IEEE.

[15] Ser, W., et al. *Detection of wheezes using a wearable distributed array of microphones*. in *2009 Sixth International Workshop on Wearable and Implantable Body Sensor Networks*. 2009. IEEE.

[16] Oletic, D., B. Arsenali, and V. Bilas, *Low-power wearable respiratory sound sensing.* Sensors, 2014. **14**(4): p. 6535-6566.

[17] Pasterkamp, H., S.S. Kraman, and G.R. Wodicka, *Respiratory sounds: advances beyond the stethoscope.* American journal of respiratory and critical care medicine, 1997. **156**(3): p. 974- 987.

[18] Kwan, A.M., et al., *Personal Lung Function Monitoring Devices for Asthma Patients.* IEEE Sensors Journal, 2015. **15**(4): p. 2238-2247.

[19] Uwaoma, Chinazunwa, and Gunjan Mansingh. "Towards Real-Time Monitoring and Detection of Asthma Symptoms on Resource-Constraint Mobile Device." In *Consumer Communications and Networking Conference (CCNC), 2015 12th Annual IEEE*, pp. 47-52. IEEE, 2015.

Fast Adder Performance in ASIC

Lee Mei Xiang
Faculty of Electrical Engineering
Universiti Teknologi Malaysia
Johor Bahru, Malaysia.
meixiang94@gmail.com

P.M. Muhammad Mun'im Ahmad Zabidi
Department of Electronic and Computer Engineering
Faculty of Electrical Engineering
Universiti Teknologi Malaysia
Johor Bahru, Malaysia.
munim@utm.my

***Abstract*— In VLSI IC design field, the performance of a chip is influenced by design environment, schematic and sizing parameter of the transistors used. Same concept go to adders IC design. Presently, the embedded system in VLSI pay more concern on area, power consumption and its performance. Nowadays, we prefer a high performance with low power consumption system. As we all know, adder is the critical circuit that full fill of those requirements. Therefore, this project aims to investigate the performance of a high performance Parallel Prefix Adder by using Quartus II and Sypnopsis tools in the target of 0.18nm Silterra Technology. The types of adder included in this project are Ripple Carry Adder, Carry Look Ahead Adder, Kogge Stone Adder and Default Adder. The objective of this project is to select the optimal transistor size in order to obtain a good trade-off between power consumption and propagation delay. At the end of this project, we find out that the performance of Kogge Stone Adder is the best compare to other adders.**

Keywords*— *Kogge Stone Adder, Ripple Carry Adder, Carry Look Ahead Adder, Parallel Prefix Adder, Area, Power Consumption, Time Delay, Sypnopsis, Propagator, Generator.

I. INTRODUCTION

In VLSI implementation, many embedded system or processors (DSP) required high performance function with low power consumption to full fill the higher quality in technology world. In a system, the most important elements always came from the lowest level. With the right usage of lowest gate level, the system will have more space to be improved.

As we all know, adder is a very basic building blocks in common data path component. It is known as an important block in many applications which need advance accelerate adder. There have so much adder architecture from previous researcher. However, the most basic adder architecture is known as Ripple Carry adder (RCA).

The most straightforward explanation of basic logic circuit for adder is shown as Figure 1. Figure 1 is known as one bit RCA or Full Adder. For two bit RCA or above, The Carry from previous bit will become the input of C in the next bit. So, now comes a problem, the delay for passing the carry to another stage will become more dominate if the number of bits of an adder increases [2].

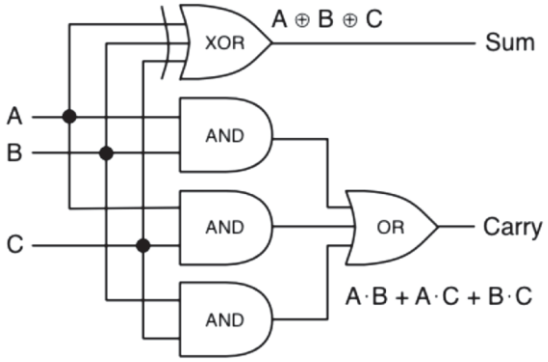

Fig. 1. Basic Logic Gate for Adder.

In order to overcome this problem, extensive research was continued to focus on improving the performance and the power consumption of adder. In VLSI implementations, Parallel Prefix Adder was proved to have better performance than previous adder.

In Parallel Prefix adder, binary addition usually presents in terms of Generation Signal (Gi), Propagation Signal (Pi), Carry Signal (Ci) and Sum Signal (Si). Each bit position will follow the range of i as i less or equal to n and more or equal to 1 ($1 \leq i \leq n$)[3].

All of these signals can be obtain from the equation below [4]:

$$G_i = a_i + b_i \quad (1)$$

$$P_i = a_i \oplus b_i \quad (2)$$

$$C_i = \begin{cases} G_i \\ G_i + P_i C_{i-1} \end{cases} \quad (3)$$

$$S_i = P_i \oplus C_{i-1} \quad (4)$$

The sum for Parallel Prefix Adder can be obtained by three stages as shown in the block diagram below [5].

Fig. 2. Block diagram in getting the sum for Parallel Prefix Adder.

According the figure above, P_i and G_i generated from pre-processing block based on equation (1) and (2). The signals will be proceed to the next stage, Prefix Carry Tree to generate carry bits signal. This stage is the part that differentiate or the

performance of an adder used. On the other hand, the final stage is aim to get the final adder result by follow the equation (4).

Figure 3 shown the interconnection for Prefix Carry Tree Block.

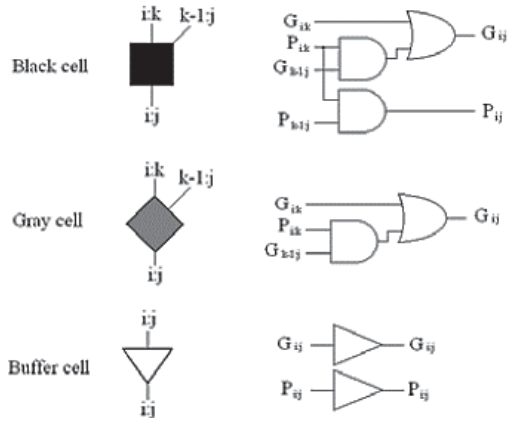

Fig. 3. Complex Logic Cell inside the Prefix Carry Tree [5]

There are a lot of Parallel Prefix adders been developed start from 1960. For example 1960: J.Sklansky–conditional adder, 1973: Kogge-Stone adder, 1980: Ladner-Fisher adder and etc [9].

The adder that we will concentrate more in this paper is Kogge Stone adder (KSA). The concept of Kogge Stone adder was developed by Peter M. Kogge and Harold S. Stone, and hence published in a seminal paper titled in 1973. It was introduced to solve a large class of recurrence problems in parallel computer such as the Illiac IV. Nowadays, KSA is known as the special and fast adder in VLSI world. It always being comprised in the architecture of three blocks, which are pre-processing, carry generator and post processing block with others Parallel Prefix adders.

Figure 4 shown the example of interconnecting of KSA in carry generator block or can be known as Prefix Tree Block.

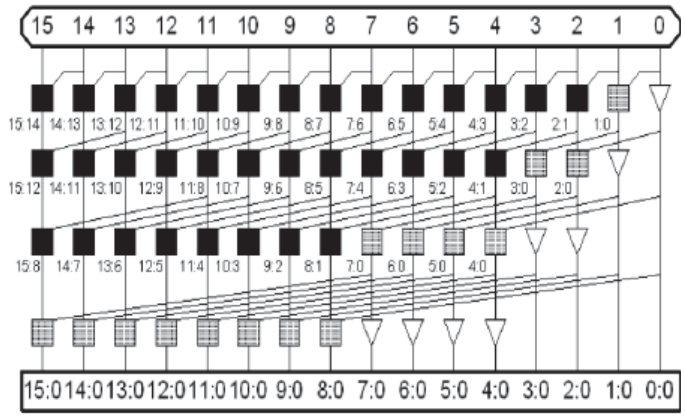

Fig. 4. 16-bit Kogge Stone Adder

In this project we will compare the characteristics of chosen adders, which are Ripple Carry adder, Carry Look Ahead adder and Kogge Stone adder. Carry Look Ahead adder (CLA) and KSA are known as Parallel Prefix Adder. However, according from previous researcher the architecture in CLA is simpler than KSA but need more time in adding.

II. METHODOLOGY

This session explains the methodology used in completing this project. Basically, there are two softwares used in this project which are Quartus II and Sypnopsis Tools. The details of the flow of project will discuss in sub-chapter. Figure 5 shows the overview of the project methodology.

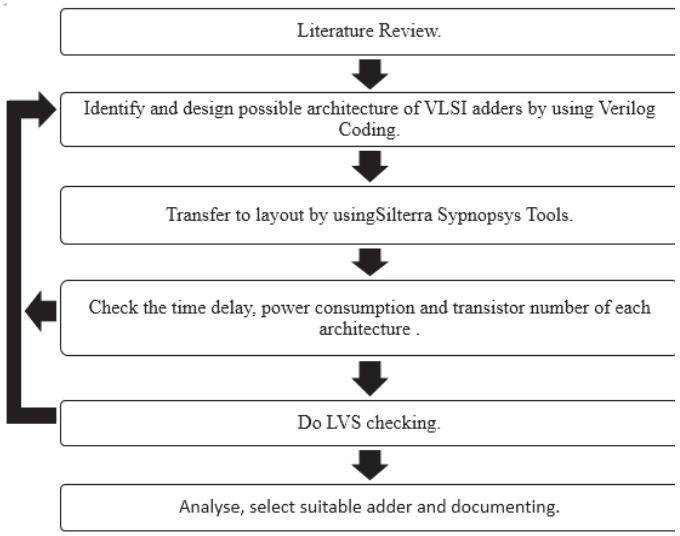

Fig. 5. Methodology Flow Chart

A. Quartus II

Before implementation the adder design into VLSI, the adders were built and went through FPGA simulation by using Quartus II. The device family used in this project is Cyclone IV GX. During the implementation, Verilog code was used to build the library cells for top-entity and test bench of each adder.

The formulae used in Ripple Carry adder, Carry Look Ahead adder and Kogge Stone adder are shown in equation below:

1) Ripple Carry Adder:

- This adder is built by various full adder blocks based on the bit number required.
- The formulae used in each full adder block is as below:

$$Sum = A\hat{}B\hat{}Cin \quad (5)$$

$$Cout = (Cin \,\&\, A)|Cin \,\&\, B|(A \,\&\, B) \quad (6)$$

2) Carry Look Ahead Adder:

- This adder is built by various propagator and generator blocks (PG) and various carrier generator blocks (PPC) based on the bit munber required.
- The formulae (7) and (8) represent PG block, formulae (9) represent PPC block and formulae (10) showed the process of adding.

$$P_i = A_i\hat{}B_i \quad (7)$$

$$G_i = A_i\&B_i \quad (8)$$

$$C_{i+1} = (P_i \& C_i) | G_i \quad (9)$$

$$Sum_i = P_i \hat{} C_i \quad (10)$$

3) Kogge Stone Adder:

- The architecture of KSA is partially alike as CLA. However, there are another type of block between PG blocks and PPC blocks which is known as Fundamental Carry Operator block (FCO).
- It is used to process the propagator and generator bits from pre-processing structure.
- In addition, the formulae in PPC block has a bit difference from Carry Look Ahead adder.
- The formulae (11) and (12) represent PG block, formulae (13) and (14) represent FCO block while formulae (15) represent PPC block and formulae (16) showed the process of adding.

$$P_{i\_j} = A_i \hat{} B_i \quad (11)$$

$$G_{i\_j} = A_i \& B_i \quad (12)$$

$$P_{i\_j-1} = P_{i\_j} \hat{} P_{i-1\_j} \quad (13)$$

$$G_{i\_j-1} = (G_{i-1\_j} \& P_{i\_j}) | G_{i\_j} \quad (14)$$

$$C_{i+1} = (P_{i\_0} \& C_0) | G_{i\_0} \quad (15)$$

$$Sum_i = P_i \hat{} C_i \quad (16)$$

- Which i represent the number of bit, and j represent the level in FCO block.

The purpose in using Quartus II is just to make sure the architecture of each adder functioned correctly. Once the outputs were verified, it will proceed to pre-layout and post-layout by using Sypnopsis Tool.

B. *Synopsis Tool*

The Sypnopsis Tools are used in mapping RTL design into ASIC design. It is done by transferring the Verilog code to layout automatically. The details for each adder will be recorded into the results for pre-layout or synthesis, post-layout or static analytic time and ICC.

The figure 6 showed the design methodology by using this method. However, some changes occur along this project as I replaced Astro by ICC shell.

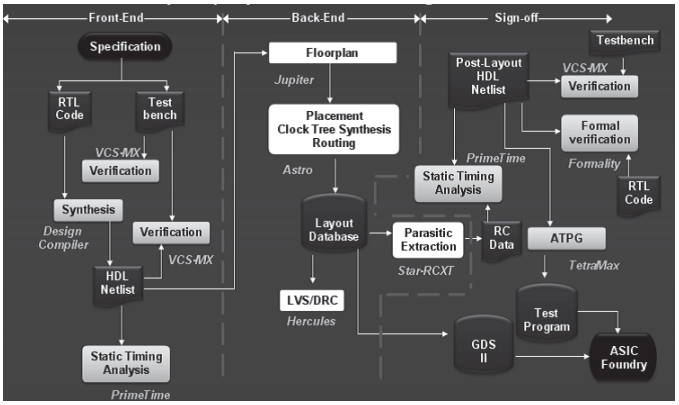

Fig. 6. Project Flow Chart by using Sypnopsis Tools

III. RESULTS

In this section, things will be discuss are about the area size, average power, total cells used and the details in static timing analysis (STA) and synthesis for each adders design by using 20 Nano seconds clock period. We do run for the waveform and RTL gate simulation in Quartus II too. However, the results from both simulations have no reference values. Hence, the two simulations are only used for determine the Verilog design code and the test bench code for each adders design functioned correctly.

For the architectures in each adder, we added the registers in the beginning and the ending point in order to make the measurement of data transferring time become more visible.

Table 1 below show the results data for each type of adder in different bits.

TABLE I. DETAILS PARAMETER FOR EACH TYPE IN DIFFERENT BITS

Type of Adders		Total Power (mW)	Leakage Power (µW)	Total Cell Area (mm^2)	Time Delay (n sec)
8 bit	RCA	0.1118	0.0094	0.0024	4.83
	CLA	0.1162	0.1031	0.0025	3.44
	KSA	0.1213	0.1240	0.0031	3.02
	Default Adder	0.1285	0.1086	0.0024	3.78
16 bit	RCA	0.2211	0.1863	0.0047	7.35
	CLA	0.2253	0.2015	0.0049	5.45
	KSA	0.2406	0.2618	0.0065	3.61
	Default Adder	0.2230	0.1961	0.0046	6.83
32 bit	RCA	0.4959	0.3724	0.0093	12.50
	CLA	0.5029	0.4004	0.0097	10.15
	KSA	0.6152	0.5932	0.0140	3.75
	Default Adder	0.1319	0.2392	0.0046	2.47

Below are the graphs for each parameters to show the relationship in each type of adders.

A. . *Total Power*

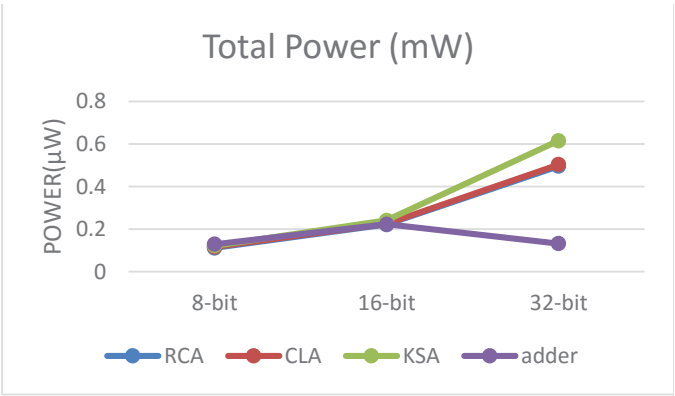

Fig. 7. Total Power in each type of adders

B. *Leakage Power*

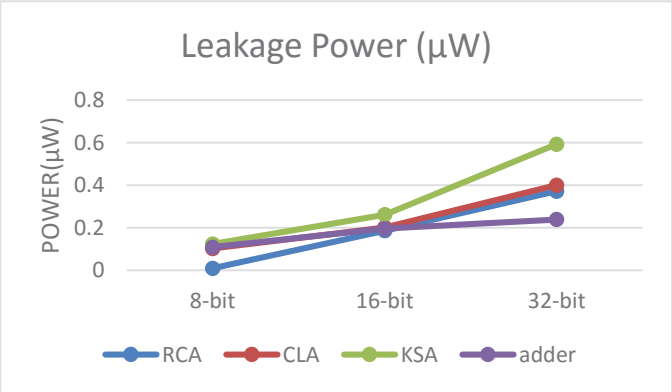

Fig. 8. Leakage Power in each type of adder

C. *Total Cell Area*

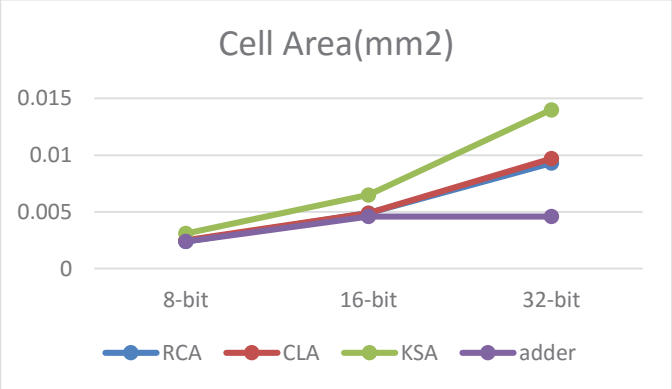

Fig. 9. Total Cell Area in each type of adder

D. *Time Delay*

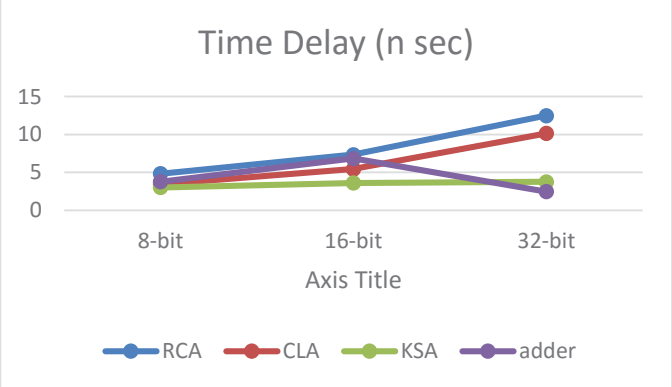

Fig. 10. Time Delay in each type of adder

IV. Discussion

Based on the results value we can clearly see that the time delay in Kogge Stone adder is the lowest from 8-bit to 16-bit. However, in term of 32-bit the lowest time delay shown is the default adder used in Sypnopsis. This is because we have no idea how the architecture of the default adder look like. We cannot conclude that default adder is always in the best performance as the performance in Kogge Stone adder show more stability than the default adder.

Next, in terms of total power usage, every adder showed almost the same value with each other from 8-bit to 16-bit. However in 32-bit, Kogge Stone adder show slightly more power usage than others but default adder showed aggressively less power usage than others. The reason had explained at above.

Furthermore, default adder showed almost balance value in leakage power, same goes to Ripple Carry Adder and Carry Look Ahead Adder. Their value of leakage power grows linearly. However, leakage power in 32-bit Kogge Stone adder increased more than others adder. Same situation goes to total cell area. From this, we can conclude that the leakage power of each adder is affected directly by the cell area of an adder.

In order to see the performance for each bit of adder, radar graph had been used. The 16-bit adder has the most reference value.

A. *8-bit Adder*

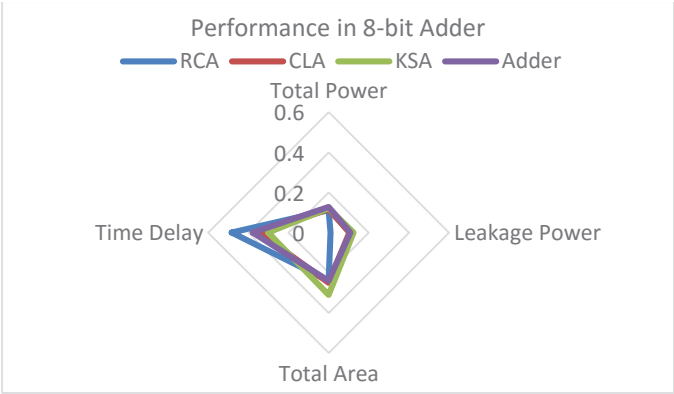

Fig. 11. Performance in 8-bit adder

Based on figure 11 above, we can see that Kogge Stone adder has the lowest time delay but the cell area is slightly larger than others. Its' power usage is almost the same with Carry Look Ahead adder and default adder in Sypnopsis. For Ripple Carry adder, it has lowest leakage power but highest time delay. It is not consider as an ideal adder used in other systems as the time delay will bring forward from one level to another level. Hence for 8-bit adders, Kogge Stone adder is more suitable to use.

B. 16-bit Adder

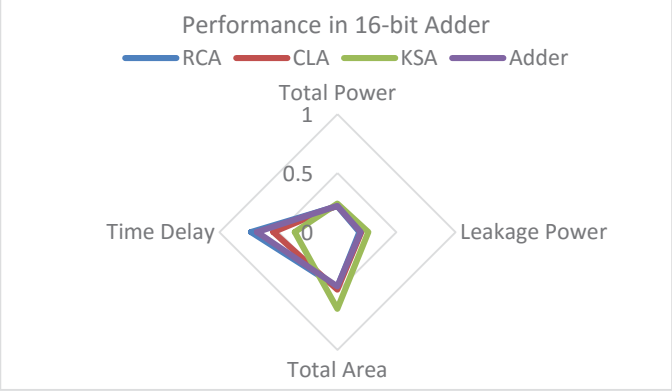

Fig. 12. Performance in 16-bit adder

Figure 12 showed the performance for each type of adder in 16-bit. As performance in 8-bit, Kogge Stone adder has the lowest time delays but highest in leakage power and cell area. However, the difference in terms of time delay is higher than the leakage power and cell area. In others meaning, Kogge Stone adder has the best performance than others with accepted power usage and cell area.

C. 32-bit adder.

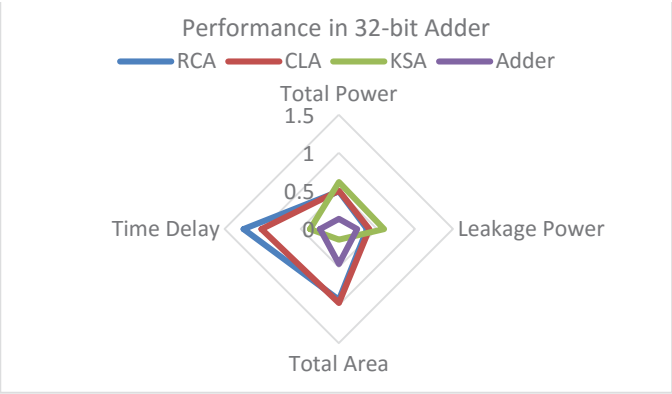

Fig. 13. Performance in 32-bit adder

Figure 13 above clearly showed that the Ripple Carry adder and Carry Look Ahead adder have the lowest performance. The time delays in RCA and CLA is too high and not suitable to be used in others system. For Kogge Stone adder, it showed a great performance in each parameters. It can be said that performance of 32-bit Kogge Stone adder is better than other bits. However, here comes to an option, default adder in Sypnopsis required lowest power usage and lowest time delays. Although it required more cell area than Kogge Stone adder, it seem to be an optimized adder to be used. However, Kogge Stone adder is better in terms of stability. The performance of Kogge Stone adder is increased linearly along its' bits. Unlike default adder, the performance are not stable in the growing bits.

V. Conclusion

From this project, we know that Ripple Carry adder has the simplest adder architecture and lowest power consumption. However, it required higher time delay due to its' serial adding process.

On the other hand, Carry Look Ahead adder as one of the prefix parallel adder has simpler adder architecture compare to Kogge Stone adder. It required lowest setup and hold time among them. However, its' time delay is the highest which is not suggested to use in this project.

Last but not least, without counting on default adder used in Sypnopsis, Kogge Stone adder has the lowest time delays and reasonable power usage and total cell area in almost all bit. We can conclude that the best performance of Kogge Stone adder showed in 32-bit. Although it used the most complicated adder structure, but it is suggested to use due to its characteristics.

As a conclusion, the results had met the objectives of this project. According the simulation results, we get a lower time delays and reasonable power usage and total cell area adder which is Kogge Stone adder. Hence, this project can be consider as hit the targets as state before.

VI. Acknowledgment

First the all, I would like to thank for Silterra by arranging the Sypnopsis Tools training and middle term clinic to help me in the process of completing this project.

Next, many thanks for CEDEC by providing the Sypnopsys Tools training and also the platform for me to complete my pre-layout and post-layout deigns.

In additional, I would like to thank Dr. Hadi for helping me in my simulation by using Sypnopsis Tools and teach me the way to analyze the data.

Last but not least, I want thank my supervisor, PM Munim as he help me in my project from the beginning until the end. Thanks for everyone that make my project a success.

References

[1] Gangula Thirupathi Reddy, D. M. C. 64 Bit Pipelined Hybrid Sparse Kogge-Stone Adder Using Different Valance. International Journal of Research Studies in Science, Engineering and Technology, 2015.

[2] Cory Merkel, D. B. 8-bit Parallel Prefix Adder Using Brent Kung Tree BIST. EECC730. November 2008.

[3] Haikun Zhu, R. G., Chung-Kuan Cheng. Constructing Zerodeficiency Parallel Prefix Adder of Minimum Depth. Ph.D. Thesis. ASP-DAC. 2005,2006.

[4] Vibhuti Dave, E. O. and Saniie, J. Performance Evaluation of Flagged Prefix Adders for Constant Addition. Ieee international conference. Faculty of Electrical Engineering, Mathematics and Computer Science, Delft University of Technology. 2006.

[5] Anas Zainal Abidin, K. K. M. S. Z. O. M. A. H., Syed Abdul Mutalib Al Junid. 4-bit Brent Kung Parallel Prefix Adder Simulation Study Using Silvaco EDA Tools. Issn: 1473-804x online, 1473-8031 print. 2015.

[6] V. Krishna Kumari, D. M. K., Y. Sri Chakrapani. Design and Characterization of Koggestone, Sparse Koggestone, Spanning tree and Brentkung Adders. International Journal of Scientific and Engineering Research. 2013.

[7] Amos R. Omondi, Benjamin Premkumar, "Residue number systems: theory and implementation", Imperial College Press, Technology & Engineering, 2007

[8] Andrew Beaumont-Smith and Cheng-Chew Lim, "Parallel Prefix Adder Design", Department of Electrical and Electronic Engineering, The University of Adelaide,5005, Australia, 2001

[9] Kostas Vitoroulis, "Parallel Prefix Adders", Concordia University, 2006

[10] VLSI Design, Technician Publications, ISBN=8184314817, 9788184314816

[11] A. P. Godse and D. A. Godse, "Digital Systems Design" - I: Technical Publications, 2008.

[12] Tien-Yu Wu, Ching-Tsing Jih, Jueh-Chi Chen and Chung-Yu Wu, "A Low Glitch 10-bit 75-MHz CMOS Vidoe D/A Converter", January 1995.

FPGA based High Speed Data Acquisition

Loh Shu Ting
Faculty of Electrical Engineering
Universiti Teknologi Malaysia
Johor Bahru, Malaysia.
stloh_1234@hotmail.com

Muhammad Nasir Ibrahim
Department of Electronic and Computer Engineering
Faculty of Electrical Engineering
Universiti Teknologi Malaysia
Johor Bahru, Malaysia.
mdnasir@utm.my

***Abstract*— Today's computing technology can do a lot of fast processing which is shown by the usage of high speed data acquisition system. But, with the current and frequently used architecture of microcontroller as the data acquisition device, it might not be the best in high speed performance. Field Programmable Gate Array which is well known with its flexibility and parallelism qualities is proposed in order to acquire data with the maximum speed available from the hardware connected with it. Not only this, this project applies a primary noise elimination feature as well as offline monitoring and storage of data. Processor of Cyclone IV, ADC0804 and RS232 Universal Asynchronous Receiver and Transmitter communication are integrated to form a fundamental data acquisition system. Very High Speed Hardware Description Language is used to create the controller program since it is well structured and has lots of available software support. The highest frequency of input signal captured is 2902 Hertz with maximum sampling frequency of 16,780 Hertz. In the future, the system can be built as an affordable device to acquire real-time biomedical signal where offline monitoring of patient's health condition can be done at home instead of medical institution.**

Keywords—Data Acquisition System (DAS); Field Programmable Gate Array (FPGA); Analog-to-Digital Converter (ADC); Very High Speed Hardware Description Language (VHDL).

I. INTRODUCTION

In data acquisition system (DAS), there are two kind of physical parameters to be interfaced with which are the analog signal from real world and digital signal from artificial world [1]. Digital system has been increasingly utilised since it eases the process of computation, control and measurement functions relating to signal processing. Thus, to communicate between analog and digital worlds, analog-to-digital (A/D) and digital-to-analog (D/A) converters are used. In this data acquisition system which deals with both analogue and digital signals, data converters are applied.

Other than data converters, components involved in DAS are transducers, amplifiers, filters, nonlinear analog functions, analog multiplexers and sample-hold circuit [1]. These components interconnect with each other to form a basic DAS as shown in Fig. 1. Input to the system might be various type of physical variables, categorised by characteristic type and measurement type. Physical variables under characteristic type include force, thermal, rate, quantity, time, chemical composition, physical properties and electrical. Whereas, variables categorised under measurement type are force, electrical, motion and time-modulated signal [2]. These physical signals are to be converted into electrical signal by transducer.

After converting into electrical signal, signal conditioner can be applied whenever necessary. Amplifier functions to amplify the amplitude of the signal to a significant level that can be detected by electronic circuit from microvolt or millivolt to 1 to 10 Volt (V) levels. Signal amplified might be affected by common-mode noise or other types of noise. Thus, a low-pass active filter can be implemented to minimise the high frequency signal components or the unwanted electronic noise. Sometimes, nonlinear analog function circuit that involves operations such as linearization, multiplication, division, squaring, and log conversion will be applied [1].

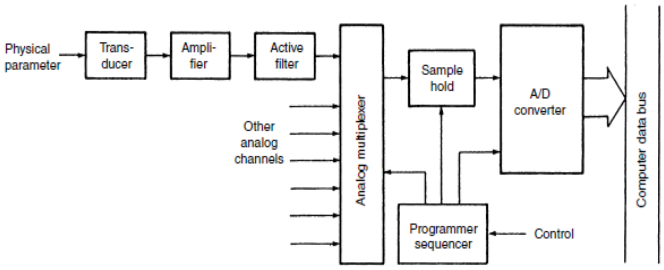

Fig. 1. Data acquisition system in general [1].

Next, the processed analog signal will be sent to analog multiplexer to choose between different channels of analog input. The selector of the multiplexer is controlled by the electronic circuit or known as programmer sequencer in Fig. 1 [1]. Prior to the conversion stage, a sample-hold circuit will acquire the signal voltage and hold the value while waiting for the A/D converter (ADC) to convert the analog value to digital form. The resultant digital data will be transmitted into the electronic circuit as input data.

The purpose of this study is to build a fundamental data acquisition system using Field Programmable Gate Array (FPGA). There are many cases of DAS built using microcontrollers and computer [2] which implemented microprocessors or microcontrollers rather than FPGAs. Therefore, in this study, self-built ADC module was used to convert analog signal to digital data controlled by Altera FPGA DE2-115 board and ADC0804 Integrated Circuit (IC). Only one channel of input was supplied to the module. The data acquired was then sent to laptop to be displayed and for further development in the future. Meanwhile, this system has the

potential to acquire real-time biomedical signals such as heart rate.

II. Literature Review On Previous Work

A. Related Work In Market

In the current market, many health-related products have been released. This is due to the rising concern of the society towards health issue. Products are sold to be portable, easy to use yet advanced. Fig. 2 show the product named Kardia Mobile, released by Alive Cor, which uses simple pulse sensor attached at mobile phone casing to measure heart rate [3]. The heart rate measured can be observed in phone with electrocardiogram (ECG) signal displayed as well as heart rate in beat per minute (bpm). This ECG data can be sent to health experts to do further analysis on one's health. But, it is using phone application and microprocessor to do the task.

Fig. 3 is known as Wireless Continuous Non-Invasive "Beat-by-Beat" Blood Pressure and Heart Rate Monitor produced by CareTaker Medical in United States [4]. This device offers continuous non-invasive blood pressure and heart rate monitoring using patented finger cuff technology. It targets for usage during patient transport and remotely after patient discharge.

Fig. 4 is a biotelemetry device called Intensive Care Unit (ICU) Telemetry created by Dextronix. This Bluetooth enabled VET-Scout heart rate monitors can deliver all ECG signals from the patient into hospital Local Area Network (LAN) via their proprietary Wireless Application Protocol (WAP)-Access Point router in real time [5]. This device applies Bluetooth when patients move outside the range of WAP access point and Virtual Private Network (VPN) or Internet to monitor patients if patients are still inside the covered range of their network. But, their patients are animals currently.

An Internet of Things (IoT) Heart Attack Detection and Heart Rate Monitor was invented by NevonProjects at India [6]. This device detects heart rate using heartbeat sensing and interfaced with microcontroller. The heart rate detected is displayed in Liquid Crystal Display (LCD) in terms of bpm values and also displayed in computer software via Internet. On the online software, user can set minimum and maximum heart rate. Whenever the user's heart rate exceeds either one of the maximum or minimum limits, the device gives out alarm to alert about the possible danger. This device uses microcontroller as the processor.

Fig. 2. ECG signal displayed in mobile phone, namely Kardia Mobile from Alive Cor [3].

Fig. 3. Wireless continuous non-invasive "beat-by-beat" blood pressure and heart rate monitor [4].

Fig. 4. ICU telemetry from Dextronix, Inc. [5].

B. High Speed Data Acquisition System Using Different Systems

In 2008, High Speed Data Acquisition System Using FPGA for LLRF Measurement and Control paper studied on a high-speed data acquisition system that employed FPGA with a fast 14-bit ADC to acquire 1.3 Giga Hertz (GHz) LLRF at sampling rate of 270 MHz [7]. Data was acquired by FPGA from ADC then transmitted to personal computer (PC) to do analysis. In this research, FPGA was used to acquire high speed radio frequency and Double Data Rate Synchronous Dynamic Random-Access Memory (DDRAM) of FPGA played a role in this DAS.

In the same year, other than LLRF, image processing was also a hot topic in research. The Platform of Image Acquisition and Processing System Based on DSP and FPGA by Yan Lei *et al.* [8] researched about real time image processing by getting data from PC, data acquired by FPGA and data processed by Digital Signal Processor (DSP). FPGA played the role of logic unit and buffer for transferring image data using its RAM and First-In-First-Out (FIFO) features. A remarkable point is FPGA was used not only due to its flexibility but also its memory feature.

Samrat L. Sabat, Ajay Kumar D and P. Rangababu [9] proposed a DAS in FPGA using Sytem-on-Chip (SoC) method with cyclic redundancy check (CRC) technique to support the error checking mechanism of DAS in the study of Reliable High Speed Data Acquisition System Using FPGA. The FPGA used was Xilinx Aurora protocol. Data of 1.25 Giga bits per second (Gbps) was transmitted using Universal Asynchronous Receiver Transmitter (UART) instead of wire. This study has focused on the capability to detect error and retransmit the data frame if error is detected. Wireless transmission method has been used since 2009.

While time went on, Song Gu and Zhou hulin [10] have studied on an image acquisition system comprised the Altera FPGA board and Nios soft-core processor as the DAS main core and published their paper, The Design of Image Acquisition and

Display System. This paper highlighted the usage of Static Random Access Memory (SRAM) in FPGA and most importantly they proved the potential of using soft core instead of hard core processor to achieve programmable SoC system.

The paper of Implementation of High Speed Distributed Data Acquisition System [11] and High Speed Data Acquisition System with Ethernet Interface [12] introduced on distributed data acquisition interface using FPGA. Both papers discussed on similar subject that was implementing a distributed data interface with 16 channels of analog inputs and data was transmitted to computer through Ethernet interface. It is clear that FPGA was used due to its flexibility in hardware, short design duration and low power consumption. The data transmission method of these papers is more advanced by using Ethernet to deliver data to a remote computer system. Very High Speed Integrated Circuit Hardware Description Language (VHDL) was the hardware description language used in this paper.

In Design of High-Speed Parallel Data Interface Based on ARM & FPGA, FPGA was integrated with Advanced Reduced Instruction Set (RISC) Machine (ARM) processor to form a parallel data interface which improved the metastability problem during data transmission between asynchronous clock-domains [13]. FPGA was used due to its parallelism and able to reconstruct characteristic. Parallel data were passed to FPGA's DDRAM then only transmitted to ARM to further process the data. This paper shows that low speed module which is the FPGA can perform high speed data acquisition which could possibly save the cost of the design.

Back to year 2013, the paper of Platform-Based Design Approach for Embedded Vision Applications [14] studied on real-time image and video processing system using Xilinx ML-507 FPGA board with Virtex-5 core. The purpose of using FPGA was the need of reusable design and flexibility. Input real-time Red-Green-Blue (RGB) analog video was converted into frames and transmitted into DDRAM of FPGA. This indicates that memory feature in FPGA is crucial in DAS.

In the High-Speed Data Acquisition System Based on FPGA in Missile-Borne Test System research paper, it proposed something different on the DAS using FPGA. The Xilinx FPGA-based DAS comprised three input analog channels with one 5M samples per second (sps) sampling rate and three 256 Megabytes (Mb) NAND Flash [15]. The collected data were stored in non-volatile Flash memory and imported into USB disk after that. The input data were echo signal, ignition signal and power signal of a fuse on the missile. FPGA was applied to test the system of fuse to ensure a precise guide and control of the missile. Again, memory and processing speed of FPGA played important roles in the system.

III. RESEARCH METHODOLOGY

A. Hardware Design

In terms of hardware, this system employs several components which are:

1) *Signal source*
2) *ADC module*
3) *Data acquisition device*
4) *Display*

Signal source consists of variable resistor with constant voltage and signals from function generator. Constant voltage from variable resistor tests for the consistency and accuracy of the data acquired by FPGA. Whereas, function generator generates waveforms of different frequencies to test for the maximum possible speed capability of FPGA and its competency to deal with different type of signals. All signals applied range from 0 to 5V.

The ADC0804 chosen is an 8-bit resolution Successive Approximation Register (SAR) ADC with total of 20 pins [16]. Among that, it has 9 input pins and 9 output pins connected to FPGA and input voltage source and 2 input pins being left unconnected. The clock of ADC is supplied by FPGA instead of using its own internal clock generator controlled by timing of resistor and capacitor. ADC0804 is then designed on a circuit board with a potentiometer and corresponding pin headers.

On the other hand, Altera FPGA DE2-115 board is chosen to be the data acquisition device. Although FPGA's clock frequency is much lower than microprocessor, but its parallelism characteristic can solve the timing issue compared to microcontroller and microprocessor which operate on fetch-decode-execute cycle. FPGA is a hardware control device and flexible, which has lesser limitations compared to MCU which has fixed hardware interconnections. The FPGA board chosen does not possess built-in ADC and has no hard processor. This is to give a flexibility to this study where not necessary board with hard processor and built-in ADC can be used as the data acquisition device.

For the connections part, General Purpose Input Output (GPIO) connector is used to connect between FPGA and ADC. The overall connection from FPGA to ADC is depicted in Fig. 5. While the connection from FPGA to PC is just done by connecting the RS232 to USB converter cable from RS232 serial port of FPGA to USB port of PC.

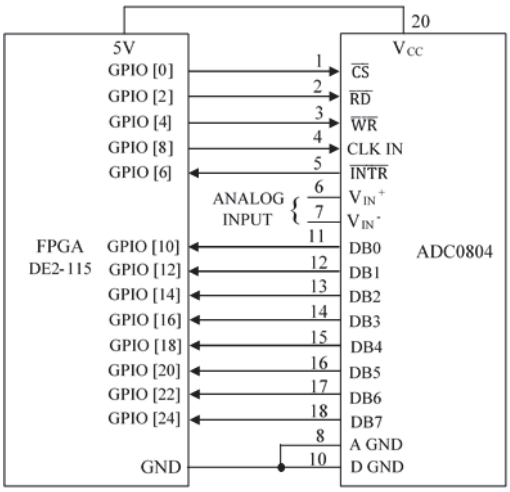

Fig. 5. Connections of ADC0804 with FPGA DE2-115.

B. ADC Controller Design

ADC0804 has minimum conversion time of 66 clock cycles of the ADC clock and maximum of 73 clock cycles of the ADC clock [16]. It can support clock frequency of 100 kHz to 1460

kHz [16]. ADC controller is then being designed using VHDL in Quartus II software by following the timing requirement of ADC0804. VHDL is a strongly and richly typed language as well as more verbose than Verilog. It makes the design self-documenting and thus permits development of reusable packages to cover functionality that is not built into the language. Strong typing allows the compiler to catch as many errors as possible in early of the validation stage.

In the controller, clock frequency of 50 MHz of the FPGA is scaled to 1389 kHz by using Equation 1 [17]. By substituting the desired new frequency which in the maximum supported clock frequency of the ADC into the equation, prescaler of 17.12 is obtained. For prescaler of 17, the new frequency calculated is 1471 kHz, while for prescaler of 18, the new frequency calculated is 1389 kHz. Therefore, prescaler of 18 is used since it does not exceed the maximum clock limit of the ADC.

$$f_{new} = \frac{f_{original}}{prescaler * 2} \quad (1)$$

f_{new} = new clock frequency
$f_{original}$ = original clock frequency

In order for the ADC to operate, an active low write and chip select signal should be given first to initiate the conversion process in ADC. Upon completion of the conversion, an active low interrupt signal is generated half clock cycle later and sent to the output pin to be detected by FPGA. By detecting this interrupt signal, FPGA will then send an active low read signal to ADC to request for the converted digital data. Once ADC detected the falling edge of the read signal, data is ready at the output pin (DB0 to DB7) after 200 nanosecond (ns) of access time [17].

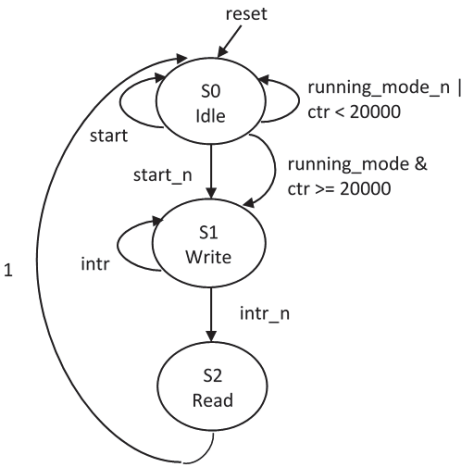

Fig. 6. Timing diagram of data output enabled [18].

The overall flow of the operation is indicated in Fig. 6 which is the FSM chart for the ADC controller. Idle state is where a counter delay of 20000 is located before proceeding to write state after the read state. Write state is the operation of sending active low write and chip select signal to ADC. Read state is the state entered when active low interrupt signal is detected and active low read and chip select signal are then being sent to ADC to access the digital bits. It will go back to idle state once the read operation is completed. Start represents the active low push button.

C. UART Controller Design

The communication tool applied in this study is RS232 Universal Asynchronous Receiver and Transmitter (UART) protocol in FPGA. This communication method is an asynchronous data transmission where no clock signal is required to send to the receiver in the transmission process [18]. In this study only transmitter is used because data is intended to send to PC and no data is to be received from PC. Prior to the sending of data, both transmitter (FPGA) and receiver (PC) must have the same timing parameter which is the baud rate [18]. Baud rate of 9600 is used to aim for a stable data transmission.

In serial communication, the parallel data bits from ADC are packed into a frame of 10 bits and being sent to PC serially where start bit is the first bit sent out of the data frame. The data frame comprises 1 active low start bit, 8 data bits with least significant bit (LSB) sent out first after the start bit and 1 active high stop bit. Start bit is used to inform the receiver that the data transmission is started. Following by the start bit are the 8 data bits and then the active high stop bit to tell the receiver that the transmission process has ended [18]. The data packet format is indicated in Fig. 7. Parity bit is known as the error checking bit. In this study, no parity bit is included. UART controller is then designed based on the data packet format in VHDL. FSM chart for the transmission process in top level entity is depicted in Fig. 8.

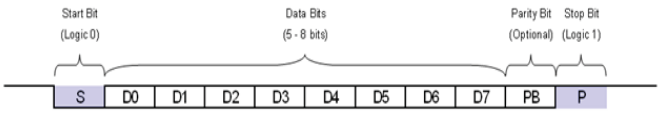

Fig. 7. UART data packet format [18].

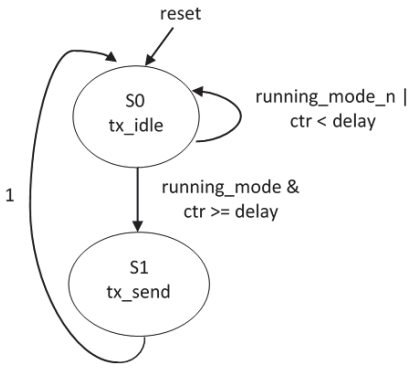

Fig. 8. FSM of initiating the UART transmission process.

IV. Result And Discussion

A. Implementation of ADC Controller

Prior to implementation on hardware, simulation was done to check the functionality of the program. Fig. 9 shows the simulation waveform of ADC controller using Quartus II ModelSim. When start signal was inserted, chip select and write signal went low for one clock cycle. The state changed from state 1 which was the idle state to state 2 which was the write state. The state maintained at state 2 until active low interrupt signal

was inserted. Read signal and chip select went low at the next clock cycle. Data was acquired once the interrupt signal detected and state changed to state 3, the read state. The state went back to idle state once no interrupt signal was detected. A fix delay was running in the idle state before going into write state. When reset signal was inserted, the data stored was cleared and state restarted at idle state.

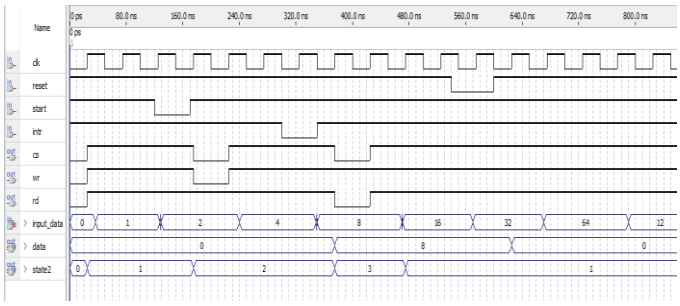

Fig. 9. Simulation waveform of ADC controller.

For the hardware part, LED display was programmed from pin LEDR0 to LEDR7 to represent the 8 bit data from ADC. LEDR0 was the LSB and LEDR7 was the most significant bit (MSB). The LED displayed can be represented in decimal values by using Equation 2.

$$\text{Digital Reading} = \frac{Analog\ Input\ Voltage \times Resolution\ of\ ADC}{System\ Voltage} \quad (2)$$

Fig. 10. Digital bits of 0b00001001 indicates voltage value of 0.174V.

B. Implementation of UART Controller

Fig. 11 shows the simulation waveform of RS232 UART transmitter controller waveform. Only transmitter is used in order to make the FPGA (transmitter) to have same baud rate with PC (receiver), the clock frequency of 1389 kHz was scaled again using Equation 1. But, in this controller, the prescaler was calculated by dividing initial frequency, 1389 kHz, with desired frequency, 9600 Hz. Prescaler of 145 was obtained. No operation was done at that stage. Data was sent to the tx_line when the clock is half of the new clock. The new clock was divided by half due to its 50% duty cycle.

In the simulation, the system clock was simulated at 20 MHz. With the prescaler set to 3, the new clock was 5 MHz. When at half of the prescaler which should be 1.5 but ended up round off to 2 in digital, it indicated the rising edge of the new clock by assuming the initial pulse of the clock was active low. Data transmission started at the rising edge of the new clock. Signal of busy was set high once start signal was asserted to represent the ongoing transmission process. It would be low again once the transmission process was completed.

By referring to the waveform, the 8-bit data was "0000 0101". After packing with the start bit and stop bit, the data transmitted in tx_line was "01010 00001". The tx_line represents the UART TXD pin of FPGA. Setting of 8 data bits, 0 parity bits, 1 start bit, 1 stop bit and baud rate of 9600 was set in the SerialPlot software. The data obtained was set to be in the format of uint_8 which means unsigned integer of 8 bits. The software also provide choices for user to record the data in text file.

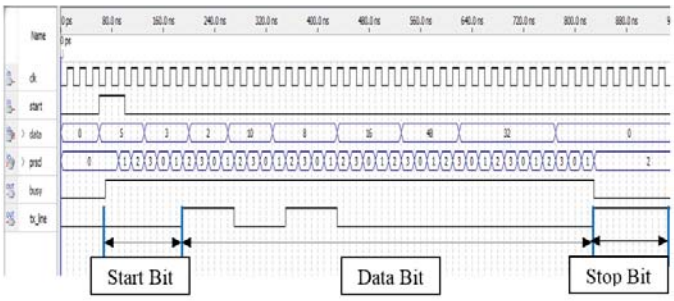

Fig. 11. Simulation waveform of RS232 UART transmitter controller.

C. Implementation of Full Data Acquisition System

Full DAS was formed by combining both ADC controller and UART-TX controller in form of component in the top level entity. The system has reset button, ADC start button, UART transmission start button, ADC interrupt signal and input data from ADC as the input. Whereas, the output consists of ADC chip select signal, ADC write, ADC read, data acquired from ADC, state for ADC operation and UART transmission line. Fig. 12 discloses the simulation waveform of overall data acquisition system where ADC and UART transmission part were combined. The ADC process was started once ADC start button was pressed which was represented by adc_start signal. When UART transmission start button, represented by uart_start signal, was pressed, the successfully acquired ADC data was then sent into the UART TXD pin which was represented by uart_txd signal. This formed the basic operation for the DAS built.

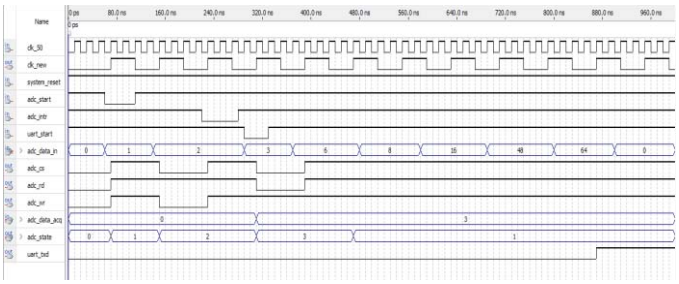

Fig. 12. Simulation waveform of full data acquisition system.

In the hardware implementation phase, the input signal was sourced from function generator with adjustable frequencies and range from 0 to 5V. When the sine wave input signal was inserted, the results was displayed at SerialPlot software in PC in form of graphics. The results obtained should be the same as the input signal waveform inserted to ADC. Fig. 13 exhibits the output digital bits for signals of frequencies 550 Hz (a), 2902 Hz (b) and 4 kHz (c). All three waveforms can roughly show back the curve of the sine wave.

The sampling rate for the ideal case which has 1389 Hz clock frequency and with only 73 clock cycles for one complete

conversion was 19.03 kHz. In fact, the real worst case maximum sampling rate for ADC0804 is 16.78 kHz with total conversion time of 82.78 clock cycles after calculating from the write and read operation in the datasheet with the system applied instead of 73 maximum clock cycles stated in datasheet [16].

Based on Fig. 13, the curve of output waveform for all three frequencies seemed to be acceptable since they show a copy of sine waves as the input signals but in fact aliasing has occurred for 4 kHz output waveform. The higher the input frequency, the more the cycles should be shown in the plot with the same time scale. But, output waveform of 4 kHz possessed less cycles of wave than 2902 kHz output waveform. It has actually surpassed the optimum range of input frequency with the sampling rate provided. Hence, it is concluded that aliasing has occurred and caused inaccurate reconstruction of output waveforms. Output waveform of 2902 Hz is behaving according to the theory thus it is an acceptable output.

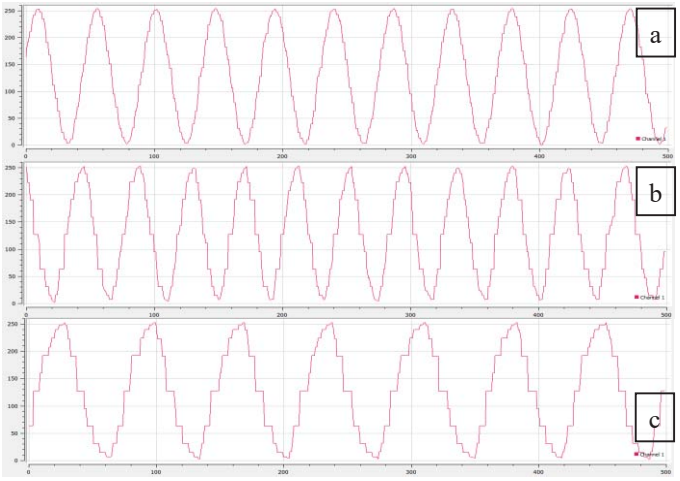

Fig. 13. Output waveform of 550 Hz (a), 2902 Hz (b) and 4 kHz (c).

V. Conclusion And Future Work

Data exists in every matter of our daily life. It is important to acquire the data so that human can become more advanced by studying the data. Basic study by applying artificial signals to the data acquisition device has been done in this project. Maximum frequency of 2902 Hz was successfully acquired by this system followed by the success of offline monitoring and data storage. Therefore, it holds the potential to further study this system.

Multichannel or high speed ADC with sampling rate of 1 Msps can be considered in order to enhance the function of the system. Signal conditioning can be implemented when real world signal is applied. A packet of data acquired from ADC can be stored in Synchronous Dynamic Random-Access-Memory (SDRAM) before sending to PC to eliminate latency between the data obtained.

References

[1] Gerd W¨ostenk¨uhler (Ed.), "132: Data Acquisition Systems (DAS) In General," Reproduced from the Handbook Of Measuring System Design, John Wiley & Sons, Ltd., 2015.

[2] Measurement Computing Corporation, Data Acquisition Handbook, A Reference For DAQ And Analog & Digital Signal Conditioning, (3rd Ed.), United States of America: Measurement Computing Corporation. 2004-2012.

[3] AliveCor, Inc., "Introducing the Kardia™ Mobile ECG," 2016. [Online]. Available: http://www.pmsinstruments.co.uk/pdf/Kardia-Mobile-Data-Sheet.pdf, [Accessed December 22, 2016].

[4] Dave Fornell and Jeff Zagoudis, "FDA approves CareTaker wireless remote patient monitor," Diagnostic and Interventional Cardiology, May 2016. [Online]. Available: http://www.dicardiology.com/product/fda-approves-caretaker-wireless-remote-patient-monitor, [Accessed December 22, 2016].

[5] Dextronix, Inc., "ICU telemetry," [Online]. Available: http://www.dextronix.com/products/icu-monitor/, [Accessed December 22, 2016].

[6] NevonProjects Software & Embedded Kits. "IOT heart attack detection and heart rate monitor," [Online]. Available: http://nevonprojects.com/iot-heart-attack-detection-heart-rate-monitor/, [Accessed December 22, 2016].

[7] H. Katagiri, S. Fukuda, T. Matsumoto, T. Miura, S. Michizono, Y. Yano and M. Yoshida, "High speed data acquisition system using FPGA for LLRF measurement and control," Proceedings of LINAC08, Victoria, BC, Canada, pp. 1042-1044, 2008.

[8] Yan Lei, Zhao Gang, Ryu Si-Heon, Lee Choon-Young and Bae Ki-Man, "The platform of image acquisition and processing system based on DSP and FPGA," International Conference on Smart Manufacturing Application, IEEE, pp. 470-473, 2008.

[9] Samrat L. Sabat, Ajay Kumar D and P. Rangababu, "Reliable high speed data acquisition system using FPGA," Second International Conference on Emerging Trends in Engineering and Technology (ICETET-09), IEEE, pp. 392-396, 2009.

[10] Song Gu and Zhou hulin, "The design of image acquisition and display system," 2nd International Conference on Education Technology and Computer (ICETC), IEEE, vol. 5, pp. 23-26, 2010.

[11] Anju P. Raju and Ambika Sekhar, "Implementation of high speed distributed data acquisition system," International Journal of Advancements in Research & Technology (ISSN 2278-7763), SciResPub, vol. 1, no. 4, pp. 1-7, 2012.

[12] Anju P. Raju, "High speed data acquisition system with ethernet interface," IOSR Journal of Electronics and Communication Engineering (IOSRJECE) (ISSN: 2278-2834), SciResPub, vol. 2, no. 5, pp. 12-17, 2012.

[13] Daode Zhang, Yurong Pan and Xinyu Hu, "Design of high-speed parallel data interface based on ARM & FPGA," Journal of Computers, vol. 7, no. 3, pp. 804-809, Academy Publisher, 2012.

[14] Jai Gopal Pandey, Abhijit Karmakar, Chandra Shekhar and S. Gurunarayanan, "Platform-based design approach for embedded vision applications," Journal of Image and Graphics. Engineering and Technology Publishing, vol. 1, no. 1, pp. 1-6, 2013.

[15] Mingyu Zhou, Xuan Zhou, Guangyu Zhen and Shusheng Peng, "High-speed data acquisition system based on fpga in missile-borne test system," Applied Mechanics and Materials (ISSN: 1662-7482), Switzerland: Trans Tech Publications, vols. 333-335, pp. 452-459, 2013.

[16] Texas Instruments Incorporated, "ADC080x 8-bit, uP-compatible, analog-to-digital converters," November 2009, Revised June 2015.

[17] Carlos, A. R., "Frequency Divider with VHDL," [Online]. Available: https://www.codeproject.com/Tips/444385/Frequency-Divider-with-VHDL, 2012. [Accessed May 15, 2017].

[18] Kong, W. W., "UART - Universal Asynchronous Receiver and Transmitter," [Online]. Available: http://tutorial.cytron.com.my/2012/02/16/uart-asynchronous-receiver-and-transmitter/, 2010 [Accessed May 15, 2017].

Automatic Locking System using CPLD

Tan Chu Wei
Faculty of Electrical Engineering
Universiti Teknologi Malaysia
Johor Bahru, Malaysia.
tcwei93@gmail.com

Mr Muhammad Arif bin Abdul Rahim
Department of Electronic and Computer Engineering
Faculty of Electrical Engineering
Universiti Teknologi Malaysia
Johor Bahru, Malaysia.
arif@fke.utm.my

***Abstract*—This paper introduce the design and implementation of complex programmable logic device (CPLD) EPM240-based locking system. This automatic locking system use password to unlock the door which replaced the traditional key methods. User is required to enter the correct password in order to unlock of the system. Alarm will be triggered for above three attempt. The software used in this project is Altera Quartus II and Verilog is used in writing the program. The CPLD EPM240 board is used to develop and boot the programming code into the project. Finally, the design is implemented on the CPLD EPM240 board with an external circuit on the bread board which consists of a 4x4 matrix keypad, a seven segment display and some important electronic components. Thus, the matrix keypad is used as input interface and electronic lock and seven segment as output interface. A electronic lock is chosen to perform the locking mechanism in this project. This interface circuit can be used to test the functionality of the design without referring to the simulation waveform. In short, the output result should be the same as expected. Generally, this password based locking system is able to increase the security level as compared to the traditional methods.**

Keywords—CPLD EPM240; Altera Quartus II; Verilog; Automatic Locking System; Password.

I. INTRODUCTION

According to the report on Crime in United States 2015, the rate of property crime was estimated at 2487.0 per 100,000 residents in year 2015[1]. Property crimes resulted in the loss of estimated at $14.3 billion per year. In Malaysia, house burglary contributed around 20 percent among the others [2]. Hence, we can concluded that house burglary is a critical concern today even though under CCTV surveillance. A survey conducted found out that the majority of the burglars will avoided homes with security system and 74 percent of failed burglaries can be credited to the audible alarm [3]. The project today aimed to minimize the rate of house burglary. The traditional method where used a key is no more safe as anyone can duplicated the key easily or forcibly break into the house by using some tools. Market today comes out with various alternatives to replace this traditional locks like electronic locks and mechanical locks. Electronic locks quite expensive where not everyone can afford to have one. Mechanical locks in the market today still considered as slow mechanism for operation and not user-friendly. Hence, from the above problems, an automatic password based locking system using CPLD is introduced. The cost of this system is affordable and it is more secure since the password entered needed to match with the predefined password which have many possibilities.

II. OBJECTIVES OF STUDY

Based on the aforementioned problem statements, the objectives of this project have been derived as following:

1. To learn the knowledge of design using hardware language and understand its importance.
2. To increase the security level of the locking system and to prevent an unauthorized unlocking of the system.
3. To give flexibility to the users to change or reset password in case the used forget the current password.
4. To give user a more affordable and cost-efficient way of locking system.

III. LITERATURE REVIEW

According to the readings, the oldest and simple locks was discovered in the ruins of the Assyrian Empire, in the city of Khorsabad near Nineveh. Nowadays, technological advances are rapidly making it possible to automate much of the works currently carried by humans. Locking system today also evolved from only the original and simple mechanical lock into the electrical lock and as well to the electronic type. Today, with the assemblage of electronic and mechanic at the locking system, the lock system has developed into a high technology styles where it needs some special authentication to unlock it. Such automatic locking system will only operate after it receives certain information [4].The example of the locking system available in the market today are biometric, security token, RFID, GSM, NFC and etc. In general, the working principle for this type of authentication locking system normally use the embedded systems to process and to verify the password that the user had entered. Such advance and automatic locking system actually trouble to the burglars as they need much time as well works to break this high-tech locking system [5].

A. Authentication Methods

1) Password Type

This type of authentications methods can considered as the most popular method where it used numerical code as the access tool. Generally, the users need to enter the correct password via keypad and unlock the system. The password normally consists of 4 to 6 digits and there are 1 million possibilities for the passwords. Such longer password actually can cause some problem especially when the users will get forgotten easily since it is difficult to memorize. According to Birget, the passwords actually have two criterions which are against each other [4]. The two

statements are password should be easily to memorize by the users and the password should be safe from the intruders.

2) Token Type

Generally, the token used by the users can be a ring, passport, card, identity card or other devices that can keep the information and data to be verified by the security system. The method implemented is RFID where it authenticates the user by using the radio wave which belongs to the token type group. Normally, the operation needed the tag to store the information as the code and usually such tag is embedded into an object for verification. The controller will then receive the serial data from the reader and control the locking system. If the code in the tag detected is correct, then the system can be unlocked, else it will remain locked. The validation for the detection field of the reader depends on the system design where it may up to several meters long [6].

3) Biometric Type

The advance type of authentication system would be the biometrics authentication where it related to the human characteristics and it used in computer science as a form of identification and access control. Such identifiers are distinctive, measurable characteristic used to describe and labeled the individuals. The example included fingerprints which are quite popular today, face recognition, voice detection, DNA, hand geometry, palm print and etc [5].

B. Existing Modal of Security System

1) Security System using Password

For this, most of the research showed that PIC as the microcontroller, Atmel's chip and FPGA are used in the implementation of this type of locking system. The reason for using PIC is because of the lower cost and simple design. In the paper of M.H. Muhammad [7], he enhanced the previous lock by adding the reset function to the lock where the users can reset the password by themselves through the microcontroller EEPROM. FPGA is used by some researchers in their findings. Sitong S., Angang T. and Decai Z [8] introduced FPGA-based electronic look. The benefits of this are that it can be easily modified as the latest design can direct programmed into the hardware without any changes needed for the hardware. Meanwhile, the drawback for this is that the price of FPGA available in the market are quite expensive.

2) Security System using Token

There are several types of token that have been introduced by the researchers which included RFID card, keys and remote controller. Based on A. Fang, X. Ye, M. Gong, W. Yang, L. Zhang in their research [9], the 32-bit ARM CPU of PHILIPS has been chosen as the core and the subsystem included RAM, ROM, Real time clock and LCD in performing this complete locking system. Such locking system applies the infrared communication module to allow the data exchanged with the door lock. RFID card of EM4100 series is used as the token to access this locking system. The specialty of this system is that we can trace for the door-open record according to the door-open time or the card numbers, without the need of the computer in performing this.

3) Security System using Biometric

Several methods were introduced and proposed for the use of biometric-based security system. The methods applied include fingerprint, voice recognition and face and iris detection. Soni-Key [10] is one of the biometric door locking system available in the market today where it used the fingerprint and voice detection in the authentication process. The aim actually to help the disable people where they had the difficulty in moving. The disadvantage for this system is that the accuracy problem as the voices are hardly constant for every access.

C. Other Scurity System

There are still some special authentications which are still not very popular in the market today. One of this is the security procedure using audio recognition which is proposed by the student from West Visayas State University [11]. For the verification process, a high-frequency audio which acts as the code and this code is combined during the access process to enable the system to trace it. There are no many experts in cracking this type of locking system yet, hence it can be said that this technology still very protected and safe. But the disadvantage is where a music player is needed to play the code and the computer needed to verify the real code generated.

D. Drawbacks of each authentication method

The token method issue is where the system only able to recognize the token itself instead of the owner of the token. This means that when the token is dropped to non-authorized people, there might use it for an illegal purpose and caused trouble [12].The main problem for the biometrics security system is that the cost is higher and the system may not able to recognize the authorized user due to the change in the personal biometric features. It can't be denied that there is some risk for using the password. The most common are where the user can't memorize their password. This result is where they will choose the common password like "123456", "000000", "123abc" and etc. Such password can be easily broken or hacked by others with the use of the dictionary attack. Besides, the bystander can simply peep the inserted password when the users not aware of it, they will just see the movement of the finger and guess the password based on the position of the keypad roughly.

E. CPLDs

CPLDs are integrated circuits that the designers will configure to implement digital hardware. CPLDs can handle significantly larger design than SPLDs but can't afford too many logic as FPGA does. [13] The main building block of the CPLDs are a macro cell, which contains logic implementing disjunctive normal form expressions and more specialized logic operations. CPLDs are better to

MCUs because parallel processing can be done in CPLDs to a large extend which means their operations actually can perform in a single clock cycle in CLPDs where this can't be done for other processors [14].In short, CPLDs actually allow the digital system design become more efficient and convenient and it brings many advantages for the hardware system development.

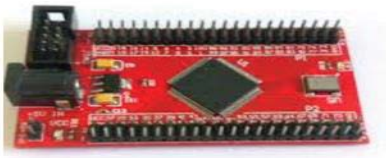

Fig. 1. *CPLD EPM240T100I5*

F. Comparison between CPLDs, FPGA and MCU

TABLE I. COMPARISON BETWEEN THE CPLDS, FPGA AND MCU

Properties	**FPGA**	**CPLD**	**Microcontroller**
Flexibility	High	Moderate	Low
Complexity	More complex than CPLD	Less complex	Most complex
Application Suitability	Parallel execution	Parallel execution	Serial execution
Processing Speed	High	High	Low
Price	High	Low	Low
Working Principle	hardware connection or wiring	hardware connection or wiring	software programming
Programming Language	Hardware Description Language:	Hardware Description Language:	C, C++, C# and etc

IV. METHODOLGY

Basically, the project divided into two parts. The first part is software part using Altera Quartus II for writing the Verilog code. Second part is hardware where programmed into the CPLD and mechanism part which included the 4x4 matrix keypad and electronic lock.

A. Software -Altera Quartus II

Verilog language is used in writing the coding. The ASM chart is shown in Fig 2. The concept of this locking system is where the users need to press # on the keypad (represent op) in order to unlock the door. If the door is not close after 10s, then the alarm will ring as well to remind the users to lock the door back. If the password enter is match with the predefined, then the door will open. The alarm will ring and the door will lock if attempt three times wrongly. In order to reset password, the user need to press * on the keypad (represent prog). The correct predefined password needed to enter and match before reset. Then the user need to enter two times the new password and hence reset process is done.

At the top level of the RTL design hierarchy, this digital system is partitioned into two units which is Control Unit (CU) and Datapath Unit (DU). DU perform all the required operations like ALU, counter, comparators, register and etc. CU tell DU what to do, in terms of switching, operation selection, data movement between ALU components and etc. The functional block diagram of DU is shown in Fig 3. The output of CU is used to control DU which included shiftA, shiftB, en2, clr2, en3, clr3 and en_timer. Meanwhile, the output of DU is send to CU for feedback signals which included match, morethanten, count2 and count4. The top level module for CU and DU is shown in Fig4. The interface of 4x4 matrix keypad and seven segment display is written is Verilog code as well. When the user press correctly the password to open, the seven segment will show O and will show P is the user press correctly for reset. Debounce code is added because there is the debouncing glitch occur when pressed the keypad. Hence, all the Verilog code is done.

Next, the behavioral simulation needs to be performed to test and verify the functionality of the design through waveform. Specific waveform simulator software namely Altera-ModelSim is required. Firstly, the project file is simulated by using the Altera-ModelSim which is invoked from Quartus II. After that, signal tracing is made to check with the desired functionality and perform verification. Thus, the verification can be done by comparing the result from the simulation with the expected result. If the result is wrong, the design stage needs to be turned back to design implementation and then debug out.

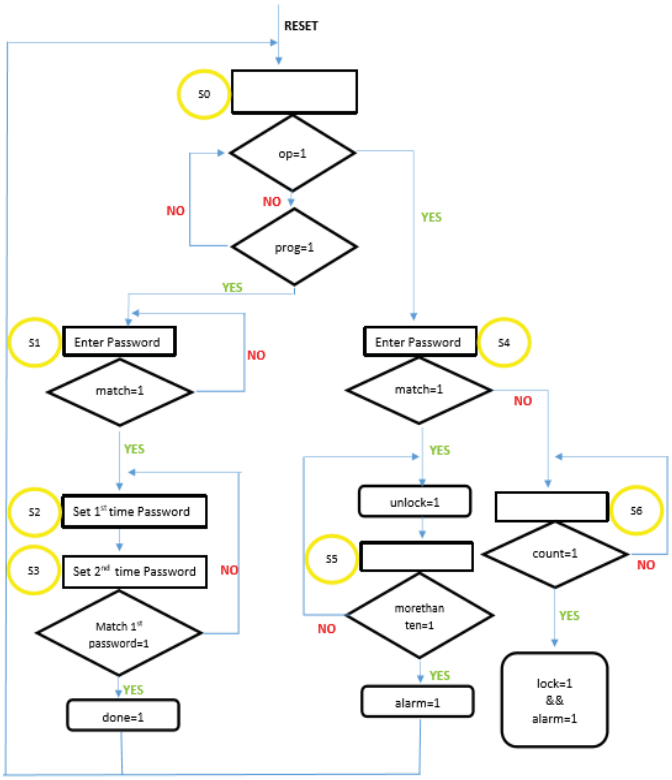

Fig. 2. *ASM Chart of the Locking System*

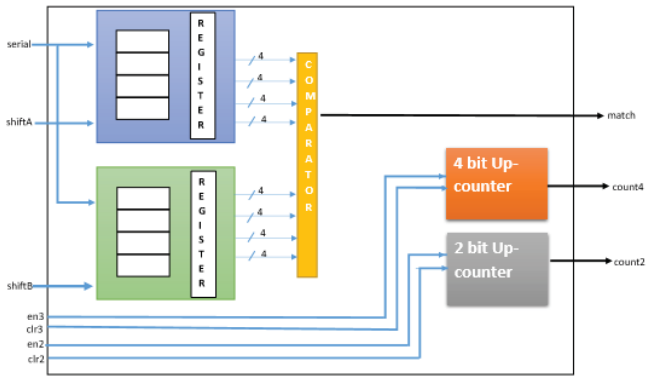

Fig. 3. *Funtional Block Diagram (fbd) for DU*

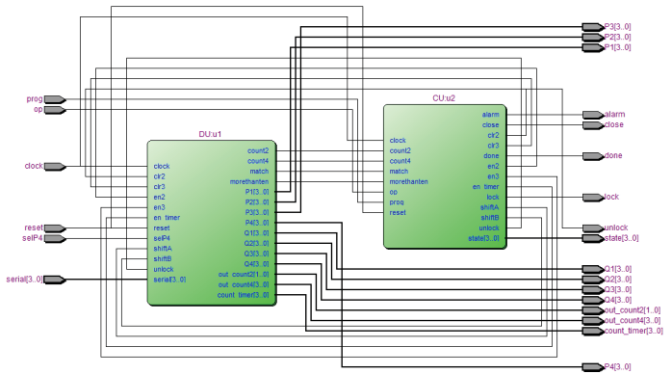

Fig. 4. *Top Level Module for Locking System*

B. *Hardware*

This part consist of CPLD EPM240, 4x4 matrix keypad, seven segment display and electronic lock.

1) CPLD Part

CPLD used as the main controller and the Verilog coding written in Altera Quartus II is then programmed inside. There are 80 GPIO pin can be used. The main reason on why CPLDs is chosen is because they are non-volatile and active at power up as long as they have been programmed at least once.

2) Keypad Part

A 4 x 4 Matrix Membrane Keypad is used in this project. In order to determine which buttons on the matrix keypad is pressed, a keypad scanner has to be designed to scan the state of all the buttons column by column and row by row for every small time interval. The keypad is scanned by switching the number of column and at the same time, it will check the state of the each row within 1ms. Therefore, the output gives a specific data to indicate which button is pressed.

3) Lock Interface Part

This part mainly concentrated on the operation of the electronic lock where the lock normally operates on certain voltage to cause the current flow in the magnetic coil. Besides, there are also voltage regulator, relays and transistors as well. The relays are used to control the direction the lock where the polarity of the lock connections is needed to exchange in order to have a different direction of the lock movement.

However, to test the functionality of the locking system module with the interface circuit, it need to program onto the CPLD and then observe the output. If it is not working, it need to return to design implementation stage to troubleshoot the problem either from the programming code or wiring. Finally, if all the designs either for interface part or the hardware part are working fine, the verification was done by comparing and checking the results between the simulation and the output of the interface. Both result should be the same.

Fig. 5. *Mechanism Part of the Locking System*

V. RESULT AND ANALYSIS

A. Simulation

Behavioral simulation needs to be performed to test and verify the functionality of the design through waveform in Quartus Altera II. There are several condition can be discusse and analyses.

I) If the user enter correct the predefined password during the reset process, then it can continue to reset a new password and after complete done will equal to 1. The out_count4 is used to count 4 digit password and state is run correctly according to the state diagram designed.

Fig. 6. *Simulation Waveform for condition 1*

II) If the user enter correct password, the door will unlock. If more than 10second after open, the door alarm will operate (close=1).

Fig. 7. *Simulation Waveform for condition 2*

III)If the user enter the password wrongly for 3 times, the alarm will operate and the door will lock. The out_count2 is used to count the number of attempt. When it is out_count2 =3 , then the alarm will toggle.

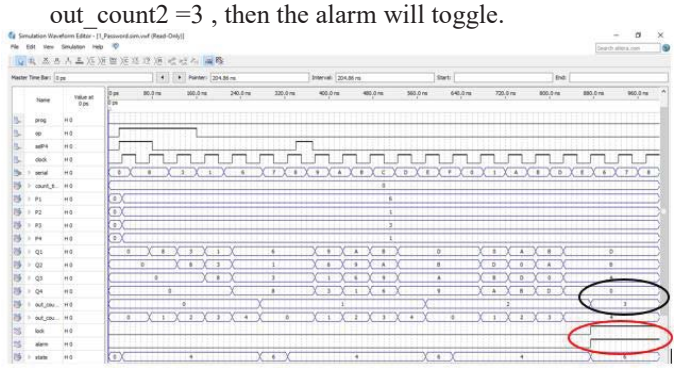

Fig. 8. *Simulation Waveform for condition 3.*

B. Hardware

Some testing are done by sending the keypad data to the system by pressing button and then display through the seven segment display. However, the seven segment display does not receive the data everytime properly. Sometime not received at all or received incorrect data and the data is sent more than one time although it is one time pressed and . It can say that the system is unstable. Problem found out where it is due to the debouncing glitch of the push buttons [14]. Hence, a debouncer designed to filter out the glitches occue when pressing the keypad.A pull up resistor is used to solve this problem. Wiring connetion is an issue as it can cause some failure result.

VI. Conclusion

This locking system using CPLD can consider as a low-cost locking system. By comparing to the other electronic locks that had the different type of authentication methods like biometrics and RFID, this lock system has the good price aspect. The goal of this project is to create a cost-effective, easy installation and user-friendly to the users. With this, the objective of this project where everyone house should at least one of this system can be achieved. If the objectives of this project can be enhanced, then the crime statics will definitely decrease. This directly increase the security level of the society and the people will live in a secure environment. Besides, the knowledge and skills of design and debugging also can be learn from this project. Such skills will be very useful in future.

References

[1] Latest Crime Statistics Released, (2016). FBI / *Crime in the United States, 2015* . Availble: https://www.fbi.gov/news/stories/latest-crime-statistics-released [Accessed December 8, 2016]

[2] 2015 Crime in the United Stated, (2015). FBI/ Property Crime. Available: https://ucr.fbi.gov/crime-in-the-u.s/2015/crime-in-the-u.s.-2015/offenses-known-to-law-enforcement/property-crime [Accessed December 8, 2016]

[3] Results from the Expat Survey on Crime in Malaysia, (2014). Andy Davison / *The Expat May 2014*. Available: http://www.expatgo.com/my/2014/06/03/results-from-the-expat-survey-on-crime-in-malaysia/ [Accessed December 8, 2016]

[4] Bill Ballad, Tricia Ballad and Erin Banks. (2011). "Access Control, Authentication, and Public Key Infrastructure." Book, Jones & Bartlett Learning, Chapter 1, pp. 13-15.

[5] James Ohwofasa Akpeninor. (2012). "Modern Concepts of Security." book, AuthorHouse, chapter 6, pp. 86-97.

[6] Dhiren R. Patel. (2008). "Information Security: Theory and Practice." Book, Prentice-Hall, Chapter 1, pp. 9-10.

[7] Muhanad Hayder Mohammed. (2012). "SECURE ELECTRONIC LOCK USING PIC 16F628A MICROCONTROLLER."International Journal of Research in Computer Science, 2 (5): pp. 43-47.

[8] Si Tong Sun et al. (2011). "The Design of Electronic Code Lock." Advanced Materials Research (Volume 267), Manufacturing Systems and Industry Application: pp. 1001-1004.

[9] A. Fang, X. Ye, M. Gong, W. Yang, L. Zhang. (2008). "The circuit designing of the intelligent door lock." 2008 ISECS International Colloquium on Computing, Communication, Control, and Management.

[10] E. Phelps, W.R. Pruehsner, J.D. Enderle (2000). "Soni-key voice controlled door lock [for disabled persons]." Bioengineering Conference, 2000. Proceedings of the IEEE 26th Annual Northeast: pp. 165- 166.

[11] J.R.R. De Josef, B.D. Gerardo, M.B.S. Concepcion, K.G.V. Oreta, YungCheol Byun. (2012). "Ultrasonic Key Recognition: Security Algorithm for Pre-composed High Frequency Sound as a Mode of Unlocking a Security Lock." 2012 IEEE/ACIS 11th International Conference on Computer and Information Science, pp. 655-660.

[12] Svigals, J. (1994). "Smartcards a security assessment." Comput. Secur. 13(2): pp. 107-114.

[13] Nagaraj Hediyal. (2011) Generic Complex Programmable Logic Device (CPLD) Board. Nagaraj Hediyal / (IJCSIT) International Journal of Computer Science and Information Technologies, Vol. 2 (5) , 2011, 2004-2007

[14] Divya K. Shah, Chaurasiya Rohit B., Devdip Sen, Shashwat Goyal (2015). Vehicle Parking System Implementation using CPLD. In 2015 International Conference on Communication, Information & Computing Technology (ICCICT), Jan. 16-17, Mumbai, India Vehicle Parking System Implementation. 2015.

GPS Tracking Device using Arduino and Smartphone

Nor Aisyah binti Abd Ghafar
Department of Electronic and Computing Engineering
Universiti Teknologi Malaysia
Skudai, Johor, Malaysia
aisyahghafar94@gmail.com

En. Kamal bin Khalil
Department of Electronic and Computing Engineering
Universiti Teknologi Malaysia
Skudai, Johor, Malaysia

***Abstract*— implementing embedded system is not restricted in one solution. It always created with multiple ability or technology combined. In this experiment, two technologies combined to construct an embedded system to able the system to track location and communicate with certain command. GPS module is used to track the location and the GSM used to send the location to the user via SMS. As the size is important in implementing higher technology, smaller size tracking device should be take in account. The control unit constructed using stand alone processor which is smaller in size and can perform based on Arduino architecture. From the experiment, the ability of the system integration is investigated in performing the output needed. As a conclusion, the system can be improved by using smaller component to reduce the size of the system. Also, before the implementation made, limitation of a processor should be take in account to avoid failure.**

Keywords—GSM module, GPS module, Arduino, Arduino bootloader, ATMEGA328P, QFD.

I. INTRODUCTION

The project will focus on application of GPS as an embedded tracking device. The design will be able to be implemented on any belongings. The important factor include small sized device to make it portable and suitable to be plug on any belongings, and have a good power management which makes the device able to operate in longer time.

The device will be able to communicate with user to send and receive information. It will be design to sent data only when needed by user. This functionality is implemented to reduce energy consumption of the device. In this case, GSM modules will be used to allow both devices communicate with each other. User can control the device and locate the item which attach to the device. GPS module will be used to track the location geometrically so that user can apply Google Maps application to track the location of the item.

In implementing small size device, Arduino Uno will be replaced with custom made control unit board which has smaller piece of processor chip and has specific function only. This is the main part of the experiment.

II. LITERATURE REVIEW

A. GPS

Global Positioning System (GPS) is widely used in many fields for many purposes as it has locating ability. It is a space-based satellite positioning that can be programmed to provide time and location it gathers on the surface of earth [1]. It communicates with Arduino via NMEA protocol.

B. GSM

Global System for Mobile Communication (GSM) was originally a European mobile communication standard that can provide outdoor high-speed mobility [3]. It can provide wide range of communication. GSM can digitize and compressed data then sends it down a channel with two other streams of user data in its own time slot. GSM operates in 900MHz, 1800MHz or 1900MHz which differ in different country [1]. It great strength is its international roaming capability [1]. It can be control by Arduino by AT command syntax.

C. Arduino

Arduino is an open source architecture. It is convenient to use due to the simplified version of C++ [2]. Also, there are many resources and libraries provided worldwide to ease user for their code execution and reference.

D. Arduino Bootloader

Two main processor chip used in Arduino board are ATMEGA328 and ATMEGA168 which especially defer in storage and limitation. Arduino board has the ability to reprogram a blank ATMEGA328 or ATMEGA168 chip to be able to follow its Arduino architecture by using Arduino Bootloader. The chip will be program as Arduino Nano. Instead of using FTDI programmer, Arduino is used as ISP [6].

E. Arduino ISP

Arduino will act as in-system programmer (ISP) to run the bootloader to the blank ATMEGA328P. This specification also allows the Arduino to acts as the programmer to the bootloaded ATMEGA328P (with ATMEGA328P on board removed). This will ease designer to wire the processor directly, even create their own custom PCB of the standalone system [5].

F. ATMEL ATMEGA Family

The ATMEL ATMEGA family is a friendly processor family with Arduino environment. It comes in three type which differ in size, i.e. through hole, Quad Flat Package (QPF) and thin quad flat pack (TQFP) which smaller in size respectively.

G. PCB

Printed Circuit Board (PCB) is a useful implementation in electronic world to reduce circuit complication and size. By using PCB, bulky jumper wire can be avoided. Designer needed to run a few processes to produce single PCB circuit. Circuit can be design using software such as EAGLE or Proteus. Basic etching process used copper board with carbon circuit design strapped on it. Professional use such as electronic

manufacturing will sent out their Gerber files to the official PCB manufacturer to be process.

H. Android based Map Application

The android application is a java based application. There are many application created. Each of them suite different consumer needs. It is design especially to create interactive and user friendly user interface environment for user without their need to seeing the process execute by the application. It can be inserted with many type of extension, i.e. Google Maps Extension with insertion of API key into the application manifest.

III. METHODOLOGY

The tracking system should consist of GPS data provider, and can be sent via wide range which is the ability of GSM. In this experiment, both are represented in separated modules which control by Arduino for communication platform.

The prototype of embedded GPS tracking system main component are GPS module, GSM module and Arduino Uno. LCD is use as information provider. The block diagram of the system in Figure 1 below is representing the basic understanding of the tracking system design:

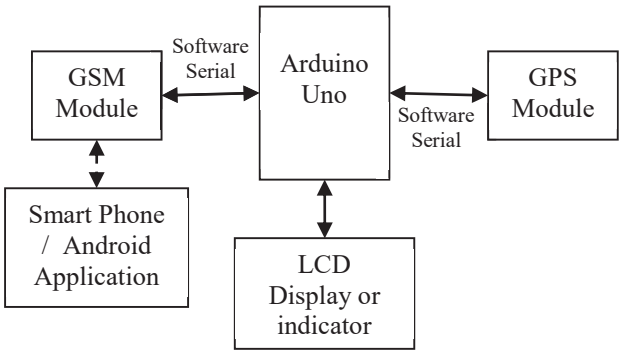

Fig.1. The prototype of embedded tracking system

The GPS and GSM are separated modules. Both communicate with Arduino from software serial. In Arduino Uno board, there are one hardware serial and one software serial provided for communication including for the purpose of flushing the codes inside the ATMEGA328 chip on the board.

The experiment is divided into 4 phase. This 4 phase is implement to firstly ensure functionality of each module and to investigate the different obtain in order integrate the system to form a standalone system. The last phase is made to improve the system by providing user application in Smartphone. The flow chart of the implementation phase is as Figure 2 below:

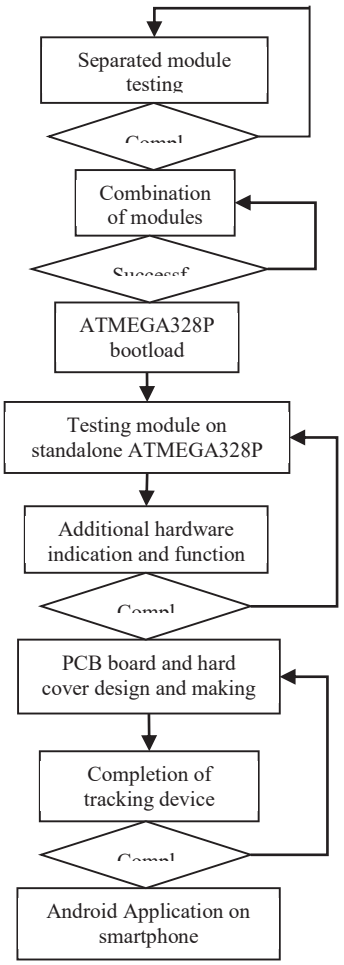

Fig.2. Flow chart of system completion

A. Phase 1 –GPS and GSM module testing

In this phase, it separated module executed using Arduino Uno. Both modules have its own protocol and syntax. After the execution of both modules is successful, the combination of both modules is executed.

B. Phase 2 –Bootload ATMEGA328P

In phase 2, a blank ATMEGA328P is burn with bootloader [5] with Arduino IDE using Arduino as ISP. The processor is configured to run as Arduino Nano. External 16 MHz crystal and reset circuit is added to the processor to complete the circuit for codes flushing purposes. The bootloading process is shown in Figure 4 below.

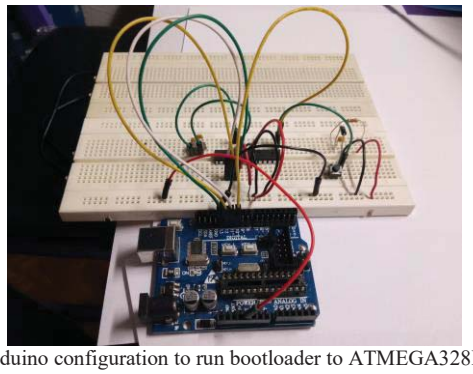

Fig. 4. The Arduino configuration to run bootloader to ATMEGA328P

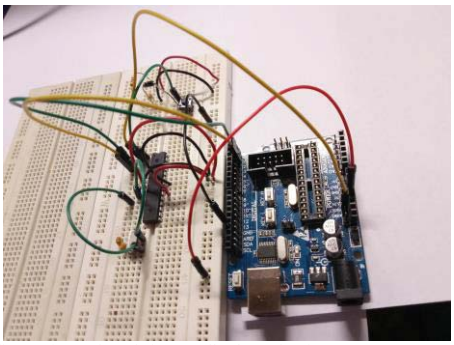

Fig. 5. the configuration of Arduino to flush codes into ATMEGA328P

After the bootloading, the circuit can now operates on its own without depending on Arduino Uno. The GPS and GSM module is tested on the ATMEGA328P according to step in phase 3 in Figure 2.

C. *Phase 3-Complete hardware circuit*

Circuit on phase 2 is redesign to reduce circuit size. QFD ATMEGA328P is used to replace through hole processor chip. PCB circuit is design with 25mm x 50mm to replace the usage of Arduino Uno.

The battery use to power the circuit is 1200mAh and 7.4 volt Li-Polymer battery. A voltage regulator is needed to regulate the voltage provided by the Li-Polymer battery to suit the operation voltage of the processor. Two type of voltage regulator is use:

- 3.3 volt output for GPS module
- 5 volt output GSM module and ATMEGA328P

In reducing the size of the device, LCD Display was replaced with Surface Mounted Device (SMD) type LED to show the status of the system. Some information showed by the LED is power, GPS module availability, GSM module availability, and battery level indicator.

D. *Phase 4-Google Map for android platform design*

The Google Map for Android platform is design using Android Studio software. The extension of Google Map is used to permit the usage of Google Map interface onto the application.

IV. Result and Discussion

The result was collected phase by phase. The result is represented below:

A. *Phase 1*

- GPS module

TABLE 1: THE RESULT OF GPS MODULE EXPERIMENT

Location	Latitude	Longitude	Error (m)
S24, Kolej Tuanku Canselor	1.556730	103.644670	3
Observatory Building (Balai Cerap)	1.569913	103.644741	5

The accuracy of the GPS has an approximate 5 meter to 10 meter error. The value provided by the GPS is calculated in the TinyGPS library. The value can be track using Google Map. The code is correct.

- GSM module

Figure 3 below shows the screenshot captured of output when command of sending message sent to the GSM. The command is sent via software serial port provided in Arduino.

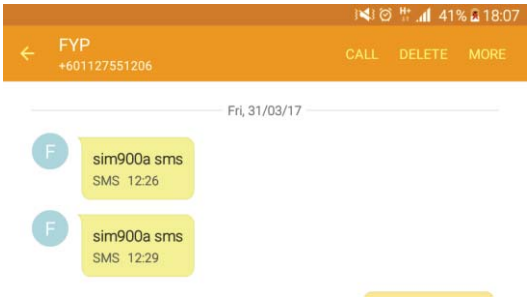

Fig.6. Message sent by GSM module in GSM testing process

- GPS and GSM module integration

Figure 6 below shows the data acquired when both modules is connected together. The GPS location is rechecked using Google Maps and the data is accurate. The combination of the two modules is successful.

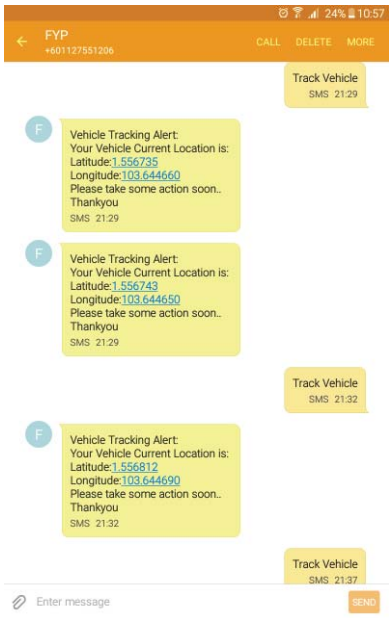

Fig.7. The output from combined module

B. *Phase 2*

- Arduino Bootload

The ATMEGA328P is successfully bootloaded with Arduino Nano firmware using Arduino as ISP.

- GPS and GSM coding testing

The stand alone Tracking device was verified. The system successfully produces output correctly as in Figure 6.

C. *Phase 3*

The Tracking device circuit was completed with additional hardware indicator. The final device is complete. The figure is as shown in Figure 7 below.

However, there is some error occurred in implementing the command. There should be two commands that the GSM need to find, i.e. “Track item” and “Alarm”. Eventually the GSM only noticing “Track item” line and ignoring the “Alarm”. Instead of that, the system work fine.

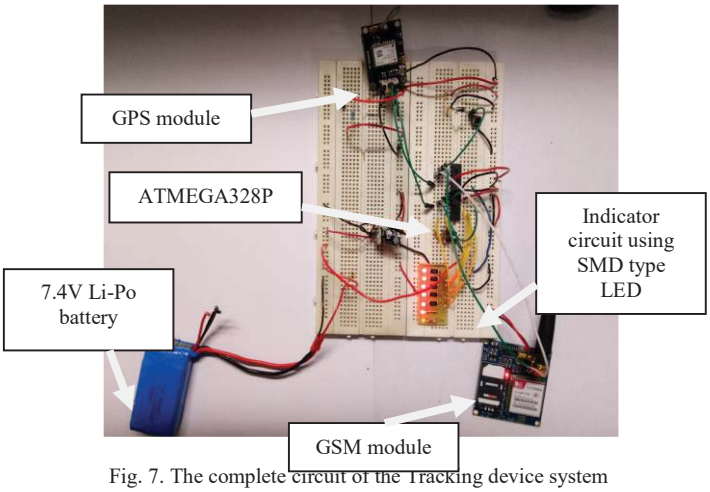

Fig. 7. The complete circuit of the Tracking device system

D. *Phase 4*

Simple Google Map application was design. The implementation only has basic Maps interface. Further knowledge needed to design a good and functional Android Application. However, the testify of the Android Application with the Tracking device in not gathered due to

V. CONCLUSION

The tracking device is working properly. The GPS can cooperate well with the GSM module using a single software serial. The data gather from the GPS is confirmed using Google Maps. The implementation of smaller circuit should be implemented carefully as the PCB board is sensitive which can cause much trouble if it done harshly.

There are several things that can be improved from the system. The Android Application can be improvise to meet consumer needs. The GSM could be replaced by RFID to increase feasibility to user because they don’t need to keep on providing money to the tracking system. Smaller size component can be used, i.e. instead of using QFD type processor, use TQFP processor which requires special tools in solder process. Battery efficiency should be study more to choose a suitable battery for the system.

ACKNOWLEDGMENT

I would like to express my gratitude to my supervisor, En. Kamal bin Khalil which has helped me in finding solution to my problem. I also would like to thanks my Final Year Project part I panel and evaluator, Dr. Usman Ullah for providing ideas to use QFD ATMEGA328P to reduce the size of the system.

REFERENCES

[1] Mohd Riyazuddin and G. Deepika, “Intelligent vehicle control and monitoring using GSM and GPS,” International Journal of Research in Advanced Engineering Technologies, Vol 6, pp.3-4, Feb 2017.

[2] Yusuf Abdullahi Badamasi, “The Working Principle of an Arduino,” Nigerian Turkish Nile University, p. 1, 2014.

[3] Chwan-Lu Tseng, Joe-Air Jiang, Ren-Guey Lee, Fu-Ming Lu, Cheng-Shiou Ouyang, Yih-Shaing Chen and Chih-Hsiang Chang, “Feasibility Study on Application of GSM-SMS Technology to Field Data Acquisition,” Computers and Electronics in Agriculture, p. 1, March 2006.

[4] Salas K Jose, X. Anitha Mary and Namitha Mathew, " ARM 7 Based Accident Alert and Vehicle Tracking System," International Journal of Innovative Technology anf Exploring Engineering (IJITEE), Vol 2, p. 2, March 2013.

[5] Rick Anderson and Dan Cervo, Pro Arduino. Technology in Action, Pp.181-184

[6] Dimitri Diakopoulos and Ajay Kapur, "HIDUINO: A Firmware for Building Driverless USB Devices using the Arduino Microcontroller," International Conference on New Interfaces for Musical Expression, pp.

Development of Medical Imaging using Ultrasound

Siti Mariana Binti Adnan
Faculty of Electrical Engineering
Universiti Teknologi Malaysia (UTM)
Johor, Malaysia
Marianaadnan94@gmail.com

Ismail bin Ariffin
Department of Electronic and Computer Engineering
Faculty of Electrical Engineering
Universiti Teknologi Malaysia
Johor, Malaysia
ismail@fke.utm.my

***Abstract*—Ultrasound is one of the medical imaging technique that does not use ionizing radiation and non-invasive. Ultrasound are used to generate image of interior part of the body especially soft tissue by transmit ultrasound into the body and detect the echoes that reflect back produce by boundaries in the body such as tissues, bone and blood vessels. The frequencies for ultrasound are higher than the range of frequency for human hearing. The frequencies that had been used in medical ultrasound are between 2 MHz to 20 MHz. The hardware development for medical ultrasound imaging consists of transmitter and receiver circuit for transmitting and receiving the ultrasound frequency. The transmitting frequencies can be choose between the range by considering the acoustic impedance and pulse amplitude loss produced by reflection. The output of the hardware are recorded and echo signal identification. The software development using Matlab also use to obtain B-mode image from Radio Frequency files by using data obtain from gelatin phantom and patient data. The quality of the image produce using the device are quite good although not as good as the ultrasound machine.**

Keywords—ionizing radiation ;non-invasive; echo signal; acoustic impedance; B-mode image; radio frequency; phantom data.

I. INTRODUCTION

Medical imaging had been discovered by Wilhelm Conrad Roetgen's with his discovery of X-ray in November 1895 [1]. Medical imaging is a technique to produce and store an image of the internal part of the body such as tissues, muscles, organs, bone and etc. by using certain sources depends on type of medical imaging system use. Medical imaging had been used for medical uses – clinical analysis, medical intervention and display the function of some organs or tissues [2].

Medical imaging system consists of X-ray, computed tomography (CT), positron emission tomography (PET), ultrasound, magnetic resonance imaging (MRI) and etc. Each type of medical imaging system have different function, uses and method that will create different type of image.

X-ray are type of radiation that able to penetrate into some solids like human body to produce image (2-dimensional image) [3]. X-ray are usually used to diagnose, monitoring and improve human health condition. Bone and joints usually use X-ray to diagnose bone-related problem such as fractures, broken or dislocated bone, arthritis, teeth decay, bone cancer, and bone infections. Besides bones, X-ray also used to evaluate chest to investigate chest symptoms – shortness of breath, chest pain and etc. for identify health conditions.

Computed tomography (CT) able to produce 2-dimensional (2D) and 3-dimensional (3D) image using X-rays to create multiple cross-sectional image or slices of the internal part of human body- tissues, bones, blood vessels at the same time [4]. CT scan able to use for assessment of body shape or body structure, diagnose diseases or cancer, measure bone strength, aid to plan for radiotherapy or surgeries and etc.[5]. The risks of using CT scan is the patient will be exposed to high dose of radiation since it is need the radiation to generate multiple cross-sectional image of the body at the same time.

Positron emission tomography (PET) is a nuclear medicine that injecting special dye that has radioactive tracers into the body to provide information about how the inner part of the body are working. PET scan are usually used to detect cancers, brain diseases, heart-related problems and organs that not function as normal [6]. The PET scan is considered to be a safe procedure since the exposure of radiation to the patient are minimal.

Magnetic resonance imaging (MRI) is a medical imaging that uses strong magnetic fields and radio waves to generate 3D image of internal human body without using ionizing radiation. MRI are used to diagnose health condition that involve soft tissues such as tumor or brain disorders that does not show on X-ray examinations, monitor medical conditions and also it can produce image for all part of the human body.

Ultrasound is one of the medical imaging technique that does not use ionizing radiation and non-invasive. Ultrasound is the transmission of mechanical vibrations that occur when sound waves are penetrate trough matter or material [7]. Ultrasound are used to generate image of interior part of the body especially soft tissue by transmit ultrasound into the body and detect the echoes that reflect back produce by boundaries in the body such as tissues, bone and blood vessels. Ultrasound consists of a few type of scanning mode, A-mode, B-mode, real-time mode, gated mode, Doppler mode, transmission mode and etc.

II. LITERATURE REVIEW

Ultrasound is widely used in medical field as the medical ultrasound imaging to capture real-time image because of the low cost systems, portable and does not use ionizing

radiation. However, standard brightness mode (B-mode) imaging cannot captured the image of highly vascularized tumor because of the poor scatter of blood. Therefore, microbubble contrast agents are injected to modify acoustic properties of the blood. Since the microbubble contrast agents are too large, the droplets had been used to replace it. Imaging system that can capture the droplet vaporization events and generate ultrasound images are develop [8].

Ultrasound also used to measure bone mineral status to identify possibility of person exposed to osteoporosis. The method used is called quantitative ultrasound (QUS) that usually focus on children. QUS devices can be used to measure two main variables, speed of sound (SoS) and broadband ultrasound attenuation (BUA) of the ultrasound waves propagate through bone tissue [9].

The used of ultrasound for bone surface detection are very useful for biopsy, orthopedic operation, and branchytherapy. The disadvantage of using B-mode ultrasound to detect bone is poor image quality captures due to shadowing, artifacts in tissue and etc. Ultrasound radio-frequency (RF) signals can be used to replace b-mode images to visualize the bone surface. There are two techniques of ultrasound radio-frequency (RF) signals that can be used to enhance the quality of bone surface visual, strain imaging and reflected power imaging [10].

There are a few ultrasound equipment that basically used to process the ultrasound image, transducer that used to transmit and receive the pulses of sound waves, computer to process the raw data into an images and store the image into the disk and monitor to display the image. Since the image quality of ultrasound is low, the advanced techniques of signal processing had been introduced to provide higher diagnostic value and high quality image [11].

The low quality of ultrasound images caused by side lobes and acoustic clutter from off-axis scatters that produce from the leakage of acoustic energy. Therefore, the techniques called frequency-space (F-X) prediction filtering or FXPX suggested as the best techniques to improve the quality of ultrasound images and visuals [12].

III. PROJECT METHODOLOGY

A. *Hardware development*

The range frequency of sound that human able to heard approximately between 20 Hz to 20 kHz [7]. The frequencies for ultrasound are higher than the range of frequency for human hearing. The frequencies that had been used in medical ultrasound are between 2 MHz to 20 MHz. The hardware development for medical ultrasound imaging consists of transmitter and receiver circuit for transmitting and receiving the ultrasound frequency. The transmitting frequencies can be choose between the range by considering the acoustic impedance and pulse amplitude loss produced by reflection.

Acoustic impedance, Z, is a measurement of resistance occur when the sound waves propagate through material. Acoustic impedance, Z, is the product of velocity of sound in the medium, v, with the density of medium, Y.

$$Z = Yv \quad \{1\}$$

The reduction in pulse amplitude during reflection are different for different interfaces. This are given in the Table 1 below [13].

Table 1: Reduction of pulse amplitude caused by reflection.

Interface	Amplitude loss (dB)
Ideal reflector	0.0
Tissue-air	-0,01
Bone-soft tissue	-3.8
Fat-muscle	-20.0
Tissue-water	-26.0
Muscle-blood	-30.0

B. *System development*

Matlab had been used to obtain the echo signal identification. From the data obtain from the scanning process, the echo signal had been generate by writing the programming on Matlab. Besides, by using Matlab, the B-mode image had been obtain from RF files from the gelatin phantom and patient data [14]. The data originally obtain for the strain imaging and for estimation of viscoelastic features.

The gelatin phantom data are obtain by using phantom derived from animal hide gelatin containing graphite scatters. The acid are injected to change the uniform properties of the phantom which softened a region in the center of the phantom with a circular cross section. The phantom was scanned by using linear array ultrasound from the Antares system while being compressed using a motion and the RF echo frames are collected at a frame rate of 2-4 frames/sec. Figure 1 below show the lab set up that had been set up to obtain the data [14].

Figure 1: Lab setup for phantom scan.

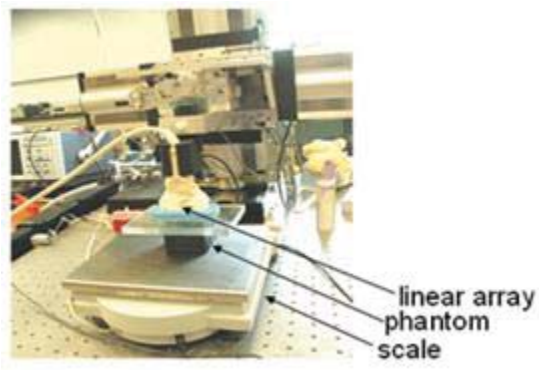

The data consists of a total of 13 RF files where each RF file contains 343 frames, with the first RF file recorded at 4 frames/sec and all subsequent RF files recorded at 2 frames/sec.

The patients data are obtain by applying a ramp-and-hold stress stimulus to the patient to initiate a creep-recovery method for imaging breast lesions. A linear transducer array from the Antares™ System is manually pressed into the skin surface scanning in the anterior-posterior direction while the patient lies on her side for an approximately 15 seconds. Figure 2 shows how the data was obtain from biopsy-verified studies and presented with non-palpable tumors initially detected by mammography [15]. The data are obtain from one of the patient diagnosed with Invasive Ductal Carcinoma (IDC) and the other one diagnosed with fibroadenoma.

Figure 2: Patient lying on her side while an ultrasound scan is taken.

The data provided 183 RF frames in total and are recorded at a rate of 17 frames/sec.

IV. RESULT AND ANALYSIS

A. *Echo Signal Identification*

As for the echo signal identification, the identification process of the signal is done to identify the location where the reflection echo are happen and the medium that cause the echo. The distance of the echo signal is measured on the sample. The unnecessary signal or artifacts had been remove after echo signal identification are done. Figure 3 shows the graph of echo signal identification from the data obtain using this hardware to scan the phantom.

B. *B-mode Image from Radio Frequency Files*

From the data obtain from gelatin phantom [14] and patient [15], the B-mode image are produce by using Matlab. Figure 4 shows the B-mode image obtain after the gelatin phantom data are process using this system while Figure 5 shows the B-mode image obtain after the patients data that diagnosed with IDC and fibroacenoma are process using this same system.

Figure 4: B-mode image obtain from RF files of gelatin phantom data.

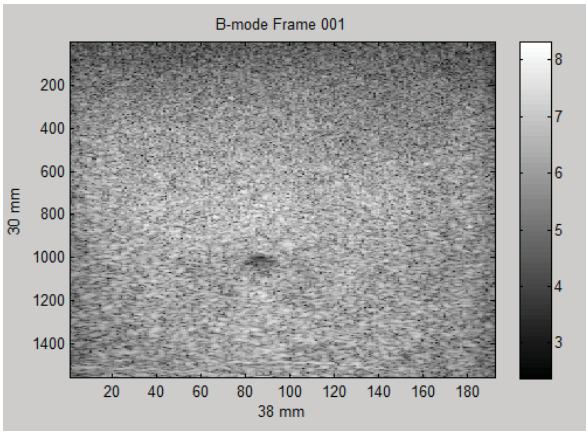

V. CONCLUSION

The ultrasound machine are too big and expensive to bring to place aside from hospital or clinic. Therefore, the simple and portable device with good quality of image and suitable to diagnose are needed. The experiment had been conduct and the device had been built to solve the problem.

The result shows that the device can obtain the data and also can diagnose any problem occur through echo signal identification. From echo signal, many problem can be detected, such as bone fracture and et cetra. Beside the device also produce a good quality of B-mode image that convert from Radio Frequency files.

REFERENCES

[1] BRADLEY, W. G. (2008). History of Medical Imaging1. Proceedings of the American Philosophical Society, 152(3), 349-361.

[2] Medical imaging. (2016, December 12). In Wikipedia, The Free Encyclopedia. Retrieved 13:00, December 12, 2016, from https://en.wikipedia.org/w/index.php?title=Medical_imaging&oldid=754400311

[3] How is an X-ray done?. (2016). NPS MedicineWise. Retrieved 20 December 2016, from http://www.nps.org.au/medical-tests/medical-imaging/for-individuals/types-of-imaging/x-rays/for-individuals/how-it-is-done

[4] Computed tomography (CT). (2016). NPS MedicineWise. Retrieved 20 December 2016, from http://www.nps.org.au/medical-tests/medical-imaging/for-individuals/types-of-imaging/computed-tomography-ct

[5] CT scan. (2016). Betterhealth.vic.gov.au. Retrieved 20 December 2016, from https://www.betterhealth.vic.gov.au/health/conditionsandtreatments/ct-scan

[6] Krans, B. (2015). PET Scan. Healthline. Retrieved 20 December 2016, from http://www.healthline.com/health/pet-scan#Overview1

[7] Shung, K. K. (2005). Diagnostic ultrasound (1st ed., pp. 5-37). CRC Press.

[8] Arena, C. B., Novell, A., Sheeran, P. S., Puett, C., Moyer, L. C., & Dayton, P. A. (2015). Dual-frequency acoustic droplet vaporization detection for medical imaging. IEEE transactions on ultrasonics, ferroelectrics, and frequency control, 62(9), 1623-1633.

[9] Baroncelli, G. I. (2008). Quantitative ultrasound methods to assess bone mineral status in children: technical characteristics, performance, and clinical application. Pediatric research, 63(3), 220-228.

[10] Wen, X., & Salcudean, S. E. (2007). Enhancement of Bone Surface Visualization Using Ultrasound Radio-frequency Signals. In IEEE Ultra. Symp (Vol. 1051, pp. 2535-2538).

[11] Kaur, K. (2013). Digital image processing in ultrasound images. International Journal on Recent and Innovation Trends in Computing and Communication, 1(4), 388-393.

[12] Shin, J., & Huang, L. (2016). Spatial Prediction Filtering of Acoustic Clutter and Random Noise in Medical Ultrasound Imaging. IEEE Transactions on Medical Imaging.

[13] Salehuddin Ibrahim., Maheza Irna Mohamad Salim, & Alwin Arul Alexander.,. (2012). Progression of SEI & SEM final year project series 1 (1st ed., pp. 115-126). Skudai: Pusat Pengurusan Penyelidikan (RMC) & Penerbit UTM Press.

[14] Insana Lab: Ultrasonic Imaging - The University of Illinois at Urbana-Champaign. (2017). Ultrasonics.bioengineering.illinois.edu. Retrieved 15 May 2017, from http://ultrasonics.bioengineering.illinois.edu/data_phantom.asp

[15] Insana Lab: Ultrasonic Imaging - The University of Illinois at Urbana-Champaign. (2017). Ultrasonics.bioengineering.illinois.edu. Retrieved 15 May 2017, from http://ultrasonics.bioengineering.illinois.edu/data_patient.asp

[16] Donald, F. (2016). Ultrasonic transmitter circuit using IC 555 - Gadgetronicx. Gadgetronicx. Retrieved 21 December 2016, from http://www.gadgetronicx.com/ultrasonic-transmitter-circuit-ic555/

[17] Donald, F. (2016). Ultrasonic receiver circuit using Opamp LM324 - Gadgetronicx. Gadgetronicx. Retrieved 21 December 2016, from http://www.gadgetronicx.com/ultrasonic-receiver-circuit/

[18] Hykes, D., Hedrick, W., & Starchman, D. (1985). Ultrasound physics and instrumentation (1st ed.). New York: Churchill Livingstone.

Model of Low Stream Power Generation System

Muhammad Nazrin Bin Jamil, Abd Hamid bin Ahmad and Azli bin Yahya
Faculty of Electrical Engineering
Universiti Teknologi Malaysia
Skudai Johor
mnazrinjamil@gmail.com

***Abstract*— The objective of this paper is to design simulate and analyze a model of low stream power generation systems. This is basically a system that generate electricity by using kinetic energy of flowing water. Instead of building a large dam and use a lot of cost, this low stream power generation system is more economical to use and it is easy to implement anywhere as long as we have a continues flowing of water. In order to analyze and gain some data, we just build the model that represent the real situation or behavior of a small river. Two DC motor was used in this model and one of them will be controlled by using controller so the rotation speed of dc motor can be control and it can be relate with the real speed of flowing water. Another dc motor will act as a generator. Because the output voltage from generator is quite small a boost converter was used to step up the voltage to the desired useful voltage so it can be used to charge the battery.**

Keywords – Low stream, kinetic energy, controller, DC motor, rotation speed, boost converter

I. INTRODUCTION

Nowadays, the awareness about the important of using sustainable energy was increasing among the people in the world. The dependence on fossils fuel, coal and natural gasses to generate electricity has caused the side effect to our environment such as air pollution, greenhouse effect and acid rain. For example, the burning of fossils fuel will release carbon dioxide to the air and it will be trap in our atmosphere. This will lead to the greenhouse effect and also the major factor to the increasing in global warming. Recent research have proven that, in every year the burning of fossils fuel will produce about 21.3 billion tonnes of carbon dioxide (Co2) and our natural resources can only absorb half from that values [1]. This is an example that show our environment are on the verge of destruction. Another things that makes our scientist worried about our non-renewable natural resources which one day will be run out. If there is no resources exist we cannot produce energy to generate electricity. Therefore, we have to find another ways to extract energy from other resources that are more sustainable and give free effect to our environment. By 2030, the world must make some international coorperation to find best way to generate clean energy and also do some advancement in energy efficiency, renewable energy technology and also promote investment in energy infrastructure and clean energy technology [2].

Low stream power generation system which is harvesting electrical energy by using kinetic energy from the flowing of water instead of potential energy of falling water. This system operates at low river current speed usually in between 0 m/s until 3 m/s [3]. This system is basically more efficient compare to wind turbine because density of water is 800 times more denser compare to air [4]. In term of physical operation and electrical component, hydrokinetic shares same similarities with wind turbine system [5]. Thus, extracting electrical energy by using kinetic energy of flowing water is more efficient even at low speed. This system does not need to build a massive building such as dam or the other things that cost consuming. Because of hydrokinetic does not need a dam, it is consider to be called free flow turbine or zero head hydro turbine [6]. The working principle of hydrokinetic by using water stream are shown in the figure below.

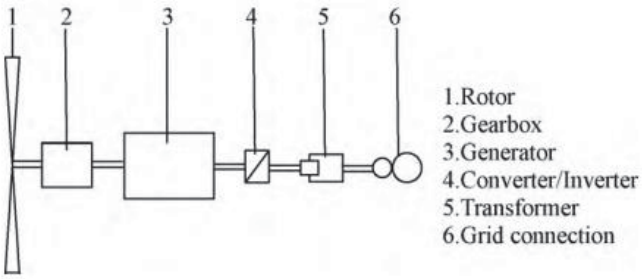

Figure 1: Principle scheme of water current turbine system

Hydrokinetic or water stream will turn the turbine blades and it will activate the generator to produce electricity. The amount of electricity that can be generate is depend on the volume, density and speed of water, type and the size of turbine blades and also depend on the type of generator. The efficiency of the hydrokinetic turbine can be estimated by using Betz limit [7]. This can be applied to all hydrokinetic that are working in free stream such as tidal and river flow [8]. The output power generate from the hydrokinetic system can be calculate by the equation below;

$$P = \frac{1}{2}\,\rho\, AV^2 C_P \quad \text{.....(1)}$$

where P is the total power output from the turbine in Watt. ρ is the density of water , A is the area of the rotor blades in (m^2), V is the velocity of water in (m/s) and C_P is the power coefficient of the turbine. However, because this is just a model and does not required actual turbine to turn generator all this parameter will not be consider. Therefore, there are many factor that must take into account in order to get the efficient way to generate

electricity from this system. Figure below show the picture of our model.

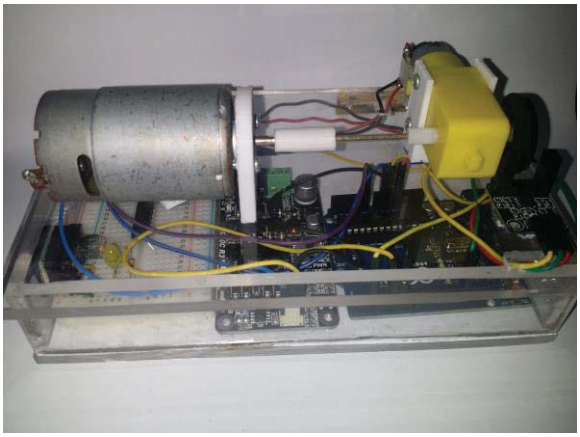

Figure 2: Finalize project model

II. DC MOTOR CONTROL

In order to make this system become more to natural like river flow. Arduino was used as a controller to control the rotation speed of dc motor. Motor driver was connected to Arduino to control the speed of dc motor. The motor driver that have been used in this system is MD10C as shown in the figure below.

Figure 3: MD10C motor driver

A. *Pulse Width Modulation (PWM)*

Function of this motor driver is to control the pulse width modulation (PWM). This PWM signal will be injected to the input of dc motor. PWM speed control works by driving dc motor with a series of pulse with a different duty cycle. Duty cycle is a fraction of high output voltage with low output voltage and at the same time the frequency of the PWM waveform is keep constant. In other words, the wider the pulse width, more voltage that will be applied to the dc motor and the rotation speed of dc motor will be increase. Figure below show the pattern of PWM waveform.

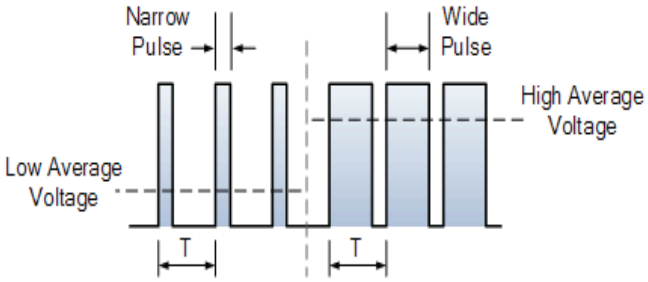

Figure 4: Pulse width modulation

III. SPEED SENSOR

Speed sensor was used to detect the rotational speed of dc motor. Speed sensor module that are used in this model is the infrared speed sensor based on the LM393 chip. This speed sensor module consist of light emitting diode that transmit infrared beam and another electronic component which is called phototransistor is to detect the present or absence of the infrared beam. For measuring the rotating speed of dc motor, an encoder disc with twenty slots was installed at the shaft of dc motor. This encoder was placed in between transmitter and receiver. The function of this encoder is to block and allow the infrared beam reach to the receiver and for one time of blocking this illumination is a one event. Basically, calculating the rotation speed is done by counting the event for a given period of time and simply dividing the number of events by the number of slots of a disc which is twenty.

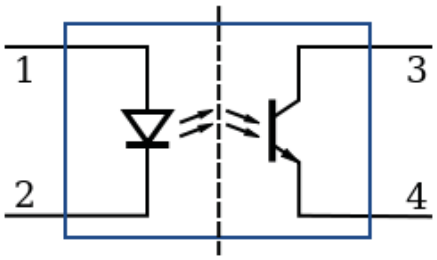

Figure 5: Schematic diagram of optocoupler

Figure 6: Speed sensor & encoder disc

A. *Relating rotational speed with river speed*

Speed of water can be measure by relating it with rotation speed of turbine. Before that, the circular motion of a rotating

turbine must be converted to linear motion of river flow. We all know that it just not simply to convert from angular velocity of turbine to speed of water because there are many parameters that must be take into account. The example of the parameters that influence the rotation speed of turbine such as water velocity, water density, turbine flow area and also some frictional losses due to drive mechanism of that turbine [9]. Because this is a simple small scale model of low stream power generation, assuming that there are no losses and can simply convert the rotation speed of turbine to speed of water. Below are the steps to calculate speed of water based on the rotation speed of the turbine and for the reference figure 7 shows the illustration of the circle.

1) Determine the diameter, D of the turbine blades.
2) Calculate the circumference, C of the turbine based of equation 2.
3) To get rate of water speed multiply circumference of turbine by the rotation speed as shown in equation 3.

$$\text{Circumference, } C = \pi \times D \quad \text{.....(2)}$$

$$\text{Speed of water , } V = C \times \textit{rotation speed} \quad \text{.....(3)}$$

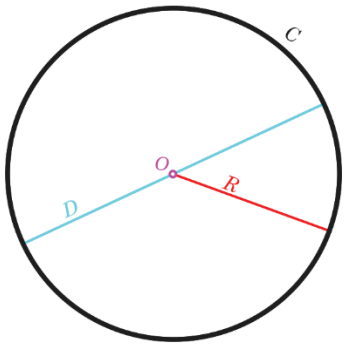

Figure 7: Circle illustration

The diameter of the turbine have been set to be 20cm in my programming that calculate the speed of water. So, the measured speed of water will be shown in meter per second (m/s). After speed of water can be measured I just control the PWM input to the motor so that water speed can be adjusted in the range from 0 m/s to 3 m/s based of the actual river current speed.

IV. VOLTAGE & CURRENT DETECTOR

Output voltage from this generator can be measured by using Arduino. Analog input for Arduino can be used to measure dc voltage in between 0V to 5V. To allow voltage greater that 5V to be measured, a voltage divider circuit can be used [10]. The voltage divider will decrease the voltage that being measured within the range of Arduino analog input.

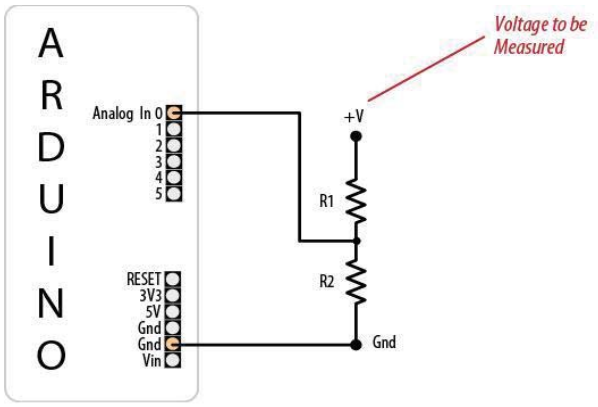

Figure 8: Voltage divider circuit

A. *Voltage measure*

The value of R1 and R2 that have been used in this model is 10kΩ and 1kΩ respectively. So the division factor value of R1 plus R2 which is 11. If we notice that 5V is Arduino analog to digital converter (ADC) reference voltage and ADC for the Arduino is a 10-bit ADC. This meaning that it has the ability to detect 1024 (2^10) discrete analog level.
To get the value of voltage, the reading of analog input must be multiply with 5 which is the reference voltage. After that just simply divided with 1024. Then to get the actual reading of measured voltage just multiply by the division factor of 11. Below are the equation that have been used to get the reading of measured voltage from generator;

$$\text{Voltage} = \left(\frac{\text{Analog input} \times 5}{1024}\right) \times 11 \quad \text{..... (4)}$$

B. *Relating ADC value to voltage*

For Arduino ADC assume 5V is 1023 and if anything value is less than 5V it will be ratio between 5V and 1023. Therefore we can simply relate this by the equation below;

$$\frac{\text{Resolution of the ADC}}{\text{System voltage}} = \frac{\text{ADC reading}}{\text{Analog voltage measured}}$$

C. *Current measure*

To get the value of current are based on the Ohm's law equation. It stated that the current through a conductor is directly proportional to the voltage [11] where the resistance is the constant. The measured voltage that are produced from the generator just simply divided with the total resistance that have been used as a division factor. The total resistance is the summation of R1 and R2 with give the value of 11kΩ and this is show in the equation below.

$$\text{MEASURED CURRENT} = \frac{\text{MEASURED VOLTAGE}}{11\text{K}\Omega} \quad \text{.....(5)}$$

V. BOOST CONVERTER

Boost converter is a DC-to-DC power converter that can step up voltage while stepping down current from its input supply to the desired output voltage. Input for the boost converter can be from any DC sources such as solar panels, batteries, DC generator and rectifiers. Process that change DC voltage to another different DC voltage is called DC to DC conversion [12]. From the power conservation equation which is P=IV output current must be lower that the input current. The main component that is use in the boost converter circuit which is at least two semiconductors component such as a diode and a transistor and energy storage elements such as a capacitor and inductor or two in combination. Figure 9 show the simple circuit of a boost converter with it basic component. Because this system was use low stream of water to generate electricity, the output that can be generate from the generator is quite small. A special chip is needed to step up dc voltage so it can be used to charge the battery.

A. Principle Operation

The working principle of boost converter is when the switch is closed inductor will store energy in form of magnetic field. When switch is opened, the magnetic field that have been created in the inductor will decrease and it create current and drive it to the load. Note that the changes in magnetic field can produce an induced electric current. The time taken for discharging the inductor must not be longer to avoid it fully discharged. So, fast switch cycle is needed to avoid fully discharged of an inductor in between charging stages. Therefore, MOSFET transistor is use as a switch and usually called as a switching transistor. High frequency square wave will be applied to the MOSFET gate.

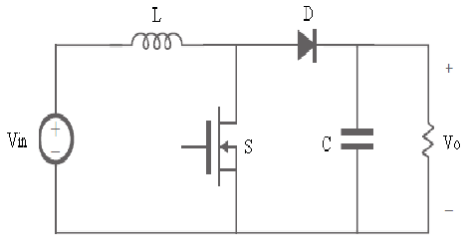

Figure 9: Boost converter circuit

VI. RESULT & DISCUSSION

All the data from this model have been recorded in the table 1 below. Data that have been collected such as voltage, current, and power that are generate from generator was get for the range speed of water that are in between 0 m/s until 3 m/s. This speed of water are based on the real river current flow that have been studied before. From the observation, the output voltage that can be generate form this system is in between 0.1V until 1.07V. This output voltage is quite small and nothing can do from this value even to light up a LED I must have an input voltage at least 1.8v.

To make output voltage from generator to become useful it need to step up this dc voltage so it can be used to supply to the load or can be used to charge the battery. Boost converter circuit can be used to step up dc voltage to the certain value that I want. But it have realize that all the boost converter design have the requirement for input voltage greater that 1V. After do some observation it have been found that one chip meet this system requirement of input voltage as low as 0.3V to 5.5V and it can step up voltage from 1.8V until 5.5V . This chip have been fabricated and boost converter circuit are intergrated in this chip. Figure 10 show TPS61200 boost converter chip that can be used to step up voltage for this system.

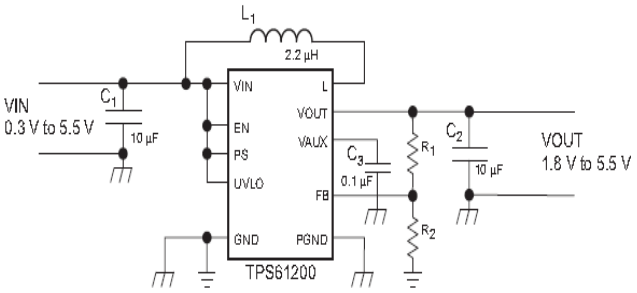

Figure 10: TPS61200 Boost converter

TABLE I.

Water Speed (m/s)	Voltage (V)	Current (μA)	Power (mWh)
0.31	0.10	8.79	3.06
0.63	0.16	14.65	8.50
0.94	0.26	23.93	22.67
1.26	0.35	31.74	39.89
1.57	0.47	42.48	71.46
1.88	0.50	45.90	83.42
2.20	0.68	61.52	149.89
2.51	0.81	73.24	212.43
2.83	0.96	87.40	305.51
3.14	1.07	97.17	373.89

VII. CONCLUSION

Because of many remote villages around the world are having the same situation where they still lack access to the electricity. This is the good option to implement this conventional hydrokinetic energy system so it can helps to improving energy supply to remote and off-grid areas where the

transmission line do not exist. This system do not require any complex infrastructure and all entire villages can get benefit of electricity from this system. We hope that this model can be a starting point for other researchers to build up this low stream power generation technology to a higher level. This system have a bright future for the low power energy harvesting technology.

In conclusion, the result presented in this paper represent for the design and analysis of this hydrokinetic system. This low stream power generation system needs to be well studied for the advancement of this technology. Because the concept of hydroelectric generation by using water stream was new compared to the conventional hydropower system. It have been a limited studies on the characteristic of this hydrokinetic system such as hydrodynamic characteristic of hydrokinetic turbine, the efficiency of the hydrokinetic system and the scientific background behind the stream energy conversion system. However the scope of this paper is limited in application in free-flowing rivers since its suitable for small scale electricity generation. This system need to be well investigated and still in their infancy. Hope that it can be useful for a better understanding of the benefit offered by this low stream power generation technology.

VIII. BIBLIOGRAPHY

[1] F. Birol, "Energy and climate change," International Energy Agency, Paris, 2015.

[2] G. Davies, "The exploration and emploitation of non-conventional hydrocarbon in Europe," *Social Affairs, Health and Sustainable Development,* p. 3, 2016.

[3] M. L. Bahaj AS, "Fundamentals applicable to the utilization of marine current turbines for energy production," *Renewable Energy ,* vol. 28, pp. 2205-11, 2003.

[4] Y. L. Maniaci D, "Investigating the influence of the added mass effect to marine hydrokinetic horizontal-axis turbines using a general dynamic wake wind turbine code," in *Oceans' 11conference*, Hawaii, USA, 19–21 September 2011.

[5] H. Zhou, "Maximum power point tracking control of hydrokinetic turbine and low-speed high-thrust permanent magnet generator design," 2012.

[6] M. J. Khan, M. T. Iqbal and J. E. Quaicoe, "River current energy conversion systems: progress, prospects and challenges," *Renewable Sustainable Energy,* vol. 12, pp. 21-93, 2008.

[7] V. M. Silantyev, "Limits of the Turbine Efficiency for free fluid flow," *Energy Resources Technology,* p. 317, December 2001.

[8] W. T. Twidell J, "Renewable energy resources," *Taylor and Francis,* 2006.

[9] A. Goude, S. Lundin and M. Leijon, "A parameter study of the influence of struts on the performance of a vertical-axis marine current turbine," *Swedish Centre for Renewable Electric Energy Conversion.*

[10] Peter, "Measuring DC Voltage using Arduino," *Starting Electronics,* 23 MAY 2013.

[11] E. L. Consoliver and G. I. Mitchell, Automotive Ignition Systems, McGraw-Hill, 1920.

[12] E. J. Carlson, K. Strunz and B. P. Otis, "A 20 mV Input Boost ConverterWith Efficient Digital," *IEEE JOURNAL OF SOLID-STATE CIRCUITS,* p. 10, 2010.

Content-Based Image Retrieval System for an Image Search Gallery Application

Nicole Tham Lei May
Faculty of Electrical Engineering
Universiti Teknologi Malaysia
Johor Bahru, Malaysia.
tlmnicole94@gmail.com

Dr. Zaid Omar
Department of Electric and Computer Engineerings
Faculty of Electrical Engineering
Universiti Teknologi Malaysia
Johor Bahru, Malaysia
zaid.fke@utm.my

***Abstract*—This study aims to introduce a user interface based Content Based Image Retrieval system by combining conventional descriptor-based similarity computation and ranking methods and the use of textual EXIF metadata in an image gallery application. In the CBIR module, we also introduce a hit-and-miss method which computes the similarity of individual regions using simple colour features to root out images that are devoid of any similarity to the query image. The project is mainly divided into three parts which are the gallery interface, the query-processing module, and the image database. This leads to a newer and more intuitive way of searching for and managing images in a database within a computer.**

I. INTRODUCTION

In recent years, rapid advances in data storage and image acquisition technologies have enabled the creation of large, ever-growing digital image collections. Images are increasingly used to convey information as they tend to contain large amounts of data. Due to the increasing difficulty in accessing and making proper use of the vast amount of information contained in digital images and videos, it is necessary to develop suitable information systems to efficiently manage these collections. Image searching is one of the most important functions that need to be supported by such systems to allow efficient browsing, searching, and retrieval.

With the improvement in quality of smartphone cameras over the years coupled with the advent of various social media platforms, smartphone users tend to take a lot of photos with their phones every day. According to a survey by personal media startup Magisto, the average smartphone user takes around 150 new photos every month. Despite this, current smartphone gallery applications are not made to keep up with huge databases of images and the only common method available to retrieve old images is to scroll through many unwanted images before arriving at the desired image. Hence, this project aims to make image galleries more organized by introducing a CBIR-based system for more convenient image searches.

Gallery applications currently available in the market today are inconvenient, images are not organized and the process of recalling old pictures is very tedious and time consuming. Moreover, conventional CBIR systems are computationally heavy for huge databases and not very suitable to be used for search applications where performance is expected to be fast while still being able to produce relevant results.

Based on the problem statements, the objectives of this study are to analyze and determine a reliable feature representation (image descriptor) to characterize images for the CBIR system.as well as to develop a more efficient CBIR algorithm utilizing textual metadata classification in order to reduce the computation time for image retrieval in a local database, to allow users to search by 'tags' used to define the images instead of input images, as well as to implement the system as a 'search' feature in an image gallery smartphone application.

For this project, various image descriptor models will be analyzed and tested in order to determine the most suitable feature representation to be used for this application. The image descriptor model will be considered in terms of retrieval accuracy, speed, and memory efficiency. A CBIR system will then be developed using the selected feature descriptor using the Euclidean distance as a similarity measure. Next, a separate TBIR system will then be developed for textual metadata classification of the images and incorporated with the CBIR system built earlier to reduce the computation time as a result of similarity computation and ranking followed by each search. An image gallery application for Android will then be developed and tested for basic gallery app functionality. Lastly the overall image retrieval algorithm will then be implemented as a search feature on the app.

The findings of this study will benefit users by introducing a more effective way of searching for images on their computers. At the same time, the system will also introduce a way to better organize and manage image collections in smartphones

II. LITERATURE REVIEW

A. *Text-Based Image Retrieval*

In most of the earlier retrieval systems, video or image contents are managed by keywords or textual metadata. [1] These systems have many advantages in terms of maintenance efficiency, user accessibility and efficiency in terms of

computation and memory consumption. However, the capabilities are limited due to the vast amount of labor required in annotating massive image collections. Moreover, there is also a problem with the subjectivity of human perception in defining different image collections as different individuals may have different ways to define the rich contents contained in a single image.

B. Feature Extraction

There are many low-level image features that can be used to characterize an image. Some commonly used features include color, texture, shape, spatial location, etc. Some CBIR approaches use a combination of more than one low-level feature to improve the retrieval performance. Color descriptor is a basic visual feature which is used to retrieve images based on the similarity of color proportion in the images. Due to its stability and robustness; application of color features has widely been accepted in numerous CBIR applications. Jalab H.A [2] implemented an image retrieval system based on color layout descriptor (CLD) which represents the spatial distribution of colors. The results have boasted very high precision and recall values. Chatzichristofis et al [3] proposed a colour and edge directivity descriptor (CEDD), which incorporates both color and texture information in a histogram. This type of descriptor is very lightweight, making it suitable to be used for large image databases; another advantage is that it requires relatively low computational power to extract from images.

One method of texture recognition is the Steerable Pyramid Model [4]. The method divides an image into a set of oriented sub-bands and low-pass residual where it is decomposed into a set of directional sub-bands and one decimated low-pass sub-bands [5]. It is a rotation-invariant and scale-invariant image descriptor and thus offers an efficient and flexible approximation of early processing in the human visual system. Gabor wavelet Transform (GWT) is the most widely used method for texture analysis and feature extraction. It uses the multi-orientation and multi-resolution approach for texture analysis and has been proven to be very efficient. Manjunath and Ma [6] have shown that image retrieval using Gabor features performs better than pyramid-structured wavelet transform (PWT) features, tree-structured wavelet transform (TWT) features and multiresolution simultaneous autoregressive model (MR-SAR) features.

C. Localized features

C. Iakovidou et. Al. revisited several well established methods from both major image description tactics (global features – local features), and re-introduced them as newer and improved feature descriptors called the SIMPLE (Searching Images with MPEG-7 Powered Localized Descriptors) family of descriptors [7] [8]. The MPEG-7 Color Layout Descriptor (CLD) [2] represents the spatial distribution of the color in images in a compact form. The image is divided into (64) 8 x 8 discrete blocks and their representative colors in the YCbCr space are extracted. The descriptor is obtained by applying the discrete cosine transformation (DCT) on every block and using its coefficients.

The produced descriptor is a 3 x 64 bin (64-Y, 64-Cb, and 64-Cr) representation of the image. The MPEG-7-like Color Edge Directivity Descriptor (CEDD) [3] is originally a global descriptor that divides an image into 1600 rectangular image areas. Those Image-Blocks are then handled independently to extract their color information (through a two staged Fuzzy Histogram Linking procedure that produces a 24-bin color histogram of pre-set colors) and texture information (employing the five digital filters proposed by the MPEG-7 EHD and using a heuristic fuzzy pentagon diagram to threshold the normalized maximum responses so as to form a 6- bin texture vector). The obtained vectors are combined in the end to form the 144 bins CEDD descriptor.

D. Performance evaluation

To estimate the degree of retrieval accuracy of a system to get an idea about its performance and reliability. For CBIR, the statistical metrics precision-recall is a widely used measurement method to validate the retrieval accuracy. Most recent literature has used this to measure the performance of image retrieval. The measurement formula is as described in equation (1) and (2).

$$P = (\text{No. of relevant images retrieved})/(\text{Total no. of images retrieved}) = r/n \quad (1)$$

$$R = (\text{No. of relevant images retrieved})/(\text{Total no. of relevant images in database}) = r/m \quad (2)$$

Precision, ‘P’ is the ratio of the number of retrieved relevant images to the all the retrieved images from the database [1] and Recall, ‘R’ is the ratio between the number of retrieved relevant images, to the total number of relevant images in the whole database. The value of precision falls as recall value rises. A system is ideal if both the precision and recall values remain high. However, no such image retrieval system exists which gives the mentioned accuracy.

III. METHODOLOGY

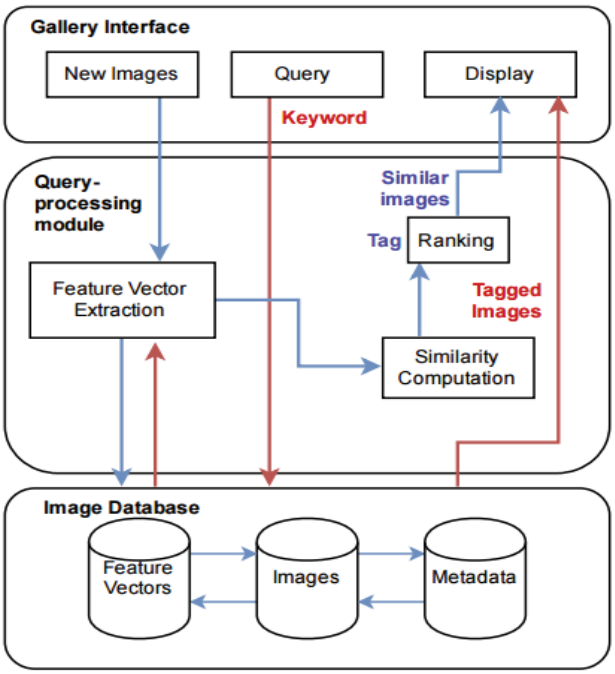

Figure 1. Summary of the system

The system consists of three components: which are the gallery interface, which handles the loading of image thumbnail, integration of search features, and tagging function, the query processing module, which is basically where feature extraction, ranking, and similarity computation is done, and lastly the image database where each image is related to its own specified 'tags' and feature vectors.

A. Query-Processing Module

The query-processing module is the basic CBIR system that takes in either textual metadata or image queries as input. When an image is tagged, the system will extract and store the feature vectors associated with that image so that when a similar text query is inputted, the system will then proceed to use the features to search for similar images in the database and automatically tag them as similar, this will reduce the computation time for the next query as the system will only have to search for images by scanning for the same tags as opposed to executing the extraction and difference calculation again. Moreover, when the user uses the same tags on another significantly different image, the system will take note regardless and will store the new feature vectors and perform computation with those features as well.

The similarity of images is determined by separating the image into 5 regions as in Figure 2, each region of the query image will be computed individually with the search image for similarity. To filter out irrelevant images, each region will be considered as a 'hit' when the similarity threshold is fulfilled, the more 'hit' an image has, the more similar.

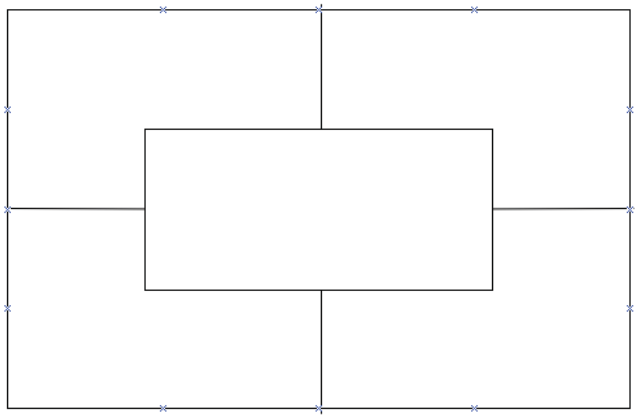

Figure 2. Regions to be computed

If a particular image has zero 'hits' it is considered as a 'miss', wherefore it will not be considered as similar and will not take into account for rankings of similarity. In order to further evaluate the relevancy of images, The MPEG-7-like CEDD [4] is used to further rank images by similarity and 'weed out' images with low similarity index by defining a suitable threshold.

B. Gallery Interface

The gallery interface gives the user options whether to search using a query image or an existing tag which are associated with features that are associated with the tagged image. The system keeps track of image 'tags' that are available in a particular database of images to ensure that only registered search queries are taken into account when the user searches for an image. If the user decides to tag an image that is significantly different from the present image. The layout of the interface is shown in Figure 3.

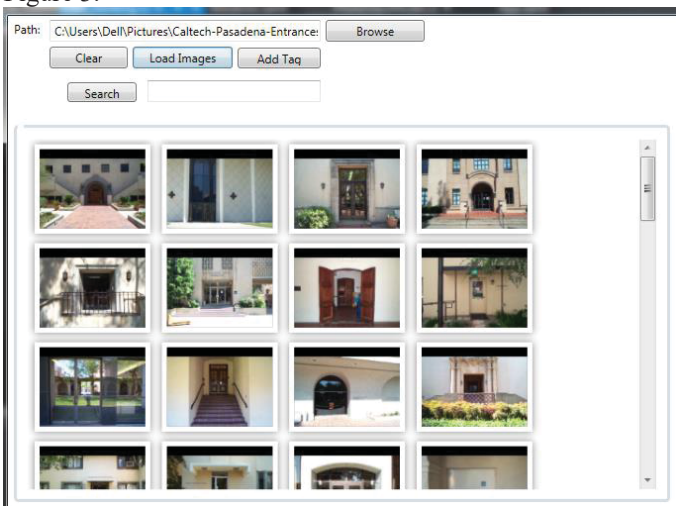

Figure 3. User interface

IV. Results and Analysis

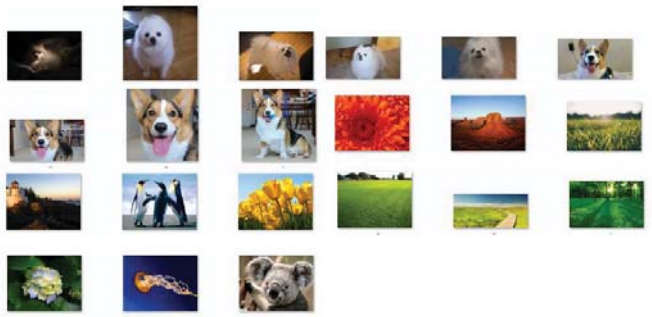

Figure 2. Database of 21 images

Figure 3. Desired results for the 1st test

Figure 4. Obtained results for 1st test

Time 5.42s for 21 images average 0.21s
Precision = 4/7 = 0.57 (57%)
Recall = 4/5 = 0.8 (80%)

Figure 5. Desired results for the 2nd test

Figure 6. Obtained results for the 2nd test

Time 5.68s average time per image 0.27
Precision = 2/3 = 0.67 (67%)
Recall = 2/4 = 0.5 (50%)

The results have shown that the system performed better on images where the object of interest is at or near the center of the image, however it is possible that lighting does have an effect on the performance as well. It is possible to further improve the results implementing a grid system to in the hit-or-miss stage to localize features rather than putting more focus on the center of the image.

V. Conclusion

References

[1] Long, F., Zhang, H., & Feng, D. D. (2003). Fundamentals of content-based image retrieval. In Multimedia Information Retrieval and Management (pp. 1-26). Springer Berlin Heidelberg..

[2] Jalab, H. A. (2011, September). Image retrieval system based on color layout descriptor and Gabor filters. I.S. Jacobs and C.P. Bean, "Fine particles, thin films and exchange anisotropy," in Magnetism, vol. III, G.T. Rado and H. Suhl, Eds. New York: Academic, 1963, pp. 271-350.

[3] Chatzichristofis, S. A., & Boutalis, Y. S. (2008, May). CEDD: colour and edge directivity descriptor: a compact descriptor for image indexing and retrieval. R. Nicole, "Title of paper with only first word capitalized," J. Name Stand. Abbrev., in press.

[4] Simoncelli, E. P., & Freeman, W. T. (1995, October). The steerable pyramid: a flexible architecture for multi-scale derivative computation. In ICIP (3) (pp. 444-447).

[5] Deselaers, T., Keysers, D., & Ney, H. (2008). Features for image retrieval: an experimental comparison. Information Retrieval, 11(2), 77-107.

[6] B. S. Manjunath and W. Y. Ma. "Texture features for browsing and retrieval of large image data" IEEE Transactions on Pattern Analysis and Machine Intelligence, (Special Issue on Digital Libraries), Vol. 18 (8), August 1996, pp. 837-842.

[7] C. Iakovidou, N. Anagnostopoulos, A. Ch. Kapoutsis, Y. Boutalis and S. A. Chatzichristofis, "SEARCHING IMAGES WITH MPEG-7 (& MPEG-7 LIKE) POWERED LOCALIZED DESCRIPTORS: THE SIMPLE ANSWER TO EFFECTIVE CONTENT BASED IMAGE RETRIEVAL", «12th International Content Based Multimedia Indexing Workshop», June 18-20 2014, Klagenfurt – Austria. M. Young, The Technical Writer's Handbook. Mill Valley, CA: University Science, 1989.

[8] C. Iakovidou, N. Anagnostopoulos, A. Kapoutsis, Y. Boutalis, M. Lux and S. A. Chatzichristofis, "LOCALIZING GLOBAL DESCRIPTORS FOR CONTENT BASED IMAGE RETRIEVAL. SIMPLIFYING THE SIMPLE FAMILY OF DESCRIPTORS", «EURASIP Journal on Advances in Signal Processing», Springer

A Computational Study on the Characterization of Blue Phosphorene Field Effect Transistor

Ridhwan Fahmi Mat Radzi
Faculty of Electrical Engineering
Universiti Teknologi Malaysia
Johor Bahru, Malaysia.
ridhwanfahmi93@gmail.com

Zaharah Johari
Department of Computer and Electronics Engineering
Faculty of Electrical Engineering
Universiti Teknologi Malaysia
Johor Bahru, Malaysia.
zaharahj@utm.my

***Abstract*—The purpose of this study is to investigate the electrical characteristic of blue phosphorene in material state and device state because new material is needed to cover and backup the material that is on it limits. The performance of the blue phosphorene in term of it electronic properties and characteristics and the comparison between blue phosphorene with others material was done. The electronic properties such as bandstructure, density of state (DOS), electron density (ED) and current-voltage (I-V) characteristic are simulated using Atomistic Tool Kit (ATK) software version 13.8.1 from Quantum Wise. The blue phoshorene also been compress and stretch to see its performance. From the simulation, when the structure become wider the bandgap will decrease. In the case of DOS, it will increase. The ED also exhibit an increment. The compress and stretch will make the bandgap smaller. The I-V characteristic, shows a linear and increase in drain current with varying back gate bias. Discussion enhance that the blue phosphore can only be used as switching device and high output device.**

Keywords— Phosphorene; bandstructure; transistor

Introduction

Phosphorene was first isolated in 2014 by mechanical exfoliation. Phosphorene predicted to be strong competitor to graphene because it has band gap. Phosphorene have many types but there are only two types that been discover that are stable to be used, which are black and blue phosphorene. The two dimensional monolayer counterpart of bulk black phosphorus, also called phosphorene (include the blue phosphorene). The few-layer related systems have generated intense theoretical mechanical, thermal and electrical properties [1,2].

Blue phosphorene which has found to be symmetrically compatible with the arsenic phase of phosphorus. Blue phosphorene is composed of a hexagonal lattice with a basic of two P atoms like the honeycomb structure of graphene [3]. Blue phosphorene has isotropic properties. The band gap for the blue phosphorene is 2 eV for it single structure [4]. There are two-atom unit cell with the zigzag structure along a1 and a2. The lattice constants for the blue phosphorene is |a1|= |a2|= 3.15 Å [5]. The inclusion of finite-temperature effects makes the blue phase thermodynamically more stable over the black phase above 135 K [6]. This blue phosphorene monolayer allotropes already proposed with stability and compatibility as in-plane heterostructures. The silicene and germanene have been recently synthesized, stanene is theoretically predicted, and all these structures exhibit the same lattice structure as a blue phosphorene monolayer [1].

I. LITERATURE REVIEW

A. Blue Phosphorene

The blue phosphorene is an isotropic with a zigzag structure the predicted value is 78 W/m-K. Blue phosphorus displays a wide fundamental band gap [5]. The advantages of blue phosphorene is its wide fundamental band gap in excess of 2 eV (Fig 1) [4]. The top view of the blue phosphorene structure illustrate the similarity with honeycomb lattice of graphite, which contains two atoms per layer per unit cell [3,4]. Form the monolayer of black phosphorus, we can be change to the blue phosphorene without changing their local bond angles and flip some of the P atoms from ‘down’ to ‘up’ position (Fig 2a) [4]. The distance covalent bond at the equilibrium distance of 2.27 Å and resulting in a large binding energy of 5.19 eV/atom [4]. The blue and black phosphorene is equally stable. The weak inter-layer interaction of 6 meV/atom holds the layered structure together at the interlayer distance d = 5.63 Å [4]. The lattice constants for the blue phosphorene is |a1|= |a2|= 3.15 Å [5]. The influence of the interlayer interaction on the in-layer structure is small, causing only a negligible change from a=3.324 Å in the bulk to a=3.326 Å in the isolated monolayer [4]. The calculated flexural rigidity value D=0.84 eV for the blue phosphorus [2].

Fig 1 : Sample of bandstructure of 2 x 3 blue phosphorene

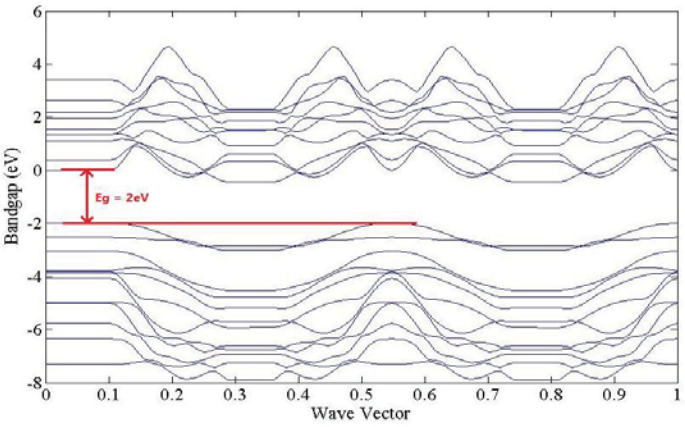

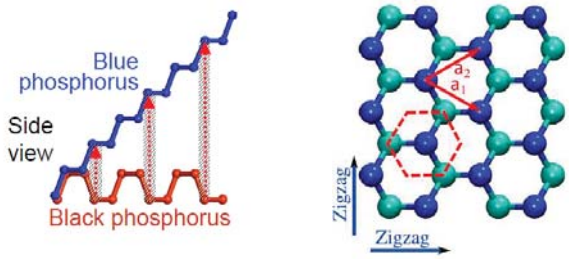

(a) (b)

Fig 2 : (a) The relation between the black and blue phosphorene structure [4]. (b) The structure of blue phosphorene [5]

II. Methodology

A. Computational Method

For this project we are using Atomistic Tool Kit Software version 13.8.1 form Quantum Wise. This software was used to run the simulation of electronics properties for blue phosphorene. This software has capabilities of simulation of electronics device structure. In addition, ATK software also has unique capabilities which focus on large scale system and it is become modern software platform that combining powerful scripting with a graphical user interface [7].

This software is used to build the blue phosphorene. The main tools used are the builder to create the blue phosphorene. The structure is then sent to script generator tool where the electronics properties can be calculated. The 2D plot as analyzer is used to view the simulation result. The data is then exported to MATLAB for re-ploting. The flow of conducting the simulation are describe in the next section.

To obtain the simulation result, there are several method can be done using ATK software, that is self-consistent Extended-Huckel Theory (EHT) [8] and Non-Equilibrium Green's Functional (NEGF) [9]. The EHT can be used to calculate the large system properties [10]. It also inexpensive for computational and have good tradeoff. For more accurate result, the several functions of EHT is used that is the generalized gradient approximation (GGA) in Density-Functional Theory as the bench-marked (DFT) [10]. The Krylov calculator is been used to calculate the bandstructure, density of state and electron density in this blue phosphorene silmulation. The Kyrov calculator is faster than the default method [11]. For the I-V characteristic the configuration for the length between right and left electrode is 6.2 nm for better geometry optimization (Fig 4). The length need to be select wisely because when the value not suitable, the bonding will be broken. The applied energy at the configuration is 2eV for both left and right electrode. The k – point sampling at Brillouin zone of 1 x 1 x 100 is been used for the material but when changing to device, k – point sampling of 100 x 1 x 100 is been used. For numerical accuracy, the density of mesh cut-off energy was assumed at 10 Hartree. The Fermi level is measured at zero parameter.

B. Creating Blue Phosphorene

In ATK, the blue phosphorene material is not exist. Therefore, it need to be create as a new material in ATK. To create the blue phosphorene, there are several steps need to be done. First, we need to create the black phosphorene using Builder in ATK. Open the crystal builder plugin and select the space group Cmca for a space group number 64 (orthorhombic). Then, insert the lattice parameter for a=3.3136 Å, b=10.478 Å and c=4.3763 Å. Next, change the element form Hydrogen to Phosphorus and change the y=0.10168 and z=0.08056 positions according to the reference. After all steps are done, press build and the black phosphorene structure is created. The trick for changing the black phosphorene into blue phosphorene is by flipping specific P atoms from a 'down' to an 'up' position without changing the local band angles (Fig 2a) [4]. Then, change the angle of whole structure from 45˚ uprise to transverse at 0˚ [7].

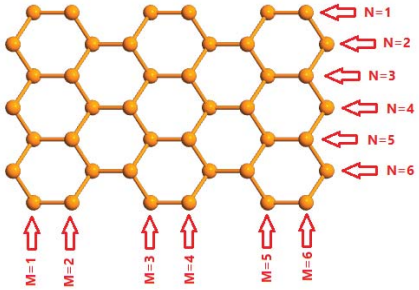

Fig 3 : Example 6 x 6 blue phosphorene structure where the N (length) and M (width)

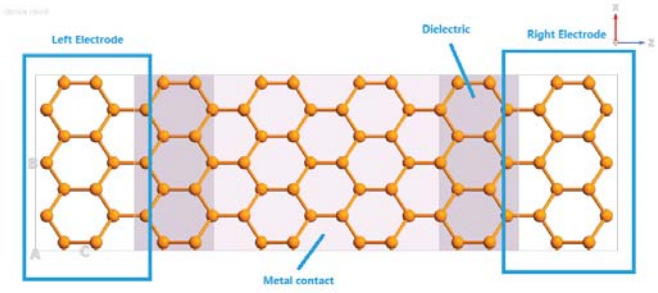

Fig 4 : The 6 x 8 blue phosphorene device structure

III. Result and Discussion

A. Eletronic Properties

1) Bandstructure

In this project, the structure is been varied by it width, W and it length, N to see the effect of it bandgap value. The upper level of the bandgap is known as conduction band and the lower is the valance band. This two also known as π and π*. The zero value of the bandgap is the Fermi energy (E=0) at the wave vector of Γ. As can be seen in Table 1, the increment of the

width and length is 4, 6, 8, 10 and 12. For varied it width, the trend for the bandgap is decreasing by the increasing of it width. For varied it length, the trend is increasing at the start and suddenly decrease. As we can see at 'n10w6' the value of bandgap decrease form 'n8w6' = 0.2181 to 0.01765 and then it increase to 0.1082 at 'n12w6' but the value is not increasing greater than 'n8w6'. It somehow like it changing state from metallic to semiconductor because at 'n10w6', the bandgap value is very small and the electron can easily jump between the valance and conduction band. The changing in width obviously can be seen correctly and stable because the decreasing is gradually as the width increase.

Table 1 : The blue phosphorene structure and it bandgap

Structure configuration	Band gap (eV)
i-Varied width	
N = 6 W = 4	0.2058
N = 6 W = 6	0.1851
N = 6 W = 8	0.15444
N = 6 W = 10	0.08544
N = 6 W = 12	0.06225
ii-Varied length	
N = 4 W = 6	0.1637
N = 6 W = 6	0.1851
N = 8 W = 6	0.2181
N = 10 W = 6	0.01765
N = 12 W = 6	0.1082

2) *Density of state*

From Fig 5, the result of DOS is varied by it width and it increment by 2. For 'n6w4', it can be seen at 0.2eV to 1eV that it contain the forbidden gap where the electron does not exist at that point. For this type of DOS, the forbidden gap is at the positive side and it mean that the blue phosphorene p-type material. The DOS is not quite similar for any of the structure when we varied width. We can see that when the width increase, the bandgap also increase.

From Fig 6, the increment is the same at width but it been varied by it length. It different when varied the width, the waveform is more symmetrical at both negative and positive side. The peak of the DOS also higher that when varied width but it the same as we expend the size of the blue phosphorene structure, the bandgap also increase. From Fig 6 also, at 'n4w6' it contain the forbidden gap but the range it different that is from 0.2eV to 1.4eV. By comparing both Fig 5 and Fig 6, when we

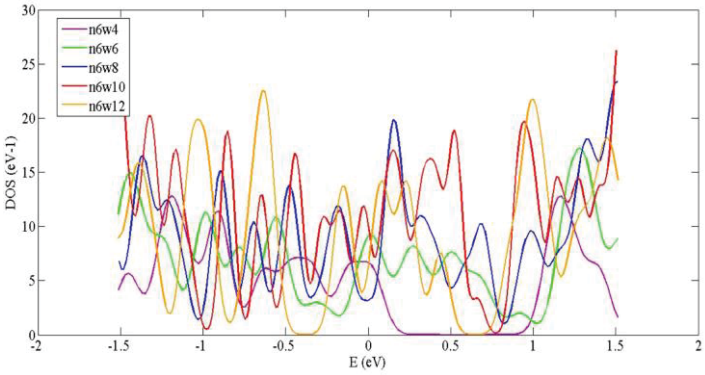

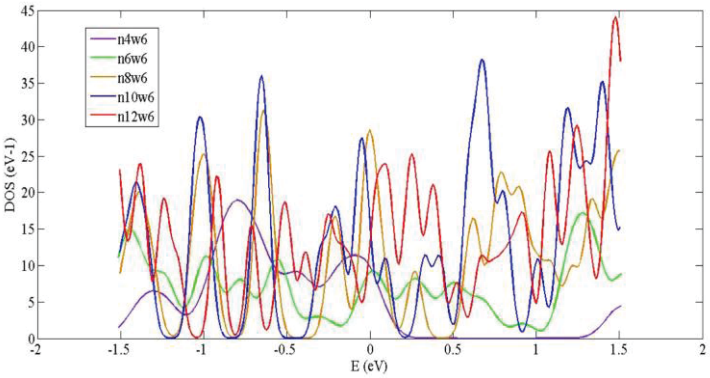

varied length, we can have higher DOS. So we know that the number available of the quantum state that within an energy range is higher when varied the blue phosphorene length.

Fig 5 : DOS for blue phosphorene when varied it width

Fig 6 : DOS for blue phosphorene when varied it length

3) *Electron density*

The electron will move for one point to another point by force. From Fig 7, it shows that the probability of the movement of electron from one point or another from three direction that is a=x, b=y and c=z axis. It also shows the effect when we varied the width and length. When we varied the width, the higher the width, the a, b and c axis also increasing. This also same as we varied the length. It show that the a-axis give higher value that the b and c axis. This because the there are many electron in the a-axis that need to be move. So, it need more force to deal with it. When we compare the result between when varied width and varied length, the most effected the ED is when we varied the width. The higher for a-axis is at 'n6w12'around 1000 $Å^{-3}$. For b and c axis, when we varied the width, for both axis b and c is getting away from each other but when we varied the length, the b and c axis is getting closely to each other. This because the structure itself, so the electron need to travel for long or short distance depend on the structure.

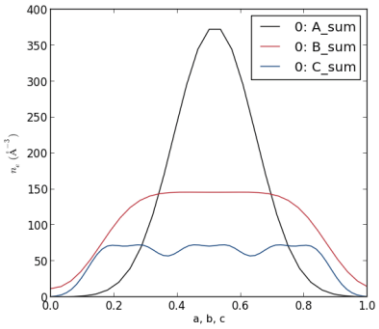

(a) n4w6

(b) n6w4

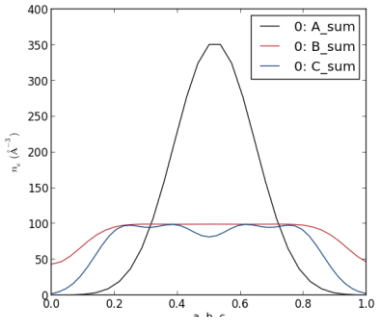

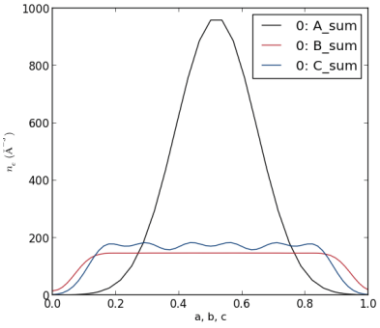

(c) n12w6

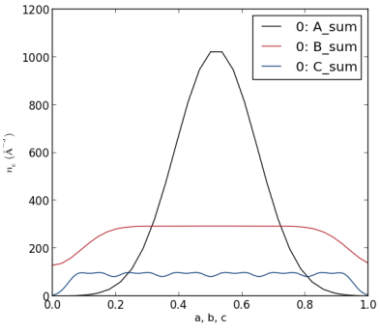

(d) n6w12

Fig 7 : The electron density at different structure

4) Compress and stretch

The structure 'n6w8' have the average range of bandgap and the structure is good enough to be used as semiconductor device. As the result from Table 2, the structure of the blue phophorene is expend when it value is positive and shrink when it value is negative. As the size of structure expand, the distance (bond length) of a1, a2 and a3 is increasing and vice versa as it shrink. At ±15% strain, the type of the structure is semiconductor to metal transition because the bandgap becoming smaller and smaller. The trend for the increasing or decreasing of the strain is the bandgap will decrease and obviously when it goes shrinking, the bandgap drastically decrease. As the original type at zero 0% strain, the blue phosphorene is indirect bandgap but it change to the direct bandgap at ±10% strain. This phenomenon could be caused by the emerging of new conduction band minimum at the Fermi level. So, it maybe can be use as optical application.

Table 2 : The percentage of strain, bond lengths, energy bandgap and type of the energy bandgap of 'n6w8' monolayer blue phosphorene before and after strain

Strain, ε (%)	Bond length (Å)			E_g (eV)	Type
	a_1	a_2	a_3		
-15	2.21	1.89	3.72	-	Semiconductor to metal transition
-10	2.22	2.00	3.94	0.06682	Direct Γ - Γ
-3	2.24	2.20	4.33	0.06712	Indirect Z- Γ
-2	2.24	2.22	4.38	0.06613	
-1	2.25	2.25	4.42	0.08661	
0	2.25	2.27	4.46	0.1544	
1	2.25	2.29	4.51	0.1144	
2	2.25	2.31	4.55	0.1081	
3	2.26	2.33	4.60	0.09427	
10	2.27	2.45	4.81	0.0712	Direct Γ - Γ
15	2.28	2.56	5.03	-	Semiconductor to metal transition

B. Transport Properties

1) I-V curve

For the I-V characteristic, the 'n6w8' structure is been used to become the device structure. As the data from Fig 8, the voltage bias is been varied from 0.5V to 2V. The changes of the voltage bias effect the value of drain current as the voltage bias become higher, the drain current also become higher. For the result, the properties of the I-V curve for blue phosphorene is linear and the output of it drain current is high. It is different cases for other material such as black phosphorene, silicon and germanium because the threshold voltage, Vth is not zero. The threshold voltage for black phosphorene is around 0.25V [5]. As for the silicon and germanium is 0.7V and 0.3V [12]. In the graph, it not shown because it not visible at the range of 0.2V. The threshold is needed to control power dissipation, limit energy consumption and maintain reliability [12]. When we have higher threshold voltage, we need higher supply voltage to on the device. In simple word, the minimum voltage needed to make the device operate. The saturation region can be found in black phosphorene, silicon and germanium. Therefore, this material can be used as an amplifier [12]. The I-V characteristic of blue phosphorene only exhibit linear region and absent of saturation. This kind of transistor can be used for low-voltage and low-power application [13]. Therefore, more work need to be done to further optimized the design to fully utilize the material.

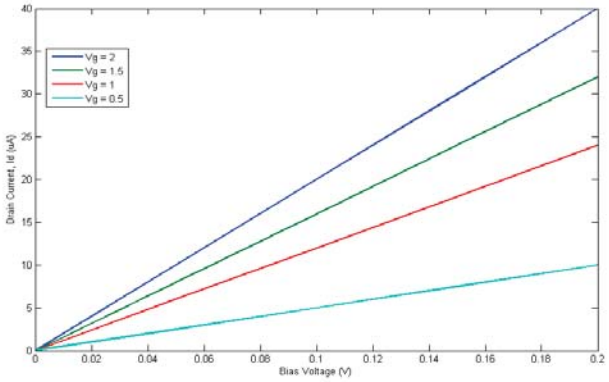

Fig 8 : The relationship between the drain current when varied bias voltage

IV. Conclusion

The simulation shows that the bandgap for 2 x 3 blue phosphorene is around 2eV. When the structure of the blue phosphorene increase, the bandgap became smaller. The trend for the DOS is when the length or width is increase, the bandgap increase. The a-axis for ED will increase when the width and length increase but at b and c axis, it depend when varied width it will getting away from each other but when varied length, it vice versa. The compression and stretching of blue phosphorene make the bandgap become smaller compare to the original state. The I-V characteristic been varied by the voltage bias and it shows that the higher the voltage bias applied, the higher the drain current, Id. It seen that blue phosphorene has zero threshold voltage and that mean it does not have saturation region. For recommendation, more work need to be done to further optimized the design to fully utilize the material.

References

[1] Soares, J. R., Almeida, R. M., Cancado, L. G., Dresselhaus, M. S., & Jorio, A. (2015). Group Theory for Structural Analysis and Lattice Vibrations in Phosphorene Systems. American Physical Society, 1-11. Retrieved October 7, 2016.

[2] H. Liu, A. Neal, Z. Zhu, D. Tomanek, and P. Ye, “Phosphorene: a new high-mobility 2d semiconductor," (2014), arXiv:1401.4133.

[3] Ospina, D., Duque, C., Correa, J., & Morell, E. S. (2016, July 29). Twisted bilayer blue phosphorene: A direct band gap semiconductor. 1-13.

[4] Zhu, Z., & Tomanek, D. (2014, April 3). Semiconducting layered blue phosphorus: A computational study. Phys. Rev. Lett., 1-5.

[5] Jain, A., & McGaughey, J. (2015, February 17). Strongly anisotropic in-plane thermal transport in single-layer black phosphorene. Department of Mechanical Engineering, Carnegie Mellon University, Pittsburgh, 1-5.

[6] Xie, J., Si, M. S., Yang, D. Z., Zhang, Z. Y., & Xue, D. S. (2014, May 20). A theoretical study of blue phosphorene nanoribbons based on first-principles calculations. 1-5.

[7] www.quantumwise.com.

[8] Stokbro, K., Petersen, D., Smidstrup, S., Blom, A., Ipsen, M. and Kaasbjerg, K. Semiempirical model for nanoscale device simulations. Phys. Rev. B, 2010. 82(7): 75420.

[9] Chen, X., Song, K., Zhou, B.,Wang, H. and Zhou, G. Dependence of transport on adatom location for armchair-edge graphene nanoribbons. 2011: 3.

[10] Raza, H. and Kan, E. C. An extended Huckel theory based atomistic model for graphene nanoelectronics. Journal of Computational Electronics, 2008. 7: 372–375. ISSN 15698025.

[11] ATK Tutorial for Molecular Devices Calculate and analyze a molecular device configuration.

[12] Ospina, D. A., Duque, C. A., Correa, J. D., & Suárez Morell, E. (2016). Twisted bilayer blue phosphorene: A direct band gap semiconductor. Superlattices and Microstructures, 97, 562–568. https://doi.org/10.1016/j.spmi.2016.07.027

[13] Júnior, C. C. S., Deotti, D., Ponte, R. M. da, Machado, M. B., & Schneider, M. C. (2012). Zero-Threshold-Voltage MOSFETs: A Survey. Student Forum - SFORUM, 1–4. Retrieved from http://www.lbd.dcc.ufmg.br/colecoes/sforum/2012/0015.pdf

Portable Electronic Biosensor for E-coli Detection

Munirah binti Ahmad Hamizan
Faculty of Electrical Engineering
Universiti Teknologi Malaysia
Johor, Malaysia.
Email: munirahahmad94@gmail.com

Dr Yusmeeraz Yusof
Department of Electronic & Computer Engineering
Faculty of Electrical Engineering
Universiti Teknologi Malaysia
Johor, Malaysia.
Email: yusmeeraz@utm.my

Abstract— This paper reports an ion-sensitive field effect transistor (ISFET) based label-free biosensor for the detection of Escherichia coli (E-coli) bacteria normally found in environment, foods, and intestines of human and animals. A portable device consists of ISFET biosensor, readout circuit, microcontroller and LCD display are built in this project. The level of E-coli present in samples is sensed by determine its concentration in CFU/ml. This fully electronic biosensor can help to improve existing method that requires specialized laboratory and personnel to perform the test. The developed device is user friendly and portable to be used anytime anywhere.

Keywords— Label-free, portable, ISFET, biosensor, E-coli

I. INTRODUCTION

ISFETs are widely used in detection of bio-chemical species and have strength creation to provide mass expenditures which of low cost, light weight, small size and fast response time [1]. The portable device consists of ISFET biosensor, readout circuit that functions to amplify the biosensor signal, and microcontroller to change analog signal to digital signal, completed with LCD display are developed in this project. By using this portable device, E-coli can be detected directly and gives real time result. This device is a user friendly device where it can be used by anyone without the need of specialized skills to perform the test and this portable device also help in improving existing methods in detection of food pathogens. The existing methods are mostly require long time to get the results, require authorized person to perform the test and hardly invasive causes the patients to feel uncomfortable when performing the test. E-coli were being selected as a target analyte because it can be contagious and effects human's intestines. There are many types of E-coli and most of the E-coli is yet harmless but can attack human and animal foods. The symptoms of E-coli infection include anemia and diarrhea. Moreover, if the E-coli bacteria getting aggressive and critical it can lead to kidney failure and worst scenario, fatal [2]. E-coli attacks human by improper foods handling, spread from person to person and contacts with animals.

II. BACKGROUND AND PROBLEM STATEMENT

In order to develop the portable device ISFET sensor, it is crucial to understand the label-free sensing principle of ISFET and the target analyte E-coli which has been chosen for the purpose of this study.

A. Label-free Biosensor

As nowadays many monitoring and analysis need to be taken from different parameters in areas like clinical, food industry, environment quality and medical, an analytical device had been develop such as biosensor. Biosensor is a device arbitrate by immunosystems, isolated enzyme, tissue, organelles or whole cell make a specific biochemical reaction to detect chemical compound by electrical, thermal or optical signal [3]. The element in biosensors is biological recognition element or bio-receptor that can detect the presence of analyte such as proteins, DNA and glucose. The reaction between bio-receptor and the target analyte create a physical or chemical response which are then will be receive by the transducer to be transform into a measurable signal. Transducer process can be electrochemical, optical, piezoelectric, thermometric, ion-sensitive, magnetic or acoustics [3].

Biosensor can be a label-free process or labeling process. For electrical and electronic use, label-free process biosensor will be use as it is related to the electrical system and component. Label-free detection is a direct transduction (electrical, mechanical or optical) where it can utilize molecular biophysical properties such as molecular charges to monitor molecular presence and activity (mass spectrometry), weight and refractive index. Label-free not using any label probes and the result are in real-time manner. The advantages of label-free biosensor are that it can give direct acquiring information and specifically use native protein and ligands as it target analyte. Meanwhile label detection method are suitable if the test that want to be conduct need abundance sample and need to be done chemically by attaching the biomolecule to any foreign particles in order to detect molecular activity and properties of a system within itself. Label process has a sophisticated preparation step where it needs to be done in low yield, combining synthesis and purification. Label processes are fluorescent probe, radioisotope, chemiluminescent and nanoparticles [4].

B. Principle of ISFET biosensor

ISFET (Ion-sensitive field-effect transistor) is any of label-free potentiometric biosensor applications particularly for detection of pH. They are applied to measure the concentration of hydrogen ions contained within solution and the measurement

using the interface potential of on the gate insulator. ISFETs also been used in the detection of chemical and biosensors. ISFET sensor is based on the modification and combination of three systems. The system is sensitive ion electrodes (ISE), pH indicator strips and optical sensors. Modification all three elements has strength creation to provide such ISFET mass expenditures which of low-cost, light weight, small size and fast response time. Since the fabrication is in direct proportion standards of Metal Oxide Semiconductor (MOS) technology, but it is also low output impedance, high-speed signals, distributed sensing, the possibility of multiplexing and temperature compensation [5].

ISFET operated on the principle of Field Effect Transistors work (FET). FET has three main terminals which are a source, drain, and gate. Of current that flows in the FET subject on the potential difference between the source and drain, and is controlled by an electric field generated from the gate voltage. Another element that affects the current flow is kind of the carrier; either electrons or holes are defined by the type of channel FET (i.e.: n-channel or p-channel). When a positive voltage is applied to the gate, it will push positive charge (hole-free) of the substrate region under the gate. Positive charges caught in the rain to the substrate, it is much of the region shortage carrier. Consequently, the depletion region consist only negative charges. These charges can move around freely because the hole will neutralize down to the substrate [6]. A positive gate voltage used will attractive negative charges (electrons) from the substrate to the channel region. The enough amount of electrons is induced under the gate will realize the inversion layer between the drain and source. When voltage difference applied between the drain and source, the current will flow through it. A gate voltage will flow controller time because it will impact inversion layer consisting of the threshold voltage (VTH). The VTH value is negative for p-channel and n-channel positive. As shown in Figure 1, ISFET structure is more similar to the Metal Oxide Semiconductor Field-Effect Transistor (MOSFET) however channel ISFET is a solution that can enable ion; hydrogen ions serve as an example for the door. Ions are interested by the surface of the sensor, and it will produce a potential difference on the door that creates the inversion layer. Where the inversion layer has been established, electrons flow from the source to the drain and the current is cascaded through the inversion layer [7]. ISFET based biosensor is essential in everyday life mainly for the biomedical field. Applications include detection of DNA, electro-immunology sensing, sensing enzyme based, live monitoring of the reaction cell, and the measurement of pH.

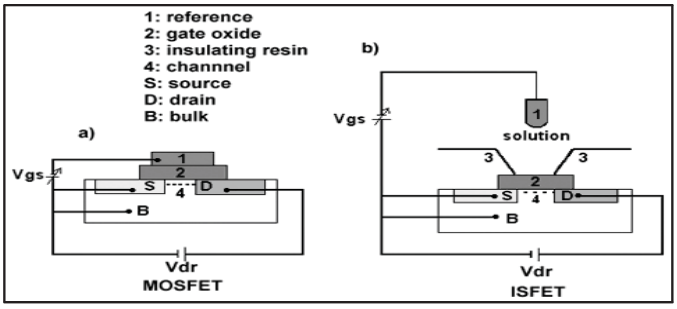

Fig. 1. The structure of MOSFET and ISFET [7].

C. *Escherichia Coli (E-Coli)*

E-coli is a gram-negative rod-shaped bacteria, which possesses adhesive fimbriae and a cell wall that consists of an outer membrane containing lipopolysaccharides, a periplasmic space with a peptidoglycan layer, and an inner, cytoplasmic membrane usually lives in human and animals intestines and act as a key to a healthy digestive tract. There are many types of E-coli and most of it is harmless but the congestive one can make the host where it lives get sick and causes illness. The most dangerous E-coli are E-coli type O157:H7 as it can cause vomiting or nausea, severe abdominal cramps, bloody diarrhea, kidney failure and the worst case scenario is fatal. The problem often occurs to an adult with a weak immune system and also children. E-coli O157:H7 have Shiga toxic that is very dangerous to human and animals intestines and can be called as Shiga toxin-producing E-coli (STEC) and there are several types of E-coli which is as harmless as O157:H7 in the STEC categories [2]. The most severe cases of E-coli infection are Hemolytic Uremic Syndrome (HUS) where it destroys red blood cells and it acquires intensive care, kidney dialysis and blood transfusion for the patients with this disease. The patient with E-coli infection can be treating as fast as two weeks periods and HUS can only be detected after one week. Centers for Disease Control and Prevention estimated about 265,000 STEC occur each year in the U.S [8].

E-coli mostly comes from improper food handlings which is contaminated foods and water like meats not cooked properly and have pink side, soft cheese made from raw milks, raw juice and untreated water or swimming in contaminated water. Secondly is infected from people to people due to feces of infected person. The infected person will touch things especially foods and the germs will affect other people. Lastly, the infection of E-coli can come from in contact with animals like cows and cattle happen to have E-coli infection. E-coli were classified under food pathogens and allergies that causes disease to human and animals need to be treated.

D. *Statement of Problem*

Food pathogens and allergies detection methods generally need to be performed by specialized personnel like doctors, gastroenterologist or dietitian who are authorized to treat patients. Likely, the result is not fully accurate and takes long time to analysis and gets the actual result. Thus, the treatment will take long time and the prevention steps will be harder if the allergy and food poisoning had become severe. In order to detect allergies and food pathogen diseases, the test need to be done in the clinic or hospital with all the right equipment use and the entire test that had been conducted are very inconvenient to the patients especially infants that still fragile and soft.

In order to get a correct result of food pathogens and allergy detection, biosensors will be introduced. Biosensor is important in clinical diagnosis where it generates different pH value in detection of DNA, sequences of amino acids, nucleotides and living cell such as protein enzyme [9]. Labeling process such as chemical detections involves many procedure to be done and resulting time analysis to be longer. Meanwhile, optical method uses fluorescent dyes that are expensive and sometimes the test conducted can produce false-positive signals due to the perturbations in molecular interactions of label molecules. It is

also require large sophisticated equipment for the detection and analysis process. In this project, the product will be fully developed by electrical based biosensor label-free which is ISFET sensor. ISFET sensor is portable, low cost, miniaturization, lightweight and suitable to be use in biosensing application. As biomolecule contains different amount of ionic charges either positive charges or negative charges, it can be detected by the gate electrode and the induced voltage can be measure by an electronic readout device.

III. METHODOLOGY

This project uses software simulation and hardware implementation. The prototype consists of ISFET biosensor, readout circuit, microcontroller and display unit. Input for the sensor is a chemical sample. When a sample is sensed by the sensor, it will produce an output voltage, VSENSE and this voltage is transferred to the electronic readout circuit. Output voltage from readout circuit, VOUT will be displayed on LCD panel and LED will show the level of E-coli present based on it concentration (CFU/ml), which is programmed in Arduino microcontroller. There are two software tools used in this project; Multisim for circuit design in electronic readout circuit and Arduino (microcontroller) for programming and display.

A. ISFET biosensor

This project used a WINSENSE ISFET pH Sensor (WIPS) product. ISFET sensor is suitable for this project because it can measure the voltage in solution that produced by the distribution of charge. It only uses a single power supply, inexpensive and lightweight. The sensing element is the metal gate of ISFET which works with a reference electrode (RE) and a chemical solution.

B. Readout Circuit

In this project, the circuit will be built based on the schematic diagram as shown in Figure 2. Readout circuit is compatible to be use with any kind of detector. 5V power supply is built by using voltage regulator LM7805 IC where it will regulate power from the 9V battery. The noise can be reduced by using capacitor at the input and output nodes of 0.1µF.The first stage are voltage follower and for the second, third and fourth stages are non-inverting amplifier. Inputs from the VSENSE that come out from the ISFET sensor are in the range of 0 to 2 V and the expected output are approximately 5V. VOUT can be getting by multiplication of VSENSE with the gain that comes from the 4 stages of amplifier. In this circuit, three non inverting amplifier and one voltage follower are use in this project. The equation can be seen as in equation (1) and (2).

$$V_{OUT} = (\frac{Rf}{Ri} + 1)V_{IN} \quad (1)$$

$$A_V = (\frac{Rf}{Ri} + 1) \quad (2)$$

The amplifier that will be use is UA741 ICs and four resistors. For the first stage the voltage follower will have the gain of Av = 1 meanwhile the second, third and fourth stage will have the gain Av of 1.25, 1.5 and 1.333 respectively.

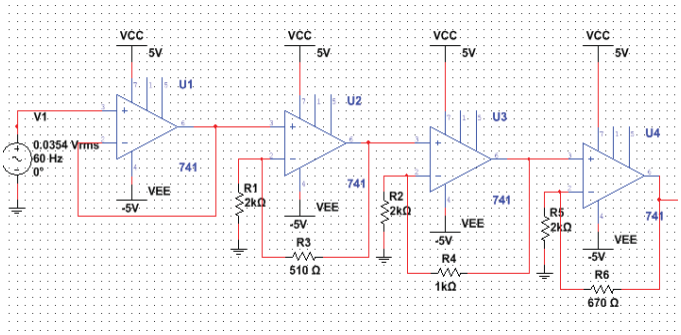

Fig. 2. Schematic Readout Circuit.

C. Microcontroller and Display Unit

Display unit consist of LCD display and LED. LCD display will show the result of the E.coli bacteria presented in the broth solution in term of voltage and the LED will show the level of E.coli present based on the colour of LED. Green LED is for the low level of E.coli concentration which is 100 and 101 CFU/ml, yellow LED for the medium of 102 CFU/ml and red LED show that highest level of E.coli present which is 104 CFU/ml. The display is controlled by Arduino board that receive voltage signal from the readout circuit which than will be programming to be converted to digital display.

D. Measurement Setup

The experimental analysis was conducted with the E-coli concentration from 10^0 to the 10^4 CFU/ml. E-coli concentration in the form of broth was keep in acidic condition as E-coli is denature at acidic condition to prevent the bacteria from alive and reproduce [2]. Before the portable electronic biosensor was being tested with the E-coli broth, calibration need to be performed in order to make sure the data get was accurate. Calibration was done by testing it with the distilled water with the 7 pH which is the voltage get is 3.965 V when detecting with the portable device. From this value, the reading of the E-coli voltage should be lower than distilled water as E-coli is in acidic. The experiment was conducted in the laboratory and environmental condition. In order to keep the result accurate, the experiment need to be conducted in 24 hours as E-coli broth can be best denature in 24 hours. The experiment was repeated three times for each E-coli concentration and proper equipment was used to prevent the contamination of E-coli broth.

IV. RESULT AND DISCUSSION

The portable electronic biosensor device was built and tested. The important part of the device is to get the adequate gain for the signal so it can be read by microcontroller and LCD display. The device was measured by setting a voltage between 0 to 2 V at the input of the VSENSE and observes the VOUT. By using the equation (2), gain is calculated and then compared with the result obtained from simulation of the circuit using Multisim software. ISFET portable device was tested with E-

coli with concentration of 10^0 to 10^4 CFU/ml and the result were analyzed.

A. *Hardware Measurement*

The readout circuit with +5V voltage regulator is tested. The input VSENSE coming from the ISFET biosensor is amplified by using the readout circuit so that the signal can be read by the microcontroller and translated at LCD display. The data for hardware measurement are tabulated in Table 1 and the comparison of gain between hardware measurement and circuit design simulation using Multisim software is shown in Table 2. From the data, the gain produced from the simulation and hardware measurement are approximately 2.5. The test concludes that the hardware and software simulation result have the same gain, A_V.

TABLE I. DATA FOR HARDWARE MEASUREMENT

VSENSE (V)	VOUT (V)
0.57	1.420
0.85	2.130
1.40	3.499
1.62	4.049
1.86	4.649

TABLE II. VOLTAGE GAIN A_V

Measurement	Voltage Gain A_v
Simulation	2.499
Hardware	2.499

B. *Biosensing Measurement*

VOUT obtained from the detection of E-coli concentration in term of CFU/ml were shown in Table 3 and the trend of the E-coli average voltage reading was shown in the form of bar chart in Figure 3. It shows that the higher E-coli concentration, the higher VOUT. The result was compared with the previous work regarding E-coli concentration, CFU/ml with impedance [2]. It stated that the higher E-coli concentration, the higher the impedance. By relating it with the Ohms law, it can be concluded that the higher the voltage, the higher the impedance as the current is constant.

TABLE III. DATA FOR E-COLI VOLTAGE READING BY USING PORTABLE ELECTRONIC BIOSENSOR DEVICE

E-COLI CONCENTRATION (CFU/ML)	VOUT (V)
10^0	3.701
	3.848
	3.834
10^1	3.882
	3.896
	3.890
10^2	3.894
	3.912
	3.903
10^3	3.907
	3.892
	3.925
10^4	3.920
	3.986
	3.894

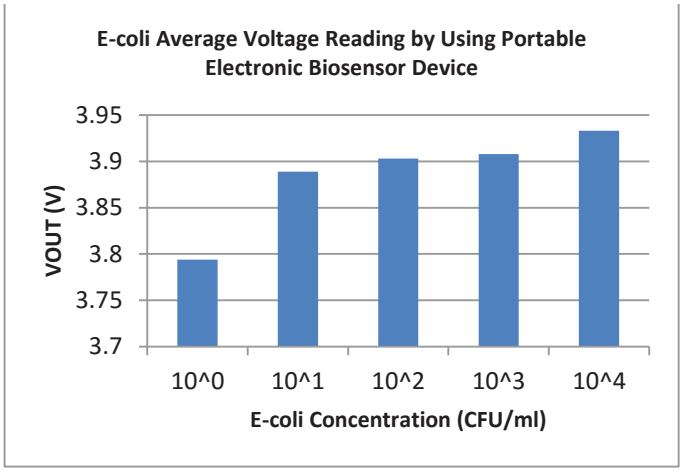

Fig. 3. E-coli Voltage Reading using ISFET Portable Device.

V. CONCLUSION

From this project, biosensor plays a crucial part in development of new technologies to the human kind. The contribution of the biosensor had been vastly used in clinical, environmental, and for forensic use. Biosensor is very efficient in detection, monitoring and analysis for biological molecules. Thus in this project, label-free portable ISFET biosensor prototype has been developed based on the electrical sensing concept. In the future, ISFET can be use not only for E-coli detection but for many other allergies and specifically differentiate between all the allergies with one portable device.

ACKNOWLEDGEMENT

The authors would like to thank the postgraduate student, Mr. Herman from Faculty of Biomedical Engineering, Universiti Teknologi Malaysia for the preparation of E-coli.

REFERENCES

[1] Lee, Chang-Soo, Sang Kyu Kim, and Moonil Kim. "Ion-Sensitive Field-Effect Transistor For Biological Sensing". *Sensors* 9.9 (2009): 7111-7131.

[2] Radke, Stephen M., and Evangelyn C. Alocilja. "A High Density Microelectrode Array Biosensor For Detection Of E. Coli O157:H7". *Biosensors and Bioelectronics* 20.8 (2005): 1662-1667.

[3] Monošík, Rastislav, Miroslav Streďanský, and Ernest Šturdík. "Biosensors - Classification, Characterization And New Trends". *Acta Chimica Slovaca* 5.1 (2012).

[4] Syahir, Amir et al. "Label And Label-Free Detection Techniques For Protein Microarrays". *Microarrays* 4.2 (2015): 228-244.

[5] Rozina Abdul Rani and Othman Sidek, Member, IEEE, ISFET pH Sensor Characterization: towards Biosensor Microchip Application, School of Electric and Electronic Engineering Campus, Universiti Sains Malaysia, Malaysia,2004.

[6] Smith, Kenneth. "The Story Behind Microelectronic Circuits". *IEEE Solid-State Circuits Magazine* 1.4 (2009): 8-17.

[7] Stern, Eric, Aleksandar Vacic, and Mark A. Reed. "Semiconducting Nanowire Field-Effect Transistor Biomolecular Sensors". *IEEE Transactions on Electron Devices* 55.11 (2008): 3119-3130.

[8] "E. Coli | Foodsafety.Gov". *Foodsafety.gov*. N.p., 2017. Web. 14 May 2017.

[9] Lazcka, Olivier, F. Javier Del Campo, and F. Xavier Muñoz. "Pathogen Detection: A Perspective Of Traditional Methods And Biosensors". *Biosensors and Bioelectronics* 22.7 (2007): 1205-1217.

Automatic Number Plate Recognition on Embedded Processor

Nurul Afida binti Rosli, Usman Ullah Sheikh
Bachelor of Engineering (Electric-Electronic)
Faculty of Electrical Engineering, Universiti Teknologi Malaysia,
81310 Johor Bahru, Malaysia.
amelfyda1403@gmail.com

***Abstract* – This research work propose an embedded car plate recognition system. This propoasal system is depends on NORCO embedded platform with an external camera. The camera will detect any motion present by subtracting two frames. Contours with alphanumeric characters are detected as car plate. This alphanumeric characters is compared with the the database in order to identify the character and give a complete car plate as a result.**

Keywords – ANPR; motion detection; plate extraction and localisation; k-NN;

I. INTRODUCTION

ANPR (Automatic Number Plate Recognition) is a powerful image processing technology which is used in identifying the car plate without human aid. It was invented in 1976 at the Police Scientific Development Branch in the UK [1]. ANPR is capable of extracting and recogniting of car plate's alphanumeric characters automatically from an image received or captured. This system can be used in many areas ways such as for speed enforcement [2]. ANPR had an accurancy of between 95% to 98% [3]. It is an inexpensive method compared to other ANPR systems [4][5].

The ANPR system involves four important stages which are motion detection, image capturing, locate and extract car plate and identify characters. In completing the whole process, a camera is used in order to detect motion and capture the image as soon as the motion is detected. ANPR can be operated in real-time where the image is obtained online or undergo offline processing. Once the image is successfully captured or received, the system will start locating and extracting the car plate within the image. It will find all the possible car plate location in the image by using method of finding contour with characters. Then, image is cropped containing only the number plate for futher processing. KNN (K-Nearest Neighbor) algorithm is used for character identification. It will compare the characters in the image with the database stored in the PC.

The rest of the paper is divided into four sections; section 2 will give an explaination regarding software and hardware models used, while Section 3 will present the simulation results of the ANPR system. Section 4 will discuss the output of the simulation and lastly the conclusion and future works is given in Section 5.

II. SYSTEM MODEL

In building a complex system such as ANPR, it involves both software and hardware models.

A. Software Model

The ANPR system can be broken down into four steps and all of that must be done correctly and follow the sequence in order to give the correct output. The steps are;

- motion detection
- capturing image
- locate and extract car plate
- identify alphanumeric characters

For motion detection, subtraction method is used where it will calculate the difference between two frames. In order to get those two frames, a USB camera is used. As tracking function is enabled by the user, the camera will snap the current image as the first frame. This frame will be used as a reference image. The second frame will be captured and will be compared continuosly with the first frame. If there is any change, the system will acknowledge the user that there is motion detected.

Next step is capturing image. When a motion is detected by the system, the camera will capture the last image in PNG format so it can undergo further processes for car plate extraction.

The image is preprocessed in order to locate and extract car plate. In this section, the system finds contour which contains alphanumeric characters. Based on observation of cars, there are few words or alphanumeric characters besides car plate such as model name of the car. To distinguish between that, the contour method is chosen as it will find the rectangle shape within the image. The image is first converted to grayscale and preprocessing will take place. During the preprocess, the system will find any rectangle shape which contains alphanumeric characters in it as high probability of car plate location. After the location of car plate is finalized, the image then undergoes filtering process which involves two different techniques. The first technique is used in order to remove of all white patches containing in the image as the image now is in grayscale format. After that, the image will undergo

second filtering method which uses pixel count method. This is to remove the other regions in the image other than the car plate region. As a result, only the car plate region is left after cropping and eliminating the unwanted region in the image. This will make the identification process easier as the system only focuses in processing the wanted region rather than the whole image. Besides, it will save the time and reduce the probability in getting false result of car plate.

The last step in ANPR is to identify alphanumeric characters from the cropped image. To do so, k-NN (k-Nearest Number) algorithm is used. Before the identifying process is started, an image containing various type of fonts is included in the system as reference to identify the alphanumeric character. The system will start analyzing the cropped image from left to the right as it is how human read the car plate. After that, the system will start the identifying process and will read the characters one by one. All of those characters are compared with the database and the system will look for the edge found in each character as important point. It will give the result based on edge found and the higher similarity between character in cropped image and database. Normally, Malaysia car plate contains from two to eight alphanumeric characters in one plate. As the system reads the characters one by one, it will be stored temporarily in string format in a variable. When all of the characters have been identified, the result is combined in a string and will be arranged from left to right. The complete detail of the software model is shown in Figure 1.

B. Hardware Model

The hardware model consists of camera for capturing the image, a NORCO CPU for processing the image and execute the algorithms and a PC.

NORCO is the main processing system and it is using Linux as operating system. NORCO used Intel chip.The USB camera will be connected to the NORCO and the image will be saved in the PC and then will be processed. The complete hardware model is shown in Figure 2.

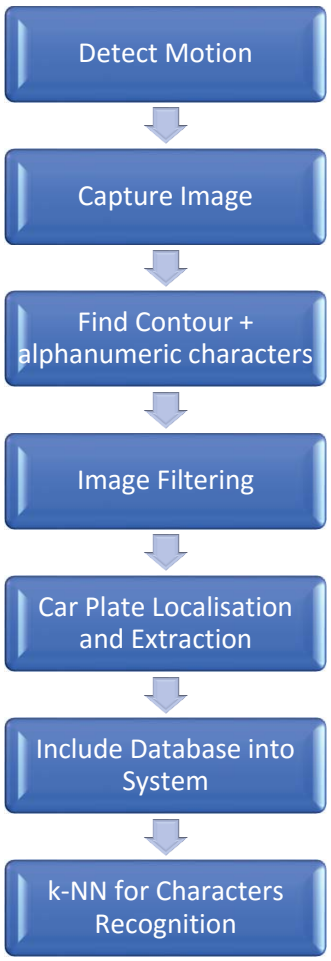

Figure 1: Steps of automatic number plate recognition software model

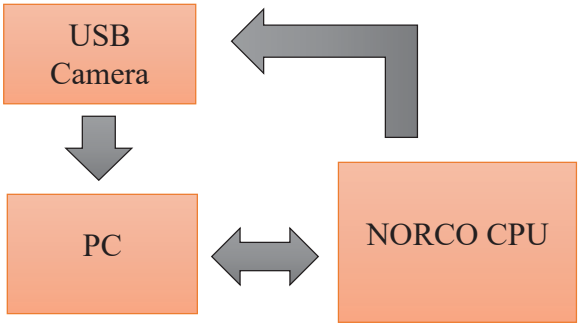

Figure 2: Hardware setup of ANPR system

III. SIMULATION RESULTS

Firstly, the camera is set up by connecting it to the NORCO through USB port. This camera will be in fixed position and standby to detect any motion and capture it. Different angle of cars in the image can be seen as it depends on the speed of the car passing the camera. The different effects of the day lights are also be considered during the processing. In this project, the images are in PNG format and the resolution is 640 x 480 pixels as shown in Figure 3.

After that, the image captured will converted

the images to grayscale as shown in Figure 4. Next, the system will look for location of car plate and will crop it. The results are shown in Figure 5 below. Contour with alphanumeric characters are detected in order to locate the car plate in the image. Once the car plate is succesfully extracted and cropped, it will undergo next process which is identify characters of car plate.

The characters will be identified from left to right and the character is read one by one and will be stored temporarily as a string. Figure 6 shows the characters are separated as highlighted with green boxes. The last step where recognition of characters takes place where k-NN method is used. Figure 7 shows the final result after identify character process.

Figure 3: Images taken using the USB camera

Figure 4: The grayscale images

Figure 5: The cropped car plates

Figure 6: Process of identifying alphanumeric characters with database

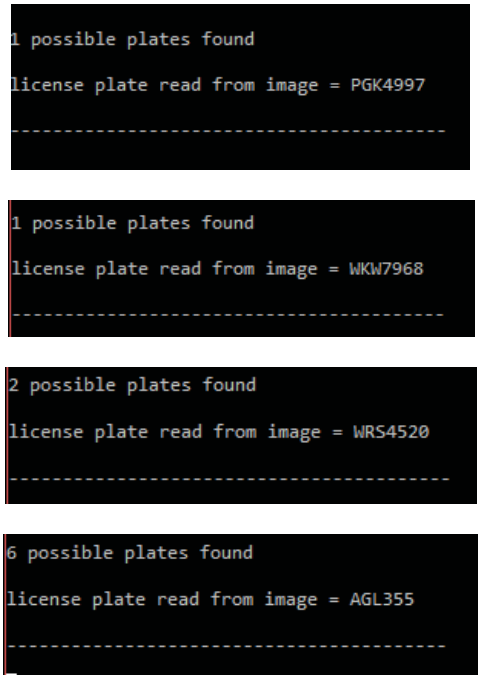

Figure 7: Recognize characters using k-NN method

But there is probability of error while running this algorithm such as the system unable to detect car plate location in the image and the system gives wrong result in recognition process. Figure 8 show some images that the system was unable to locate car plate. Figures 9, 10 and 11 show the error in the recognition process. Sometimes, the system fail in recognize the characters correctly and read it as other character where confusion occurred. Table 1 below shows some confusion in recognize the characters.

Figure 8: Failure in locating the car plate

Figure 9: Some images that gave wrong result of recognition

Figure 10: Some characters that are not being recognized

Figure 11: The wrong results of character recognition

IV. DISCUSSION

In this paper, an embedded ANPR is presented. This system use series of image processing techniques in detecting motion, extract and identify characters of car plate. The system uses the NORCO platform and it can function in real time.

This ANPR has been tested with many images and it only can detect car plates in daylight condition. Besides, it also can detect car plate in various angles. That the result of recognition process depends on the image quality and size of car plate.

The simulation also gave some incorrect results. One of the factor is distance where it effects the size of car plate. If the car plate is too small, the system cannot recognize it. Next factor is quality of the images. If the image is blurred, the system may not be able to locate the car plate. Besides, double line car plate also makes the system fail locating the car plate as the size of plate is larger than usual. In this system, it is designed to specific acceptable size of car plate. In addition, there is also case where the system is unable to recognize all the characters in the car plate and confusion occurs between characters. The analysis is done using 40 different images and the results are as below.

- Ability to locate car plate = 95%
- Correctness of recognition process (per plate) = 52.5%
- Correctness of recognition process (per character) = 91.67%

Table 1: Confusion between characters

Car plate	Readable plate	Error
PJH 1533	PJH 533	Missing 1
JEJ 9891	JEJ 889	9 read as 8 Missing 1
WGL 7848	W0L 7848	G read as 0
WGR 3464	W0P 3464	G read as 0 R read as P
JDM 8434	JUM 8434	D read as U
WRV 4648	VR4 4648	W read as V V read as 4
WQT 5934	W0T 593J	Q read as 0 4 read as J
DBC 8969	DBC S969	8 read as S
KCT 4439	KCT 4459	3 read as 5
NBX 4672	NBX 4872	6 read as 8

V. CONCLUSION AND FUTURE WORK

In this paper, embedded car plate recognition is presented. The camera used in this project has low resolution and is unable to detect fast motion. Other than that, the recognition process is too sensitive to different size of car plate, blurred image and reflection at car plate itself. OCR (optical character recognition) can be used to overcome these problems as OCR has large reference database.

VII. REFERENCES

[1] M. T. Qadri and M. Asif, "Automatic Number Plate Recognition System for Vehicle Identification Using Optical Character Recognition," 2009 International Conference on Education Technology and Computer, Singapore, 2009, pp. 335-338.

[2] Optasia Systems Pte Ltd, “The World Leader in License Plate Recognition Technology” Sourced from: www.singaporegateway.com/optasia, Accessed 22 November 2008

[3] Li Bo, Zeng Zhi-yuan, Study and Realization for License Plate Recognition System. Digital Eng.and Emulation Research, vol 231, pp. 262- 268, April 2007.

[4] J. W. Hsieh, S. H. Yu, and Y. S. Chen. Morphology based license plate detection from complex scenes. 16th International Conference on Pattern Recognition (ICPR’02), pp. 79–179, 2002.

[5] K.K. Kim, K.I., Kim, J.B. Kim, and H.J. Kim, “Learning-Based Apporach for License Plate Recognition” Proceedings of IEEE Signal Processing Society Workshop, Vol. 2, pp.614-623, 2000.

Wearable Translation Device on Intel Edison

Afiq Syazwan bin Yusof
Faculty of Electrical Engineering
Universiti Teknologi Malaysia
Johor Bahru, Malaysia.
afiqsyazwanyusof@gmail.com

Dr Usman Ullah Sheikh
Department of Electronic and Computer Engineering
Faculty of Electrical Engineering
Universiti Teknologi Malaysia
Johor Bahru, Malaysia.
usman@fke.utm.my

***Abstract*—The basic of this project is to create eyeglasses that help user to understand text from another language instantly. The materials used to create this piece include: camera module, Intel Edison, and speaker. The techniques used in order to develop this system include: image processing, object character recognition, cloud computing services and text to speech system. The aim is to create a wearable computer device that is easy to use for translating language.**

***Keywords*—Text to Speech (TTS); Object Character Recognition (OCR); Internet of Things (IoT).**

I. INTRODUCTION

Malaysia is a multiracial society and tourist site. In sign boards, name place and even the text in shopping complex, there are many different languages implement in each place. Sometimes the tourist confuses and do not understand the simple text guide if they did not understand the language. By using character recognition technology, it enables instant language translation for users travelling abroad to read restaurant menus, sign board and other documents.

Although nowadays there are applications in smartphones that can translate language, the aim of this is to develop a wearable gadget that is easy to use and do not need too much handling. So, we don't need to every time open our smartphones to understand foreign language just for a simple text. The spectacle language translation is some other approach to overcome language barrier.

Wearable devices are electronic technologies or computers that are incorporated into items of clothing and accessories which can comfortably be worn on the body. These wearable devices can perform many of the same computing tasks as mobile phones and computers [1]. The designs often incorporate practical functions and features. Nowadays many wearable small devices had been built. The small and powerful sensor technologies had been developed for this wearable technology to collect and deliver information on the surroundings.

The objectives of this project are to use a small and fast microprocessor to create a wearable gadget that helps user to understand text from other language instantly. The scope of the project is to design the spectacle that can be implemented with electronic components. The system will be programed using Javascript and access key from Microsoft azure is use to access its services. The translation language is limited to Malay and English. It will then give audio playback to the user.

. The Intel Edison as in fig. 3 is use as the microcontroller for this project because of its small size and high processing rate. It also has built-in wifi that can be integrated with Internet of Things [2].

Internet of Things is the concept of basically connecting any device to the Internet. This includes everything from cellphones, coffee makers, washing machines, headphones, lamps and wearable devices [3]. In this case, this wearable gadget is need to connect with the internet to have access to the Microsoft cognitive services.

Microsoft Cognitive Services are a set of APIs, SDKs and services available to developers to make their applications more intelligent, engaging and discoverable [4]. Cognitive Services provides the best services to manipulate the application to become even better. It helps to build powerful applications that can provide easy handling and interaction to user.

Microsoft Cognitive Services provide the ability to build apps with powerful algorithms using just a few lines of code [5]. It works across devices and platforms, and with continuous enhancement, it's easy to set up. Some of the services that Cognitive Services offers are such as Language, Speech, Vision, Search, and Knowledge APIs.

For algorithm, the Cognitive Services APIs are available through RESTful services that can leverage to create the interaction and communication from any device [5]. Javascript language programming will be used for the post request coding.

II. METHODOLOGY

In this project, the spectacle was design using Solidworks software. The design as in fig. 1. The design is then printed in 3D printer machine. The small 7.4V lipo battery as in fig. 2 is used to power on the Intel Edison. Intel XDK as in fig. 4 is used to program the hardware. The operation of the system is explained as follows;

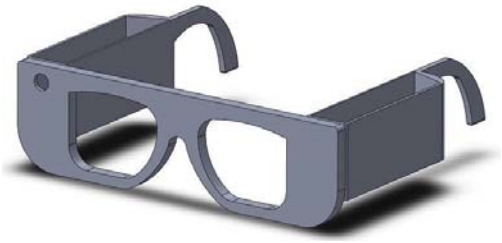

Fig. 1. 3D rendering of the spectacle design

Fig. 2. 7.4V Lipo battery

Fig. 3. The Intel Edison module

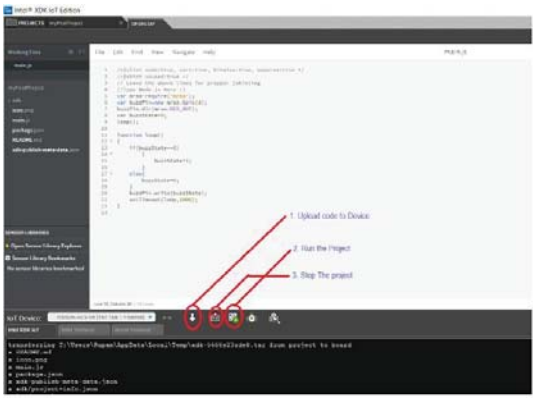

Fig. 4. Intel XDK software screenshot

A. *Image taken using camera*

Camera module VC0706 as shown in Fig. 5 is used because of its small size and high-speed capture rate. It can be connected to Edison via UART or SPI with baud rate 115200. VC0706 library was used to take the picture. The image capture will be on 640 × 480.

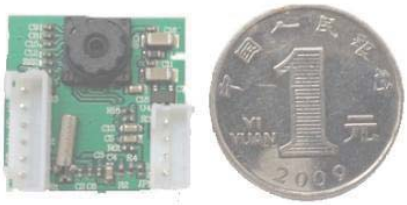

Fig. 5. Camera module

B. *Upload image to Dropbox*

The image that had been taken is then uploaded to Dropbox to obtain the URL. The access token is needed to access the link. The library "drobox-upload" was used for this step and it will provide the image link from Dropbox. Fig. 6 shows where to get the access token from Dropbox.

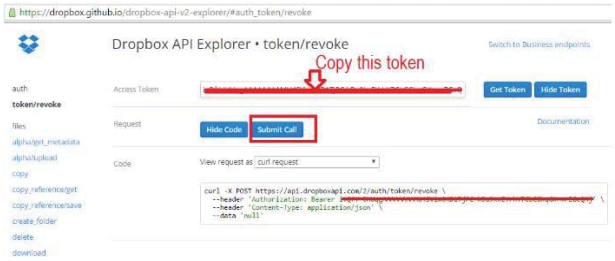

Fig. 6. Token to access Dropbox.

C. *Extract text using Computer Vision API*

The cloud-based Computer Vision API provides developers with access to advanced algorithms for processing images and returning information. By specifying and sent an image URL, Microsoft Computer Vision algorithms can analyze visual content in different ways based on inputs and user choices [6]. One of the choices is OCR API. OCR technology detects text content in an image in any background as long as the language is understandable. It automatically detects the language. OCR saves time and provides convenience used to recognize text in image. This type of API can correct the rotation of the recognized text, in degrees, around the horizontal image axis as seen in fig. 7. The received link from Dropbox will extract the text from image. The obtained text was then sent to text translator API.

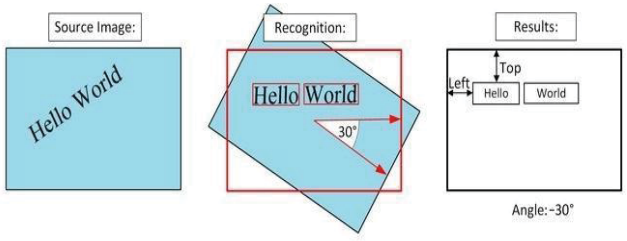

Fig. 7. OCR orientation

D. *Translate text using Text Translator API*

The Microsoft Translator API can be used to translate speech and text through a REST API. It translates text from one language into text of another language. The API automatically detects the language of the received text before

translating it in the chosen language. This translation API service supporting multiple languages such as Malay, Japan, English, Mandarin and many more. The translated result was then send to Bing speech API.

E. Convert text to speech using Bing Speech API

Bing Speech API offer a speech-to-text, text-to-speech, and language understanding capabilities delivered through the cloud. Text to speech algorithms from Bing speech API is use to convert text type to the audio type. It similar like apps converting text into audio that can be played back to the user [7]. The output produces the json format for spoken text. The json format is then write and save in the wav file.

F. Play wav file using Bluetooth audio

The Bluetooth audio will be connected to Edison and it needs a few commands and settings to be detected. The wav file was then played by the Bluetooth audio and give audio output to the user. Gst-launch command is use in order to play the wav file.

III. RESULT

The operation of the system is as follows. The user presses the capture button to give signal to camera module to take the image. The Camera is connected to Intel Edison via serial communication. The image as in fig. 8 is then uploaded to Dropbox to get the URL link. Fig. 9 shows example link from Dropbox. The link is then sent to OCR cognitive service to extract text from the image. Fig. 10 shows example of the obtained text from image while fig. 11 shows the json format of the output. The text in English is then translated to Malay using Translator API. After that it is converted to speech using TTS API and give json format as in fig. 12. The content-type in json format is write and save in wav file. Finally, the wav file is played through the audio speaker.

Fig. 8. Example image taken

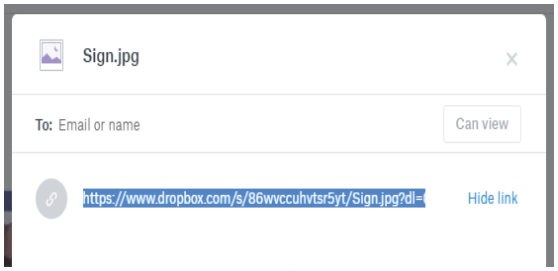

Fig. 9. Dropbox URL

Fig. 10. Text detected from image

Fig. 11. Text detected in json format

```
HTTP/1.1 200 OK
Content-Length: XXX
Content-Type: audio/x-wav

Response audio payload
```

Fig. 12. Example TTS output response

IV. CONCLUSION

One key advantage of this implementation is its simplicity and speed, which makes it feasible for wearable gadget. This project can read image in texts on sign board and simple phrases. The user can understand the text by listening to the audio playback from the wearable gadget. However, the available languages are limited. For this project, the only available languages are Malay and English. Future work should focus on extending the localization algorithm to process text from multiple languages.

REFERENCES

[1] Tehrani, Kiana, and Andrew Michael. "Wearable Technology and Wearable Devices: Everything You Need to Know." Wearable Devices Magazine, WearableDevices.com, March 2014

[2] Dr Jon Harrop, "What is is Intel Edison for?", 10 Nov 2014

[3] Jacob Morgan, Forbes Contributors, "A simple Explanation of The Internet of Things", 13 May 2014

[4] Jordan Novet, "Microsoft launches Cognitive Services based on Project Oxford and Bing", 30 March 2016

[5] Kasam Shaikh, "A Look at Cognitive Services", 12 December 2016

[6] JuliaNik, Roy Harper, Moe Ibrahim, Kristine Toliver, "Computer Vision API Version 1.0", 6 Feb 2017

[7] Priyaravi20, Maria Ines Parnisari, Itechedit, "Bing Speech API Overview, 28 Feb 2017

[8] A. B. Kevin, "Power System Security," [Online]. Available: http://www.citeseer.ist.psu.edu/387125.html, [Accessed January 9, 2005]

Carbon Based Nitrate Sensor for Agricultural Application

Mohamad Aris Bin Ibrahim, Suhana Binti Mohamed Sultan
Faculty of Electrical Engineering
Universiti Teknologi Malaysia
Johor Bahru, Malaysia.
maris7@utm.my

***Abstract*—This research is about to analysis the behavior of carbon material due to solutions sensor device in resistor form. The selected solutions are related with agricultural application which is in soil fertilizer. The mentioned resistors are Nanocrystalline graphite (NCG) and Screen-printed electrode (SPE).**

Keywords—Solution sensor device; Nanocrystalline graphite; Screen-printed Electrode;

I. INTRODUCTION

In agricultural field, there are very little research on measuring the soil fertility using solid state device. The common sensing applications that had been developed are on gas sensor and humidity sensor only. The purpose of the configuration for soil's condition is to enrich and monitor the soil fertility. In order to do that, a device to measure solution's concentration need to be developed because the fertility of the soil is based on the condition of solutions inside the soil. There are several types of fertilizer that may affect the soil fertility. One of them is synthetic fertilizers such as Ammonium Sulphate, Potassium Nitrate, and Phosphorus. The purpose of these fertilizers are to supply nutrients to the plant. Plants need these nutrients to make component for plant growth such as carbohydrates and proteins. The estimation percentage of these fertilizers for the soil are based on the type of plant. Commonly, the percentage is nitrogen-10, phosphorus-10, and potassium-20[1]. For example, if the total volume of solution is 100L, nitrogen will be 100 mL, phosphorus equal to 100 mL, and potassium will be 200 mL.

Previously, there have been several work regarding the soil fertility such as monitoring the condition of nitrogen in plant by using digital image processing [2]. It is important to constantly monitor nitrogen content in soil because excessive amount can be hazardous to the plant as well as human being. The condition of nitrogen solution was estimated by sampling the images of certain parts of the plant, such as leaf, tree branch, and tree root. The fertility condition of these parts was monitored by comparing the samples' images with the good one. This method can only estimate the condition of nitrogen solution in soil whether it is in suitable range or not. Unfortunately, this technique is expensive and time consuming.

In this work, resistance's concept is applied to design the sensor device to measure nitrogen in aqueous solution. The resistor structure is much simpler compared to transistor or diode base device which are more complicated. The basic equation governing the resistive-based sensor is Ohm's Law:

$$V = IR \tag{1}$$

V: voltage supply
I: current
R: resistor

The commercial resistor that available at the market is made by Silicon (Si) and it is a passive resistor type. The resistance value is fix and cannot be adjusted. In this project, non-Si materials were explored. Therefore, the resistance value can be adjusted base on the external effect, that is the concentration of nitrate-based solution.

In this project, the analysis had been taken by two types of resistors which are Nanocrystalline Graphite (NCG) and Screen-Printed Electrode (SPE). These two resistors are made of carbon material. Carbon has the potential towards sensing properties. Previously, there have been various sensor devices being developed using carbon-based such as temperature sensor, humidity sensor, and glucose sensor [3]. Therefore, this work studies the feasibility of carbon material to sense the presence of weak acids. The selected solutions which will be used in this work are Potassium Nitrate (KNo_3) and Ammonium Sulphate$(NH_4)_2SO_3$,

A. Carbon

Carbon exist in many different forms. The most extensively studied are graphite, diamond, and amorphous carbon. The physical properties of carbon vary widely with the allotropic form such as graphite is not transparent and diamond is highly transparent. The permittivity of carbon is $(3-60)\text{x } 10^{-5}$ohm. m, depending on its form [4].

The future flexible devices based on existing Si technology have become a challenge due to its compact fabrication. The

new semiconductor, graphene, based technology creates an alternative way to overcome such limitations of Si technology. Graphene, a one-atom-thick

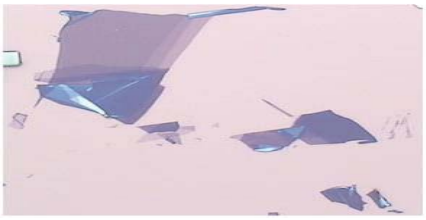

Figure 1: Multilayer graphene by exfoliation method [5].

planar sheet in a two-dimensional (2D) network of sp^2 hybridized carbon atoms packed into a hexagonal structure. It has recently attracted much attention in the scientific community for its potential applications in printed flexible electronics due to its excellent electronic and mechanical properties. Graphene is a thin layer of graphite. To obtain the graphene layer, exfoliation process for graphite material could be done. Figure1 shows the example of graphene produced by exfoliation method.

However, exfoliation technique does not promise large area for device fabrication. Hence, nanocrystalline graphite is another form of carbon material which has some interesting properties. It consists of grain boundaries that enhance the sensitivity of the film.

Another form of device which will be used in this project is Screen Printed Electrodes (SPE). This fast and cost-effective technology might be suitable to produce electrochemical (bio)sensors for biomedical, agri-food and environmental applications. The advantages of SPE include sensitivity, selectivity, possibility of miniaturization and mass-productivity which is suitable to the design of portable and cost effective measuring system [6].

II. Methodology

A. Nanocrystalline Graphite (NCG)

NCG film was deposited with a 9 nm thick onto SiO_2/Si substrate using a catalyst-free plasma enhanced chemical vapour deposition (PECVD) technique [7]. The NCG film is then patterned into a 1.3 mm x 15.4 mm strips for resistive sensing. The resistance of NCG is determined by the thickness of NCG's layer deposited on the substrate. The resistance also can be influenced by external force such as the concentration of the solutions. The characteristics of NCG will change if there is any selected solution dropped on it's surface.

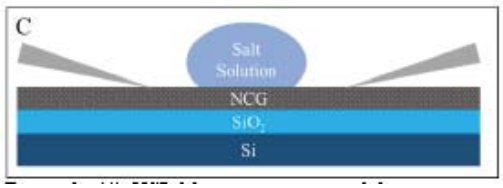

Figure 2: Cross-sectional view of the NCG strip fabricated [8].

The electrical resistance of the strip was measured using a standard 2-point probe resistive measurement with a probe spacing of 5 mm using a Keithley 2100 high precision multimeter. For NCG analysis, the ammonium sulphate solution had been prepared with three different concentrations; 0.01M, 0.1M, and 0.5M. The solution was dropped on the top surface of NCG film as shown Figure 2. Figur 3(a) shows a droplet of salt solution on NCG film.NCG is a semi-metal and has low resistivity. The presence of solutions, some conductive ions, at the grain boundary provides a conductive path for the charge carriers and also lowering the overall conductivity. When the concentration of ammonium sulphate is increased, the number of conductive ions available for charge transport is increased. With this activity, the average resistance of NCG will be decreased.

B. Screen-Printed Electrode

The technology of designing SPE is quite interesting which is the deposition layers of special inks or pastes onto an insulating substrate. The pastes mentioned can be made of materials that suit with the purpose of that particular SPE, which contains functional materials such as cofactors, stabilizers and mediators [9]. The examples of these materials that can be applied are graphene, carbon, silver and gold. The application of SPE becomes more common since the lower cost and easy to fabricate. In this work, the selected materials are carbon paste. As mentioned, the characteristics of graphene-based SPE are almost same with carbon-based SPE.

Screen-Printed Electrode (SPE) had been analyzed with semiconductor device analyzer, B1500. The solution was dropped at the top of carbon surface as shown in Figure 3(b).

C. Resistivity ,ρ

The analysis has been taken with the constant area, A and length, L. The only changes in this analysis is the resistivity, ρ of these resistors. The equation need to be considered regarding the analysis of resistance is:

$$R = \frac{\rho L}{A} \quad (2)$$

where R = resistance(Ω), ρ= resistivity (Ωm) L= length (m) and A = area (m^2)

As mentioned earlier, the value of resistivity, ρ is fixed base on the type of materials. Fortunately, it can be manipulated by adding external force onto that particular material such as drop a weak acid onto it. Somehow, the resistivity of semiconductor materials varies depend on the level of doping [7]. Besides, temperature is one of the components that influence the measurement. However, the temperature of this analysis is fixed which is at room condition, 24℃.

D. Solution

Different types of solutions with different concentrations are needed in order to analyse these resistor behaviours. The solutions need to be prepared carefully. The selected solutions are ammonium sulphate and potassium nitrate. Both of these solutions were prepared with 0.25 M,0.5 M,0.75 M and 1.0 M. Firstly, 1 M of stock solution need to be prepared for each of them. After that, that particular stock solutuon can be diluted based on needed concentration by using de-ionize water (DI water). The dilution process can be done by using Equation (3).

$$M_1V_1 = M_2V_2 \qquad (3)$$

M_1: the initial molarity
V_1: the initial volume
M_2: the final molarity
V_2: the final volume

III. Results & Discussion

Figure 4 and 5 show the changes of current on SPE electrode before and after the reaction with ammonium suphate and potassium nitrate, respectively. X-axis represent the time in second and y-axis represent the current in mA. Results show that the relationship of the concentration of weak acid solutions influence the resistivity of these resistors. The current value increased instantly after introducing the salt solutions on the carbon surface. The changes of current values are base on the changes of the value of solutions' molarity. The changes of current in Figure 4, the reaction between SPE and ammonium sulphate,are higher compare to Figure 5, the reaction between SPE and potassium nitrate. This result shows that SPE is more sensitive towards ammonium sulphate than potassium nitrate.

The results of the experiment had been further analyzed to determine the sensitivity. The sensitivity of SPE were calculated to see the performance of SPE due to sensor device. The average of initial value and final value of reaction are tabulated in Table 1. In order to determine the sensitivity, Equation (4) is used:

$$sensitivity = \frac{|initial\ value\ of\ resistance - final\ value\ of\ resistance|}{initial\ value\ of\ resistance} x100 \qquad (4)$$

The value of resistance can be determining from results in table 1 by using equation (1). The voltage supply for the analysis is constant which is 5V dc.

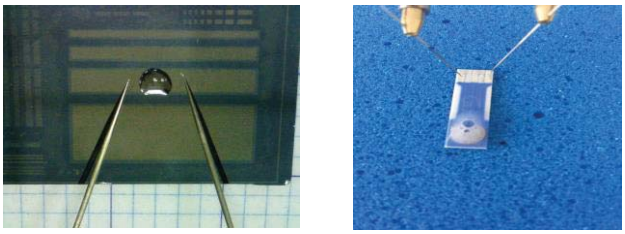

Figure 3: (a) Nanocrystalline Graphite (NCG) sample (b) Screen-printed Electrode (SPE)

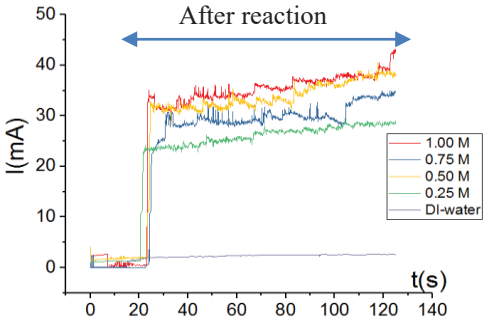

Figure 4: The current, I(mA) response of SPE react with ammonium sulphate.

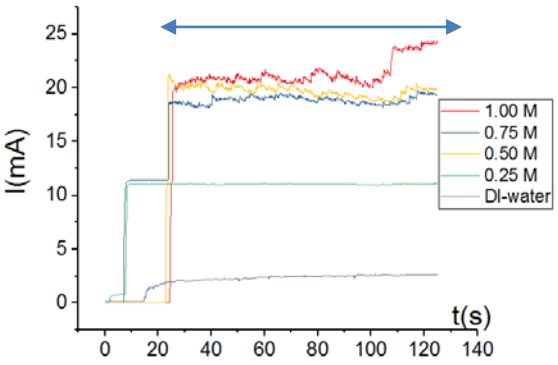

Figure 5: The current, I(mA) response of SPE react with potassium nitrate

From the Table 4, it shows that the result of sensitivity of SPE due to ammonium sulphate and potassium nitrate. The large difference between before and after reaction occur made the sensitivity of SPE become high and some of them almost approace to 100%. It seen like the SPE electrode has a very good sensitivity due to salt solution such as ammonium sulphate and potassium nitrate.

Subsequently, results from SPE were compared with the measured values using NCG material which were measured previously. Table 5 summarizes the sensitivity extracted from NCG device. The sensitivity of NCG and SPE due to both solutions were analyzed to determine which are the best resistor for sensor device.

Figure 6 shows the sensitivity of NCG and SPE reacted with ammonium sulphate and potassium nitrate. X-axis represent the molarity (M) of these solutions and y-axis represent the sensitivity of NCG and SPE. Theoretically, the graph of sensitivity (%) again molarity(M) is linear. The graph of NCG shows the increasing of sensitivity simultaneously with molarity. For SPE, it seen like the sensitivity of SPE reach a high value of sensitivity. From these results, maybe the analysis of SPE need to be done with lower molarity or lower voltage supply to get the smooth linear graph. The result shows that the sensitivity of SPE is higher than NCG either with ammonium sulphate or potassium nitrate. These result are because of the rate of change of current due to reaction with salt solution of SPE are higher than NCG.

Table 1: The measured current response of the SPE electrodes towards salt solutions

Molarity (M)	Ammonium sulphate, $(NH_3)_2SO_4$		Potassium nitrate, KNO_3	
	Initial I (A) $(x10^{-3})$	Final I (A) $(x10^{-2})$	Initial I (A)	Final I (A) $(x10^{-2})$
0.25	1.2700	2.6072	$5.65x10^{-4}$	1.1049
0.50	1.8270	3.3861	$1.23x10^{-8}$	1.9663
0.75	0.1170	2.9780	$1.00x10^{-6}$	1.7835
1.00	1.3500	3.5527	$4.99x10^{-8}$	2.1283

Table 2 : The resistance values of the SPE electrodes towards salt solutions.

Molarity (M)	Ammonium sulphate, $(NH_3)_2SO_4$		Potassium nitrate, KNO_3	
	Initial I (Ω)	Final I (Ω)	Initial I (Ω)	Final I (Ω)
0.25	3937.00	191.777	8849.57	452.530
0.50	2736.73	147.663	$4.065x10^{8}$	254.285
0.75	42735.0	167.898	$5.00x10^{6}$	280.348
1.00	3703.70	140.738	$1.002x10^{8}$	234.929

Table 3: The resistance values of NCG towards salt solutions.

Molarity (M)	Ammonium sulphate, $(NH_3)_2SO_4$		Potassium nitrate, KNO_3	
	Initial I (Ω)	Final I (Ω)	Initial I (Ω)	Final I (Ω)
0.10	142981.30	270523.00	280434.80	49452.00
0.50	279208.10	228396.10	275476.00	81032.00

Table 4: The extracted values of the sensitivity of SPE

Molarity(M)	sensitivity (%)	
	KNO_3	$(NH_3)_2SO_4$
0.10	17.63	5.17
0.50	29.42	18.15

Table 5: The extracted values of the sensitivity of NCG film

Molarity(M)	sensitivity (%)	
	KNO_3	$(NH_3)_2SO_4$
0.25	94.90	95.13
0.50	100.00	94.60
0.75	100.00	100.00
1.00	100.00	96.20

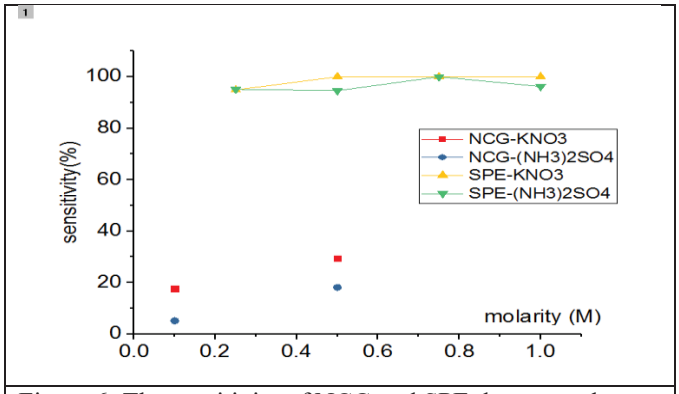

Figure 6: The sensitivity of NCG and SPE due to weak acids.

IV. Conclusion

SPE resistor is more compatible to use as solution's sensor device due to high sensitivity. But, it has a limitation which is can't stand with high concentration (molarity, M) solution such as 1M of potassium nitrate. This limitation might be as a boarder to that particular solution's sensor device.

V. REFERENCE

[1] M.L. Vitosh. Wheat Fertility And Fertilization. FILE; 22.17,Field Crops-Wheat.2003.

[2] Rafael F. Muñoz-Huerta. A Review of Methods for Sensing the Nitrogen Status in Plants: Advantages, Disadvantages and Recent Advances. 16 August 2013.

[3] D.D.L. Chung. Carbon materials for structural self sensing, electromagnetic shielding and thermal interfacing. Composite Materials Research Laboratory, University at Buffalo, State University of New York, Buffalo, NY 14260-4400, USA. 2012

[4] Wikipedia. "carbon". Available : https://en.wikipedia.org/wiki/Carbon. Accessed: april 2017.

[5] Sam Vaziri, Fabrication and Characterization of Graphene Field Effect Transistors, Royal Institude of Technology (KTH). June, 2011.

[6] Elena Jubete, Screen-printing technology for (bio)sensor manufacture;a success story. IK4- CIDETEC, San Sebastian, Spain.2015.R. Nicole, "Title of paper with only first word capitalized," J. Name Stand. Abbrev., in press.

[7] "Radio-Electronic.com" [online]. Available : http://www.radio-electronics.com/info/formulae/resistance/resistivity-basics-formula-equation-units.php

[8] Salleh. "nanocrystalline graphite thin film resistors for sensing ionic concentrations in aqueous solutions". Unpublised.

[9] Y. Yorozu, M. Hirano, K. Oka, and Y. Tagawa, "Electron spectroscopy studies on magneto-optical media and plastic substrate interface," IEEE Transl. J. Magn. Japan, vol. 2, pp. 740-741, August 1987 [Digests 9th Annual Conf. Magnetics Japan, p. 301, 1

MEMS Fabry-Pérot Albumin Sensor using PDMS Thin Film

Khoo Ming Kwan
Faculty of Electrical Engineering
University Technology Malaysia
81310 UTM Johor Bahru, Johor, Malaysia
mingkwan93@live.com

Suhaila Isaak
Dept. of Electronic and Computer Eng.
Faculty of Electrical Engineering
University Technology Malaysia
81310 UTM Johor Bahru, Johor, Malaysia
suhaila@fke.utm.my

Abstract—Microalbuminuria is a term to describe a moderate level of albumin in urine. A gradual increase of albumin level may indicate signs of a health problem such as diabetes, high blood pressure, and endothelial dysfunction. This paper details the fabrication and characterization of flexible sensor thin film on albumin level detection. Sodium urate solution has been used to act as the urine sample. Each molecule in the solution has its own unique absorption and reflection spectrum. Hence that Beer Lambert Law is utilized. Beer Lambert law stated that there is relationship between absorbance and concentration of an absorbing species in a solution. The results show a spectral shift and increase in vividness of light with sodium uric at different concentration as a substitute of urine samples. The transmittance and reflection of Polydimethylsiloxane thin film have been determined. This sensor prototype creates an alternative for albumin detection.

Keywords—MEMS, Microalbuminuria, PDMS, Fabry-Pérot Interferometer, early detection, Albumin, Dipstick, Spectrometer

I. INTRODUCTION

Microalbumin is a scientific term describing the presence of albumin level present in urine. A presence of albumin may indicate the sign of kidney damage [1]. Patient with high risk of progressive kidney damage shows an increased presence of protein in their urine. The higher the albumin level, the more vulnerable the patient toward kidney function failure [2][3].

TABLE I. CLASSIFICATION OF MICROALBUMINURIA WITH DIFFERENT TIME OF COLLECTION [4]

Spot Collection	*Timed Collection*	*24-Hour Collection*	*Category*
Less than 30 mcg/mg creatinine	Less than 20 mcg/min	Less than 30 mg	Normal
30-300 mcg/mg creatinine	Less than 20 mcg/min	30-300 mg	Microalbuminuria
More than 300 mcg/mg creatinine	More than 200 mcg/min	More than 300 mg	Clinical albuminuria

Source: Bishnu Prasad Devkota, Microalbumin: Reference Range, Interpretation, Collection, and Panels.

Based on the Table I, differentiation between a healthy person and unhealthy person can be done quickly using dipstick method as that are the two extreme value. But to detect the microalbuminuria among the sample of people, a dipstick method maybe not accurate as the dipstick will only shows two result positive (Clinical albuminuria) and negative (Normal).

Comparing with techniques in Table I, 24-hour collection is the preferred technique. This is because, the ratio of albumin/creatinine shows similarity with the screening tools for the diabetic nephropathy [5][6]. On the contrary, results of 24-hour urine collection for the albumin gives a wide range of excretion of albumin in urine. As the ratio of albumin and creatinine from the urine collected in the morning considered a valid test. This is because of the ratio of albumin and creatinine will be affected as the target will consume food and started to exercise [4].

As most of the compound absorbs and reflects light with a specific range of wavelength, scientist use these properties to detect chemical compound. A spectrophotometer is the machine that able to use these as advantage to detect compound in a sample.

In dipstick method, strips with different reagents is made into contact with urine. The strips will then show the result by changing in the strip color to determine the patient health condition.

There are both advantages and disadvantages of both of the two conventional method which is dipstick method and spectrophotometer. In dipstick method, the detection of microalbumin is not very accurate as there is the need to reconfirm the sample if the patient suffers progressive kidney failure. This is because dipstick only give a qualitative analysis. The advantage of dipstick is giving an immediate result. In spectrophotometry, the analysis of the albumin level is accurate as they show the ratio of albumin and creatinine. But this method are not as portable as dipstick method.

Thus, an alternative method that able to fit into the category of both advantages of both method is proposed. The objective of this paper is to fabricate the sensor unit and obtain its characterization and to open up possibility of using the same mechanism of MEMS detection but using different method and different structure of the device.

II. LITERATURE REVIEW

A. Dipstick

In dipstick method, result can be either positive (color change) or negative (no change in color). The results are positive when the concentration of the albumin is within 20 to 30 mg/L [13]. Diluted or concentrated of urine sample will often give false positive and false negative results of the test [7]. Often,

this method use the chemical properties of the urine chemical composition to change the color of the dipstick.

B. *Spectrophotometer*

Spectrophotometer is an instrument to determine the light absorbs by the compound. The intensity of the light beam that passes through a sample will be calculated. This instrument able to determine the amount of a known chemical substance. The sample will be illuminated with monochromatic light and its light that able to transmit through sample will the detected by photodetector. Spectrometer use albumin/creatinine ratio to measure the concentration of the albumin in urine as this is the method used by hospital in medical checkup. This is because our body will filter creatinine at a same rate, thus by comparing the creatinine and albumin will determine the body albumin excretion rate. If the ratio of albumin/creatinine is within 30-300 µg/mg, the patient will be classified as microalbuminuria. This is the technique that uses quantitative method which different from dipstick method.

C. *Microelectromechanical system (MEMS)*

MEMS are the technology of microscopic devices, which uses moving part as part of the device/system. In this project, the moving part will be the thin film itself. This type of sensor is based on the surface stress which including the capacitive type, piezo resistive type, and optical read-out type [14]. Optical read-out type is the most sensitive among all the type because of high conversion efficiency from mechanical to optical read-out signal [15] [16]. This system use Fabry-Prtoy interference to produce such effect with two partially reflective surface aligned parallel together to produce interference of concentric rings.

D. *Fabry-Perot Interferometer*

Fabry-Perot is an application of wave interference in optics. Equation 1 describe the interference occur in the interferometer.

$$\delta = \frac{2\pi nd\ cos\theta}{\lambda} \equiv p\pi \tag{1}$$

Where δ represent the phase of the light, n represent the refractive index of the medium between the two surface, d represent the thickness of the thin film and θ represent the angle of the refracted ray, and p represent an integer number. From the equation 1, the light transmitted is a periodic function of δ that varies between maximum and minimum as δ changes shown in equation 2 and 3.

$$I_{max} \qquad \delta=p\pi, \text{ p is an integer} \tag{2}$$

$$I_{min} \qquad \delta = (p + \tfrac{1}{2})\pi \tag{3}$$

E. *PDMS*

PDMS is acronym for Polydimethylsiloxane, which belong to a group of polymeric organosilicon or can be referred as silicones [17]. PDMS is the choice of the project because of its characteristic which s optically clear, inert, nontoxic and non-flammable. Most of the application such as contact lenses, medical devices to elastomers are made from PDMS. In biomedical microelectromechanical systems (bio-MEMS), soft lithography is used frequently in microfluids. It has hydrophobic surfaces making it easy to attract protein molecule. Another advantage of PDMS is it is a low cost, easy fabrication and good flexibility that make it suitable candidate for prototype of MEMS microalbumin detections [19].

III. METHODOLOGY

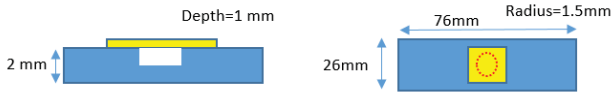

Fig. 1. Final dimension of the sensor (a) side view (b) top view

A. *Introduction*

In this following chapter, the fabrication of the device will be explained. From the fabrication of the PDMS to the thermal bonding of the glass slide with PDMS will be explained. In addition, the setup of the spectrometer to test the device fabricated will also explained in this session. Figure.1 shows the design of the sensor.

B. *Fabrication of PDMS thin film*

PDMS thin film is the core unit of the device. To fabricate thin film with minimum thickness, spin coater is used to create the result. In this fabrication, SYLGARD 184 Silicone Elastomer is used. The kit consists of both the base and curing agent. Firstly, a finite volume of the base is transferred into petri dish using a plastic pipette. After the base is transferred, the curing agent of SYLGARD 184 will then transferred in the petri dish that contained the base. The mixing of both the base and curing agent should be in the ratio of 10:1, the base is 10 part while the curing agent is 1 part. The mixture will then mix throughout using plastic pipette, bubble will be seen in the petri dish as the curing agent is taking effect. The mixture should be mix until bubbles is visible within all the surface of the mixture. The mixed elastomer will be place in the spin coater with setting pre-set setting in the spin coater. After spinning, the mixture is sealed and sit for the cure. The process of curing will take place approximately 24 hour. A detailed information of the volume of base, curing agent, spinning speed is as shown in the Table II.

In this fabrication, the thin film needed to be peel off from the base. In the Table II it shows the result when the curing time for the PDMS was reached and ready to be peeled off. Most of the time the PDMS thin film experience tear as a result of overstressing the thin film during peeling off. Only in one method, the thin film able to extract out from the petri dish base. This because in other method, the volume of PDMS after low spinning process hinder the PDMS thin film to be peeled from its base. Any coating speed higher than 1000rpm with 5ml base volume of PDMS will make the thin film too thin to be peeled off, while any volume lower than 5ml of the base volume will also make the thin film too thin to withstand the peeling force during peeling the film from its base.

TABLE II BASE VOLUME, CURING AGENT VOLUME, SPIN SPEED AND RESULTS

Base Volume (ml)	Curing Agent Volume (ml)	Spin Speed (rpm)	Results
2	0.2	1000	Thin film experience tear when peeling off from petri dish
3	0.3	1000	Thin film experience tear when peeling off from petri dish
4	0.4	1000	Thin film experience tear when peeling off from petri dish
5	0.5	1000	Able to peel off form petri dish
5	0.5	1100	Thin film experience tear when peeling off from petri dish
5	0.5	1200	Thin film experience tear when peeling off from petri dish

C. *Glass Slide*

Glass is chosen as the substrate for the thin film because it is transparent. There are many type of glass in the market, namely borosilicate glass, commercial glass, glass fiber, lead glass etc. The choice of glass in this project is optical grade glass, which is the microscopic glass. Figure 2 shows the first design of the microscopic glass slide.

Fig. 2. First design on microscopic glass slide

The depth of the trench is half of the microscopic slide thickness which is 0.5 mm. The trench is created by using a glass drill bit of 5mm. The problem of using the first design for the microscopic glass slide is small opening area because the trench is created using the drilling technique. As the microscopic glass slide is only 1 mm thick, drilling a trench with a 0.5mm thick using glass drill bit of 5mm only give a small opening as the length of the drill bit is 0.5cm, the opening created will be as small as 0.1cm.

Another problem of creating a trench in the microscopic glass slide is the transparency of the trench created. During the drilling on the glass, the glass surface will become white, this is because the surface of the glass in the trench is crack and this will greatly affect light going through the trench. In addition, the area surrounding of the trench experience cracking because area surrounding the trench supposed to be the part of the hole. Therefore, creating a trench with 1mm thickness of the glass is impossible.

The alternative to solve the problem cause by creation of the trench on the microscopic glass slide is to drill through the microscopic glass slide. Using a 5 mm of the glass drill bit to drill 1mm thickness of microscopic glass will only create a radius of 1.5mm of hole. The drilled microscopic glass slide is stacked with another microscopic glass slide thus creating an air gap for the light to interfere.

D. *Assembling All Part Together*

From the PDMS thin film to the drilling process, all the parts are ready to be assembled. The first step of assembling the parts is cutting the PDMS thin film into small part. Since the drilled hole is very small, the dimension of the thin film is only limited by a dimension of $1cm^2$ which is enough to cover the drilled hole. After that, the thin film is stick on top of the drilled microscopic glass slide. One of the method to stick the thin film is by using thermal bonding. The oven must pre-heat to 80°C first before thermal bond the two pieces together. Apply gentle pressure to the thin film and the drilled microscopic glass on each other and bake in the pre-heated oven at 80°C for over 1 hour. The thermal bonded PDMS with drilled microscopic slide leave only one side of the hole on the slide. Another microscopic glass slide, was used to cover the back side of the microscopic glass slide. Two glass slide is then seal together using silicone sealant.

IV. Result and Analysis

In the following topic, results gathered on experiment will be analyzed and discussed. As the objective of this project is to develop a microalbumin sensor using alternative approach. The sensor fabricated will put into test for its performance and further identifying if the method work for the stated detection method. The data from HR4000CG-UV-NIR Ocean Optics have been analyzed using Microsoft Excel.

A sensor made from PDMS have been tested with the spectrometer to validate the effectiveness of the sensor. A normal microscopic glass has been illuminated with light source and the light is then channeled into horizontal direction with a fiber optic. The light source has been illuminated through the glass with 10681 counts at 643.41nm. Figure 3 shows the spectral range of glass illuminated with light source.

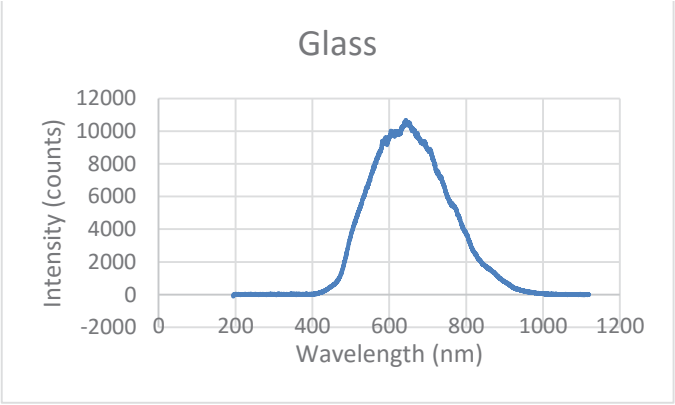

Fig. 3. Spectral range of the Glass

This step is taken to identify the spectral range of the light source with microscopic glass slide. In Figure 3, the spectral range of the light source is in the range of 400nm to 1000nm which is in line with the range of visible light spectrum (400nm-700nm) and in near infra-red range.

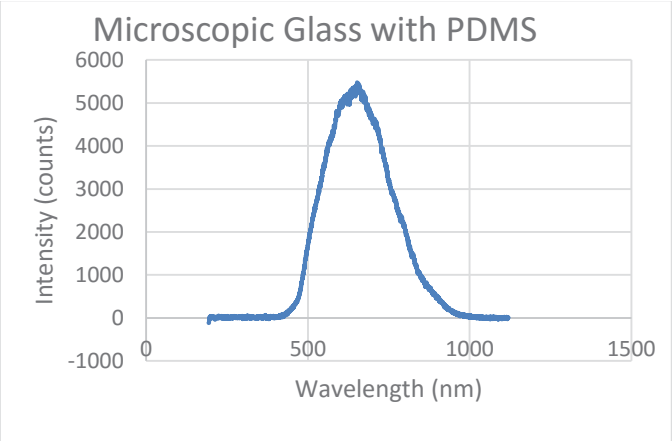

Fig. 4 Spectral range of microscopic glass slide with PDMS

In Figure 4, the result from microscopic glass slide with PDMS shows a smaller intensity counts. This is because the PDMS surface along with the air gap and the microscopic glass surface create a partial transmittance and reflection from low refractive index to high refractive index (PDMS is approximate to 1.4), through air gap and then finally through the bottom part of microscopic glass slide (approximate 1.52). Based on Fresnel equations [ref], the reflectance and transmittance relationship are as follow.

$$T_P = 1 - R_P \tag{4}$$

$$T_s = 1 - R_s \tag{5}$$

$$R = \frac{1}{2}(R_S + R_P) \tag{6}$$

Where T_S is the transmittance of s polarized light, R_S is the reflectance of s polarized light, while T_P and R_P represent the transmittance and reflectance of p polarized light. From the equation 4, 5 and 6 respectively, the relationship of transmittance and reflectance can be as simple as the equation 4.4. This equation does not take transmittance and absorbance into account as the light travel in the bulk where Beer-Lambert law applied.

$$T = 1 - R \tag{7}$$

The intensity count in Figure 4.2 is 5324 count at wavelength 643.41. Reflectance of the microscopic glass slide with PDMS can be calculated using the difference of transmitted light as in the calculation in below. In the calculation below, the PDMS thin film have approximate same coefficient for reflectance and transmittance.

$$T_{PDMS} = \frac{5324}{10681} = 0.498$$
$$R_{PDMS} = 1 - 0.498 = 0.502 \tag{8}$$

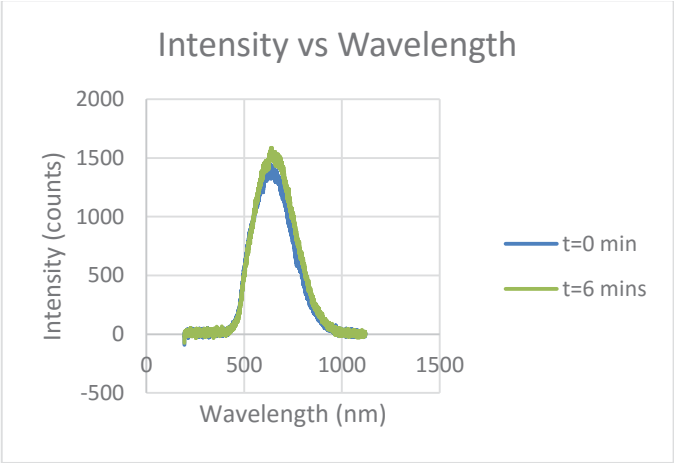

Fig. 5. Intensity vs wavelength with sodium urate of concentration 15mg/dL.

After the testing the microscopic glass slide on spectrometer without sodium urate solution on top of the PDMS surface, the next step of the experiment will involve with different concentration of the sodium urate solution. Figure 5 shows the spectral range of light with sodium urate concentration of 15mg/dL.

Based on Fig 4.3, there is an obvious drop in the intensity of the spectrometer reading at t = 0 minute. This is because the solution was applied on the surface by dropping a solution on top of the PDMS thin film. This action further adds another interface for light to travel which comply with the Fresnel equation. The peak intensity for t = 0 minute is 1448 counts at 621 nm. Notice that there is an increase of intensity at the sixth minute, this is because both the solution droplet and PDMS thin film form a negative meniscus convex lens (converging meniscus) which brings parallel lights to a focus as shown in Figure 6. Figure 7 shows spectral shift with two different Full Width Half Maximum (FWHM), one with small FWHM and another one with large FWHM. In this experiment, the spectral range of the light is a large FWHM as the light source is not a monochromatic light source and the lens form from the deflection of the PDMS thin film, therefore the transmittance change is very small. In addition to these criteria, the result of the spectral change will be more obvious as the air cavity and the thickness of PDMS is in the magnitude 0f hundred nanometer.

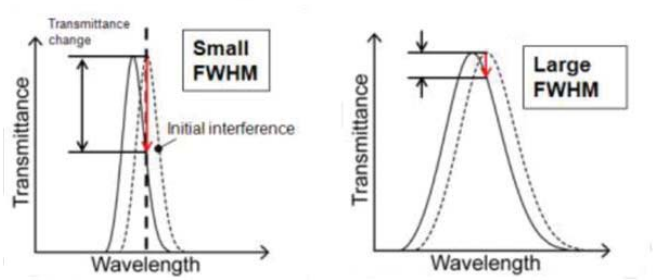

Fig. 6. Spectral shift with (a) small FWHM (b) large FWHM

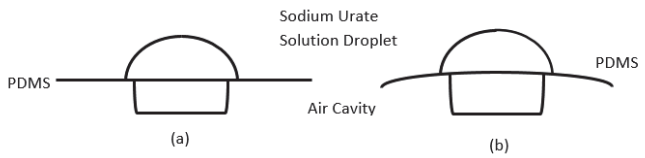

Fig. 7. The geometry of the thin film (a) before thin film deflect (b) after thin film experience a small degree of deflection.

In Figure 7, the deflection of the PDMS thin film will not only form a converging meniscus but also a larger air cavity. At the sixth minute, there is a slight change for the peak as the spectral experienced redshift from the original spectral range this is because the air cavity in the sensor is increases as the distance from the bottom of the PDMS thin film to the top of the second microscopic glass interface increases. The deflection of the PDMS thin film is because of adsorption of uric acid on the PDMS surface, creating a surface tension thus the thin film deflects.

In conclusion, the fabrication method for the sensor able to produce a sensor capable to detect sodium urate, one of the component present in urine. Further fabrication proposed such as immobilization of antibody for albumin on the PDMS surface will greatly increases the selectivity of the sensor as this sensor will be use on urine sample to detect microalbumin.

V. CONCLUSION

Microalbumin early detection give doctors more time to cure a patient before the condition get worse. In conventional detection method, dipstick and spectrophotometer enable a person to detect microalbumin, but dipstick only gives qualitative results while spectrophotometer gives quantitative results. But spectrometer do not grant a doctor to test urine sample on the spot. In this early prototype, an alternative method to detect microalbumin was proposed. Results shows a promising result as the PDMS thin film able to detect sodium urate, a substitute for urine sample. The spectral shift of the spectral range proposed that the PDMS experience adsorption from the reaction of sodium urate. Further development such as immobilization of microalbumin antibody on PDMS thin film and built in photodiode will enable the full integration of the microscopic glass slide into a back-end detector.

REFERENCES

[1] K/DOQI.Clinical practice guidelines for chronic kidney disease: evaluation, classification, and stratification. Am J Kidney Dis 2002;39:S1-266

[2] Rossing P, Hommel E, Smidt UM, Parving HH (1994). Reduction of albuminuria predicts beneficial effect on diminishing the progression of human diabetic nephropathy during antihypertensive treatment. Diabeteologia; 37:511-6.

[3] Apperloo AJ, De Zeew D, De Jong PE (1994). Short term antiproteinuric response to antihypertensive treatment predicts long-term GFR decline in patients with non-diabetic renal disease. Kidney Int: S174-8.

[4] Bishnu Prasad Devkota,Microalbumin: Reference Range, Interpretation, Collection, and Panels,
http://emedicine.medscape.com/article/2088184-overview, Jan 2014.

[5] Edgar V Lerma,Proteinuria. Medscape Reference.
http://emedicine.medscape.com/article/238158-overview, Dec 2016.

[6] Vecihi Batuman, Diabetic Nephropathy
http://emedicine.medscape.com/article/238946-overview, Sep 2016.

[7] Toto, R. D. (2004). Microalbuminuria: definition, detection, and clinical significance. The journal of clinical hypertension, 6(s11), 2-7.

[8] Qiu, T., Huang, G., Yang, X., Ma, L., & Yang, X. (2011). Palmtop spectrophotometer for DNA and protein measurement in micro-nanoliter assays. Paper presented at the Journal of Physics: Conference Series.

[9] Takamoto, A., Sugahara, K., Shibahara, T., Katakura, A., Matsuzaka, K., & Sugihara, N. (2013). Screening for oral mucosal diseases by a portable spectrophotometer: Comparison between color difference and epithelial thickness. Journal of Oral and Maxillofacial Surgery Medicine, and Pathology, 25(4), 314-327.

[10] Anjalidevi, B. (2011). Prediction of microalbuminuria by using spot urine samples and regression analysis to convert spot microalbumin values to 24 hours microalbuminuria.

[11] Lin, Julie; Hu, Frank B.; Curhan, Gary C. (2010-05-01). Associations of diet with albuminuria and kidney function decline. Clinical journal of the American Society of Nephrology: CJASN. 5 (5): 836–843. doi:10.2215/CJN.08001109. ISSN 1555-905X. PMC 2863979. PMID 20299364.

[12] Wiseman, M. J.; Hunt, R.; Goodwin, A.; Gross, J. L.; Keen, H.; Viberti, G. C. (1987-01-01). Dietary composition and renal function in healthy subjects. Nephron. 46 (1): 37–42. ISSN 1660-8151. PMID 3600911.

[13] Lucy E. Yaguo Ide, Nwadiuto A. Akani, Microalbuminuria: It's Significance, risk factors and methods of detection, The Nigerian Health Journal, Vol. 11, No 1, January - March 2011

[14] Hiroki Oyama, Kazuhiro Takahashi, Nobuo Misawa, Koichi Okumura, Makoto Ishida and Kazuaki Sawada (2012), A MEMS Based Fabry-Perot Protein Sensor with Reference Sensor, The 14th International Meeting on Chemical Sensors

[15] H.P. Lang, M.K. Baller, R. Berger, Ch. Gerber,J.K. Gimzewski, F.M. Battiston, P. Fornaro, J.P.Ramseyer, E. Meyer and H.J. Guntherodt (1999), An artificial nose based on a micromechanical cantilever array, Analytica Chimica Acta 393,p.59 doi: 10.1016/S0003-2670(99)00283-4

[16] D. A. Raorane, M. D. Lim, F. F. Chen, C. S. Craik,and A. Majumdar (2008), Quantitative and label-free technique for measuring protease activity and inhibition using a microfluidic cantilever array, Nano letters, vol. 8, pp. 2968-2974; doi:10.1021/nl8019455

[17] "Linear Polydimethylsiloxanes" Joint Assessment of Commodity Chemicals, September 1994 (Report No. 26) ISSN 0773-6339-26

[18] S. Grilli; V. Vespini; P. Ferraro (2008). Surface-charge lithography for direct pdms micro-patterning. Langmuir. 24 (23): 13262–13265. doi:10.1021/la803046j. PMID 18986187.

[19] Zhang, B.; Dong, Q.; Korman, C. E.; Li, Z.; Zaghloul, M. E. (2013). Flexible packaging of solid-state integrated circuit chips with elastomeric microfluidics. Scientific Reports. 3: 1098. Bibcode:2013NatSR...3E1098Z. doi:10.1038/srep01098.

[20] King-Ning Tu (2010). Electronic Thin-Film Reliability (pp 120), Cambridge University Press.

Noninvasive Jaundice Detector using Integrated Textile Color Sensor

Eliza Liyana Hanim Binti Mamat
Faculty of Electrical Engineering
University Technology Malaysia
81310 UTM Johor Bahru, Johor, Malaysia.
diana_liyana@yahoo.com

Suhaila Binti Isaak
Dept. of Electronic and Computer Eng.
Faculty of Electrical Engineering
University Technology Malaysia
81310 UTM Johor Bahru, Johor, Malaysia
suhaila@fke.utm.my

***Abstract*— Jaundice is common in new-born that cause skin and cornea of the eyes become yellow due to high bilirubin levels in blood. The side effect of jaundice can be prolong if the bilirubin level is high and untreated. Non-invasive technique is highly demanded in medical industries. The aim of the project is to develop integrated non-invasive jaundice detector with textile material. This sensor has been designed on cotton material for in-house usage and parents can monitor their new-born regularly. The detector consists of three light emitting diode (LEDs) with various wavelength as light source and photodiode. OPT101 monolithic photodiode has been use as detector to detect the jaundice level based on light absorbance method. The light absorbance level has been measured using power meter. The LED intensity has been tested to determine the observance level of the sample. The absorbance and concentration relationship based on Beer-Lambert Law are explain in this paper. The output of the system would be useful since parents can refer to doctor immediately if the infant at critical condition.**

Keywords—jaundice; beer-lambert law; OPT101.

I. INTRODUCTION

In late of 18th centuries, the first jaundice disease has been reported. The data regarding the condition of the liver as the relationship between liver and jaundice has been collected and analysis. Based on that, the main factor of jaundice is detected which is due to meconium as when there is a delay in passage of meconium. Besides that, somnolence, poor feeding and cerebral are also factor of jaundice in new-born [1]. Meconium is composed of materials ingested during the time of neonatal still in the uterus. Meconium consists of intestinal epithelial cells, lanugo, mucus, amniotic fluid, bile and water [2].

The best way to treat neonatal jaundice is by breastfeeding because milk will cause more bowel movements, and continue increasing the amount of bilirubin eliminated in infant's stool [1,3]. On the other hand, phototherapy has been widely used in jaundice treatment for more than four decades. The phototherapy treatment also treat jaundice effectively where the special light is used to reduce number of bilirubin in the infant's body. The design of devices has been developing throughout the year, with the aim of reducing bilirubin level at shorter exposure duration [4].

The best method to detect bilirubin level in body is by performing blood test because most of the bilirubin in the blood. To perform blood test, a blood sample is needed to test the bilirubin level. The blood sample usually taken from the infant by pricking infant's heel [5]. Alternatively, a urine test also method to detect bilirubin level in body. The difference is urine test is the test to detect substances called urobilinogen. These substances are produced whenever there is a reaction between bacteria and bilirubin in the digestive system [6].

II. LITERATURE REVIEW

A. *Non-invasive method*

In non-invasive technique, blood samples are not required for measure the concentration of the bilirubin. This technique only involves light, which is reflected and absorbance by the skin. Its help to find how much red blood cell are broken down and to find out the level of bilirubin. This technique is less painful, reduce traumatize and produce fast result [7].

B. *Kramer's rule: visual inspection*

Each of the body part has been divided into five zone, head and neck, upper trunk, lower trunk and thighs, arms and lower legs and the last is palms and soles. Figure 1 show the zones of Kramer's rule use to visual inspection. The value of bilirubin concentration in blood will be based on yellowness of skin. The yellowness of skin is due to bilirubin itself. This type of bilirubin is identifying as unconjugated bilirubin that bound with albumin that flow around the blood system [8].

Figure 1 Zones of Kramer's rule

Table 1 states that each prediction value of total serum bilirubin (TSB) concentration for each yellowness zone. The TSB is increasing by 50µmol/dL per zone. Each zone represents the jaundice level condition by normal, medium and critical condition. The TSB concentration value is based on physical colour of skin. As an example, if the TSB is 150µmol/dL, it means the infant need to be treat immediately.

Table 1 Total serum bilirubin per zone.

Zone	Definition	Total serum bilirubin (µmol/L)
1	Head and neck	100
2	Upper trunk	150
3	Lower trunk and thighs	200
4	Arms and lower legs	250
5	Palms and soles	>250

C. *Beer-Lambert Law*

The interaction of light with human tissue in the form of a absorption and concentration is mainly described by using Beer Lambert law. It says that 'A' is absorbance is proportional to the 'c' concentration of solution and 'Ɛ' is specific extinction coefficient [9].

$$A = \varepsilon \times c \times d \quad (1)$$

Besides that, absorbance can also determine by measure the power of LED without sample, Pin and power of LED with sample, Pout.

$$A = \log \frac{Pin}{Pout} \quad (2)$$

Electromagnetic wave motion involves the propagation of energy from a source to a detector. The energy transported per time can be represent as power of LED with sample. The light intensity, I can be measure by obtained area of LED.

$$I = \frac{Pout}{area} \quad (3)$$

III. Methodology

The system is developed to absorbance level of jaundice for various concentration sample by changing the light intensity. The absorbance was calculated from the power captured by power meter. The baby is supposed to keep his finger on an opening to provide on sensor enclosure. In this system, LED is used as light source and OPT 101 photodiode is used as detector. Figure 2 show the block diagram of the system.

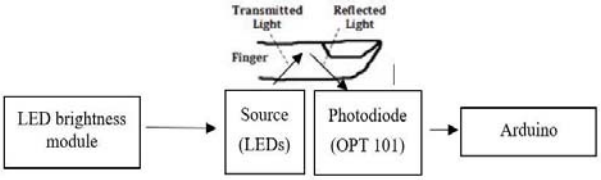

Figure 2 Block diagram

A. *Super bright LED*

The super bright LED is 5mm in diameter round which has an ordinary iron silver-plated pin. The super bright LED has high- brightness, low-power consumptions with high reliability and stability. This super bright LED is colorless and transparent, precision better optical design, the formation of a specific viewing angle with a uniform intensity distribution. In this system, there are three LED with different wavelength has been used which is red, green and blue. The reason of choosing these wavelength is because they are light sensitive photoreceptor cells in the human eyes and respond most to yellow.

B. *OPT 101*

To implement the study photodiode have been used in this study. OPT101 has been used for this integrated consolidation of photodiode and trans impedance amplifier on a single chip. The photodiode directly connected to the amplifier circuit to detect the intensity of light. In monitoring process, the photodiode OPT101 is used.

IV. Result and Discussion

In the following topic, results gathered on experiment will be analyzed and discussed.

A. *Relationship between absorbance and intensity*

The relationship between absorbance of bilirubin and intensity was determined by measuring the absorbance for different intensity at a fixed wavelength and concentration by using power meter. The absorbance of bilirubin is inversely proportional to intensity that has been reflected from the sample. Figure 3 show the calibration curve. Calibration curve is plotted to determine the mathematical equation that relates bilirubin absorbance and concentration.

The value of absorbance is obtained by using equation (2) and value of intensity is obtained by using equation (3).

$$A = \log \frac{0.0000164}{0.0000059} = 0.443991836 \quad (4)$$

$$I = \frac{0.0000059}{6.1575} = 1.55E - 06 \quad (5)$$

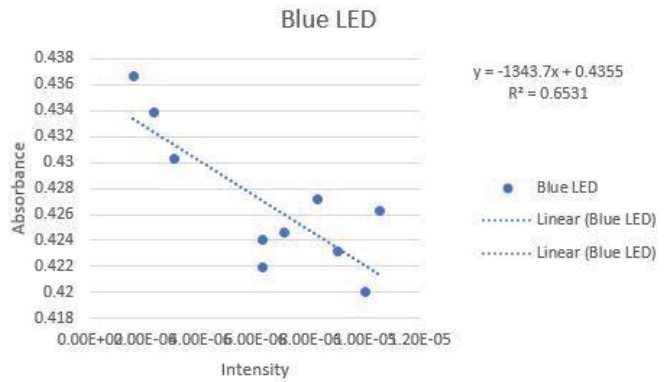

a) Blue LED

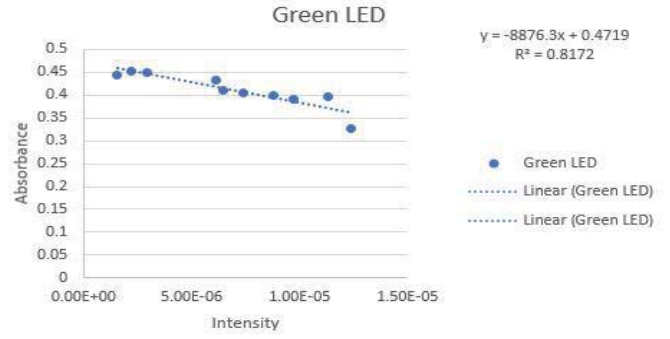

(b) Green LED

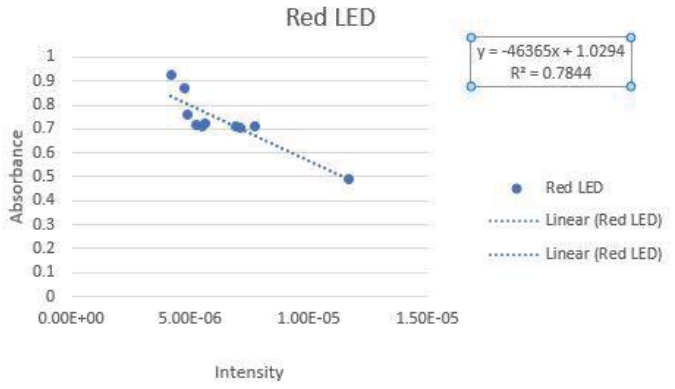

(c) Red LED

Figure 3 Calibration curve of absorbance vs intensity with fix concentration

From the calibration curve, a linear equation for each LED is obtained. The value of the correlation for all LED is closely approaching to 1, which indicates that there is a strong positive linear relationship between intensity and absorbance. It also means that absorbance of bilirubin and intensity of LED tends to increase and decrease proportionally.

B. Relationship between absorbance and concentration

The relationship between absorbance of bilirubin and concentration is determined by measuring the absorbance for different bilirubin concentration at a fixed wavelegth using power meter. Figure 4 show the relationship of absorbance and concentration of bilirubin. Based on the graph, the absorbance of bilirubin is directly proportional to concentration of bilirubin. This is proven of Beer-Lambert law where the absorbance increase as the concentration increase. As increasing concentration, less light reflected back to the photodiode because more light are being absorbed by the sample.

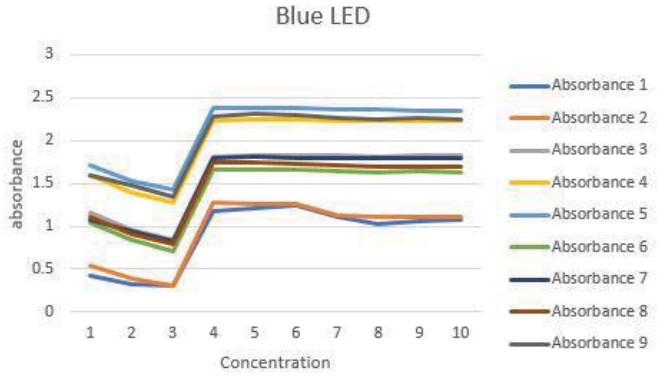

a) Blue LED

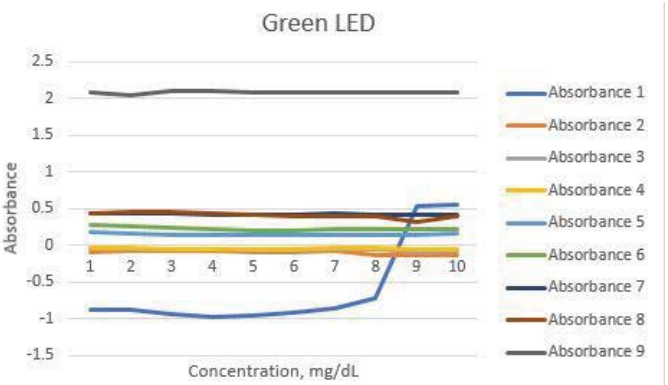

(b) Green LED

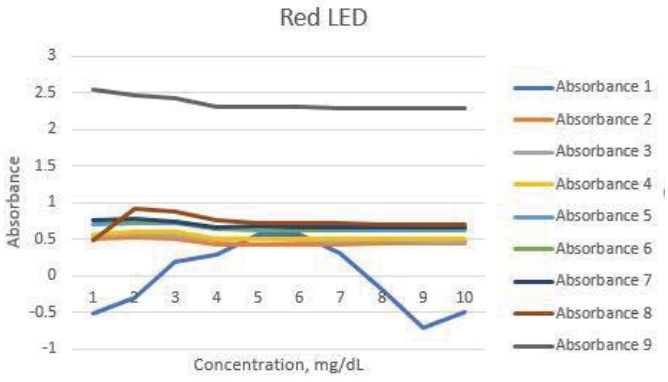

(c) Red LED

Figure 4 Relationship of absorbance and concentration

Based on figure 4, Blue LED show constant result of absorbance with difference concentration. Based on CIE chromaticity diagram, blue wavelength has high percentage of absorption of yellow wavelength.

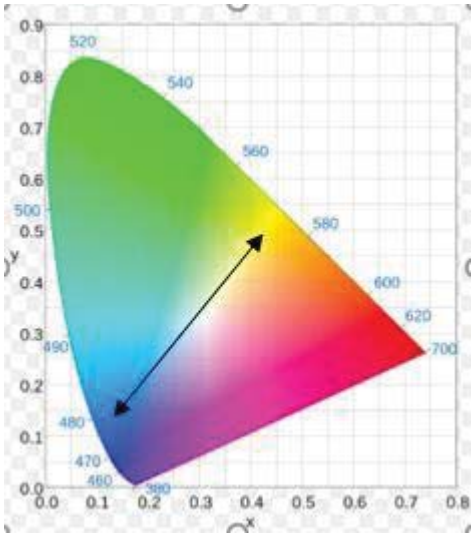

Figure 5 CIE chromaticity diagram

V. CONCLUSION

As conclusion, the jaundice level is successfully identify based on the relationship between absorbance and intensity and relationship between absorbance and concentration. Increasing concentration of bilirubin will lead increasing value of absorbance due to less light reflect to the photodiode. This statement has proven with Beer-Lambert law where the absorbance is directly proportional to concentration. The value of the correlation for all LED is closely approaching to 1, which indicates that there is a strong positive linear relationship between intensity and absorbance.

REFERENCES

[1] Thimotee Baumes, Jean Baptiste. Traite De L'Amaigrissemwnt Des Fans. 1st ed. 1806.

[2] "Meconium Aspiration". Kidshealth.org. N.p., 2016. Web. 21 Dec. 2016

[3] "Infant Jaundice Lifestyle And Home Remedies - Mayo Clinic". Mayoclinic.org. N.p., 2016. Web. 21 Dec. 2016.

[4] Brennan, Dan. "Treating Newborn Jaundice". WebMD. N.p., 2016. Web. 21 Dec. 2016.

[5] "Newborn Jaundice - Diagnosis - NHS Choices". Nhs.uk. N.p., 2016. Web. 17 Dec. 2016.

[6] "Jaundice - Diagnosis - NHS Choices". Nhs.uk. N.p., 2016. Web. 17 Dec. 2016.

[7] Ankan Gupta, Ashok Kumar, and Preeti Khera. "Method And Model For Jaundice Prediction Through Non-Invasive Bilirubin Detection Technique". International Journal of Engineering Research and V4.08. 2015.

[8] Mohammed, M. F., Matti D. J. and Mohammed, R. K. 2012. Detection the ratio of bilirubin in human body using laser technology. International Journal of Modern Engineering Research (IJMER), 2(4), pp. 1947-1950.

[9] R. Shriram, M. Sundhararajan and N. Daimiwal, "Effect of change in intensity of infrared LED on a photoplethysmogram," 2014 International Conference on Communication and Signal Processing, Melmaruvathur, 2014, pp. 1064-1067

Fabrication and Characterization of Reduced Graphene Oxide Schottky Back-to-Back Diode

Wan Fahim Asqalani Bin Wan Yusof
Faculty of Electrical Engineering
Universiti Teknologi Malaysia
Johor Bahru, Malaysia.
fahimasqalani@gmail.com

Shaharin Fadzli Bin Abd Rahman
Department of Electronics and Computer Engineering
Faculty of Electrical Engineering
Universiti Teknologi Malaysia
Johor Bahru, Malaysia.
shaharinfadzli@utm.my

***Abstract*—Graphene is a single atomic layer that consists of carbon atoms which are bonded in hexagonal honeycomb structure. In recent years, graphene has drawn much attention and intensively researched because of its promising prospect to current nanoelectronics demands. It also opens up new possibilities in electronic devices. Graphene is still in research process and still not applicable in large commercial or industrial productions yet but to achieve the potential application of graphene, controlling and manipulating its properties are very crucial. Recent year there are always a great progress in this industry and definitely will revolutionize the world. This project focuses on fabrication and characterization of a back-to-back schottky diode from graphene derivative while extracting the parameters related to sensing application. This can be done by fabricating the device using techniques like chemical exfoliation, filtration as well as transferring pattern to substrate. the device is characterized by I-V measurement.**

Keywords—graphene; back-to-back; schottky diode; reduced graphene oxide;

I. INTRODUCTION

A single layer or monolayer of graphite is called graphene which known as a wonder material nowadays. Recent studies have revealed that individual graphene sheets have astonishing electronic transport properties [1]. Although graphene can be formed into other structures to make it more stable and reactive, but just a monolayer of graphite which is graphene also has its own structure and different reaction to other concentration or substances. Since graphene has a very high charge carrier mobility and high surface to volume ratio properties which can affect the adsorbed molecules conductivity thus very attractive and suitable for molecular sensing applications [2]. A lot of studies have been done in demonstrating potential application for molecular detection based on changes of work function [3], conductance [3][4], surface waves frequency, [4] together with Fermi level

Just like metal-semiconductor junction, Graphene can form a schottky junction with other conventional semiconductors like Silicon(Si) and Germanium(Ge) [1-5]. Chemical sensor based on reverse-biased graphene/Si schottky diode has been developed that reveals a particularly high bias-dependent molecular detection sensitivity and low operating power compared to resistive based diode. Although there are many types of sensor configurations, Schottky diode is expected to be a suitable one that answers the worldwide demand for sensors [6].

Graphene can form a junction by contact with 2D and 3D semiconductors which have a characteristic of rectifying and can act as an extremely good schottky diode [15]. The junction formed was called Graphene-Semiconductor junction and it can be a part of devices with a wide range of applicability[16]. Graphene-semiconductor junction has a feature which capable for schottky barrier height to be tuned [1-4][17]. This feature provides a platform for study of interface transport mechanism, photo-detection, solar cells, high speed communication as well as sensing applications [1]. In this project, Graphene used as a metal and having a contact with a conventional semiconductor which is Silicon[1][2][4].

Diode that was formed at the junction can be used as sensor. Graphene with one atom thick layer structure allows molecules to be absorbed on the surface thus changes the graphene Fermi level, and therefore tailored the Schottky barrier height of the junction. The barrier height of the diode changes when there is a change in the work function of the metal. The barrier height is proportional to the work function of the metal. The work function change when there is a change of the concentration of the graphene or the doping levels of the graphene is decreased or increased. The variations in barrier height will also alter the current and the voltage of the diodes [5][6]. The barrier height is increasing as it was acting like resistance and will decrease the current, thus will increase the voltage of the diodes [8-10].

This approach focused on the material which is the reduced graphene oxide (rGO), one of graphene derivative that having a contact with silicon wafer. It is significant to fabricate and characterize a back-to-back schottky diode from reduced graphene oxide -silicon- reduced graphene oxide junction. Extraction of junction properties, namely barrier height(ϕBO), ideality factor (n) and series resistance (Rs) is also required. The device will be used as a specific sensor for example ethanol sensor and tested.

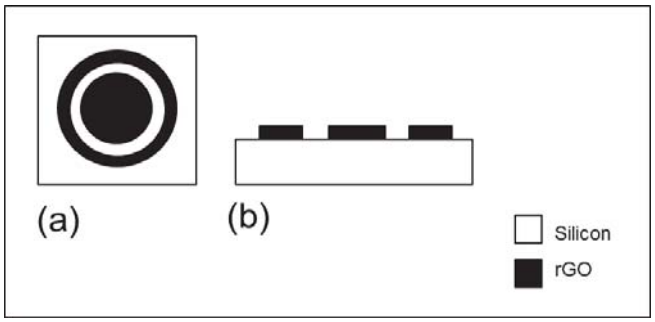

Fig. 1. Device structure of schottky back-to-back diode (a) Top view, (b) Cross-sectional view

II. EXPERIMENTAL PROCEDURE

The desired fabricated device had a reduced graphene oxide in contact with n-type silicon wafer substrate with resistivity of 1-10 ohm, as shown in Fig. 1. The outermost circular pattern of reduced graphene oxide had a diameter of 5mm. The filter used for the graphene oxide (GO) film was 0.2 µm membrane filters (cellulose nitrate) with diameter of 47 mm. The graphene oxide film was prepared by vacuum filtration. The significant for this technique was for separating a solid product from a solvent or liquid reaction mixture. The mixture in this experiment was 1 mg/ml equivalent to 1000 ppm graphene oxide solution. The solution was poured through a filter paper. The graphene oxide was trapped by the filter and the liquid was drawn through the funnel into the flask below, by a vacuum.

For graphene oxide patterning, the process flow can be shown in Fig. 2. Active photoresist printed circuit board(PCB) was used to make a mold. The printed mask covered the photoresist part was exposed to UV light. Due to active type photoresist, energy from the light dissociates the sensitizer and break down the cross-links. Exposed resist dissolve in developer solution (Sodium hydroxide, NaOH). The remaining part will be the same that on the mask.

To create a permanent pattern on the circuit board, etching process need to be done. Etching will remove material from areas identified by the lithography process (not masked by photoresist). A wet etching method was used that required liquid etchant solution such as hydrogen peroxide. The chemical will transport of by-products away from surface. The printed circuit board would be used as a base for making mold with PolyDimethylsiloxane (**PDMS**).

PolyDimethylsiloxane (PDMS), which is a Si based organic polymer that can be used in a lot of applications like soft lithography, fabrication of microfluidic devices and etc. A ratio of 9: 1 was used between the PDMS and its curing agent. In order to ensure the PDMS mold was uniformly cross linked, the curing agent must be distributed uniformly by whisking the mixture vigorously with a spatula. Then, the mixture was placed in a bell-jar connected to a vacuum pump to remove bubbles. After, the PDMS mixtures obtained bubbles free condition, leave the mixture for about half day before stripping off from the circuit board.

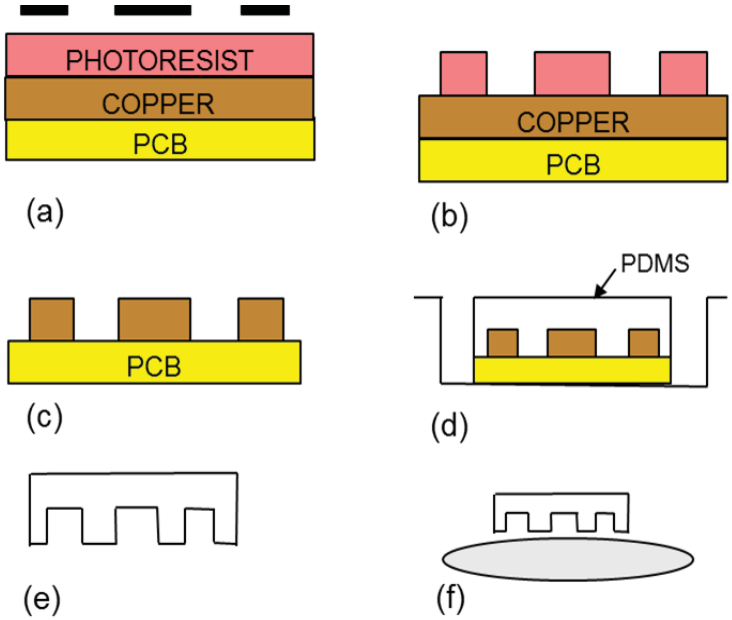

Fig. 2. Process flow for rGO patterning (a) active photoresist PCB covered by mask, (b) develop PCB, (c) PCB after etching, (d) coat the PCB with PDMS, (e) Stripping the PDMS, (f) PDMS stampped onto the filter to pattern the GO.

The PDMS was used as a stamp to peel off the undesired part of the graphene oxide filter. Due to rough surface of the printed circuit board, the PDMS was not sticky enough to peel off the graphene oxide. A PVA glue was needed for this particular part. To get a uniformly distributed glue on the PDMS, the small amount of glue was placed on a slides glass and was spin in the spin coater. The spin parameters for the first and second set was 300 and 5000 rpm respectively. The PDMS was put on the coated slides glass and distributed the glue uniformly without gave up too much pressing force. The PDMS then transferred on the graphene oxide filter and using the stamping method to pattern the GO.

Transferring the graphene oxide filter to silicon wafer required a careful handling of the sample. Dropped a little of water onto the filter that were placed on the silicon wafer. The significant for this method was that water would be absorbed by the filter and the water molecule will be in between graphene oxide and the filter itself. Put a lot of force when pressing the graphene oxide on the silicon substrate. The graphene oxide can form a contact with silicon substrate. The sample then diluted into acetone solution to dissolve the filter. The proposed material was reduced graphene oxide which is one of graphene derivatives, reduction process was done after transferring the GO to the silicon substrate. The process uses ascorbic acid as the reducing agent. The sample was heated at 90°C in 500 ml 1 Molar of ascorbic acid for about one hour. The fabrication process was completed and further characterization of I-V measurement required.

III. RESULTS AND ANALYSIS

A. Vacuum filtration

Fig. 3 shows the image of graphene oxide, GO after vacuum filtration process of 1000 ppm GO solution. This process take about an hour to complete .

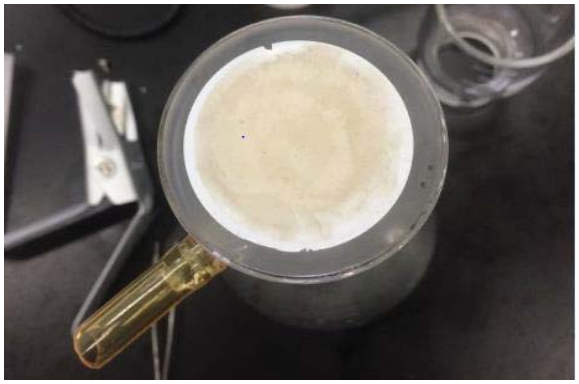

Fig. 3. Graphene oxide film

B. Graphene Oxide Patterning

Fig. 4 shows the result of GO patterning process. Active type photoresist PCB will give a same shape as the mask used during exposure and the end result after etching can be referred to Fig. 4(a). The mold in Fig.4(b) was obtained after pouring the mixture of PolyDimethylsiloxane (PDMS) and its curing agent. The mixture inversely follows the shape of the base which is the PCB after completely harden. Due to the rough surface of the circuit board, the PDMS does not have enough stickiness to peel off the undesired GO film. To overcome this problem, a PVA glue was used and the results can be shown in Fig. 4(c). the different form of pattern was due to the uniformity of the glue that was coated on the mold.

C. Reduced Graphene Oxide (rGO) –Silicon Contact

The transferring process of graphene oxide to silicon substrate was the most challenging process. Several techniques was used for this particular process. The pattern from the graphene oxide film cannot be transferred perfectly to the substrate due to some factors that affect the quality of transferring. One of the factors is handling the sample in the acetone solution. A clumsy movement can cause the GO to dilute with the filter in the solution. A good amount of force given during pressing the film onto the substrate also plays an important part in achieving a good quality of pattern transferred. The sample undergoes a reduction process after transferring to reduce oxide from the GO. Reduced Graphene Oxide (rGO) contact with silicon substrate formed after the reduction process using ascorbic acid.

Fig. 5 shows the result of pattern transferred to the silicon. The images were taken using a microscope.

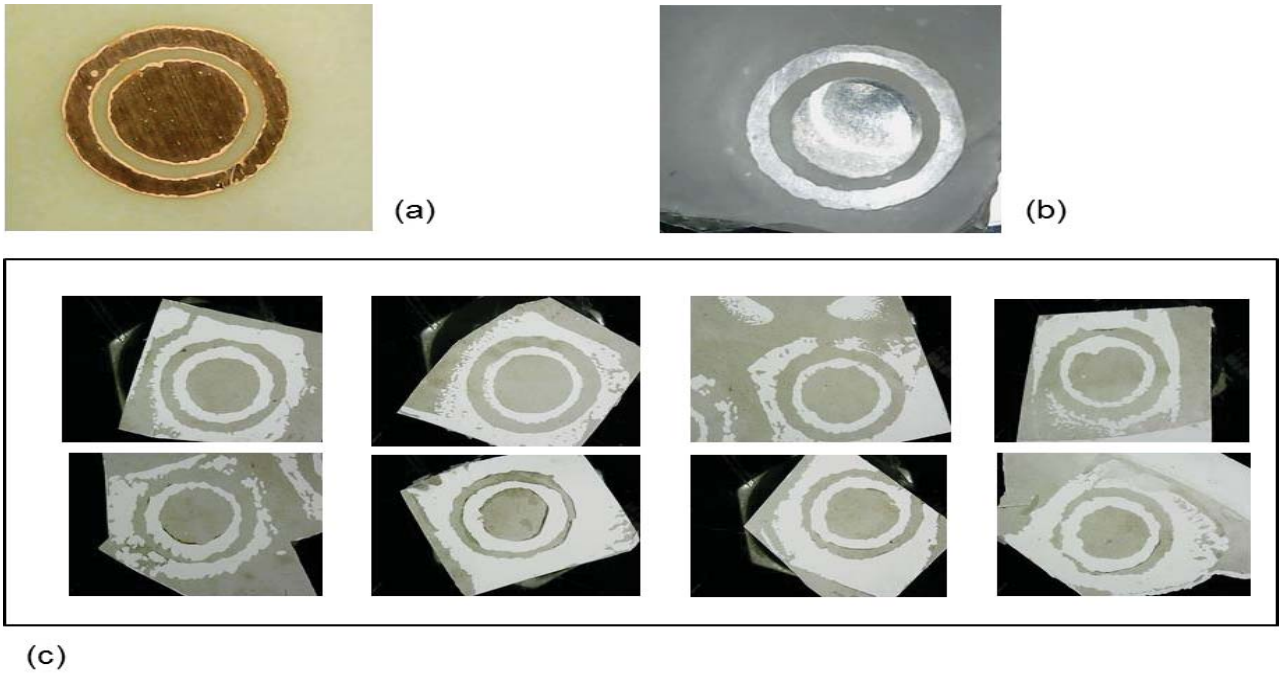

Fig. 4. Images of GO patterning process, (a) pattern on PCB, (b) mold using PDMS, (c) images of GO film after patterning that was cut into pieces

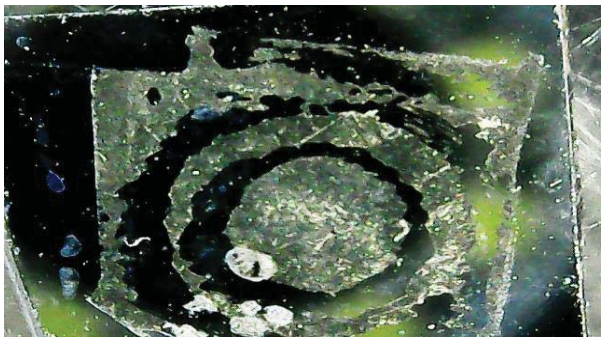

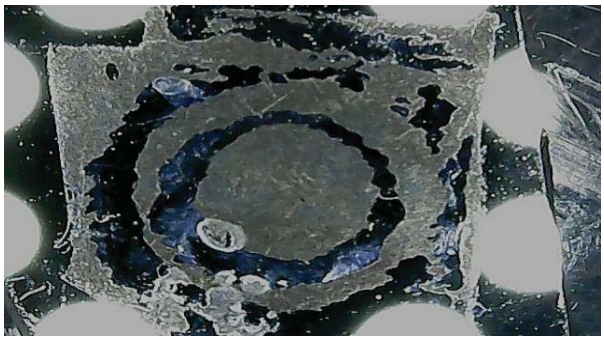

D. Ethanol Sensing

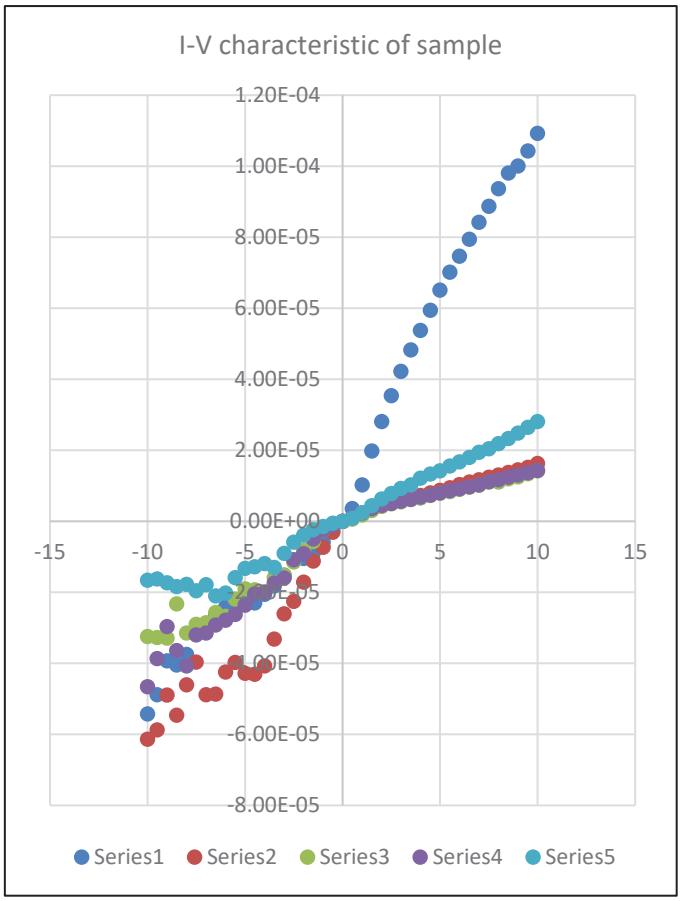

Fig. 6. I-V characteristic of the sample

Figure above describe the I-V characteristic of the sample. Series 1 refers to normal condition of the sample when taking the measurement while series 2-5 was the sample condition when ethanol was dropped on the sample at different time. An atom thick layer of rGO allows the ethanol molecules to be absorbed and changes the doping concentration. This will tailored the work function of the graphene. When increasing the work function, the current will be decreasing.

IV. CONCLUSION

In conclusion, graphene based sensor is likely to be developed due to the remarkable properties and high sensitivity as a sensor. This can be observed in several researches that successfully produced a single schottky diode structure based on graphene. The back-to-back structure is hopefully become a step up for the sensing applications. The operation surely has no issue due to the reverse bias operation which proven to give a better sensitivity. Moreover, the reduced graphene oxide (rGO) is easy to be prepared and less cost compared to some materials. Lastly, graphene/semiconductor heterojunctions are promising devices in future for real-life applications and an interesting platform for research.

ACKNOWLEDGMENT

The author would like to thank his supervisor, Dr. Shaharin Fadzli Abd Rahman for his supervision, guidance and knowledge throughout this research.

REFERENCES

[1] A. K. Singh, M. A. Uddin, Prof. T. S. Sudarshan, Dr. G. Koley, "*Tunable Reverse-Biased Graphene/Silicon Heterojunction Schottky Diode Sensor*", (2014)

[2] Yanbin An,Ashkan Behnam, Eric Pop,and Ant Ural, Appl. Phys. Lett. 102, 013110 (2013)

[3] M. W. Nomani , R. Shishir , M. Qazi , D. Diwan , V. B. Shields ,M. G. Spencer , G. S. Tompa , N. M. Sbrockey , G. Koley , Sens. Actuators, B 2010 , 150 , 301 .

[4] S. Rumyantsev , L. Guanxiong , R. A. Potyrailo , A. A. Balandin ,M. S. Shur , IEEE Sens. J. 2013 , 13 , 2818 .

[5] A. Ashour, M. Saqr, M. AbdelKarim, A. Gamal, A.Sharaf, 8th int. conference on Sensing Technology, Sep.2-4, 2014

[6] Kim, H.-Y.; Lee, K.; McEvoy, N.; Yim, C.; Duesberg, G. S. Nano Lett. 2013, 13 (5), 2182−2188

[7] Adenilson J Chiquito1, Cleber A Amorim1, Olivia M Berengue1,Luana S Araujo1, Eric P Bernardo1 and Edson R Leite2, J. Phys.: Condens. Matter 24 (2012) 225303 (7pp)

[8] Ng H T, Han J, Yamada T, Nguyen P, Chen Y P and Meyyappan M 2004 Nano Lett. 4 1247

[9] W. Park, J. Hu, L. a. Jauregui, X. Ruan, and Y. P. Chen, "Electrical and thermal conductivities of reduced graphene oxide/polystyrene composites," Appl. Phys. Lett., vol. 104, pp. 1–13, 2014.

[10] S. Pei and H. M. Cheng, "The reduction of graphene oxide," Carbon N. Y., vol. 50, no. 9, pp. 3210–3228, 2012.

[11] L. Meng and S. Park, "Preparation and Characterization of Reduced Graphene Nanosheets via Pre-exfoliation of Graphite Flakes," vol. 33, no. 1, pp. 209–214, 2012.

[12] K. S. Novoselov, V. I. Fal′ko, L. Colombo, P. R. Gellert, M. G. Schwab, and K. Kim, "A roadmap for graphene," Nature, vol. 490, no. 7419. pp. 192–200, 2012.

[13] Donal A. Neamen, “Semiconductor Physics and Devices” 4th edition New York: McGraw-Hill. (2012)

[14] B. L Sharma. "Metal Semiconductor Schottky Barrier Junctions and Their Applications". New York: Plenum Press (1984)

[15] An, X.; Liu, F.; Jung, Y. J.; Kar, S. Nano letters 2013, 13, (3), 909-916

[16] Ural, A. In Fabrication and Characterization of Photodetectors Composed of Graphene/Silicon Schottky Junctions, 225th ECS Meeting (May 11-15, 2014), 2014; Ecs.

[17] Sung, C.-Y.; Lee, J. U. IEEE Spectrum 2012, 49 (2), 32−59.

Low Cost Direct Laser Writing using Blu-Ray UV Laser Module

Ang Yong Xian
Faculty of Electrical Engineering
Universiti Teknologi Malaysia
Johor Bahru, Malaysia.
yxang2@live.utm.my

Shaharin Fadzli Bin Abd Rahman
Department of Electronics and Computer Engineering
Faculty of Electrical Engineering
Universiti Teknologi Malaysia
Johor Bahru, Malaysia.
shaharinfadzli@utm.my

***Abstract*—Lithography is important in device fabrication. Varieties of articles and journals have discussed the usage of illuminator sources and different methodology to manipulate the power intensity of the sources in pattern transferring process. In addition to controlling the intensity of the light sources, positioning system of both the photomask and wafer is also the critical factor that influences the final resolution of the fabricated device. In this paper, mask-less photolithography using a relatively lower cost approach can achieve up to 50µm.**

Keywords—*Photolithography; Direct Writing; Mask-less; UV Laser, Resolution*

I. INTRODUCTION

Device fabrication is one of the important process in manufacturing the fundamental electronic components made up of electronic circuit and system [1]. Technology used for device fabrication keeps advancing to produce devices with improved accuracy to meet the designed specifications. The typical basic flow of device fabrication is as shown in Fig.1.

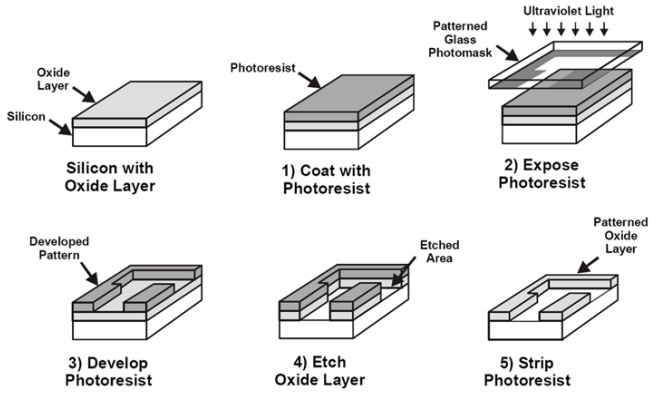

Fig. 1. Basic Process Flow of device fabrication.

At first, the process starts with the development of a thin film called photoresist on the substrate. The process is then proceeded with photolithography. A pattern transfer is done by using a photomask and light source. Photoresist reacts with the light source and a desired pattern is formed. The oxide layer is then etched and the pattern is actually transferred from the photoresist to the oxide layer. Finally, the photoresist is removed.

From the process flow, the lithography process is obviously significant. It determines the final resolution of the device. In the market, machines setup to carry out a photolithography process are complex and differ in functionality depends on the types of devices. The resolution of the fabricated devices ranges from micrometers to nanometers. TABLE I implies the significance of photolithography process. 35% of total wafer processing cost comes from lithography process.

TABLE I. RELATIVE COSTS OF PROCESS IN DEVICE FABRICATION

Manufacturing Process Step	Percentage of Wafer Processing Cost per Square Centimeter*
Lithography	35%
Multilevel materials and etching	25%
Furnaces and implants	15%
Cleaning/stripping	20%
Metrology	5%

*Excludes packaging, test, and design costs.

ASML, Nikon and Canon are the major vendors of the lithography machines in the world. The machines available in the market are essentially invested by semiconductor manufacturer for commercial activities.

Application of photolithography in device fabrication includes the fabrication of microfluidic channels [2] and planar passive elements [3]. These are the materials being studied in current research trends.

Commercialised lithography system such as mask aligner and laser writing system is expensive. Researchers or educators who involve in a small-scale research project may have limited access to such lithography systems. Low-cost machines which perform photolithography for individual research are seldom available in the market. This causes the disconnection between scientific theory and real life application [4,5,6,7].

As solution, a low-cost direct laser lithography system is proposed. Direct laser writing technique used in photolithography is highly flexible and fabricates single device without the usage of photomasks [8,9,10]. The system can be realised by utilising an ultraviolet laser found in Blu-Ray laser pick-up module inside a HD-DVD writer. Hence, design and construction of a simple direct writing system is feasible. This

features reduces the cost-of-ownership of the photolithography system that is to be owned by users for non-commercial purposes. This assists in the research of microstructure system.

In this work, a direct laser writing system using ultraviolet (UV) laser module is designed and constructed. The direct writing process for microdevice fabrication is optimised.

II. METHODOLOGY

A. System Design

Overall design of the direct laser writing system is shown in Fig. 2. Fig. 3 shows the side of the system. Laser pick-up module is attached to the frame with an adjustable holder. Besides, adjusting micrometers are adapted to stepper motors using coupling. The stepper motors are powered using DC power supply and controlled by Arduino Board.

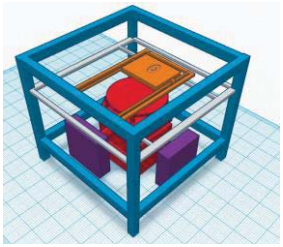

Fig. 2. 3D schematic view

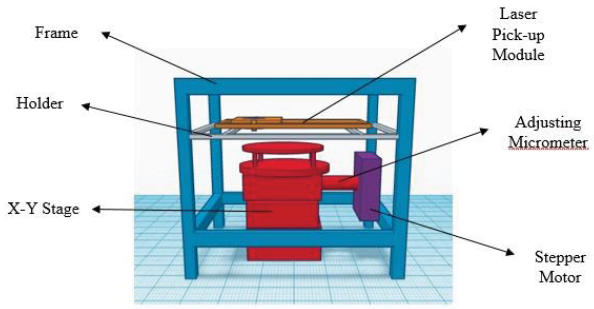

Fig. 3. Side view of system design

B. Hardware Components

1) Laser Pick-up Module: A cheaper blue-violet diode is obtained from the PHR-803T Blu-Ray pick-up manufactured by Toshiba. This pick-up module as shown Fig. 4 is mainly used in Xbox 360 HD-DVD drive. It is available as the spare part in the market.

Fig. 4. Extracted laser pick-up module

The laser diode is sensitive to electrostatic discharge (ESD). Care has to be taken when handling the laser diode to make sure touching on diode does not destroy the diode. The blue-violet diode of 405nm wavelength used in PHR-803T is most likely to be GH04P21A2GE. This is because there are no data specifications given by the original equipment manufacturer (OEM). From the datasheet of the GH04P21A2GE, the operating current of the laser diode has to be lower than 100mA to avoid reducing the life time of the diode. The performance of the violet diode is tested and verified using constant current source using Keithley 2400 SourceMeter. The power intensity of the laser varies dependind on the driving current. Photoresist is sensitized by sufficient power intensity of the UV light with certain range of wavelength. SPR 6809 positive photoresist is a broad spectrum of light-sensitive glue. Hence, tuning of the driving current is important to obtain the value of the optimum power intensity (driving current).

2) Constant Current Source: A current source is required to power on the laser diode. To ensure the normal operation of laser diode, a constant current source is designed. Before tested with the laser diode, the circuit is tested with dummy loads.

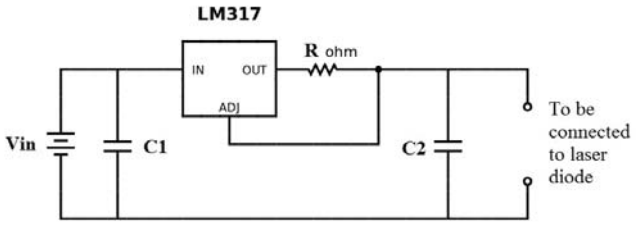

Fig. 5. Constant current source circuit

Assume Vin= 9V, C_1=0.1μF, C_2=1μF, R=1.25/Iout

IC LM317 is used in the current source circuit. Since the recommended maximum Iout is 100mA, the minimum value of R is set to 12.5 ohm. Resistor R in Fig. 5 can be added with a potentiometer in series to adjust for desired Iout. However, to avoid possible damage to the diode, the potentiometer is only adjusted when the circuit is switched off. Before using laser diode, test the constant current source using dummy load.

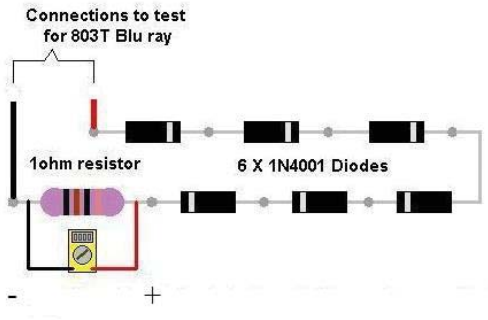

Fig. 6. Dummy loads to represent laser diode

Dummy load of laser diode is constructed using six 1N4001 diodes connected in series. Reading of the voltmeter across the 1 ohm resistor will be the current flows through the load measured in mA.

3) Linear X-Y Stage: The stage is available in the market or can be built up using cheaper materials. There are two axes of positioning micrometer to adjust the linear movement of the stage. The laser pick-up module is attached to the external frame of the X-Y stage and installed at a position right above the stage. The position of the pick-up module is fixed.

Fig. 7. Linear X-Y stage

A wafer or PCB board is placed on the stage and below the pick-up module during writing process. The coverage of the exposure area is determined by the maximum extension of the two adjusting micrometers. A complete revolution of the micrometer thimble results in linear movement of 0.5mm. Sensitizing of the photoresists depends on laser power intensity (constant current supply) and also writing speed (exposure time). Thus, the experimental data from manipulating these two parameters is to be investigated. By tuning the parameters properly, the writing process is optimised.

4) Stepper Motor: The X-Y stage is to be connected with stepper motors. The micrometers are adapted to the stepper motors using coupling. Choice of the stepper motor influences the resolution and speed of the driver system [11]. Repeatability of translation in X and Y has to be tested since an open loop system of driver would be used.

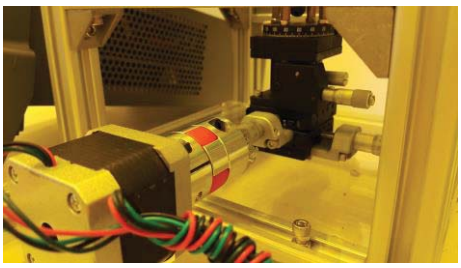

Fig. 8. Stepper motor adapted to the linear stage via coupling

5) Controller: The stepper motor is driven by A4988 driver and controlled using Arduino Board. The driver allows full step which is 200 steps for a complete rotation of the stepper motor. This means the motor rotates at 1.8 degree for each step. 12V DC power supply with proper current rating for Arduino and stepper motor driving system are considered properly.

C. System Integration

Individual hardware parts are constructed and tested with functionality. Troubleshooting is performed to eliminate and correct any errors. After the verification of individual parts, system integration is done and completed.

D. Lithography Process

The writing process is tested with 1cm x 1cm silicon wafers. The procedures are stated as followed.

1) Cleaning of silicon wafer: The wafers are immersed into acetone inside a beaker and then placed in ultrasonic bath for 5 minutes. This step repeated with ethanol and then deionised (DI) water. The wafers are dried using hand blower.

2) Spin Coating: A thin layer of photoresist is coated on the suurface of the wafer using spin coater.

3) Soft Bake: The coated wafer is baked under 90°C for 5 minutes.

4) Direct Writing: The wafer undergoes writing process with different driving current and exposure time.

5) Development: The wafer is immersed in developer for 45 seconds and then in distilled water for 45 seconds.

E. Observing

The samples are observed under the microscope and the images are captured using AmScope. The resolution of the line is determined by taking the ratio of the pixel of sample line to the pixel a standard 0.1mm line.

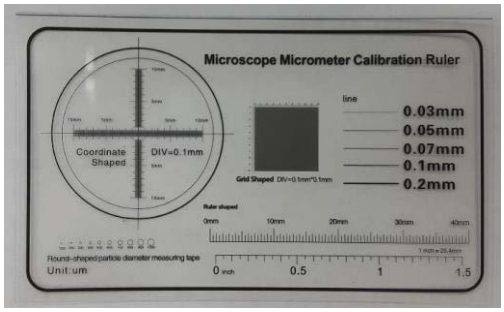

Fig. 9. Standard 0.1mm line in calibation ruler

III. Results and Discussion

A. Direct Writing System

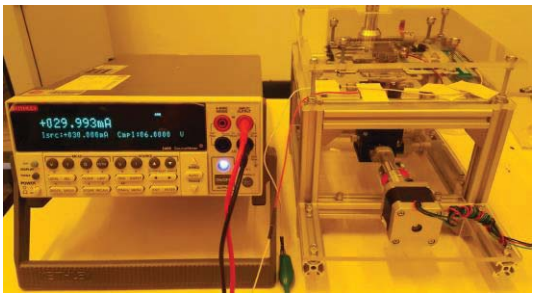

Fig. 10. Direct writing system with current source

The maximum range of the exposure area of the direct writing system is 12mm x 12mm.

B. *Blue-Violet Diode*

TABLE II. PERFORMANCE OF UV LASER DIODE

Driving Current (mA)	Forward Voltage (V)
5	3.37
10	3.67
15	3.90
20	4.11
25	4.33
30	4.54
35	4.73
40	5.00
45	5.17
50	5.33

C. *Line Resolution*

All lines are set to be produced at 5mm in length. Appropriate setting is done to adjust the rotational speed of stepper motor. The rotational speed is directly related to the exposure time (writing speed) of the sample.

TABLE III. LINE WIDTH OF EXPOSED SAMPLES

Exposure Time (s)	Line Width with Varying Driving Current		
	30mA	40mA	50mA
4	N/A	0.32 mm	0.47 mm
20	0.05 mm	0.41 mm	0.60 mm
40	0.07 mm	0.44 mm	1.18 mm
60	0.08 mm	0.56 mm	N/A
80	0.11 mm	0.61 mm	N/A

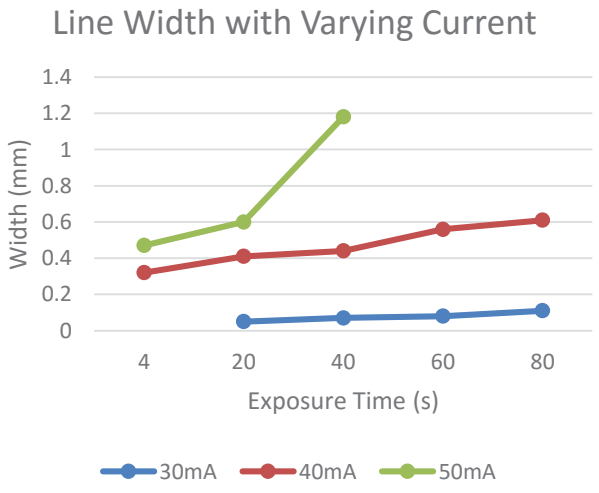

Fig. 11. Line width of the samples by controlling the current and exposure time

Fig. 11, shows the results of exposure samples by manipulating exposure time and the driving current. The lower the current, the thinner the line of the exposed sample. The 30 mA of current produces better results compared to 40mA and 50mA.

Shorter exposure time results in high resolution of the line. However, the control of the line becomes difficult because the writing speed is fast. Insufficient exposure time is unable to remove the photoresist deep enough and thus results in failure of the writing process.

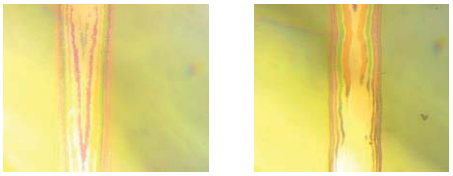

Fig. 12. Samples exposed using 30mA in 20s and 80s (under microscope)

From Fig. 12, the results show small incompleteness in the removal of the photoresist. This is due to the problem in adjusting suitable distance between sample and laser. In other words, the distance is not constant across all the exposure area due to inclination of the sample.

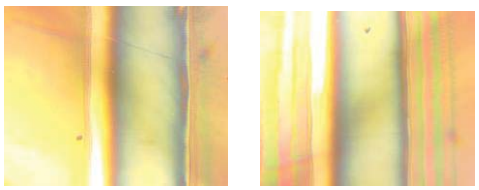

Fig. 13. Samples exposed using 40mA in 20s and 40s (under microscope)

From Fig. 13, the results show expected completeness in the samples. However, the resolution is not high. Although faster writing speed (shorter exposure) can be achieved, the control of the writing process becomes harder.

Fig. 14. Samples exposed using 50mA with 4s, 20s and 40s

Fig. 14 shows that driving current of 50mA in 40s produces overexposure. This means the direct writing process only requires low current (low power intensity) of laser diode.

CONCLUSION

The results of the experiment have shown that the direct writing process using UV laser is feasible. 0.05mm is the resolution achieved by using 30 mA current in 20s exposure. More optimization need to be done to improve the resolution of the samples. Higher resolution requires better focus over the exposure area and appropriate low power intensity of the laser and shorter exposure time of the sample.

REFERENCES

[1] M. J. Madou, "Fundamentals of Microfabrication and Nanotechnology Volume II: Manufacturing Techniques for Microfabrication and Nanotechnology," 3rd ed., Boca Raton: CRC Press. 2011, pp. 3-97.

[2] Burdallo, I., Jimenez-Jorquera, C., Fernández-Sáanchez, C. and Baldi, A., "Integration of Microelectronic Chips in Microfluidic Systems on Printed Circuit Board," Journal of Micromechanics and Microengineering, IOP Publishing Ltd., pp. 1-7, 2012

[3] Rajan, D. K. and Lekkala, J., "A Maskless Exposure Device for Rapid Photolithographic Prototyping of Sensor and Microstructure Layouts," Procedia Engineering, Elsevier Ltd., pp. 3-97, 2010

[4] Márquez-Segura, E., Otero, P., Camacho-Peñalosa, C., and Zürcher, J.-F., "A Very Low-Cost System for Photoresist Coating of Microwave Substrate Boards for Educational Purposes," International Journal of Electrical Engineering Education, pp. 93-105, 2006

[5] Musgraves, J. D., Close, B. T. and Tanenbaum, D. M., "A Maskless Photolithographic Prototyping System Using A Low-Cost Consumer Projector and A Microscope," American Journal of Physics. Vol. 73 (No. 10), 2005, pp. 980-990. American Association of Physics Teachers.

[6] Menon, R., Patel, A., Gil, D. and Smith, H. I. , "Maskless Lithography. Materials Today," pp.26-33, 2015, Elsevier Ltd

[7] Gabran, S.R.I., Mansour, R. R., Salama, M. M. A. ," Maskless Pattern Transfer Using 355nm Laser," Optics and Lasers in Engineering, pp.710-716, 2012, Elsevier Ltd.

[8] Lee, K. N., Shin, D. S., Lee, Y. S. and Kim, Y.K., "Protein patterning by virtual mask photolithography using a micromirror array," Journal of Micromechanics and Microengineering, pp.19-25, 2002, IOP Publishing Ltd.

[9] Singh, R. K. and Sharma, R., "Techniques Used for Mask Less Lithography. International Journal of Science and Research (IJSR)," pp. 135-138, 2013

[10] Chang, H. W., Lee, H. W., Lin, C. T. and Wen, Z. Q., "Development of Blue Laser Direct-Write Lithography System," International Journal of Engineering and Technology Innovation. Vol. 2 (No. 1), pp. 63-71, 2012, Taiwan Association of Engineering and Technology Innovation (TAETI).

[11] Campbell, R. A. A., Eifert, R. W. and Turner, G. C. , "Openstage: A Low-Cost Motorized Microscope Stage with Sub-Micron Positioning Accuracy," Public Library of Science (PLOS) ONE, pp.1-18, 2014

IoT: Smart City Automated Parking System

Ng Sea Kun
Faculty of Electrical Engineering
Universiti Teknologi Malaysia
Johor Bahru, Malaysia.
seakun11@gmail.com

Dr. Puspa Inayat Khalid
Department of Electronic and Computer Engineering
Faculty of Electrical Engineering
Universiti Teknologi Malaysia
Johor Bahru, Malaysia.
puspa@fke.utm.my

***Abstract*—The purpose of this project is to develop an Android mobile application and a Windows Form application to work as the IoT (Internet of Things) part of the Smart City Automated Parking System. A database was created which stores all the information and details. The host computer which the database is located in, acted as a server in the overall system. This project was proposed due to the severe problem of traffic congestion and lack of parking spaces especially in the urban areas during the rush hours. This system was designed aiming to reduce the fuel and time consumed in the seeking of vacant parking spaces during peak hours, as well as to optimize the parking facilities space usage and ease the management of the parking system. MySQL Database was used in this project, via the assistance of Xampp and phpMyAdmin. The Android application was developed using Android Studio, whereas the Windows application was developed using Microsoft Visual Studio. The mobile application was designed to access to the server according to the IP address, read the PHP script and execute the SQL statement within. On the other hand, the Windows application set the database as a binding source and refer to the database for the query of data. The Android application was successfully developed for the user-end service purpose, which allows the users to check the availability of the parking facilities and to operate with the automated parking system for the parking service. The Windows Form application on the other hand, allows the management officers to view the information and details of the users, parking facilities, and records of the parking services, and acts as the monitoring software.**

Keywords—smart city, automated parking, server, database, Android application, Windows Form application

I. INTRODUCTION

Smart city is now one of the hottest trends among the main directions of science and technology development. A smart city is defined as a city where information and communications technology (ICT) is applied in the city planning for the development of a high quality living environment and infrastructures which are sustainable and optimizing the management of resources [1]. The main concept in the city planning for a smart city is real-time information sharing and how information resources are interconnected, while optimizing the cost and benefit, to increase the quality of life of citizens, in terms of power efficiency, transportation, safety and security [2].

The urban population has been increasing rapidly in most of the developed and developing countries, including Malaysia [3]. And this results in the problem of overwhelming number of vehicles, faced by the populated urban region. However, public transport system is not well-organized in Malaysia and this would cause a higher possibility that people who need to travel frequently will have to own a car for convenience [4]. As the number of registered vehicles increases in Malaysia, especially in the urban area, the problem faced by the mass in traffic congestion and lack of parking spaces are getting more serious. Being difficult in seeking a vacant parking space has been a common issue in some frequently-visited places such as shopping malls and office buildings. This problem could be worsen during peak hours, for instance, in the case of shopping malls during weekend and holiday seasons. Other than wasting time, fuel energy is also wasted when one needs to drive around to look for vacant parking space in the parking lot. Although there are parking-assisting system, which provides real-time information about the parking spaces, there is still room for further improvement. In order to cope with this issues, smart city parking system which provides automated parking service offers the greatest convenience and experience to the drivers, and a better operating system of the parking management.

The Smart City Automated Parking System proposed in this paper is designed to arrange and park the cars with the automated platforms, which minimize the energy and time required to move the cars, and establish a connection between the users and the system. A mobile application was developed so as the users will receive a notification message when the car is parked, and it can also be used to call for the car to be transported to the pick-up point. This aims to reduce the energy and time consumed to seek a vacant parking space in the parking facilities, as well as to optimize the parking facilities space usage and ease the management of the parking system.

II. METHODOLOGY

A. MySQL Database Server

A database server was created for the access of the automated parking system, the users' mobile application and the Windows application. The MySQL database was created using Xampp and phpMyAdmin. Five tables were created in total for the overall process: *users, admin, userpassword, parking*, and *records*. The *users* table was created to store the details of the users, including their first name, last name and email address. The *admin* table was developed to store the admin account and its password for the access of the Windows application which could only be accessed for monitoring purposes by the management team. The *userpassword* table was used to store the users' account and their password which is to be referred for the login function. The *parking* table stored the data of the parking facilities including their status, whether vacant or not. Lastly, the

records table recorded all the users' activities related to the parking facilities and the time of the particular activities occurred. The host computer of the database thus served as a server in this system.

B. Android Mobile Application

An end-user Android mobile application was developed to directly connect the users to the parking system. The users would be updated by the real-time information of all the parking facilities through the mobile application. A parking availability function was designed for the users to check the parking facilities availability. The mobile application also allowed the users to park the vehicle in the parking facilities using the mobile application. The mobile application was developed using Android Studio software. In the application code, it stored the IP address of the server, which is the host computer of the database. When the mobile application called for a particular function, it would access to the PHP script saved in the server and execute the SQL statement written in the PHP script. For instance, INSERT statement would be executed when a new row is to be added into the database table and UPDATE statement would be executed when a status is to be updated in the database table. In the mobile application, several activities were designed for different interfaces in the mobile application for different functions.

C. Windows Management Application

A Windows application was developed for the management purpose which enables monitoring of the system and database. The application was designed to carry out three main functions: users-viewing, parking-facilities-viewing, and record-viewing. The database was linked to the application by setting the database as the binding source of the application. When the application was used to view the data, the application would access to the database via the connection obtained by the binding source. The database would be accessed as well in the search function of the different pages.

III. RESULTS

In this project, an android mobile application and a Windows form application were developed in order to work at the user-end and the management end in the Smart City Automated Parking System.

A. Android Mobile Application

An android mobile application was developed to make the overall procedure of parking the vehicle into the automated parking system easier and faster. At the first interface of the mobile application, the log-in page would request for the username and password. Otherwise, the users would have to register for a new account in order to continue using the service.

The number of remaining vacant parking space could be viewed for all the parking facilities. For this project, 2 different parking facilities were created as shown in Figure 1.

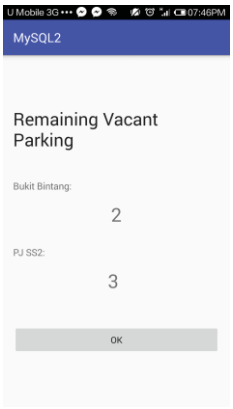

Fig 1. The interface of the Android application showing the remaining available parking spaces in different parking facilities.

For the parking service, the mobile application would request for an operation code which would be shown by a terminal in the parking facilities. After the automated parking service started, the application would enter an interface that would display the starting parking time and current time as shown in Fig 2. This information would help the users to easily estimate the duration of the parking service. In this interface, the users could also end the parking service. When the retrieving function was activated in mobile application, other than sending the instruction to the system, the mobile application would also update the status of the corresponding parking space to "Occupied" from "Empty".

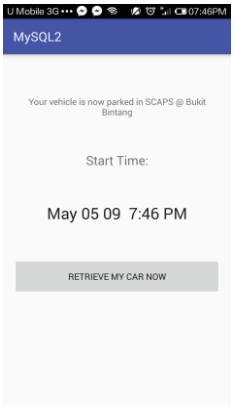

Fig 2. The interface of the Android application showing the starting time of the parking service

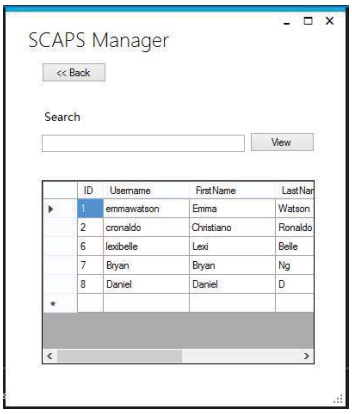

Fig 3. The user-viewing function allows the admin the view the details of all the users and search for desired result.

B. *Windows Form Application*

The application started from a login page which only reads the username and password keyed in and compares in the database and finds if there is any matching pairs. If the username and password matched, the admin were allowed to enter to the next interface. The interface allowed the admin to choose among the three main functions, which are the users viewing, parking spaces viewing and records viewing as shown in Fig 5.

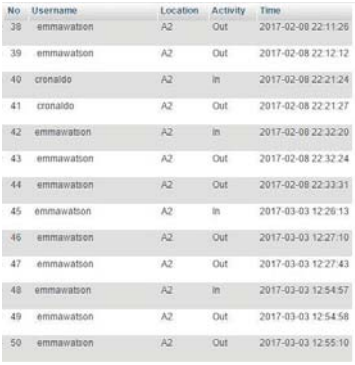

Fig 4. The records of the users using the parking services are recorded in the database and can be viewed for the monitoring purposes by using the developed Windows application.

Fig 5. The three main functions of the Windows Form application are the users-viewing, parking facilities status-viewing, and records viewing.

In both the records-viewing and users-viewing functions, search function was designed to allow the admin to find the desired result in the shortest time as shown in Fig 3. By entering the keyword, the application compared the keyword and all the relevant details of the users and displayed the shortlisted result. In the parking facilities status-viewing function, the admin can select only the parking facilities that he/she wish to view.

IV. Discussions

Via the mobile application developed, the users could always be updated with the parking availability before parking and also the current parking duration when they are using the parking service. After registering as a new users, the user's details needed to be stored in the user database and the user then could log in using the new user account.

There were 2 main services provided by the mobile application: the parking availability checking and the parking service. The parking availability checking enabled the users to check the availability of each parking facilities before heading to that area so that they could plan their journey better.

The mobile application would request for an operation code which would be shown by a terminal in the parking facilities for the parking service. This procedure was designed to ensure that the users are in the correct automated platform of the parking facilities. If the entered operation code matched one of it of the vacant parking spaces, the automated parking operation began.

The Windows form application was developed for the management purpose which enables the management officers to monitor and manage the users account, parking facilities and the records of the parking services used by all the users.

When any function was chosen, the application would access to the database and display the desired result in the data grid. By entering the keyword, the application compared the information and keyword and displayed the shortlisted result.

In the overall operation of the parking system, operation code system is applied in order to ensure that there is no mistake for the users to clearly state which automated platform the vehicle is on. For future development, the operation code can be replaced by QR code to ease the procedure and to reduce the possibilities of errors. The users can just scan the QR code shown in the mobile application using the built-in QR code scanner in the mobile application. The mobile application should be able to interpret the QR code and get to know which automated platform is in operation.

After the users park the vehicle, the starting time of the parking service is shown in the interface. For future improvement, the feature showing the current duration of parking service and the current parking fees can be added.

Payment function can also be added so that the users can proceed to the online payment function after they end the parking service. Online payment service makes the overall system more convenient. The membership function may be applied as well for more convenience.

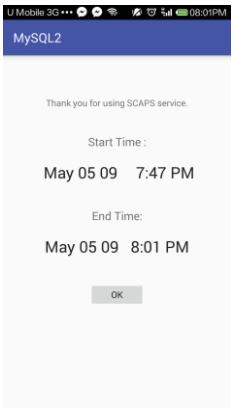

Fig 6. The interface of the Android application showing the starting time and the end time of the parking service.

For the Windows management application, the function of surveillance camera monitoring can be added into the application as well so that the overall monitoring of the parking facilities can be done by using only one software.

V. Conclusion

The IoT part of the Smart City Automated Parking System is successfully developed. It is able to work closely with the automated system as a server of the overall system. The time spent and fuel wasted in the parking spaces seeking process can be reduced by implementing the system.

References

[1] Parishwad, O. and Singh, T., 2014. Analysing and Rating Smart City Development in India. Journal of Civil Engineering and Environmental Technology (JCEET), p.54.

[2] Kyriazis, D., Varvarigou, T., White, D., Rossi, A. and Cooper, J., 2013, June. Sustainable smart city IoT applications: Heat and electricity management & Eco-conscious cruise control for public transportation. In World of Wireless, Mobile and Multimedia Networks (WoWMoM), 2013 IEEE 14th International Symposium and Workshops on a (pp. 1-5). IEEE.

[3] Idris, M.Y.I., Tamil, E.M., Noor, N.M., Razak, Z. and Fong, K.W., 2009. Parking guidance system utilizing wireless sensor network and ultrasonic sensor. Information Technology Journal, 8(2), pp.138-146.

[4] Nurdden, A., Rahmat, R.A.O.K. and Ismail, A., 2007. Effect of transportation policies on modal shift from private car to public transport in Malaysia.Journal of applied Sciences, 7(7), pp.1013-1018.

[5] R. Lu, X. Lin, H. Zhu and X. Shen, "SPARK: A New VANET-based Smart Parking Scheme for Large Parking Lots," in Proceedings of IEEE INFOCOM'07, 2007.

[6] Wang, H. and He, W., 2011, April. A reservation-based smart parking system. In Computer Communications Workshops (INFOCOM WKSHPS), 2011 IEEE Conference on (pp. 690-695). IEEE.

[7] Shaheen, S.A., C.J. Rodier and A.M. Eaken, 2005. Smart parking management field test: A bay area rapid transit (bart) district parking demonstration. http://pubs.its.ucdavis.edu/download_pdf.php?id=44.

[8] Chinrungrueng, J., U. Sunantachaikul and S. Triamlumlerd, 2007. Smart parking: An application of optical wireless sensor network. Proceedings of the International Symposium on Applications and the Internet Workshops, January 15-19, 2007, Hiroshima, pp: 66-69.

[9] Nam, T. and Pardo, T.A., 2011, June. Conceptualizing smart city with dimensions of technology, people, and institutions. In Proceedings of the 12th Annual International Digital Government Research Conference: Digital Government Innovation in Challenging Times (pp. 282-291). ACM

[10] Zanella, A., Bui, N., Castellani, A., Vangelista, L. and Zorzi, M., 2014. Internet of things for smart cities. IEEE Internet of Things Journal, 1(1), pp.22-32.

[11] 11. Su, K., Li, J. and Fu, H., 2011, September. Smart city and the applications. In Electronics, Communications and Control (ICECC), 2011 International Conference on (pp. 1028-1031). IEEE

[12] Bushro B.A., 2014, June. Interactive car parking system. UTM.

[13] Hanif, N.H.H.M., Badiozaman, M.H. and Daud, H., 2010, June. Smart parking reservation system using short message services (SMS). In Intelligent and Advanced Systems (ICIAS), 2010 International Conference on(pp. 1-5). IEEE.

[14] Polycarpou, E., Lambrinos, L. and Protopapadakis, E., 2013, June. Smart parking solutions for urban areas. In World of Wireless, Mobile and Multimedia Networks (WoWMoM), 2013 IEEE 14th International Symposium and Workshops on a (pp. 1-6). IEEE.

[15] Norasmawani N., 2015. Smart Parking System With Indoor Navigation. UTM.

[16] Alliance, O.H., 2011. Android overview. Open Handset Alliance.

[17] Elgin, Ben, 2005. "Google Buys Android for Its Mobile Arsenal". Bloomberg Businessweek. Bloomberg. Retrieved February 20, 2012.

[18] "Android NDK Native APIs". developer.android.com. Retrieved June 10, 2015. "The Android NDK provides a set of native headers and shared library files that has gradually increased with successive releases of new Android API levels."

Development of Automatic Test Pattern Generation

Tang Soon Loong
Faculty of Electrical Engineering
UniversitiTeknologi Malaysia
Johor Bahru, Malaysia.
soonloong93@hotmail.com

Norlina binti Paraman
Department of Electronic & Computer Engineering
Faculty of Electrical Engineering
UniversitiTeknologi Malaysia
Johor Bahru, Malaysia.
pnorlina@utm.my

***Abstract*— This paper proposes the algorithm of automatic test pattern generation (ATPG). The main purpose of this work is to develop a simple and fast ATPG tool in order to detect any stuck-at fault in logic circuit. This can be achieved by implementing PODEM algorithm and D algorithm into the system to generate test patterns which are able to expose the particular stuck-at fault. To develop this ATPG tool, C++ programming language will be used with an Integrated Development Environment (IDE) software in order to build and debug it. The system requires a circuit file and will undergo several process such as circuit levelization, fault collapsing and forward implication to obtain the correct test pattern for every fault. The main outcome of this ATPG tool is to generate test pattern for all stuck-at fault and compute fault coverage for a circuit. Therefore, this ATPG tool is useful it is a simple, fast and cost efficient test generation software.**

Keywords—PODEM, fault, algorithm, circuit, pattern, tool

I. INTRODUCTION

Automatic Test Pattern Generator (ATPG) is an automated electronic design technology that is used to generate test pattern to test a digital circuit. The generated test pattern enables automatic test equipment to differentiate between the actual circuit behavior and the faulty circuit behavior by observe the output from the circuit [1]. There are two main types of ATPG which are combinational ATPG and sequential ATPG. Combinational ATPG method allows testing the logic circuit without flip-flops with only requires one test pattern for a test. In the other hand, sequential ATPG method is used mostly in logic circuit with flip-flops and it searches for a sequences of test pattern to expose certain fault in the faulty circuit. Due to the present of memory element, the difficulty in controlling and observing the internal signal of a sequential circuit is higher than combinational circuit.

Besides that, there are some cases that ATPG unable to generate a test for a particular fault [2]. This happens when the fault may be undetectable intrinsically and thus no test pattern is able to detect that fault. The next possible case is a test pattern that expose the fault exists but ATPG algorithm fails to find it. Overall, the effectiveness of ATPG system is determine by the number of faults that it can detect in a faulty circuit, the number of generated test pattern and the fault coverage of the circuit.

Nowadays, there are many kinds of ATPG tools can be found in the market. Some open source tools are available for public to freely download but the functions of it are limited. On the other hand, some ATPG tools requires the user to pay and purchase the license for certain time period which is very costly for the user. Conventionally, test vector can only be found by performing algorithmic method to the faulty circuit and analyses manually. However, this will take some times to analyze the faulty circuit and find the suitable test pattern to detect fault.

Therefore, the objective of this study is to develop acomplete ATPGsystem. It is able to generate test pattern which can expose stuck-at fault, determine the number of fault in a circuit and compute the fault coverage. This ATPG system will also help to reduce the time consume to generate test pattern for faulty circuit.

In addition, this project will involve programming part which requires C++ programming language to develop the ATPG tool. This programming language is a general-purpose language and it is widely used in desktop application, servers and many other applications. The most important feature is object-oriented programming feature which allow programmer to create different classes in a software. Therefore, it is one of the programming language that is suitable to develop this ATPG system.

II. LITERATURE REVIEW

In digital very-large-scale integration (VLSI) testing, ATPG plays an important role in detect and expose fault in a circuit [3]. There are two different test that can be perform on a circuit which are structural test and functional test. Generally, structural test is used on ATPG because of the performance of it is higher than functional test. Besides that, algorithm for ATPG is important in order for the ATPG to generate test pattern for combinational logic circuit. Test pattern which are produced are applied to the primary input and the effects will be observed from the primary output of the circuit. Hence, two most known algorithms for combinational circuit are D algorithm and PODEM algorithm are further studied and implemented in ATPG.

In the world of digital, Boolean algebra comprise of logic 0 and 1 is used to represent and study the behavior of digital circuit. Previously, two copies of circuit which are good circuit and faulty circuit are analyzed to determine the behavior of the circuit [2]. This is not efficient and impractical since two copies of circuit is required for each fault in the circuit.

Therefore, Multi-valued algebras is introduced to solve the previous issue [1]. It uses special symbol to represent the logic level of both good circuit and faulty circuit. There are 2 types of notation in ATPG algebra that are Roth's Algebra and Muth's Addition. Roth's Algebra is commonly used in combinational

ATPG while Muth's Addition is applied in sequential ATPG. Moreover, both algebras utilized two logic values to represent good and faulty circuit where first value is logic value of good circuit and second value is logic value of faulty circuit.

In these algebras, there are three notations are introduced to represent the condition of the circuit namely, D, $\overline{D}$, and X. The alternative representation for D is 1/0. This means that the logic value of line is 1 in normal condition and 0 when the fault is present in the circuit [3]. Similarly, $\overline{D}$ can be represented with 0/1 where logic value 0 for normal circuit condition and 1 for faulty circuit condition. Besides that, X is used to represent the situation when the logic value of both normal and faulty circuit are unknown. Thus, it is computationally faster to represent logic level for both circuit in algebras, rather than one of them at a time.

TABLE I. MULTI-VALUE ALGEBRA

Symbol	Alternative Representation	Fault-free circuit	Faulty Circuit	
D	1/0	1	0	Roth's Algebra
$\overline{D}$	0/1	0	1	
0	0/0	0	0	
1	1/1	1	1	
X	X/X	X	X	
G0	0/X	0	X	Muth's Addition
G1	1/X	1	X	
F0	X/0	X	0	
F1	X/1	X	1	

There are several previous study which had been done by other researcher. One of the study is improved path sensitizing method in test pattern generation by Chuan Wang Chang. He stated that his method accelerates any path sensitizing when propagate the fault to the primary output [4]. This is done by propagate the stuck-at fault on a stem which is a fan-out node to its respective fan-out branches and desensitizing one or more input lines of a reconvergent gate when the particular fault unable to propagate through the gate. The advantage of this method is it will reduces the time taken to generate test pattern while the disadvantage is it will not perform well when the circuit has too many fan-out branches. Another ATPG study is a SAT-based ATPG system done by Huan Chen [5]. His idea is based on modern Boolean Satisfiability (SAT) method and implement on ATPG to optimize the ATPG system. His system integrates different fundamental models which consists of Fault Database, SAT-based ATPG Engine and Structural ATPG Engine. The advantages of his system is less time required for test generation while disadvantage is it is platform dependent. Prof. Dong S. Ha proposed ATALANTA test pattern generation [6]. The method implemented FAN algorithm and parallel pattern fault propagation technique for fault simulation to the ATPG system. The advantage of his system is it can be used for test pattern generation and fault simulation while the disadvantage is it cannot be applied on the sequential circuit.

III. RESEARCH METHODOLOGY

Generally, this project is divided into 2 main parts to make sure the troubleshoot process and development of software proceed in an order manner. The first part of the project is compile and build the automatic test pattern generation tool into a command line program. After that, the next part is to generate a result file which contains all the outputs after a circuit is simulated by the program. Users will be able to view the information of circuit and every test pattern generated for each fault in that circuit from the result file.

A. Overall Project Flow

The overall design of this project can be split into 2 important stages that are test pattern generation and file generation. The first stage which is test pattern generation is mainly focus on generate test pattern and obtain the fault coverage for a gate-level circuit. In the other hand, the second stage which is file generation. It focus on generate an output file which contains every test pattern and information of a circuit.

The first stage starts when the system receives gate level netlist as input. The netlist file will be open and read by the system. Next, it will perform D algorithm and PODEM algorithm on the circuit. After performing the algorithms, test patterns will be generated by the system. The generated test pattern will detect most of the stuck-at fault in a circuit.

The second stage begins after test pattern is generated from the first stage. Then, the program will create a text file and write all the generated test pattern and the percentage of fault coverage to the file. The result file is then save into the computer at the same directory as the ATPG program.

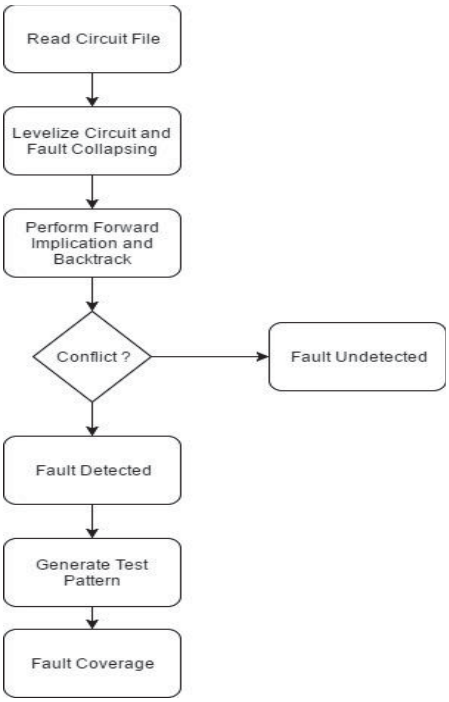

Fig. 1: Proposed methodology

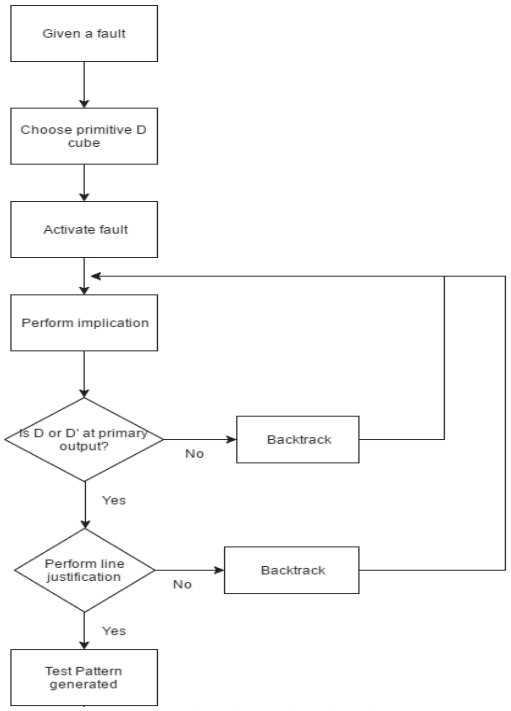

Fig. 2: Flowchart of D algorithm

B. D algorithm

Besides that, D algorithm will be covered in this project and this algorithm uses Muth's algebra. Firstly, a specific stuck at fault will be given in the circuit either it is stuck-at 0 or stuck-at 1 fault. After that, a primitive D-cubes which are singular covers with multiple value algebra will be selected based on the D-cube table. This is important in fault propagation and forward implication.

Next, stuck-at fault at fault site is activated with a logic value that is opposite of the fault circuit. This is normally done to trigger the stuck-at fault and is known as fault activation. It is then followed by forward implication process. This process is executed to determine the gate output value according to the input value. It is can be done by referring to the lookup table of logic gate. The primary output will be observed to check whether the fault is successfully propagated to output or not. If the fault is not observed at the primary output, the system will backtrack to perform forward implication and assignment different logic value to the particular line.

After the fault has successfully driven to the primary output, line implication will be performed. It will determine all unassigned gate input for specified output. This process is can be done by referring the logic gate lookup table. If there is any conflict happens, it will backtrack to perform forward implication again and change the logic value of the line. After line implication is complete, a test pattern will be generated by the system that can expose the given fault. The generated test pattern will be then feed into a fault simulator.

C. PODEM algorithm

PODEM algorithm limits its search space only to primary input of the circuit. The primary objective of the algorithm is to sensitize the fault and propagate it to the primary output. Once the fault is sensitized, the next objective is changed in order to propagate the selected fault to a primary output of the circuit. Forward implication is used in next step to determine the output of logic gate based on its input. This is performed to propagate the fault to primary output. Another function which is known as backtrace will be executed after that to determine one of the values of primary input. For every primary input that is assigned, logic simulation is performed to check for two conditions that are disappearance of fault propagation path which is also known as X-PATH CHECK and desensitization of the fault in the circuit. When one of the two condition stated above is breached, the program will backtracks and changes the logic value assigned to the most recent primary input. This process of assigning logic values to primary input is repeated till all primary inputs form a valid test pattern or no more combinations of primary input are possible. If there are no test pattern can be generated for the fault, the fault is considered as untestable fault.

IV. RESULT AND DISCUSSION

A. Result

This ATPG program requires a circuit file as an input for it to simulate. The circuit file must be written in .ckt format and the circuit diagram is shown in Figure 3. Every line on the circuit is assigned with different number by user so that it will be easier for the program to analyze it. The circuit file will be opened and read by the program after the program is initialized. To start the

program, users have to enter "podem [circuit filename]" at the command prompt window as shown in Figure 4.

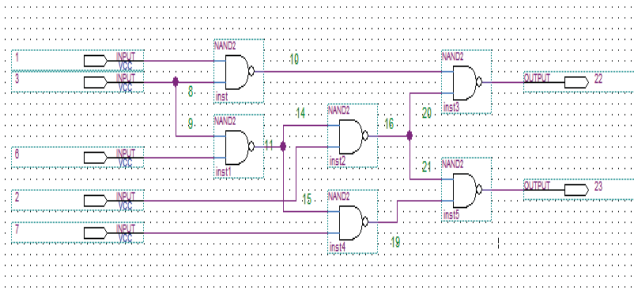

Fig. 3: Circuit diagram

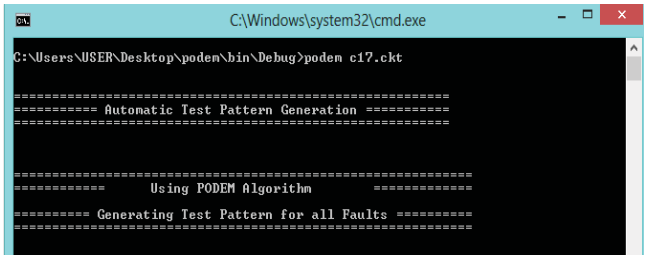

Fig. 4: Command line for program initialization

After the circuit is successfully analyzed by the program, it will produce a simulation result on the command prompt window. Figure 5 shows the simulation result after the circuit file is successfully analyzed. It can be seen that there are total of 33 test patterns generated for the circuit and the fault coverage is 97.0588%.

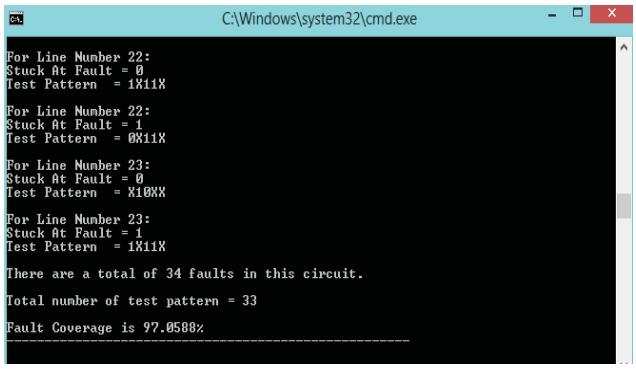

Fig. 5: Simulation result of ATPG

Besides that, the program will also display the circuit information such primary input, primary output, line number, line type and gate input as Figure 6. The line type will determine whether it is a primary input, branch or gate output. For line type number representation, 0 represent primary input, 1 represent branch while 6 represent NAND gate output.

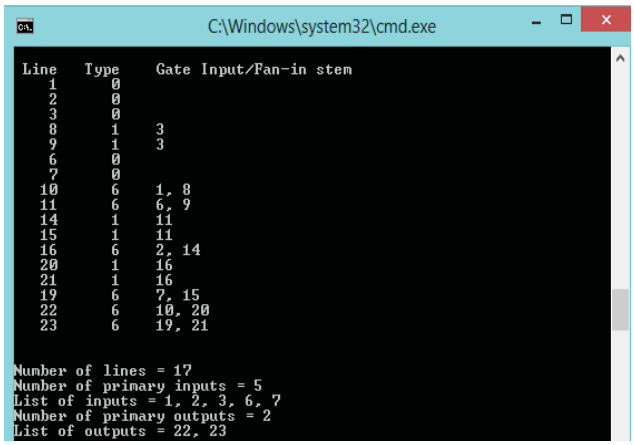

Fig. 6: Circuit information

After that, it will also generate a text file named reportFile.txt after the simulation process is completed. The generated file contains information such as test pattern for every fault, number of line, number of input and output, total number of faults and fault coverage of the circuit. Users are able to view the generated file and store it in everywhere for future use.

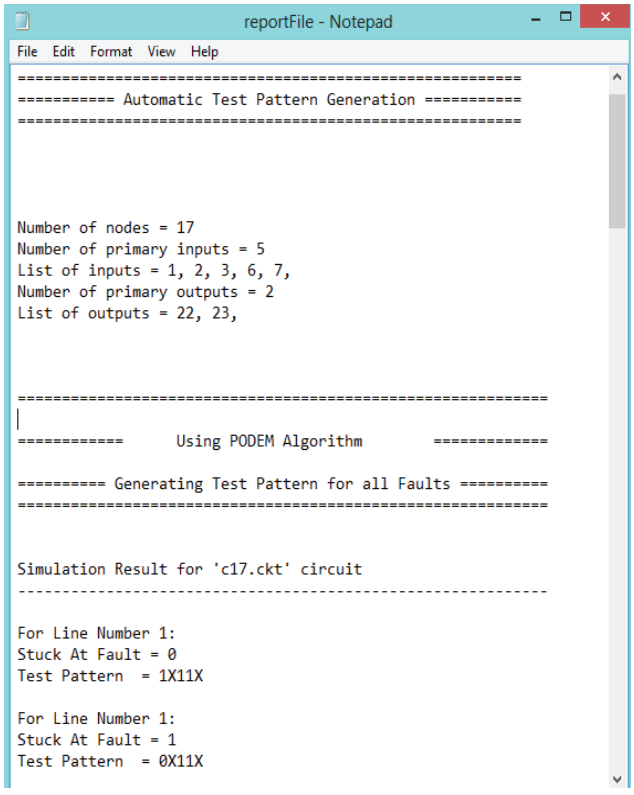

Fig. 7: Result of Text File

In addition, users can also obtain the fault coverage and total number of fault in a circuit from the text file. From Figure 8, there is a stuck-at 1 fault at line 21 which are undetected by the program and test pattern cannot be generated for that particular fault. This is due to the particular fault cannot be propagated to primary output of circuit.

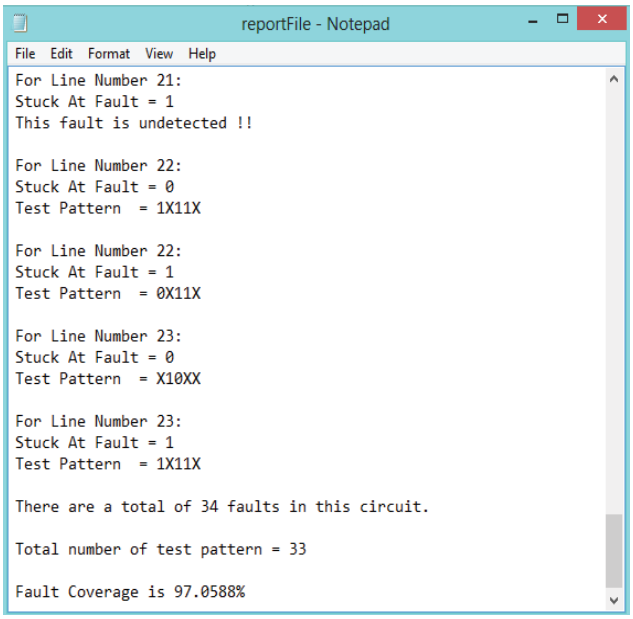

Fig. 8: Result of fault coverage

B. *Missing circuit file condition*

There are two conditions where the ATPG program will not functioned correctly. The first condition is when the circuit file is not included in the input command of the program. This cause the program unable to start because it does not have a circuit file to simulate. The program will display a format error as in Figure 9 when this condition happens.

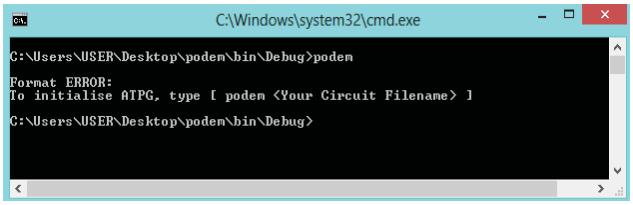

Fig. 9: Error when circuit file not included

The other condition is when the circuit file that is entered in the command does not match the file name in the directory. This cause the program unable to search the particular circuit file in the directory. Therefore, it will show an error as in Figure 10.

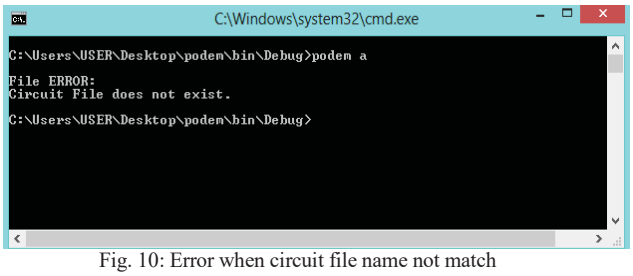

Fig. 10: Error when circuit file name not match

V. CONCLUSION

In a nutshell, gate level ATPG is developed in order to generate test pattern, perform fault simulation and determine fault coverage of a circuit. It is also helps in reducing the time consume to generate test pattern and save cost. In addition, the concept of D algorithm and PODEM algorithm are used in this project while C++ programming language is used to build the ATPG tool. The development of ATPG has brought many benefits and solve various issue in testing of IC. Therefore, ATPG tools is very important to improve the effectiveness of VLSI circuit testing.

REFERENCES

[1] Laung-Terng Wang, Cheng-Wen Wu, Xiaoqing Wen. *VLSI Test Principles and Architectures*. Elsevier. 2006.

[2] Michael L. Bushnell and Vishwani D. Agrawal. *Essentials of Electronic Testing for Digital, Memory & Mixed-Signal VLSI Circuits.* Kluwer Academic Publishers. 2000.

[3] Tom Kirkland and M.Ray Mercer. *Algorithms for Automatic Test Pattern Generation*. IEEE Transactions Design and Test of Computers, vol. 5, no. 3, pp. 43-55, 1988.

[4] Chuan-Wang Chang and Shie-Jue Lee. *An Improved Path Sensitization Method in Test Pattern Generation for Combinational Circuits*. National Sun Yat-Sen University; 1995.

[5] Huan Chen and Joao Marques-Silva (2012). *TG-Pro: A SAT-based ATPG System*. Journal on Satisfiability, Boolean Modeling and Computation 8, 83-88.

[6] H. K. Lee and D. S. Ha. *Atalanta: An efficient ATPG for combinational circuits*. Technical report, 93-12, DEE, Virginia Polytechnic Insitute and State Univ.; 1993.

[7] Miron Abramovici, Melvin A. Breuer and Arthur D. Friedman. *Digital Systems Testing and Testable Design*. John Wiley & Sons. 1990.

[8] Mark Lee. C++ Programming for the Absolute Beginner 2nd Edition. *Cengage Learning PTR*. 2009.

[9] John Sunwoo, Vishwani D. Agrawal. *A New ATPG Algorithm for 21st Century: The Simplest But Powerful.* Auburn University; 2001.

[10] U. Gliser and H.T. Vierhaus. *MILEF: An Efficient Approach to Mixed Level Automatic Test Pattern Generation*. German National Research Center for Computer Science; 1992.

[11] P. Goel. *An Implicit Enumeration Algortihm to Generate Test for Combinational Logic Circuit*. IEEE Trans. Comput., vol. C-30, pp. 215-222, 1981.

[12] M. H. Schulz, E. Trischler, T. M. Sarfer. *SOCRATES: A Highly Efficient ATPG System.* EEE Trans. CAD, vol. 7, pp. 126-137, Jan. 1988.

[13] CodeBlocks Manual. Retrieved from CodeBlocks website: http://www.codeblocks.org/home

[14] T. Larrabee. *Test pattern generation using Boolean satisfiability*. IEEE Transactions on Computer-Aided Design of Integrated Circuits and Systems, 11(1):4–15, 1992.

pH Monitoring for Arowana Fish

Muhammad Azmel Bin Jamaludin
Faculty of Electrical Engineering
Universiti Teknologi Malaysia
81310, UTM Johor Bahru, Johor, Malaysia.
Email: muhammadazmel94@gmail.com

Dr Norlaili Mat Safri
Department of Electronic & Computer Engineering
Faculty of Electrical Engineering
Universiti Teknologi Malaysia
81310, UTM Johor Bahru, Johor, Malaysia.
Email: norlaili@utm.my

Abstract*— Portable pH sensor are currently use for fishery system. Fish keeper needed a pH sensor to know the pH value for water either good quality or not. Ion-Sensitive Field-Effect Transistor (ISFET) is one type of the potentiometric sensors which is broadly used for pH detection. ISFET sensor used as part of a portable pH sensor monitoring. Water quality plays an important role on production and healthy of fish. Thus, the fish keeper need to recognize how to keep the water in good quality. Objective of this project was to continuously monitor pH of water in fish tank or aquarium and to alert user of water pH condition. The pH value is displayed by using LCD and out of specification specified, the system will send an alert message to fish keeper. This project aims at improving awareness of water quality even when user is not around near the fish water tank.

Keywords*— ISFET biosensor, Readout circuit, Vsense, Output Voltage.

I. INTRODUCTION

Arowana fish or sometimes called dragon fish is kind of expensive and super popular fish amongst the fish aquarium community due to its prehistoric cosmetic appearance. Arowana fish need to be more attention cause by there are carnivores, through will generally eat anything that are nearby it. The arowana eating habits produce a lot of waste [1]. Thus, fish keeper need to pay extra attention to water conditions (Ammonia, Nitrite, Nitrate). Changing about 25% to 33% of the week is advisable, or better yet, 20% twice a week [1]. Observe about pH ranges that are suitable for them which is 6.5-7.5. Ion-sensitive field-effect transistor (ISFET) has been introduced by Dr. Piet Bergveld in 1970 for measuring ions concentration in a solution. ISFET biosensor are widely use in detection of chemical and biosensor and have strength creation to provide ISFET mass expenditures which of low cost, light weight, small size and fast response time. The portable device for fish tank consisting ISFET biosensor, readout circuit, microcontroller, LED, display unit and GSM module. Readout circuit function to amplify the voltage output that produce by the biosensor. Next, Arduino Uno as microcontroller; to change the analog signal to digital signal for display unit which is LCD display and lastly an alert system which it will send message to fish keeper by using GSM module. Arduino will convert the voltage signal from readout circuit to exactly pH value in LCD display. The LED will operate in case of pH value are not in particular range for Arowana fish. If pH value are suitable for Arowana fish, LED green will light up and otherwise is LED red will light up as an indicator of danger.

II. BACKGROUND AND PROBLEM STATEMENT

In order to develop the pH monitoring for Arowana, it is important to understand the portable ion-sensitive field-effect transistor based biosensor, Arowana fish and ammonia conversion characteristics in a closed recirculating aquaculture system which has been chosen for the main purpose of this studies.

A. Portable Ion-Sensitive Field-Effect Transistor Based Biosensor.

Ion-sensitive field-effect transistor (ISFET) as a sensor for pH detection due to its capability which is enables direct electrical measurement without using any other chemical labels or additives [2]. Thus, Ion selective membrane of the ISFET is used to trap the ions for example hydrogen or hydroxide and the interfacial potential changes at the gate insulator will produce the output either in current or voltage value.

ISFET is any of label-free potentiometric biosensor applications particularly for detection of pH value. They are applied to measure the concentration of hydrogen ions contained within solution and the measurement using the interface potential of on the gate insulator. ISFETs also been used in the detection of chemical and biosensors. ISFET sensor is based on the modification and combination of three systems. The system is sensitive ion electrodes (ISE), pH indicator strips and optical sensors. Modification all three elements has strength creation to provide such ISFET mass expenditures which of low-cost, light weight, small size and fast response time. Since the fabrication is in direct proportion standards of Metal Oxide Semiconductor (MOS) technology, but it is also low output impedance, high-speed signals, distributed sensing, the possibility of multiplexing and temperature compensation [4].

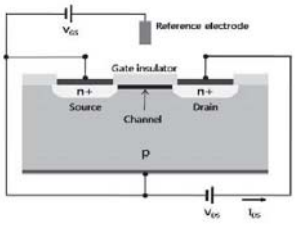

Fig. 1. Schematic of ISFET

Figure above show that how ISFET operated based on field-effect transistor (FET) working principle and its structure is similarly to the Metal Oxide Semiconductor (MOS) FET. Ion-selective membrane, electrolyte and a reference electrode is replaced with the metal gate. Biomolecules which is ionic charges will produce a potential difference between source when interaction with gate insulator and it will create an inversion layer in a channel [2].

The flow of electron from source to drain and it can generate current. If positive voltage is applied on the gate, the positive charges which is free holes will repel from the region of substrate under the gate. Next it will become far from carrier-depletion region. When the neutralizing holes are going down substrate will make these charges can move freely [2].

B. Arowana Fish

Arowana fish can be a great species because it is bigger than other. Certain varieties can be grow up to about four feet long. They also comes from primitive origins (Jurassic Age), and certain varieties are nicknamed 'Bony Tongued Fish' [1]. Arowana fish are kind of carnivores species that it will eat anything that nearby from it. So Arowana fish should be fed maybe 3 times a day and must ensure prepare an important balanced diet just like for most other fish.

The eating habit of Arowana fish produce many of byproducts of organic waste which is Ammonia, Nitrite and Nitrate that are breaking down the water conditions. Thus, fish keeper need to pay extra attention due to this scenario and keep maintain the pH ranges that are suggested for these species. A cold temperature might be kill them.

A good healthy Arowana fish can be grow up to at least 24 to 30 inches [1]. Other species can become bigger which 48 inches in wild. Arowana fish might be able to live for many years and well care it can be up until more than 20 years. If keeping aquarium temperature towards the lower end, they may look young longer than they would in higher temperature. Need to pay particular attention to each Arowana fish's needs below.

C. Ammonia Conversion Characteristics in a Closed Recirculating Aquaculture System.

In the recirculating aquaculture system (RAS), Nitrification and denitrification were commonly used to decrease the ammonia and nitrate concentration. If the aquaculture system not operate properly, two kinds of bacteria will showed up due to the increasing of nitrification activity [3].

The two of bacteria are ammonium-oxiziding bacteria (AOB) and nitrite-oxidizing bacteria (NOB). The research prove that this ammonia conversion in a closed recirculating aquaculture system which is nitrification and aerobic denitrification can nicely in aerobic and low chemical oxygen demand (COD) [3].

D. Statement of Problem

As Arowana fish is a kind of fish that require special care and the price of each of this species can go up to $300,000 [5], it is important for the owner of Arowana fish to make sure that their fish will stay healthy. In addition, Arowana fish can still be alive even though the owner are not around to look after their fish. Arowana fish needed a suitable pH for continuity of life and the most suitable pH for the fish is around 6.5 until 7.5. Arowana fish cannot live in acidity and alkaline water as the water in that pH can be poisoning for the pulmonary system of the fish. Hence, Arowana fish cannot breathing properly and can cause fatal where the fish can only live only up to 20 minutes.

In order to overcome the situation and to help the owner of Arowana fish, biosensors will be use as a tool to check the pH of the aquarium's water. Biosensor is a new electronic technologies that can detect different pH value where it can gives reading in term of voltage and biosensor had been widely use in detection of DNA, sequences of amino acids, nucleotides and living cell such as protein enzyme [6]. Labeling process such as chemical detections involves many procedure to be done and resulting time analysis to be longer. Meanwhile, optical method uses fluorescent dyes that are expensive and sometimes the test conducted can produce false-positive signals due to the perturbations in molecular interactions of label molecules. It is also require large sophisticated equipment for the detection and analysis process. In this project, the product will be fully developed by electrical based biosensor label-free which is ISFET sensor. ISFET sensor is portable, low cost, miniaturization, lightweight and suitable to be use in detection of pH application. As biomolecule contains different amount of ionic charges either positive charges or negative charges, it can be detected by the gate electrode and the induced voltage can be measure by an electronic readout device.

III. METHODOLOGY

This pH monitoring for Arowana fish consists of ISFET biosensor, readout circuit, microcontroller, display unit and GSM Module. Input for the sensor is a chemical sample. When a sample is sensed by the ISFET biosensor, it will produce an output voltage, VSENSE and this voltage is transferred to the electronic readout circuit. Output voltage from readout circuit, VOUT will be displayed on LCD panel and LED will show the either pH value more acidic or alkaline compare to ideal pH ranges that suitable for Arowana fish, which is programmed in Arduino microcontroller. There are software tools used in this project which is Arduino (microcontroller) for programming, display unit and GSM Module.

A. ISFET biosensor

This project used a WINSENSE ISFET pH Sensor (WIPS) product. ISFET sensor is suitable for this project because it can measure the voltage in solution that produced by the distribution of charge. It only uses a single power supply, inexpensive and

lightweight. The sensing element is the metal gate of ISFET which works with a reference electrode (RE) and a chemical solution.

B. Readout Circuit

In this project, readout circuitry is specifically used for obtaining and amplifying the sensed voltage from ISFET sensor. Readout circuit is compatible for any types of detector. The readout circuit for this project is a multistage amplifier as shown in Figure 3.4. This project uses three UA741 ICs and four resistors. First stage is the voltage follower (VO1) that has a unity gain (Av≈1). Second and third stages of amplifier are non-inverting amplifiers with the gain, AV of 1.25 and 1.5 respectively. Figure 2 shows the schematic of the readout circuit.

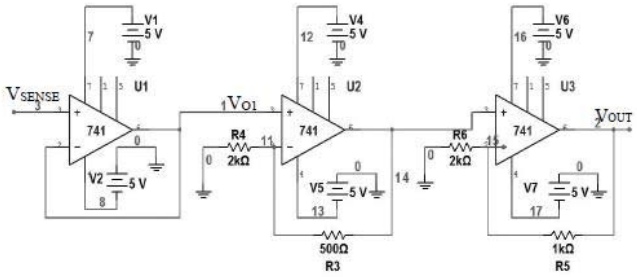

Fig. 2. Schematic Readout Circuit.

C. Microcontroller and Display Unit

Display unit consist of LED display and LCD. LCD display will show up the pH value of water conditions in fish tank for Arowana. Red LED means that the pH value to acidic from the safe zones for Arowana fish. Green LED indicate that pH value more than 7.5. The display is controlled by Arduino board that receive voltage signal from the readout circuit which than will be programming to be converted to digital display and lastly it will display pH value and other cases it will send message.

D. Power supply

In this project, the 5V power supply is built from the regulated power source by using LM7805 IC. LM7805 IC regulates the power supply from a battery of 9V. The noise that appears during the regulation can be reduced by adding a capacitor at the input and output nodes. Figure 3 shows the LM7805 regulator circuit.

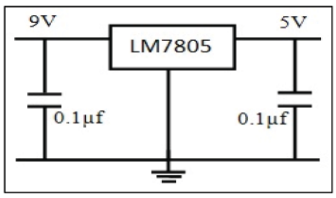

Fig. 3. LM7805 circuit diagram.

E. Display Unit

Display unit for this project consists of LCD and LED. LCD is to display the pH value whether it in range for Arowana fish or not. LED is to activate the light; red LED for acidity (pH< 6.5) and green LED is for alkaline (pH> 7.5). This display unit is controlled by Arduino board that receives a voltage signal from the sensor circuit which is being converted using Arduino programmable language code.

IV. Result and Discussion

This pH monitoring for Arowana project was built up and test. Important things in this project is to transfer the output voltage from ISFET biosensor and reference electrode form Winsense Kit (WIPS) to exact pH value at the end. The pH value will show at display unit and will be send message if pH value which can cause Arowana fish to die.

A. Hardware Measurement Winsense Kit

The Winsense kit consists ISFET, Reference Electrode (RE), read-out circuit box and certain buffer solutions. Three input signal terminals drain terminal (D), source terminal (S), and gate terminal (G) are connected to ISFET drain, source terminals and the RE, respectively. The read-out circuit box have 5 terminals which is V+, D, S, G, and ground (GND). Voltmeter has been used to measure the output signal across the 2 terminals: V+ and GND terminal.

The output signal has been collected for 3 testing buffer solution. Table 1 shows the data from this experiment. 3 buffer solutions which have pH value of 4, 7 and 10. The output range of Winsense Kit are 0-2 V. The voltage output from buffer solution are 727mV for buffer acid, 820mV for neutral and lastly 890mV for alkaline. The graph that shows in Figure 4 is about Vsense versus pH value. It shows when the solution is more alkaline, Vsense is increased and otherwise it will decreased.

TABLE I. DATA FROM WINSENSE KIT

pH value	Voltage (mV)
4	727
7	820
10	890

TABLE II. DATA FOR SENSOR CHARACTERISTIC

Element	pH value	Vsense (V)
Johnson nourishing body wash	5.5	3.427
Buffer solution	7.03	3.508
Handwash	9.5	3.672

B. Biosensing Measurement ISFET Sensor Characteristic

Result of Vsense (V) get from detection of ISFET portable device and Winsense Kit in Figure 5 below. It shows the higher

pH value, the higher Vsense. This result will be used to get equation of straight line.

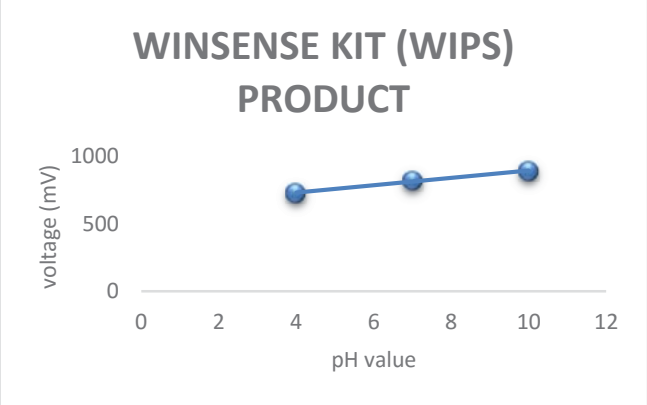

Fig. 4. Vsense versus pH value.

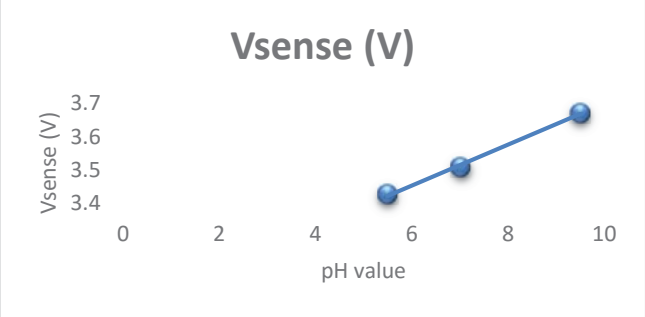

Fig. 5. E-coli Impedance Reading using Microelectrode Array Biosensor [2].

From the result, the sensitivity of ISFET can be calculated based on the formula 4 and 5. The data in the result will be plot to fitting curve with linear trend line and acquire the sensitivity from the graph. The sensitivity will be coded in the Arduino language programming for the device to work on the relevent range.

V. CONCLUSION

In nutshell, biosensor plays the crucial part in this project. . It only uses a single power supply, inexpensive and lightweight Biosensor is very efficient in detection, monitoring and analysis for biological molecules. Thus in this project, GSM module will help to develop as an alert system which it can send message to fish keeper in case of the pH value outrange of safe zones. In the future, ISFET can be used not only for pH detection but for many other specification of biosensor in one portable device.

ACKNOWLEDGEMENT

The authors would like to thank Fakulti Kejuruteraan Elektrik (FKE) for giving funding and providing a Final Year Project course for student to improve learning platform in research and development form from syllabus that was learned. Many thanks to Assoc. Prof. Dr Norlaili Binti Mat Safri as my final year project supervisor for her support, knowledge and guidance given from beginning until finish.

REFERENCES

[1] "Arowana Fish". *Aquaticcommunity.com*. N.p., 2017. Web. 14 May 2017.

[2] Rozina Abdul Rani and Othman Sidek, Member, IEEE, ISFET pH Sensor Characterization: towards Biosensor Microchip Application, School of Electric and Electronic Engineering Campus, Universiti Sains Malaysia, Malaysia,2004.

[3] Ammonia Conversion Characteristics in a Closed Recirculating Aquaculture System, Guang-Yu Wang (2009)

[4] Rozina Abdul Rani and Othman Sidek, Member, IEEE, ISFET pH Sensor Characterization: towards Biosensor Microchip Application, School of Electric and Electronic Engineering Campus, Universiti Sains Malaysia, Malaysia,2004.

[5] "This Fish Is Worth $300,000". *New York Post*. N.p., 2017. Web. 14 May 2017.

[6] O. Lazeka, F.J.D. Campo, F.X. Munoz,Pathogen Detection: a perspective of traditional methods and biosensors, Biosensor and Bioelectronic 22, 1205-1217,2007.

Fall Risk Analysis Among Elderly using Kinect Sensor

Liyana Syafiqah Jasni
Faculty of Electrical Engineering
Universiti Teknologi Malaysia
Johor Bahru, Malaysia.
liyanaajasni@gmail.com

Nor Aini Zakaria & Nasrul Humaimi Mahmood
Department of Electronic and Computer Engineering
Faculty of Electrical Engineering
Universiti Teknologi Malaysia
Johor Bahru, Malaysia.
norainiz@utm.my

***Abstract*— Elderly people have a high tendency to fall due to the lack of ability to walk, with limitations in bending and stability. The objective of this work is to determine the factors of fall risk of a person using a Kinect Sensor to track and capture the movements of a person by capturing the skeleton image of a human. In this work, a machine learning algorithm is used to produce and show the skeleton image of human body which utilizes Microsoft Kinect Sensor and MATLAB software to capture the movement's parameters of a person based on the joint coordinates obtained. There are 27 samples used to complete the Timed Up and Go (TUG) test, 20 of them are adults which aged between 23 years to 63 years old and another 7 are elderly people which aged more than 65 years old. The test is conducted based on the standard test procedure by using Kinect Sensor with the aid of MATLAB software, which is used to track and view the skeleton image of a person. The subject is classified as a faller if they complete the TUG test is more than 13.5 seconds. From the TUG test, the results indicated that the sensitivity and specificity are 54.55% and 87.50% respectively based on the truth and test result table. The fall risk factors are determined by the distance and the angle between the joints for non-fallers and fallers. The result of this work found that the joints angle are able to determine the factors of the fall risk of a person.**

Keywords*— Kinect Sensor, MATLAB, Timed Up and Go test, joints angle

I. INTRODUCTION

A *fall* was defined as any event that led to an unplanned, unexpected contact with a supporting surface [1]. Most of older people nowadays have a high tendency to fall but not because of they get older and falls is happened. Many possible causes older people might have such as a medical problem or disease. Furthermore, they also might had a history of fall or had been into an accident whether in serious or not. So, they will have a high risk factors that fall event is happened to them.

The second leading cause of accidental or unintentional injury death worldwide is falls [2]. This is due to the older people who have a high tendency to fall in order their balancing and how they walk is one of the fall risk factor where fall event can happen. Older people that more than 65 years old are suffer the greatest number of fatal falls and estimated 420 000 individuals die from falls in each year which over 80% are in low-and middle-income countries [2].

Moreover, the therapist used several test method to detect a fall risk of a person such as Sit-Stand Test, Timed Up and Go (TUG) Test, Walking Test and many methods that related to the walking test. From this test, the only result that can be obtained is the time duration of the patient takes to complete the test. Every test has been set their threshold time. If the patient exceed the threshold time, then a fall risk of a person is detected.

The TUG test is only help to show an event of the falling of a person with give a result by the time taken for a person to complete the test in seconds. Hence, this test is manually controlled by the user with using a stopwatch to record the time taken of the subject to complete the test. The Kinect Sensor is introduced to use for the classification and quantitative analysis between a faller and a non-faller. Otherwise, not only using TUG test method can determine the fall risk of a person, the function of Kinect Sensor device and MATLAB software also can use to obtain the data of joint coordinates from the skeleton image of a person that detected using Kinect Sensor and show the data in MATLAB.

The objectives of this work are to identify between faller and non-faller from the time taken of the subjects complete the TUG test in seconds, and to show and obtain the data of X, Y and Z joint coordinates of the subjects while doing TUG test from MATLAB and Kinect software. After the data is obtain, it is used to calculate the distance and the angle of joints between a fallers and non-fallers. Lastly, one of the objectives of this study is to help the therapist in rehabilitation purpose by detecting the factor that cause fall to happen.

There are 27 subjects to complete the test, 20 of them are adults which aged between 23 years to 63 years old and another 7 are elderly people which aged more than 65 years old. In addition, MATLAB software is used to run the source code to show the skeleton image of a person and obtain the data of joint coordinates of the subject from the Kinect Sensor while the subject doing TUG test until complete. Then, the result of the data that show in MATLAB is calculated and analyzed to find a fall risk factors by finding the distance and the angle of joints between a faller and non-faller.

II. LITERATURE REVIEW

There are many technologies and techniques that used to detect a fall of a person. One of the technologies that widely used is a wearable sensor such as accelerometer [3], where this device is used to detect a fall of a person. This device is attached to the part of human body to capture their movements and obtained the movement data [4]. Furthermore, this device could be measured

the acceleration of gravitational information [5]. When this device exceeds the specific threshold value, a fall of a person is detected. Moreover, accelerometer device are small in size, lightweight, cheap, and mobile. Besides, the person need to wear this device continuously to detect a fall event happen but sometimes the person had forgot to wear this device and a fall event cannot be detected [6].

Kinect Sensor is introduced where this device able to detect a 3D body movement of a person using its RGB, depth and infrared sensor that can recognize 20 point main body joints [7]. The infra-red LED, the depth camera is independent of illumination of lights and can work well in weak light condition even in a dark room [8]. Typical camera cannot determine the depth of the human body or skeleton tracking image. With the help of the depth camera, the distance from the top of the person to the floor can be simple calculated [9]. In addition, Kinect sensor generates a depth map in real time, where each pixel corresponds to an estimate of the distance between this device and the closet object in the scene at that location of the pixel [10]. Then, the map shows that the applications of the Kinect system will track the different parts of the body of a person accurately in 3D. Hence, Kinect Sensor device also used for gaming and entertainment that provided by the identity technology behind Microsoft's Kinect for the Xbox 360 by combining with multiple technologies based on the use of depth-sensing, RGB cameras, and careful user interaction design [11]. Besides, Kinect sensor is a helpful device in rehabilitation. The cost of Kinect device is affordable price as their technology equipped. This sensor also demonstrates a good accuracy compared to ViCON system [7].

ViCON system is a system that captures the kinematic and kinetic motion of a people. In [7], this system includes with about 8 cameras while in [18] consists of 6 cameras that used to track and capture a full body of a person. From this, the ViCON system need to use more cameras to capture a motion of people and obtained a good accuracy kinetic data. In addition, ViCON uses camera with light capture scheme to capture the motion [7]. Then, this will enable the system to capture many points of kinematics that depends on the specified joints and be represented as kinematic movements. The camera that used in ViCON system can be operated in a dark room or any places. This is because; the camera lights are brighter than any source of light in that place. So, this system is mostly accurate and has a high accuracy but very high cost system.

Besides TUG test, Five-Times-Sit-to-Stand (5STS) is one of the methods of Sit-Stand Test that able to detect a fall risk of a person [12]. In this method, the patient need to sit and stand for five times as quickly with arms folded, to check the balancing of the patient and also factors of physiological such as vitality and pain. A Sit-to-Stand test cycle was split up into four phases: sitting, sit-to-stand transition, standing and stand-to-sit transition phase [12]. The time duration of movements of the patient were recorded during the 5STS test for make a comparison and evaluate the differences between the fallers and non-fallers, the analysis of covariance (ANCOVA) system is used [12]. Other than that, besides 5STS test, Sit-to-Stand test is aim to create an experiment for collecting human movement data with emphasis on compromised movement due to back pain [13].

While, The Timed Up & Go (TUG) test is a simple test and quick functional mobility test that requires a subject to stand up, walk 3 meter, make u-turn, walk back again and finally sit down [14, 15, 16]. Based on [17], the test record the time duration of the patient doing the test until complete that measured in seconds. If the subject exceed the threshold time, the fall risk of a person is obtained. Besides, this test is really sensitive and specific measure of probability for falls and gives a reliable score. TUG test also be able to differentiate the patients from the healthy subjects and correlated well with plantar flexor strength, gait performance and walking endurance in chronic stroke subjects [14].

III. METHODOLOGY

A. *Time Up and Go (TUG) Test*

Timed Up and Go test or also known as TUG test is a walking test that are commonly used by therapists to detect fall risk of elderly person. In this work, a number of 27 subjects which are divided into two groups, adults and elderly which aged from 23 to 63 years old for adult group and 65 years old and above for elderly group to undergo the TUG test. Prior to the TUG test, the subjects are interviewed to get their information such as age, gender, weight, height, and history of serious injury before, and history of operation before. These information are used to discuss in discussion part

The Kinect Sensor is placed with the height of 1 meter from the ground and 3 meters away from a chair that faced the sensor. An 'X' mark is placed 2 meters away from the chair as the sensor device is unable to detect the whole skeleton image if an 'X' mark is placed 3 meter away from that chair.

The subject is asked to sit on the arm chair and face directly to the sensor device that was placed straight in front of the chair. Firstly, the subject is asked to stand from the sitting position and this position is called as in Sit-to-Stand (STS) position. Next, the subject is asked to walk for 2 meters until the subject reached the 'X' mark. Then, the subject need to make U-turn once reaching the 'X' mark and walk again for another 2 meters to the chair. Lastly, once the subject has done with walking and turning, the subject needs to sit again on the chair and this position is called as Back-to-Sit (BTS) position. The TUG test setup is shown in Fig. 1.

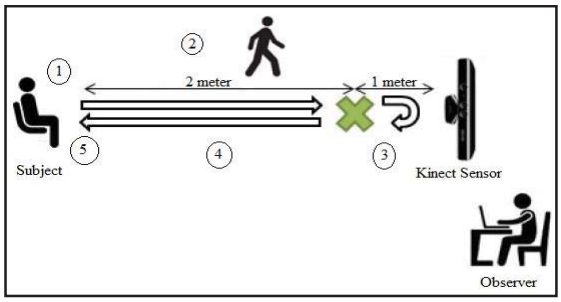

Fig. 1. Timed Up & Go test setup

The parameter obtained from the TUG test is the time taken for the subject to complete the test that is measured in seconds. The starting time is from the subject start to get up from the chair and the stop time is when the subject sits back on the chair. A

fall is detected when a person completes the TUG test with more than 13.5 seconds and classified as a faller [17].

B. Kinect Sensor

A Kinect Sensor Xbox 360 device is able to track skeleton points of the human body joints to build a visual body structure of a person. This sensor is equipped with a RGB camera (640x480), an infrared camera capable of producing depth images (640x480), depth sensor, audio microphone array and a motorized tilt as shown in Fig. 2.

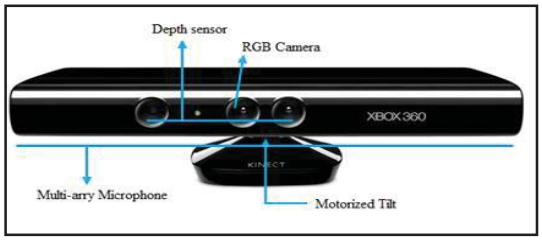

Fig. 2. Kinect Sensor

The RGB camera is function as to capture colour image and also to stores three-channel data in 1280x960 resolutions where the three-channel is the three letters of R, G and B, are stand for 'Red', 'Green', and 'Blue' colours respectively. The sensor can detect within in range of distance from 1.2 metre to 3.5 metre. But, when the subject is detected too near to the camera or beyond 3.5 metre, the sensor is unable to make any detection of the person image.

Meanwhile, the function of depth sensor is to capture the depth image with the motion of a person while moving. In this device, there is a infrared light where the infrared emitter will emit the infrared beams. Then, the beam that is reflected to the sensor will detected by the depth sensor and converted into depth information and it able to measure the distance between the sensor and the subject.

There are four microphones in this device and functioned as to record the audio and to capture the surrounding sound as the audio microphone array. This is also able to detect the location of where does the sound came from by using this specification, with the aid from the motorized tilt and also able to detect the audio wave direction.

Before the test to start, the Kinect Runtime version 1.7 and Kinect SDK version 1.8 has to be downloaded in the personal computer. The 'Kinect for Windows Sensor' is installed and act as the support package installer in MATLAB where 'supportPackageInstaller' can type at MATLAB console and search a 'Kinect for Windows'. When the installation is finished, Kinect Runtime version 1.7 and Kinect SDK version 1.8 installed. Then, 'imaqhwinfo('Kinect');' is typed at the command window to confirm whether the installation is successful or not. If there is an answer from that command, then it means that the installation is successful.

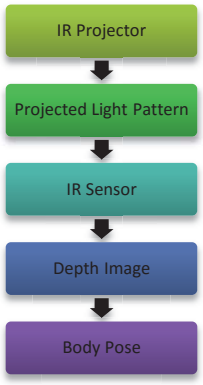

Fig. 3. A process to show the skeleton image

Thus, a machine learning algorithm is used in this work such as randomized decision forest algorithm [19] that used for segmentation part prediction and estimate the body pose from the depth image, and the mean-shift algorithm is used for joint estimation and it fast mode-finding algorithm [20]. It can observed part centre is offset by pre-estimated value. The Microsoft Kinect Sensor and the MATLAB software programming are utilize to capture the movement of a person parameters that based on the data of joint coordinates obtained as shown in Fig. 3.

In this work, there are two source codes need to run using MATLAB that able to detect a skeleton image, namely skeleton viewer source code and a skeleton tracking source code. The skeleton viewer source code that keeps the data of points of the skeleton in a person where are the total of the data points of the skeleton are 20 points or joint in a normal person as shown in Fig. 4. Then, when the number of points of skeleton have been identified, two specific two points are will produce a pairs where the joints are connected in order to produce a larger parts of body such as spine, left hand, right hand, left leg and right leg.

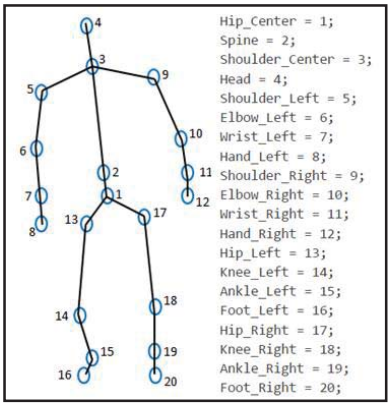

Fig. 4. Skeleton image of human

The data of joint coordinates in MATLAB are collected while the subjects doing the TUG test until complete. The data obtained is used to calculate and analyze the distance and the angle between the joints for fallers and non-fallers. A fall person has lost balance and due to that, a certain angle between the orientation of body and the ground floor is generated [21]. In this work, right hip, right knee, and right ankle joints are chosen to calculate the distance and the angle of the joints. Fig. 5 shows the joint of a human body that is used to calculate the distance

and the angle between the joints. The results are plotted as a line graph using Microsoft Office Excel 2007. The average angle values for each joint are calculated and the range angle value of the joints between fallers and non-fallers are determined. A discussion must be made using the information that is obtained from the interview session. A faller subject have a higher range value of the angle joint due to less bending that they can made.

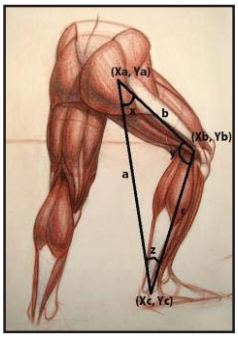

Fig. 5. Example of joint coordinates that used for analysis.

These are the equations that are used to calculate the distance and the right hip angle between the joints.

$$distance = \sqrt{\{(X_2 - X_1)^2 + (Y_2 - Y_1)^2\}} \quad (1)$$

$$a = \sqrt{\{(X_a - X_c)^2 + (Y_a - Y_c)^2\}} \quad (2)$$

$$a^2 = b^2 + c^2 - 2bc\cos x \quad (3)$$

$$\cos x = \left(\frac{a^2+b^2-c^2}{2ab}\right) \quad (4)$$

$$x = cos^{-1}\left(\frac{a^2+b-c^2}{2ab}\right) \quad (5)$$

Equation (1) shows a general equation to calculate the distance between joints from the data obtained in MATLAB. So, (2) is used to calculate the distance between hip and ankle joint, a as shown in Fig. 5. Equation (3) is used to calculate the angle of joints which further derived as (4) and (5) and used to calculate the right hip angle. These equations are derived to calculate the angle of right knee and right ankle joint.

IV. Results and Discussions

The TUG test has been conducted with 27 subjects, who are classified as faller and non-faller that based on the time taken for the subject to complete the TUG test. Adult subjects were from UTM students while elderly subjects were from a nursing home located at Taman Nesa, Skudai, Johor Bahru. If the subject completes the test more than 13.5 seconds, then the subject is classified as a faller. So, for non-fallers, 19 subjects are detected and 8 subjects are detected as fallers.

TABLE I. TRUTH AND TEST RESULT

TEST RESULT	TRUTH		TOTAL
	Faller	Non-Faller	
Positive	A *True Positive* (6)	B *False Positive* (2)	8
Negative	C *False Negative* (5)	D *True Negative* (14)	19
TOTAL	11	16	27

Once the subjects are classified as faller and non-faller, the sensitivity and specificity of the test is determined by the truth and test result table as shown in Table I [22]. The truth columns shows to determine either the subject is a faller or a non-faller, while the test result columns shows either the result is a positive or negative results. In addition, sensitivity values shows the capacity to detect fall events, while specificity shows the capacity to detect non-fall events. These measurements are used to describe the performance of the tests that are used to classify between the fallers and non-fallers According to the truth and table result, the calculation of sensitivity (6) and specificity (7) are shown as below:

$$Sensitivity = \frac{A}{A+C} \cdot 100\% \quad (6)$$

$$= \frac{6}{6+5} \cdot 100\% = 54.55\%$$

$$Specificity = \frac{D}{D+B} \cdot 100\% \quad (7)$$

$$= \frac{15}{15+2} \cdot 100\% = 87.50\%$$

Fig. 6 shows the line graph, angle against time (in seconds) of right hip angle are plotted for each non-faller. From the graph, the average of the value of the angle is calculated to determine the minimum and the maximum range values for non-fall subject. Fig.7 and Fig. 8 are shows the line graph of right knee and right ankle angle respectively for non-fall subject. The same procedures are used to determine the range values for right knee and right ankle joint.

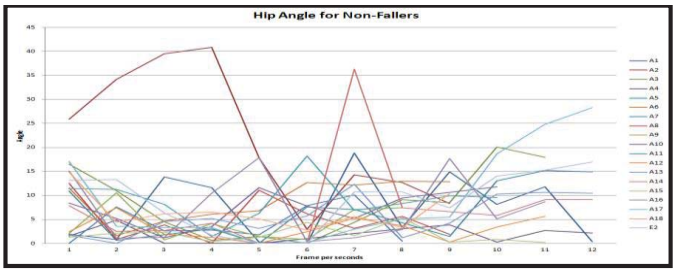

Fig. 6. The angle of right hip joint for non-fallers.

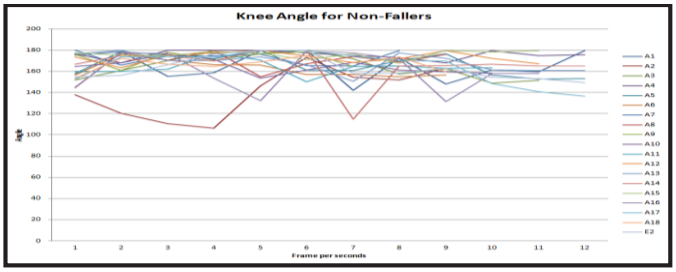

Fig. 7. The angle of right knee joint for non-fallers.

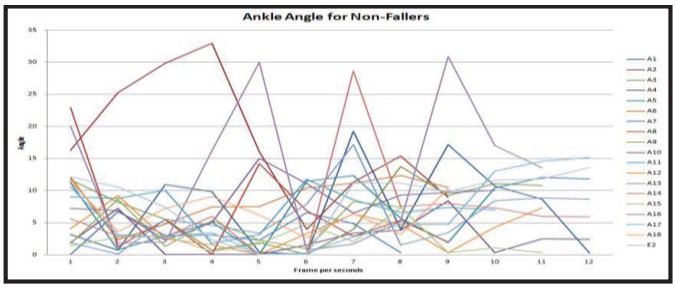

Fig. 8. The angle of right ankle joint for non-fallers.

Moreover, Fig. 9 shows the line graph of right hip angle for each faller subjects. From this graph, the average of the value of the angle is calculated to determine the minimum and the maximum angle values for fallers. Fig.10 and Fig. 11 are shows the line graph of right knee and right ankle angle respectively for fallers. The same procedures to determine the range values for right knee and right ankle joint are applied.

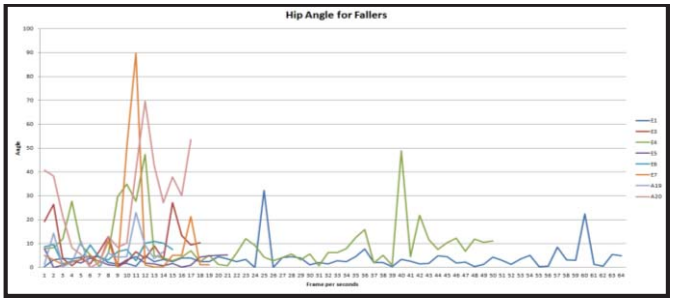

Fig. 9. The angle of right hip joint for fallers.

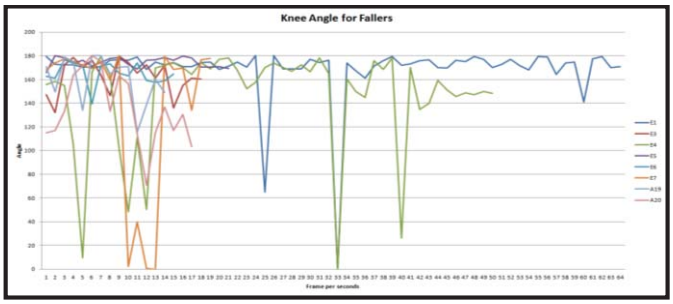

Fig. 10. The angle of right knee joint for fallers.

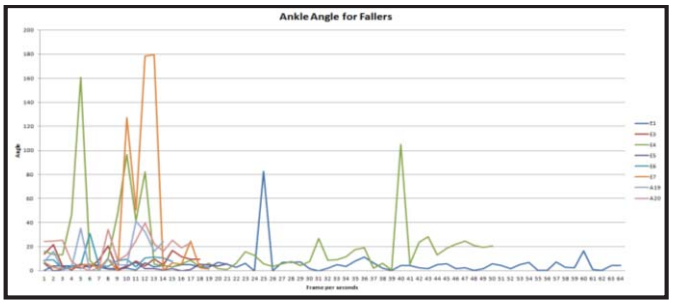

Fig. 11. The angle of right ankle joint for fallers.

TABLE II. THE RANGE VALUE OF ANGLE AT EACH JOINTS BETWEEN FALLER AND NON-FALLER

Angle (Degree)	Category	
	Non-Faller	Faller
Right Hip	4.272 - 9.278	2.811 - 24.453
Right Knee	162.309 - 171.304	117.076 - 173.782
Right Ankle	4.425 - 8.872	3.407 - 44.470

Then, from the range values obtained, one subject is chosen from each category to show the graph pattern which have meet the range of the angle values calculated, angle of joints against time per second, while they undergo TUG test. Hence, in that graph shows the time when the subject done the steps in TUG test such as sit, walking and make u-turn.

Fig. 12. Subject A10 in the sitting position.

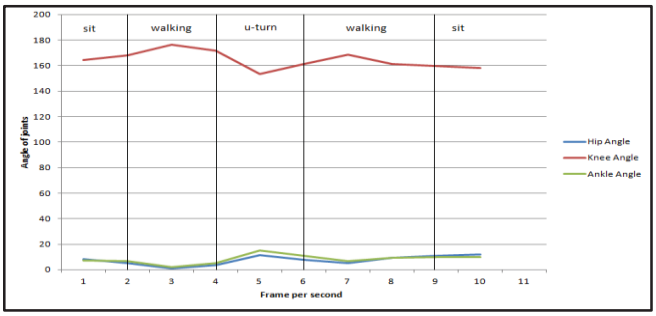

Fig. 13. The angle of three joints for Subject A10.

Fig. 13 shows the graph for Subject A10 as shown in Fig. 12, female, 23 years old is chosen as non-faller. She completed the TUG test in 9.45 seconds and do not have any history of falling event or had been in serious injury. Furthermore, she is an healthy person. The way she walked to complete the TUG test also was like as normal person. Based on the Fig. 13, it shows that the angle values of three joints are in range value of angle for non-faller that has been calculated before. So, Subject A10 do not have any factor of fall risk.

Fig. 14. Subject E1 in the walking position.

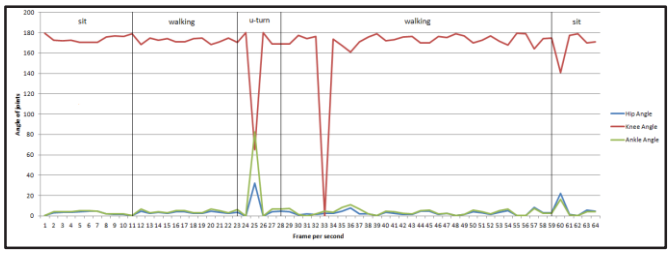

Fig. 15. The angle of three joints for Subject E1.

Fig. 15 shows the graph for Subject E1 as shown in Fig. 14, female, and 76 years old is chosen as faller. She completed the TUG test in 68.44 seconds and has history of falling event and had been in serious injury for years ago at her house. From that incident, her upper right leg that between hip and knee operated where a metal was inserted to replace her bone. She is not able to walk like normal person and need to use a support stand to walk. Based on the Fig. 15, it shows that the angle values of three joints are in range value of angle for faller that has been calculated before. So, Subject E1 has a factor of fall risk and have a high tendency to fall.

V. CONCLUSIONS

Overall, this study has achieved all the objectives where the factors of fall risk among elderly can be determined by the angle between the joints from the data of joint coordinates extracted from the skeleton image that appeared in MATLAB using Kinect Sensor that is used to capture the movement of a person while the person completes the TUG test. The angle of the joints for elderly tends to be in the higher range due to less bending that can be made compared to normal person. The TUG test is also helpful in classifying the subjects who have a fall risk based on the time taken to complete the test. A person that takes more than 13.5 seconds to complete the TUG test will be classified as a faller.

REFERENCES

[1] Shumway-Cook A, Brauer S and Woollacott M., "Predicting the Probability for Falls in Community-Dwelling Older Adults Using the Timed Up & Go Test," Physical Theraphy, Vol. 80, No. 9, pp. 896-903, September 2000.

[2] Falls and Older Adults (accessed on 5 December 2016). NIHSeniorHealth website: https://nihseniorhealth.gov/falls/causesandriskfactors/01.html

[3] Yanjun Li, Gan Chen, Yueyun Shen, Yihua Zhu and Zhen Cheng, " Accelerometer-Based Fall Detection Sensor System For The Elderly," IEEE CCIS Journal, pp. 1216-1220, 2012.

[4] Yueng Santiago Delahoz and Miguel Angel Labrador, "Survey on Fall Detection and Fall Prevention Using Wearable and External Sensors," Sensors, pp. 19806-19842, 2014.

[5] Jason Cody, Subir Biswas and Karin PfeifferWearable, "Sensor Technology to Measure Physical Activity," Sept. 15, 2010. (accessed on 21 December 2016). http://msutoday.msu.edu/news/2010/wearable-sensor-technology-to-measure-physical-activity/

[6] Arti Jagtap and Yogesh Angal, "Microsoft Kinect Sensor for Fall Detection in Homes of Older People," International Journal of Advance Research in Electronics and Communication Engineering (IJARECE), Vol. 5, Issue 7, pp. 2110-2112, July 2016.

[7] Wan Zharfan Wan Zainal Abiddin, R. Jailani, Abdul Rahman Omar and Ihsan M. Yassin, "Development of Matlab Kinect Skeletal Tracking System (MKSTS) for Gait Analysis," IEEE, pp. 216-220, 2016.

[8] Zhen-Peng, Junhui Hou, Lap-Pui Chau and Nadia Magnenat-Thalmann, "Fall Detection Based on Body Part Tracking Using a Depth Camera," IEEE Journal of Biomedical and Health Informatics," Vol. 19, No. 2, pp. 430-439, March 2015.

[9] Lei Yang, Yanyun Ren and Wenqiang Zhang, "3D depth image analysis for indoor fall detecttion of elderly people," Digital Communicatons and Networks , pp. 24-34, 2016.

[10] Chanjira Sinthanayothin, Nonplas Wongwaen and Wisarut Bholsithi, "Skeleton Tracking using Kinect Sensor & Displaying in 3D Virtual Scene," International Journal of Advancements in Computing Technology (IJACT), Vol. 4, No. 11, pp. 213-223, June 2012.

[11] T. Leyvand, C. Meekhof, Y. C. Wei, J. Sun and B. Guo, "Kinect Identity: Technology and Experience," in Computer, vol. 44, no. 4, pp. 94-96, April 2011.

[12] Andreas Ejupi, Matthew Brodie, Yues J.Gshhwind, Stephen R.Lord, Wolfgang L.Zagler and Kim Delbaere, "Kinect-Based Five-Times-Sit-to-Stand Test for Clinical and In-Home Assesment of Fall Risk in Older People," S.Karger AG, Basel, Gerontology, Vol. 62, pp. 118-124, 2016.

[13] Eric Acorn, Nikos Dipsis, Tamar Pincus and Kostas Stathis, "Sit-to-Stand Movement Recognition Using Kinect,' Springer International Publishing Switzerland, pp. 179-192, 2015.

[14] Ng. SS and Hui-Chan CW, "The Timed Up & Go test : Its Reliability and Association with Lower-Limb Impairments and Locomotor Capacities in People with Chronic Strokes," Arch Phys Med Rehabil, Vol. 86, pp. 1641-1647, August 2005.

[15] Tiago S. Alexandre, Debora M. Meira, Natalia C. Rico and Simone K. Mizuta, "Accuracy of Timed Up and Go Test for screening risk of falls among community-dwelling elderly," Rev Bras Fisioter, Vol. 16, No. 5, pp. 381-388, 2012.

[16] Emma Barry, Rose Galvin, Claire Keogh, Frances Horgan and Tom Fahey, "Is the Timed Up and Go test a useful predictor of risk of falls in community dwelling older adults: a systematic review and meta-analysis," BMC Geriatrics, 2014.

[17] Podsiadlo D. and Richardson S, "The timed "Up & Go":a test basic functional mobility for frail elderly persons," J Am Geriatr Sac, Vol. 39, No. 2, pp. 142-148, 1991.

[18] Ajay Kapur, George Tzanetakis, Naznin Virji-Babul, Ge Wang and Perry R. Cook, "A Framework for Sonification of Vicon Motion Capture Data," Proc. of the 8th Int. Conference on Digital Audio Effects (DAFX-05), Madrid, Spain, September 20-22, 2005.

[19] J. Shotton et al., "Real-time human pose recognition in parts from single depth images," CVPR 2011, Providence, RI, 2011, pp. 1297-1304.

[20] Y. C. Chen, H. J. Lee and K. H. Lin, "Measurement of body joint angles for physical therapy based on mean shift tracking using two low cost Kinect images," 2015 37th Annual International Conference of the IEEE Engineering in Medicine and Biology Society (EMBC), Milan, 2015, pp. 703-706.

[21] Jiajia Wang, "Fall Detection System Based On Angle Change Rate With Kinect Sensor," Global Journal for Research Analysis (GJRA), Vol. 5, Issue 7, pp. 128-129, July 2016.

[22] Fadzlin Shuhada binti Mazlan, "Fall detector using Kinect Sensor," Ijazah Sarjana Muda Kejuruteraan (Elektrik-Elektronik) Tesis, FKE, UTM, 2016

IoT based Monitoring of Baby's Body Temperature

Fatin Nadia Binti Mohd Saleh
Faculty of Electrical Engineering
Universiti Teknologi Malaysia
Johor Bahru, Malaysia.
nadiasaleh77@yahoo.com

Dr Nor Aini Zakaria / Dr Mohd Azhar Abdul Razak
Department of / Centre of
Faculty of Electrical Engineering
Universiti Teknologi Malaysia
Johor Bahru, Malaysia.
norainiz@utm.my/ mohdazhar@fke.utm.my

***Abstract*: This proposed design of a monitoring device which is small, lightweight and portable with wireless interface capability. This system monitor the vital parameter which is the body temperature by using a wearable sensor and the information will be transferred to their parents through a wireless network. Example hazardous cases include overheating (fever), under heating and high temperature that change over a predefined time period. The effectiveness of the system is as a preventive measure against febrile seizure that lead to an epilepsy. By measuring this vital parameter, it can be done under risk situation conveyed to the parents with alarm triggering system to initiate the proper control actions whenever an abnormal condition occur. The system is extended for interfacing with the mobile phones to enable remote monitoring. Architecture of the system consists of a wearable sensor for monitoring the vital parameter and a sound buzzer where all of the component be controlled by a single microcontroller, the ESPresso Lite V2.0 based on ESP8266 and supplied by the lithium ion polymer battery. Even though the system is more focusing on temperature monitoring only, it can be further expanded or upgrade to monitor other vital parameter such as heart rate, oxygen saturation, respiration rate or any other parameter.**

Keywords: Baby monitoring; Vital parameter; Microcontroller; Wearable Sensor; Wireless Connected

I. INTRODUCTION

As we knew, the only way on how babies could express themselves is by crying. During the sleep, in times of illness and in case of birth defects is the most needed time where the baby need to be monitored regularly. Different complications may present and cause an unexpected death at the age of baby's life of six months and below. This is the critical age that need fully supervising by the parents. The most crucial thing monitored by the doctor is the baby's body temperature. Body temperature is a complex, non-linear variable that is subject to many sources of internal and external variation [1].

Fever is the part of the body's natural method of baby against infection. Elevated body temperature are considered one of the most common symptom diseases [3]. Febrile seizure is a well-known condition in the medical field where kids go under convulsion due to high fever or due to sudden rise of temperature[]. The rapid increase of body temperature in a short period of time may happen at the same time the fever seizure. Normal body temperature of baby three months and below is 36.0 °C to 37.4°C. For temperature around 37.5°C to 38.4°C, this is classified as the low grade fever temperature. Elevated temperature is the critical range of body temperature that need to be aware which is from 38.5°C to 40.0°C. Too high body temperature may lead to febrile seizure among babies. The problem is most of the parents outside are not aware as the baby's body temperature gets higher. As long as the baby achieved a high grade fever temperature, the possibility of the baby affected by a seizure is higher. Therefore, this prototype are create to monitor the baby's body temperature and immediately send an alert to the mother whenever an abnormal body temperature is occur. Abnormal situation is when the body temperature suddenly fluctuate from the normal body temperature.

This proposed body temperature monitoring system create a peace of mind to loved ones when they are away from their mother as they can get an update status of their child [5]. The sensor will sense the body temperature and then data is transferred to a server connected by a Wi-Fi interface module used as a platform for the baby to communicating with the mother. The information will be stored in the cloud then will be send to cell phones through application made to notify the parents.

II. LITERATURE REVIEW

A. Exsting Research Findings

Many home-care monitoring system are available nowadays but most of the system are specially designed for aged people and patients. These system can monitor their health status, automatically send out emergency signals, and have other functions [5]. Children and adults require different type of care since a children are totally dependent for their normal functions on someone else. Babies could not give any feedback about their discomfort or any health status. Caring methods for babies are not the same as the babies cannot give any feedback about their discomfort or health complaints. Hence, a home-care system or monitoring system that are specially designed for babies is today's need which would substantially lighten parents especially mother's burden [5]. For support this requirement, many research papers and patents of healthcare application are studied.

B. *Infromation for the Mothers*

From the various sources that have been figure out from the existing monitoring device available, it have shown that understand various feedback by their children create an interest from parents. The common concerns are:

1. Understand what the child are trying to communicate when they makes some sound [2].
2. Immediate and appropriate actions to be taken when children shown some abnormal symptoms [2].
3. Health condition of child when sick while the mother is away from them [2].

C. *Benchmarks for the babies body temperature*

A list of body temperature benchmarks have been obtained to facilitate the design of the sensor and signal processing unit. Table 1 shows the temperature measurement for armpit and skin for a references.

TABLE 1: BENCHMARK OF BODY TEMPERATURE

Body temperature	Location	Normal temperature	Fever temperature
	Armpit	35.5 – 37.0 °C	> 38.5°C
	Skin	29.0 – 34.0 °C	> 35.2 °C

D. *Existing Child Monitoring Technologies*

Some early efforts and developments in sensor technologies and wireless communication technologies include the design of miniaturized wireless monitor for long term monitoring of newborns. It will monitor the vital signal from the baby such as oxygen blood level, heart rate, respiration rate, body temperature, body posture, legs activity, and transmit the signals over wireless network. Efforts toward miniaturized the form factor and improving the comfort of the system have been made. The system was fixed on the newborn foot. By including all of the most important signals for pre-screening which is the proposed solution designed and give an early warning about possible life threatening situations using low energy wireless communication with smart phones [1]. In context of child monitoring by a working mother, a mother can monitor their baby vital signal through distance. The technology involves in monitoring the continuous measure temperature, heart rate and motion, and send it to server where the data is processed. A processed biological information of a baby are sent to a mother and generates an alert system if the condition of baby are found abnormal. This alert messages are transmitted to support system and nearby health clinics in emergency situation.

III. METHODOLOGY

The architecture of the overall system are shown on the figure 1. It consists of both hardware and software. A sensor of LM35 are controlled by the Arduino ESPresso lite 2.0 microcontroller, to sense the body temperature. An Arduino microcontroller is commonly used in designing devices because it is open source electronics prototyping platform. The ESPresso microcontroller will send a data to server. The data will be stored on the cloud server. In this project, data are stored on the thingspeak.com and also the blynk.com. The processed biological information (human body temperature) then will be sent to android on a mother cell phone through a Wi-Fi interface. For Wi-Fi interface, ESP8266 module is used as a medium to create a connection wirelessly. To view the data for a mother, android is choose by creating an application on it. Blynk Apps is preferable due to it user friendly device. Figure 2 is showing the application that will be used in this project to display body temperature of the baby.

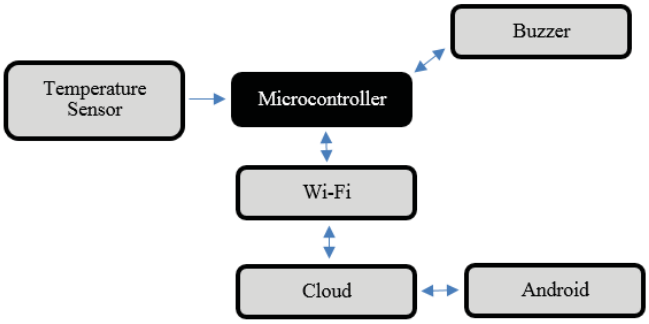

Figure 1 Block diagram of the proposed project design.

Figure 2 Blynk Application

Below are the subsections that provide more details of the component that being used in this project?

A. *Temperature Sensor*

A wide range of real time devices and sensors, have been developed for clinical research and health monitoring in recent years. LM35 sensor is a type of sensor's where output is an analog DC voltage signal and it can measure temperature range from -40 °C to =125 °C which is suitable

enough to measure targeted human body temperature. This type of sensor are preferable in this project is because it is suitable for the baby as it not cause any harmful since it is only require a small output voltage. With the accuracy of ±0.5 °C, it can be converted from voltage to degree Celsius based on the function,

$$Temp\ (C) = Output\ Voltage * V_{INPUT}/1024 \quad (1)$$

Input voltage is 3.3V from the Arduino ESPresso. The placement of the sensor is important for accurate measurements therefore to reduce discomfort to the babies, the sensor is located on the baby's foot just like on the figure 3 below but this project are more focusing on display the baby's body temperature on an android not LCD.

Figure 3 Monitoring device on the baby's foot

B. *Buzzer*

The Lilypad buzzer is being used to trigger an alarm whenever the body temperature is higher than normal condition is occur. This is to give an awareness to the people nearby the baby. The loudness of the chosen buzzer may not interrupt the baby during the sleep.

C. *Lithium Ion Polymer Battery*

LiPo (lithium ion polymer) battery are preferable for this project design because of its structure where is thin, light and powerful. The output ranges from 4.2V when completely charged to 3.7V. This battery had a capacity of 800mAh. It is also a rechargeable battery by using a USB cable.

D. *MicroController*

All of those components in this system such as LM35, buzzer, will be controlled by a single microcontroller. According to the system requirements, espresso lite 2.0 (Arduino type) was chosen as the best controller due to its weight and sizes. Espresso lite 2.0 is an Arduino-compatible Wi-Fi development board based on an earlier beta version (V1). The core hardware inside the espresso lite V2.0 is Espressif system's ESP8266 WROOM-02 Wi-Fi module and is programmable using the Arduino IDE.

Figure 4 ESPresso Lite V2.0

IV. RESULTD & DISCUSSION

A. *Program Testing*

For testing purposed, ESPresso board was connecting to a laptop by Wi-Fi to ensure the consistency data transfer and the wireless communication. The ESPresso lite 2.0 had to be programmed by using an Arduino IDE software to read the data from the wearable sensor and send the data through connected Wi-Fi to the laptop. The data will be stored on the thingspeak.com and then it will gives result on twitter account immediately. Figure 5 shows the result for the program testing that has been conducted.

(a)

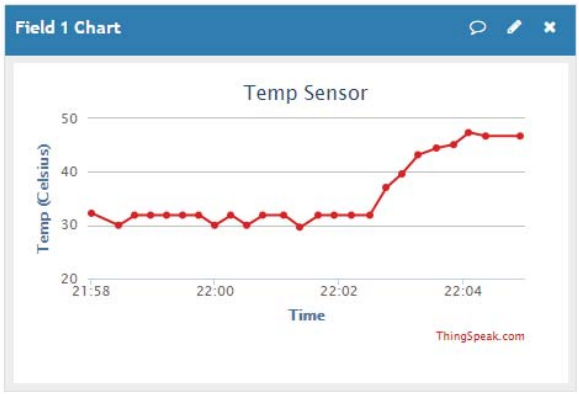

(b)

(c)

Figure 5 (a) Result of Wi-Fi connected from serial monitor Arduino Espresso (b) Server data be stored (c) Alert phone display via twitter account

Figure 5(a) show a display results from serial monitor of Arduino IDE software where the sensor of LM35 starts to measure the body temperature. Espert showing that an Arduino ESPresso connecting with thingspeak.com to store the data. This is just for the status connecting of Wi-Fi between the board and server. In figure 5(b), LM35 sensor will sense the body temperature for every 20 seconds, and then thingspeak server will show the result in terms of graph for data analyzing. A sudden increase on temperature showing on the graph is to relate with the changes of human body temperature. This method is create by putting the sensor close to the fan of laptop. For the last figure of 5(c), this is actually to create a notification and awareness to the mother whenever the baby's body temperature is higher. For experiment, the statement is pop up on the twitter timeline as the temperature is reached 32 °C and above.

B. Apps Montoring

The system have been tested using the application that function as a medium for mother-child communicating. There was no real body being tested during the experiment because it might create harmful to the babies, and so, the system was tested on a room temperature. This application is used to show the display temperature detected by the sensor. Figure 6(a) is to show the status of hotspot Wi-Fi from the phone is connecting the Blynk application and the ESPresso microcontroller. For every one second delay, the data from the ESPresso microcontroller will transfer data to blynk cloud and display on the mobile android. Figure 6(b) shows the actual view if a mother want to know the body temperature measurement of their wellbeing. Whenever the body temperature reached the higher grade fever temperature, this application will turn out the notification for mother awareness. The measurement shows on the figure 6(b) is only the room temperature for testing program.

```
[3774] Connected to WiFi
[3774] IP: 192.168.43.63
[3774]
    ___  __          __
   / _ )/ /_ _____  / /__
  / _  / / // / _ \/  '_/
 /____/_/\_, /_//_/_/\_\
        /___/ v0.4.7 on Arduino

[5001] Connecting to blynk-cloud.com:8442
[5199] Ready (ping: 2ms).
[62373] Connecting to blynk-cloud.com:8442
[65652] Login timeout
[68652] Connecting to blynk-cloud.com:8442
[71015] Login timeout
[74015] Connecting to blynk-cloud.com:8442
[80889] Connecting to blynk-cloud.com:8442
[87073] Login timeout
```

(a)

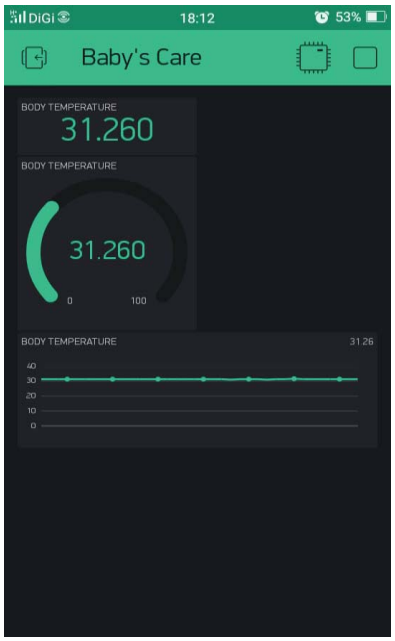

(b)

Figure 6 (a) Status of Wi-Fi connected to an Arduino (b) Mother's phone display through an Apps

C. Result of Sensitivity Test

Table 2 illustrates the data obtained during the sensitivity test. The result shows the reading of body temperature measurement at different placement of sensor to measure the accuracy. By referring the experimental results on table 2 below, the digital thermometer and DNT thermometer was used as a reference for the calibration and verification of LM35 sensor and MCP9700 (Lilypad temperature sensor). Figure 7 is the image of two types of the digital thermometer that being used in this experiment.

TABLE 2: MEASUREMENT OF TEMPERATURE

Sensor Placement	Number of Trial	Digital Thermometer (°C)	DNT Thermometer (°C)	Temperature Sensor LM35 (°C)	Temperature Sensor MCP9700 (°C)
Under Arm	1	35.60	36.20	35.45	33.79
	2	36.10	36.60	36.09	34.11
	3	36.10	36.40	35.77	34.11
	4	36.10	36.50	35.77	34.11
	5	36.30	36.40	36.09	33.79
Under Elbow	1	35.50	35.50	35.13	32.82
	2	35.40	35.80	35.13	33.47
	3	35.30	35.50	35.13	33.14
	4	35.50	35.80	35.13	33.14
	5	35.50	35.70	35.13	33.47
Under Knee	1	35.10	35.40	34.48	33.14
	2	35.00	35.50	35.13	33.79
	3	35.30	35.90	35.13	33.47
	4	35.50	36.20	35.77	33.47
	5	35.50	36.20	35.77	33.47

When taking the measurement, the sensor and thermometer was placed on the recommended part and count for ten second before record the temperature measurement in Celsius for one minute. The gap for every trial is one minute. Based on the results of measurement and calibration from table 2, MCP9700 sensor measurement is not the same or close to the digital thermometer. The difference in Celsius is too big compared to LM35 is more accurate and reliable. Besides that, in terms of safety, using Lilypad temperature sensor might be dangerous to the baby due to current flow from wired to the attached sensor on the cloth.

Figure 7 DNT Digital Thermometer (left) and Digital Thermometer (right)

D. Device Evaluation

The placement of the sensor that function to carry a task of measuring the body temperature was located on the baby's foot. It will sense the baby's body temperature through the skin of the baby. By placing the sensor on foot, it may reduce the baby's discomfort if the baby is sleeping. By then, the device system can measure the body temperature continuously. From the figure 8, for the final over view of the system, the sensor that attached to the baby's foot will be connect with casing containing a lithium ion polymer battery and also an espresso board.

Figure 8 The design that will be implement on baby's foot

V. CONCLUSION

The quality of baby and parents communication can be improved by proposed a suitable monitoring device which is less expensive and yet, it is easy to be implement. There are many benefits can be obtained in terms of electrical properties such as the power consume by the device to carries out several task including sense the baby's body temperature and transferred data from the microcontroller to the external system by a connected Wi-Fi interface. This is a convenience system design that can monitor the baby's health condition from any distance. Besides, this system can be future upgrade by adding another sensor to monitor different type of vital sign such as heart rate, respiration rate, humidity and oxygen saturation.

REFERENCES

[1] Mairo Leier, Gert Jervan. "Miniaturized Wireless Monitor for Long Term Monitoring of Newborns", 2014.
[2] Elham Saadation, Shruti Priya Iyer, Chen Lihui, Owen Noel Newton Fernando. "Low Cost Infant Monitoring and Communication System", 2011.
[3] Baker Mohammad, Hazem Algebra, Reem Ashour, Hani Saleh. "Portable Wireless Biomedical Temperature Monitoring System: Architecture and Implementation"
[4] Md Asaduzzaman Miah, Mir Hussin Kabir, Md.Siddiqur Rahman Tanveer and M.A.H.Akhand. "Continuous Heart Rate and Body Temperature Monitoring System using Arduino UNO nad Android Device", 2015.
[5] Savita P.Patil, Manisha R.Mhetre. "Intelligent Baby Monitoring System", 2014.
[6] Greg Kelly, ND "Body Temperature Variability (part 1): A Review of the History of Body Temperature and its Variability Due to Site Selection, Biological Rhythms, Fitness and Aging", 2006.
[7] Alina Arulsamy, Bey Hing Goh, Mohd Farooq Shaikh, "Current Status of Epilepsy in Malaysia and Way Ahead", 2015.
[8] Nur Herzatil Aqmar Binti Ghazali, "Human Body Temperature Monitoring With Short Message Service (SMS)", 2011/2012.
[9] Salomi S.Thomas, Mr Amar Saraswat, Anurag Shaswat, Dr, Vishal Bharti, "Sensing Heart Beat and Body Temperature Digitally using Arduino".
[10] Zhihua Zhu, Tao Liu, Guangyi LI, Tong Li and Yoshio Inoue, "Wearable Sensor System for Infants", 2015.

Ankle Rehabilitation with Feedback Ankle Gait System

Abdul Rahim Bin Tahir
Department of Electronic and Computer
Universiti Teknologi Malaysia
43500 Skudai, Johor
abdzrahimtahir@gmail.com

Nasrul Humaimi Bin Mahmood
Department of Electronic and Computer
Universiti Teknologi Malaysia
43500 Skudai, Johor
nasrulhumaimi@utm.my

***Abstract*— The ankle represents one of the most complex bone structures in human body and the overall ankle motion is therefore complicate. In addition, motion analysis of ankle is a key issue in ankle rehabilitation and in developing an ankle rehabilitation device. Based on the analysis of the structure of ankle and its motion, this paper proposed two types of motion modes of ankle, according to the modes, two different kinds of rehabilitation robots are proposed respectively. Then the mechanical design, the kinematics and workspace analysis are derived for the proposed rehabilitation robots.**

Keywords- Ankle Rehabilitation, Dorsiflexion, Plantarflexion, Ankle Gait System, Inertia Measurement Unit(IMU), Gyroscope, 3D Printing, Machine Learning, General User Interface, Unaffected Ankle, Affected Ankle

I. INTRODUCTION

The establishment of rehabilitation therapy strategic for the purpose to treat foot gait problem are increasing concern nowadays. The ankle rehabilitation in Malaysia are dynamically increasing due to number of people having ankle problem are increasing. Researcher and rehabilitation product development are competing each other to produce the best rehabilitation ankle solution [1]. The dysfunction of the ankle foot is complex that may leading to less efficient gait and amplified fall risk [2]. The tibialis anterior musculature facilitates dorsiflexion [3]. Proper ankle dorsiflexion is critical throughout the stance and swing phase of gait. For example, proper dorsiflexion enables toe clearance during swing [4]. With the correct activation of dorsiflexion musculature adverse and inefficient motor patterns during gait, such as circumduction, may be avoided.

Gait and other human movement patterns have been successfully identified through the accelerometer platforms and software applications. The synthesis gyroscope sensor technology and machine learning has led to the development of a novel ankle rehabilitation system that may be utilized at a setting of the subject's preferred convenience. The device consists of a 3D printed ankle rehabilitation system that provides resistance through an elastomer band. A software application enabling functionality of gyroscope platform that is mounted to the footplate with an adhesive medium. The gyroscope signal data can be conveyed through ankle gait system as a text file. Using the derived feature set of the data, machine learning can be applied to classify between an affected ankle and unaffected ankle. This first endeavor forges a broader goal of being able to determine through machine learning when a subject's therapy should be modified based on objective sensor quantification in synthesis with machine learning. The objective of the research is to demonstrate from an engineering proof of concept perspective the capacity to utilize gyroscope sensor applications to evaluate a subject's rehabilitation status in combination with machine learning for a portable ankle rehabilitation system.

II. BACKGROUND

The ankle dorsiflexion provides significant contribution throughout the gait cycle. The gait cycle can be discretized into two phases: stance and swing. Stance constitutes 60% of the gait cycle, and swing represents 40% of the gait cycle. During the initiation of the stance phase the tibialis anterior provides eccentric contraction, for which the ankle foot complex decelerates. This subphrase is denoted as controlled plantar flexion. Intuitively, controlled plantar flexion facilitates the ankle foot complex by providing coordinated contact with the ground surface [6,7,11].

Another phase of gait that the dorsiflexes provide major contribution is during swing. Swing involves the leg clearing the ground, while continuing in fluid forward progression. The proper activation of the tibialis anterior sustains orientation the ankle joint during swing, mitigating foot drop that can lead to the potential for stumbling during the synchronous transition from swing to stance [6,7,11].

Fig. 1. Basic ankle movement (Dorsiflexion or Plantarflexion)

In the event of insufficient strength for the tibialis anterior, multiple gait pathologies can arise. As a compensatory strategy to foot drop, circumduction patterns can develop, such that the leg trajectory is no longer isolated in parallel to the sagittal plane but also somewhat perpendicular. Insufficient strength of the ankle dorsiflexed, especially during eccentric contraction during

the controlled plantarflexion subphrase of stance can lead to foot slap, which entails greater loads about the leg [5,6,7,11].

Clinical success of ankle strengthener systems has been successfully implemented for rehabilitation therapy. Conventional strategies have applied progressive strengthening to the ankle dorsiflexed [12,13,14]. In particular, strengthening techniques for improving the ankle dorsiflexed musculature have advanced gait quality for subjects with hemiparesis [15,16,17]. However, the transition to a fully homebound setting with remote connectivity between therapist and subject would be highly advantageous.

A further evolution of a homebound strengthening device can be realized through integration of a smartphone sensor and machine learning. The smartphone is equipped with multiple sensors, such as an accelerometer and gyroscope. Equipped with a diverse software application package, the smartphone can convey its sensor measurement by wireless connectivity to the Internet as an email attachment. The wireless sensor capability of the smartphone has resulted in the remote positioning between experimentation site and post-processing resources. In essence a subject using the smartphone for acquiring movement features can readily select a setting of the subject's preference, such as a homebound environment. The smartphone functioning as a wireless accelerometer and gyroscope platform has been successfully demonstrated for the quantification of human movement characteristics [8,18].

The gyroscope signal data from the smartphone equipped with a software application to function as a wireless gyroscope platform can be refined into a feature set for classification through machine learning. Processing the feature set with machine learning application enables automated diagnostic classification. The support vector machine constitutes a promising machine learning scenario. The support vector machine has been successfully conducted for biomedical applications, such as for the classification of a hemiplegic patellar tendon reflex pair and gait status [9,19].

The support vector machine demarcates between two classes of the feature set, such as pair of legs (affected and unaffected) through the implementation of a support vector. Using a mathematical procedure, the feature set is processed to a hyperspace. With the application of a kernel the hyperspace is condensed to a hyperplane. At the hyperplane, a support vector is applied to delineate between the two classes of the feature set [19,20]. The support vector is particularly useful for binary classification of two disparate classes of the feature set, such as a pair of legs (affected and unaffected) [9,19,20].

The research objective is to apply machine learning, such as a support vector machine, to classify between an ankle pair (affected and unaffected) using an ankle rehabilitation system. The results are attained from the perspective of engineering proof of concept. The feature set is derived from a gyroscope platform and it conveyed by Arduino and ankle gait system as text file and save to computer.

III. METHODOLOGY

The process developing use agile method of development to develop the ankle rehabilitation system that involve process of modulation and integration of multiple sub system. The system involves multiple subsystem such as mechanism, electronic, analysis and GUI. The mechanism part, first it is a basic SolidWorks designing to rendering a basic mechanism of ankle rehabilitation design. The prototype version that were design evolve for 3D print, which consisted of the material acrylonitrile butadiene styrene (ABS). The bottom of 3D print side support was stronger by put rubber to reduce impact to 3D print. An elastomer band was to ensure subject foot are tightly attach to mechanism.

Next, electronic and sensor are the most important part in this research that in order to measure the degree of ankle bend during dorsiflexion and plantarflexion strengthening. Sensor for measuring is I use one off-the-shelf 6-degree-of-freedom MPU6050 (Figure 1(d)) to measure the orientations of the foot. The IMU provide data from two types of MEMS sensors: 3-axis accelerometer and 3-axis angular rate gyroscope. A non-chip sensor fusion algorithm derives the 3D orientation of the IMU circuit board using the sensor inputs. This IMU is not expensive and it is very accurate, as it contains 16-bits analog to digital conversion hardware for each channel. Using IMUs that mounted on the foot, I compute the ankle joint angle by differencing the orientation vectors of the IMU.

Fig. 2. Inertial Measurement Unit (IMU) Mpu6050

In order to collect data of degree of ankle movement using orientation vector of IMU, I was implement Kalman filter to filter out the unwanted signal while reading data.

The microcontroller control by GUI to select whether to collect data or not. In order to measure each repetition of the ankle rehabilitation system, the smartphone equipped with software to function as a wireless gyroscope platform was mounted to the foot plate through an adhesive. The subject's foot was mounted to the footplate through a flexible strap.

With the data acquired for a specified quantity of repetitions using the ankle rehabilitation system and measured through GUI application. The set of data was consolidated into text file (.txt) from GUI application that collect the data.

Fig. 3. General User Interface(GUI) for collect data

Engineering proof of concept was achieved by evaluating as many subject as can. The subject applied the ankle rehabilitation system for 5 repetitions to both the affected ankle and unaffected ankle. The subject's ankle characteristics were measured through a gyroscope that attached by adhesive to the footplate of the ankle rehabilitation system that functioned as a gyroscope platform through a software application. The ankle gait system application acquired data for a duration of 40 seconds, which was sufficient to record 5 repetitions per ankle. The following experimental protocol was applied:

A. *Mount the gyroscope to the footplate of the 3D printed ankle rehabilitation system through an adhesive.*

B. *Secure the foot to the ankle rehabilitation system through a flexible strap.*

C. *Upon activation of the gyroscope signal, instruct the subject to conduct 5 repetitions of contracting the ankle's dorsiflexor musculature and ankle's plantarflexion musculature.*

D. *Activate the recording of the gyroscope signal from the ankle gait software application.*

E. *Once the recording sample is completed convey the gyroscope signal as a text file and save into computer for post-processing of the feature set.*

IV. Result

The ankle rehabilitation system equips with inertia measurement unit(IMU) and general user interface function to collect, analysis and give the result to the user. This rehabilitation system being built to work in setting of subject choice, such as homebound, office or rehabilitation center. The raw signal data to measuring the angle movement about ankle's dorsiflexion and plantarflexion from IMU being process and collect using GUI. The data is measuring angle of ankle dorsiflexion and plantarflexion of affected ankle movement contrast to unaffected ankle movement. The analysis system can facilitate acuity only to therapist to analysis the subject's rehabilitation status for any calibration or modification of therapy. Figure 1 illustrate the ankle rehabilitation system with subject foot mounted to footplate with IMU sensor.

A. *Normal or unaffected ankle movement*

Figure below presents a considerable disparity between the waveform of unaffected healthy leg or healthy ankle. The waveform is present the data gait movement of a person for dorsiflexion movement and plantarflexion movement. From the data of this person he has 49.32 degree of dorsiflexion and has 25.34 degree of plantarflexion. From the survey form that answer by subject, found out that the subject is active workout in gym and active playing futsal.

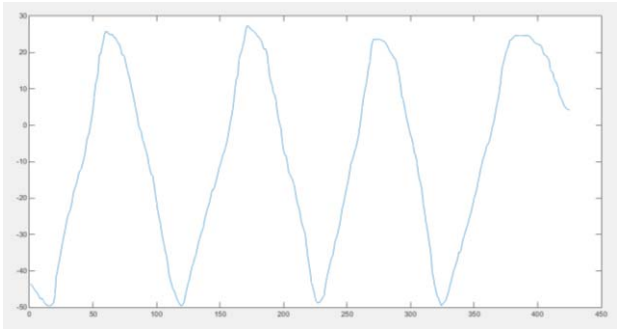

Fig. 4. Subject C raw data graph of angle movement vs time taken

The figure below present a feature data set of subject B's that have healthy ankle. Subject B is a 23-year-old and he still studying in university. Subject B is performed healthy and active lifestyle. He is a hiker, and he going through high intensive training and active runner. The figure present waveform of subject data gait movement for dorsiflexion movement and plantarflexion movement. From the waveform, found that the person has 65.3 degree of dorsiflexion and has 19.75 degree of plantarflexion.

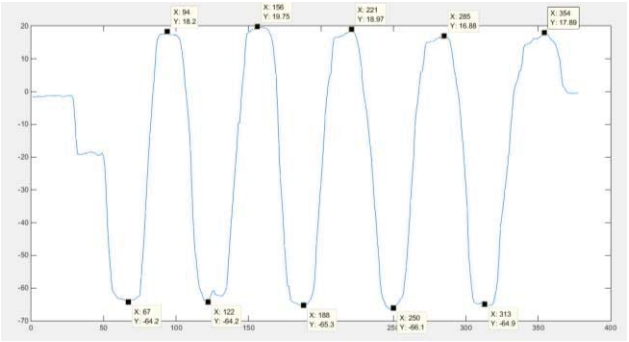

Fig. 5. Subject B raw data graph of angle movement vs time taken

B. *Abnormal or affected ankle movement*

The figure below present a gait pattern of a subject that have unhealthy ankle. Subject C is 64 years old, housewife and she having middle foot arthritis. The figure present waveform for dorsiflexion movement and plantarflexion movement of the subject. The resulted waveform show us that the person has 21.3 degree of dorsiflexion and 9.144 degree of plantarflexion.

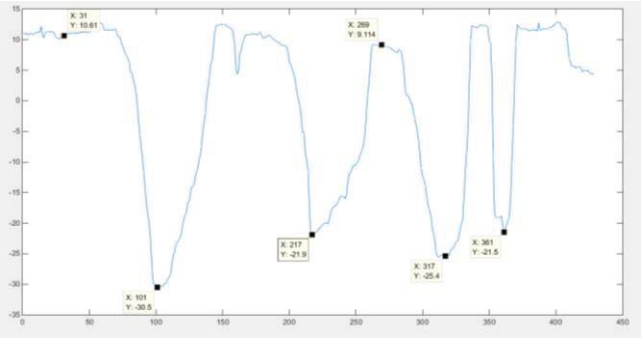

Fig. 6. Subject C raw data graph of angle movement vs time taken

C. Comparing data between affected and unaffected ankle

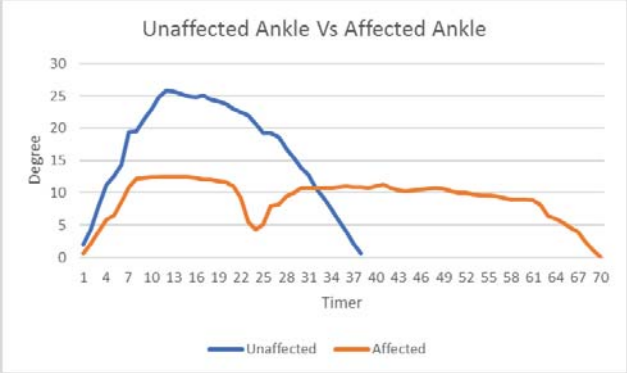

Fig. 7. Graph of unaffected ankle vs affected ankle data for plantar flexion

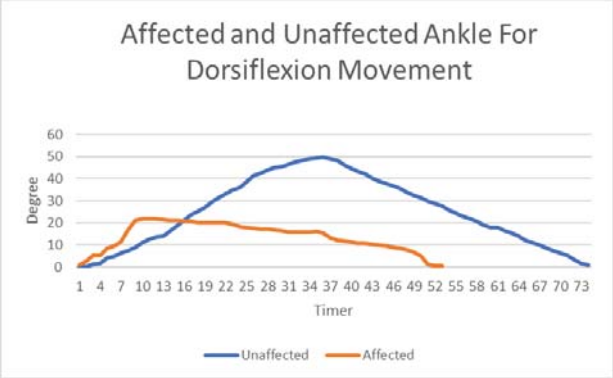

Fig. 8. Graph of unaffected ankle vs affected ankle data for dorsiflexion

D. Statistical data

TABLE I. STATISTICAL OF ALL DATA TAKEN

Statistical	Value	
	Plantarflexion	Dorsiflexion
Minimum	9.144	21.3
Maximum	39.3	64.5
Mean	27.951	40.951
Std. Dev.	4.167	9.089

The ankle gait system function well to collect data of the subject. After collecting data done the data going through an analysis as in figure 7 to learn as many data as possible to get differentiate the maximum, minimum and mean data of the angle as in Table 1. From the data, the ankle gait system need to calibrate to adjust with the result of the user data to find is there any problem with the subject ankle.

V. FUTURE IMPROVEMENT

Future improvements of the ankle rehabilitation system are envisioned. As opposed to using an elastomer band, a motorized actuator can be applied. With an actuator both concentric and eccentric therapy strengthening of the ankle can be developed. A localized gyroscope sensor could be applied to the footplate with wireless transmission to a smartphone for access to the Internet. Other machine learning algorithms could be considered for classification suitability. Machine learning may enable phased classifications for the rehabilitation process in order to establish optimized therapy.

VI. CONCLUSION

With the incidence of traumatic brain injury and associated motor impairment, such as ankle dorsiflexion and ankle plantarflexion, a novel rehabilitation devices can facilitate the therapy process. The presented ankle rehabilitation system entails the amalgamation of 3D printing, gyroscope platform, and machine learning. A support vector machine achieved 97% classification based on a feature set acquired from a gyroscope signal for a affected ankle and unaffected ankle while using the ankle rehabilitation system. The ankle rehabilitation system was primarily constructed from a 3D print, and resistance was provided through an elastomer band. The intrinsic characteristics of the ankle rehabilitation system facilitate operation in the environment of a subject's preference, such as a homebound setting. A therapist can remotely evaluate a subject's response to a therapy prescription, and modify the strategy accordingly. Machine learning classification is envisioned to augment the therapist's decision process and acuity.

REFERENCES

[1] M. D. Faul, M. M. Wald, L. Xu, and V. G. Coronado, "Traumatic brain injury in the United States; emergency department visits, hospitalizations, and deaths, 2002-2006," *Atlanta (GA): Centers for Disease Control and Prevention, National Center for Injury Prevention and Control, Division of Injury Response*, Mar. 2010.

[2] D. G. Everaert, R. B. Stein, G. M. Abrams, A. W. Dromerick, G. E. Francisco, B. J. Hafner, T. N. Huskey, M. C. Munin, K. J. Nolan, and C. V. Kufta, "Effect of a foot-drop stimulator and ankle–foot orthosis on walking performance after stroke a multicenter randomized controlled trial," *Neurorehabil. Neural Repair*, vol. 27, no. 7, pp.579-591, Sep. 2013.

[3] R. R. Seeley, T. D. Stephens, and P. Tate, *Anatomy and Physiology*. New York: McGraw-Hill, 2003.

[4] P. M. Mills, R.S. Barrett, and S. Morrison, "Toe clearance variability during walking in young and elderly men," *Gait Posture*, vol, 28, no. 1, pp. 101–107, Jul. 2008.

[5] R. LeMoyne, C. Coroian, T. Mastroianni, and W. Grundfest, "Virtual proprioception," *J. Mech. Med. Biol.*, vol. 8, no. 3, pp. 317–338, Sep. 2008.

[6] B. H. Dobkin, *The Clinical Science of Neurologic Rehabilitation*. New York: Oxford University Press, 2003.

[7] J. Perry, *Gait Analysis—Normal and Pathological Function*. Thorofare, NJ: Slack, 1992.

[8] R. LeMoyne and T. Mastroianni, "Use of Smartphones and Portable Media Devices for Quantifying Human Movement Characteristics of Gait, Tendon Reflex Response, and Parkinson's Disease Hand Tremor," A. Rasooly and K. E. Herold, *Mobile Health Technologies: Methods and Protocols*. New York: Springer, 2015, pp. 335-358, Ch 23.

[9] R. LeMoyne, W. T. Kerr, K. Zanjani, and T. Mastroianni, "Implementation of an iPod wireless accelerometer application using machine learning to classify disparity of hemiplegic and healthy patellar tendon reflex pair," *J. Med. Imaging Health Inform.*, vol. 4, no. 1, pp. 21-28, Mar. 2014.

[10] R. LeMoyne, W. Kerr, T. Mastroianni, and A. Hessel, "Implementation of machine learning for classifying hemiplegic gait disparity through use of a force plate," *In Proc. 13th Int. Conf. IEEE Machine Learning and Applications (ICMLA)*, Detroit, MI, Dec. 2014, pp. 379-382.

[11] R. LeMoyne, "Advances regarding powered prosthesis for transtibial amputation," *J. Mech. Med. Biol.*, vol. 15, no. 1, Feb. 2015.

[12] A. Lesic and M. Bumbasirevic, "Ankle fractures," *Current Orthopaedics*, vol. 18, no. 3, pp. 232-244, Jun. 2004.

[13] C. W. Lin, C. E. Hiller, and R. A. de Bie, "Evidence-based treatment for ankle injuries: a clinical perspective," *J. Man. Manip. Ther.*, vol. 18, no. 1, pp. 22-28, Mar. 2010.

[14] C. Kisner and L. A. Colby, *Therapeutic Exercise: Foundations and Techniques*, Philadelphia, PA: F.A. Davis, 2012.

[15] T. H. Kim, J. S. Yoon, and J. H. Lee, "The effect of ankle joint muscle strengthening training and static muscle stretching training on stroke patients' C.O.P sway amplitude," *J. Phys. Ther. Sci.*, vol. 25, no. 12, pp. 1613–1616, Dec. 2013.

[16] S. S. Ng and C. W. Hui-Chan, "Contribution of ankle dorsiflexor strength to walking endurance in people with spastic hemiplegia after stroke," *Arch. Phys. Med. Rehabil.*, vol. 93, no. 6, pp. 1046-1051, Jun. 2012.

[17] S. S. Ng and C. W. Hui-Chan, "Ankle dorsiflexion, not plantarflexion strength, predicts the functional mobility of people with spastic hemiplegia," *J. Rehabil. Med.*, vol. 45, no. 6, pp. 541-545, Jun. 2013.

[18] R. LeMoyne and T. Mastroianni, "Implementation of a smartphone as a wireless gyroscope application for the quantification of reflex response," *in Proc. 36th Int. Conf. IEEE EMBS*, Chicago, IL, Aug. 2014, pp. 3654-3657.

[19] R. K. Begg, M. Palaniswami, and B. Owen. "Support vector machines for automated gait classification," *IEEE Trans. Biomed. Eng.*, vol. 52, no. 5, pp. 828-838, May 2005.

[20] M. Hall, E. Frank, G. Holmes, B. Pfahringer, P. Reutemann, and I. H. Witten, "The WEKA data mining software: an update," *ACM SIGKDD explorations newsletter*, vol. 11, no. 1, pp. 10-18, Jun. 2009. New York: Oxford University Press, 2003.

Implementation of Parallel Harris Corner Detector on FPGA

Wong Kien Liong
Faculty of Electrical Engineering
Universiti Teknologi Malaysia(UTM)
Johor, Malaysia.
liong-93@hotmail.com

Dr. Nasir Shaikh Husin
Department of Electronic and Computer Engineering
Faculty of Electrical Engineering
Universiti Teknologi Malaysia(UTM)
nasirsh@utm.my

***Abstract*— Many methods have been used to detect corners in an image, such as SUSAN and Harris corner detector (HCD). The performance of HCD is better than other methods in terms of stability and accuracy, especially for a noisy image. HCD has been used in many applications of image processing such as object recognition. However, HCD requires a substantial amount of time to detect the corners. This paper discusses the implementation of parallel HCD on Field-Programmable Gate Array (FPGA). The parallel implementation is able to reduce the time required to detect corners in an image. It also optimizes the resource utilization, throughput and latency compared with other implementations. The hardware implementation of parallel HCD was tested using the Verilog testbench, enveloped by a Matlab testbench. An image is divided into two halves and each half is processed by a HCD in parallel. Each image passes through various modules such as spatial derivatives, Gaussian filter, Harris response and finally non-maximum suppression before the corners are detected. Matlab testbench is used to validate the results of the hardware architecture. The corners detected using HCD hardware are compared with the results from Matlab to check the accuracy of the hardware implementation.**

Keywords—Parallel Harris Corner Detector; Spatial Derivatives; Gaussian Filter; Harris Response; Non-maximum Suppression

I. INTRODUCTION

High level computer vision is used in the detection of classes of object in an image, object recognition, and classification of images for medical as well as scientific applications [6]. All of these operations rely on low-level processes, such as corner detection. Intersection of two edges is defined as a corner [9]. A corner is a point where there are two dominant and different edge directions in a local neighborhood of that point. Harris corner detector (HCD) algorithm is widely used in many applications such as object recognition and corner detection. There are many others methods for corner detection such as SUSAN and Minimum Intensity Change (MIC), but their performance with noisy image is poorer than the HCD algorithm in term of stability and accuracy. However, HCD is time consuming For computer vision systems, high-speed corner detection is essential for motion detection and object recognition [6, 10]. So, we need to reduce the time required for corner detection in an image. This paper presents the hardware implementation of parallel HCD algorithm on Field Programmable Gate Array (FPGA), which can reduce the time required for corner detection in an image as well as optimizes the resource utilization, throughput and latency.

II. LITERATURE REVIEW

Many methods have been used to detect corners on different platforms. This section discusses some of the previous works that are related to HCD and also implementing HCD on FPGA.

A. Corner Detection

Using computer vision systems is one of the methods for corner detection and also for extracting certain kinds of features. It can also infer the contents inside an image. Corner detection is frequently used nowadays in the applications of motion detection, 3D modeling, panorama stitching, video tracking, image registration as we11 as object recognition[6]. Corner detection is related with the topic of interest point detection [9]. HCD algorithm which is developed by C. Harris and M. Stephens in 1988 can detect the location of corner points within an image. The intrinsic properties of corner points had made using of HCD algorithm frequently in the computer vision system applications such as object recognition [6]. A corner can be defined as the intersection of two edges. It can also be defined as a point which contains 2 dominant and different edge directions in a local neighborhood of that point [11]. HCD algorithm can easily recognize the corner by looking at the intensity values within a small defined window or area within an image which have high gradient values in all directions [2]. If a corner is exists within an image, shifting the window in any direction such as X-direction and Y-direction will produce a large change in appearance or high changes in intensity exist in more than one direction. Figure 1 shows the type of regions in an image [8].

B. Mathematical Description of Corner Detection

Calculating the sum of squared difference between the region of interest and nearby shifted regions can help to identify the corner within a region of interest [2]. Figure 2 shows the sum of square difference formula for identifying the corner.

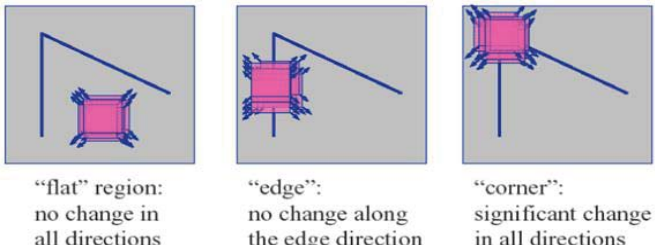

Fig.1. Type of regions in an image.

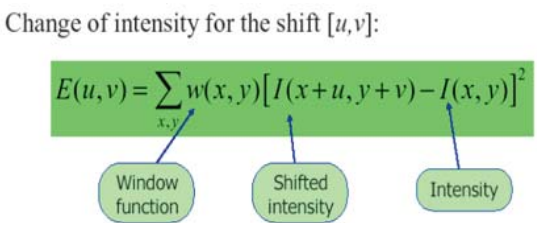

Fig.2. Sum of square difference formula for identifying the corner.

This formula will calculate the difference between region of interest and shifted region by summating the squared differences pixel by pixel. Input image is represented by the function *I* in the formula. The *(x, y)* coordinate specifies the region of interest. The *(u, v)* coordinate specifies the offset of the shifted region from the region of interest.

C. Moravec's corner detector

Moravec' s corner detector is introduced in 1980 [1]. It can easily recognize the point by looking through a small window [1]. If a corner is exists, shifting a window in any direction should give a large change in intensity [1]. However, there are some weaknesses for the Moravec's corner detector. For example, noisy response due to a binary window function, only a set of shifts at every 45 degree is considered and only minimum of E which is shown in the figure 2 is taken into consideration [1]. However, HCD which is introduced in 1988 by Harris and Stephens is able to solve all of these critical problems.

D. Harris Corner Detector

HCD is introduced by C. Harris and Stephens in 1988 to solve the weakness of Moravec's corner detector. For the noisy response due to a binary window function that occurred in Moravec's corner detector, HCD use a Gaussian filter which is able to filter the noise inside an image. In Moravec's corner detector , only a set of shifts at every 45 degree is considered but HCD consider all small shifts by Taylor's expansion[5]. The idea of HCD is formulating the gradient to detect response at any shift and find the local maxima in the auto-correlation surface *M* which is given by matrix M as shown at equation 1 at below [2]. M is actually a 2×2 matrix computed from image second derivatives [2].

$$M = \begin{bmatrix} A & C \\ C & B \end{bmatrix} \quad (1)$$

where A = Gaussian filtered second derivatives, Ix^2

B = Gaussian filtered second derivatives, Iy^2

C = Gaussian filtered second derivatives, $IxIy^2$

Below are the steps for HCD. The first derivatives of an image is calculated by using the kernel in Figure 3 and then the first derivatives, *Ix* and *Iy* are used for calculating the second derivatives, Ix^2, Iy^2 and *Ixy* of the image.

-1	0	1

Fig.3. Kernel for the estimation of image derivatives

Gaussian Filter is applied to the second derivatives, Ix^2, Iy^2 and *Ixy* to produce the filtered spatial derivatives, A, B and C which the noise already removed. The equation for Gaussian Filter is shown at the equation 2, 3 and 4 at below.

$$A = \omega \otimes Ix^2 \quad (2)$$

$$B = \omega \otimes Iy^2 \quad (3)$$

$$C = \omega \otimes IxIy \quad (4)$$

The corner response is calculated based on the filtered spatial derivatives by following the equation in 5 at below. Equation 5 is derived based on the steps in figure 4.

$$R = Det(M) - k(Trace(M))^2 \quad (5)$$

where k is a constant set to 0.06.

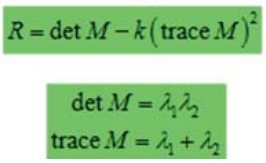

Fig.4. Steps to derive the Corner Response, R.

If its response is an 8-way local maximum, a corner pixel with a positive response is selected as a corner. 8-way local maximum means that the pixel is greater than all the 8 neighborhood pixels. If their responses are both negative and local minima in either the X or Y direction, edge region pixels are selected as edges.

E. Previous work of Implementation of Harris Corner Detector

Previous works for Implementations of HCD on FPGA for gray-scale images are found in [10]. Color images are not within the scope of this work is not used.

The work in [11] presents a pipelined architecture for maintaining a data width of 8-bits during calculating of the Harris response. This had caused regions of saturated response occurred in the response image. In order to remove this effect, further filtering was applied on the response of the saturated

regions before selecting the local maxima. However, this had also caused extra cost in area and latency. In this work, the experiment concluded that the problem of saturated response is not eliminated by the filtering operation. The final results are not satisfactory.

The work in [12] developed a local processing architecture that will exploit the data locality for reducing the line buffers used in the pipeline. An excessive amount of combinational logic is used for calculating the Harris response for each local stream of the processed image. The work in [11] had used a total of 26 line buffers, a total of 20 line buffers are used in [14] , while only seven line buffers is used in the architecture in [7]. This reduction had cause utilizing a large amount of slice registers as well as limiting the Non-maximum window to smaller size which is 3x3. This will reduce the accuracy of the final result. In the same paper, new architecture was generated to solve this problem. However, a total of 12 line buffers had been utilized with additional consumption of slice registers. These two architectures are referred as (1) and (2).

The work in [13] uses four stage pipeline which are derivative generator, Gaussian filtering, measuring the response, and non-maximum suppression. It used Block RAMs (BRAMs) at the beginning of each stage. It is excessive and should be reduced.

In [10], an improved non-maximum suppression method was introduced. It is able to reduce the total hardware consumption and was implemented as a branch of the pipeline to save the additional time consumed throughout this process. The benchmarking results were produced from OpenCV library running on a desktop computer. The platform used (Zedboard development system) featured an on-board DSP for speeding up the throughput and minimizing the Look-Up Tables (LUT) consumption. The results obtained without using the DSP is added for comparison. The summary of the previous works related to HCD and FPGA platform is shown on Table 1.

The work in [3] uses four stages for implementation of HCD which are spatial derivatives, Gaussian Filtering, Harris Response and Non-maximum Suppression. However, too much logic elements are used in the non-maximum suppression stage because it utilizes more resources than the other three stages. Logic elements used in non-maximum suppression stage needs to be reduced. Second, if multiple pixels in the 7x7 neighborhood have the same maximum value, all the multiple pixels are selected as corners. In addition, although this architecture achieves a high throughput but it also causes high latency.

III. Research Methodology

Throughout this chapter, it is going to explain about the methodology and design flow of hardware and software for the implementation of parallel HCD on FPGA. The simplified working process for the parallel HCD is shown at the figure 5 at below to ease the understanding about the overall working process of parallel HCD.

In this work, the proposed parallel HCD actually is divided into many parts. After we input an image into MATLAB, MATLAB will divide the picture into two equal half. MATLAB will generate the data file contains the image gradients. First, the data file of the top half image and bottom half image will go through the spatial derivatives at the same time to generate second derivative. Next, both second derivatives will go through the Gaussian Filter to remove the noise. Then, the filtered second derivatives will go through the Harris Response and finally it reached the Non-maximum Suppression to detect the corners in the top half and bottom half image. The corners data file generated by the hardware is read by the MATLAB to convert it into the square matrix. MATLAB will combine the result of top half and bottom half image and finally it becomes one combined image only. Figure 6 shows the functional block diagram of parallel HCD.

Table 1: Summary of previous work related to HCD.

Title	**Platform**	**Drawback**
A multi-resolution FPGA-based architecture for real-time edge and corner detection[11]	Altera Arria V	Saturated response. More logic elements.
An efficient FPGA implementation of the Harris corner feature detector[10]	Xilinx Zynq-7000	More logic elements Low F_{max}
An FPGA sliding window-based architecture HCD[12](1)	Xilinx Spartan 6	Not accurate. Low F_{max}
An FPGA sliding window-based architecture HCD[12](2)	Xilinx Spartan 6	Low F_{max}
Low Cost Pipelined FPGA Architecture of HCD for Real-Time Applications[14]	Altera Cyclone IV	More logic elements
Implementation of HCD on FPGA[3]	Altera Cyclone IV	More logic elements

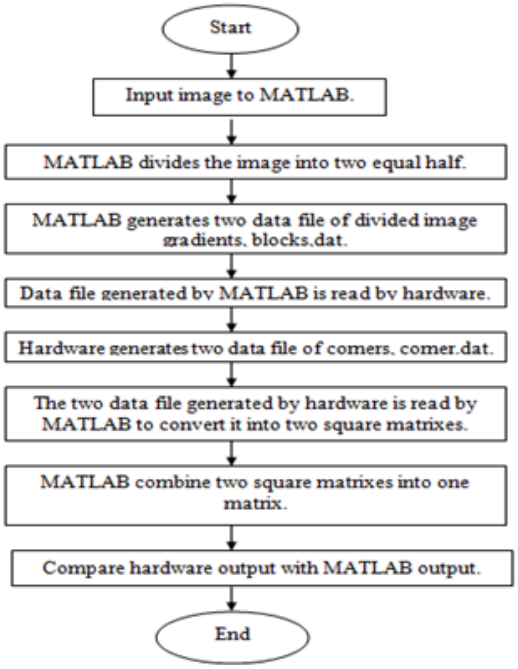

Fig.5. Working process of parallel HCD

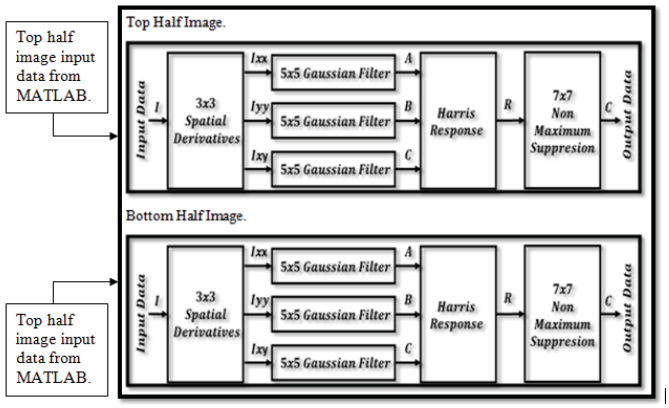

Fig.6. Functional Block Diagram of parallel HCD.

A. *Spatial Derivatives*

Spatial derivative is used to produce the first derivatives, *Ix* and *Iy* and second derivatives, *Ix2*, *Iy2* and *IxIy*. The first derivatives is produced by using the Prewitt Operator in X and also Y direction. Prewitt operator is constructed based on 3 x 3 operator approximation. Smoothing element is added to the masks by dividing the mask values with 3. So, every row or column of the mask is having an averaging effect. Figure 7 at below shows the derivatives kernel for Prewitt operator in X and Y direction.

However, second derivatives, *Ix2*, *Iy2* and *IxIy* are produces by squaring and multiplying the first derivatives, *Ix* and *Iy*. The spatial derivatives module is divided into First_Derivative module and also Second_Derivative module. For the first derivatives module, the input is the 8 bit data which is actually the binary data of an image that is generated by the MATLAB and the output is the 9 bits first derivatives, *Ix* and *Iy*. However for the second derivatives module, the input is the 9 bits first derivatives, *Ix* and *Iy* and the output is the second derivatives, *Ix2*, *Iy2* and *IxIy*.

$$1/3\begin{bmatrix}-1 & -1 & -1\\ 0 & 0 & 0\\ 1 & 1 & 1\end{bmatrix} \quad G_y \qquad 1/3\begin{bmatrix}-1 & 0 & 1\\ -1 & 0 & 1\\ -1 & 0 & 1\end{bmatrix} \quad G_x$$

Figure 7: Derivatives kernel for Prewitt operator in Y and X direction

B. *Gaussian Filtering*

Gaussian Filter is the second stage in the HCD which is used to remove the noise in the image before corner detection. 3 Gaussian filters are used for the 3 second derivatives. Each of the Gaussian Filter is divided into horizontal Gaussian and also Vertical Gaussian. The Gaussian Filter operator is a 2-D convolution operator which will be used for blurring the images and removing noises [4]. However, 1x5 kernel followed by 5x1 kernel with standard deviation of 1 and scaled by a factor of 256 is used throughout this project in order to ease the implementation of parallel HCD and reduce the logic elements. All multiply operations are transformed into shift operations because the kernels value for 1x5 kernel and 5x1 kernel are constant. The 2-D 5x5 Gaussian filter is shown in figure 7. The 2-D 5x5 Gaussian filter is separated into two 1-D Gaussian filter which are 1x5 and 5x1 Gaussian filters. It is in Figure 8.

$$1/256\begin{bmatrix}1 & 4 & 6 & 4 & 1\\ 4 & 16 & 26 & 16 & 4\\ 6 & 26 & 41 & 26 & 6\\ 4 & 16 & 26 & 16 & 4\\ 1 & 4 & 6 & 4 & 1\end{bmatrix}$$

Fig.7. 2-D 5x5 Gaussian filter

$$1/256\begin{bmatrix}14 & 63 & 103 & 63 & 14\end{bmatrix} \qquad 1/256\begin{bmatrix}14\\ 63\\ 103\\ 63\\ 14\end{bmatrix}$$

Fig.8. 1-D Gaussian filter (a) 1x5 (b) 5x1

C. *Harris Response*

Harris Response is the third stage in the parallel HCD. It is used to calculate the Harris Response, R. The 30 bits filtered second derivatives from the Gaussian Filter is the input to the Harris Response. All the second derivatives will arrive at the same clock cycle to Harris Response so that delay slice registers and row buffers are not required at this stage. The

output of this stage is 32 bits Harris Response, R. The filtered second derivatives from the Gaussian Filter will go through square module, multiplier module or adder module before storing in the registers. After that, it will go through the subtract module or square module and the results will stored in another inner registers. Finally, it will go through a subtract module and the result will stored in the last inner register. Almost all the registers in the Harris Response are 60 bits wide due to the multiplication and squaring process. At the last register inside the Harris Response, the output of Harris Response is located from bit 5 until bit 36. The algorithm of Harris Response is shown at equation 6 at below.

$$\text{Harris Response},, R = (AB - C^2) - k(A + B)^2 \quad (6)$$

k is empirically set to $0.04 - 0.06$.

However throughout this project, we are going to set the value of the constant k to 0.0625 which is larger than the original Harris algorithm. This can help to ease the implementation of hardware because 0.0625 can be implemented only through an arithmetic right shift of 4-bit. This approximation does not affect the accuracy of our result noticeably. If we get the Harris Response, R in negative value, it will be set to 0. The highest value of the response R is able to be represented by 32 bits and will not getting any saturated area in the response image.

D. Non maximum Suppression

Non-maximum Suppression is the final stage for parallel HCD. It will filter out all the values of the pixels which are non-maximum in their local neighborhood inside a window. Non-Maximum Suppression module iterates over every pixel in certain image area. Throughout this project, 7x7 non-maximum suppression windows are used to compare the pixels of the image. A large non-maximum suppression window will help to select the strongest corner within certain image area. For every pixel in the image, 48 neighborhood pixels surrounding that pixel are compared. If the pixel is not the maximum in that neighborhood, the pixel value will be set to zero. If the pixel is the maximum in that neighborhood, it is compared with certain threshold, T. If the maximum pixel in that neighborhood is greater than the threshold, T, it will be set to one which represent that a corner exists in that corner, otherwise it will be set to zero. 48 parallel comparators with seven stages of pipelining registers are required for the non-maximum suppression operation. The maximum values of each row in the 7x7 non-maximum suppression window are extracted by the first three stages of pipeline stage. After that, the maximum values of each row in the 7x7 non-maximum suppression window are extracted by the next three stages of pipeline stage. The last pipeline stage is required for the thresholding or compared with threshold value. There 3 sub-modules inside the Non-maximum Suppression, which are BRAM, Max7 and Max6. Sub-modules Max7 and Max6 are needed in order to obtain the maximum pixel value among the 48 neighboring pixels at certain window and also for extracting the center pixel at certain window. The pixels of seven rows were received by non-maximum suppression from BRAM module. The first pixel for every row is delayed by 7 clock cycles in order to have a 7x7 window. Except for the middle row, all pixel values from others rows are sending to Max7 module to obtain the maximum pixel value in that image area. Max6 module will process pixels value from the middle row to find the maximum pixel value in the middle row and hold the center pixel inside the pipelining registers until the output of Max7 modules and Max6 modules are ready. Predefined threshold, T will be compared with the maximum pixel value out of the 48 neighboring pixels. If the pixel value is greater than the predefined threshold, T, it will be selected as a corner, otherwise it will be set to zero or means that no corner exist.

IV. Results And Discussion

Throughout this chapter, it is going to discuss about the results of corner detection from the hardware and also the software of parallel HCD. After that, both the results from software and also hardware are being compared and analyzed. The 256 x 256 pixels of *blocks.gif* image is used as the input image for the parallel HCD.

A. Results from FPGA Hardware

As discussed as before, the hardware of parallel HCD is implemented inside the Quartus and simulated with the modelsim. After that, Matlab is used to show the results from the hardware. The figure 9 shows the results of corner detection from the hardware of parallel HCD for the *blocks.gif* image.

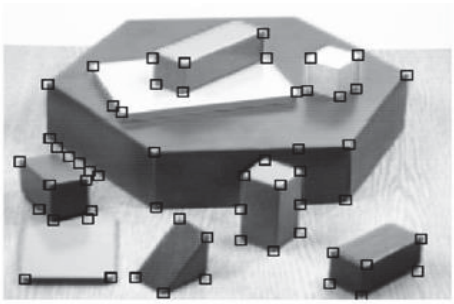

Fig.9. Results of corner detection from the hardware architecture of parallel HCD.

B. Results from Matlab Software

The results from the software of parallel HCD are generated from the Matlab software. The algorithm for the parallel HCD is written as a testbench inside the Matlab software. Figure 10 shows the results of corner detection from the Matlab software of parallel HCD for the *blocks.gif* image.

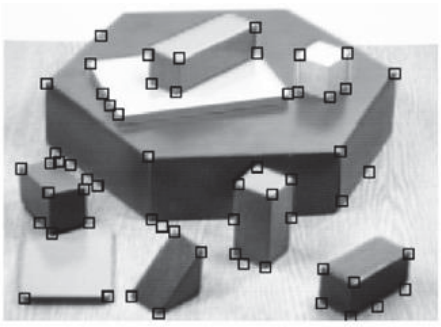

Fig.10. Results of corner detection from the software of parallel HCD.

C. Analysis and Comparision

After comparison the results from the hardware architecture and also the Matlab software, the results from the hardware and also the software is almost similar. However, there is a slight differences in corners detected which are due to the thresholding process in hardware architecture, mismatching of the result of X-direction and Y-direction as well as line buffering from the non-maximum suppression stage. For the Matlab software, the thresholding process occurred in Harris Response module with threshold value of 5000 whereas the thresholding process for hardware architecture occurred in non-maximum suppression stage. The threshold value in hardware is adjusted empirically because we are limiting the result of Harris Response, R from 66-bits to 32-bits in the third stage.

D. Recommendations and Future Improvements

This design is dividing the image into two half for running through the parallel HCD. However, the future improvements can divide the image into four parts for running through the parallel HCD in order to further reducing the latency and execution time. The future improvements also required for the non-maximum stage by reducing the logic elements utilized at that stage. The output of non-maximum suppression stage should also be improved because at current state, if multiple pixels in the 7x7 neighborhood have the same maximum value, all the multiple pixels are selected as corners. This can be solve by using Adaptive Non-maximum Suppression (ANMS) module.

V. Conclusion

In conclusion, a pipelined architecture is proposed to implement the parallel HCD on FPGA for real time applications. The parallel HCD had successfully being implemented on FPGA. This architecture is pipelined into several stages. So, a higher throughput is achieved. This implementation was divided into four stages which are spatial derivatives, Gaussian smoothing, Harris Response and Non-maximum suppression. The time required for corners detection in an image for the parallel HCD is being reduced compared with the previous work of HCD. The execution time and latency is improved and also better resource utilization compared with previous work. The results from the hardware architecture of parallel HCD is also accurate after benchmarked with the results from the Matlab software.

Acknowledgment

First and foremost, I would like to thank the God for removing all the obstacles and difficulties when I completing this project. Next, great appreciation is giving to my parents because they always support me and gives me motivation and strength especially when I am facing problems and unable to continue for my project. In addition, I also would like to thank Dr. Nasir Shaikh Husin who is the supervisor for my Final Year Project. He had taught me on lots of concept about the HCD and also the skills to use the Quartus and Modelsim software. I am very appreciated for his teaching, guidance and advices. Last but not the least, I also want to thank for all my friends and others people who had help me to complete this project.

References

[1] Moravec, H.P,(1980).Obstacle avoidance and navigation in the real world by a seeing robot rover, DTIC Document.

[2] Loundagin, J,(2015). Optimizing Harris Corner Detection on GPGPUs Using *CUDA,*

Available at: http: // digitalcommons.calpoly.edu/cgi/ viewcontent. cgi article= 2473 & context=theses.

[3] Mohammed Omar Awadh Al-Shatari,(2016) . Implementation of Harris Corner Detector on FPGA, Universiti Teknologi Malaysia : MEE thesis.

[4] Edmund Lai,(2010).*Gaussian Filtering*. University of Auckland New Zealand.

Available at: https://www.cs.auckland.ac.nz/c ourses/compsci3 73s1c /Patrices Lectures /Gaussian%20Filtering_1up.pdf

[5] Yates, R.,(2009). *Fixed-point arithmetic: An introduction*. Digital Signal Labs. 81(83): p. 198.

[6] Mainali, P., et al. Lococo,(2010). Low complexity corner detector in Acoustics *Speech and Signal Processing (ICASSP)*. 2010 IEEE International Conference on: IEEE.

[7] Gonzalez, R.C, and Woods,(2002). *R.E. Digital Image Processing (2nd .edition).* New Jersey: Prentice Hall Inc.

[8] A. Noble (1989). *Descriptions of Image Surfaces (Ph.D.).* Department of Engineering Science, Oxford University: p. 45.

[9] Leonardo Trujillo and Gustavo Olague (2008). *Automated design of image operators that detect interest points.* Evolutionary Computation: p. 483–507.

[10] Chao, T.L. and K.H. Wong(2015). An efficient FPGA implementation of the *Harris corner feature detector*. in *Machine Vision Applications (MVA).* 2015 14th IAPR International Conference on: IEEE.

[11] Possa, P.R(2014), A multi-resolution fpga-based architecture for real-time *edge and corner detection.* Computers, IEEE Transactions on, **63**(10): p. 2376-2388.

[12] Amaricai, A., C.-E. Gavriliu, and O. Boncalo(2014). *An FPGA sliding window-based architecture harris corner detector*. in *Field Programmable Logic and Applications (FPL),* 2014 24th International Conference on,IEEE.

[13] Hsiao, P.-Y., C.-L. Lu, and L.-C. Fu(2010). *Multilayered image processing for multiscale Harris corner detection in digital realization.* Industrial Electronics, IEEE Transactions on, 57(5): p. 1799-1805.

[14] Orabi, H., N. Shaikh-Husin, and U.U. Sheikh (2015). *Low cost pipelined FPGA architecture of Harris Corner Detector for real-time application* in *Digital Information Management (ICDIM).* Tenth International Conference ,IEEE.

Natural Language Processing Engine for On-The-Go Application

Muhammad Hadi Asyrafi Bin Abdul Halim
Faculty of Electrical Engineering
Universiti Teknologi Malaysia
Johor Bahru, Malaysia.
hadiasyrafi94@gmail.com

Dr. Musa bin Mohd Mokji
Department of Electronic and Computer Engineering
Faculty of Electrical Engineering
Universiti Teknologi Malaysia
Johor Bahru, Malaysia.
musa@fke.utm.my

***Abstract*— A popular goal of researchers in the field of data mining and artificial intelligence today is the natural language processing by computers. As we all know, computers generally didn't have the capability to individually process natural language, the language that human used every-day. This project aims to apply Natural Language Processing (NLP) in creating a processing module targeted towards mobile devices in on-the-go applications. In this fast moving world today, time is gold. Hence, this module will introduce features that will be beneficial for everyday usage, travelers, students and even professional workers. It hopes to increase in user productivity while reducing time consume skimming through text traditionally. This processing engine accepts commonly used information files ranging from documents, images, audio files and even Wikipedia articles. Text processing features available are Automatic Text Summarization, Semantic Analysis, Language Detector and Keyword Highlighting. The coding will be solely written in Python programming language as they are simple yet powerful while also support related libraries for NLP and text extraction.**

I. INTRODUCTION

This project aims to build a dedicated natural language processing engine for mobile devices targeted for on-the-go application. It will consist of 2 parts which is input preprocessing, natural language processing engine which is the main part of this project. These 2 parts will be combine together and wrapped by a graphical user interface (GUI) to create an intuitive and fully functional text processing engine for on-the-go application in mobile devices. The program will be coded in Python together with several related libraries already available for usage.

The preprocessing module are mainly responsible for converting input from several sources into Python's string to be fed to the main processing engine afterwards for further processing. A powerful library called 'textract' is used for this. Besides browsing local documents, preprocessing module also supports text extraction from Wikipedia. Wikipedia's article scraping are chosen to be integrated into the program due to its popularity and usability as information source nowadays. In-order to extract news articles from websites, the use of APIs and RSS feeds are indeed the simplest approach available. Data accessed through this manner comes in structured form making it easier to process. However, not all websites provide these features and sometimes even if they are available they are not maintained regularly [1]. This is where web scraping comes in. Web scraping is a technique of extracting information from websites and transforms them from unstructured form into a structured format [2]. A Python library named 'BeautifulSoup' will be used to assist in HTML parsing. The document later will undergo HTML tags stripping which will only leave text document for further processing.

The second module is the text preprocessing engine for Natural Language. "In contrast to artificial languages such as programming languages and mathematical notations, natural languages have evolved as they pass from generation to generation, and are hard to pin down with explicit rules" [3]. These natural language text which are in the form of unstructured data cannot be processed directly by computers [4]. Hence, Natural Language Toolkit, or NLTK in short which provides rich libraries for solving the complex nature of natural language related programming in Python are used to help with the processing tasks. Some of the most important features of this libraries that are used within this program are Tokenization, Part-of-Speech (POS) tagging and stop-words identification. Processing tasks that are handled by this module includes language detector, keywords highlighting, sentiment analysis and text summarization.

These three parts will be combined together into a running program which will automatically classify newly published news from several assigned websites immediately in real time. Web scraper will pass extracted news for preprocessing using NLTK library and later will be classified by SVM classifiers. The resulting classification will be cross-referenced with human based classification of the exact material for accuracy evaluation. Time taken for each classification will also be taken as one of the performance indicators of the system.

II. EASE OF USE

A. Selecting a Template (Heading 2)

First, confirm that you have the correct template for your paper size. This template has been tailored for output on the A4 paper size. If you are using US letter-sized paper, please close this file and download the file "MSW_USltr_format".

B. Maintaining the Integrity of the Specifications

The template is used to format your paper and style the text. All margins, column widths, line spaces, and text fonts are prescribed; please do not alter them. You may note peculiarities. For example, the head margin in this template measures proportionately more than is customary. This measurement and others are deliberate, using specifications that anticipate your paper as one part of the entire proceedings, and not as an independent document. Please do not revise any of the current designations.

III. PROJECT METHODOLOGY

This project consists of 2 parts or modules which is input preprocessing and natural language processing. Each part needs to work harmoniously with each other for achieving the desired outcome.

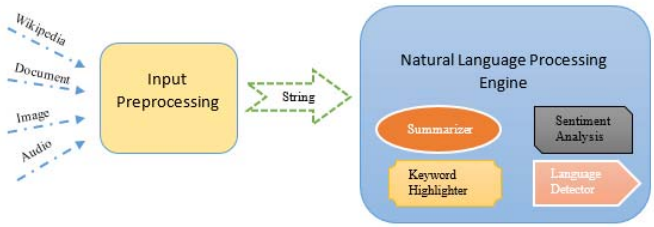

A. Input Preprocessing

The main role of this module is processing and converting any supported input file fed into the system into Python's string data type. This is because the main module of NLP processing accepts only string type of data for processing. The library used for this feature is called textract. Textract provides a single interface for extracting data from multiple file types by having dependencies on several related established libraries for Python such as python-docx, tesseract-ocr, pdftotext, python-pptx, and SpeechRecognition.

In addition to local text extraction using textract, this preprocessing module also integrated Beautiful Soup into the module. Beautiful Soup is a powerful open source HTML parsing library. Urllib2 is another important library that is used to fetch HTML documents online. Combining these 2 libraries together, a web scraper dedicated for Wikipedia text extraction is employed. "Web scraping is a computer software technique of extracting information from websites" [2]. It deploys an autonomous bot or program code that goes inside any given website refers by its URL as endpoint and extract relevant information according to the programmer specification. The information from websites are usually in HTML format. In this project, the web scraper will be programmed to extract text only from Wikipedia articles. Other junk data that may compromises NLP processing unit such as table, image and charts will also be filtered out. Below are listed some of the supported data types available:

Category	File Type	File Extension
Document	Text File	.txt
	Power Point Presentation	.pptx
	Portable Document Format	.pdf
	Word Document	.doc .docx
	Open Document Text	.odt
Image	Portable Network Graphic	.png
	Graphic Interchange Format	.gif
	Joint Photographic Expert Group	.jpg .jpeg
Audio	MPEG Audio Layer-3	.mp3
	WAVE Audio Format	.wav
	OGG Vorbis File Format	.ogg

B. Natural Language Processing Engine

This NLP module will rely mostly on Natural Language Toolkit (NLTK) an open source library for language processing in Python. Using this library, features including Tokenization, Stop Words Identification and Part-of-Speech Tagging are the one will be most commonly used. Tokenization is the process of splitting words individually in the whole text and part-of-speech such as nouns, verbs, and adjective will later be assigned by POS-tagger to the individual words. In every language, there exists stop words which are common and carries little to no meaning and are not useful for processing. Some example of these words in English vocabulary are 'a', 'an', 'and', 'are', 'it', and 'of' [13]. These basic features will be the foundation of more complex features available inside the module. Depending on the application, these features combining with several algorithms will produce Language processing features which are Summarization Algorithm, Keyword Highlighting, Semantic Analysis and Language Detection.

The first feature included in the module is Text Summarization Algorithm. There are so many approaches and techniques introduced on this particular topic. For this project, a technique published by H.P Luhn in IBM Journal April 1958 is used. It is one of the simplest technique available. According to Russel (2013), the paper by H.P Luhn talks on a summarization

technique which filters out sentences containing frequently appearing words that appear near one another. In another sense, this method is based principally upon sentence detection and frequency analysis within sentences [13].

The idea is that important sentences are the one that contains frequently occurring words. This is true except for stop-words which are frequently appearing but carries less significant. Hence, stop-words are filtered out. "In order to score each sentence, the algorithm in score_sentences applies a simple distance threshold to cluster tokens, and scores each cluster according to the formula (1)" [13]. Each sentence will be scored using the formula and later be filtered out using statistical threshold by computing mean and standard deviation for the scores obtained. Even-though this method is simple and performed well on most cases, its downturn is that it doesn't consider sentences on a deeper semantic level.

$$\frac{(significant\ words\ in\ cluster)^2}{total\ words\ in\ cluster} \quad (1)$$

Reading plain text is rather daunting and boring task for most human. In-order to counter this, NLP processing module also features a simple keyword highlighting algorithm. There are so many other methods available for this feature, each with their own set of rules of determining what are the important words with respect to individual sentences or even the whole text. However, for this module one of the simplest approach are employed. After tokenization, each individual word are tagged with POS. Words that are tagged with either NN (noun, singular), NNS (noun, plural), NNP (noun, proper singular) and NNPS (noun, proper plural) are considered as important. These tags are usually associated to the main topic in a specific sentence. After finish tagging, the text will be re-written with selected keywords bolded.

This next feature aims to guess the sentiment of a text document as a whole determining whether it is positive or negative. This feature is useful when dealing with a bunch of long reviews to gain insight on something. This method relies on several dictionaries which are negative, positive, inverse, decrementing, and increasing list of words. Negative and positive dictionaries contain hundreds of respective tone words which are retrieved from a paper by Bing Liu et.al (2005). Inverse dictionaries contain words that invert a certain word sentiment for example 'not' and 'would not'. Decrementing and increasing dictionaries contain words that lowers or increases semantic value of the words preceding it. Text input then will be tokenized to their individual words and compared with the available dictionaries and scored according to their positivity and negativity. The final value will be added up, positive value shows a positive sentiment and vice versa.

The last feature available inside this processing module is the language detection. The algorithm for this feature relies on the use of pre-defined stop-words inside NLTK library. The method behind this feature is that each tokenized word will be cross referenced with stop-words of each language available inside the library. The language with the most number of similarities is chosen as the natural language of the text. There are 13 available stop-word's languages available which are Danish, Dutch, English, Finnish, French, German, Hungarian, Italian, Norwegian, Portuguese, Spanish, Swedish and Turkish. To account for Malay, I have created my own set of stop-words for Malay language. So, there are a total of 14 languages that can be detected by this feature.

IV. RESULT AND ANALYSIS

A. Summarization Analysis

For analyzing the summarization of textual document using this module, 10 BBC news articles are retrieved from their websites. The graph below shows percentage of summarization achieved by each article respectively. To conclude, the summarization percentage ranges between 65.78% to 82.01% with the average of 75.76%. Approximately ¼ of the total text remained for each summarization.

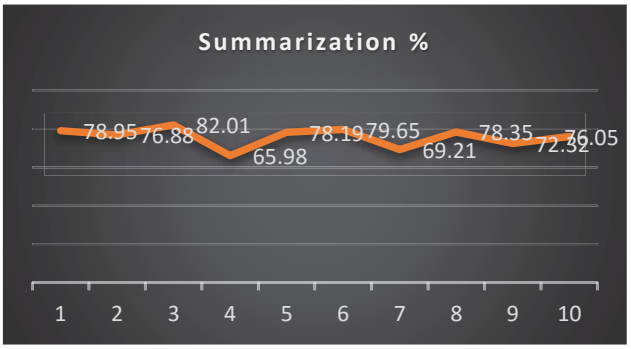

B. Semantic Analysis

Semantic analysis deals with determining positive or negative tone of a text. Samples are taken from movie rating website called imdb. These samples are chosen from such websites because movie reviews are generally strongly bias towards one sided. In addition, star rating in such websites helps to define the sentiment for comparison. Review with rating below 4 are considered as negative while rating of above 7 are considered as positive. 50 negative reviews and 50 positive reviews are extracted randomly from several movies for sampling. From the results, we can clearly see that hit (accurate analysis) make up 83% of the total analysis. The percentage error of this feature for this particular case are 17% as shown.

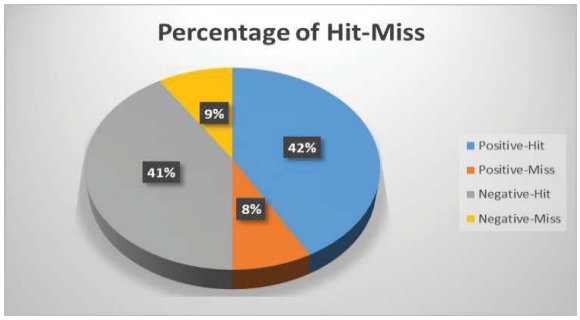

C. *Language Detection*

This subtopic will be discussing the result of analysis of language detection feature in this NLP processing module. For each language, 5 random text containing mainly short stories are extracted online for analysis accounting for a total of 70 textual document. These texts are ran through the module and the resulting language detection are compared with the original language of the text. The result clearly shows a 100% accuracy for all languages detection.

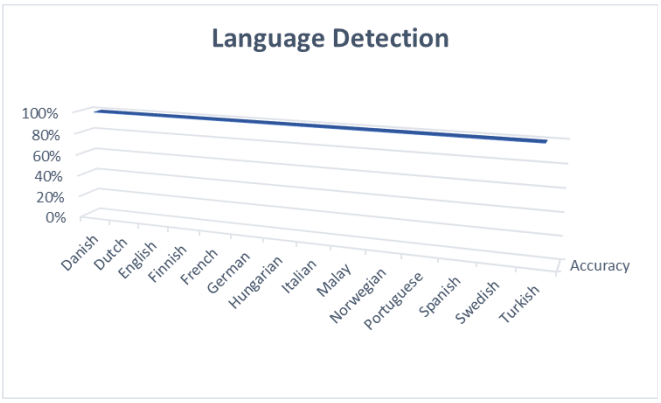

The system should be able to automatically extract news articles directly after published on given websites and later classify the news into its respective category. This program is expected to be running in background all the time as to do classification in real time. This project can be considered as successful only if the accuracy of news classification rise above 80% of the time. In addition, the running program should not eat up too much computer resources such as RAM and CPU while also didn't burden the internet traffic by much. This is also the indicator that the program is written and executed successfully.

V. CONCLUSION

Natural Language Processing is not an entirely new field to be studied. The rapid growth of Artificial Intelligence had indeed gives us new perspective on solving problems that we deal with daily. NLP processing features introduced in this project only are only some of the possible applications in intelligent information management. This project is hoped to later pave the way how we deal with this vast volume of information called as Big Data in the near future.

REFERENCES

[1] [1] H. Brody, 08 December 2012. [Online]. Available: https://blog.hartleybrody.com/web-scraping/.

[2] [2] S. Ray, 22 October 2015. [Online]. Available: https://www.analyticsvidhya.com/blog/2015/10/beginner-guide-web-scraping-beautiful-soup-python/.

[3] [3] S. Bird, E. Klein and E. Loper, Natural Language Processing with Python, O'Reilly Media, 2014.

[4] [4] M. I. Rana, S. Khalid and M. U. Akbar, "News classification based on their headlines: A review," in Multi-Topic Conference (INMIC), Karachi, 2014.

[5] [5] T. Joachims, Learning To Classify Text Using Support Vector Machines, Kluwer Academic, 2001.

[6] [6] Y.-H. Chen and S.-F. Li, "Using latent Dirichlet allocation to improve text classification performance of support vector machine," in 2016 IEEE Congress on Evolutionary Computation (CEC), Vancouver, BC, 2016.

[7] [7] A. Dragland, 22 May 2013. [Online]. Available: http://www.sintef.no/en/latest-news/big-data--for-better-or-worse/.

[8] [8] D. Gutierrez, 5 June 2015. [Online]. Available: http://insidebigdata.com/2015/06/05/text-analytics-the-next-generation-of-big-data/.

[9] [9] J. Victor, 26 October 2011. [Online]. Available: http://www.sharemarketschool.com/how-does-news-affect-stock-prices/.

[10] [10] W. Zhou and C. Lili, "The algorithm of text classification based on rough set and support vector machine," in Future Computer and Communication (ICFCC), Wuhan, 2010.

[11] [11] L. Cui, F. Meng and Y. Shi, "A Hierarchy Method Based on LDA and SVM for News Classification," in Data Mining Workshop (ICDMW), Shenzen, 2014.

[12] [12] S. M. H. Dadgar, M. S. Araghi and M. M. Farahani, "A novel text mining approach based on TF-IDF and Support Vector Machine for news classification," in Engineering and Technology (ICETECH), Coimbatore, 2016.

[13] [13] C. D. Manning, P. Raghavan and H. Schütze, Introduction to Information Retrieval, Cambridge University Press, 2008.

[14] [14] 31 August 2004. [Online]. Available: http://jmlr.csail.mit.edu/papers/volume5/lewis04a/a11-smart-stop-list/english.stop.

[15] [15] [Online]. Available: http://scikit-learn.org/stable/modules/svm.html.

[16] [16] S. P. Ponzetto, Knowledge acquisition from a collaboratively generated encyclopedia, Heidelberg: Akademische Verlagsgesellschaft, 2009. 2005]

QR Code based Entrance Gate System

Zaemah binti Ahmad
Faculty of Electrical Engineering
Universiti Teknologi Malaysia
Johor Bahru, Malaysia.
zaemah_ahmad@yahoo.com

Dr. Musa bin Mohd Mokji
Department of Electronic and Computer Engineering
Faculty of Electrical Engineering
Universiti Teknologi Malaysia
Johor Bahru, Malaysia.
musa@fke.utm.my

***Abstract*— Nowadays, case involved crimes such as robbery, kidnapping and burglary has increased especially at the residential area. Thieves are no more afraid with the surrounding where many of lately incident happened during day hours. One of the contributing reason for this is, it is difficult to control people that enter and go out from a residential area. Currently, most of the security system focus on using access card for the owner of the gated residence only. Besides, some residential area can just provide security system which placed a guard in front of the residential area which the security is still on the less secure because they cannot control the people going in and out from the residential area. Therefore, this project has been developed to improve the card system in order to make the residential area more secure and can be applied to residential type of entrance only. This project will be using QR code as an access to the residential area. QR code will be given by the owner of the housing area as invitation for the guest to enter the housing area. There will be a website for the owner to key in the data of the guest. The data will be stored in a database. In this project, 000Webhost (free webhost) is used to build the website. In addition, this project used Visual Studio 2015 with add of ASP.net to create the QR code. As a conclusion, this type of security system is automated and practical, hence make the residential area more secure.**

Keywords— Visual Studio; QR code; security system; residence

I. INTRODUCTION

By years, the number of residential area keep increasing and some of residential area provide security system and some might not have. Most of terrace type of houses does not have any security applied for the residence. However, at the apartment or luxurious housing area, there are security system applied which by providing a guard at in front of the residence or by providing access card to the owner of the residence or both. Lack of security system lead to crimes, but it is hard to control the people coming in and out of a residence to make the residence is secured.

Some residential area provide security guard in front of the residence. Besides, there are some residential area that used RFID card to access the residential but it just applicable to the owner of the house in the residential area and for the guest, they need to place their identity card or driving license and write their name in a guest book record. However, by placing identity card or driving license break the rule and not applicable to place identity card to the guard at the guard house. Unsecure security system lead to the crimes at the residential area. A residential area should be safe by having applicable security system to avoid and decrease crimes. Therefore, this project is proposed to make a proper and safer security system by applying QR code.

QR (Quick Response) code is a machine readable optical label with information on the associated on the item or product. It conveys information by arrangement of its dark and light element. The objective of this project is to automate entrance gate system, to apply QR code as an easy and secured access for owner of the residence and guest and to develop a secured system for entrance gate system. However, this project is limited and will only solve for relatives and friends type of guest only. It is also limited for web base only but can be access with any type of gadget that can browse through internet and this project will provide a file of recorded data consists of (name, NRIC, plate number, phone number, address and visit date) only.

II. LITERATURE REVIEW

This chapter will discuss the previous work that has been done in order to improve the system and the application of QR code as by now, there is no application of QR Code on entrance of residential yet. However, QR Code has been used in several of application such as marketing, healthcare and warehouse and logistic as QR Code can store a large amount of data in a smaller space.

A. Security guard

There are some residential area that use this type of security which placing a guard in front of the entrance of the residential. A guardhouse will be placed in front of the residential where the guard will be placed there. Guests that want to enter the residence, they need to leave their identity cards or licenses at the guardhouse and write their name in the record book.

B. Access using RFID card

Some of residence area provide a RFID card to the owner of the house. RFID is a group of technologies refer as Automatic Identification and Data Capture (AIDC) where this method automatically identify object, collect data and enter those data directly into the computer systems. The owner of the house in that resident area will be given that card and they will touch that card at the entrance gate that will allow the gate to open. However, it is just applied to the owner whereby the guest of that want to enter the resident needs to record their name in the record book at the guard house.

C. QR code as attendace system

In 2014, Fadi Masalha had proposed student attendance system which to reduce burden of maintaining manual records and saved time. To generate QR Code with specific information, the system requires a simple log in process through its server by the class instructor. Then, the instructor will displays an encrypted QR Code to the students and students can scan the displayed QR Code using the system Mobile Module. [1]

D. Online banking using QR code

In 2014, Sonawane Shamal had design a QRP, a secure authentication system by combining a password and a camera equipped mobile phone. [2] The mobile phone is acting as an authentication token. When user goes for online banking, after opens the bank website, a registration QR Code will be display on the page and user can scan the QR Code image with the QR Code scanner. The generated string is automatically entered into the login page and the homepage of bank opens if the network is available on smart phone.

E. QR code as security solution

In 2012, Sankara Narayanan discussed on attack via QR Codes and security solution. The attack happens when user scans the code, he/she is directed towards a website and malicious file downloads in the user's device without the knowledge of the user. The solution to this problem is downloading an app on the phone which provides a preview to each code before its open a webpage reader. By this way, user can see if they are not visiting the correct site if the code is hijacked. Thus, secured usage is ensure and data security is enhanced.

F. Implementation of QR code in healthcare

In 2015, Jyoti Patel had proposed an integrated system for the use by healthcare personnel within hospitals and it is adapted to smartphone, tablets and handheld devices. The main purpose of generating QR Codes is engaging the patients' attention and emotions through their smartphones as patient always lose paper hand-outs, care instructions, and appointment cards, but they rarely misplace their smartphones. [3]

III. Methodology

In order completing this project, some software is used to generate the QR code and designing the webpage. Below are the software used in this project and the project overview:

A. Visual Basic Studio 2015

Visual Basic Studio is used to develop computer programs. This software supports different programming languages such as C, C++, VB.NET, C# and F#. Visual Studio also include a code editor that support syntax highlighting and code implementation. This project used this software to encode and decode the QR Code based on the information given. The interface of Visual Basic Studio is shown in Figure 1.

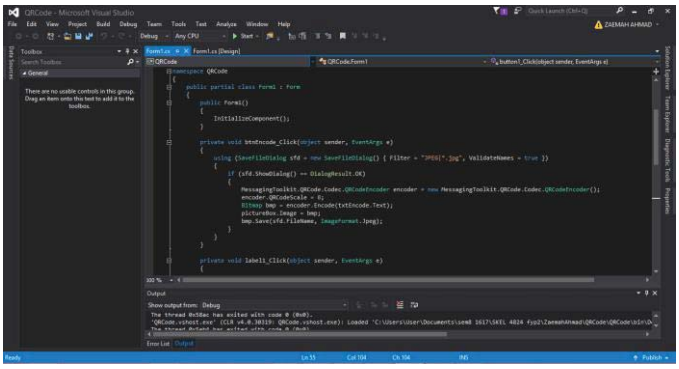

Figure 1: Interface of Visual Basic Studio 2015

B. 000Webhost

000Webhost is a free web hosting provided a service to create website with PHP, MySQL, and Cpanel. Figure 2 and Figure 3 shows the interface of 000Webhost and MySQL respectively. It is easier to create website and upload it to the internet as 000Webhost provide free server and database. In this project, this tool is used to create the website of the invitation form for the user to fill in the details of the guest. Then, the details of the guest will be save to the database provided by the webhost which is MySQL. MySQL is an open-source database management system (DBMS) that manages databases and connects them to software. Therefore, MySQL is used to connect the website with Microsoft Visual Studio.

Figure 2: Interface of 000Webhost

Figure 3: Interface of MySQL

C. Project Overview

Figure 4 shows the overview of the operation of this project from start to the end.

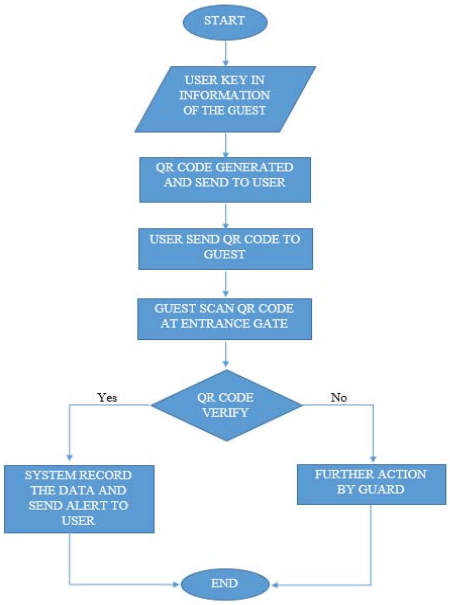

Figure 4: Project Overview

To see the project flow clearly, the system of this project can be divided into two categories. First, the system conduct for the resident and second is the system at the entrance of the residence which is at the guard house. Figure 5 shows the process flow at the resident side, while Figure 6 shows the process flow at the guard house side.

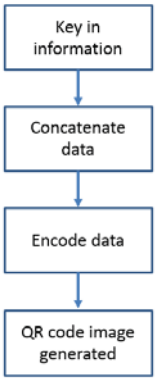

Figure 5: Process Flow at Residence Side

Figure 5 shows the flow that need to be taken by the residents when they want to invite guest to their house. Firstly, they need to browse the link of the website and fill in the details required. The details will be store in the MySQL database and the system will concatenate data from database to the system in the computer at the guard house. Next, the data will be encoded and QR code will be generated and ready for used.

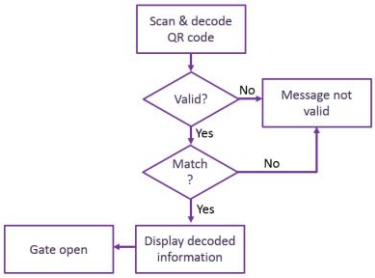

Figure 6: Process Flow at Guard House Side

Figure 6 shows the process flow that happen at the guard house of the residence. When guest scan the QR code at the guard house, the QR code will be decoded by the system in the computer at the guard house. The QR code will be verified either it is valid generated from the website provided or not. If the QR code is not valid, which by the QR code is generated from different QR code generator, the message shows 'Not Valid' will be display on the screen of computer at the guard house. Instead, if the QR code is valid, the system will check either the data in the QR code is match or not with the data filled by the resident in the website. If the data is not match, the message 'Not Valid' will be display and if the data is match, the system will undergo next process. Next, the system will display the decoded information of the user from the QR code on the computer's screen at the guard house and the gate will open.

IV. Result

QR code is encode and decode by using Visual Basic Studio 2015 based on the information filled in the website provided. Below are the results from this project.

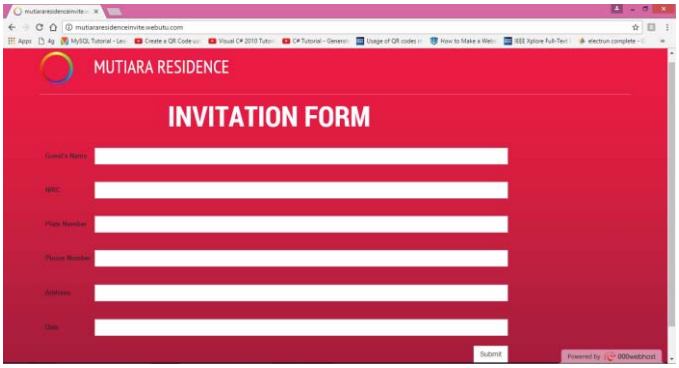

Figure 7: Website for the residence to fill in the details of the guest

Figure 8: QR code generated 1

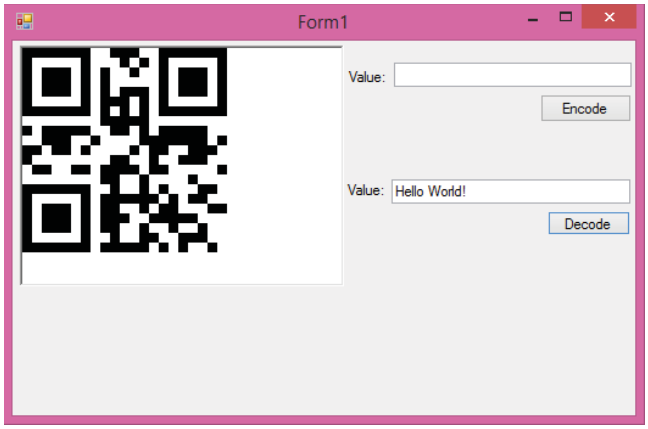

Figure 9: Interface for decode the QR code

Figure 10: QR code generated 2

V. Discussion and Conclusion

Figure 8 shows the interface from Visual Basic Studio 2015 to key in the data needed and the generated QR code based on the information. Instead, Figure 9 shows the decoded QR code by selecting the QR code image that needed to decode and the information decoded is place at the space provided above the 'Decode' button.

However, if we encode the same information, the QR code generated will not be the same. As Figure 10, the QR code generate with the same information as in Figure 8, but the result will not be the same as the QR code produced in Figure 8. It shows that, even the QR code is generated with the same information, but it can only be used once per scan.

As a conclusion, all the objectives stated at the beginning of this project is achieve successfully. Even though all the objectives are achieved, some improvement need to be done for further development. In this project, the QR code is just apply to the guest type of relatives and friends only and entrance of residence.

References

[1] Fadi Masalha, Nael Hirzallah, "Students Attendance System Using QR Code", Volume 5, Issue 3, International Journal of Advanced Computer Science and Applications, 2014, pp. 75-79.

[2] Sonawane Shamal, Khandave Monika, Nemade Neha,"Secure Authentication for Online Banking Using QR Code", Volume 4, Issue 3, International Journal of Emerging Technology and Advanced Engineering,march 2014,pp. 778- 781.

[3] Madhuri Chaudhari, Jyoti Dighe, Supriya Gadhave, Snehal Khairnar, Prof. Sonal Gore,"Data Management and Prediction about Health Status to Support Health Care System Using QR Code", Volume 5, Issue 11, International Journal of Advanced Research in Computer Science and Software Engineering, November 2015,pp. 412-415

[4] K.H Pandya, H.J. Galiyawala, "Survey on QR Codes: in context of Research and Application", Volume 4, Issue 3, International Journal of Emerging Technology and Advanced Engineering, march 2014, pp. 258-262

[5] P. Pramkeaw, T. Ganokratanaa and S. Phatchuay, "Integration of Watermarking and QR Code for Authentication of Data Center," 2016 12th International Conference on Signal-Image Technology & Internet-Based Systems (SITIS), Naples, Italy, 2016, pp. 669-672.

[6] Z. Čović, Ü. Viktor, J. Simon, D. Dobrilović and Ž. Stojanov, "Usage of QR codes in web based system for the electronic market research," 2016 IEEE 14th International Symposium on Intelligent Systems and Informatics (SISY), Subotica, 2016, pp. 187-192.

[7] Sago Brad, "The Usage Level and Effectiveness of Quick Response (QR) codes for Integrated Marketing Communication Purposes among College Students", International Journal of Integrated Marketing Communications, vol. 3, no. 2, pp. 7-17, 2011

[8] S. Okazaki, A. Navarro, S. Campo, "Cross-Media Integration of QR Code: A Preliminary Exploration", Journal of Electronic Commerce Research, vol. 14, no. 2, pp. 137-148, 2013.

QRS Complex Detection

Nursaiful Hadi bin Sulaiman
Faculty of Electrical Engineering
Universiti Teknologi Malaysia
Johor Bahru, Malaysia.
nursaifulhadi@gmail.com

Dr. Mohd Afzan bin Othman
Department of Electronic and Computer Engineering
Faculty of Electrical Engineering
Universiti Teknologi Malaysia
Johor Bahru, Malaysia.
afzan@fke.utm.my

***Abstract*—A QRS complex detection algorithm was proposed as the algorithm is powered up three times in order to discriminate any baseline wander contaminated in the Electrocardiogram (ECG) signal and at the same time to improve the visibility of P, Q, R, S and T waves. The proposed algorithm was developed using MATLAB. The important characteristic of this proposed algorithm are simple algorithm as we intended to embedded the algorithm on a Arduino based microcontroller (for the next project) and yet the proposed algorithm is accuracy enough to locate QRS complex which is then used to calculates important ECG parameters such R-R interval, heart beat per minute, QRS durations and etc. Theses ECG parameters are essential in determining the heart condition. The results were shown by using GUI MATLAB which features the number of Q, R and S wave, the plot of the ECG signal graph, R-R interval, the calculation of heartbeat and the QRS interval. The performance of the proposed algorithm was verified by using MIT-BIH Normal Sinus Rhythm Database from Physiobank resulted in 91.53% precision for R peak detection, 77.41 % precision for Q wave detection and 87.77% precision for S wave detection.**

Keywords—Electrocardiogram(ECG);MATLAB;R-R interval

I. INTRODUCTION

A reliable QRS complex detection is essential in order to determine one's heart condition. From QRS complex, the other important waves of Electrocardiogram (ECG) signal such P wave, Q wave, R wave, S wave and T wave can be located and then interpreted by calculating the parameters to verify any signs of cardiac disease from the ECG. These parameters include RR interval, ST segment, QT interval and PP interval.

When there are slightly changes in the ECG waves, it will signed any abnormalities occurs during heart contractions. Thus the physician will know that someone is having a cardiac disease and will identify the kind of disease by just looking at the parameters calculated above. Thus, an accurate QRS complex detection capability is a must in order to avoid any false detection which resulting wrong diagnosis to a patient.

A. Basic Function of Heart

Human heart has four chambers that act together to pump blood throughout the whole body. The two small upper chambers are called atria and the larger lower chambers are called ventricles [1]. The right atrium receives oxygenated blood coming back from the body via two large veins which are the superior vena cava and inferior vena cava. This blood is pumped by the right atrium into the right ventricle, which then pumps the blood into the lungs. The blood is oxygenated. After that, the blood comes back into the left atrium, which is then pumped into the left ventricle. The blood is pumped back by the left ventricle to the circulatory system via the aorta which is the largest artery in the body. The process of pumping blood by heart muscles will produce an electrical activity of the heart and is captured as ECG signals.

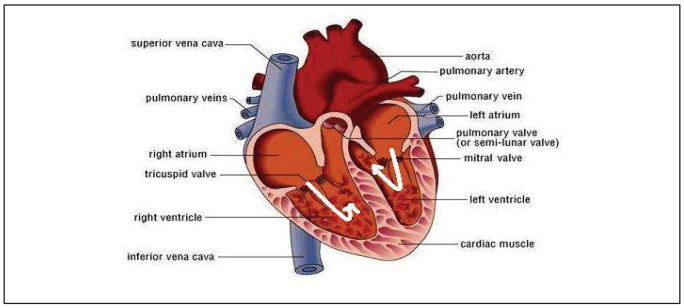

Fig. 1. *The Human Heart.*

B. Conduction System of the Heart

Human heart is known to be myogenic. Signal is generated from the heart itself which is by the pacemaker cells within the cardiac muscle. Cardiac myocytes are actually auto rhythmic because their ability to depolarize at the same interval spontaneously [2]. The conduction system of the heart has constant pattern as shown below:

- The chambers of the heart pump with the automatic discharge of electricity from the sinoatrial (SA) node. This is the essential and natural pacemaker which is located in the right atrium. On average, there are 60 to 100 times discharge per minutes. This node initiates each heartbeat and also determine the heart rate [1].
- When the SA node discharges, both atria contract, and the electrical impulse is relayed to the atrioventricular (AV) node, located between the two ventricles [1]. This node acts as the impulse gateway from atrium to ventricles and the surrounding fibrous skeleton acts as an insulator to prevent the electrical impulse from getting to the ventricles from other routes [2]. The contraction process of atria is known as atrial depolarization, and is denoted as P wave on the ECG waveform.

- Atrioventricular (AV) bundle also known as bundle of His which is the route for the impulse to leave the AV node [2].
- Then, the electrical wave is transmitted from the AV node to the lower chambers of the heart which are ventricles via the bundle branches [1]. This process is illustrated by wave in ECG signal.
- The ventricles will contract and pump blood to the whole body. The atrium and ventricle contractions is 0.12 and 0.20 seconds when in normal delay [1]. On the ECG, the R wave marks the left ventricle contraction while S wave marks the right ventricle contraction.
- The nerves that spread throughout the ventricular myocardium, Purkinje fibers will disperse the electrical impulse to the myocytes [2]. This process is marks as T wave in ECG where is it is indicate that heart's muscle of ventricles return to its normal shape, relax and ready to receive the next signal.

The electrical impulse flow is shown in the block diagram of the cardiac conduction system in Figure 2 below:

Fig. 2. *Block diagram of cardiac conduction system.*

The detection of QRS complex based on the algorithm using MATLAB software are based on the normal sinus heart rhythm. Heart rhythm has special features on their signal because of its quasi-periodic wave, which means that the signal is repetitive according a certain of time. Normal heart wave basically shows P, Q, R, S and T wave. These waves are actually the indication of heart activity. Atria depolarization indicated by P wave. QRS interval shows ventricular depolarization and T wave as the ventricular repolarization. Figure 1.1 shows the signal of the heart which consists of P, Q, R, S and T waves.

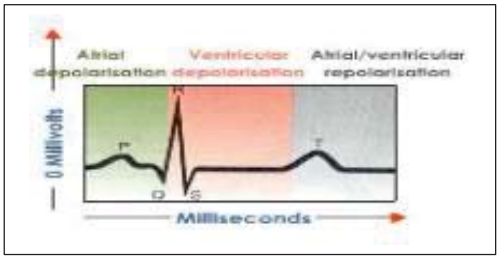

Fig. 3. Characteristic of Heart Rhythm.

The R-R interval in the normal heart wave has less than 1 second which is approximately 0.8 seconds. This means these R-R intervals will indicate the rate of human heart which is normally 60 to 80 beats per minute (bpm). Missing or irregular wave can cause heart problem or arrhythmia.

QRS complex detection is difficult to recognize, not only just need to refer to the physiological variable of the QRS complexes, but also there are many types of noise present in the ECG signal. These noises include the baseline wander, motion artefacts and high frequency noise interference. In this project, these noises were reduced by using a filter that was proposed by Pan and Tompkins, 1985.

The popular signal feature used to locate the QRS complex is the R wave because the algorithm can provide the straightforward information to implement. These R waves can be used to detect the heartbeat using R-R interval. However, the detection of the R waves alone is insufficient enough for QRS complex detection. To achieve the proper detection, others parameters must be put under consideration so that Q and S waves can be detected correctly. The Q and S waves detection is not a simple job as both waves were similar in shape from one to another.

II. Literature Review

A. *Pan and Tompkins algorithm*

Pan and Tompkins algorithm was developed to process ECG data in order to cut off noises without cutting off other information. The Pan and Tompkins algorithm, need several process which are band pass filter, derivative equation, squaring function and moving window integration [3].

- Band pass Filter

Band pass filter is used to reduce unwanted noise in the ECG signal by making it same as the spectrum of the average QRS complex [3]. The band pass filter reduces the influence of muscle noise, 60Hz power line interference, baseline wander as well as the T wave interference [4]. This filter is the cascade from the low pass filter and high pass filter. The number of order used is second order low pass filter. The transfer function of the filter is as follows:[3]

$$H(z) = \frac{(1-z^{-6})^2}{(1-z^{-1})^2} \tag{1}$$

The output equation of the filter is shown in (1)

$$Y(nT) = X(nT) * H(z) \tag{2}$$

where T is the sampling period, X(nT) as the input, H(z) as the filter and Y(nT) as the output after convolution with low pass filter [3].

The transfer function of a high pass filter is

$$H(z) = \frac{(-1+32z^{-16}+z^{-32})^{-32}}{(1+z^{-1})} \tag{3}$$

The output equation of the filter is

$$Y1(nT) = Y(nT) * H(z) \tag{4}$$

where Y(nT) from (4) as the input, H(z) as the high pass filter and Y1(nT) as the output after convolution with high pass filter [3].

- Derivative Filter

Derivative filter's function is to differentiate the signal to produce the QRS complex slop information after filtering [9]. The derivative filter in Pan and Tompkins algorithm uses 5 point derivative and the transfer function of the filter is as follow:

$$H(z) = (\frac{1}{8T})(-z^{-2} - 2z^{-1} + 2z^{1} + z^{2}) \quad (5)$$

where Y1(nT) from (4) is the input convoluted with the derivative filter H(z) and Y2(nT) is the output [3].

- Squaring Function

After differentiation is squaring function, where it is executed at every point, squaring point by point. All the data points are made into positive data and does nonlinear amplification of the output of the derivative highlighting the bigger frequencies [3].

$$Y3(nT) = [Y2(nT)]^2 \quad (6)$$

where Y2(nT) from (6) becomes the input for this process and Y3(nT) as the output.

- Moving Window Integration

Moving window integration is for averaging signal function. This process is to get the waveform feature information in addition to the slope of the R wave [9]. The calculation is based on the following equation:

$$Y4(nT) = \frac{1}{N}[Y3\{nT - (N-1)T) + Y3(nT - (N-2) * T) \cdots Y3(nT)] \quad (7)$$

where N is the number of samples in the width of the integration window [3]. A big N means wide window and will cause the QRS and T waves to merge while too narrow will cause few number of QRS complexes to produce several peaks in the signal [3].

B. Applications of Adaptive Filtering

Adaptive filter essentially minimizes the mean-squared error between a primary input, which is the noisy ECG, and a reference input, which is either noise that is correlated in some way with the noise in the primary input or a signal that is correlated only with ECG in the primary input [4]. An adaptive recurrent filter structure is used to acquire the impulse response of the normal QRS complex. These are the basic adaptive filter structures used which are the mean-squared error (MSE), the least-mean squares (LMS) algorithm, the adaptive recurrent filter (ARF) and reference impulse detection. The adaptive filter extracts the signal, or eliminates the noise by minimizing the MSE between the primary and the reference inputs [4].

III. Methodology

For the detection for the QRS complex, there are several methods was proposed by researchers. Every method has its own pros and cons in classifying the abnormalities of the heart such as have higher sensitivity, lower specificity or lower accuracy. In this project, ECG signals of normal sinus rhythm were obtained from MIT-BIH Normal Sinus Rhythm Database from Physiobank. This database is a large and widely recognized database. Eighteen records were taken from the website. From the records, we take two samples of one minute interval with different start time and end time. The records were verified by the professional physicians. The records also included the actual number of normal sinus rhythm (R wave), the R-R interval, sampling frequency and others. Thus, from the actual records, we can compare with the algorithm used in the MATLAB software using the methods below:

A. Band pass filter

Band pass filter is used to reduce unwanted noise in the ECG signal by making it same as the spectrum of the average QRS complex [4]. The bandpass filter reduces the influence of muscle noise, 60Hz power line interference, baseline wander as well as the T wave interference [5]. This filter is the cascade from the low pass filter and high pass filter. The number of order used is second order low pass filter. The transfer function of the filter is as follows as (1).

For this algorithm, we used second order band pass butterworth filter type. The frequency used for high pass filter is 1Hz and the low filter is 30Hz. The filtered data then is plotted and the result showed the ECG signal which consists of P, Q, R, S and T wave.

B. Powered Output

After the signal is filtered, the detection for QRS complex was continued using power of three to the sample ECG signal to get the smooth signal and acquire the more visible Q and S wave. The equation is shown below:

$$outpower = output\hat{}3 \quad (8)$$

Output was taken after the ECG signal was filtered. The outpower is the multiplication of the outpower data by three times.

C. Detection algorithm

Then, without using Matlab function, we decided to just detect the QRS complex by using simple algorithm. The simple algorithm is used rather than build in function of peak detection (in Matlab) is used because, once this propose algorithm is successfully detect the QRS complex, then we try to implement it as a system on chip by using Arduino (later for the next project). So simple algorithm yet accurate is a must in our design. If we opted for already developed peak detection algorithm function in the MATLAB, we afraid the algorithm will be too complex to embedded on the Arduino. After going through the processes, the data using the proposed algorithm and the annotation from Physiobank were compared and recorded in the tables.

D. Global Use Interface(GUI) MATLAB

To get the results shown easier, GUI MATLAB is created. The GUI showed the plot of the detection of QRS complex in 10 seconds interval samples, the number of Q, R and S detection, the R-R interval, the calculation of heartbeat and the QRS interval.

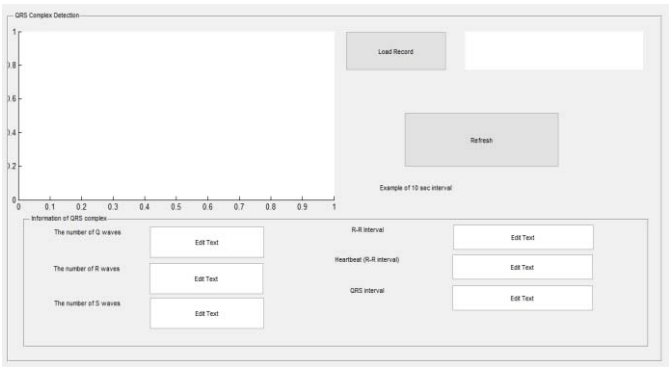

Fig. 4. *Example GUI MATLAB*

IV. RESULTS & DISCUSSIONS

The results were measured and recorded in the table below with comparison with the actual MIT-BIH Normal Sinus Rhythm Database from the Physiobank.

TABLE I. COMPARISON BETWEEN R WAVE DETECTION (PROPOSED ALGORITHM) WITH ACTUAL R WAVE FROM PHYSIOBANK

	R wave detection by proposed algorithm		Actual R wave from Physiobank		Accuracy (%)	
Records	Data A	Data B	Data A	Data B	Data A	Data B
nsr16265	95	106	95	106	100	100
nsr16272	76	65	52	62	68.42	95.38
nsr16273	110	74	110	74	100	100
nsr16420	76	76	76	76	100	100
nsr16483	98	94	98	94	100	100
nsr16539	93	64	93	64	100	100
nsr16773	89	68	89	68	100	100
nsr16786	75	71	75	71	100	100
nsr16795	96	100	62	64	67.39	64
nsr17052	63	60	63	61	100	100
nsr17453	103	87	103	87	100	100
nsr18177	85	88	85	88	100	100
nsr18184	78	80	78	80	100	100
nsr19088	95	94	95	94	100	100
nsr19090	86	75	86	75	100	100
nsr19093	64	72	64	72	100	100
nsr19140	77	80	77	80	100	100
nsr19830	111	113	111	113	100	100

Table I shows the comparison between R peak detection using propose algorithm with the actual R peak detection provided by Physiobank. From Table 1, all records shows 100% accuracy in detecting R wave except two, nsr16272 and nsr16795, with accuracy of 68.42% and 67.39% respectively using data A. From our observation we found that, ECG signal of nsr16272 and nsr1795 has a few large signals that caused the peaks were detected in the range of the proposed algorithm.

TABLE II. COMPARISON BETWEEN Q WAVE DETECTION (PROPOSED ALGORITHM) WITH ACTUAL Q WAVE FROM PHYSIOBANK

	Q wave detection by proposed algorithm		Q wave detection from Physiobank		Accuracy (%)	
Records	Data A	Data B	Data A	Data B	Data A	Data B
nsr16265	58	71	95	106	61.05	66.98
nsr16272	88	66	52	62	59.09	93.93
nsr16273	62	55	110	74	56.36	74.32
nsr16420	89	85	76	76	85.39	89.41
nsr16483	82	88	98	94	83.67	93.62
nsr16539	89	64	93	64	95.70	100
nsr16773	124	74	89	68	71.77	91.89
nsr16786	53	54	75	71	70.67	76.06
nsr16795	37	39	62	64	59.67	60.93
nsr17052	82	77	63	61	76.83	77.92
nsr17453	151	139	103	87	68.21	62.58
nsr18177	44	44	85	88	51.76	50.00
nsr18184	94	99	78	80	82.98	80.80
nsr19088	78	63	95	94	82.11	67.02
nsr19090	84	83	86	75	97.67	98.80
nsr19093	77	108	64	72	83.12	66.67
nsr19140	81	82	77	80	95.06	97.56
nsr19830	90	86	111	113	81.08	76.11

Table II shows the comparison between Q wave detection (proposed algorithm) with actual Q wave from Physiobank. The number of Q wave detected supposedly same with the R wave because the ECG signal is in normal rhythm signal. For normal sinus rhythm, for every R waves must consist of Q wave and S wave. From our observation, nsr 16795 in data A shows the lowest accuracy which is 38.54% and the highest accuracy is 100% using nsr16539 in data B. The reason why the Q wave detection are vary with the R peak detection because some of the values are included in range of the developed algorithm to detect Q wave.

TABLE III. COMPARISON BETWEEN S WAVE DETECTION (PROPOSED ALGORITHM) WITH ACTUAL S WAVE FROM PHYSIOBANK

	S wave detection from Physiobank		S wave detection by proposed algorithm		Accuracy (%)	
Records	Data A	Data B	Data A	Data B	Data A	Data B
nsr16265	92	105	95	106	96.84	99.06
nsr16272	59	62	52	62	88.14	100
nsr16273	107	74	110	74	97.27	100
nsr16420	76	76	76	76	100	100
nsr16483	45	49	98	94	45.92	52.13
nsr16539	42	64	93	64	45.16	100
nsr16773	89	68	89	68	100	100
nsr16786	42	70	75	71	56.00	98.59
nsr16795	61	61	62	64	98.39	95.31
nsr17052	61	59	63	61	96.83	98.33
nsr17453	97	87	103	87	94.17	100
nsr18177	85	88	85	94	100	93.62

nsr18184	78	80	77	80	98.72	100
nsr19088	95	94	95	80	100	85.11
nsr19090	86	75	86	82	100	91.46
nsr19093	64	72	65	72	98.46	100
nsr19140	77	80	76	75	98.70	93.75
nsr19830	111	113	18	24	16.22	21.23

Table III shows comparison between S wave detection (proposed algorithm) with actual S wave from Physiobank. From the observation, the detection of S wave is better than Q wave. This can be shown that almost all the data are 90% and above precision. The least precision data are nsr16483 and nsr 19830. The reason why the S wave detection are different with the R peak detection because some of the values are out of range of the developed algorithm to detect S wave.

The total average accuracy for R peak detection in data A is 90. 87% and 92.19% in data B. For the Q wave detection in data A is 75. 68% and 79.14% in data B. For the S wave detection in data A is 85.05% and 90.48% in data B.

Fig. 5. *Example GUI MATLAB using nsr19090 record.*

Figure 4 shows the example of GUI MATLAB using nsr19090 record in 1 minute interval within time 15 hours 14 minutes until 15 hours 15 minutes. The graph showed the data is plotted in 10 seconds interval and detection of Q, R and S wave. The number of R-R interval and the QRS interval are measured. For the heartbeat signal can be calculated using formula:

$$Heartbeat = 60/RRinterval \quad (9)$$

Fig. 6. *Example GUI MATLAB using nsr16420 record.*

Figure 5 shows the example of GUI MATLAB using nsr16420 record in 1 minute interval within time 10 hours 13 minutes until 10 hours 14 minutes. The detection of QRS, R-R interval complex, QRS interval and the calculation of heartbeat are shown.

Besides from the results shown, the main reason why Q and S wave are hard to detect is the filter used to remove noise is not good enough. This will cause the data losses. The data is too small is also another reason why the detection is difficult to find.

For the GUI MATLAB, we use it for simpler approach to get the data easier and comfortable as the data we used are quite a lot which is 18 records in different one-minute interval samples. The interface we used included the graph of the 10 seconds interval, the number of Q, R and S wave, the R-R interval, the calculation of the heartbeat and the QRS interval.

V. CONCLUSION

The developed algorithm used in this project can be used to detect R wave as the accuracy of R wave detection is around 91.53% which is including nsr16272 and nsr1795, while the accuracy will be 100% if we excluding both records. As for the S wave, the algorithm can be used after modification of developed algorithm as the accuracy is around 87.77%. The detection of Q wave need to improve because it have low accuracy which is 77.41%.

After the improvement and modification of the developed algorithm to get the QRS complex detection, we can further continue to study with other database from the website to know comparison between the normal heart signal and the abnormal heart signal or arrhythmia. The classification of arrhythmia can be known from the R-R interval and the calculation of the heartbeat. This can be used for the needed patients to get earlier diagnosis without having a long time waiting in the health facility. The data can be transmit online to

the health facility and let the physicians or doctors do the diagnosis process. As a conclusion, the approach we used to get the QRS complex detection need to be improved especially in detecting the Q and S waves.

REFERENCES

[1] DailyCare Biomedical Inc. , 2016

[2] Saladin, KS & Wynsberghe, DV 2002, Anatomy & Physiology: The Unity of Form and Function with OLC Bind-in Card, 3rd edn, The McGraw-Hill, N.Y.

[3] J. Pan and W. J. Tompkins, "A real-time QRS detection algorithm." IEEE Trans. Biomed. Eng., vol. BME-32, pp. 230-236, 1985.

[4] Nitish V. Thakor and Yi-Sheng Zhu, "Applications of Adaptive Filtering to ECG Analysis : Noise Cancellation and Arrhythmia Detection." IEEE Trans. Biomed. Eng Vol. 18. no 8. August 1991

[5] Qiuzhen Xue, Yu Hen Hu and Willis J. Tompkins, "Neural-Network-Based Adaptive Matched Filtering for QRS Detection" IEEE Trans. Biomed. Eng Vol. 39. no 4. August 1997

[6] Fokkenrood, S., Leijdekkers, P. and Gay, V., 2007, Ventricular tachycardia/fibrillation detection algorithm for 24/7 personal wireless heart monitoring. International Conference on Smart Homes and Health Telematics, pp. 110-120. Available from: SpringerLink

[7] Dizon, L. and Johansson, M., 2014. Atrial Fibrillation Detection Algorithm Evaluation and Implementation in Java. Master's thesis, School of Technology and Health.

[8] Dash, S., Raeder, E., Merchant, S. and Chon, K., 2009, 'A statistical approach for accurate detection of atrial fibrillation and flutter'. 36th Annual Computers in Cardiology Conference (CinC), pp. 137-140. Available from: IEEE.

Electrochemical Deposition of Zinc Oxide Thin Film for Solar Cell Application

Amer Safri Hamidi
Department of Computer and Electronic Engineering
Faculty of Electrical Engineering
Universiti Teknologi Malaysia
Johor Bahru, Johor
amersafri@gmail.com

Mastura Shafinaz Zainal Abidin
Department of Computer and Electronic Engineering
Faculty of Electrical Engineering
Universiti Teknologi Malaysia
Johor Bahru, Johor
m-shafinaz@utm.my

***Abstract*—This paper reports on deposition process of Zinc Oxide (ZnO) using a simple electrochemical deposition setup. The ZnO thin film was deposited on the Aluminium (Al) substrate in an aqueous solution of Zinc Chloride ($ZnCl_2$) at room temperature using two terminal electrochemical cell consist of positive and negative electrode. Two types of Al substrate were used, which are Al foil and Al plate. Al foil or Al plate as the negative electrode and Platinum (Pt) wire or Zinc (Zn) plate as the positive electrode. A constant current density of 10 A/m^2 was applied in the experiment. 5mM $ZnCl_2$ and 0.1M potassium chloride (KCl) support solution act as the electrolytic solution. The experiment was carried out by varying the concentration of $ZnCl_2$ electrolyte solution and KCl supporting solution. Three different mixture of electrolyte solution and supporting solution, 125 ml of $ZnCl_2$ + 25 ml of KCl, 100 ml of $ZnCl_2$ + 50 ml KCl and lastly 75 ml $ZnCl_2$ + 75 ml KCl. Each of the samples were undergo 30 minutes of deposition process. At the end of the experiment, the morphologies and properties of ZnO were determine right after the electrodeposition process by studying the result from Single Electron Microscope (SEM) and Energy Dispersive X-ray spectroscopy (EDX). The nanostructructures of the ZnO are nanosheet network. Photoconductivity test also being tested to determine the current-voltage (I-V) characteristic of each samples. From all the samples tested, the most conductive and sensitive toward light response is obtained for sample D. The results convince the potential of utilizing simpler setup and produce good characteristic of ZnO film for cell application.**

Keywords— ZnO, thin films, electrodeposition, $ZnCl_2$, KCl, photoconductivity test, solar cells

I. INTRODUCTION

Zinc Oxide (ZnO) is one of the widely used material in industry. ZnO are applied in the production of paints, rubber, plastics, catalysts, ceramic, pharmaceuticals and others [1]. In electrical and electronics industry, ZnO is used in ingredient of phosphors and as a transparent electrode. From 1930s, ZnO has been seen as one of the promising material for electronic for many decades. ZnO is a compound semiconductor with a wide bandgap of 3.37 eV and listed in the class of transparent conducting oxides (TCO) [2]. Another examples of important oxides are tin and indium oxide. Recently, ZnO thin films become a key components and take a major part in most thin film solar cells. This is because the films can be produce in a large-scale without having to spend a lot of money. ZnO is one of the reactive material and deposition of this semiconductor can be performed under various mild condition. On the other hand, the improvement in properties of ZnO thin films become a challenges in the production and R&D of photovoltaics.

Nowadays, the world is facing critical issues such as climate changes due to greenhouse effect [3]. One of the answers to overcome this problem is to use renewable energies which can provide a long term solution to the world energy demand in a sustainable way. Solar energy carries the potential of becoming the largest renewable energy sources. The conversion of electricity from sunlight by photovoltaic (PV) solar modules has increased and the production cost have been reduced year by year. Currently, most of the solar cells used is crystalline silicon solar cells based on silicon wafers with a thickness of around 150–300μm. However, high temperature is needed to produce thick silicon wafers and a very pure silicon is totally expensive as well as some of other materials [4]. Therefore, cost-effective thin-film solar cells may replace the current PV solar modules as it can absorb most of the sunlight with only a few micrometers of film thickness. This type of ZnO solar cells can become a huge prospect in the future because of low material consumption, effective energy conversion, simple production techniques and can produce efficiently by large areas deposition.

II. METHODOLOGY

In this experiment, the configuration of two terminal electrodes in a 150 ml beaker was used to deposit the ZnO thin film on the Al substrate. This configuration as shown in Figure 1 comprises an Al substrate as the cathode electrode and Pt wire or Zn plate as the anode electrode. A power source supplied the desired current density needed during the electrodeposition process. Al was used because it is one of the active metal and easy to react during electrochemical deposition process.

Before starting the experiment, the surface of the substrate was cleaned first using deionized (DI) water to avoid any contamination because DI water are free from any mineral ions such as calcium, sodium and copper [5]. A mixture of $ZnCl_2$ aqueous solution and supporting electrolyte 0.1M KCl were used as the precursor. The major advantages of using $ZnCl_2$

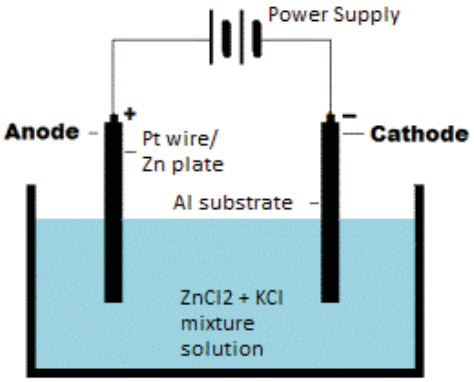

Fig. 1. The configuration of two terminal electrochemical cell

aqueous solution as the electrolyte are the solution are easy to handle, low cost and moderate toxicity. Varying the electrolyte concentration in electrochemical deposition can alter the band-gap and lattice constant of the thin film. Basically, the deposition time will be kept in 30 minutes and current density of 10 A/m^2. After the electrochemical deposition process, all of the samples were put in the petri dish before being kept in a closed place.

Characterization of surface morphology of ZnO thin films were done by using Scanning Electron Microscope (SEM). Energy Dispersive X-ray (EDX) also was used to identify the elements present on the sample surfaces.

A. Al Foil Negative Electrode and Pt Wire Positive Electrode

Firstly, Al foil was wrapped around a glass sides. Most of the glass slide are 25.4x76.2 mm in size. The back side of the Al substrate were covered with cellophane tape. The cellophane tape acts as insulator. Figure 2(a) shows the Al foil sample before being deposited. Three Al foil samples with the same dimension were prepared to deposit the ZnO thin film on the substrate in three different mixture of solution. The first solution was 125 ml $ZnCl_2$ + 25 ml KCl. The second was 100 ml $ZnCl_2$ +50 ml KCl and the third solution was 75 ml $ZnCl_2$ + 75 ml KCl. All of the samples were soaked half of their size. Therefore, the area of dipped Al foil samples in the solution were 25.4x38.1 mm.

The total current density needed was 10 A/m^2. In other to obtained the desired current density, Equation (1) was applied where J is the current density, I is the current supplied by the power source and A is the area of dipped Al foil in the electrolyte.

$$J = \frac{I}{A} \qquad (1)$$

$$10\ A/m^2 = \frac{I}{0.0254\ x\ 0.0381\ m}$$

$$I = 0.01\ A$$

Hence, the current of 0.01 A was applied using power source to get the current density of 10 A/m^2.

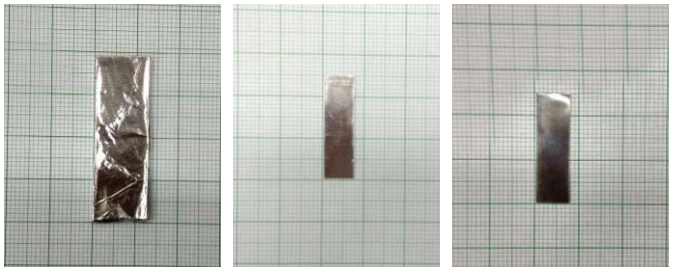

(a) (b) (c)

Fig. 2. (a) Al foil with 25.4x76.2 size sample (b) Al plate with 50x15 mm size sample (c) Fig. 4. Zn plate with 50x15 mm size sample

B. Al Plate Negative Electrode and Pt Wire Positive Electrode

Basically, three Al plates with the approximate size of 50x15 mm were prepared. The backside of the Al plates were covered with cellophane tape. The Al plate sample used was diplay as in Figure 2(b). The Al plates were soaked half of the size in three different mixture of solution as the same as in section A. The total dipped area of Al plates were 25x15 mm.

As previous experiment A, the desired current density was 10 A/m^2. Applying Equation 1,

$$10\ A/m^2 = \frac{I}{0.025\ x\ 0.015\ m}$$

$$I = 0.004\ A$$

Thus, the current that need to be supplied by the power source was 0.004 A.

C. Al Plate Negative Electrode and Zinc Plate Positive Electrode

In this experiment, three Zn plates as in Figure 2(c) with the average weight of 1.0598 g and size of 50x15 mm was used as the positive electrode. The negative electrode were Al plates, as shown in Figure 2(b).Same as previous experiment, the cellophane tape were attached at the back of the Al plates. This experiment still using the same mixture of solution, as mention in the previous section. The total dipped area of Al plates were 25x15 mm. As the size of the samples were

TABLE I. THE CONDITION FOR THE SAMPLES

Sample	Anode	Cathode	Electrolyte
A	Pt	Al foil	125 ml $ZnCl_2$ + 25 ml KCl
B	Pt	Al foil	100 ml $ZnCl_2$ +50 ml KCl
C	Pt	Al foil	75 ml $ZnCl_2$ + 75 ml KCl
D	Pt	Al plate	125 ml $ZnCl_2$ + 25 ml KCl
E	Pt	Al plate	100 ml $ZnCl_2$ +50 ml KCl
F	Pt	Al plate	75 ml $ZnCl_2$ + 75 ml KCl

G	Zn	Al plate	125 ml $ZnCl_2$ + 25 ml KCl
H	Zn	Al plate	100 ml $ZnCl_2$ +50 ml KCl
I	Zn	Al plate	75 ml $ZnCl_2$ + 75 ml KCl

similar to those samples in Experiment B, the current applied by the power source was 0.004 A.The conditions applied for all samples prepared in this work are summarized in Table 1. Current density was kept for 10 A/m^2 and the deposition time was 30 minutes for all samples.

III. Results and Discussion

A. ZnO growth on sample

After 30 minutes of electrodeposition process, the deposited ZnO could be seen on all of the Al substrate in each experiment using the naked eyes. Figure 3 shows the deposited ZnO thin film on all of the type of Al substrate.

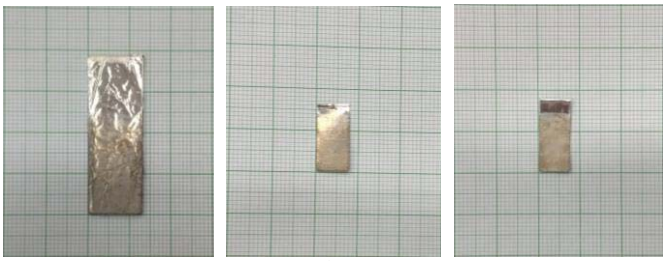

(a) (b) (c)

Fig. 3. (a) Electrodeposited ZnO on Al foil (b) electrodeposited ZnO on Al plate for Pt wire as positive electrode (c) electrodeposited ZnO on Al plate for Zn plate as positive electrode

B. Morphology Study on Nanostructures of ZnO Thin Films

When the oxygen is present as the precursor, ZnO electrodeposition would comply with the following equations:

$$O_2 + 2H_2O + 4e \rightarrow 4OH^-$$

$$Zn^{2+} + 2OH^- \rightarrow Zn(OH)_2$$

$$Zn(OH)_2 \rightarrow ZnO + H_2O$$

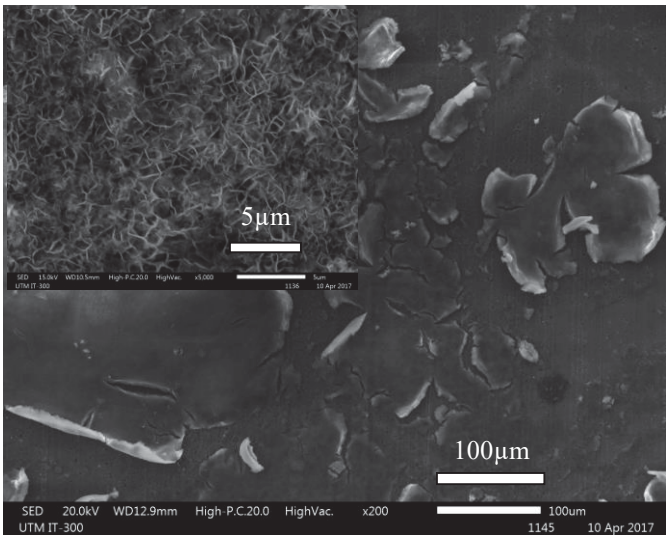

Fig.4. SEM image of ZnO thin film on Al foil (Sample A)

First, the electrolyte contains zinc cation and other anion. Then, the reduction of oxygen on the surface of the Al substrate leads to the adsorption of hydroxide ion. the precipitation of zinc hydroxide take places near the surface of the substrate generated by hydroxide ion. Finally, ZnO is formed and this process in known as the deposition of ZnO [6].

Many interesting features were unveiled from the Scanning Electron Miscroscope (SEM) images. In this experiment, the images of Scanning Electron Microscope (SEM) were taken for three each type of substrate, which are Al foil with Pt wire as positive electrode,, Al plate with Pt wire as positive electrode and Al plate with Zn plate as the positive electrode. All of those three samples have similar nanostructure which are ZnO nanosheet networks [7]. This networks are slightly curved and have an uneven surface morphology on a large scale.

First of all, The SEM image of ZnO thin film grown on the Al foil in the mixture of 5mM $ZnCl_2$ and 0.1M KCl solution

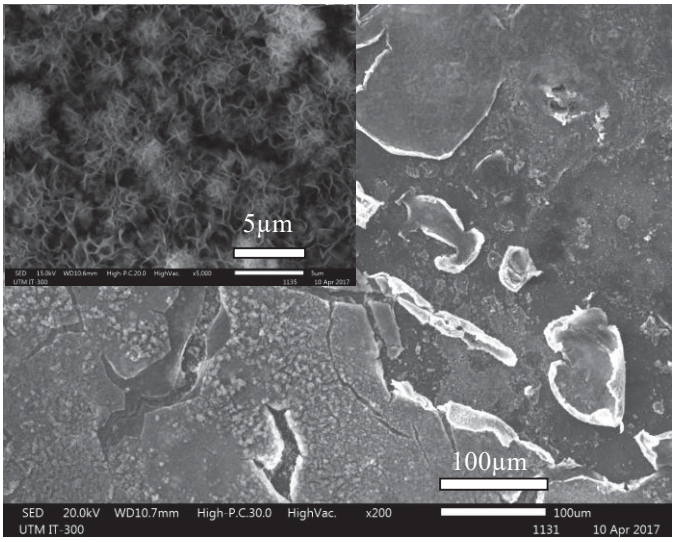

Fig.5. SEM image of ZnO thin film on Al plate (Sample D)

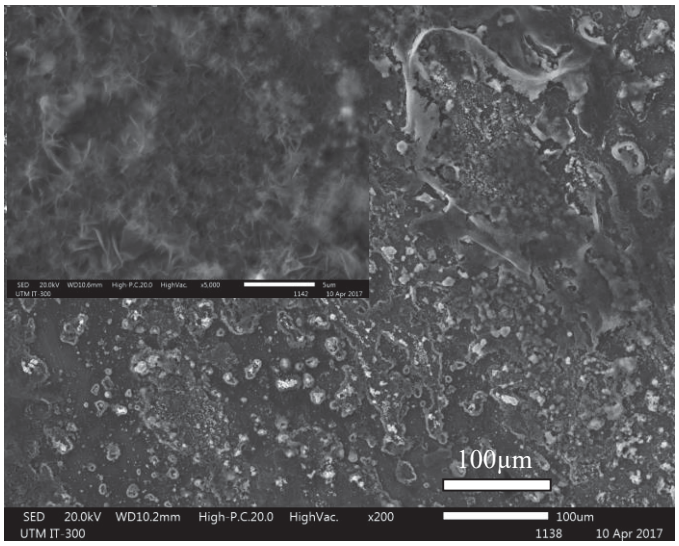

Fig.6. SEM image of ZnO thin film on Al plate for Zn plate (Sample G)

are shown in the Figure 4. The magnification scale of 100µm shows the crack and peeling morphology ZnO thin film. Electrodeposited ZnO on Al plate in Figure 5 have even, uneven and crack morphology at the same time. Meanwhile, the thin film of ZnO in Figure 6 has irregular shapes and is divided into smaller pieces.

C. Chemical Composition of the ZnO Thin Film

The EDX can reveal the information and composition of ZnO thin film on the substrate which had been prepared after the electrodeposition process. From the Figure 7 and Table 2, Al has the higher weight percentage which is 36.69% as it is the substrate used in the experiment. The image from the EDX also proved the presence of ZnO thin film on the substrate surface. The weight percentage of Zn is 25.49% and O is 27.59%, indicate that the ratio of Zn:O is almost 1:1. There are also some element such as Cl and K presence on the surface of the surface due to the mixture of solution used in the experiment.

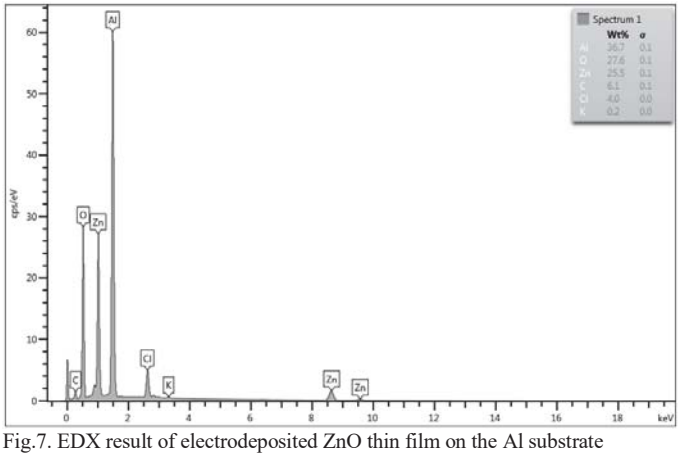

Fig.7. EDX result of electrodeposited ZnO thin film on the Al substrate

TABLE II. ELEMENT AND WEIGHT PERCENTAGE

Element	Wt%	Wt% Sigma
C	6.09	0.15
O	27.59	0.07
Al	36.69	0.08
Cl	3.98	0.02
K	0.17	0.01
Zn	25.49	0.07
Total:	100.00	

D. Photoconductivity Test

Material becomes more conductive when absorb the electromagnetic radiation such as ultraviolet light, infrared light or visible light. This optical and electrical phenomenon is known as photoconductivity. When light is absorbed by a material such as a semiconductor, the number of free electrons and electron holes changes and raises its electrical conductivity [8]. The electrons in semiconductor become excited due to light penetration which then receive enough energy to cross the band gap or to excite the impurities within

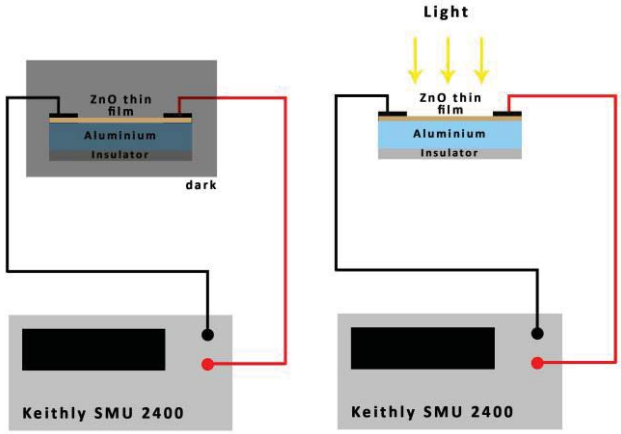

(a) (b)

Fig. 8. Photoconductivity test (a) dark condition (b) light condition

the band gap. When applying a bias voltage across the semiconductor, a variation of current can be measured due to the changes in electrical conductivity of the material [9]. In this experiment, Keithly instrument SMU 2400 was used to find out the I-V characteristic of each sample. Two measurement condition, dark and light were taken during the photoconductivity test.

Figure 8 display the setup of the photoconductivity test.Each sample were left for 3 minutes in both dark and light condition to reach the equilbrium before taking the results. In Figure 9 shows the graph of Al foil samples in dark and light condition. Slope of I-V line of sample C is the steepest in both dark and light condition followed by sample B, sample A and

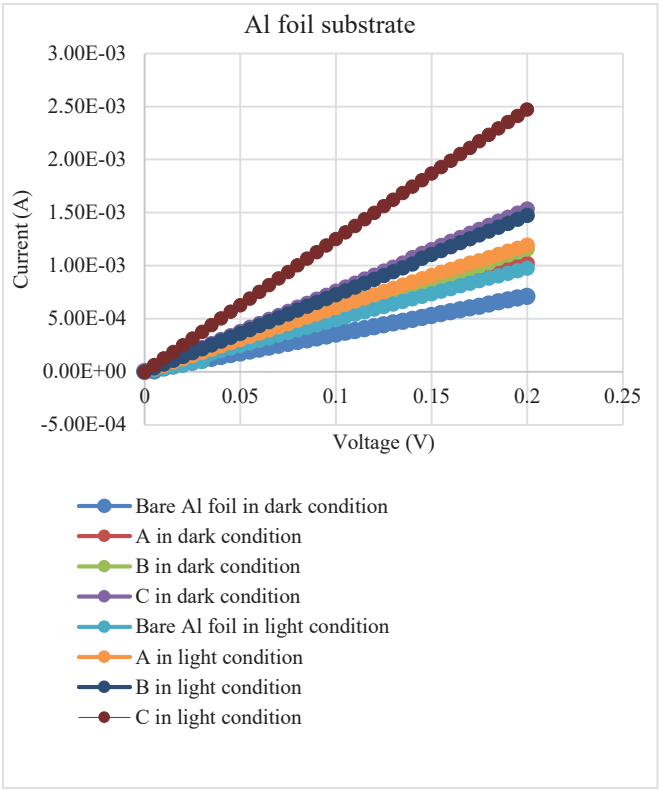

Fig. 9. Graph of Al foil samples

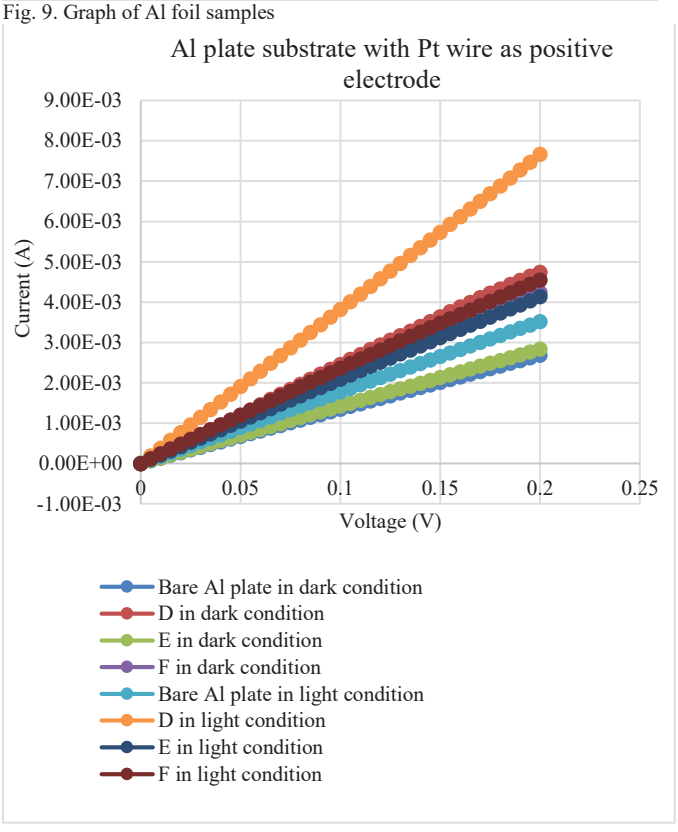

Fig. 9. Graph of Al plate samples for Pt wire as the positive electrode

bare Al foil. The difference of current at 0.2 V of sample C is also the highest compared to other samples. This indicate that sample C has better photoconductivity and sensitivity toward the light.

The graph of Al plate samples with Pt wire as positive electrode is shown in Figure 9. Sample D has the best photoconductivity as it has the steepest gradient in both dark and light condition. This is because sample D has higher concentration of $ZnCl_2$. Meanwhile, sample F has poor sensitivity toward light because the difference of the current in dark and light condition at 0.2 V are the smallest.

For Figure 10, the sample with the best photoconductivity are sample H. On the other hand, sample H has moderate sensitivity toward light because the diference of the current for dark and light condition are moderate.

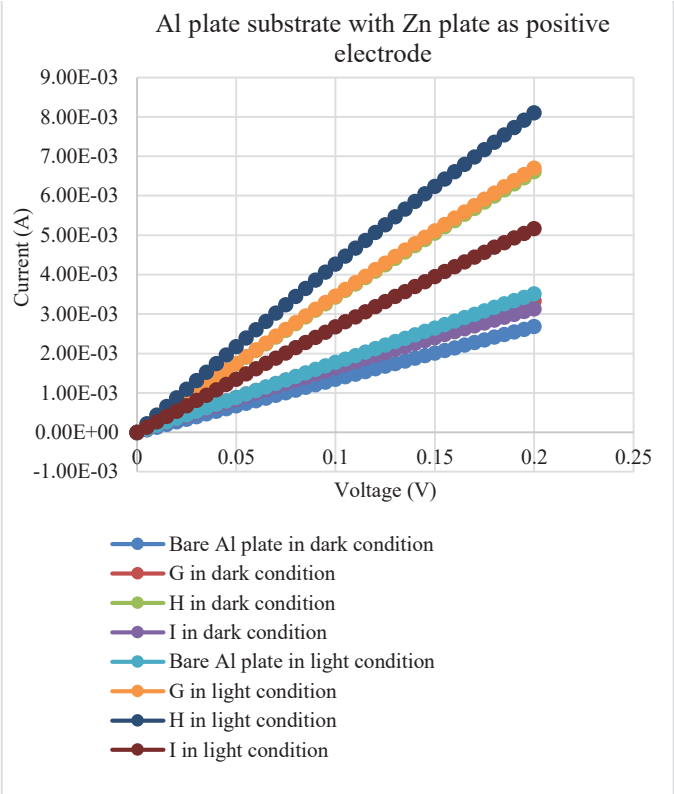

Fig. 10. Graph of Al plate samples for Zn plate as the positive electrode

IV. CONCLUSION

ZnO thin film are formed by electrochemical deposition of $ZnCl_2$ with KCl as supporting solution. The nanostructure of the thin film was confirmed by using SEM and the coimposition of the element on the surface substrate was done by using EDX. The photoconductivity of each sample by studied and the performance of the samples show that the they can be a promising solar cell. Another important part that need to be understand is the growth mechanisms of ZnO. The factor of the gowth mechanisms also need to be studied more for better understanding of the electrochemical deposition process.

Acknowledgement

REFERENCES

[1] A. Moezzi, A. M. McDonagh, and M. B. Cortie, "Zinc oxide particles: Synthesis, properties and applications," *Chem. Eng. J.*, vol. 185–186, pp. 1–22, 2012.

[2] B. Zhou, X. Han, Q. Feng, and M. Tao, "Green electrodeposition of ZnO as a TCO in terawatt solar cells," *Conf. Rec. IEEE Photovolt. Spec. Conf.*, pp. 2030–2033, 2012.

[3] M. Henini, *Handbook of Thin-Film Deposition Processes and Techniques*, vol. 31, no. 3. 2000.

[4] K. L. Chopra, P. D. Paulson, and V. Dutta, "Thin-film solar cells: an overview," *Prog. photovoltaics*, vol. 12, no. 23, pp. 69–92, 2004.

[5] P. Singh and A. Kabalan, "Electrochemical atomic layer deposition of a CdTe/PbTe superlattice for the absorber layer of a solar cell," *Conf. Rec. IEEE Photovolt. Spec. Conf.*, pp. 2548–2552, 2012.

[6] G. Jiangfeng, D. Zhaoming, D. Qingping, X. Yuan, and Z. Weihua, "Controlled Synthesis of ZnO Nanostructures by Electrodeposition Method," *J. Nanomater.*, vol. 2010, pp. 1–6, 2010.

[7] M. K. Gupta, J. H. Lee, K. Y. Lee, and S. W. Kim, "Two-dimensional vanadium-doped ZnO nanosheet-based flexible direct current nanogenerator," *ACS Nano*, vol. 7, no. 10, pp. 8932–8939, 2013.

[8] M.H.Huang, S.Mao, H.Feick et al., "Room-temperature ultraviolet nanowire nanolasers," *Science*, vol. 292, no. 5523, pp. 1897–1899, 2001.

[9] M. Sathya, A. Claude, P. Govindasamy, K. Sudha, and A. Claude, "Growth of pure and doped ZnO thin films for solar cell applications," vol. 3, no. 5, pp. 2591–2598, 2012.

Automated Current Control for Pulse Anodic Etching of Porous Silicon

Ahmad Bukhairi Md Rashid and Mastura Shafinaz Zainal Abidin
Department of Computer and Electronic Engineering
Faculty of Electrical Engineering
Universiti Teknologi Malaysia (UTM)
Johor Bahru, Johor
m-shafinaz@utm.my

***Abstract*— This paper reports on development of a low cost, user friendly device to control the pulse current setting specifically for anodic etching of porous silicon. Basic current control circuit with digital potentiometer as load across emitter (R_E) is used to control the value of the current. An Arduino Uno microcontroller is used to control the duty cycle and the amount of current to feed into the circuit. A cell phone with the aid of an app is the medium for user interface. The connection between mobile phone and Arduino board is establish via a Bluetooth module HC-05. The devices able to produce output current in range of 2mA to 57mA depends on the value of digital potentiometer. The process of current control in anodic etching is expected would be simplified with the presence of this devices.**

Keywords—pulse current; direct current; anodic etching; digital potentiometer.

I. INTRODUCTION

The most common method to produce porous silicon (PS) is by using anodic etching as introduced by Canham [1]. This method uses direct current (DC) as the input. Usually, Hydrofluoric Acid (HF) is used as electrolyte where it involves the reaction between HF and the Silicon (Si). However, other solution such as mixture of acetonitrile (CH3CN) or dimethylformamide (C3H7NO) with HF also can be used [2]. This self-adjusted mechanism process basically occurs at the pore of the tips [3]. In anodic etching, the process of etching is slow down by the reduction of the HF concentration inside the pore depending on the reaction between HF and Si [3]. Significantly, the output of the process will form bubble on the wall surfaces of pores. Hence, this will induce a non-homogeneity gradient along the depth [2]. As the consequence in device application, the performance of the optical devices will be decreasing and cause the structure to have mechanical instabilities [1].

Hou X-Y et al has suggested that if positive pulse is used, the HF concentration inside the pore can be recovered which useful to enhance the etching process [3]. It has been proven that various characteristic of PS might be produced using pulse anodic etching [1-4]. There are several parameters in pulse anodic etching that need to be determined for optimum experimental condition such as duty cycle, frequency and etching time. In generally, many applications nowadays prefer to use dry etching compare to wet etching due to better yield. However, there are still several advantages of wet etching compare to dry etching such as low cost, high etching rate and good selectivity for most material [5].

Table 1 shows the summary of the parameter used in pulse anodic etching as reported in [2,3,6].

Table 1 : Parameter in Pulse Anodic Etching

Reference	Duty Cycle	Frequency (HZ)	Current Density (mA/cm^2)
[2]	• 0.5	• 50 • 500 • 1000	• 10 • 50
[3]	• 0.05 • 0.2	• 100 • 2000	• 2 • 10

It is found that the PS produced by anodic etching will have smaller mean roughness than DC anodic etching [2]. However, if the frequency of pulse anodic etching is increased to 100Hz, mean roughness will increase as well. In contrast, the roughness become low at higher current density. This occurred due to increment in pore size when high current is being applied. It also been concluded that the optical properties is strongly dependent on the duty cycle and the frequency of the applied current.

On other hand, [3] has concluded that pulse anodic etching is more effective way than DC etching method to prepare light emitting PS. Thicker and more uniform PS layers with high photoluminescence intensity are easier to be prepared. Therefore, pulse anodic etching can be said will give better output compare to DC anodic etching.

II. METHODOLOGY

The concept devices are constructed based on the basic current control circuit concept. Figure 1 shows the schematic of the circuit. The circuit required 20V input voltage obtained from DC power supply. Zener diode (1N4740A) has the reverse voltage of 10V. BD435 is choose as it has low V_{BE} in order for the transistor to turn on. The load (anodic etching setup) is

replaced by resistor and is connected to the current sensor module. The current sensor is connected in series to the collector of the transistor. By assuming that the value of the current across the load is the same as the current across R_E (digital potentiometer), the current that need to be feed to the circuit can be controlled by altering the value of the digital potentiometer. The voltage across R_E is fix at around 2V. This will allow the system to vary the value of the current from 2mA until 200mA.

A relay is used to produce the pulse output of the circuit. Both relay and digital potentiometer are connected to Arduino and is programmed based on the user's need. Users only need to key in the required value into app in the smartphone. Then, the entered data will be send to Arduino with the aid of Bluetooth Hc-05 module. As the data is received, Arduino will execute the command and run the program. The data inserted by the user is in the form of current, Ton, Toff and etching time. Figure 2 shows a screenshot of the apps. This app has been developed by using MIT App Inventor [7,8]. The common pin is connected to V_{CC} while NO (Normally open) pin is connected to load. In normal condition, there will be no current that can flow through the load as the circuit is open. A is connected to pin 5 Arduino while B is connected to ground. Whenever relay received signal form Arduino, the circuit will be complete and the load will receive the current. Then, Arduino will stop from sending the signal and the circuit will be open again. So, the timing when Arduino send signal and stop from sending the signal is used to make the pulse output. Ton is counted when Arduino is sending the signal while Toff is when Arduino stop sending the signal. This will produce pulse output.

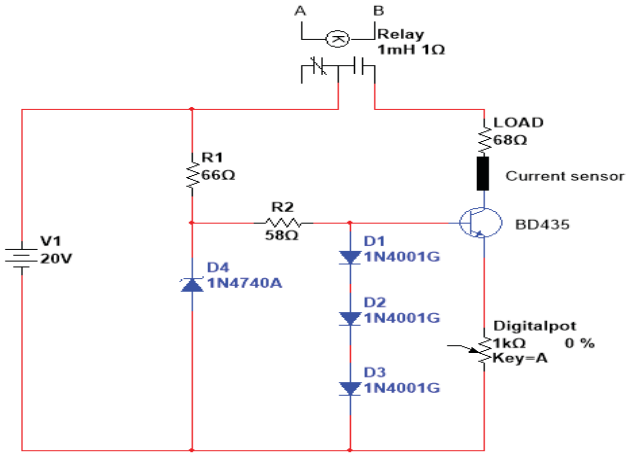

Figure 1 : Schematic of the circuit

Figure 2 : Screenshot of The App

III. RESULT AND DISCUSSION

Based on the datasheet, digital potentiometer used consists respective of 100 multiplexers that represent a value of resistance on respective stage. However, the real value may be varied by 2% from the desired value. The potentiometer is used first calibrated, and it is found that the real value of the digital potentiometer is varied between 0.03% to 194% from the desired value. This result exceeds too far from specification is datasheet. During data collection, it is noticed that the value of digital potentiometer is very unstable when the value of resistance is high. As the value of resistances decrease, they become more stable. However, user need to be careful as sometimes, digital potentiometer does not select the right stage based on the input parameter. For an example, user has entered the value 50 (for stage no 50). Instead of going to stage no 50, digital potentiometer will go to stage 100 that gives the lowest resistance. Figure 3 shows the variation of the digital potentiometer with its respective value.

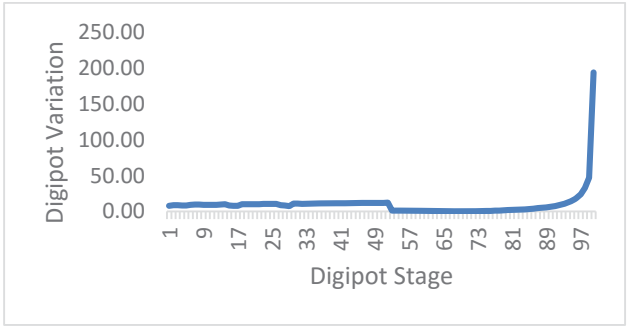

Figure 3 : Digipot Variation

Figure 4 represents the value of the digital potentiometer stage with its respective value when the multiplexer is moved from 1 to 100. Based on the graph, no discrepancy found in the value of the resistance at low range, however when the value of resistance is high, big difference between measurement and theoretical value is observed. The variation is the highest at multiplexer equal to 100. The measured value is 29.4 Ω while the theoretical value is 10Ω. This value is depending on mechanical of the digital potentiometer which is hard to be controlled.

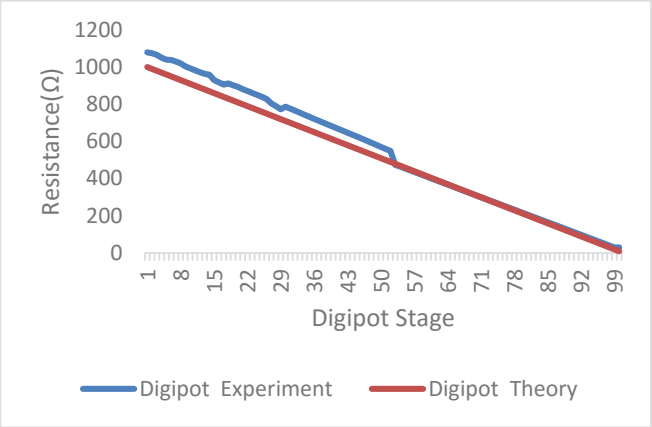

Figure 4 : Digipot Resistance VS Digipot Stage

Figure 5 represents the value of the current across digital potentiometer against digital potentiometer multiplexer stage for both theoretical and measured value. Based on the graph, the value of current for measured and theoretical are almost similar. The clear different that been observed is when the value of digital potentiometer stage is around 90, where the value of current for theoretical value is higher than measured value. This difference may be caused by the value of the digital potentiometer that are not the same as the theoretical value. As depicted in Figure 3, the variation is very high when the value of digital potentiometer stage is around 90. The resistance of measured value is also too high, which give good agreement to Ohm's law where low current is produced.

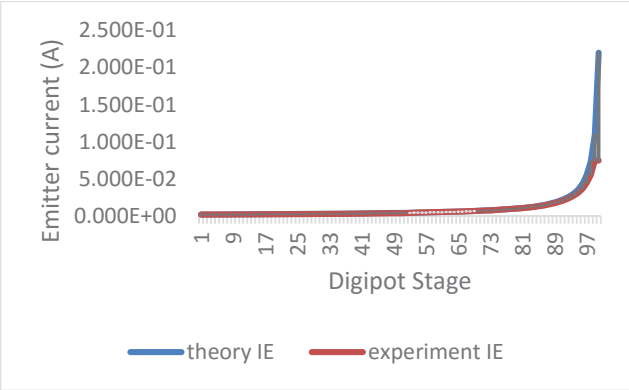

Figure 5 : Emitter current VS Digipot stage

Figure 7 shows the value of current across digital potentiometer and across the load. Figure 6 shows the value of voltage across the load against digital potentiometer stage. For testing purpose, the load is replaced by 68 Ω resistor. The voltage value increased throughout the experiment as the resistances of digital potentiometer decreased. The voltage across the load is measured and is recorded. Then, the value of current is obtained using Ohm's Law. Based on the graph, the difference between current across digital potentiometer and load are very small. Therefore, this supports the earlier hypothesis that load current is equal to I_E.

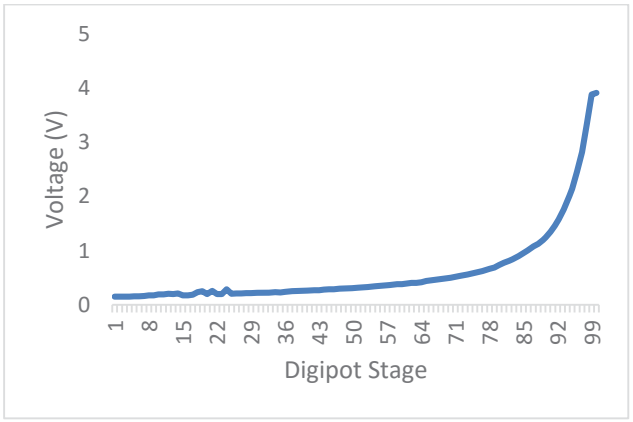

Figure 6 : Voltage Across Load VS Digipot stage

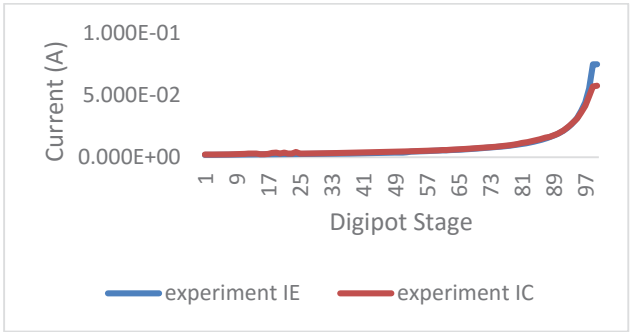

Figure 7 : Current VS Digipot Stage

Figure 8 shows partial waveform of pulse output when the circuit is running. It is clearly can be seen that, the pulse has very fast rise time and fall time. The amplitude of the pulse depends on the voltage of the load. During Ton, a very stable output can be achieved. However, during Toff, the output is not very stable but it did not affect the overall process of anodic etching. The switching mechanism by using relay can be said to be good so far.

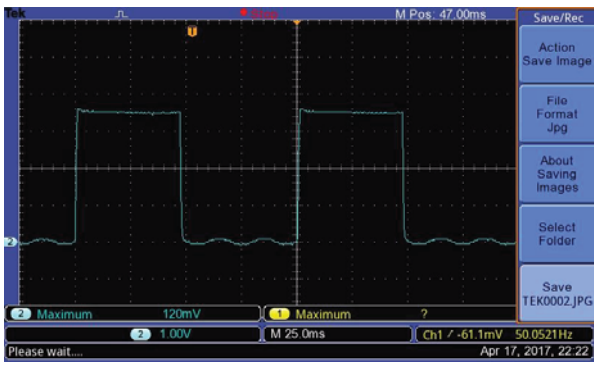

Figure 8 : Pulse output across load

IV. CONCLUSION

As a conclusion, a device to control current setting value for anodic etching is successful developed. The process is control by Arduino by receiving data from app through mobile phone. By using basic current control, there is a potential to create low cost device that can produce pulse output while give the user authorities to control the current. However, further study is needed to find the solution for the instability digital potentiometer resistance. A more accurate and stable component are needed so that the control abilities of the resistances can be improved. For further enhancement, it is recommended that relay is replaced by mosfet as the effect of using relay for switching for a longer time is still unclear. There might be possibilities that the relay may burn. Thus, mosfet could be used and the problem regarding voltage across Gate to Source can be solve by using mosfet driver. Some study indicated that mosfet driver can supply higher current to mosfet so that the voltage supply can be enough to turn on the mosfet.

REFERENCES

[1] J. Escorcia and V. Agarwal, "Effect of duty cycle and frequency on the morphology of porous silicon formed by alternating square pulse anodic etching", physica status solidi (c), vol. 4, no. 6, pp. 2039-2043, 2007.

[2] J. Escorcia-Garcia, O. Sarracino Martínez, J. Gracia-Jiménez and V. Agarwal, "Porous silicon photonic devices using pulsed anodic etching of lightly doped silicon", Journal of Physics D: Applied Physics, vol. 42, no. 14, p. 145101, 2009.

[3] X. Hou, H. Fan, L. Xu, F. Zhang, M. Li, M. Yu and X. Wang, "Pulsed anodic etching: An effective method of preparing light- emitting porous silicon", Applied Physics Letters, vol. 68, no. 17, pp. 2323-2325, 1996..

[4] P. Myers, "Michael J. Sailor: Porous Silicon in Practice. Preparation, Characterization and Applications", Chromatographia, vol. 76, no. 11-12, pp. 721-721, 2013.

[5] C. Erli, "Introduction to Nanofabrication", III. Wet and Dry Etching, 2004.

[6] L.T. Canham, Appl. Phys. Lett. **57**, 1046 ~1990!.

[7] D. Wolber and H. Abelson, App Inventor, 1st ed. Sebastopol: O'Reilly, 2011.

[8] H. Rim, "Android App. Implementation Teaching using App. Inventor for Elementary school students", Journal of Korea Multimedia Society, vol. 16, no. 12, pp. 1495-1507, 2013.

System Integration of Heart Screening Device with development of Android based Application

Teh Her Tee And Dr Ismahani binti Ismail
Electronic & Computer Engineering (ECE) Department
Faculty of Electrical Engineering
Universiti Teknologi Malaysia
Skudai, Johor Bahru, Malaysia
ismahani@fke.utm.my

Dr Jasmine Hau Yuan Wen
IJN-UTM Cardiovascular Engineering Centre
Faculty of Biosciences and Medical Engineering
Universiti Teknologi Malaysia
Skudai, Johor Bahru, Malaysia
hauyuanwen@biomedical.utm.my

***Abstract*— This paper presents the system integration of current existing in-house heart screening device with the development of Android based application. Cardiovascular disease (CVD) is the number one cause of death globally. There is a design of in-house heart disease screening device for arrhythmia detection with self-interpretation algorithm and wireless communication. However, once the arrhythmia is detected and warning is given by the device, the sending of raw ECG data to seek for professional opinion is not user-friendly. Hence, the development of Android based application to the heart screening device enable the direct transmission of raw ECG data via Bluetooth from wireless ECG acquisition unit to the Android application for more user-friendly data storage and data transfer to seek for professional opinion if arrhythmia is detected from the heart screening device. The Android mobile app also enable the display of real-time ECG chart plotting when receiving the ECG signal. Besides, there is also user-friendly graphical user interface (GUI) design for the application as well. The design of the application is installed and test run on the real mobile device.**

Keywords—android; arrhythmia; Bluetooth; electrocardiogram (ECG); GUI; JAVA; real-time;

I. INTRODUCTION

Cardiovascular disease (CVD) is the number one cause of death globally [1]. Based on World Health Organization (WHO), it estimates that 36% of the Malaysian population died in cardiovascular diseases [2]. According to Datin Dr Liew Yin Mei, medical director of the Heart Foundation of Malaysia, CVD continues to be the leading cause of mortality in Malaysia [1] . According to WHO, there are 50% to 70% of people did not aware of their heart condition because they were lacking of frequent heart monitoring [3]. However, a frequent screening of heart condition able to detect the abnormality in the early stage.

Some of the CVDs are resulted from arrhythmias. Arrhythmia is an abnormal heart rhythm or improper beating of heart caused by the abnormal electrical activity of the heart. There are various types of heart rhythm disorders such as PVC, PAC, AFIB and so on. Normally, arrhythmias can be detected by monitoring the electrocardiogram (ECG). ECG is a non-invasive method to record the human's heart electrical activity by placing sensors at limb extremities and body of the subjects.

Hence, a light-weight and cost effective ECG device with self-arrhythmia interpretation is desired, not only to enable the outpatient to perform home monitoring for frequent cardiac condition checking, but also small clinic and general hospital in rural area to provide arrhythmia screening. There is a current in-house heart screening device existed. This heart screening device is equipped with the self-interpretation algorithm and wireless communication between the ECG acquisition unit the device itself. However, the raw ECG data can only be stored in the SD card of the device itself and is not user-friendly to send the raw ECG data to seek for professional opinion if the arrhythmia warning signal is detected since the sending of data required the transfer of SD card.

Therefore, this paper presents a design of Android based application with the help of Bluetooth wireless communication to receive and store the raw ECG data directly from the ECG acquisition unit. Besides, the Android based application also enable the plotting of real-time ECG chart on the screen of application at the moment it is receiving raw ECG data from the wireless ECG acquisition unit. With the development of this Android application will ease the transfer of ECG data and make it more user-friendly.

II. LITERATURE REVIEW

A. Electrocardiogram

Every heart will produce a small electrical impulse in order to make the heart contract by spreading the electrical impulse throughout the whole heart muscles. Electrocardiogram (ECG) is a tool that can be used to measure this heart electrical activity. Various types of heart disorders can be determined by analyzing the patterns of the ECG signals, such as abnormal heart rhythms and heart attack [4].

Fig. 1 shows the normal waveform pattern that produced by the ECG. As it can be seen from the waveform, it normally consists of P wave, QRS complex and T wave. Every interval and segment will have its own functions that had shown in the figure below.

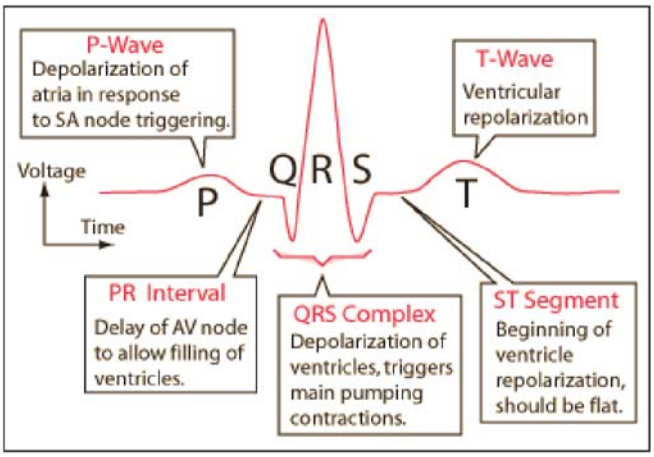

Fig. 1. Normal Waveform pattern of Electrocardiogram

B. *Arrhythmia*

As mentioned in the last section, a heart will produce tiny impulse in order to make the heart muscles to contract. An arrhythmia is referring to the change of the patterns or sequences of the electrical impulse to be different as compared to the normal patterns. For examples the abnormal heart beat pattern may be too fast, too slow or erratically. This may cause the heart to be beat too fast, too slow or erratically as well and hence, affect the blood pump effectiveness [5]. The examples of the types of arrhythmia are Left Bundle Branch Block (LBBB), Right Bundle Branch Block (RBBB), Premature Atrial Contractions (PAC), Premature Ventricular Contractions (PVC), Ventricular Tachycardia (VTACH), Atrial Fibrillation (AF) and Atrial Flutter (AFL).

C. *Android*

Android is a Linux kernel based mobile operating system that developed by Google in the year of 2005 [6]. This operating system is targeted for the touchscreen mobile devices such as smartphones and tablets. Android offers a unified approach to application development for mobile devices and based on Java programming language. In the other word, the developers need only develop for Android, and their applications should be able to run on different devices powered by Android. The development of Android based mobile applications can be done by using Android Software Development Kit (SDK), which is equipped with the necessary development tools, such as software library, virtual emulator based on QEMU, debugger, documentation and tutorials [7]. The source code for Android is always available and released under free and open source software license. The integrated development environment (IDE) that can be used together with Android SDK to develop Android application are Eclipse using the Android development tools plugin, Android studio, Google App inventor and so on. The reason why Android based operating system is chose in this project is due to many advantages, which are the codes are open source, larger developer and community research, increased market, inter-app integration and Android OS is the largest operating system used by most of the mobile phone worldwide.

D. *Review on previous in-house Arrhythmia screening device*

Previous in-house design of arrhythmia screening device, Throb is an arrhythmia screening device that can classified four types of arrhythmia, with the self-interpretation and touchscreen graphical user interface features. Fig. 2 shows the previous in-house Throb arrhythmia screening device with wireless communication. The system is built based on System-on-Chip (SoC) technology where all the controllers are located in targeted platform, VEEK-MT, which utilizes Altera Cyclone IV chip. The device uses a reference code in the demonstration disk from ALTERA VEEK-MT kit packaging called Picture Viewer. In previous work, the top-level application software is executed by NIOS II Processor is modified to create an easy-to-use arrhythmia screening device [8].

The device also equipped with wireless ECG acquisition unit that used to obtain raw ECG data from users. The ECG acquisition unit consists of OLIMEX SHIELD-EKG-EMG prototype board stacked with Arduino Uno as microcontroller and Cytron Bluebee with XBee shield prototype board for the wireless communication feature design. The raw ECG data is obtained from the users by using the passive electrode and then amplified by the OLIMEX SHIELD-EKG-EMG prototype board [9]. The raw ECG data will then send to Throb for classification and result display through Bluetooth. Besides, the device has user-friendly and multi-touch screen GUI. Users are able to store their medical information and observe their ECG in graphical form [10].

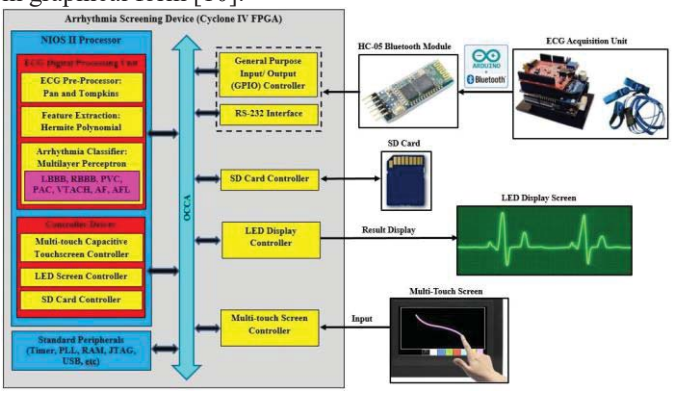

Fig. 2.Top level system architecture of the previous in-house arrhythmia screening device

III. METHODOLOGY

A. *Scope of study*

The scope of study for this project is to integrate the system of heart screening device by designing and developing an Android based mobile applications that enable the transmission of raw ECG data between ECG acquisition unit and Android mobile app via Bluetooth, real-time ECG chart streaming plotting and for data storage in internal memory of the mobile devices. The top level system architecture of the heart screening device and the scope of study in red bracket for this project is as shown in Fig. 3 below.

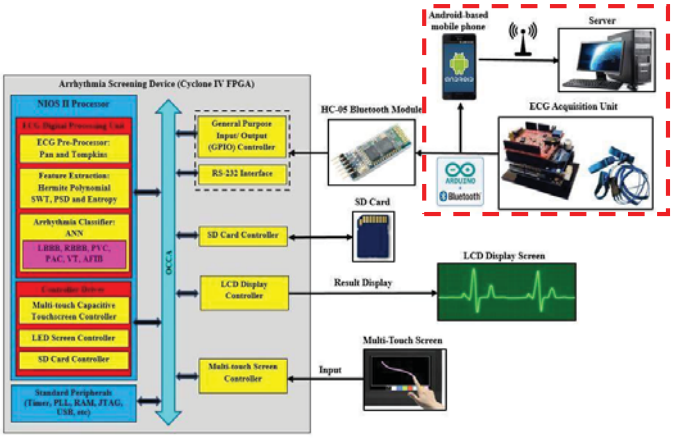

Fig. 3.Top level system architecture of the heart screening device and the scope of study

B. *Overall System Design Flow*

Fig. 4 shows the overall system design flow of the heart screening device with Android based application. The system starts with the raw ECG signal obtain through the wearing of passive electrode to both hands and right leg of the users as input of the system. The signal obtained is then be amplified by OLIMEX SHIELD-EKG-EMG prototype board and then transmitted to Android based application pre-installed in mobile phone through Bluetooth. This can be done with the aid of Cytron Xbee shield with Bluebee module prototype board with Arduino Uno as microcontroller. The Android application will then receive raw ECG data and save these data in internal memory of the mobile device. At the same time, there will also be a display of real-time ECG chart plotting on the screen on mobile device.

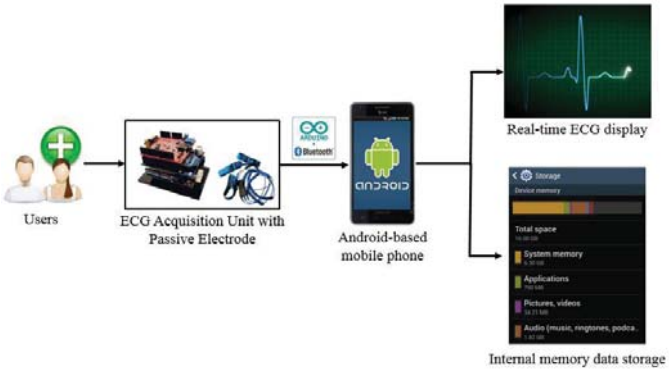

Fig. 4. Overall system design flow

C. *Project implementation*

In this project, the implementation will be divided into two parts, which are the Bluetooth wireless communication design for ECG acquisition unit and the Android based application design development.

Bluetooth design for ECG acquisition unit

ECG acquisition unit is used to obtain the real-time raw ECG signals from the patient or users. ECG acquisition unit consists of 3 components, which are the Olimex Shield-EKG-ENG Prototype Board, Arduino Uno Board and Cytron Bluebee module with Xbee Shield. Fig. 5 shows the stackable ECG acquisition unit with passive electrode.

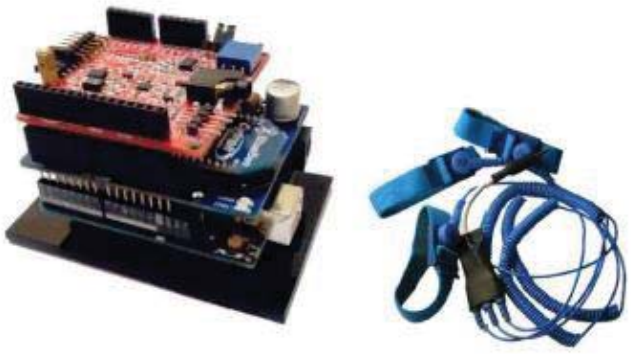

Fig. 5.Wireless ECG acquisition unit with passive electrode

Olimex Shield-EKG-ENG prototype board is used together with passive electrode in order to amplify the small ECG signal obtain through the electrode. Arduino Uno is a microcontroller board that uses an AVR microcontroller called ATmega328. It is used as a control unit to obtain ECG signal from the analogue pin of Olimex Shield-EKG-ENG Prototype Board and transmit the signal through Bluetooth to the heart screening device by using Cytron Bluebee module with Xbee Shield. Cytron Bluebee module with Xbee Shield is a Bluetooth module with 2 operations modes that can be acted as master or slave. In this project, it is used to transmit the ECG data from the ECG acquisition unit to the heart screening device for further classification purpose [6]. The summary of the function of each part of ECG acquisition unit are as shown in Table 1.

Table 1: Summary of functionality of ECG acquisition unit components

ECG acquisition unit components	**Function**
1. Olimex Shield-EKG-ENG Prototype Board	Used to amplify the small ECG signal obtained by using passive electrode.
2. Arduino Uno Board	Act as control unit for the operation in ECG acquisition unit.
3. Cytron Bluebee module with Xbee Shield	Transmit ECG data to heart screening device through Bluetooth.
4. Passive electrode	Used to obtain the ECG signal by wearing it to both hands and right leg of the users.

Before uploading the Arduino coding for raw ECG data transmission, the Cytron Bluebee module with XBee shield need to be set as slave or server which listen and wait for incoming Bluetooth connection request from server after turn it on. This can be done by switching the Bluetooth module to AT MODE and enter the following AT command as shown in Table 2. After the Bluetooth module set to slave, upload the Arduino sketch design for raw ECG data transmission to the Arduino Uno board.

Table 2: AT command to set Bluetooth module as slave

AT Commands	Function
AT+ORGL	Reset to defaults
AT+RMAAD	Clear any paired devices
AT+ROLE=0	Set mode to SLAVE
AT+UART=57600,0,0	Set baud rate to 57600
AT+NAME = ARR-SCREENING-DEVICE	Set the name of the Bluetooth device
AT+ADDR	Get the address of the slave

Android based application

Android based application is designed to receive the real-time raw ECG data for displaying the real-time ECG chart plotting and the data storage purposes. The design of Android application can be divided into two parts, which are the Bluetooth connection features, and data receiving for real-time plotting and storage in internal memory. Besides, there is also user-friendly GUI designed for the application.

Android based application is designed and implemented by using Android studio IDE with SDK tools. The GUI page mapping of Android application is as shown in Fig. 6.

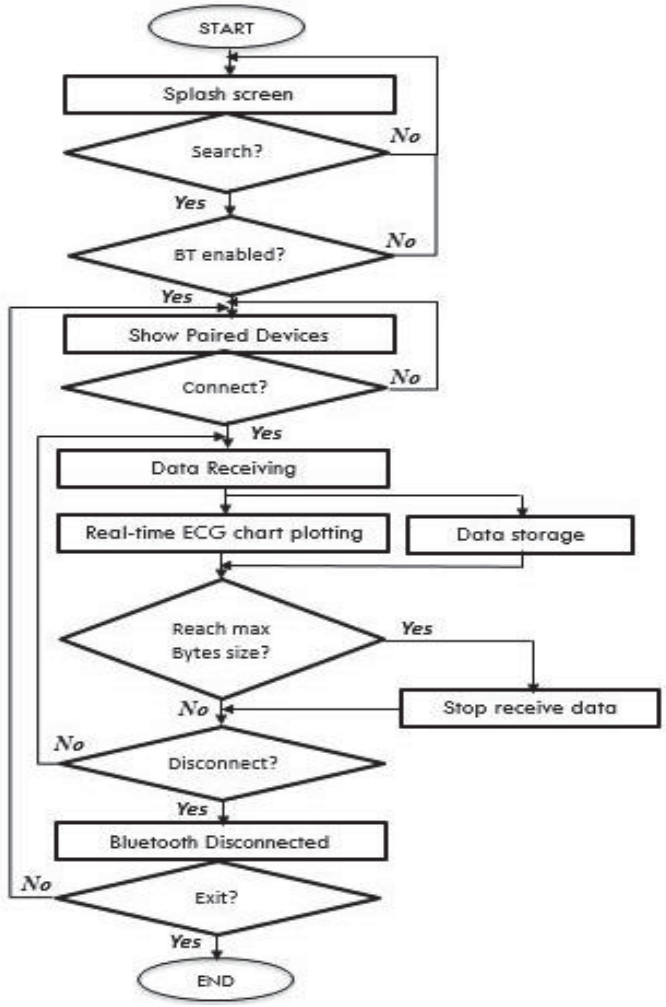

Fig. 6. The GUI page mapping of Android application

IV. RESULT AND DISCUSSION

The outcomes of this project can be divided into two parts, which are the user-friendly touchscreen GUI page mapping and the text file that created in internal memory of mobile devices to store raw ECG data.

A. Page mapping of Graphical User Interface

The Android based application is installed and run on Samsung Galaxy S5 mobile device. Fig. 7 shows the initial starting page when open the application. After the search button is pressed, the device will check for the Bluetooth either is it enabled or not. If no, a dialog box will prompt to ask the users to enable the Bluetooth as shown in Fig. 8. Else, a list of paired Bluetooth devices with this mobile phone will be shown on the page as illustrated in Fig. 9.

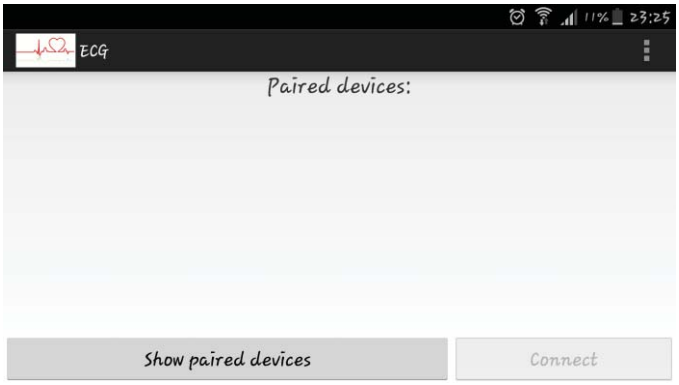

Fig. 7. Initial starting page of the application

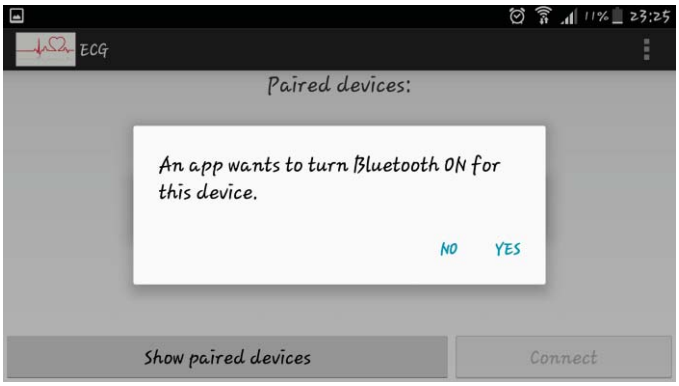

Fig. 8. Dialog box prompt to ask for Bluetooth enable permission

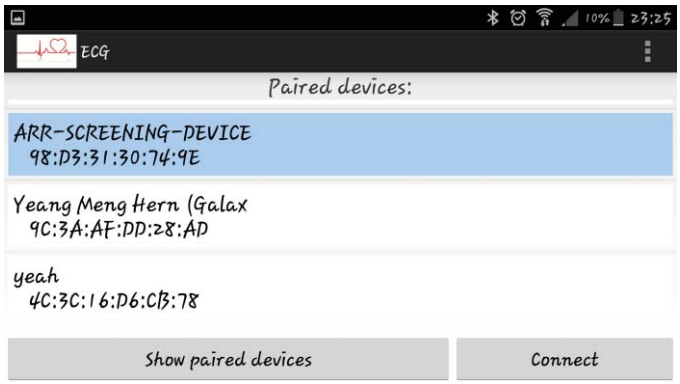

Fig. 9. Display of Bluetooth paired devices in a list

The user will then search for the wireless ECG acquisition unit (ARR-SCREENING-DEVICE) and connect with it. After the Bluetooth connection is established, the data received will display as the text view and the real-time ECG chart is plotting on the screen as shown in Fig. 10. When the disconnect button is pressed, the Bluetooth connection will lost.

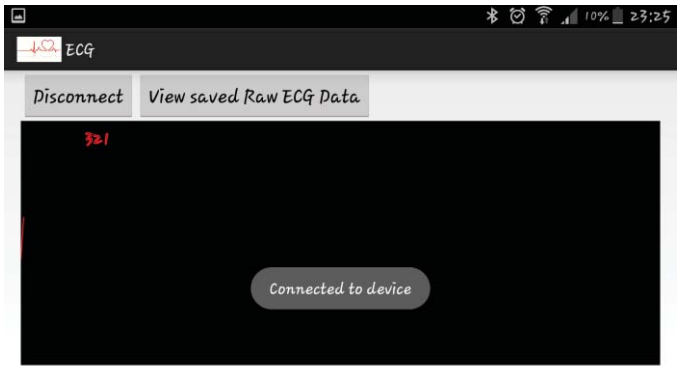

Fig. 10. Display of real-time ECG chart plotting and data received on the screen

B. *Data storage as text file in internal memory*

While displaying the real-time ECG chart and data in the screen, the application also create a text file in "ECGData" folder and write the received raw ECG data to the file for storage in internal memory of the mobile device in background. The naming of text file will be based on the date and time where the file created. Fig. 11 shows the text file created and the raw ECG data stored inside the text file.

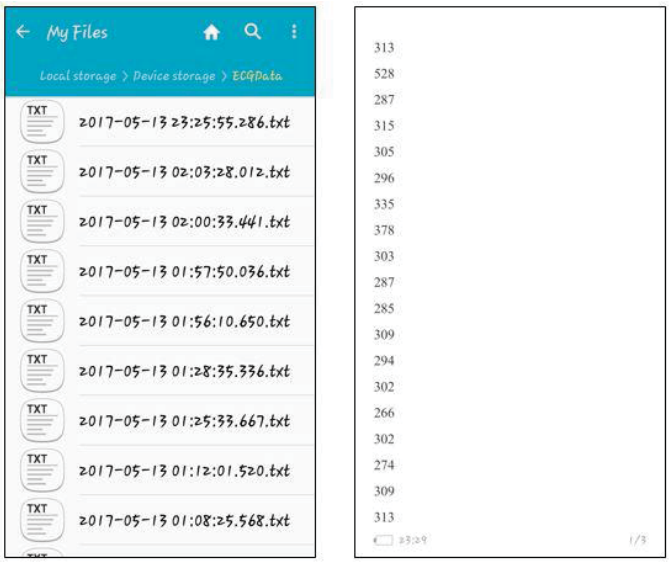

Fig. 11. Text file created in ECGData folder and the raw ECG data stored inside the text file.

V. CONCLUSION

In conclusion, this paper represented about system integration of heart disease screening device with the design implementation of Android based mobile applications features. The Android based application is designed to receive the raw ECG data from the wireless ECG acquisition unit after the Bluetooth communication is established between them and display the real-time ECG chart plotting on the screen while receiving the data. Besides, the received ECG data can also be saved into a text file in the internal memory of mobile device. Furthermore, the Android application also equipped with user-friendly graphical user interface (GUI). The purpose of add on this features is to prepare the system of heart screening device for further Internet of things (IoT) purposes. The future work recommended for this project is to improve the system of the Android application with direct IoT features within the system.

ACKNOWLEDGMENT

First and foremost, we would like to express our sincere appreciation to my supervisor, Dr Ismahani binti Ismail and my co-supervisor, Dr Jasmine Hau Yuan Wen for giving us continuous support, guidance and the invaluable assistance to us during the whole project implementation journey. Besides, we would also like to acknowledge Universiti Teknologi Malaysia for providing us the facilities of lab and equipment during our project implementation period. Last but not least, we would also like to thanks to the Master student of Biochip and Medical SoC laboratory UTM who is also the mentor of this project, Lim Huey Woan for her support, advices and technical guidance to us.

REFERENCES

[1] F. Ho, "Healthy Hearts," *The Star Online*, 2013. [Online]. Available: http://www.thestar.com.my/lifestyle/health/2013/09/29/healthy-hearts/.

[2] [2] H. W. Lim, M. Syafiq, M. Sani, A. Hashim, and Y. W. Hau, "Throb : System-on-Chip based Arrhythmia Screener with Self Interpretation," pp. 30–36, 2015.

[3] [3] H. W. Lim, "The Design of Atrial Fibrillation Classification on System-on-chip Based Arrhythmia Screening Device," 2015.

[4] Dr Tim Kenny and Dr Colin Tidy (2015, Sept 22), "Electrocardiogram (ECG)," Patient: Trusted Medical Information and Support. Available: http://patient.info/pdf/4692.pdfR. Nicole, "Title of paper with only first word capitalized," J. Name Stand. Abbrev., in press.

[5] American Heart Association. (2016, Sept), "Introduction of Arrhythmia," About Arrhythmia. Available: http://www.heart.org/HEARTORG/Conditions/Arrhythmia/AboutArrhythmia/About-Arrhythmia_UCM_002010_Article.jsp#.WFqG41N9600M. Young, The Technical Writer's Handbook. Mill Valley, CA: University Science, 1989.

[6] Wikipedia, Android (operating system). Available: https://en.wikipedia.org/wiki/Android_(operating_system)

[7] Suhas Holla, Mahima M Katti, "ANDROID BASED MOBILE APPLICATION DEVELOPMENT and its SECURITY," International Journal of Computer Trends and Technology- volume3Issue3, 2012.

[8] LIM HUEY WOAN, "The Design of Atrial Fibrillation Classification on System-On-Chip based Arrhythmia Screening Device," 2015.

[9] W. J. Mun, "Embedded System Design of Arrhythmia Screening Device with Wireless Communication," 2016.

[10] Mohammad Syafiq Afendi, "Interactive on-board touchscreen graphical user interface design for system-on-chip (soc) based arrhythmia screener," 2016.

Implementation of Bluetooth Low Energy Controller - Link Layer

Ihsan Fahim Bin Yusri, Ismahani Binti Ismail & Izam Bin Kamisian
Faculty of Electrical Engineering
Universiti Teknologi Malaysia
Johor Bahru, Malaysia.
ismahani@fke.utm.my

***Abstract*—In order to integrate Bluetooth into System-on-Chip (SoC), Intellectual Property (IP) was needed. However, the existing IP for Bluetooth was expensive and it reaches million range. This paper describes the implementation a part of Bluetooth Low Energy (BLE) IP which is Link Layer Controller and transmits data using Bluetooth packet format. Bluetooth privacy and protocol are excluded in this paper. The Link Layer have five states which are standby, advertising, scanning, initiating and connecting and it communicates by using either advertising channel packet or data channel packet. Verilog HDL was used in designing the link layer and the result was verified/simulated using vector waveform. The design is able to establish and terminate a connection by communicating using both Bluetooth channel packet. Design for control unit and datapath unit for the controller was described in this paper. The implication of this paper was it is able to implement Bluetooth Link Layer and transmit data by using Bluetooth channel packet format.**

Keywords—Bluetooth Low Energy; Link Layer Controller; System-on-Chip; Intellectual Property.

I. INTRODUCTION

Nowadays, Bluetooth is a common wireless device that uses in many things such as smartphone, laptop, infotainment and television. Bluetooth is managed by Special Interest Group (SIG) for short distance, low power and low-cost communication that uses radio technology. Bluetooth used to exchange data between two devices but it is not as fast as other wireless communication modes. The purpose of Bluetooth is to eradicate the use of cords, cable, adapters and permits the electronic devices to link wirelessly with each other [1].

There are two options to integrate a Bluetooth technology into SoC design. First, connect the system with Bluetooth chipset module externally and bulky. Second, reuse Intellectual Properties (IP) core integrate inside the SoC by plugin the existing Bluetooth block inside the system [2]. However, Bluetooth IP is needed to integrate Bluetooth into a SoC and the price for the IP license is in the range $1 million [3]. In order to build an IP from scratch, a significant number of resources and implementation of both hardware and software parts which has thousand pages of Bluetooth specification need to be studied [2]. The architecture of Bluetooth had been described by Hydon [4] in Fig.1. Bluetooth can be separated into three basic part. The first part is the application that is a software stack that provides access and support to the users. Second part is the host which is a software protocol stack and lastly the controller is the implementation of the service provided for the host part [5,6].

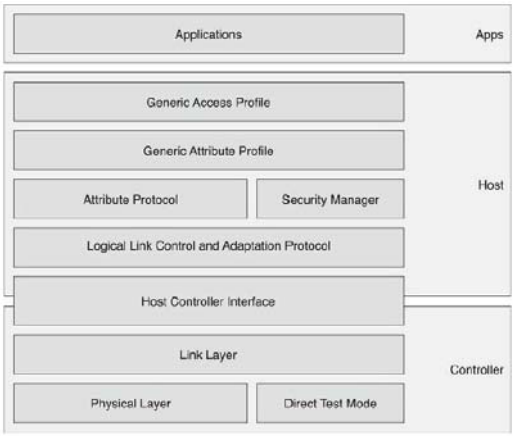

Fig. 1. The Bluetooth architecture [4].

BLE controller specification [5] defines a Host Controller Interface (HCI) layer, link layer and a physical layer. HCI is an intermediate layer that interconnects between the software stack and hardware stack and translates the software data into the basic register of the Link Layer. However, the Link Layer is a digital and the Physical layer is an analog part of the controller. The Link Layer control the data operation from establishing a connection to terminate a connection. All the communication are using a packet of data bits. This paper is to design existing IP specification for BLE Link Layer Controller state machine and its flow control.

The scope of this work is to design a part of existing IP for BLE Link Layer by following the specification that has been standardized by Bluetooth SIG. The design is able to get the Bluetooth into a connection state and transfer a data. This paper does not consider the Bluetooth protocol and privacy.

II. LITERATURE REVIEW

A. Related Work

In Wiecha paper [5] describe about the architecture and design for BLE controller. There are three points that can be extract from his works. First, in order to provide an easier integration with various architecture and increase flexibility, two separated clock domains was used. Second, the intermediate later which is software was implemented to simplify the

hardware parts. The purposed of this layer was to minimize hardware area and power consumption. Lastly, he introduced to use a Single Port RAM (SPRAM). As the result, it make the chip size smaller and reduce the number of registers in the design.

The usage of energy for BLE has been studied [7] and it ended consume extremely little energy. However, the experiment shows that it also has a drawback and restraint and BLE still can be improved. Implement Adaptive Frequency Hopping (AFH) to reduce interference and during connection event, allow more packets can be send.

B. Link Layer Specification

The Link Layer describes how two devices transmit information between one another. The definition detail of a packet, advertising channel and data channel are also included. In addition, procedures for discovering other devices, advertising data, making a connection, managing connection, and sending data within the connection are described in the Link Layer [4].

1) Link Layer State Machine

The process of the Link Layer can be represented in terms of a state machine. At a time, there is only one state in the Link Layer state machine allows being active. Fig. 2 illustrates the state machine for the Link Layer which consists of five states: Standby, Advertising, Scanning, Connection and Initiating [8].

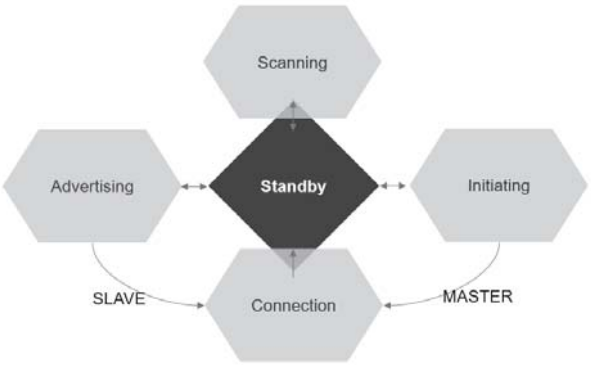

Fig. 2. State diagram of the link layer state machine [8].

2) Air Interface Packet

There are two types of packets that being used in Bluetooth channel packet such as advertising channel packet and data channel packet. There is only single packet format in the Link Layer. It is used for both advertising and data channel packet. There are fields in packet format and the structure is illustrated in Fig. 3. The first to be transmitted is Preamble, followed by the Access Address, Protocol Data Unit (PDU) and Cyclic Redundancy Check (CRC) [4].

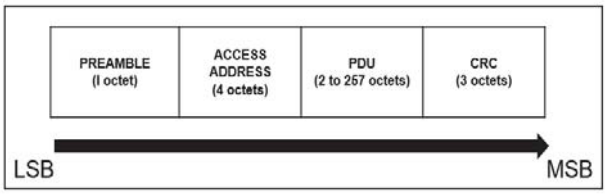

Fig. 3. Link layer packet format [8].

The preamble is used for frequency synchronization, and Automatic Gain Control (AGC) training and symbol timing estimation that executes in the receiver. There are two types of an eight-bit preamble in all Link Layer packets which are 10101010b and 01010101b.

For all advertising channel packets, the Access Address shall be same which have a value of 8E89BED6 in hexadecimal. However, in every connection of the Link Layer between two devices, it will have a different data channel packets Access Address. In initiating state, a random 32-bit value is generated and transmitted as the Access Address in a connection request.

Once a packet is sent, the PDU can be either advertising PDU or data PDU channel packets. The last field is CRC and the purpose of the CRC is for an error checking.

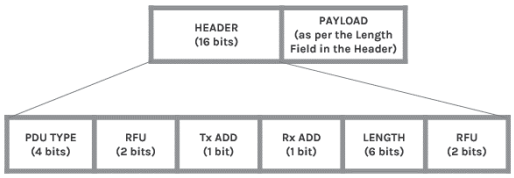

Fig. 4. Advertising channel PDU [8].

Fig. 4 shows the PDU for advertising channel. It consists of a header with 16-bits and a changeable size of the payload. There are six other fields inside the advertising channel PDU header field. The first 4-bit indicates the PDU type. The PDU types consist of advertising, scan request and response, connect request and reserve. In the TxAdd and Rxadd field of the header, information detailed to the types of PDU is defined for each advertising channel PDU separately. The Length field in the header defines the length of the payload field in octet. 6 to 37 octets is the range for the Length field. Lastly, the PDU is specified by the advertising channel PDU's Payload fields. The Reserved in the PDU types will not be sent and upon receipt, it will be ignored [8].

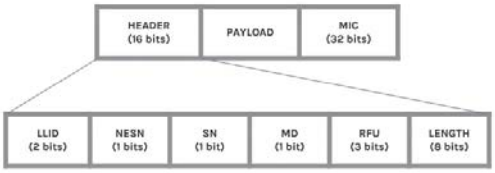

Fig. 5. Data channel PDU [8].

The data channel PDU has a slightly different from advertising channel PDU. It also has a header with 16-bits similar to the advertising channel PDU. A variable size payload and might include a Message Integrity Check (MIC) field. Fig. 5 illustrate the data channel PDU, its header and its payload. LL Data PDU and LL Control PDU can be selected in the Header's LLID field. To select the PDU, these 2-bits vectors are given: Reserve, LL Data PDU and LL Control PDU. The NESN field and SN field of data channel PDU describe as Next Expected Sequence Number and Sequence Number, respectively. The MD field of data channel PDU is described as More Data. Lastly, the size of the Payload and MIC is specified in the Length field.

3) Connection and Close Event

Before a connection is established, the link layer shall transmit an advertising channel packet. The communication between advertising and initiating state will continue until both of them move to the connection state. In Connection events, the connection state Link Layer will only send data channel packet. The same data channel index will be used for all packet in the connection event, the master will send at least one packet to the slave for each connection event. During the connection event, both master and slave will alternately transmit and receive packets. A device become a master when it enter connection state from initiating state. However, a device become a slave when it enter connection state from advertising state.

The connection event is considered establish whereas both master and slave remain to transmit packets between one another. The connection event shall be terminated if the master does not receive any packet from the slave. However, either both devices are able to close the connection event [8].

III. METHODOLOGY

This section discusses the methodology in implementation the link layer including software that is used and its program language. The flowchart of the approach used is illustrated in Fig. 6.

The project started with determination of the scope and make a documentation for the specification of the link layer such as its state machine and packet format. Next, implement the design by following the specification. Datapath Unit (DU) was designed first and followed by Control Unit (CU). Then simulate the design for verification. Finally, combine both CU and DU and simulate it. It can be verified by making sure the final module can transmit and receive a right packet. User inputs were used as the information and data from host since these data are needed to be extracted and received from HCI.

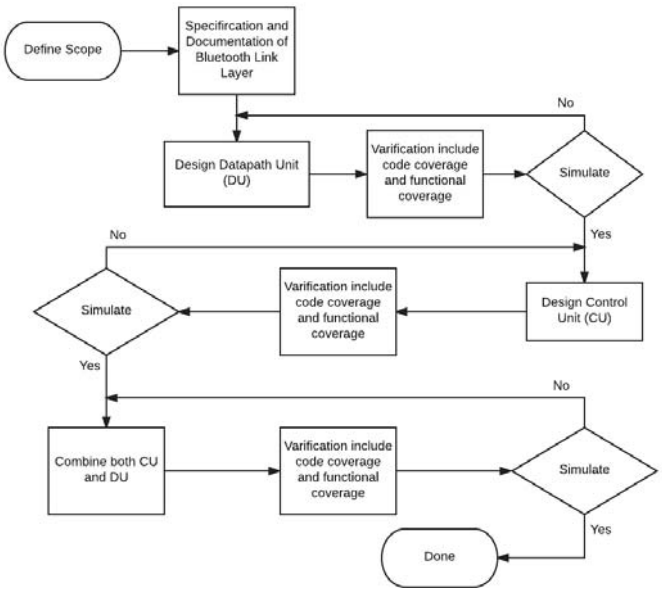

Fig. 6. Flowchart for implementation and designing the link layer.

This project used Quartus II as the main software to design the Link Layer. Quartus II, is a programmable logic device design software produced by Altera. Verilog was used to write a text-based description of a digital circuit for design entry, pre-synthesis simulation and logic synthesis of the Link Layer. Design module was divided into a hierarchy of modules, from the general at the top, to the specific at the bottom. The combination of two approaches in designing which are top-down approach and bottom-up approach was used. The design was also run and simulated by using Quartus II to get a vector waveform simulation.

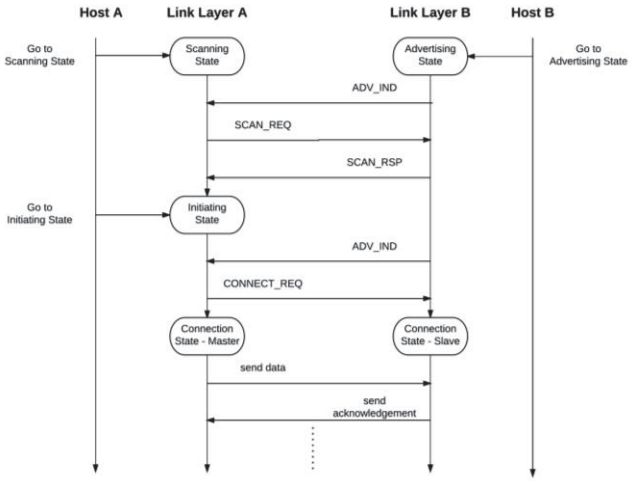

Fig. 7. Flow control for link layer establish a connection [6].

In order to establish a connection between two devices, a steps or flows of communication between these devices need to be made. Fig. 7 shows the flow control between device A and device B. First, the advertiser advertises and scanner that hear it will sent a scanning request. The advertiser replies it with scanning response and the scanner receives it. With host instruction, scanner moves to initiating state. Here, the initiator will send a connect request to the advertiser. Lastly, both devices move to connection state. Master sends the first data packet to slave and slave will send an acknowledgement back to master. This process will keep sending alternately until the data is completely sent.

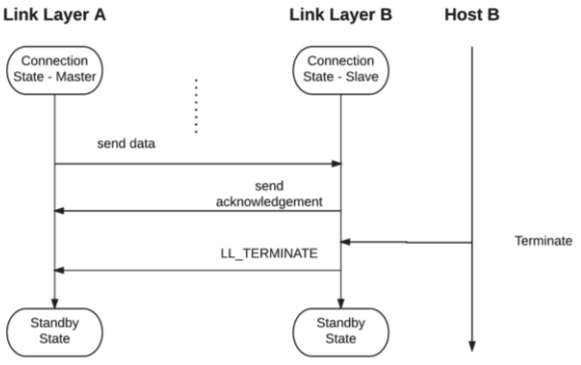

Fig. 8. Flow control for link layer terminate a connection [6].

Once the data is received, the connection will be closed. Either master or slave role can terminate the connection. Once the host instructs link layer to close the connection, the device will send a terminate PDU to other device as illustrated in Fig.

8. When the connection is closed, both devices move back to the standby state.

Link Layer consisted of two major modules which is DU and CU. For DU, it involves transmitter, receiver and timer. On the other hand, CU was designed to control the flow of the states, process it and send back to DU for further instruction. Information below shows the circuit part for the link layer:

A. Minor module (Level 2 Hearachy)

1) Transmitter.

Transmitter was used to transmit a bit-by-bit. PISO register was used as shown in Fig. 9. Both advertising packet and data packet will use the same transmitter and all data were instructed by host or user.

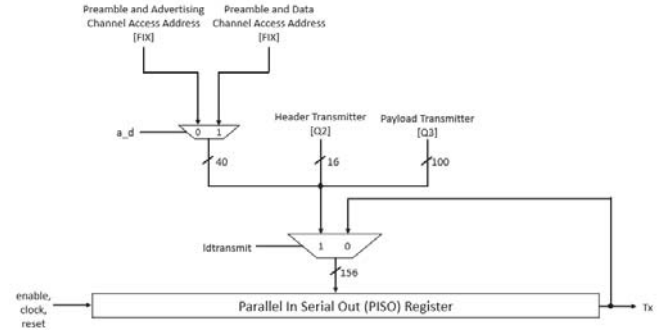

Fig. 9. Level 2 Hearachy for datapath transmitter.

2) Receiver.

When a data is received, it goes into PISO register until the packet is fully received. Then, the packet will load into a register and check what the packet channel is. PDU, receive device address and receive data was retreated. The circuit is illustrated as below in Fig. 10.

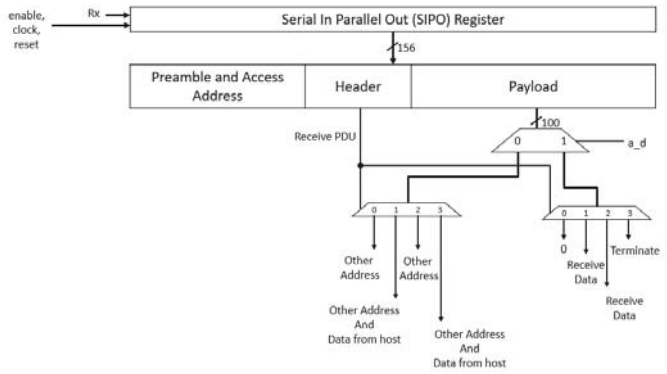

Fig. 10. Level 2 Hearachy for datapath receiver.

B. Major module (Level 1 Hearachy)

1) Datapath Unit.

DU consists of three major modules which are transmitter, receiver and timer. All the inputs data were given by CU except data that will be transmitted. The other minor module such as PDU selector and input header and payload were not illustrated in Fig. 11.

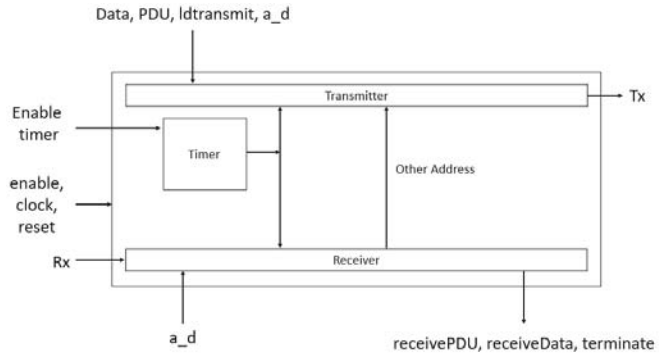

Fig. 11. Level 1 Hearachy for Datapath Unit.

2) Control Unit.

CU was designed based on the five states as described in literature review section. However, in every states has a sub-states to control it flow to transmit and receive. Fig. 12 shows the block diagram for CU with its inputs and outputs.

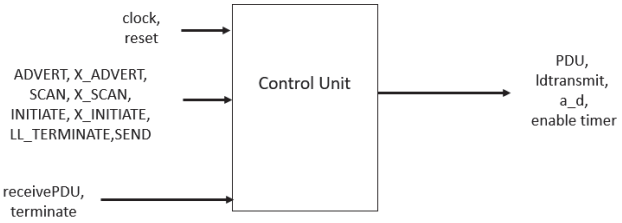

Fig. 12. Level 1 Hearachy for Control Unit.

C. Top Level Entity

The top entity for designed link layer was combination of both CU and DU. All the state and sub-states were being controlled by CU and instruct DU to be executed. Fig. 13 illustrates that 'Data' is the input data that want to be transmitted to other link layer and 'receiveData' is the receive data from other link layer.

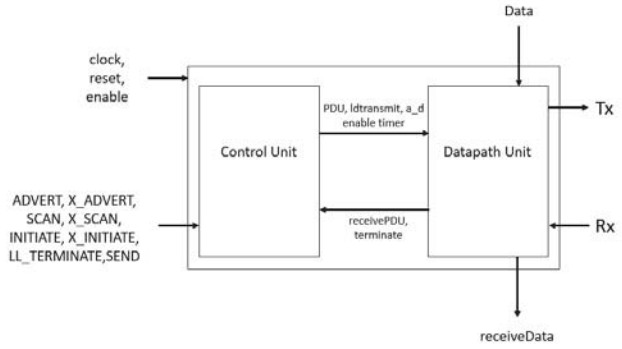

Fig. 13. Top Entity Module for Link Layer.

IV. RESULT AND DISCUSSTION

In order to show that the design is working, two link layer were connected (link layer A and link layer B). Link layer A will be an advertiser and link layer B will be a scanner and initiator. Fig. 14 shows connection that being made between two modules that produced by netlist RTL viewer Quartus II.

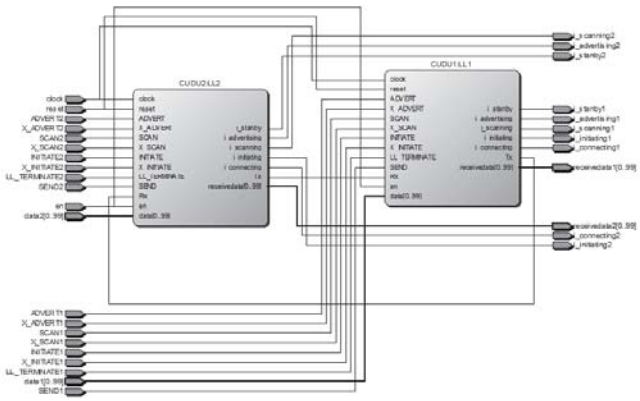

Fig. 14. Netlist RTL viewer Quartus II for connection between two modules.

The design then being simulated by using vector waveform. Input from host to change the link layer states was replaced with user input. ADVERT to enter advertising state, X_ADVERT to exit advertising state, SCAN to enter scan state, X_SCAN to exit scan state, INITIATE to enter initiate state, X_INITIATE to exit initiating state, LL_TERMINATE to terminate a connection and SEND to send a data were the inputs. In simulation, link layer 1 transmit as Tx and link layer 2 transmit as Rx.

First the link layer 1 will go to advertising state and link layer 2 go to scanning state. Link layer 1 transmit ADV_IND PDU and link layer 2 received it. After that, link layer 2 send a SCAN_REQ to link layer 1 to ask for further information from host 1. Then, link layer 1 send its information as SCAN_RSP as shown in Fig. 15.

Next, link layer 2 went to initiating state and listen to advertising state from link layer 1. When it receive a packet, link layer 2 send a CONNECT_REQ to link layer 1 and both link layer went direct to connection state. Link layer 1 become a slave role and link layer 2 become a master role. The master will send a data and slave shall receive it. User gives an input 'SEND' to master and data will be transmitted.

The data that being transmit was from 'data2' to 'receivedata1'. Fig. 16 shows the data in octet '0123456789ABCDEF123456789' was transmitted and received correctly.

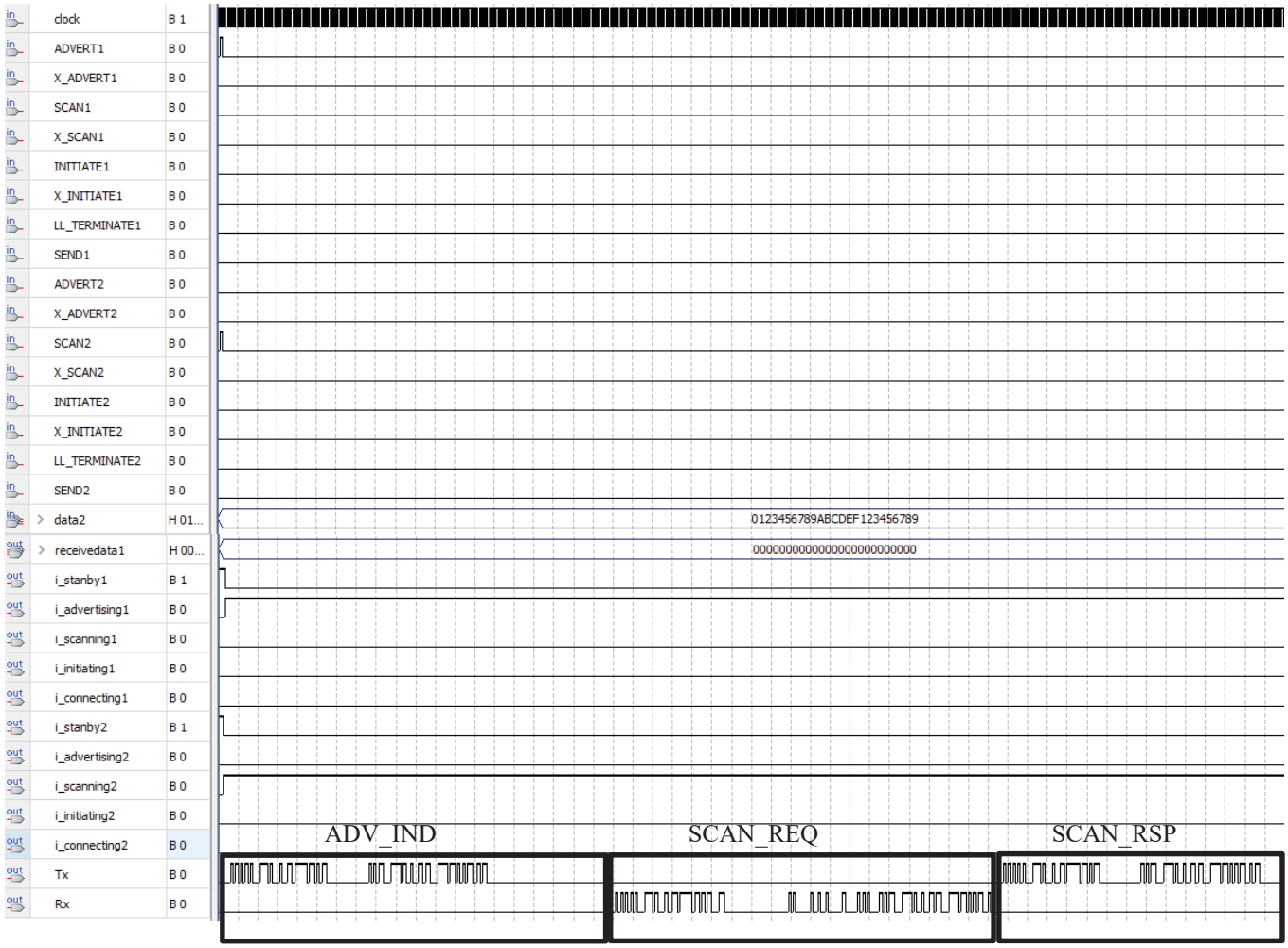

Fig. 15. Output Vector Waveform for advertising and scanning.

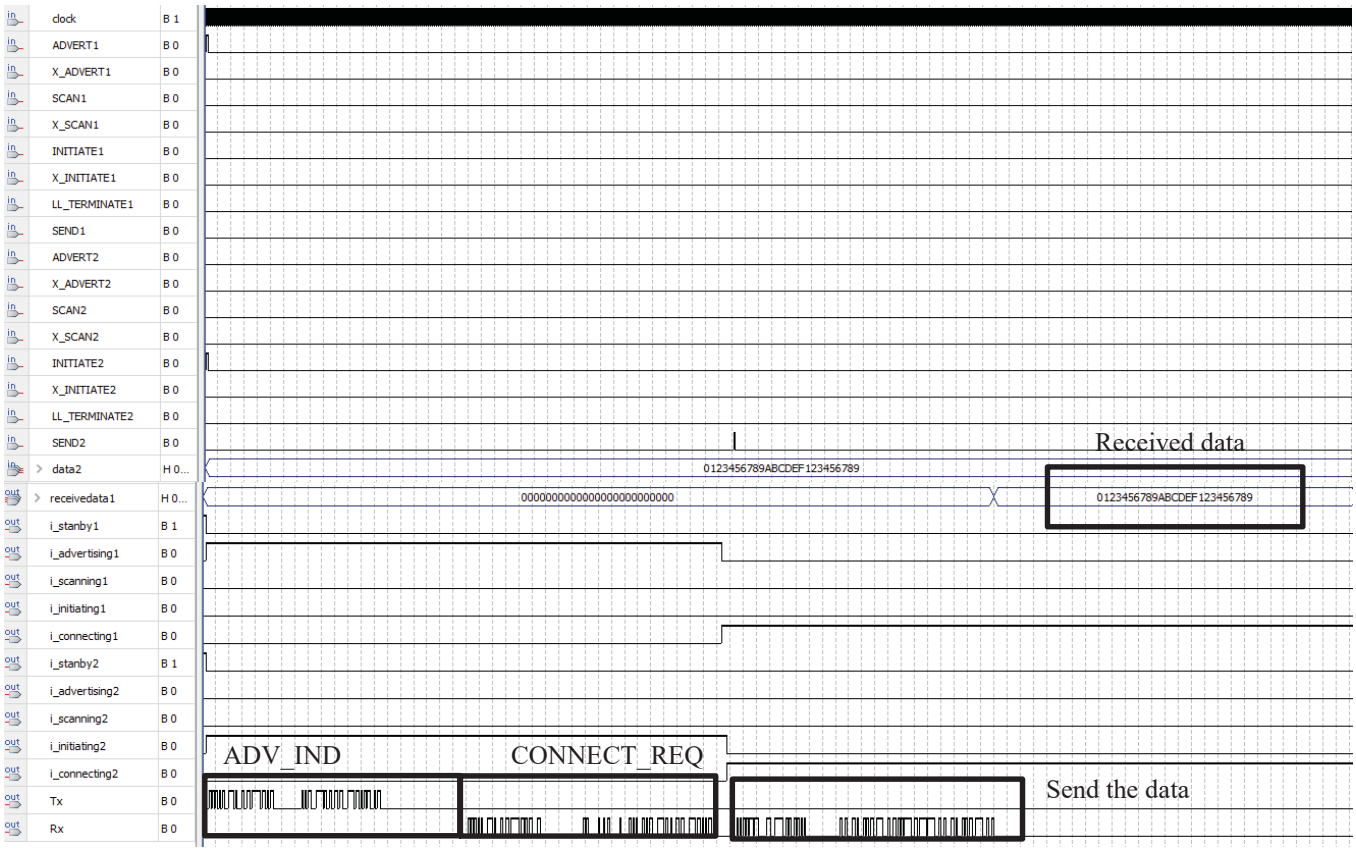

Fig. 16. Output Vector Waveform for estabish a connection and receive data.

V. CONCLUSION

BLE has a different architecture compare to other version of Bluetooth. The implementation of Bluetooth Link Layer was following the specification that has been standardized by Bluetooth SIG.

This implementation and design was successfully be implemented by using Verilog code. The designed link layer able to transmit and receive using Bluetooth advertising and data packet format. The Bluetooth state machine and its flow control was implemented from established to close a connection. Link Layer able to advertise a packet and scan or listen to other packet. During the connection state, data can be transmit and receive correctly.

In order to integrate BLE into SoC, further implementation of other layers, stacks and all Bluetooth protocol need to be design as well. With a complete Bluetooth IP, a short distance communication with ultra-low power consumption can be implemented in any SoC.

REFERENCES

[1] P. McDermott-Wells, "What is Bluetooth?," in *IEEE Potentials*, vol. 23, no. 5, pp. 33-35, Dec. 2004-Jan. 2005.

[2] K. Sairam, N. Gunasekaran and S. Redd, "Bluetooth in wireless communication", IEEE Communications Magazine, vol. 40, no. 6, pp. 90-96, 2002.

[3] P. Corcoran, "The Internet of Things: Why now, and what's next?," in *IEEE Consumer Electronics Magazine*, vol. 5, no. 1, pp. 63-68, Jan. 2016.

[4] R. Heydon, Bluetooth low energy: the developer's handbook, 1st ed. Upper Saddle River N.J.: Prentice Hall, 2013.

[5] P. Wiecha, M. Cieplucha, P. Kloczko and W. A. Pleskacz, "Architecture and design of a Bluetooth Low Energy Controller," *2016 MIXDES - 23rd International Conference Mixed Design of Integrated Circuits and Systems*, Lodz, 2016, pp. 164-167.

[6] W. Stallings, Data and computer communications, 1st ed. Harlow: Pearson, 2013, pp. 42-44.

[7] M. Siekkinen, M. Hiienkari, J. K. Nurminen and J. Nieminen, "How low energy is bluetooth low energy? Comparative measurements with ZigBee/802.15.4," *2012 IEEE Wireless Communications and Networking Conference Workshops (WCNCW)*, Paris, 2012, pp. 232-237.

[8] *Specification of the Bluetooth System*, Bluetooth SIG (Special Interest Group), Inc. Std., Rev. 4.1, Dec. 2013. [Online]. Available: http://www.bluetooth.org

Implementation of Actor-based JPEG Encoder on Xilinx Field-Programmable Gate Array

Gan Yi Reng
Faculty of Electrical Engineering
Universiti Teknologi Malaysia
Johor Bahru, Malaysia.
yanyireng@gmail.com

Dr. Ab Hadi Bin Ab Rahman
Department of Electronic and Computer Engineering
Faculty of Electrical Engineering
Universiti Teknologi Malaysia
Johor Bahru, Malaysia.
hadi@fke.utm.my

***Abstract*— This paper presents that an actor-based JPEG encoder is implemented on Genesys 2 board, a Kintex-7 FPGA using a high-level dataflow programming language, called the Cal Actor Language (CAL). Hardware description language (HDL) code is generated for hardware implementation from a Reconfigurable Video Coding (RVC)-CAL JPEG encoder. CAL is specified at high-level therefore increases design productivity for algorithmically complex application. The current RVC-CAL JPEG encoder is available online and in this work, there are several platforms that we can implement JPEG encoder with CAL specification and I have implemented in FPGA fully and general-purpose processor. Hardware implementation analysis has been done to evaluate the clock frequency, latency, slice LUT, slice register, and power. Comparison with software has been done in terms of speed, frequency, power, and energy.**

Keywords— JPEG encoder, FPGA, Cal Actor Language, Implementation, Genesys 2

I. INTRODUCTION

In this era of globalization cum fast-paced world, the complexity of digital signal processing is increasing with a tremendous rate and it is getting more and more complicated. Therefore, from the journal [1], an approach for unified hardware and software synthesis initiating from the same program design is developed. The language used in this report is Cal Actor language (CAL) [2]. We can observe that from the past, CAL language is used to generate hardware code in [3,4] with the OpenDF framework.

By using CAL language, it is easier for us to construct the design of program especially digital signal processing program such as JPEG encoding. Targeted platforms like single-core processors, multi core processors, and programmable hardware use CAL to compile. Apart from that, CAL is also widely applied in video processing and compression. As a classic example, CAL language is adopted by the Moving Picture Experts Group (MPEG) Reconfigurable Video Coding (RVC) [5] working group as an effort of standardization.

There are several platforms where we can implement RVC-CAL JPEG encoder, like fully FPGA, Embedded Linux, computer (PC) or even Java (in Eclipse). What is the performance of RVC-CAL JPEG encoder on FPGA (Genesys 2) and PC? The JPEG encoder which will be used in this project is from ORCC which is an Eclipse based open source Integrated Development Environment. [6][7] The RVC-CAL JPEG encoder have been tested using Virtex 6 FPGA in [1]. Instead of designing JPEG Encoder using hardware description language (HDL), CAL is used and then generates the HDL code using ORCC compilation. Comparing the performance of CAL specification JPEG encoder with other specification JPEG encoders can help the industry to improve the performance in term of speed and power consumption of devices like smartphone or camera, thus providing a better customer experience.

II. LITERATURE REVIEW

A. Cal Actor Language (CAL)

Cal Actor Language is a programming language which is based on Actor model of computational for dataflow system. [2] It is actually a part of the Ptolemy II project [10] at the UC Berkeley. What is an actor? It is a modular component that encapsulates its own state. By having connection at the FIFO channel, each actor can communicate with each other. We can control the action of an actor by manipulating the state variables, actions, procedures global parameter, finite state machine and function which is programmed in the actor. Since CAL can be compiled into hardware and software implementation, it has a wide range of application. In this project, RVC-CAL language which is a subset of CAL is used for JPEG encoder implementation on FPGA. Figure 1 shows the CAL computing model.

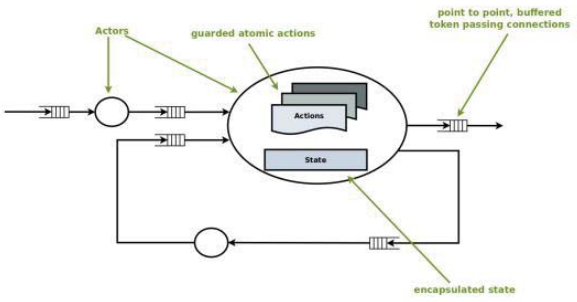

Fig. 1. CAL computing model. [1]

From Table I, we can observe the difference between the common approaches that we use for software/hardware implementation which are C/C++ programming and

Verilog/VHDL versus the later approach which is by using CAL. For regular and basic design, VHDL is one of the efficient approaches. However, when it comes to an algorithmically complex and application which involves a lot of process, productivity using VHDL reduces. Therefore, another way can be done to handle this issue which is by using CAL approach. Due to the actor based programming, we can design the algorithm more effectively and by using one approach we can implement into both software and hardware platform.

TABLE I. COMPARISON OF DIFFERENT PROGRAMMING LANGUAGE

Language	C/C++	Verilog/VHDL	CAL
Complexity of algorithm	Low	High	Low
Time consuming	Short	Long	Short
Implementation platform	Software	Hardware	Software & hardware
Power	High	Low	Low
Performance	Low	High	High

B. *Open RVC-CL Compiler (ORCC)*

After we design a network of RVC-CAL actors, the network of actors can be compiled through Open RVC-CAL Compiler (ORCC) to generate the implementation code. [11] From [1], we understand that using Backends of ORCC compilation, RVC-CAL code can be converted into targeted specific code like C language, C++, Java, LLVM, VHDL and XLIM. Figure 2 shows that the CAL code passing through ORCC Frontend to translate it to Intermediate Representation. Next the translated code will go through specific Backend. If we want to convert to C language, thus it will enter C Backend.

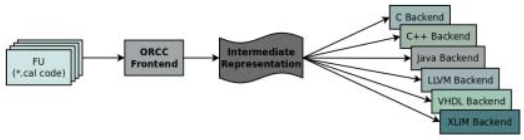

Fig. 2. ORCC framework chain. [1]

For this project, I chose C Backend to convert CAL code to C code so that I can implement it on the software as it is compatible to multiple platforms like Windows, Linux, Mac OS X etc. On the other hand, to implement on FPGA board, the RVC-CAL JPEG Encoder is going through VHDL backend to produce its VHDL code. The overview of the project is showed in Figure 3.

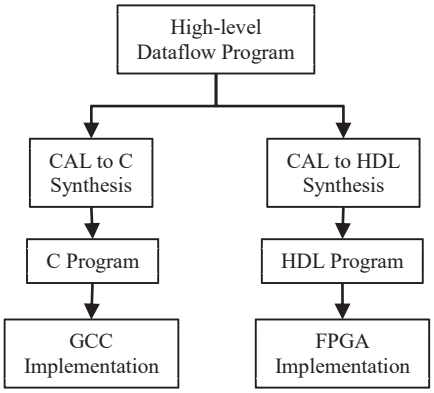

Fig. 3. Flowchart of usage of dataflow language in this project.

C. *RVC-CAL JPEG Encoder*

Joint Photographic Experts Group (JPEG) encoder with RVC-CAL specification is implemented in this project. As shown in Figure 4, Raster 4:2:0 YUV acts as the input for the JPEG encoder. The reason the JPEG encoder use this format as input is because it is the output of the input camera. Figure 5 shows the YUV 4:2:0 Macro-Block representation. [1] There are six actors in the JPEG encoder as shown in Figure 3 which are Raster To MB, FDCT, Quant, Huffman, Merger and Streamer. Compared to the traditional it has not much difference, which also passing through process of FDCT, entropy encoding and so on.

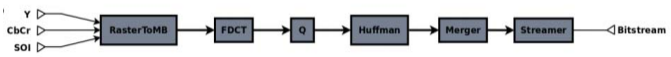

Fig. 4. The RVC-CAL specification JPEG Encoder.

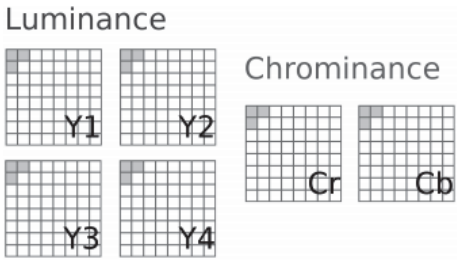

Fig. 5. The YUV 4:2:0 Macro-Block representation.

For the first actor, which is Raster to Macro Block (MB), Y, Cb, Cr and Size Of the Image (SOI) are the inputs of the actor. Next, the data from Raster to MB will go through Forward Discrete Cosine Transform (FDCT). Actors of FDCT and Quantization are working in 8 x 8 block level. After processed by Huffman actor, two bit streams will be generated which is for luminance and chrominance respectively. These two bit-streams is then entering merger which are merged into one and the necessary information will be added in the Streamer actor to form a working JPEG bit-stream.

Comparing the RVC-CAL JPEG encoder in [1], the Raster actor is having a single block output to FDCT actor and a single output to Quantization actor as shown in Figure 6.

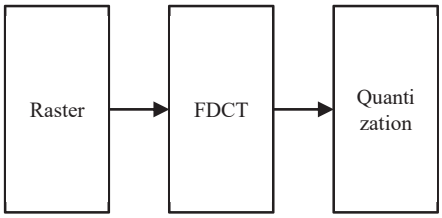

Fig. 6 Existing RVC-CAL JPEG encoder network of Raster-FDCT-Quantization.

III. Research Methodology

The process of development of the project is as illustrated as in Figure 8. This project is started by setting up the required software in the computer, such as Xilinx Vivado, Eclipse, Mingw and Cmake. The following step will be acquiring the RVC-CAL JPEG encoder and it is set up in Eclipse. For implementation on FPGA part, by using ORCC compilation, RVC-CAL JPEG encoder is synthesized into Verilog and C code by using VHDL backend and C backend respectively. Next, the C code of JPEG encoder is then compile to executable file using Cmake and Mingw. This is to ensure the coding is working after it is synthesized from RVC-CAL. For the generated VHDL code, it is synthesized into a bit stream using Xilinx Vivado. This bit stream is for us to program the FPGA and act as a JPEG encoder.

In order to implement the RVC-CAL JPEG encoder on Genesys 2, the output from the encoder is connected to an UART controller as shown in Figure 7 so that the image data can be sent to PC. From Figure 9, we can observe that there are three main blocks in the HDL program. The raw image is actually inserted in the RVC-CAL JPEG encoder before it is synthesized into VHDL code in Eclipse. To obtain the encoder output, a high Encoder_ack signal need to be send to the encoder so that it will start to process the raw image and compress it into JPEG format. Whenever the data is processed, there will be a high Encoder_send signal to indicate that the data is ready. The data output from the encoder is 8 bits wide and it is send to the UART controller before it is sent to PC. Encoder_send signal is set as the enabler of the UART controller so that the 8 bits data is processed and transfer serially to PC. As the input clock frequency of Genesys 2 board is 200MHz, after running analysis in Vivado Design Suite, I found that the encoder is unable to run at such highspeed. Thus, a clock divider is applied in the implementation to set the input clock of the encoder as 100MHz.

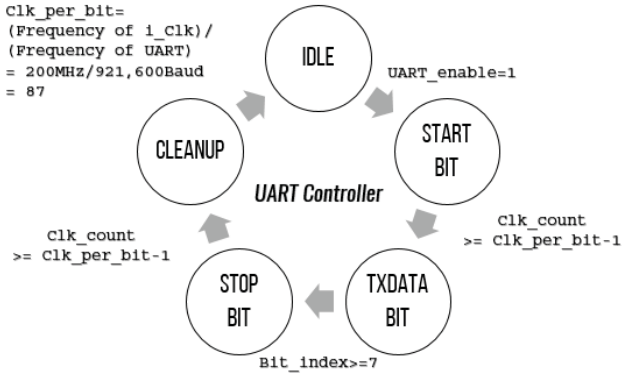

Fig. 7. State diagram of UART controller.

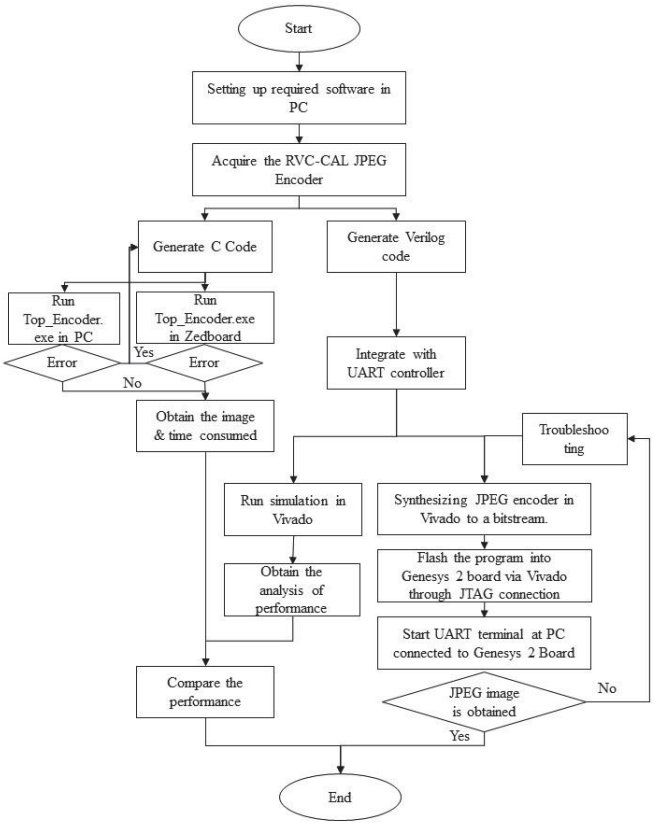

Fig. 8. Workflow of project.

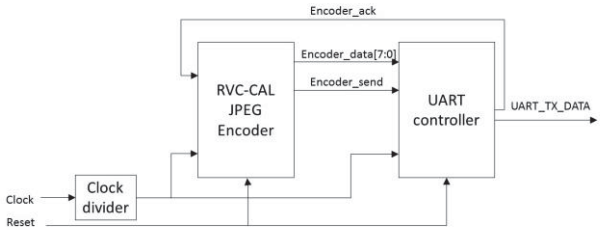

Fig. 9. Block diagram of implementation of RVC-CAL JPEG encoder on Gnesys 2 board.

IV. Result and Discussion

For this project, it is divided into two parts, which are software and hardware. In the software part, I obtained the RVC-CAL JPEG encoder from Github and import into Eclipse with ORCC compatible. After the RVC-CAL JPEG encoder is imported, the xdf file of the JPEG encoder project is opened. It is as shown in Figure 10, where the upper part is the JPEG codec and the lower part of Figure 10 is the RVC-CAL JPEG encoder. We can observe that there are networks of actors. When we double-click a specific actor, we will enter the CAL code of the actor and we edit the code there. For software implementation,

it is implemented on general purpose processor and Xillynux in Zedboard.

In Figure 11, it shows the output JPEG image of the RVC-CAL JPEG encoder. For the left image in Figure 11, it is the output of GCC implementation while for the right image is the output image of Genesys 2 board implementation.

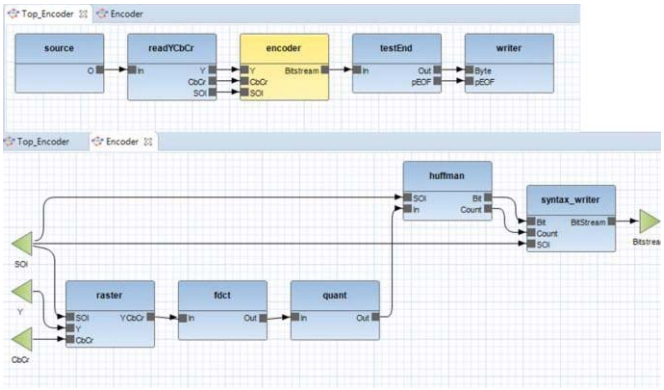

Fig. 10. Network of RVC-CAL JPEG encoder.

Fig. 11. Output image of RVC-CAL JPEG encoder.

In line with the objective of this project which is to implement RVC-CAL JPEG encoder on Xilinx based FPGA, Genesys 2 board, analysis on this implementation is conducted. The latency of the encoder is 341779 clock cycles. The maximum operating frequency of the encoder is 105MHz.The total on-chip power by the encoder is 0.278W. Table III shows the resource utilization of the implementation.

Table II shows the comparison in term of time taken to encode one image, together with the clock frequency and the power consumption of the implementation. From Table 4.4, we can see that with implemented FPGA consume the least power and time than another implementation. However, as it is integrated with UART controller, the time needed increase tremendously as the speed is limited by the UART controller. Even though with GCC implementation is only 15.2% slower than implement using FPGA fully, but the power consumption is much higher.

TABLE II. COMPARISON IN CLOCK CYCLE, MAXIMUM FREQUENCY & ON-CHIP POWER

RVC-CAL JPEG Encoder Implementation	Time Taken (T)	Clock Frequency(F)	Power(P)	Energy (E) E=P*T
FPGA	3.255ms	200MHz	0.27W*	0.879mJ
FPGA with UART	49.7ms	200MHz	0.278W*	13.82mJ
GCC	3.75ms	2.9GHz	15W**	56.25mJ
Xillynux @ Zedboard	8.37ms	100MHz	5W***	41.85mJ

* Based on implemented design

** Average power consumption of Intel i5 43000U processor

***Based on the power consumption of Zynq

TABLE III. RESOURCE UTILIZATION

Resource		LUT	LUTRAM	FF	BRAM
Original RVC-CAL JPEG Encoder	Utilization	9862	923	5932	34
	Available	203800	64000	407600	445
	Utilization%	4.84	1.44	1.46	7.64

V. CONCLUSION

In conclusion, the RVC-CAL JPEG encoder is implemented on Genesys 2 board successfully. The output image is sent to PC from Genesys 2 board through UART-USB port. With a single source of CAL specification JPEG encoder, it can be implemented in several platforms by synthesize the coding to C code through Cal2C tool and Verilog code through Xronos tool.

Hardware implementation which is using Genesys 2 board of RVC-CAL JPEG encoder have a better performance than software implementation through GCC. In term of time, it is 15.2% faster than that which implemented using GCC and 157.14% faster compared to embedded Linux implementation (Xillynux in Zedboard).

REFERENCES

[1] E. Bezati, H. Yviquel, M. Raulet and M. Mattavelli, "A unified hardware/software co-synthesis solution for signal processing systems," Proceedings of the 2011 Conference on Design & Architectures for Signal & Image Processing (DASIP), Tampere, 2011, pp. 1-6.

[2] J. Eker & J. Janneck, “CAL Language Report” University of California, Berkeley, Technical Report ERL Technical Memo UCB/ERL M03/48, 2003.

[3] S. S. Bhattacharyya, G. Brebner, J. W. Janneck, J. Eker, C. von Platen, M. Mattavelli, & M. Raulet, “OpenDF: a dataflow toolset for reconfigurable hardware and multicore systems.” SIGARCH Comput. Archit. News, 36(5):29–35, 2008.

[4] J. W. Janneck, I. D. Miller, D. B. Parlour, G. Roquier, M. Wipliez and M. Raulet, "Synthesizing hardware from dataflow programs: An MPEG-4

simple profile decoder case study," 2008 IEEE Workshop on Signal Processing Systems, Washington, DC, 2008, pp. 287-292.

[5] Shuvra S. Bhattacharyya, Johan Eker, Jörn W. Janneck, Christophe Lucarz, Marco Mattavelli, Mickaël Raulet "Overview of the MPEG Reconfigurable Video Coding Framework," Journal of Signal Processing Systems, 2009.

[6] "ORCC JPEG Encoder Download Site" [Online]. Available https://github.com/orcc/orc-apps/tree/master/JPEG/src, [Accessed October 8, 2016]

[7] "ORCC Official Website" [Online]. Available http://orcc.sourceforge.net/, [Accessed September 10, 2016]

[8] J. Balladini, R. Suppi, D. Rexachs and E. Luque, "Impact of parallel programming models and CPUs clock frequency on energy consumption of HPC systems," 2011 9th IEEE/ACS International Conference on Computer Systems and Applications (AICCSA), Sharm El-Sheikh, 2011, pp. 16-21.

[9] Mittal and Sparsh, "A survey of techniques for improving energy efficiency in embedded computing systems". IJCAET. 6 (4), 2014, pp. 440–459.

[10] "The Ptolemy Project", Department EECS, University of California, Berkeley, [Online]. Available http://ptolemy.eecs.berkeley.edu, [Accessed September 30, 2016]

[11] M. Wipliez, G. Roquier, and J. Nezan, "Software Code Generation for the RVC-CAL Language," Journal of Signal Processing Systems, 2009.

[12] Gregory K. Wallace, "The JPEG still picture compression standard, Communications of the ACM - Special issue on digital multimedia systems," 34(4), 1994, pp30-44.

[13] "ORCC Installation Tutorial", [Online]. Available http://orcc.sourceforge.net/getting-started/install-orcc/[Accessed September 10, 2016]

[14] "Java Official Website", [Online]. Available https://www.java.com/en/[Accessed September 10, 2016]

[15] "Vivado Design Suite User Guide Design Flows Overview, [Online]. Available" http://www.xilinx.com/support/documentation/sw_manuals/xilinx2015_1/ug892-vivado-design-flows-overview.pdf[Accessed October 15, 2016]

[16] "Vivado Design Suite User Guide Design Analysis and Closure Techniques", [Online]. Available https://www.xilinx.com/support/documentation/sw_manuals/xilinx2014_1/ug906-vivado-design-analysis.pdf, [Accessed October 15, 2016]

Cloud based Solar Powered Irrigation System

Erra Elvyna anak Langeh @ Randin
Faculty of Electrical Engineering
Universiti Teknologi Malaysia
Johor Bahru, Malaysia.
erraelvyna@yahoo.com

Dr. Fauzan Khairi Che Harun
Department of Electronics
Faculty of Electrical Engineering
Universiti Teknologi Malaysia
Johor Bahru, Malaysia.
fauzan@fke.utm.my

***Abstract*— Plants is one of the important resources for human being in the world. To ensure the plants to grow healthier, irrigation system is one of the beneficiary method towards plant. However, the current system of irrigation is an open loop system and will continuously watering the plants during the setting time in a certain period. This system lead to a water wastage where 70% of water in the world is only used in agriculture sector. The other problem faced if using a conventional method is less effective monitoring method. As a human being, they are not able to monitor their plants regularly and may cause a poor planning on plants monitoring. This situation will affect the plant's condition. Thus, to make sure plant will always be in a good condition this project is introduced. In this project, the device is powered by using solar, communicate with the user through Wi-Fi (cloud based), portable, affordable and friendly user. Furthermore, this project is using Espresso Lite as a controller and uses 2 input sensors which is temperature and humidity sensor to detect the surrounding condition, and moisture sensor to detect soil humidity. The output of the system is solenoid valve which controlled by relay driver and is driven at 12V DC which converted from 7V of battery using DC-DC converter. The solar panel is not only used to power up the system, but also to charge the battery using solar charger. The battery will be used during night time and when there is no sun. This proposed project aim to produce a low cost system design, reduce water wastage and provide a mobile monitoring for the users.**

Keywords—irrigation system; cloud based; Espresso Lite; solar panel

I. INTRODUCTION

Agriculture sector plays an important role to deliver the product from the plants to the living things on the earth nowadays [1]. Elements produced by plants are air, food, water, habitat, medicine and climate. Air is the main resources for all the living things as every second all human being will inhale an oxygen and exhale carbon dioxide. Oxygen is the product of photosynthesis process by the plants [2]. Without air, living things will not able to survive. Human being and animals need food for their body to have an energy. Majority, 7,000 of different species of plants used as food resources for the human being.

Having food only is not enough for the human being refill their body's energy. Water is another key element for the living things to survive. Plants distributed and purify the water on the earth. Apart from that, plants make up the backbone of habitat for all the living things. Almost all the people around the world use different species of plants as their primary health care and are more effective using a traditional method [3]. The benefit of keeping plants on the earth is they help to keep the carbon dioxide produced from the burning of fossil fuel out of the atmosphere and keeping the earth in a healthy environment. The irrigation system has already been developed to help manage the plants in the agriculture sector in order to keep them in good and health condition. The system's example are sprinkler, drip, surface and including conventional method. But this system is an open loop system and it will keep watering the plants on the setting time [4].

II. LITERATURE REVIEW

A researcher from Institute of Information Technology, Bardoli, Gujarat, India study on the traditional farm-land irrigation techniques. The objectives of this paper is to provide an automatic irrigation system which able to save time, money and human energy. In their data collection, they found out that after 30years in the future the world will face a serious problem in food resources. On the other hand, farmers also suffer from lack of rains and scarcity of water [5]. Development of Smart Irrigation System was introduced by researcher from Amrita School of Engineering, India in 2015. They discovered that the problems faced by the world nowadays is water scarcity and agriculture demand the water usage the most. The objective of this research paper is to be able to save 80% of water used and at the same time able to save the time [6].

Apart from that, researchers from Gujarat, India proposed solution to reduce the energy crisis among the Indian farmers. The system is using a solar photovoltaic to power up the system and by using this method, an irrigation system with eco-friendly solution are able to be provided. Other than that, the solutions is also low in maintenance, low cost and is flexible. The system is flexible because the position of the panels is not necessarily fixed in one position. They can be anywhere which up to 20 meter from the pipe [7]. Another researcher from India, Andhra Pradesh is developing an autonomous irrigation system which integrate with photovoltaic energy in order to reduce the cost of power. Furthermore, their objective is to monitor the water supply, temperature, and the soil autonomously. The system also implement GSM and motor control to irrigate the plants. The special of this system is the system has an ability to change according to the situation such as crops, weather conditions and soil. Thus, the system is also cheaper and efficient [8].

III. PROJECT METHODOLOGY

The process of completing this project is divided into four phase. The first phase is doing on the project proposal. Once the proposal has been approved, the second phase is begin. The second phase is focusing on the hardware and software development. Entering the third phase which to clarify the second phase by analyzing and make sure the system able to operate as the desired system. The final phase is to complete the documentation of the project. Figure 3.1 shows the project flow chart which summarize the project methodology.

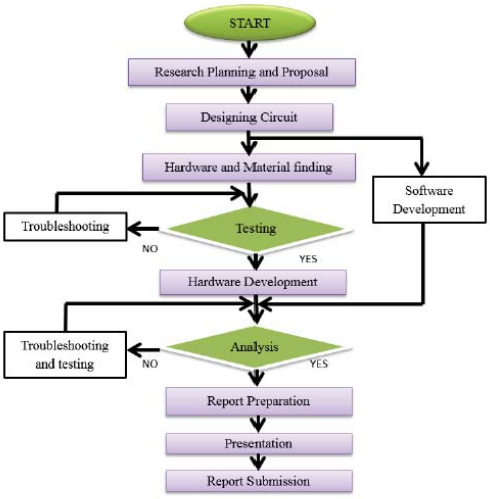

Fig. 1. Project Flow Chart

A. *Schematic Design*

The circuit design are developed and design by using the existing standard circuit. The software used is Altium Designer Summer 09. Existing drivers and sensors has been integrate in one PCB in order to minimize the space. The standard circuit of the drivers and sensors are able to be access in the particular datasheet using the recommended circuit design. Below is the schematic design of each of the drivers and sensors and the PCB design of the overall circuit.

The schematic consist of the schematic for relay driver (Fig. 2), moisture sensor (Fig. 3), solar charger (Fig. 4), controller pinout (Fig. 5), output connection (Fig. 6) and the overall schematic design of the system (Fig. 7).

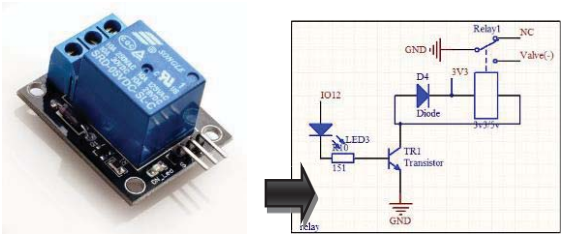

Fig. 2. Schematic of relay driver

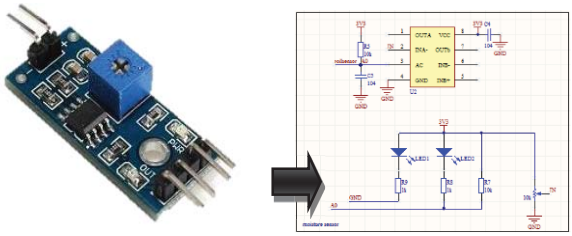

Fig. 3. Schematic of moisture sensor

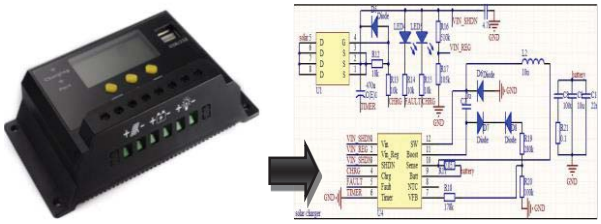

Fig. 4. Schematic of solar charger

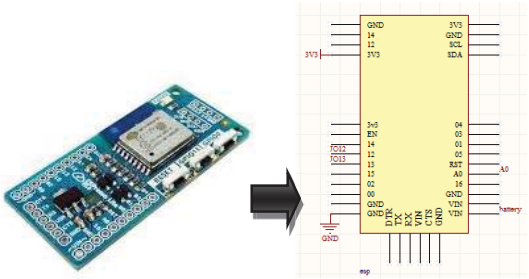

Fig. 5. Schematic of Espresso Lite pinout

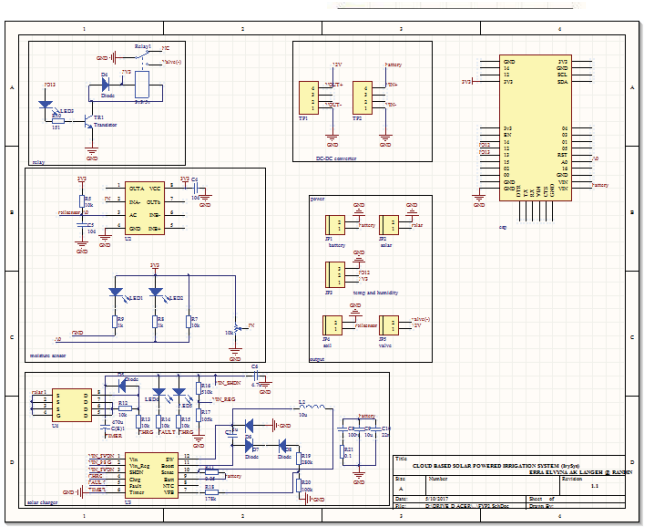

Fig. 7. Schematic design of the system

B. PCB Design

PCB design will be depending on the schematic design. In this stage, the size of the PCB will be determine. The smaller the components used in the PCB, the smaller the PCB size will be. Fig. 8 shows the PCB design for top layer and bottom layer of the device.

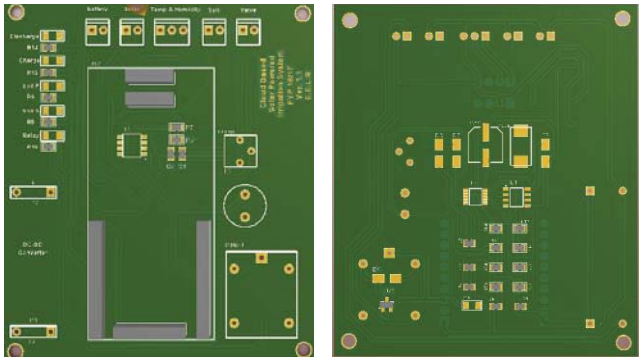

(a) (b)

Fig. 8. (a) top layer of PCB; (b) bottom layer of PCB

C. Mechanical Design

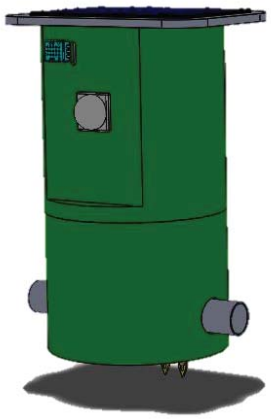

Fig. 9. Mechanical design

In hardware part, the design consist of solar panel attached on top, temperature and humidity facing outwards, PCB and battery placement inside the upper part of the box, and valve and soil sensor placement inside the bottom part of the box. In order to fabricate the system, 3D design has been done as a guide before the metal works. The mechanical design is important in order to determine the circuit design. The mechanical design will determine the placement of the PCB, battery, sensors and some other components.

D. Software Development

This project used Arduino IDE to program the controller. Temperature and humidity, and moisture sensor will be the input data while relay driver will be the output data of the system.

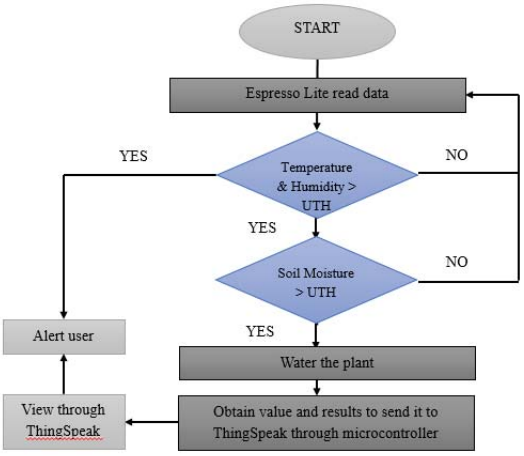

Fig. 10. Flowchart of the program

The device will be powered up and Espresso Lite will start to read the data. First, it will check on temperature and humidity sensors. Once the sensors is higher than the upper threshold value, it will check on the next data from the moisture sensor. If the moisture sensor value is reach higher than upper threshold, relay driver will trigger the opening of the solenoid valve and watering the plant. The value and results obtain from the system will be send to the cloud and user able to access on it anytime and anywhere.

E. System Overview

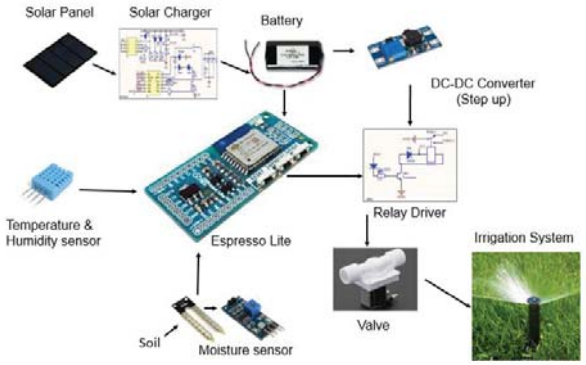

Fig. 11. System overview

Solar panel will connect to the solar charger in order to charge the battery. The battery will used to power up the controller and the sensors. At the same time 7V of battery will step-up to 12V of solenoid valve so the relay driver able to trigger the valve once there is a signal receive from the controller.

IV. Results and Discussion

Table 1 shows the reading from temperature and humidity sensors in different surrounding condition. Three different reading which is normal, hot and cold is taken.

Table 1 Temperature and humidity sensor reading

Sensor	**Relative**		
	Normal	***Hot***	***Cold***
Temperature (℃)	20 - 28	29 - 35	16 - 19
Humidity (%)	55 - 65	65 -70	40 - 55

Table 2 shows the reading from soil sensor in three different moisture. The reading taken is in water, humid soil and dry soil.

Table 2 Soil sensor reading

Sensor	**Data (%)**		
	In water	***Humid soil***	***Dry soil***
Soil	100 - 400	400 - 700	700 - 950

The data from the sensor will be display on ThingSpeak webpage where user able to access the data anytime and anywhere. Fig. 12 shows one of the sample for data display in ThingSpeak.

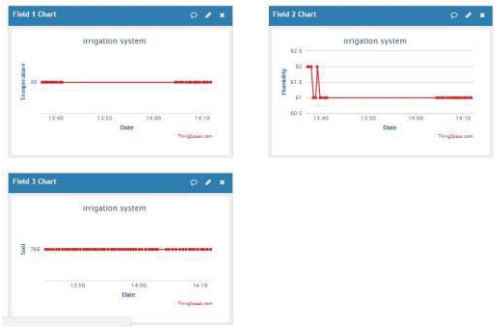

Fig. 12. ThindSpeak display

This monitoring will help the user to monitor their plants through the smartphone or any electronic device. Users should be worry-free since their plants is under a smart monitoring from the device. Apart from that, this project also expected to be able to produce a low cost system design. A low cost system design will be more helpful when the device is ready to be commercialized in the market.

V. Conclusion

As a conclusion, 70% of water is consumed by agriculture sector and this may lead to the water wastage. Thus, to reduce these problems, the best is to provide an automated irrigation system. This system is powered by solar so the users do not need to worry about the power supply or battery. Users able to interact and monitor the device using Wi-Fi service during their convenient time. This device is also an affordable, portable and friendly user.

REFERENCES

[1] David Tilman, Kenneth G. Cassman, Pamela A. Matson, Rosamond Naylor, Stephen Polasky (2002), "Agricultural sustainability and intensive production practices" Nature 418, 671-677, August 2002.

[2] Anne Marie Helmenstine (2017), "What Are the Products of Photosynthesis?," ThoughtCo, Science.

[3] Gerard Bodeker, K.K.S. Bhat, Jeffrey Burley, Paul Vantomme (2003), "Medicinal plants for forest conservation and health care" Food And Agriculture Organization Of The United Nations, 2003.

[4] A. Tagar, F. A. Chandio, I. A. Mari, B. Wagan (2012), "Comparative Study of Drip and Furrow Irrigation Methods at Farmer's Field in Umarkot" World Academy of Science, Engineering and Technology 69 2012.

[5] Karan Kansara, Vishal Zaveri, Shreyans Shah, Sandip Delwadkar, Kausal Jani (2015), "Sensor based Automated Irrigation System with IoT : Technical Review" International Journal of Computer Science and Information Technologies (IJCSIT). Volume 6, Issue 6, 2015, ISSN: 0975-9646.

[6] S.Darshna, T.Sangavi, Sheena Mohan, A.Soundharya, Sukanya Desikan (2015), "Smart Irrigation System" IOSR Journal of Electronics and Communication Engineering (IOSR-JECE). Volume 10, Issue 3, June 2015.

[7] V. B. Shinde, S. S. Wandre (2015), "Solar Photovoltaic water pumping system for irrigation: A Review" African Journal of Agriculture Research. Volume 10, 2015, ISSN: 1991-637X

[8] Dhana Lakshm. N, Gomathi K.S (2015), "Smart Irrigation System Autonomous Monitoring and Controlling of Water Pump by using Photovoltaic Energy" SSRG International Journal of Electronics and Communication Engineering (SSRG-IJECE). Volume 2, Issue 11, 2015.

Control of Electrical Discharge Machining (EDM) Servomechanism Model using Arduino

Muhammad Hilman Bin Zulfadzli
Faculty Of Electrical Engineering, Universiti Teknologi Malaysia, 81310 Skudai,Johor Bharu

Azli Bin Yahya
Faculty Of Electrical Engineering, Universiti Teknologi Malaysia, 81310 Skudai,Johor Bharu

Abstract - **Electrical Discharge Machining (EDM) is known as non-traditional or non-conventional that is used to remove or erode material. The material must be a conductive material so that the machining can be processed. Servomechanism, dielectric system, power supply, and workpiece holding system are few of the important components of EDM that need to be considered when designing EDM machines. However the idea of this project is mainly for learning purposes where the 3D model of EDM is only designed to maintain its constant gap between the tool electrode and workpiece by using ultrasonic sensor as feedback controller to the system. Thus this paper will discuss and explain the whole design process and its performance.**

I. INTRODUCTION

In early 1770, there is an English Scientist called Joseph Priestly that has invented the erosive effect of Electrical Discharge Machining (EDM). EDM is an electro-thermal non-traditional machining process, the synonym name for this EDM are spark eroding, spark machining, die sinking, burning, wire burning or wire erosion [1]. EDM provides the best solutions to machine in terms of high-strength, corrosion and wear-resistant materials. The 3 parameters are important in manufacturing in order to protect the quality of metal and its surface roughness. Thus, EDM equipment is very useful for modern manufacturing systems such as finishing parts for automotive industry, surgical and aerospace [2,3].

EDM machine can be labelled as complex machine where the process is hardly to be understood. Therefore, it is crucial for people to learn the basics of EDM before doing the actual eroding process using EDM machines. A simple 3D model is suitable to be created as to show how tool electrode can maintain its constant gap from the workpiece. Tool feed mechanism is the most important part where it controls the movement of electrode either raising or lowering it to maintain desired gap.

II. TYPES OF EDM

There are 2 types of EDM which is Die-sinking EDM and Wire-cut EDM. In Die-sinking process, it involved two metals submerged in dielectric fluids and this is where the eroding process takes place due to spark jumps across the gap between tool electrode and workpiece [4]. Whereas wire-cut known as spark EDM is an electro-thermal production process where it uses of thin single-strand metal wire and submerged in de-ionized water that able to conduct electricity which allows the wire to cut through metal by heat from the electrical sparks.

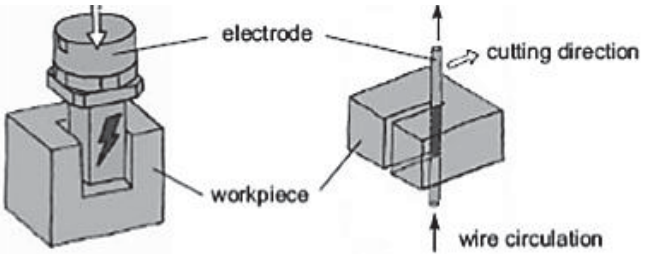

Figure 1: Die Sinking & Wire cut EDM process

A. *Parameters of EDM*

EDM is a controlled metal-removal process that uses eroding effect to cut material by means of electric spark erosion to produce desired shape. The sparks occurred between the workpiece and electrodes which can be considered as the cutting tool which are created in a dielectric fluid [5-9]. In order to produce the spark, electrode and workpiece has to be conductive and there should be no mechanical contact between the workpiece and the electrodes during the whole eroding process [7,10-12]. Studies shown that the capacity or volume removed by a single spark in EDM is small, which in the range of 106-104 mm^3, but the process of producing the sparks is repeated typically around 10000 times per second [7,13].

B. *Constructing of EDM*

The parts of EDM machines are separated into 5 major components which are Work-piece, Tool-Electrode, Dielectric Fluid, Servo System, Power Supply, and also DC pulse generator. Figure 2 shows a simple schematic process of EDM.

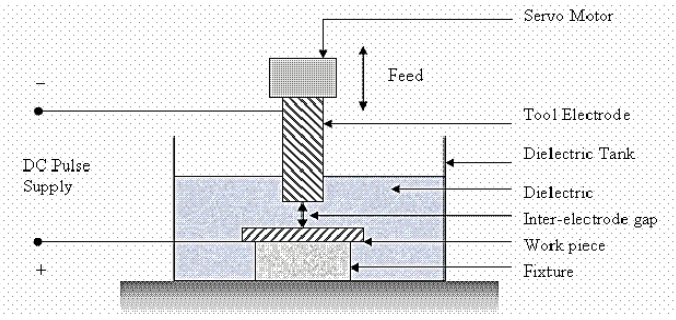

Figure 2: Simple Schematic of EDM process

1) Work-piece materials

A variety of metals can be cut by using EDM machines as long as it is conductive [7,11,14,15]. The types of metal or alloy that can be shaped using this method are titanium alloy, copper, carbon tool steel, nickel alloys, ceramics, and others[11,16-18].

2) Tool-Electrode

The type of electrodes that normally used in EDM machines are those that are highly conductive which normally made of copper, graphite, brass, tungsten, silver and others [4,7,18].

3) Dielectric fluid

The setup of EDM machines consists of a tank where dielectric fluid will be filled in it. Both electrode and workpiece will be immersed in the dielectric fluid [4,7,18].

4) Tool feed mechanisms

The function of tool feed mechanism is to move the tool or electrode either raising or lowering it to keep a constant gap automatically between the electrode and workpiece [4,7,11,18,19].

5) Power Supply

Power supply is the most crucial thing for every electronics machines or devices. In EDM systems, power supply is used to transform alternating current (AC) from the main utility supply into direct current (DC) to drive the EDM machines and thus producing spark at the machining gap [4,7,18].

6) DC pulse generator:

DC pulse generator is responsible for supplying pulses at a certain voltage and current for a specific amount of time. There are few types of pulse generator which are the RC type, transistor type, and transistor type iso-pulse generators [4,7,18,19].

C. Important Parameters of EDM

i. Process Parameters
ii. Performance Parameters

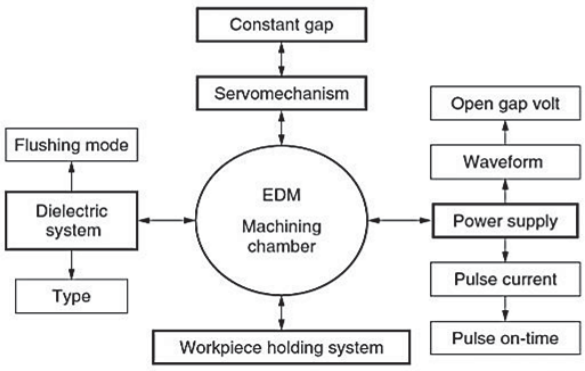

Figure 3: Parameters of EDM

Figure 3 shows the basic setup requirements of EDM machines. Performance measures of EDM's machining process can be controlled through Process Parameters [7,20,21].

1) Electrical Parameter

a) Polarity

The polarity of electrode is cathode and polarity of work piece is anode. This is because more material is removed from positive edge than the negative edge during material removal process. The polarity usually determined by experiments conducted together with other important considerations such as work material, tool material and others [20].

b) Discharge Voltage

The open gap voltage creates an ionization path through dielectric fluid when it reaches a certain level which allow current to flow. The current flow will cause the voltage to drop and stabilizes at the working gap level. Voltage discharge is associated with spark gap and the breakdown strength of the dielectric. [7,20,21]

c) Peak Current

Peak current measured in unit of amperage defined as the amount of power used in EDM. Current increases during pulse on time (T_{on}) until it reaches a level known as peak current. This factor is important in EDM because machined cavity resembles the tool electrode and excessive wear will affect the accuracy of the machining. New material for electrode such as graphite can work on high current without causing much damage. [7,20,21].

d) Pulse Frequency

Number of cycles produced across the gap in one second is known as pulse frequency. A smoother surface finish can be produced with a short pulse on-time that will remove a small amount of material and form a small crater with less thermal damage to the work piece [7,20,21].

$$\text{Pulse Frequency (kHz)} = 1000/\text{Total cycle time (us)}$$

e) Pulse On Time (T_{on}) and Pulse Off Time (T_{Off})

The Pulse On Time is duration for current to be allowed to flow per cycle and Pulse Off Time is the interval between previous T_{on} and the next T_{on}. During this time, molten materials solidified and washed out from the spark gap [21].

f) Electrode Gap

Working gap can be controlled using the tool servo-mechanism employed in EDM to the set value. The servo-mechanism system is normally designed to respond to average gap voltage as shown in Figure 2.

g) Duty Cycle

Duty cycle is denoted by τ which defined as a percentage of the pulse on-time over the total cycle

time. Total cycle time can be calculated by summing the pulse on-time and pulse off-time [20].

2) Non-Electrical Parameters

Other than electrical parameters, EDM also have non-electrical parameters such as electrode lifts time, working time, nozzle flushing, gain and type of dielectric. Type of dielectric fluid used must be quick recovery after breakdown and high dielectric strength, effective quenching and flushing ability, good degree of fluidity and easily available [7,20]

3) Powder Based Parameters

There are many parameters such as powder concentration, types of powder, powder size and etc. To avoid wastage of kerosene oil, the powder mixed electric discharge machining (PMEDM) is used. [20]

4) Electrode Based Parameters

Table below describe technical and economic considerations of various materials that used as electrode [20].

Table 1: Various Materials for Electrode

No.	Material	Wear Ratio	Material Removal Rate	Fabrication	Cost	Application
1.	Copper	Low	High on rough range	Easy	High	On all metal
2.	Brass	High	High only on finishing	Easy	Low	On all metals
3.	Tungsten	Lowest	Low	Difficult	High	Small holes are drifted
4.	Tungsten, copper alloy	Low	Low	Difficult	High	Used higher accuracy work
5.	Cast iron	Low	Low	Easy	Low	Used on few materials
6.	Steel	High	Low	Easy	Low	Used for finishing work
7.	Zinc based alloy	High	High on rough range	Easy	High	On all metals
8.	Copper graphite	Low	High	Difficult	High	On all metals

D. Characteristics of EDM

Specification of a simple EDM machining by mechanism process and other important performances are as shown in table 2 [21].

Table 2: Specifications of EDM

Mechanism of process	Controlled erosion (melting and evaporation) through a series of electric spark
Spark gap	0.010- 0.500 mm
Spark frequency	200 – 500 kHz
Peak voltage across the gap	30- 250 V
Metal removal rate (max.)	5000 mm^3/min
Specific power consumption	2-10 W/mm^3/min
Dielectric fluid	EDM oil, Kerosene liquid paraffin, silicon oil, deionized water etc.
Tool material	Copper, Brass, graphite, Ag-W alloys, Cu-W alloys .
MRR/TWR	0.1-10
Materials that can be machined	All conducting metals and alloys.
Shapes	Microholes, narrow slots, blind cavities
Limitations	High specific energy consumption, non conducting materials can't be machined.

III. EDM SERVOMECHANISM

As we know, EDM is a non-contact process. Hence, this EDM model plays an important role in determining the gap between electrode and workpiece. This model is only for learning purposes for beginners. The whole progress of EDM model will be explained in this section.

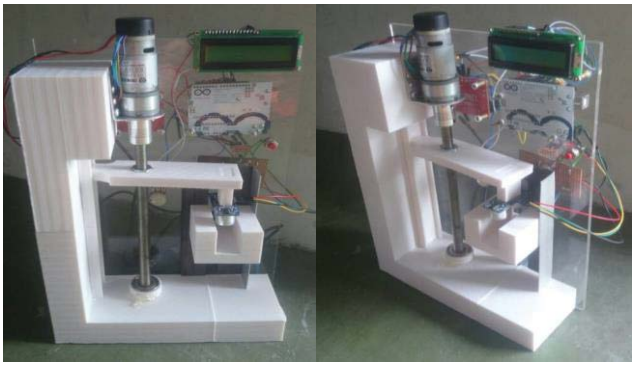

Figure 4: Final 3D EDM Model

A. 3D drawing

For this project, Solidwork software was used to draw the 3D drawing of the project parts. The white block in Figure 4 shows the product of 3D design after been printed using 3D printing machine.

B. Arduino

Arduino as the microcontroller to control electronic parts such as LCD,DC Geared Motor, Motor driver and Ultrasonic. Due to various type of Arduino, Arduino Uno has been selected in this project because its input/output pin is enough to control all electronic components.

C. LCD Display

LCD screens are user friendly and energy efficient compared to Cathode Ray Tube (CRT). LCD functioned as to display image or words on screen where it will display whatever is been programmed in arduino regarding to this EDM model.

D. DC Geared Motor

It is important to choose the right DC motor because DC motor function as to lift up the electrode. The higher the torque of DC motor, the more powerful it can lift up load. In this project, small torque of DC motor is used due to less heavy load. DC motor is controlled by Pulse Width Modulation (PWM) signal which is the speed and can be controlled forward and backward by the microcontroller Arduino.

E. Ultrasonic sensor

In maintaining the gap between electrode and workpiece, one of the mechanism to measure the distance is by using ultrasonic sensor. Sensitivity of ultrasonic sensor used for this 3D model is average. This ultrasonic sensor been placed under the electrode to measure the distance to the workpiece.

IV. Results & Analysis

Few experiments were conducted to determine the gap between tool electrode and workpiece by using ultrasonic as the sensor of the EDM model. The length is measured using a ruler and 3cm is set to be desired length during the whole experiment. Whenever a workpiece is pulled down by 1cm from its origin position, the servo mechanism will then response by lowering the tool electrode closer to workpiece until approximate of 3cm gap is achived. The results are tabulated as shown in tables.

Table 3: Gap measurements by EDM servomechanism model using Arduino (Exp.1)

Interval	Measurement	Error (%)
1	3.3	10
2	3.3	10
3	3.3	10
4	3.3	10
5	3.4	13.3

Table 4: Gap measurements by EDM servomechanism model using Arduino (Exp.2)

Interval	Measurement	Error (%)
1	3.4	13.3
2	3.3	10
3	3.3	10
4	3.2	6.67
5	3.3	10

Table 5: Gap measurements by EDM servomechanism model using Arduino (Exp.3)

Interval	Measurement	Error (%)
1	3.3	10
2	3.3	10
3	3.3	10
4	3.2	6.67
5	3.3	10

Table 6: Gap measurements by EDM servomechanism model using Arduino (Exp.4)

Interval	Measurement	Error (%)
1	3.2	6.67
2	3.3	10
3	3.4	13.3
4	3.3	10
5	3.3	10

Table 7: Gap measurements by EDM servomechanism model using Arduino (Exp.5)

Interval	Measurement	Error (%)
1	3.2	6.67
2	3.3	10
3	3.3	10
4	3.2	6.67
5	3.3	10

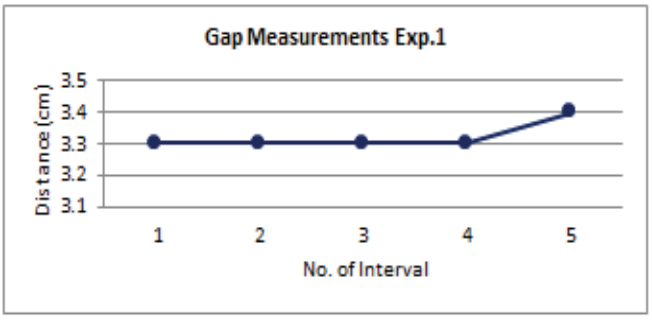

Graph 1: Results obtained from Exp.1

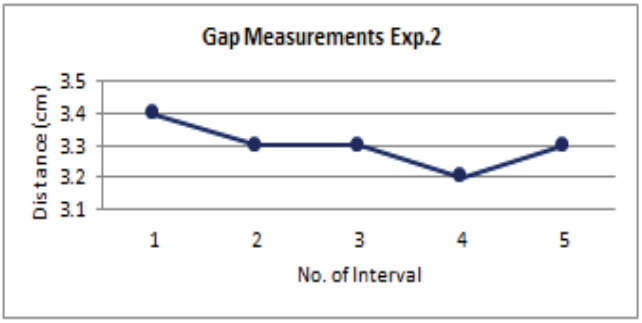

Graph 2: Results obtained from Exp.2

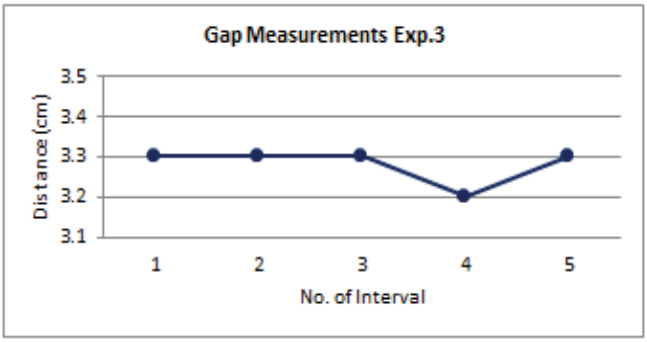

Graph 3: Results obtained from Exp.3

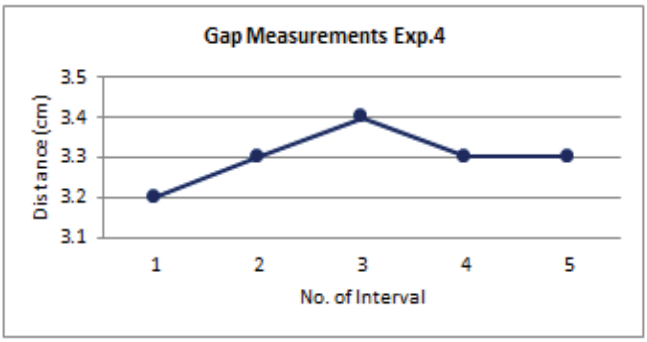

Graph 4: Results obtained from Exp.4

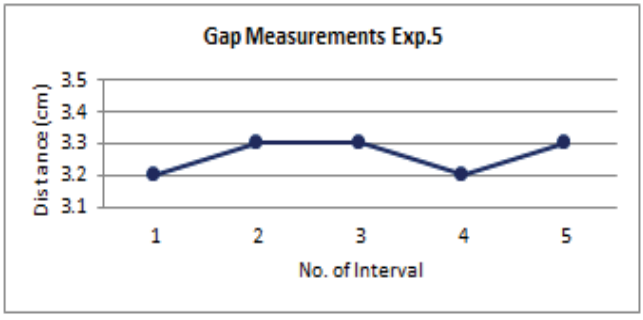

Graph 5: Results obtained from Exp.5

Table 8: Summary Measurements for all Experiments

	Interval 1	Interval 2	Interval 3	Interval 4	Interval 5
Exp1	3.3	3.3	3.3	3.3	3.4
Exp2	3.4	3.3	3.3	3.2	3.3
Exp3	3.3	3.3	3.3	3.2	3.3
Exp4	3.2	3.3	3.4	3.3	3.3
Exp5	3.2	3.3	3.3	3.2	3.3

The tabulated tables shows a repeatitive of five time tests to study the performance of the designed EDM model as to identify whether the gap measured are repeatable and reproducible. The error in percentage has been calculated by following the formula of percentage error :

$$\text{Percentage Error (\%)} = \frac{(Actual - Measurement)}{Actual} \; x \; 100\%$$

From the plotted line graphs in Graph 1 and 3, it can be seen that the gap measurements are almost giving a consistent reading at each interval which is by 3.3cm. Experiment 2, Experiment 4, and Experiment 5 however shows a fluctuate readings in the range of 3.2cm to 3.4cm.

Table 8 shows the summary of gap measurements for all the Tests and from the data, it shows that 3.3cm distance is frequently measured for 17 times. While the least counted measurement is 3.4cm for only three times. The other five times intervals are measuring gap distance of 3.2cm which is the closest reading to the desired gap.

V. DISCUSSION

It is understood that the desired gap measurement is 3cm. However, the nearest reading that can be obtained by the designed EDM model is 3.2cm and the furthest distance measured is 3.4cm which brings to maximum of 0.4cm difference from desired gap. There are several factors that may contribute to such slight difference of measurement and one of them may due to the types of components used or how the 3D EDM model is designed.

The overall performance and accuracy of this EDM model is in average level. From the results, nearly all measurements at each interval achieved below 10% of percentage error with reading of 3.3cm. The percentage error of the model is not consistent may due to less sensitivity of ultrasonic sensor. This explains why the plotted line graphs in Graph 2, 4 and 5 are fluctuating. A more sensitive ultrasonic sensor can produce better and more consistent results. However the performance of the selected ultrasonic sensor used for this project is still acceptable since the model able to produce a repeatable of 3.3cm gap for 17 times (68%) out of 25 trials.

Other factors that may contribute to inconsistent measurements are parallax error which may happen while taking the readings using ruler and also external movement of the servomotor itself. Untighten of the 3D blocks or any parts of the model may cause incorrect readings as well. For an example, a poor mounting angle of ultrasonic sensor or the blocks attached to it will disturb the transmission of wave signals from the sensor. Thus, it is crucial to make sure that the sensor is perpendicular to the target in order to receive the maximum wave energy reflecting back to it. Proper alignment becomes even more important as the sensing range increases.

VI. CONCLUSION

The intention of designing this EDM model is for learning purposes whereby it is only focusing on y-axis movement of the tool electrode by lowering it whenever the workpiece is pulled down or away from it. Ultrasonic sensor will send out signals and the signals will be reflected back once it reaches the surface of the workpiece. The traveling time taken by the wave signal will determine whether the distance is far or near. The main idea of this project is to maintain a constant gap between tool feed and the workpiece. This model is successful to function as planned whereby the servomechanism can operate automatically whenever the ultrasonic sensor encounters bigger distance from the workpiece. Therefore, this model can be used as study purposes for beginners to learn the basic operation of EDM process.

Using voltage divider would be one of the best methods to have constant gap distance between tool electrode and workpiece due to its ability to provide more accurate and reproducible reading. But, to create such voltage divider is complex making it hard to be implemented on this EDM model. Another alternative method to get accurate reading would be using highly sensitive ultrasonic sensors whichever available in the market. However, bear in mind that highly sensitive sensor would cost more and since this project is only for learning purposes, thus it is reasonable to use sensors or components which are affordable.

By considering all of the possible factors that may affect the readings of the designed EDM model, it can be concluded that the model is capable to reproduce the same length of measurements but poor in accuracy with a maximum difference by 0.4cm from desired gap. This project succeeds to achieve highest percentage error by 10%. The mentioned factors may be one of the causes to these inaccurate readings and therefore it is advisable to ensure these factors be neglected in the near future.

REFERENCES

[1] Kulbir Singh, “Effect of various parameters in metal cutting,” *Journal of Mechanical Engineering,* 2015, v 1, paper 4.

[2] ("FAQ : What are the problems with laser cutting of aluminium and how do i overcome them?")

[3] K.H. Ho, S.T. Newman, State of the art electrical discharge machining (EDM), International Journal of Machine Tools & Manufacture 43 (2003) 1287–1300.

[4] Dewangan, Shailesh Kumar. *Experimental investigation of machining parameters for EDM using U-shaped electrode of AISI P20 tool steel*. Diss. National Institute of Technology Rourkela (India, 2010).

[5] S. Singh, S. Maheshwari, P.C. Pandey, Some investigations into the electric discharge machining of hardened tool steel using different electrode materials,

Journal of Materials Processing Technology 149 (2004) 272–277.

[6] C.J. Luis, I. Puertas, G. Villa, Material removal rate and electrode wear study on the EDM of silicon carbide, Journal of Materials Processing Technology 164–165 (2005) 889–896

[7] Choudhary, Sushil Kumar, and R. S. Jadoun. "Current advanced research development of electric discharge machining (EDM): a review." *International Journal of Research in Advent Technology* 2.3 (2014): 273-297.

[8] Kunieda M. and Yoshida M., "Electrical Discharge Machining in Gas", Annals of the CIRP, 46/1, 143-146, 1997

[9] Furudate C. and Kunieda M., "Gap Phenomena in Dry WEDM", DenkiKakou-Gijutsu (in Japanese), 26/83, 21-27, 2002.

[10] Pawade, M. M., and S. S. Banwait. "An Exhaustive Review of Die Sinking Electrical Discharge Machining Process and Scope for Future Research." *Proceedings of World Academy of Science, Engineering and Technology*. No. 78. World Academy of Science, Engineering and Technology (WASET), 2013.

[11] Raju, Leera, and Somashekhar S. Hiremath. "A State-of-the-art Review on Micro Electro-discharge Machining." *Procedia Technology* 25 (2016): 1281-1288.

[12] J.H. Zhang, T.C. Lee and W.S. Lau, "Study on the electro-discharge machining of a hot pressed aluminum oxide based ceramic", J. Mater. Process. Technol. 63, 908–912, 1997.

[13] Kulbir Singh, "Effect of various parameters in metal cutting," *Journal of Mechanical Engineering,* 2015, v 1, paper 4.

[14] Reddy, C. Bhaskar, G. Jayachandra Reddy, and C. Eswara Reddy. "Growth of Electrical Discharge Machining and Its Applications–A Review." *International Journal of Engineering Research and Development e-ISSN* (2012): 13-22.

[15] Webzell, S., The first steps in to EDM in Machinery, 159, (4040) Findlay Publ. Ltd, Kent, p.41, November, 2001

[16] Schubert A, Zeidler H, Hahn M, Hackert-Oschätzchen M and Schneider J. Micro-EDM milling of electrically nonconducting zirconia ceramics, Procedia 2013; CIRP 6: 297-302.

[17] Hyun-Seok TAK, Chang-Seung HA, Dong-Hyun KIM, Ho-Jun LEE, Hae-June LEE and Myung-Chang Kang. Comparative study on discharge conditions in micro-hole electrical discharge machining of tungsten carbide (WC-Co)
material, Transactions of non-ferrous materials Society of China 2009;19 s114-s118.

[18] http://www.globalspec.com/learnmore/materials_chemicals_adhesives/electrical_optical_specialty_materials/electrical_contact_electrode_materials/edm_electrode_materials (Accessed on 10/12/2016)

[19] Abbas, Norliana Mohd, Darius G. Solomon, and Md Fuad Bahari. "A review on current research trends in electrical discharge machining (EDM)." *International Journal of machine tools and Manufacture* 47.7 (2007): 1214-1228.

[20] Singh, Sharanjit, and Arvind Bhardwaj. "Review to EDM by using water and 2powder-mixed dielectric fluid." *Journal of Minerals and Materials Characterization and Engineering* 10.02 (2011): 199.

[21] Equbal, Azhar, and Anoop Kumar Sood. "Electrical Discharge Machining: An Overview on Various Areas of Research." *Manufacturing and Industrial Engineering* 13.1-2 (2014).

Electrical Discharge Machining (EDM) Power Supply Current Control for Roughing and Finishing Process

Mohd Hazroy Bin Hasbullah
Faculty of Electrical Engineering, Universiti Teknologi Malaysia, 81310 Skudai, Johor Bahru

***Abstract*—Electrical Discharge Machining (EDM) is a type of non-traditional manufacturing process of shaping material (workpiece). In EDM process, it can produce "spark" between an electrode (wear) and a workpiece. In addition, EDM also must use conductive material to make it work as well. Electrical Discharge Machining has been widely used for manufacturing such as aerospace, automotive, electronic industries and biomedical industries due to its contactless process. This paper reviews how to design and develop power supply for EDM.**

I. INTRODUCTION

Power supply is the main key in EDM because it controls the amount of energy used. It also give an advantages in EDM which is maintain the spark level and make sure it get constant discharge in breakdown form [1]. Power supply also has time controller which is the time using to control the flow of current through the pulse depends on length of time. In EDM, the voltage and current level have low and high. It depends on what type of application they want to shape. Every electrode has different type of thermal conductivity and melting point [2]. Use low and high current are needed to get the better result in term of surface finish and surface roughness of the workpiece.

In addition, choose the suitable power supply is very important in EDM process because power supply is the main role in EDM system. In other word, it is the mother of the system. Provide consistent and repeatable power to the EDM circuits will give the system life and work properly. There are two types of major DC source power supply which are Linear Power Supply (LPS) and Switching Mode Power supply (SMPS). Choosing Linear Power Supply or Switching Mode Power Supply, it depends on application of the power result.

II. DESIGN OF POWER SUPPLY

A. *The basic pulse power supply of EDM*

Transform electric energy into energy of heat is a processing method of EDM. To remove the material from the workpiece, pulse voltage must be added between the electrode (tool) and workpiece [3]. The electric energy will produce a sparks between the electrode tool and the material workpiece. To ensure it turn in constant processing, sparks must be control by the removal rate of material [4]. It is very important if dealing with tiny surface that need to use high accuracy such as in Micro EDM. It need very tiny of removal rate per spark to ensure it can obtain surface machine in high quality [5]. Besides that, it related to the removal rate per spark and how much energy release from each part of discharge pulse [6]. This source of electric energy pulse is the product between voltage discharge and current discharge by the pulse. After that, the contribution of pulse frequency to the metal removal rate of the material workpiece [3]. It show that, the pulse voltage and pulse current and its own frequency will give a good performance on the machine part through the workpiece. To get a high quality of surface machine, pulse duration must be in short period in order to get more efficient compare to the reducing the peak value of the current discharge [3]. There are two type of pulse power supply generator as shown in Fig. 1 and Fig. 2.

The red circle in the Fig. 1, is the EDM pulse generator system. But in this project it will focus on DC power supply only which is LPS and SMPS.

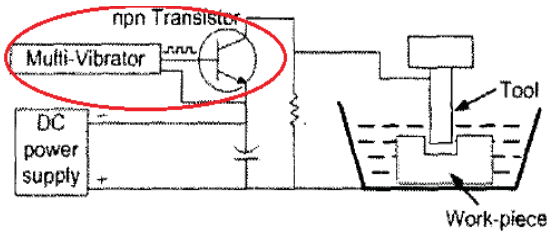

Fig. 1 DC power supply and pulse generator with n-p-n transistor [6],[7].

B. *The Basic Linear Power Supply (LPS)–Operational Amplifier (Op-Amp) Series Regulator.*

Linear Power Supply (LPS) has been used widely in industry all around the world for a very long time. Even now, LPS are being useful in certain wide range of application such in aerospace, automotive and electronic industry [8]. LPS will work by drop the DC voltage by itself. It also has low operating frequency which is 50 to 60 Hz [9]. But, from this type of power supply it might help EDM to achieve the quality of the product produce. Even though it has low power efficiency, but some application in EDM need low current to prevent it from damage the workpiece. In other word, low current power supply only suitable for electrode tool that can conduct low current. Every electrode has different type of thermal conductivity and melting point such as Brass, Aluminums, Copper and more [9].

The topology circuit has been use in this LPS is Op-Amp Series Regulator [10]. Fig. 2 shows how operational amplifier (op-amp) is used in closed-loop voltage regulator series. Operational amplifier transistor Q_2 which replaces the series transistor regulator circuit with feedback has open loop gain, Ao high that can be used to increase the gain of the feedback loop from the output to the transistor Q_1 [11]. Feedback loop

gain should be high so that small changes in the output voltage V_O can be detected and corrected immediately.

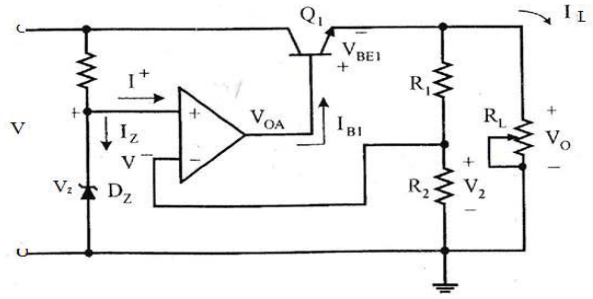

Fig. 2 Op-Amp Series Regulator circuit [11].

Referring to Fig. 2, the op amp is a comparator or an error amplifier for comparing the voltage V_2 with the reference voltage V_Z which aims to drive the transistor Q_1 either increase or decrease the output current, I_L. Resistor R_3 is used to limit the current through the Zener diode D_Z in order to operate in the breakdown regions. I_Z current is constant because the current = 0 A where it can retain the value of the reference voltage, V_Z [11]. The function of other components such as the pass transistor Q_1, Zener diode D_Z and a resistor R_1 and R_2 are the same as the components in series transistor regulator circuit with feedback.

Resistors R_1 and R_2 constitute a voltage divider circuit which produces a voltage V_2 which is proportional to the output voltage, V_O. V_2 voltage will turn feedback to the inverting input of the op amp, in which V^-,

$$V_2 = V^- = [R_2 / (R_1+R_2)]V_0$$

$$\text{or} \quad V^+ = V^- = V_Z$$

If the voltage is not inverting op amp, V^+ or voltage Zener diode, V_Z slightly larger than the voltage inverting op amp V^-, the output voltage of the op amp, V_{OA} is positive, where $V_{OA} = A_O (V^+ - V^-)$ and A_O is the loop gain amp open [11]. In other words, the V_{OA} voltage proportional to the voltage (V_Z-V_2).

Circuit operation more easily understood when the load resistance, R_L is reduced suddenly. If the resistance R_L is reduced, the voltage V_O decreases. If the voltage V_O decreases, the voltage V_2 also decreases, the V_{OA} voltage is increased, and voltage V_Z is considered to be fixed. V_{OA} voltage increase will cause an increase in the flow of Q_1 transistor where the current I_{B1} will increase and so the output current, I_L will also increase. The increase will compensate for the reduction in I_L current load resistance, R_L and the voltage V_O will return to its original value. The opposite would happen if the resistance R_L increase [11].

Referring to Fig. 2, the operational amplifier acts as an inverting amplifier with no Zener voltage V_Z as the input voltage and the voltage gain,

$$A = (V_O / V_Z) = 1 + (R_1 / R_2)$$

which voltage V_{BE1} can be ignored [11].

The regular output voltage can be summarized as follows:

$$V_O = [\ 1 + (R_1 / R_2)]\ V_Z$$

C. The Basic Switch Mode Power Supply (SMPS) – Buck Converter

SMPS circuit is more complex than LPS but SMPS is more efficient than LPS. Transistor will operate as a switch which is ON state or OFF state condition. The losses will happen between the load and input, but it only takes in small part resistive. It has very high operating frequency which is 20 kHz to 1 MHz [9]. This power supply always use by manufacturer now days for high current application in EDM. But, in some cases it might not get good surface roughness and surface finish because of the application is not suitable [12]. So, it depends on type of power supply the manufacturer use on the electrode onto workpiece.

Today, Most of the power supply is in switching form because it provides high efficiency performance to the whole system [4], [13]. Even, switch mode power supply will produces a little amount of losses at the output power. Semiconductor transistor will contribute of high efficiency in SMPS. It is because of the combination of filter electronic component which is diode, capacitor, inductor and switching controller.

With advancement of technology that never stop until now, switch mode power supply are already in form of digital. The application of controller switching digital such as micro-controller is use to control more precisely the transistor state which is ON state or OFF state [14]. Actually, switch controller which is at pulse generator will produce series of continuous pulse width modulation (PWM). This is how pulse width can be modulated and gives effect in the whole power system. Fig. 3, the different type of PWM generation by changing the duty cycle. The power supply output voltage will maintain in normal condition of pulse operating.

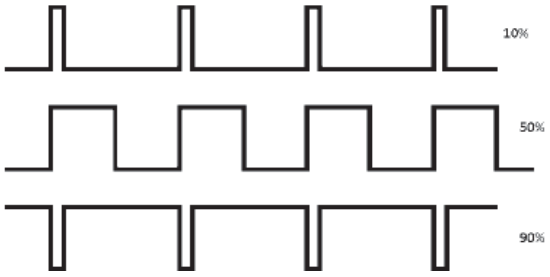

Fig. 3 Different type duty cycle of PWM generated [15].

With 90% of pulse width modulation (PWM), this pulse can make transistor to be ON in longer period. So, when output voltage power supply dropped, the transistor during ON state will give more flow of current through it and at the same time the output voltage will rise back to its normal condition [11].

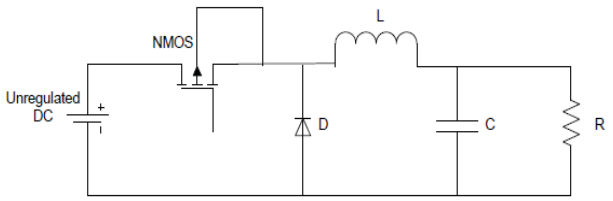

Fig. 4 The Buck Converter [13]

Fig. 4 is the topology circuit that use for SMPS which is Buck converter. The transistor will be act as main role in this power system because it gives a great impact on the efficiency of the whole power supply system. The device characteristic of transistor gives good contribution because it will act as a closed switch during ON state and it will act as opened switch during OFF state. Besides that, it produces zero loss of heat dissipation during closed and opened switches. Equation for basic power is P= IV, it means that the power will occur when the voltage and current exist at the same time [13].

Now, the discussion will be expanded into several parts best on component are used to design buck converter in Fig. 4 which are metal oxide semiconductor field effect transistor (MOSFET), electronic component such as diode, inductor and capacitor.

1) Switching Component (MOSFET)

Metal Oxide Semiconductor Field Effect Transistor (MOSFET) is widely used in manufacturing process of power supply. Selection on power MOSFET is one of the applications in Switch Mode Power Supply (SMPS). Thera are two types of power MOSFET has been used in industry. The type is n-channel and p-channel enhancement mode of MOSFET. Enhancement mode MOSFET, it will operate in normally OFF state that need a triggered pulse or a voltage bias to make the device turn ON [16]. Despite that, n-channel is more suitable compare to p-channel type. This is because the cost and performance of n-channel is better than p-channel. MOSFET also has good performance in term of frequency because in industry they really need very high frequency in switching [13].

However, larger gate voltage is needed in MOSFET in order to turn it ON when use larger input voltage. Fig. 5 shows the plotting characteristic of current-voltage, $V_{DS(sat)}$ is referred to the input voltage. High input voltage is needed in order to switch and gate voltage, V_{GS} must be in high state [16]. When voltage is applied, the gate voltage will become higher than input voltage [13]. Actually, MOSFET is voltage control device. Its mean the performance of the device depends on the voltage control, for instance, the flow of current through the drain, I_D [13].

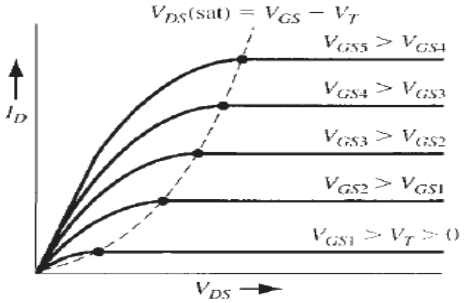

Fig. 5 I-V characteristic of n-channel MOSFET [16].

2) Diode for Buck Converter

When diode in forward biases condition, it will become a short circuit. From that, it will allow a small amount of current flow through the diode. And then, forward voltage drop will occurs across the diode. Depend on the quality of diode, 0.2-3V is the range of voltage drop across the diode. Besides that, power dissipation at the diode will also exist concurrently whenever diode is conducted. When the quality of diode is good, the voltage across the diode is small, and it will be good for diode because it less of power losses [18].

In condition of reverse biased diode, diode will become an open circuit. Open circuit means that there is no flow of current through it except breakdown will happen in the diode. To protect the diode from damage, the reverse voltage must be lower than the reverse blocking voltage of the diode [18]. Fig. 6 shows the characteristic diode graph. The graph shows the characteristic of the forward and reverse bias of the diode.

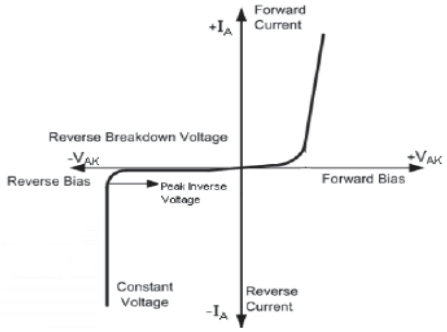

Fig. 6 Forward and reverse bias characteristics of the diode [17].

In buck converter, diode will function as forward bias and reverse bias and simultaneously MOSFET will operate in ON and OFF state. The frequency must be high enough in order to make PWM controller switching the MOSFET. The diode may act with two part in the buck converter, first part is reverse voltage need to be block in order to ON the switch. In the second part, diode will make a path for current to easily can stored in the inductor and will release it when open circuit happen [19].

3) Inductor for Buck Converter

Inductor is one of the important part in the buck converter. If the buck converter circuit don't have this component, it will not work properly. Inductor will be function as to store the charge (current) when voltage is applied on it. It has same characteristic as capacitor which is charge and discharge. It also has two place of voltage potential on it. Despite that, charge and

discharge also happen in the inductor. But, inductor will operate in two type of different part which is continuous and discontinuous current mode. The continuous current mode (CCM) can produce enough current in the output part to make sure it sustains the output voltage of the buck converter. For discontinuous current mode (DCM), it happen when the output voltage suddenly drops and the current through the buck converter will not enough. If buck converter needs more current through it, CCM will give sufficient amount of current.

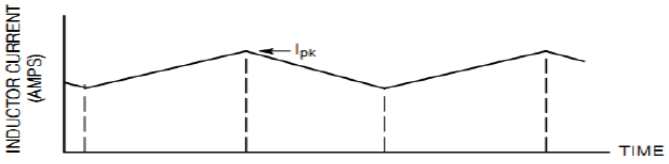

Fig. 7 Continuous current mode waveform of Inductor [20].

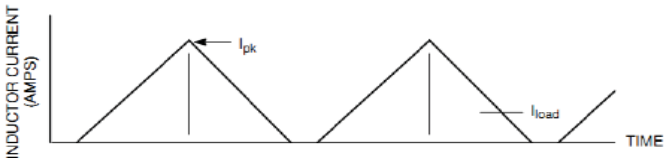

Fig. 8 Discontinuous current mode waveform of Inductor [20].

4) Capacitor for Buck Converter

Capacitor is a type of filter is needed in buck converter circuit. Capacitor can be place at input or output area. Charge and discharge happen when there is voltage applied on the capacitor. To make sure the ripple current and voltage decreased, the capacitor must charge and discharge very fast. To make it charge and discharge fast, bigger capacity of capacitor are needed. The equation of capacitor is,

$$C = Q / V$$

Base on the equation above, charge (Q) must be constant. Capacitor is inversely proportional to the voltage. It means that, if the voltage is lower, the capacitor will become bigger. To reduce to voltage drop across the capacitor, capacity of capacitance must be bigger. In other words, voltage at the output can be more stable if the capacitor size is bigger. Fig. 9 shows the voltage ripple at the output.

Fig. 9 The waveform of the output ripples voltage [19].

III. METHODOLOGY

A. Calculation for Linear Power Supply (LPS)

Design requirement for LPS, Input voltage for this power supply is 24Vdc and output current range between (0 - 0.5) A.

$$\text{Output voltage, } V_O = [\ 1 + (R_1 / R_2)]\ V_Z,\ V_Z = 6.2$$

$$15 = [\ 1 + (R_1 / R_2)]\ 6.2$$

$$1 + (R_1 / R_2) = 15 / 6.2$$

current, I^- can be ignored,

$$I_1 R_2 = V_Z,\ I_1 = 1m$$

$$R_2 = 6.2 / 1m = 6.2kohm$$

then, $$1 + (R_1 / 6.2k) = 15 / 6.2$$

$$R_1 = 8.8kohm$$

Ignored current, I^+, the input voltage is,

$$V_i = I_3 R_3 + V_Z$$

then, $$I_3 = I_Z = (V_i - V_Z) / R_3,\ I_Z = 15mA$$

$$15m = (24 - 6.2) / R_3$$

$$R_3 = 1.19kohm$$

B. Calculation for Switching Mode Power Supply (SMPS)

When applied this component calculation in real life work project, must choose component value higher than the calculated value for the safety in the circuit. Design requirement for SMPS, Input voltage for this power supply is 24Vdc and output current range between (0.5 - 1) A.

Inductor, $$L = (\ V_{in} - V_{out}\ )(\ D / F_{sw}\ ) / I_{ripple}$$

$$D = V_{out} / V_{in} = 20 / 24 = 0.8333$$

$$I_{ripple} = 0.3(\ I_{Load}\ ) = 0.3(\ 1\ ) = 0.3A$$

then, $$L = (\ 24 - 20\ )(\ 0.8333 / 100kHz\ ) / 0.3$$

$$L = 111uH \text{ (minimum value)}$$

Diode, $$I_D = (\ 1 - D\ ) .\ I_{Load}$$

$$I_D = (\ 1 - 0.8333\ ) .\ (1) = 0.167A$$

From calculated value above, must choose diode with high current rating than this calculated value.

Output capacitor,

$$C_{out} = \Delta I(\Delta T) / [\ \Delta V - (\ \Delta I\ )(\ ESR\ )\ ]$$

$$\Delta T = D / F_{sw} = 0.8333 / 100k = 8.333u$$

$$\text{Define } \Delta V = 50mV$$

$$ESR = 0.03 \text{ ohm}$$

then, $$C_{out} = 0.3\ (\ 8.333u\ ) / [\ 50m - (\ 0.3\ )(\ 0.03\ )\ ]$$

$$C_{out} = 60.97uF \text{ (minimum value)}$$

Input Capacitor:

$$C_{in} = \Delta T / [\ (\ V_{ripple} / I_{ripple}\ ) - ESR\ ]$$

$$I_{ripple} = I_{Load} / 2 = 1 / 2 = 0.5A$$

$$\text{Define } V_{ripple} = 200mV$$

$$ESR = 0.12 \text{ ohm}$$

then, $$C_{in} = 8.333u / [\ (\ 200m / 0.5\ ) - 0.12\ ]$$

$$C_{in} = 29.76uF \text{ (minimum value)}$$

C. Simulation results of LPS and SMPS using NI Multisim

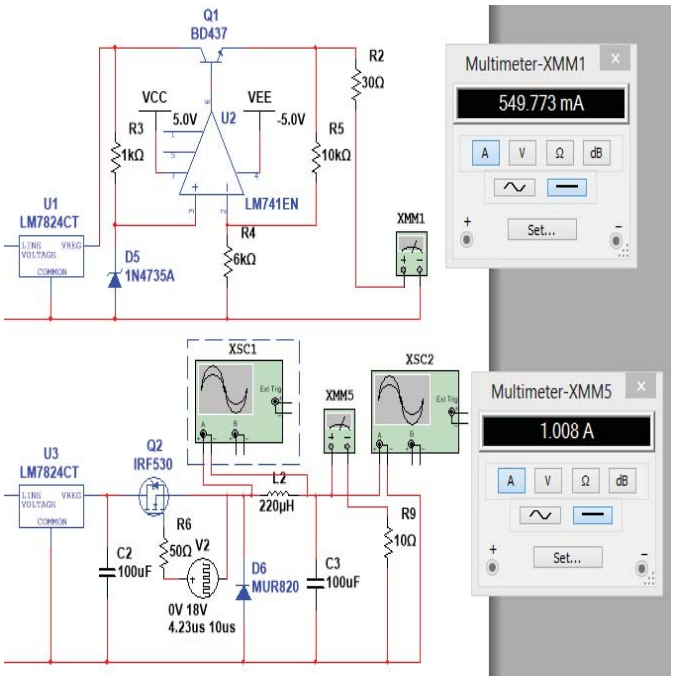

Fig. 10 LPS output current is 0.54A and output current for SMPS is 1.0A..

The design specification for LPS and SMPS is to control the output current (0 – 0.5)A for LPS and (0.5 – 1)A for SMPS. Base on Fig. 10, output current will change if the value of resistance change. In Fig. 10 output resistance for LPS is 30 ohm and it will give output current 0.54A. While, SMPS will give output current 1A if output resistane is 10 ohm.

IV. RESULT AND DISCUSSION

From the calculation and simulation before this, now time to develop the hardware for LPS and SMPS. Fig. 11 shows the whole circuit combination between LPS and SMPS. First of all, convert 240V AC voltage to 36V AC. Use center tapped transformer which is 18-0-18Vac. Combine this two secondary output and it will give 36V AC. After that use bridge rectifier and capacitor as filter to give regulated voltage DC which is 50V. From the design specification, input voltage for both LPS and SMPS must be 24V DC. Use voltage regulator LM7824 to give input voltage 24V for both power supply.

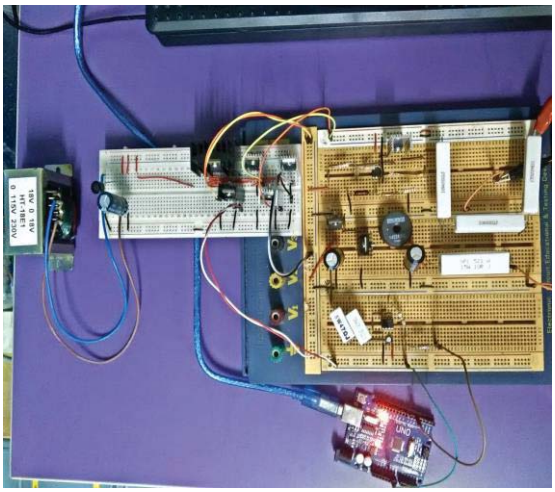

Fig. 11 Combination of LPS and SMPS.

Fig. 12 is circuit of LPS which use op-amp LM741 and BJT transistor BD437. Voltage regulator LM7805 and LM7905 is use for V_{CC} and V_{EE}.

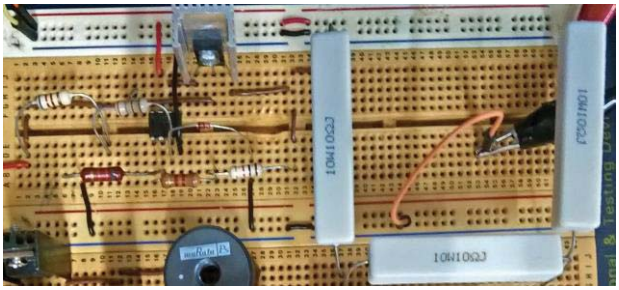

Fig. 12 LPS circuit.

Fig 13 shows the SMPS circuit connection. Use MOSFET driver which is HCPL 3120 opto-coupler to give high voltage to switch ON the MOSFET and Arduino as PWM signal. Red rectangular shape in Fig. 13 is the MOSFET driver. Use MOSFET IRF530 and diode MUR820 similar during the simulation circuit using NI Multisim.

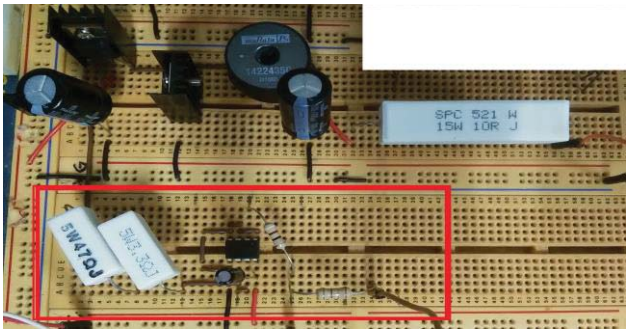

Fig. 13 Buck Converter and MOSFET driver.

Fig. 14 Test 30 ohm at LPS as output load.

Fig. 14 shows that the output current 0.54A is same as simulation result in Fig. 10. 30 ohm resistor is used to measure the output current by using digital multimeter. Fig. 15 also shows the output current is same as simulation which is use 10 ohm resistor will give 1A output current. It proves that the simulation result and real life work is working properly.

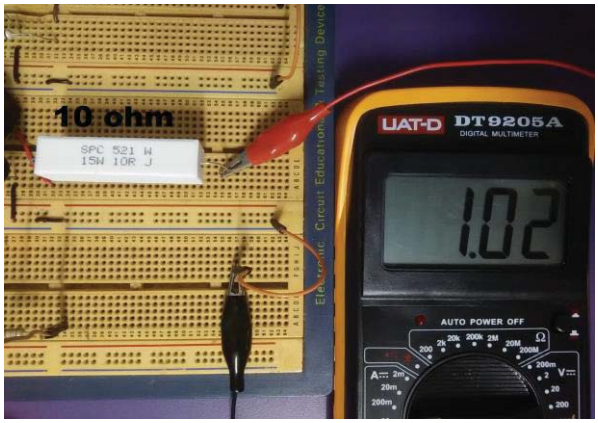

Fig. 15 Test 10 ohm on the SMPS as output load.

V. CONCLUSION

Op-amp series regulator (LPS) is the easier part to handle compared to buck converter but must be careful. To choose type of transistor want to use for op-amp output connected to gate transistor must check the transistor datasheet first. Maybe during the simulation it will work and does not have any error. Make sure, during handling the project must check voltage across collector and emitter V_{CE}. If the V_{CE} is bigger than 4V it will burn the transistor.

Next, cannot use one voltage regulator LM7824 into two different circuits because it will drop the voltage below than 24V. The solution is using each voltage regulator for each part of circuit. Must choose good heat sink to reduce heat from other part of component are heated. Last but not least, to build a power supply is not easy if you do not like to explore and troubleshoot by your own self.

REFERENCES

[1] F. Time-courses, *Advanced Analysis of*. 2012.

[2] A. Moarrefzadeh, "Study of workpiece thermal profile in Electrical Discharge Machining (EDM) process," *WSEAS Trans. Appl. Theor. Mech.*, vol. 7, no. 2, pp. 83–92, 2012.

[3] F. Han, L. Chen, D. Yu, and X. Zhou, "Basic study on pulse generator for micro-EDM," *Int. J. Adv. Manuf. Technol.*, vol. 33, no. 5–6, pp. 474–479, 2007.

[4] Y. Yang, Z. Yanqing, and Z. Yang, "Design of Pulse Power for EDM Based on DDS Chip," pp. 10–12, 2010.

[5] F. Han, S. Wachi, and M. Kunieda, "Improvement of machining characteristics of micro-EDM using transistor type isopulse generator and servo feed control," *Precis. Eng.*, vol. 28, no. 4, pp. 378–385, 2004.

[6] B. Sen, N. Kiyawat, P. K. Singh, S. Mitra, J. H. Ye, and P. Purkait, "Developments in electric power supply configurations for electrical-discharge-machining (EDM)," *Proc. Int. Conf. Power Electron. Drive Syst.*, vol. 1, pp. 659–664, 2003.

[7] T. Masuzawa, *Electrical Discharge Machining*, vol. 75, no. 1. 2009.

[8] H. J. Zhang, "Basic Concepts of Linear Regulator and Switching Mode Power Supplies," Linear Technol. Appl. Note, vol. 140, no. October, pp. 1–16, 2013.

[9] M. A. Erawan, Y. Azli, K. Nor Hisham, S. Syahrullail, A. B. Zurkarmawan, and A. Trias, "Power Generator of Electrical Discharge Machining (EDM) System," *Appl. Mech. Mater.*, vol. 554, pp. 638–642, 2014.

[10] F. Schulman, W. C. Scott, and W. H. Woodward, *Power supplies.*, Second Edi., no. July. Elsevier Inc., 1967.

[11] D. Kumar, N. Beri, and A. Kumar, "Study of Overcut During Electric Discharge Machining of Hastelloy Steel With Different," *Int. J. Adv. Eng. Technol.*, vol. 2, no. I, pp. 306–312, 2011.

[12] M. E. Carl Sommer and Steve Sommer, "Complete EDM Handbook," pp. 139–153, 2005.

[13] S. Power and A. Supplies, *Libro - Sanjaya Maniktala - Switching Power Supplies.pdf*.

[14] O. Access, "UNIVERSITI TEKNOLOGI MALAYSIA DECLARATION OF THESIS / UNDERGRADUATE PROJECT PAPER AND COPYRIGHT Name of Supervisor : Dr . Azli bin Yahya Date," vol. 16, no. April, 2010.

[15] N. G. P. Chew, C. O. F. Creep, U. Different, C. Of, and O. Access, "Universiti Teknologi Malaysia," *Notes*, vol. 16, no. November, 2008.

[16] On-Semiconductor, "Switch Mode Power Supply," p. 72, 2104.

[17] SME, "Electrical Discharge Machining (EDM)," 2001.

[18] K. Ojha, R. K. Garg, and K. K. Singh, "MRR Improvement in Sinking Electrical Discharge Machining : A Review," *J. Miner. Mater. Charact. Eng.*, vol. 9, no. 8, pp. 709–739, 2010.

[19] U. Esme, A. Sagbas, and F. Kahraman, "Prediction of surface roughness in wire electrical discharge machining using design of experiments and neural networks," *Iran. J. Sci. Technol. Trans. B, Eng.*, vol. 33, no. B3, pp. 231–240, 2009.

1D and 2D Simulation of IBC Solar Cell

Ady Putra Anizad
Department of Electronic and Computer Engineering
Faculty of Electrical Engineering
Universiti Teknologi Malaysia
Johor Bahru, Malaysia.
adyputraanizad@gmail.com

Dr. Amirjan Nawabjan
Department of Electronic and Computer Engineering
Faculty of Electrical Engineering
Universiti Teknologi Malaysia
Johor Bahru, Malaysia.
amirjan@utm.my

***Abstract*—This paper reports on simulation of Interdigitated-Back Contact solar cell in order to increase the efficiency of the cells. The simulation programs used are SARAH for 1D and PC2D for 2D as they are based on Excel and easy to used. The parameters that have been alter in order to increase the efficiency are thickness of the solar cells and the lifetime of the carrier in the cells. It is proved that the thinner solar cells may have higher efficiency than the thicker cells and the carriers' lifetime also affecting the efficiency of the solar cells.**

Keywords—efficiency; thickness; lifetime; simulation

I. INTRODUCTION

The significant increment of innovative work in the zone of photovoltaic (PV) systems in recent years have made the PV power generators a plausible option energy resource that complements other energy sources in hybrid energy systems. The increasing efficiency of solar cells as well as the improvements of manufacturing technology of solar panels contribute to the trend of fast increase of the PV energy use. The PV generators can either be grid connected (operate in distributed generation systems) or can operate in remain solitary (autonomous) systems[1]. Photovoltaics are a key innovation choice to understand the move to a decarbonized energy supply[2]. The solar resources in Europe and world-wide are plentiful and can't be cornered by one nation. Regardless for what reasons, and how quick the oil cost and energy cost increment later on, PV and other renewable energies are the only ones to offer a decrease of cost, instead of an increment in the future [3].

However, the maximum efficiency of PV that have been achieve were below 30%[6]. In order to keep up with the PV energy demand, improving the efficiency of PV cell itself is a must. The main parameters in PV are short-circuit current, ISC, open-circuit voltage, VOC and efficiency, η. Those parameters are affected by the thickness of the cells and carrier lifetime in the cells. Therefore, in order to obtain better PV productivity, these two factors are need to be adjusted.

II. BACKGROUND

This chapter discuss on developing a higher efficiency IBC solar cell by improving the parameters required which is open-circuit voltage, short-circuit current and fill factor.
Improvement of solar cell have become interesting lately due to the popularity and user's demand statistic in recent years.

A. Interdigitated-Back Contact Solar cell (IBC)

Apart from traditional PV configuration, rear contact solar cells move all or part of the front contact grids to the rear of the device hence accomplish conceivably higher efficiency. The higher efficiency potentially results from the lessened shading on the front of the cell and is valuable in high current cells such as concentrators or large areas. IBC is one of the rear contact solar cell design[5].

By putting both contacts on the rear of the cell, rear contact solar cells eliminate shading losses altogether. By utilizing a thin solar cell produced using superb material, electron-hole pairs generated by light that is absorbed at the front surface can still be gathered at the rear of the cell[6]. Such cells are especially useful in concentrator applications where the impact of cell series resistance is greater. An extra advantage is that cells with both contacts on the rear are easier to interconnect and can be put nearer together in the module since there is no space between the cells required[7].

Efficiency of IBC are significantly higher than traditional cell, reaching 20% of efficiency is no longer a myth for PV industries. Many research conducted have surpass 20% efficiency by using various fabrication process and several parameters improvement[4]. Therefore, IBC are known to have high potential in PV industries.

B. Efficiency, η

Improving the efficiency is not an easy work to do, literally the efficiency is the most regularly utilized parameter to think about the execution of one solar cell to another. The definition is proportion of vitality yield from the solar cell to input energy from the sun[8]. The efficiency relies on the spectrum and intensity of the incident sunlight and the temperature of the solar cell. Therefore, to measure the efficiency, a controlled condition is expected to contrast the performance of one device to another[4][9].

$$\eta = \frac{V_{OC} I_{SC} FF}{P_{in}} \quad (1)$$

III. METHODOLOGY

This project will be using two simulation programs simultaneously. Then base on both result, the result will be

compare to obtain an accurate simulation result. The simulation programs that will be used are SARAH for 1D and PC2D for 2D. Both programs will be running on Microsoft Excel software, which allows for direct visual mapping between the grid elements and the solution mesh[21][22].

However, several parameters from 1D simulations were unable to synchronize to 2D simulation programs. Therefore, there was some different between those two simulations result.

For both simulation, the thickness of the cells and the carrier lifetime will be manipulated. Then, the most suitable thickness and lifetime was chosen to create an improved IBC solar cell.

A. Thickness of the Cells

The thickness of the cells has been varied from 50 to 500 micrometers in order to determine the best thickness to choose for further improvement.

B. SRH Lifetime

Similar to previous step, the lifetime of the carrier will manipulate ranging from 300 to 3000 microseconds. The most suitable lifetime will be pick to optimized the parameters of the solar cells.

IV. Result and Discussion

The result of the simulations has been organized in the form of graph to make it easier to understand the trend of efficiency against thickness and lifetime.

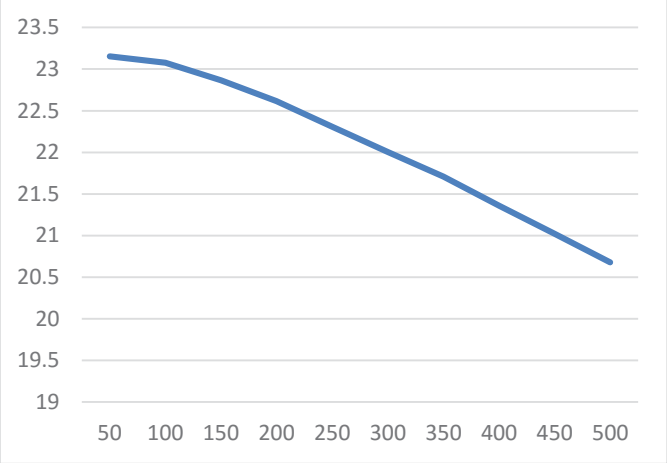

Fig. 1: Graph of efficiency vs thickness.

From the graph in Fig. 1., the efficiency is inversely proportional to the thickness of the cells. This is due to the thinner cells have a better light trapping properties. Furthermore, the thicker cells may have problems with recombination process because the electrons may have recombined before they arrive at the metal contact of the cells. In order to overcome the problem face for thicker cell, extending the bulk lifetime will be the solution.

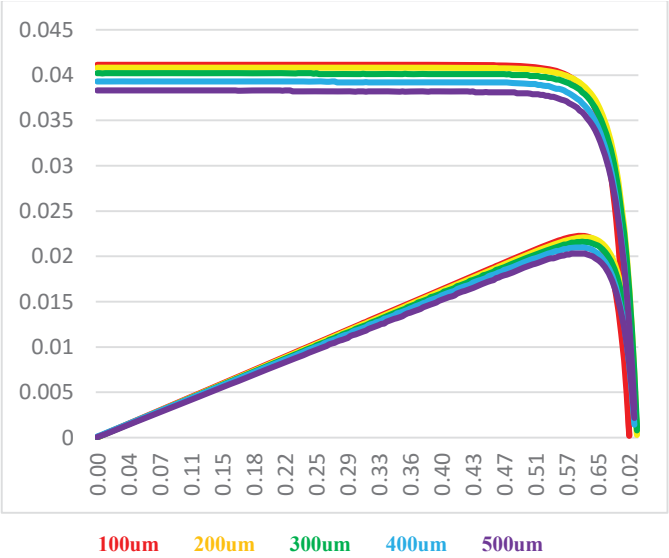

Fig. 2: IV curve for different thickness in 1D.

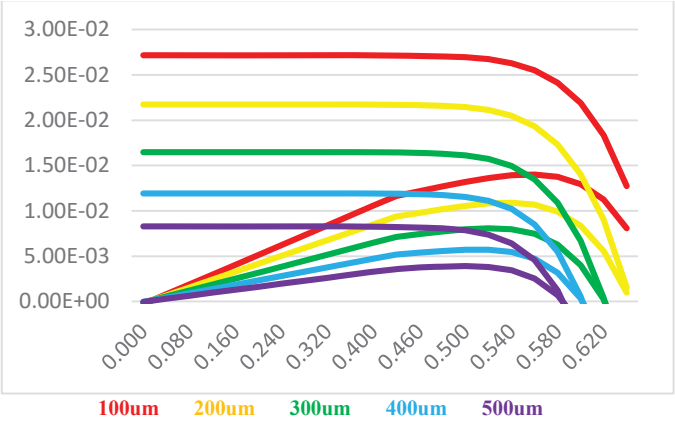

Fig. 3: IV curve for different thickness in 2D.

However, iv curve required from Fig. 1 were differ from Fig. 3 where for 1D simulations the thinner cells have higher I_{SC} but lower V_{OC} and 2D simulations the thinner cells have higher both *Isc* and V_{OC}. This unexpected result was due to parameters that was unable to be synchronize for both simulations that have been state before. Fortunately, the result in terms of efficiency are still valid because both simulations that have been made show that the thinner cells will have higher efficiency than thicker cells.

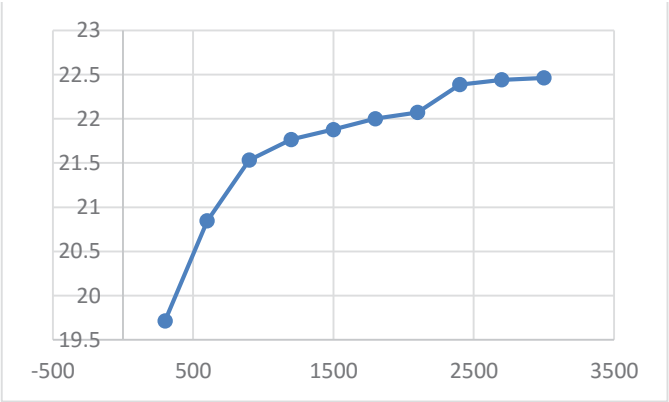

Fig. 4: Graph of efficiency vs SRH lifetime.

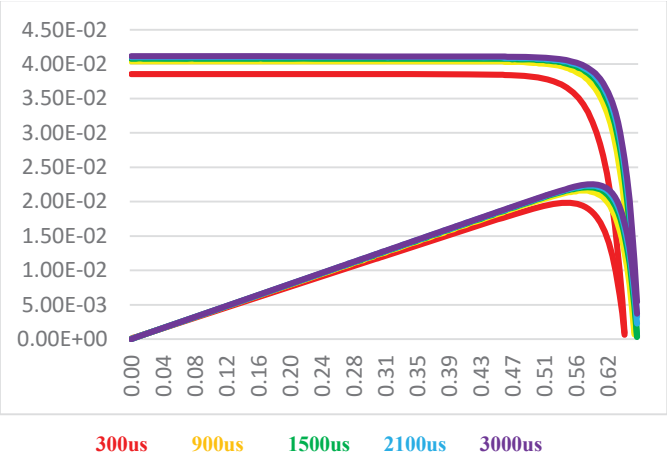

Fig. 5: IV curve for different SRH lifetime.

Fig. 5 Show that extending the bulk lifetime also increase the efficiency. This is because when the bulk lifetime is longer, recombination losses effect which affecting both *Isc* and V_{OC}. Typically recombination will happen on surface which is called surface recombination or in the bulk which is called bulk recombination[23]. For longer lifetime, the recombination were minimize and *Isc* will increase because less electron were recombined during travel.

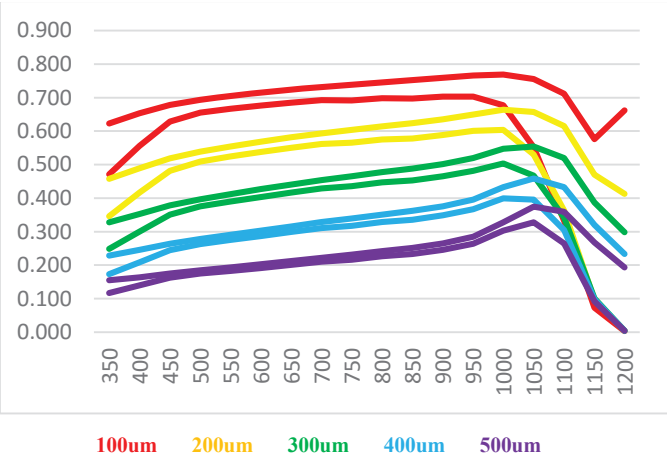

Fig. 6: Graph of External Quantum Efficiency and Collection Efficiency for different thickness.

Last but not least, Fig. 6 shows that the External Quantum Efficiency, EQE and Collection Efficiency for the thinner cells is higher than thicker cells due to thinner cells will allow light to travel further into the cells. While quantum efficiency ideally has the square shape shown above, the quantum efficiency for most solar cells is reduced due to recombination effects. The higher the wavelength of the light, the deeper light will travel into the cells. However, after 1000um of wavelength, the efficiency is dropping due to rear surface recombination.

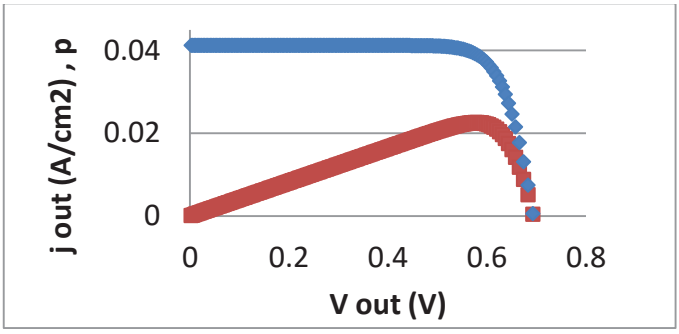

Fig. 7: IV curve for final result.

Table 1: Data for final result.

Parameter	Value	Unit
Thickness	150	um
SRH lifetime	3000	us
Voc	693.34	mV
Isc	41.25	mA/cm2
Vmpp	578.05	mV
Jmpp	39.10	mA/cm2
FF	79.01	%
Eta	22.60	%
Pin	10	W

From Table 1, the efficiency of the solar cells can be obtained through equation (1).

$$\eta = \frac{VocIscFF}{Pin}$$
$$= \frac{(693.34m)(41.25m)(79.01)}{10}$$
$$= 22.5971\%$$

V. Conclusion

In summary, it is possible to achieve efficiency higher than 20% by altering the parameters of the cells. However, others factor that affecting the performance of the cells also need to be consider to prevent the efficiency of the cells decrease. The final result was achieved by choosing the best thickness and also the most suitable lifetime.

References

[1] PV/wind/tidal/battery A. Askarzadeh, "Electrical power generation by an optimised autonomous system," IET Renew. Power Gener., Aug. 2016.

[2] K. Kusakana, "Optimal scheduled power flow for distributed photovoltaic/wind/diesel generators with battery storage system," IET Renew. Power Gener., vol. 9, no. 8, pp. 916–924, Nov. 2015.

[3] Chakrabarty, I. H. Sahputra, O. A. Restrepo, O. Bouhali, and N. Mousseau, "Arc '16," pp. 16–19, 2016.

[4] M. A. Green et al., "Solar cell efficiency tables (version 49)," Prog. Photovoltaics Res. Appl., vol. 25, no. 1, pp. 3–13, Jan. 2017.
[5] H. Steinkemper, M. Hermle, and S. W. Glunz, "Comprehensive simulation study of industrially relevant silicon solar cell architectures for an optimal material parameter choice," Prog. Photovoltaics Res. Appl., vol. 24, no. 10, pp. 1319–1331, Oct. 2016.
[6] B. P. Rand, J. Genoe, P. Heremans, and J. Poortmans, "Solar Cells Utilizing Small Molecular Weight Organic Semiconductors," Prog. Photovolt Res. Appl., vol. 15, no. February 2013, pp. 659–676, 2007.
[7] M. K. Mat Desa et al., "Silicon back contact solar cell configuration: A pathway towards higher efficiency," Renew. Sustain. Energy Rev., vol. 60, pp. 1516–1532, 2016.
[8] R. Stropnik and U. Stritih, "Increasing the efficiency of PV panel with the use of PCM," Renew. Energy, vol. 97, pp. 671–679, 2016.
[9] T. Markvart and L. Castener, Practical Handbook of Photovoltaics: Fundamentals and Applications. Elsevier Ltd, 2003.
[10] J. L. Sawin, K. Seyboth, and F. Sverrisson, Renewables 2016: Global Status Report. 2016.
[11] M. A. Green et al., "Solar cell efficiency tables (version 49)," Prog. Photovoltaics Res. Appl., vol. 25, no. 1, pp. 3–13, Jan. 2017.
[12] M. Nayfeh, M. Stupka, T. Al Saud, and M. Alsalhi, "Silicon nanoparticle photovoltaic devices," 2006.
[13] M. Dahlinger and K. Carstens, "Optimized Laser Doped Back Surface Field for IBC Solar Cells," Energy Procedia, vol. 92, pp. 450–456, 2016.
[14] P. Narchi, T. Bearda, M. Foldyna, P. Prod'homme, and P. Roca i Cabarrocas, "Interdigitated back contact silicon solar cells: Diode and resistance investigation at nanoscale using Kelvin Probe Force Microscopy," in 2016 IEEE 43rd Photovoltaic Specialists Conference (PVSC), 2016, pp. 3082–3085.
[15] H. S. Radhakrishnan et al., "Module-level cell processing of silicon heterojunction interdigitated back-contacted (SHJ-IBC) solar cells with efficiencies above 22%: Towards all-dry processing," in 2016 IEEE 43rd Photovoltaic Specialists Conference (PVSC), 2016, pp. 1182–1187.
[16] G. Nanda, R. Dash, S. C. Swain, G. Jha, R. Kumar, and R. Siddiqui, "A review on different types of PV testing and their optimization," in 2016 International Conference on Circuit, Power and Computing Technologies (ICCPCT), 2016, pp. 1–5.
[17] P. Saint-Cast, M. Padilla, A. Kimmerle, and C. Reichel, "An Analytical Model for Interdigitated Back Contact Solar Cells," IEEE J. Photovoltaics, vol. 4, no. 1, pp. 114–121, Jan. 2014.
[18] A. bin Nawabjan, "Development of a HWCVD epitaxial IBC solar cell as a test platform for novel antireflection and light trapping schemes," 2016.
[19] K. Ramanathan et al., "Properties of 19 Á 2 % Efficiency," vol. 230, no. February, pp. 225–230, 2003.
[20] S. Issue, "Thin-film Silicon Solar Cell Technology," vol. 142, no. November 2003, pp. 113–142, 2004.
[21] P. A. Basore and K. Cabanas-Holmen, "PC2D: A Circular-Reference Spreadsheet Solar Cell Device Simulator," IEEE J. Photovoltaics, vol. 1, no. 1, pp. 72–77, Jul. 2011.
[22] "PV Lighthouse." [Online]. Available: https://www.pvlighthouse.com.au/. [Accessed: 15-May-2017].
[23] "PVEducation." [Online]. Available: http://www.pveducation.org/. [Accessed: 15-May-2017].

IoT based Smart Classroom System

Edward Chan Kam Fai
Faculty of Electrical Engineering
Universiti Teknologi Malaysia
Johor Bahru, Malaysia.
edward0117@live.co.uk

Dr Mohd Afzan Bin Othman
Department of Electronics & Computer Engineering
Faculty of Electrical Engineering
Universiti Teknologi Malaysia
Johor Bahru, Malaysia.
afzan@utm.my

***Abstract*—Internet of Things (IoT) is no doubt will be the new revolution in the era of Industry 4.0, where every object will be connected to the server or internet for data processing and control. The attendance system that we currently use now is recorded by signing our signature on a piece of paper, which makes tracking and processing troublesome, it will need to be digitalized by using various sensors and module on it. Our conventional classroom system now do not have the feature of energy saving, which contribute to high cost in paying electrical bills. Thus is this paper, an IoT based Smart Classroom System which consist of various sensors to record the attendance and implement an energy saving technology is presented. The attendance data will be digitalized and send to the server to be processed automatically, the tracking can be viewed in a website. Through the energy saving technology, students or lecturer do not purposely need to switch off the air conditioning and lights each time they leave the class. Overall, the whole system will increase efficiency in terms of attendance recording and processing and save huge amount of cost spend in electrical bill.**

Keywords—Radio Frequency Identification (RFID); Smart Attendance System; Server; Database; Energy Saving System; Wireless Sensor Network (WSN)

I. INTRODUCTION

The rate of the student attendance is crucial as students will perform well in exams and practical lab if they go to classes consistently. Some of the students may not understand this and will think of it as a time wasting session that they will skip it.

In UTM, the attendance system is important as it will deter the rate of student skipping class due to boredom, they will need at least 80% of the attendance marks in order to be eligible in taking the final exam of that particular subject. It is necessary for each of the lecturer to record each and every student attendance, so that to evaluate the rights of them to take the final exam. The traditional attendance system is not efficient as it uses paper to record down the signature signed by each and every student, after that the paper is passed around while in the class. This will cause distraction among students, where their attention is supposed to be at the lecturer. The students may missed out some important facts and tips in the class. In addition, lecturers have to waste a huge amount of effort to calculate the attendance rate manually or by input typing [7]. This can put a great deal of stress in lecturers' workload. Not to mention that they have to bring the attendance sheet every day to the class.

This is where the Internet of Things (IoT) attendance system comes in. The purpose of this project is to create a platform in terms of a smart classroom system that will bring accessibility to students and especially to lecturers. Attendance system is a system that is use to record students' attendance in a particular subjects or class, this system is applied to every quarter of the world including industries, working place and etc. RFID stands for Radio Frequency Identification, it uses radio frequency (RF) signal to read data stored in the RFID chip attached with an object. As of now, the students' matric card have RFID chip inside that is unused until now. That is why RFID attendance is the most suitable technology to be used in this project.

Another feature of this project is the WSN energy saving technology implementation in it. Wireless Sensor Network (WSN) is a network of nodes (wireless sensor and actuator) that connected with each other. Through the network, the nodes pass the data from one to another to enable effective data transmission to a main location. With this technology, the system can automatically shut down electrical appliance when no one is at the classroom. Electrical consumption is getting higher and higher each day, it is mainly contributed by the usage of air conditioning. The main problem of this is the unwillingness of the students and some lecturers to switch it off after the class ends. To solve this, WSN based technology is implement in this project. Sensors will be installed at the ceiling of the classroom to detect human movement, whenever there is no one in the class in a period of the time, the sensors will automatically send radio frequency (RF) signal to the a microcontroller to switch off those appliances to save energy.

II. RELATED WORKS

A number of related work is in the implementation of RFID attendance system, some is specific in the hardware design and some is concentrating in the back-end database system.

Mahesh Sutar has designed and implemented a RFID attendance system with some algorithm of taking in attendance data and put in to the correct database for user to view it [1]. There are five different levels of accesses which are the Administrator, Lecturer, Student, University, Administration and the Guest. Each of the user will have limited access and interfaces according to the user level. This is for security and privacy purposes. Fabio J. Costa reviewed various hardware module to implement a low cost but yet effective RFID attendance system to be implemented in class [2]. He used

various low cost development board and module such as Arduino Uno (a micro controller), real time clock module (to have a time parameter inside Arduino), Ethernet shield (to enable connection to the server via Ethernet) and RFID reader (to scan RFID tag). All of these can be get below RM100 in most of the local stores and can be produced in a great numbers. This is suitable to huge sum of indoor environment like classrooms and lecture halls in UTM to be integrated.

Subramany implemented a Heating, ventilation and air conditioning (HVAC) control technique in a office environment by integrating with various sensors module to increase the accuracy to detect human presence in a indoor area [4]. The sensors used are temperature, humidity and CO2 sensor module that were installed in each room. The sensors is connected to a wireless module to send necessary data to the base microcontroller to control the flow and temperature of air supplied into each room. Muhammad After revolutionize the traditional HVAC system that rely on wired temperature regulators and thermostats into a smarter form so that the system will have more optimized algorithm with minimum human supervision [3]. In his work, the algorithm he proposed is a balancing the trade-off between communication frequency of wireless sensors and effectiveness of HVAC system so that to maintain thermal comfort and maximize the battery life of the wireless sensors. The algorithm is devised through multiple simulations to find out the pattern through different scenario ie. different in average room temperature over time.

Amir R. Atabekov from Kennesaw State University done a project of Smart Classroom System but in a different approach. He explored mostly of indoor localization in terms of the same project by implementing the smart chair in the classroom [9]. The chairs all are connected to each other in the WSN, the data of the student is sent to the server for attendance tracking. There is a project that track attendance using RFID too, to enable effective acknowledgement to the student, Arulogun O. T. design the system to send out notification in terms of mobile app or an email to the students and lecturer[10].

III. Research Methodology and Design

A. Smart RFID Attendance System

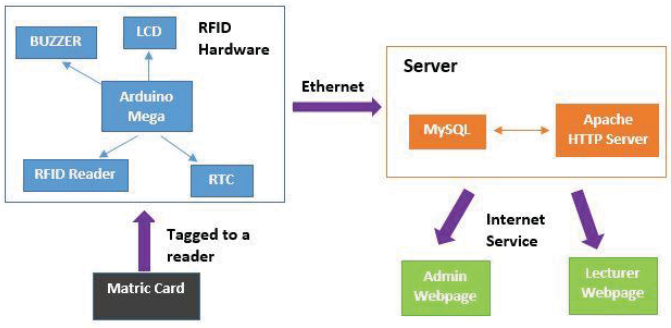

Fig. 1. Process of RFID Attendance System

The RFID attendance system consists of hardware and software part of it. The hardware part consists of several low cost development shield and module. The microcontroller used is Arduino Mega, it is based on the ATmega2560. It has 54 digital IO, among of the 54, 14 of them can be used as a PWM pins, 4 UART, and crystal oscillator of 16 MHz. Real Time Clock module of DS1302 is used as a time keeping chip to have a time parameter in the microcontroller. Arduino LCD shield is used as a display for the status in taking the students' attendance. The Arduino Ethernet Shield is used to connect to the server and the database of the system. Meanwhile, RFID reader, MFRC522 is selected to detect the different identity of the RFID tag inside every matric card in each of the students in the university. The frequency band of the RFID is a low frequency of 125 kHz-134 kHz, the max range is 5m from the reader. As for the software part of the system, the web interface using several web programming like Hypertext Preprocessor (PHP), Hyper Text Markup Language (HTML), Cascading Style Sheets (CSS), Apache HTTP Server and MySQL. PHP is a scripting language for the server side of the system, it manage the algorithm of the data flow between the data from hardware to the storage side in database. HTML and CSS is a web programming to structure and style your webpage. With these two languages, the form or slots for user to log in or a graphic user interface (GUI) was created to display the necessary information in the webpage. Apache HTTP Server is a software to develop a free-source HTTP server in any local computer that will provide a secure and efficient HTTP services. Lastly, MySQL open-source relational database management system (RDBMS), it is used as a database system to save in tables, queries, reports and other subjects with necessary data inside.

Fig. 2. RFID Attendance prototype

The students will first take their attendance by tagging their matric card to the RFID reader, the RFID of the student and the time at that instances is send to the database in the server through Ethernet connection. The server will check the availability of the students whether he is in the correct class, time, subjects and day, before the data is successfully saved in the MySQL database. A 'Welcome <name of the student>' will be displayed in the LCD display in the hardware if the attendance is successfully taken amidst all the detailed checking of the information. This is necessary as students might cheat their way to scan in a different class but in the same time to take their attendance. A website to check the attendance status is designed, it have a login for different user. (Refer Figure 3). Currently,

only lecturer and admin is given the ID and password to access the website.

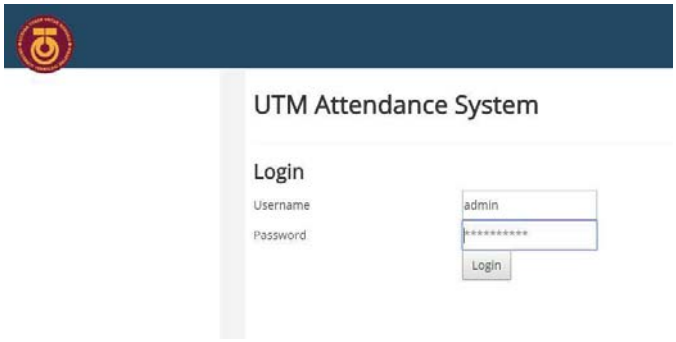

Fig. 3. Design of the Website

Lecturers can log into the server webpage to check the students' attendance rates. They can check back the student's attendance in previous date, change the status of attendance in case of medical leave, and attendance for each of the student.

There is an account for admin in the website, they can have direct access to all the settings and configurations of the server and database system. Whenever a modification of the system is needed, admin can login with their account to do their work.

The website, admin can

- Create a new ID and password to access the website
- Can register any new student with Name, RFID number and Matric Number
- Can register the subjects taken by the students
- Can register any new subjects with necessary info like ID, Name, Day, Time Start and End, Class ID and Name of lecturer
- Create an attendance table in the database from selecting the subject and day of the subject

B. *WSN based Energy Saving System*

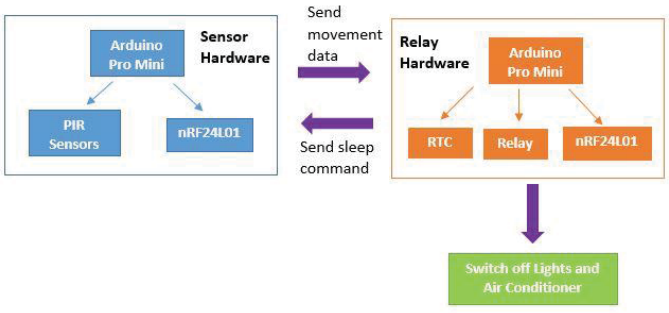

Fig. 4. Process of WSN Energy Saving System

The Smart Energy Saving is a technology that provides comfort, smart and energy saving indoor environment. Passive Infrared Sensor (PIR sensor) is used in order to detect human movement in the class that is controlled by a micro controller which is Arduino Pro Mini. The arduino is connected with a RF wireless module, nrf24l01, which can send data wirelessly. A relay module is placed inside the electrical box in each of the class to switch off electrical appliances in the classroom or lecture halls. It will be controlled by the same Arduino as before and is connected with nrf24l01 as the receiver of the RF signal or packets as shown in Figure 5.

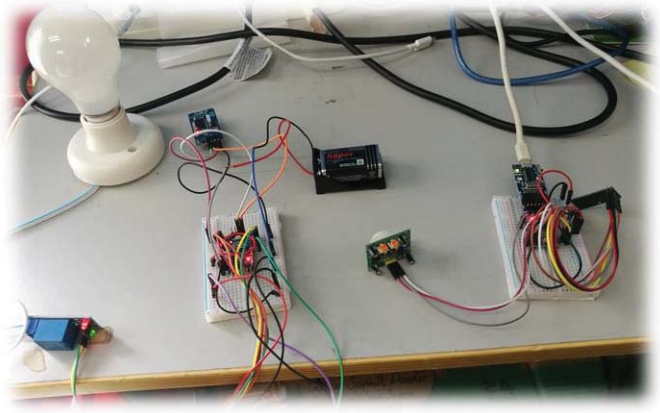

Fig. 5. WSN Power Saving System prototype

In the design, there will be two node with microcontroller (MCU) with it, they are called PIR Node and Relay Node, the PIR node will be connected to a PIR sensor and nRF24L01 wireless communication module while the Relay Node will be connected with 1 Channel Relay, Real Time Clock (RTC) and nRF24L01. Whenever there is no human movement, the PIR sensor will trigger the MCU in the 'PIR node' to wait for a period of a time, in this time, if there is still no human movement detected then only it confirms no human is in the class thus it will send a trigger message to the relay node through RF using nrf24l01. The relay node will then switch off the electrical appliance in the room through controlling the IO of 1 channel relay.

Likewise, if there is a constant human movement detected, if there is a content movement in a period of time, thus it confirms there are human movement in the class and send a RF signal to the Relay Node to switch on the lights. To really have an energy saving within the prototype, the RTC is necessary as when the time is either a weekends or after 6pm (end of any class), the Relay Node will be triggered to activate the sleep function, the sleep time is different for weekday and weekends. Before the Relay Node sleep, it will send a RF signal to the PIR Node to ask it activate the sleep function, then it will sleep as well. By the time it reaches the university opening time, both of the node will wake up automatically.

IV. Results

A. *Smart RFID Attendance System*

When lecturer log into the system with their ID and password, the home interface that they will see includes some necessary info of the subject (see Figure 6).

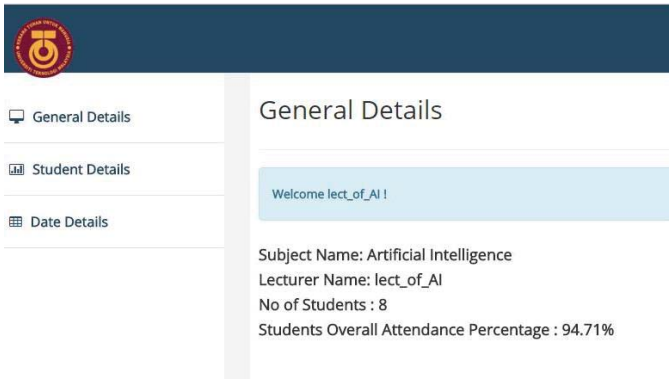

Fig. 6. Design of the Website for Lecturers

Features in the Lecturer website includes

1) Student Details

- Can check and track each of the student overall attendance as shown in Figure 7.
- In case of medical leave, lecturer can change the status of the attendance for it.

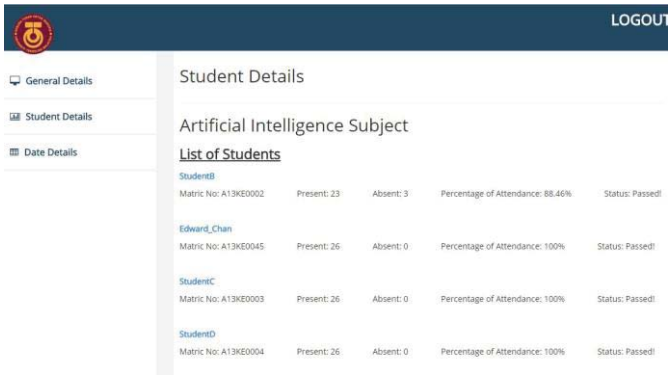

Fig. 7. Design of the Website for Lecturers

2) Date Details

- Can check back the student attendance of the any class as shown in Figure 8.

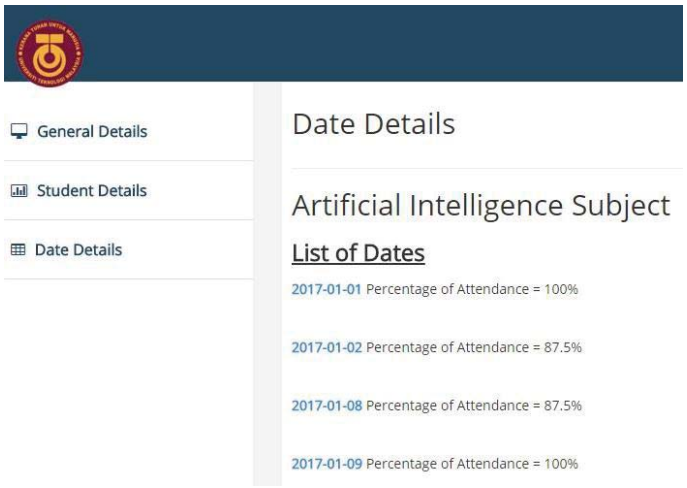

Fig. 8. Design of the Website for Lecturers

Features in the Admin website includes

1) Home Dashboard

- Can access each and every table in the MySQL as shown in Figure 9.

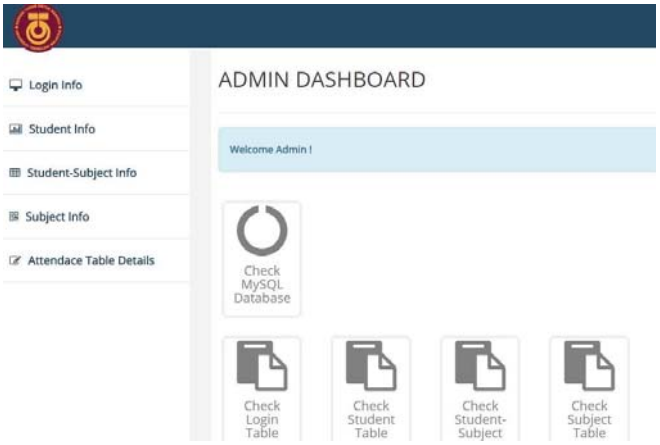

Fig. 9. Design of the Website for Admins

2) Login Info

- To create a new ID and password to access the website as shown in Figure 10.

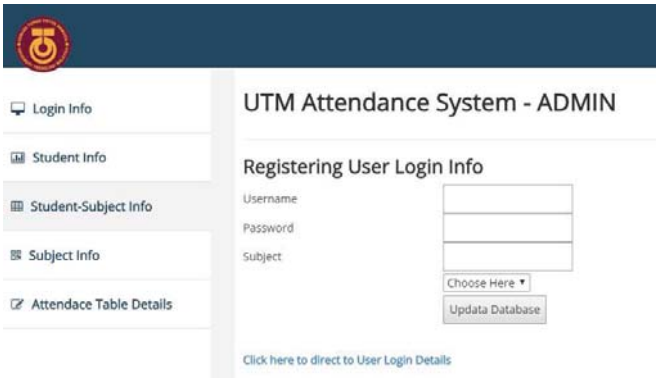

Fig. 10. Design of the Website for Admins

3) Student Info

- Can register any new student with Name, RFID number and Matric Number as shown in Figure 11.

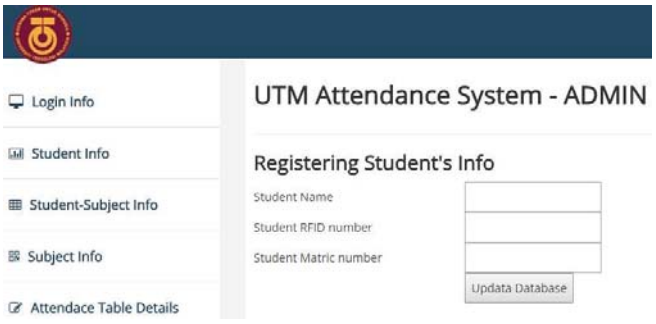

Fig. 11. Design of the Website for Admins

4) Student-Subject Info

- Can register the subjects taken by the students as shown in Figure 12.

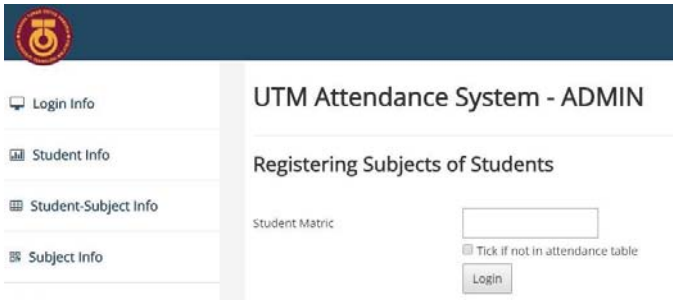

Fig. 12. Design of the Website for Admins

5) Subject Info

- Can register any new subjects with necessary info like ID, Name, Day, Time Start and End, Class ID and Name of lecturer as shown in Figure 13.

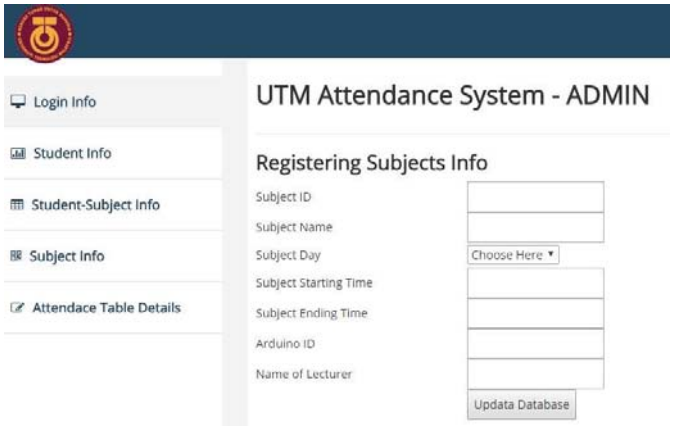

Fig. 13. Design of the Website for Admins

6) Attendance Table Details

- Create an attendance table in the database from selecting the subject and day of the subject as shown in Figure 14.

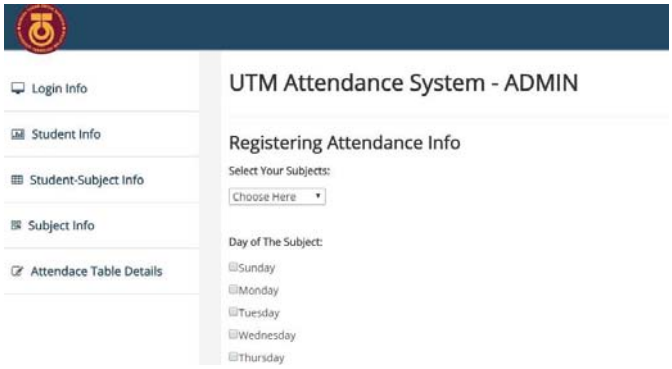

Fig. 14. Design of the Website for Admins

B. WSN based Energy Saving System

The system is implemented in Arduino connected with PIR sensor and communicate using nRF24L01 RF module, when there is a continuous no human movement or human movement in 4 seconds, then the PIR node will send a Radio Frequency (RF) message to the Relay Node to switch off and on respectively.

1) No human movement

- When there is no movement, the arduino will keep on counting for 4 more seconds (refer Figure 15), if still no human movement, then it will send a Radio Frequency (RF) message to the Relay Node to switch off the lights.

```
humanCount : 0  noHumanCount : 1
humanCount : 0  noHumanCount : 2
humanCount : 0  noHumanCount : 3
humanCount : 0  noHumanCount : 4

STATUS:
Confirmation that no human movement in the class!!
Sent order of 2
```

Fig. 15. Case Results of No Human Movement in Class

2) Human movement

- When there is no movement, the arduino will keep on counting for 4 more seconds (refer Figure 16), if still no human movement, then it will send a Radio Frequency (RF) signal to the Relay Node to switch on the lights as shown in Figure 17.

```
humanCount : 0  noHumanCount : 1
humanCount : 0  noHumanCount : 2
humanCount : 1  noHumanCount : 0
Motion detected!

humanCount : 2  noHumanCount : 0
humanCount : 3  noHumanCount : 0
humanCount : 4  noHumanCount : 0

STATUS:
Confirmation that human movement is present in the class!!
Sent order of 5
```

Fig. 16. Case Results of Human Movement in Class

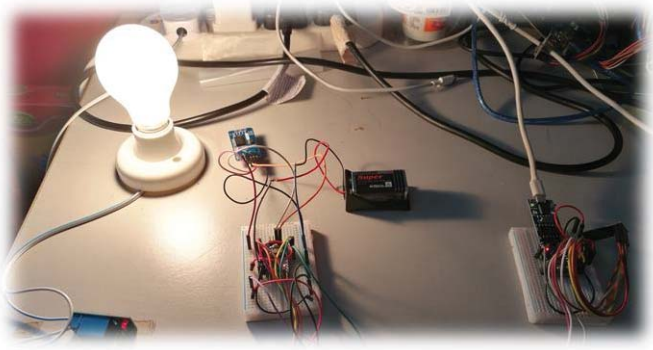

Fig. 17. Picture of the prototype of Human Movement present

V. CONCLUSION

The proof of the results and some literature reviews show that this Iot based Smart classroom system that consist of the smart attendance system and WSN power saving technology will be successful and can be worked inside any classroom. Further development in the design of the system will be needed to enable full system to be ready to be implemented in every classroom throughout the whole university. The energy consumption spent in classroom for air conditioned and lights will be significantly reduced to channel more fund in research and facilities etc. This smart attendance system will benefit not only for students but for lecturers especially in reducing their daily workout. When their work is reduced, they can concentrate more in their research and bringing knowledge to every students in the university to be graduated as top local university in Malaysia.

REFERENCES

[1] Mahesh Sutar, Mahesh Patil and Sachin Waghmare (2016), "Smart Attendance System by using RFID In IOT", International Journal of Advanced Research in Computer Engineering & Technology (IJARCET)

[2] Fábio J. Costa, Samuel Pereira, Ana Rosmaninho, Micael S. Couceiro Carlos M. Figueiredo, Victor Santos, N. M. Fonseca Ferreira (2012), "Low-Cost Access Management System in an Educational Environment", Instituto Superior de Engenharia de Coimbra.

[3] Muhammad Aftab (2013), "Engineering WSN for Smart Air-conditioning system", Massachusetts Institute of Technology.

[4] Rahul Subramany (2013), "WSN for HVAC Control", University Of Florida.

[5] "Arduino instructions." [Online]. Available: http://www.ladyada.net/learn/arduino/ M. Young, The Technical Writer's Handbook. Mill Valley, CA: University Science, 1989.

[6] Amir Atabekov, Jing He and Patrick Otoo Bobbie (2013), "Internet-of-Things-basedFramework to Facilitate Indoor Localization Education", Kennesaw State University.

[7] Cheah Boon Chew,Manmeet Mahinderjit-Singh, Kam Chiang Wei, Tan Wei Sheng, Mohd Heikal Husin, Nurul Hashimah Ahamed Hassain Malim (2015), "Sensors-enabled Smart Attendance Systems Using NFC and RFID Technologies", International Journal of New Computer Architectures and their Applications (IJNCAA)

[8] Pushpa S. Gagare., Priyanka A. Sathe, Vedant T. Pawaskar., Sagar S. Bhave (2014), "Smart Attendance System", International Journal on Recent and Innovation Trends in Computing and Communication

[9] Amir R. Atabekov (2016), "Internet of Things-Based Smart Classroom Environment", Kennesaw State University

[10] Arulogun O. T., Olatunbosun, A., Fakolujo O. A., and Olaniyi, O. M. (2013), "RFID-Based Students Attendance Management System", International Journal of Scientific & Engineering Research Volume 4, Issue 2

[11] Jeremy Blum (2013). "Exploring Arduino: Tools and Techniques for Engineering Wizardry".Crosspoint Boulevard Indianapolis : John Wiley & Sons, Inc.

[12] W. Durfee (2014), "Arduino Microcontroller Guide". University of Minnesota Press

Implementation of 2-D Discrete Cosine Transform (DCT) on Programmable System-on-Chip (SoC)

Chan Jia Ching
Faculty of Electrical Engineering
Universiti Teknologi Malaysia
Johor Bahru, Malaysia.
icebryanchan@gmail.com

Dr. Ab. Hadi Bin Ab. Rahman
Department of Electronic and Computer Engineering
Digital Signal & Image Processing Research Group
Faculty of Electrical Engineering
Universiti Teknologi Malaysia
Johor Bahru, Malaysia.
hadi@fke.utm.my

***Abstract*—Full hardware implementation, i.e. FPGA performs well with a high-performance result, but with the sacrifice of flexibility. On the other hand, full software implementation, i.e. computation using an operating system, provides a great flexibility where many variables or functions can be changed easily, but with a relatively slower speed performance. This work presents hardware-software co-design, which is an intermediate between full hardware and full software implementation, using Xilinx Zynq-7000 Programmable SoC (Zedboard). Xilinx Zedboard consists of built-in ARM processors and CLB FPGA fabric, in which they can be made to communicate with each other by using a Linux Distribution, called Xillinux. Xillinux provides a AXI bus IPs core for the Xilinx Zedboard so the data can be sent between the ARM processors and CLB FPGA fabric through a simple first in first out (FIFO) system. This work is to improve the Discrete Cosine Transform (DCT) which is the most compute intensive part of a JPEG encoder. As one of the benefit of the software-hardware co-design, the whole work uses only C programming language which provides great flexibility. Result shows that using software-hardware co-design, when the number of inputs are large, the performance of the program is doubled the full software design, up to the hardware limitation of the software-hardware co-design.**

Keywords—Xilinx Zedboard; Xillinux; Software-Hardware co-design; Discrete Cosine Transform (DCT); Hybrid System; JPEG encoder

I. INTRODUCTION

Full hardware implementation will always produce high speed and real-time result, but it is very hard to design and very time-consuming due to its complexity. Related knowledge requirement sometimes can be the bottleneck for hardware design as hardware designers need to be really good at the target hardware. Besides, hardware systems are difficult to be changed or adjusted after the final product stage, due to the lack of flexibility and lack of user's interface. Time taken to debug or maintain a hardware design can be as long as designing a whole new hardware product. Hardware design is often used in real-time embedded system where the hard deadline of a process must be full-filled, if not, fatal error will occur. Therefore, hardware implementation is widely used in embedded system design like television, washing machine, car air bag system and so on. Hardware implementation languages like Hardware Description Language (HDL) or Verilog are usually very challenging to be mastered even for those who are well-experienced in related field.

Software implementation using high level languages like C++ or Java will result in easier work due to its very high flexibility and easy debugging process. Besides, high level language programming usually comes with a lot of integrated development environment (IDE) and good compilers, allowing errors to be detected and suggestions given are usually accurate. However, software implementation does not guarantee to fully optimize the resource available. For example, in a gcc compiler environment, even with -O3 optimization level, the resources like Random Access Memory (RAM) or Central Processing Unit (CPU) is not necessarily fully utilized, resulting in a relatively slower execution speed than hardware implementation [1]. To solve the wastage of resources, parallel algorithm programming is usually used, however at the same time, it requires very high skills and experience in order to make a good parallel algorithm. Apart from that, the relatively slow speed of software implementation will eventually become more significant when the data to be processed becomes larger.

Software-hardware co-design utilizes the usage of both software and hardware, as the name describes. Some part of the design is running by the hardware part while the remaining part is running by the software part. Both of the resources in CPU and Field-programmable Gate Array (FPGA) are fully utilized by this method of co-design. Besides, this methodology also provides an alternative speed-up ranging in between full hardware and full software implementation. At the same time, this work will overcome the complexity faced by the full hardware implementation. However, co-design will face the challenges of establishing handshake between both CPU and FPGA, as well as transferring data in between. Another issue faced by the co-design is the transfer time is very significant when processing with small data or simple calculation. Therefore, co-design is often suggested to be used in large data processing or intensive programs only.

This project will attempt to improve the DCT of a JPEG encoder where it takes up the most programming time of the whole program, using software-hardware co-design on Xilinx Zedboard.

II. 2-D Discrete Consine Transform (DCT) of JPEG Encoder

A. *Joint Photographic Expert Group (JPEG) Encoder*

The JPEG image compression standard [2][3] was developed by Joint Photographic Expert Group. The JPEG compression principle is making use of controllable losses to reach high compression rates. Therefore, JPEG images are generally smaller size compared to RAW or YUV images.

JPEG Encoder generally converts a RAW format file into JPEG format and since the file size are reduced during the conversion, JPEG encoding is sometimes called JPEG compression [4]. The level of conversion or compression can be adjusted according to the user's desire, allowing a satisfied balance between output file size and image quality. Since JPEG encoding or JPEG compression is a lossy process, the higher degree of compression will result in smaller file size but at the same time, lower image quality [5]. The Fig.1 shows a basic JPEG encoder and its components. This work will focus only the DCT part of the JPEG encoder.

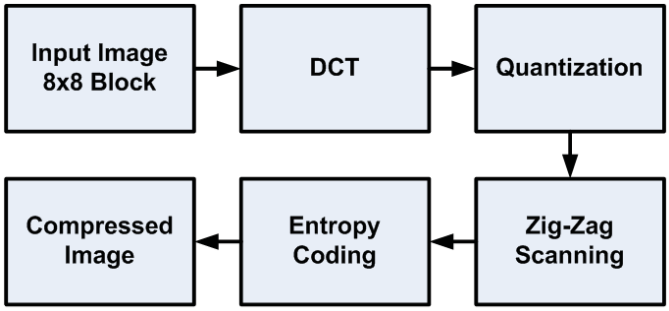

Fig. 1. A basic JPEG encoder flow chart

B. *2-D Discrete Cosine Transform (DCT)*

Discrete Cosine Transform (DCT) is a mathematical tool that is mostly used in image or video compression, i.e. JPEG, MPEG-4 AVC/H.264, HEVC. DCT transforms data from time or space domains into frequency domains for removing data redundancies in a lossy compression, as down sampling and quantization is irreversible [6]. A fast DCT is necessary for encoding or decoding images with large resolutions or videos with high frame rate [7].

The 2-D DCT calculation has a high degree of computation complexity [8]. There are many algorithms to compute the 2-D DCT coefficients [9] [10] and the algorithm chosen in this paper is based on two 1-D DCT. In an 8x8 input matrix or input block, the first 1-D DCT is running row-wise while the second 1-D DCT is running column-wise based on the outputs from the first 1-D DCT. This simple pipelined algorithm reduces the complexity of the calculation factor by four [11].

The simplified version of a fast 1-D DCT can be shown clearly in Fig. 2.

```
x0 = ind0 + ind7;
x1 = ind0 - ind7;
x4 = ind1 + ind6;
x5 = ind1 - ind6;
x2 = ind2 + ind5;
x3 = ind2 - ind5;
x6 = ind3 + ind4;
x7 = ind3 - ind4;

xa = pmul_1_2(x3);
x3 = pmul_1_1(x3);
xb = pmul_1_2(x5);
x5 = pmul_1_1(x5);

x3 = x3 + xb;
x5 = x5 - xa;

xa = pmul_2_2(x1);
x1 = pmul_2_1(x1);
xb = pmul_2_2(x7);
x7 = pmul_2_1(x7);


x1 = x1 - xb;
x7 = x7 + xa;
xa = x1 + x3;
x3 = x1 - x3;
xb = x7 + x5;

x5 = x7 - x5;
x1 = xa + xb;
x7 = xa - xb;
xa = x0 + x6;
x6 = x0 - x6;
xb = x4 + x2;
x2 = x4 - x2;
x0 = xa + xb;
x4 = xa - xb;

xa = pmul_3_2(x2);
x2 = pmul_3_1(x2);
xb = pmul_3_2(x6);
x6 = pmul_3_1(x6);

x2 = xb + x2;
x6 = x6 - xa;

outd0 = x0;
outd1 = x1;
outd2 = x2;
outd3 = x3;
outd4 = x4;
outd5 = x5;
outd6 = x6;
outd7 = x7;
```

```
pmul_1_1( x){
   return ( x - (x>>3) - (x>>7) );
}

pmul_1_2( x){
   return ( (x>>3) - (x>>7) +  (((x>>3) - (x>>7) - (x>>11))>>1 )   );
}

pmul_2_1( x){
   return ( (((x >> 9) - x)>>2) - ((x >> 9) - x));
}

pmul_2_2( x){
   return (x>>1);
}

pmul_3_1( x){
   return ( ((x + (x>>5))>>2) + (x>>4) );
}

pmul_3_2( x){
   return ( (x + (x>>5)) - (( x + (x>>5))>>2) );
}
```

Fig. 2. Fast 1-D DCT algorithm

For the 2-D DCT, it is implemented by using two 1-D DCT and it can be shown in Fig.3.

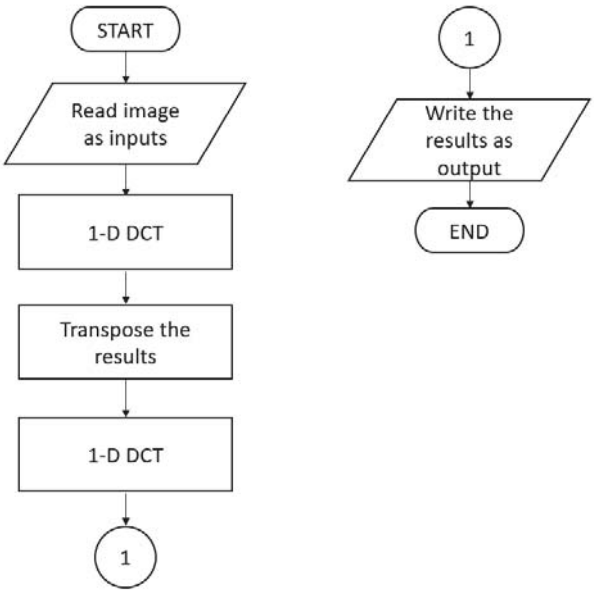

Fig. 3. Fast 2-D DCT work flow chart

III. Implementation of Full Software Program and Software-Hardware Co-Design Program

A. Xilinx Zynq-7000 (Zedboard)

Xilinx Zynq-7000 Programmable SoC, which is called Zedboard, consists of one embedded chip of a dual-core ARM Cortex-A9 MP Core microprocessor and a FPGA Fabric. Basically, the Zedboard can be divided into two parts, namely Processor System (PS) and Programmable Logic (PL). The dual-core ARM processor runs at a maximum frequency of 677MHz while the maximum frequency of PL or FPGA Fabric is determined by the design or by default it is 100MHz [12] [13]. PS is made up of ARM microprocessor, SDRAM, flash memory controllers, peripherals as well as general-purpose input/output (GPIO) [13]. Zedboard can be used to connect with a host machine through Universal Asynchronous Receiver/Transmitter (UART) or through a memory card with bitstream file generated by Vivado software [14]. Due to its PS and PL property, Zedboard is widely used in researches or projects involving hardware-software co-design [15] [16] [17] [18] [19] [20].

B. Hardware-Software Co-design using Xillybus

Hardware-software co-design means breaking down an application into two parts where a certain part of the application is handled by PS and the remaining part is handled by PL. In a fully FPGA or full hardware environment, FPGAs generally have lower computing power than x86 CPUs [15]. Despite the lower computing power, FPGAs application can sometimes outperform the CPUs, especially in image processing system or signal processing system [15]. Implementing the computing power of FPGAs into x86 CPUs or ARM processors can potentially improve the performance of ARM processors in executing certain tasks which are usually the expertise of FPGAs only [15] [16]. Application logic can be accelerated efficiently using hardware-software co-design too [17]. For example, with hardware-software co-design using Xillybus as IP core, throughput of transfer rate can be as fast as 350MByte/s [21]. Xilinx Zynq-7000 Programmable SoC (Zedboard) is one of the suitable board to implement hardware-software co-design because it integrates ARM based Processing System (PS) and Programmable Logic (PL) [17].

The user logic can be first written in any hardware programming language, then some parts of the user logic can be written in Java or other high-level programming language to support the operation of user logic [18]. After that, Xillybus IP can be used to connect AXI ports and FIFOs with I/O devices on Xillinux [18].

In a hardware-software co-design implementation, when an application logic is called, the processor passes the configuration header and messages to the hardware accelerator to compute the message [19]. In the case of using Xillybus IP core or Xillinux operating system, the hardware accelerator would be the Xillybus IP core and the FIFOs used in the Programmable Logic (PL) [15] [17] [19].

C. Xillybus IP Core

Xillybus is a Direct Memory Access (DMA)-based IP core for data transport in between a FPGA and a host machine. In other words, Xillybus is a bridge for Processor System (PS) and Programmable Logic (PL) for data transferring. Xillybus supports wide range of products and board including Altera and Xilinx devices [21]. FPGA application logics connects to the Xillybus through standard FIFOs. The Xillybus IP core then connects directly to the PS. Data transfers are easy since PS can handle the files in and out from PL through the Xillybus. The operation can be represented in Fig.4. On host machine or PS side, there is no need for software library, any programming language can be used to access Xillybus streams without any new specific extensions.

Fig. 4. FPGA block diagram of Xillybus IP core

D. Xillinux by Xillybus

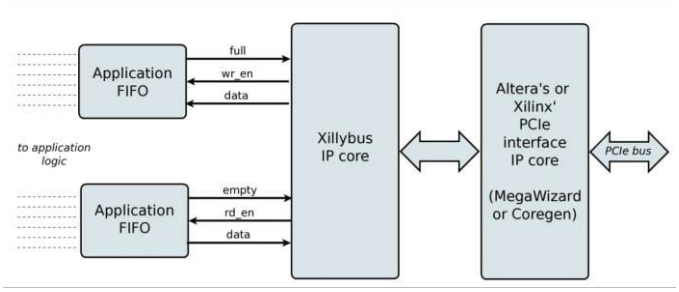

Xillinux is a Linux distribution with additional feature like FGPA code kit. Just like any other Linux distribution, Xillinux allows Xilinx products, including but not limited to Zedboard, to run a graphical desktop with the support of keyboards, mouse, monitor screen and many other input output devices. The main feature or purpose of this Linux distribution is to make the integration between Processing System (PS) and

Programmable Logic (PL) simple and easy. Xillinux uses SD card as its hard disk and it comes with a built-in PL development kit. The development kit allows Xillybus to be piped with the PS (ARM processors for Zedboard). Application logic can be connected to the FIFOs in PL and plain files can be send in and out using simple operations from Xillinux. Demo configurations of Xillybus IP core is also included by default in Xillinux. Xillybus IP core can be explained more clearly in Fig.4.

E. Wrapper Function and Synthesized Function for Programmable Logic (PL)

Wrapper function is responsible for the interface between the PS and the PL. Inside the wrapper function, pragma directives are used to interface with the Xillybus IP core. Wrapper function works like the main function in a simple C program which will later make calls to the calculation function which is called synthesized function [22]. Programmer or user needs to decide how a normal program will separate into software part and hardware part. For the hardware part of a program, it will be included in the synthesized function. This part of the program will be running in the PL as the hardware part of the software-hardware co-design. In this work, the whole 2-D DCT will be put inside the synthesized function to maximize the performance. The wrapper function together with the synthesized function will then be debugged and synthesized by Vivado HLS. After that, the synthesized hardware code will then be exported into RTL in dcp format which will later be combined with Verilog code of the provided firmware for Xillinux, in order to generate a bitstream file. The bitstream file be will copied into the SD card where the Operating System of Xillinux is installed. When the Xillinux is booted up with the new bitstream file, the hardware code is ready to be used. Any changes to be made on the hardware part of the code must be done starting from the step of designing the wrapper and synthesized function.

F. Host Program for Processing System (PS)

A program has been separated into software part and the hardware part. After the PL is ready with the desired synthesized function, a host program is written and compiled in PS to communicate and work with the function inside the PL. The PS and PL are interconnected with two standard FIFOs, one for sending data from PS to PL and another is vice versa. Therefore, it is wise to make use of basic parallel programming which includes a simple forking in the host program. The host program is forked into two processes, which are writing and reading data. This will prevent the processing from stalling due to lack of data to process or output data to be cleared up. Arrays are also used to send blocks of data into PL for processing and receive processed blocks of data from PL. These approaches will reduce but not totally eliminate the I/O overhead as well as the impact of software-hardware latencies [22].

The host program written in this work will read a text file containing the input blocks and then sends to PL for DCT before outputting the resulting blocks into a new text file. The host program or the software part of the program is responsible for reading inputs and writing outputs in the software environment. A detailed flow chart is shown in Fig. 5.

Fig. 5. Flow chart of the host program interacting with the Programmable Logic

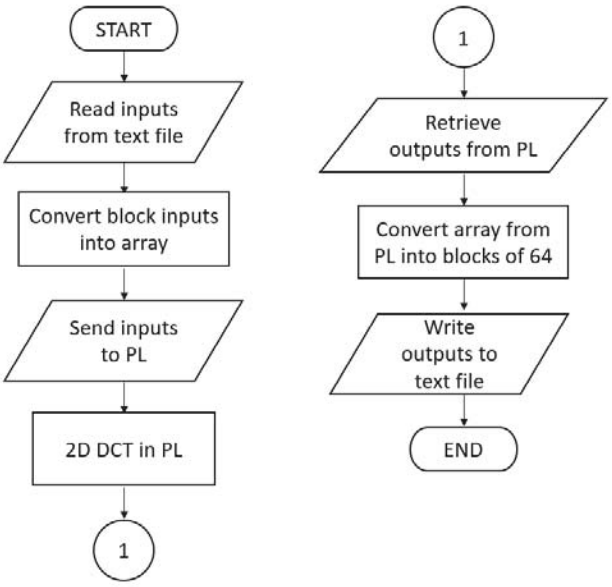

The host program is coded so that a unit of data is basically a block of 8x8 data which is compatible with the 8x8 DCT running inside the PL. This is very important as the output from the PS must be the same as the input for the PL and vice versa. It is to ensure the reliability and the functionality of the whole software-hardware co-designed program.

G. In-code Performance Profiling

In order to compare the performance between the software-hardware co-designed program and the full software designed program, a c program with exactly the same functions is written and compiled in the Xillinux environment.

In this work, in code performance profiling is used to ensure the accuracy of the result because an external profiler might cause a heavy load on the operating system. Therefore, to ensure an unbiased profiling, the timing interval must be logical.

Since both of the programs are having the same functionality, it is safe to put the profiling interval as the beginning of the main function and just before the main function ends. The resulting time taken for executions is then noted down for further analysis.

IV. Result and Analysis

Both of the full software program and software-hardware co-designed program are executed for different numbers of 8x8 blocks. Numbers of blocks are set to 100, 1000, 2000, 3000, 4000, 5000, 6000, 7000, 8000, 9000, 10000, 12000, 14000, 16000, 18000, 20000, 22000, 24000, 26000, 28000, 30000, 32000 and 34000 respectively. Each execution is repeated for at

least 100 times in order to obtain the average execution time for each number of blocks processed.

Since the Xillybus driver is using the on-board FIFO for the data transfer in between Processing System and Programmable Logic, the limitation of the co-designed program is at the 34000 blocks of 8x8 data. Feeding a single execution with more than 34000 blocks of data will result in overflow of FIFO and halting of Xillybus devices. However, on the other hand, for the full software designed program, there is no limitation on the number of blocks processed since it is using the caches and storage in the Processing System itself. If more than 34000 blocks of data are desired for the software-hardware co-designed program, the program can be rerun with different inputs.

The results are plotted in the graph as shown in Fig.6. Do note that the graph is not using constant scale for x-axis.

As shown by the graph, both programs show linear relationship between the number of blocks processed and the time taken to complete the given tasks. As the number of blocks increases, the time taken to complete the DCT of the blocks increases linearly.

Initially, when the number of blocks fed into the DCT for both programs are below 7500 blocks, the software-hardware co-designed program shows relatively slower performance up to 1 second difference than that of full software designed

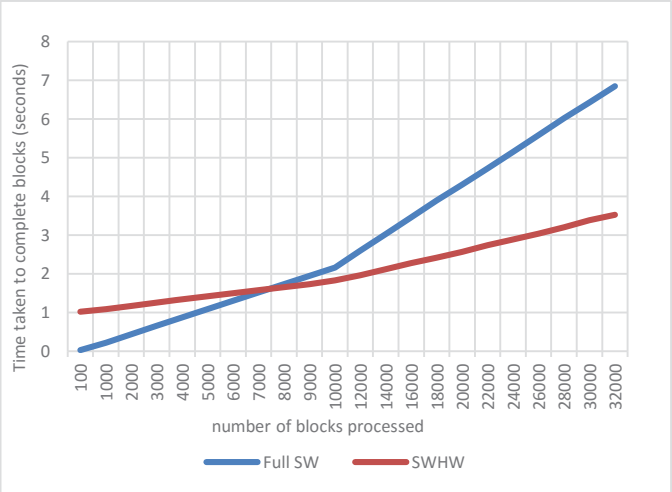

Fig. 6. Graph of time taken to execute DCT of 8x8 blocks against number of blocks processed

program. This is mainly due to the input/output (I/O) communication time is relatively large when handling small number of blocks. Besides, an idle function of 1 second is included in the co-designed program in order to prevent the Xillybus devices from stalling and it is necessary to keep the program functioning as expected.

However, both of the line graphs crosses over at approximately 7500 of blocks where the performance of co-designed program has caught up on the performance of software designed program. At this number of blocks processed, the time taken for I/O has become more insignificant compared to the performance of Programmable Logic.

Both line graphs continue to increase linearly with a constant gradient respectively after exceeding 7500 blocks of data processed. However, the performance difference between both programs is becoming bigger. The gradient of full software program execution time (0.213 milliseconds/block) is greater than that of software-hardware co-designed program (0.077 milliseconds/block). This means when the amount of input or blocks in this case increases, the advantage of using software-hardware co-design is becoming more significant.

Thus, from the result shown, software-hardware co-design is suitable for programs that deal with large amount of data. In this work, less than 7500 blocks of data are considered as small amount and the DCT design should be done just by using full software design.

However, nowadays with the advanced growing technology in image processing and cameras, even smartphone cameras are generally above 8 megapixels. This means JPEG encoder nowadays requires the capability to handle more than 125,000 blocks of data if a block contains 8x8 of pixels.

Fig. 7 illustrates clearly how the software-hardware co-designed program outperforms the full software designed program. The full software designed program shows a constant throughput of 0.3 megapixels per second despite the increase of pixels to be processed. However, the throughput of co-designed program increases linearly over the increase of pixels to be processed up to 0.58 megapixels/second at 2 megapixels. Fig. 7 also shows that the throughput of co-designed program outperforms that of full software designed program once the processed pixels exceed 480,000 pixels or 0.48 megapixels.

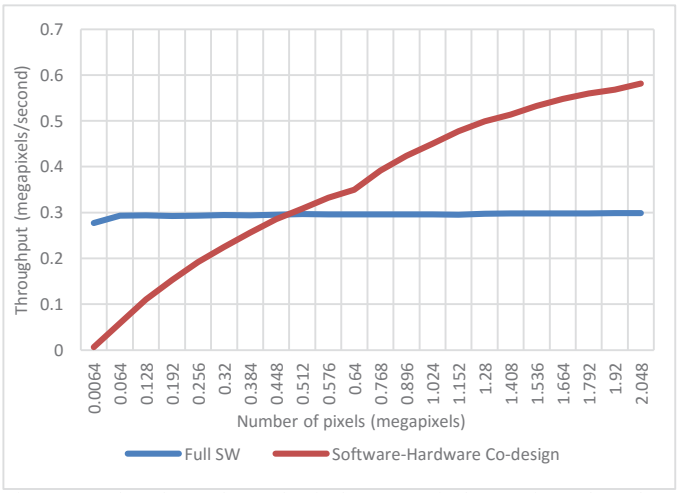

Fig. 7. Graph of number of pixels (megapixels) against throughput (megapixels/second)

Therefore, in other words, DCT of a modern JPEG encoder can be further improved by using software-hardware co-design implementation, due to large data processing.

V. Conclusion

In conclusion, DCT of a JPEG encoder can be greatly improved when implemented using software-hardware co-design simply because images produced and captured in this era easily exceed 7500 blocks of pixels or 0.48 megapixels. By using software-hardware co-design, the performance of DCT

can be improved significantly and the JPEG encoder can run at faster rate for larger image processing in bundles.

Software-hardware co-design inherits the benefits of both full software and full hardware implementations, which are great flexibility and great performance respectively. During the implementation, no HDL or Verilog code is required. The software-hardware co-designed program is fully developed using C programming language only, which provides a great flexibility in function declaration and memory allocation as well as debugging process. Only a little knowledge on sending data through the FIFO in between the PS and PL is required in the program development.

The result also shows that the performance of the software-hardware co-designed program is almost doubled the performance of full software program when it is running at its full capacity and capability.

The limitation of software-hardware co-design is that it is not suitable for small data processing as the time taken for I/O data transfer is significant when processing small amount of data. A faster bridge can be used in between the CPU and the FPGA but it can only reduce the I/O time taken but not totally eliminate it, not to mention increasing the cost of hardware design.

Another challenge for the engineer or programmer in general software-hardware co-design is the establishment of handshake and data transfer between the CPU and the FPGA. In this work, however, the challenge is overcome by using Xillinux which is a type of Linux distribution that contains Xillybus IP core drivers. Xillybus drivers is only available for Xilinx products and software-hardware co-design is made easy by the tutorials provided in the Xilinx and Xillybus official websites. For other System on Chips (SoC), engineer or designer requires knowledge in configuring the SoC itself in order to come out with a good software-hardware co-design which can have a performance ranging in between full software and full hardware design.

Further work of the software-hardware co-design will include but not limit to Artificial Intelligence (AI) applications and big data analysis. Both of the mentioned applications are processing hungry and usually deal with large amount of data. Weather forecast using AI is an example of intensive processing program. This is where the software-hardware co-design comes into its benefits. With the flexibility to maintain and debug, and the at the same time, greater performance than full software design, the productivity and reliability of the applications can be further improved.

REFERENCES

[1] E. Bezati, H. Yviquel, M. Raulet and M. Mattavelli, "A unified hardware/software co-synthesis solution for signal processing systems," Proceedings of the 2011 Conference on Design & Architectures for Signal & Image Processing (DASIP), Tampere, 2011, pp. 1-6.

[2] The International Telegraph and Telephone Consultative Committee (CCITT). “Information Technology – Digital Compression and Coding of Continuous-Tone Still Images - Requirements and Guidelines”. Rec. T.81, 1992.

[3] W. Pennebaker, J. Mitchell. JPEG Still Image Data Compression Standard, Van Nostrand Reinhold, USA, 1992.

[4] K. Sakiyama, P. R. Schaumont and I. M. Verbauwbede, "Finding the best system design flow for a high-speed JPEG encoder," Proceedings of the ASP-DAC Asia and South Pacific Design Automation Conference, 2003., 2003, pp. 577-578.

[5] Haines, R. F. and Chuang, S. L. The effects of video compression on acceptability of images for monitoring life sciences experiments. 1992.

[6] J. Miano. *Compressed Image File Formats* – JPEG, PNG, GIF, XBM, BMP, Addison Wesley Longman Inc, USA, 1999.

[7] D. F. Chiper, "A new VLSI algorithm for a high-throughput implementation of type IV DCT," 2016 International Conference on Communications (COMM), Bucharest, 2016, pp. 17-20.

[8] L. V. Agostini, I. S. Silva and S. Bampi, "Pipelined fast 2D DCT architecture for JPEG image compression," Symposium on Integrated Circuits and Systems Design, Pirenopolis, 2001, pp. 226-231.

[9] Y. Arai, T. Agui, M. Nakajima. “A Fast DCT-SQ Scheme for Images”. Transactions of IEICE, vol. E71, no. 11, 1988, pp. 1095-1 097.

[10] M. Kovac, N. Ranganathan. “JAGUAR: A Fully Pipeline VLSI Architecture for JPEG Image Compression Standard”. Proceedings of the IEEE, vol. 83, no. 2, 1995, pp. 247-258.

[11] V. Bhaskaran, K. Konstantinides. Image and Video Compression Standards Algorithms and Architectures – Second Edition, Kluwer Academic Publishers, USA, 1999.

[12] “ZedBoard Technical Specifications” Internet: http://zedboard.org/content/zynq-fpga-fabric-clock-speed, [May. 14, 2017]

[13] Xilinx. Zynq-7000 All Programmable SoC Overview, 2013.

[14] Hazarika, O. and Mishra, A. K. A Review of Hardware Platforms for Whitespace Communication. In: White Space Communication. Springer. 33–48. 2015.

[15] Lin, Z. and Chow, P. Zcluster: A zynq-based hadoop cluster. Field-Programmable Technology (FPT), 2013 International Conference on. IEEE. 2013. 450–453.

[16] Powell, A. and Silage, D. Statistical performance of the ARM cortex A9 accelerator coherency port in the xilinx zynq SoC for real-time applications, 2015.

[17] Sugimoto, N. and Amano, H. Hardware/software co-design architecture for Blokus Duo solver, 2014.

[18] Ohkawa, T., Yokota, T. and Ootsu, K. A prototyping system for hardware distributed objects with diversity of programming languages design and preliminary evaluation, 2013.

[19] Ahmed, K. E. and Farag, M. M. Hardware/software co-design of a dynamically configurable SHA-3 System-on-Chip (SoC), 2015.

[20] Fadzil, F. B. Signal Modulation Using Embedded Linux on Xilixn Zynq Progammable SoC, 2015.

[21] Preußer, T. B. and Spallek, R. G. Ready PCIe data streaming solutions for fpgas, 2014.

[22] “FPGA coprocessing for C/C++ programmers (part II)” Internet: http://xillybus.com/tutorials/vivado-hls-c-fpga-howto-2 [May. 14, 2017]

Sub-band Frequency Analysis of Brain Electrical Activity based on Graphic Rule

Nurul Aisyah Hiwani
Faculty of Electrical Engineering
Universiti Teknologi Malaysia
Johor Bahru, Malaysia.
aisyahhiwani@gmail.com

Norlaili Mat Safri
Department of Electronic and Computer Engineering
Faculty of Electrical Engineering
Universiti Teknologi Malaysia
Johor Bahru, Malaysia.
norlaili@utm.my

***Abstract*— This paper aims to design filter and transfer function based on sub-band frequency using MATLAB and investigate the sub-band frequency analysis of brain electrical activity based on preferred and non-preferred graphic rule. Two subjects which are preferred and non-preferred graphic rules were selected randomly. The raw data of EEG were used as case studies to analysis sub-band frequency in brain activity and the data was filtered using Butterworth filter according to sub-band frequency. Fast Fourier Transform (FFT) was done by using data of sub-band frequency to converts a signal from its original domain (often time or space) to frequency domain and vice versa. Fast Fourier Transform (FFT) also to determine the power content of the six sub-band frequency. Then, normalization was done to get normalized power in percentages from power spectrum density based on sub-band frequency in each channel of EEG. The result showed that preferred subject was better in recognize and plan shape before drawing during performing tracing and gazing tasks compared to non-preferred subject.**

Keywords— Handwriting; Electroencephalogram; Fast Fourier Transform; Graphic Rule; Sub-band Frequency; MATLAB

I. INTRODUCTION

Handwriting development begins at an early age[1]. Even though children start writing between three and four years of age, their handwriting progresses from irregular and unsteady to smooth and consistent when they are in pre-school and early elementary grades[1]. Handwriting is the process of writing that involves an activity using a pen or pencil on a paper by hand. It also determine the style of people's writing. Every people have different style and pattern of writing either good or bad. Without consistent exposure to handwriting, students can experience difficulty in a certain process of handwriting as commonly required for better achievement in reading and writing including retrieving letters from memory [2][3], reproducing letter on paper [2][3], spelling accurately [2], extracting meaning from text[4] and interpreting the context of words and phrases [3].

Handwriting can determine whether people follow graphic rule or not. Graphic rule planning includes identifying the first point or location to draw (starting rule) and deciding the sequence of strokes (progression rule)[5]. There are two types of graphic rule such as preferred graphic rule and non-preferred graphic rule. Starting at the top and then progressing downward or at the left and moving rightwards is known as non-preferred strategy[6]. On the other hand, starting at the bottom and moving upwards or at the right and moving leftwards is known as preferred graphic rule[6]. Furthermore, drawing is a simple step but the sequence of movement is different for each person. Children always tend to choose the simplest way by copying geometric shape. Firstly, they will visualize the shape of a geometric. Then, they will decide the sequences of stroke that demand less movement to complete the geometric shape. From drawing based on the graphic rule, brain activity can be determined by using Electroencephalogram (EEG). EEG also can show brain activity between preferred graphic rule and non-preferred graphic rule.

Electroencephalogram (EEG) is used to measure the electrical activity of brain. It is one of the first methods of non-invasively observing human brain activity. Generally, in normal persons, the brain waves were classified into six groups which were called in sub-band frequency such as delta, theta, alpha, beta, gamma and high gamma. Each frequency bands has different mental condition[7]. The Delta band frequency ranges between 0 and 4 Hz and they occur in deep sleep. The Theta band have frequencies between 4 and 8 Hz and they are related to the creativity and intuition. The Alpha band are rhythmic waves occurring at a frequency ranges between 8 and 13 Hz, which are found in all normal persons when they are awake in a quiet, resting state of cerebration[8]. The Beta band have a high frequency ranges between 13 and 31 Hz because the person was in active thinking state like doing problem solving. The Gamma band have higher frequency ranges between 31 and 51 Hz and the High Gamma band have the highest frequency ranges between 51 and 120 Hz and they occur in motor function like information processing and learning. Sub-band frequency was used to filtered EEG signal to analysis brain electrical activity based on preferred and non-preferred graphic rule by using Fast Fourier Transform (FFT).

Therefore, analysis was focused on determining transfer function of sub-band frequency using MATLAB and investigate the sub-band frequency analysis of brain electrical activity based on preferred and non-preferred graphic rule.

II. LITERATURE REVIEW

A. Brain activity

Brain is an important organ of the human central nervous system and is a highly complex organ. The brain controls virtually every functions of the human body[9]. The brain consists of three components which are cerebrum, cerebellum and brainstem. In cerebrum, there are four cerebral lobes such as frontal, parietal, temporal and occipital lobes as shown in Fig. 1 [10]. The frontal lobe generally controls planning, reasoning, movement, and some aspect of speech while parietal lobe processes touch and sensation information including pressure, pain and position of the body[9]. Then, the temporal lobe relates to hearing, speech perception and some kinds memory task and finally the occipital lobe processes and interpret visual sensory information[9]. From the regions of brain, the graphic and non-graphic rule follower during drawing task can be determined by using EEG. The EEG signal can be analyzed to determine the connections between each channels of brain based on sub-band frequency.

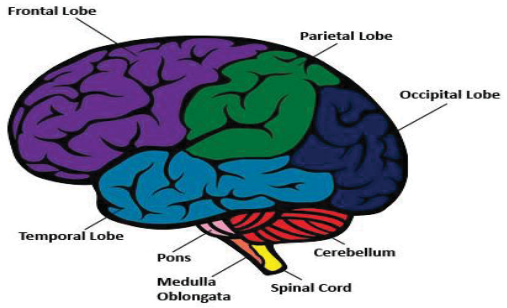

Fig. 1 Brain Regions [11]

B. Design filter of sub-band frequency

Signals may contain many frequency components. Some of them may be of interest like frequency bands of EEG rhythms; others like power line artifacts may be undesired[12]. To removed artifacts of signal filter was used. The characteristics of a filter such as the cut-off frequency, the amount of attenuation of the unwanted spectral components, steepness of the filter and the order of the transfer function. There are two types of filter such as FIR and IIR filters. Table II show functions for designing FIR filter and table III shows functions for designing IIR filter using MATLAB software[12].

TABLE II Functions for designing FIR filter

Type	Functions
fir1	Allow for design of classical low pass, band pass, high pass and band stop filters.
fir2	Allow specify arbitrary piecewise linear magnitude response.
firls	Allow specify arbitrary piecewise characteristics of magnitude response and minimizes the sum of squared errors between the desired and actual magnitude response based on algorithm.
firpm	Function implements the Parks-McClellan algorithm. It designs filters that minimize the maximum error between the desired frequency response and the actual frequency response.

TABLE III Functions for designing IIR filter

Type	Function
butter	Butterworth filter gives smooth and monotonic magnitude response function.
Cheby1	Designs Chebyshev Type I filter. These filters are equiripplein the passband and monotonic in the stopband.
Cheby2	Designs Chebyshev Type II filter. Filters are monotonic in the passband and equiripple in stopband.
ellip	Designs elliptic filter. Elliptic filters offer steeper rolloff characteristics than Butterworth or Chebyshev filters, but are equiripple in both passband and stopband.

C. Fast Fourier Transform (FFT)

Fast Fourier Transform (FFT) may be a potential tool to analyzed the neural signals, particularly the electrophysiological signals either on the scalp or from the deep brain implants. Theoretically, FFT show its application in cortical source estimation of the scalp human EEG data [13]. FFT method is very useful in analyzing the EEG data based on the types of brain waves. Besides, FFT is used to extract the statistical features from six different frequency bands such delta, theta, alpha, beta, gamma and high gamma band. The types of brain waves generated then can be further related to the certain mental condition of the subject when solving a task [14][15].

Fast Fourier Transform (FFT) is a mathematical procedures where transforming a signal from time domain to frequency domain. Discrete Fourier Transform (DFT) converts a finite sequence of equally-spaced samples of a function into an equivalent-length sequence of equally-spaced samples.

The continuous Fourier transform is defined as equation (1) [16]:

$$f(v) = F\iota[f(t)](v)$$

$$= \int_{-\infty}^{\infty} f(t)e^{-2\pi vit}dt \quad (1)$$

While Discrete and Inverse Fourier Transform is defined as equation (2) & (3) [16]:

$$Fn = \sum_{k=0}^{N-1} fk\, e^{-2\pi ink/N} \quad (2)$$

While for the inverse transform:

$$Fn = \frac{1}{N}\sum_{n=0}^{N-1} fn\, e^{2\pi ink/N} \quad (3)$$

where Fn is discrete–time signal with a period of N. The Fourier transform is operates in continuous function form. In EEG application, FFT is extremely important in extracting useful information from EEG signal based on the type of brain waves generated[7]. FFT also to determine the power content of the sub-band frequency.

III. METHODOLOGY

A. MATLAB Design

Firstly, to design the filter of sub-band frequency, a number of order and suitable filter need to be determined. The type of filter used is Butterworth digital filter. The reason of choosing Butterworth filter is because this filter gives smooth and monotonic magnitude response function. The roll off rate is faster than Bessel and Chebyshev [17]. Since this filter is frequency-based, the effect of filtering can be easily understood and predicted by referring to the cut off frequency, passband frequency or stopband frequency [17]. Practically, choosing a cut-off frequency is easier than estimating the error in raw data. However, as compared to the other frequency-based filter, Butterworth's pulse response is better than Chebyshev and its rate of attenuation is better than Bessel.

As we know, the design will not be complete without filter order. Second order filter was chosen because it was simple, small and are used extensively in many applications [18]. In second order filter, the roll off after the cut-off frequency on a bode plot is -40 dB/decade as opposed to -20 dB/decade for a first order filter which means it has significantly greater attenuation outside the pass band and a sharper cut-off[18]. Second-order filters may roll off at different rates initially depending on their Q factor, but approaching the same final rate of 12 dB per octave.

To design sub-band frequency, sampling frequency and cut off frequency for each sub-band need to be determined. During taking signal activity of brain the sampling frequency was 1000 Hz. The cut off frequency of sub-band frequency is shown in Table IV.

TABLE IV Cut off Frequency of Sub-Band Frequency[7]

EEG Frequency Bands	Cut off Frequency (Hz)
Delta	0-4
Theta	4-8
Beta	8-13
Alpha	13-31
Gamma	31-51
High Gamma	51-120

After cut off frequency for each sub-band was determined, filter was designed using MATLAB R2008a software. From the information that have been mentioned earlier, second order Butterworth filter was designed to get transfer function for each sub-band frequency.

B. Fast Fourier Transform (FFT)

The second part is plotting brain electrical activity based on sub-band frequency between the regions of brain by using FFT. FFT is used to determine the power content of the sub-band frequency. The resulting waveforms can be displayed as a brain map which will show the scalp distribution of the power within each frequency band[19].

From the filtered EEG data, the FFT was done by using MATLAB code such as Y=fft to get power spectral density based on sub-band frequency during gazing, tracing and control activities. This is because characteristics of the filtered EEG signal to be analyzed are computed by power spectral density (PSD) estimation in order to selectively represent the EEG samples signal [20]. However, six frequency bands contain the major characteristic waveforms of EEG spectrum.

Power spectral density was normalized from unit of power into percentages by using formula shown in equation (4) for delta bands. The similar methods is applied for other frequency bands as well. The data in percentages more easily to compare between control, gazing and tracing tasks.

$$EEG\ bands = \frac{\sum_{f=0Hz}^{4Hz} P(f)}{\sum_{f=0Hz}^{120Hz} P(f)} \times 100\% \quad (4)$$

Then, control task was comparing with gazing and tracing task at each regions of brain to get a significant different. Lastly, the final results will shows sub-band frequency analysis of brain electrical activity based on graphic rule.

IV. RESULT & DISCUSSION

Design filter based on sub-band frequency by using MATLAB has been done to get transfer function. The sub-band frequency are delta, theta, alpha, beta, gamma and high gamma. After that,, transfer function of sub-band frequency was used to obtain power spectral density by using FFT.

A. Transfer function of sub-band frequency

Second order Butterworth filter was used to design filter based on sub-band frequency. Then, second order Butterworth filter are simulated by using MATLAB and get the transfer function based on sub-band frequency from design filter. From transfer function of each sub-band frequency, input-output relationship can be determine as shown in Table V.

TABLE V Input-output relationship based on sub-band frequency

Sub-band	Input-Output Relationship
Delta	$y(n) = 0.0001551x(n) + 0.0003103x(n-1) + 0.0001551x(n-2) + 1.9645y(n-1) - 0.9651y(n-2)$
Theta	$y(n) = 0.0001551x(n) - 0.0003103x(n-2) + 0.0001551x(n-4) + 3.962y(n-1) - 5.889y(n-2) + 3.8922y(n-3) - 0.9651y(n-4)$
Alpha	$y(n) = 0.0002414x(n) - 0.0004827x(n-2) + 0.0002414x(n-4) + 3.9475y(n-1) - 5.8517y(n-2) + 3.8607y(n-3) - 0.9565y(n-4)$
Beta	$y(n) = 0.003x(n) - 0.0059x(n-2) + 0.003x(n-4) + 3.8098y(n-1) - 5.4744y(n-2) + 3.5166y(n-3) - 0.8522y(n-4)$
Gamma	$y(n) = 0.0036x(n) - 0.0072x(n-2) + 0.0036x(n-4) + 3.7039y(n-1) - 5.2586y(n-2) + 3.3883y(n-3) - 0.8372y(n-4)$
High Gamma	$y(n) = 0.0357x(n) - 0.0713x(n-2) + 0.0357x(n-4) + 2.9905y(n-1) - 3.6756y(n-2) + 2.1846y(n-3) - 0.542y(n-4)$

B. *Fast Fourier Transform (FFT)*

FFT analysis to determine the power content of the six sub-band frequency. This method can be done by using MATLAB where power spectral density of sub-band frequency can be determined. The FFT was done between preferred and non-preferred graphic rule. Fig. 2 shows Preferred graphic rule during control, gaze and trace tasks while Fig. 3 shows Non-preferred graphic rule during control, gaze and trace tasks.

Fig. 2 and Fig. 3 shows that there are significant differences of power spectrum for all frequency bands during controlling, gazing and tracing tasks for EEG channels that are related to the subjects performance based on graphic rules.

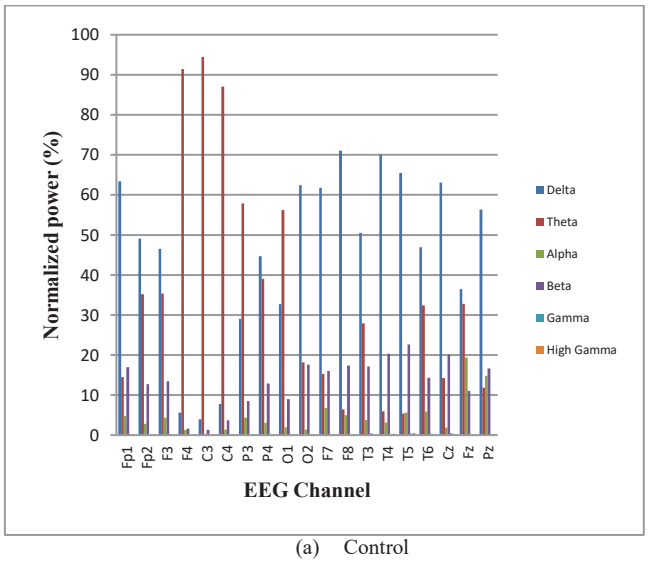

(a) Control

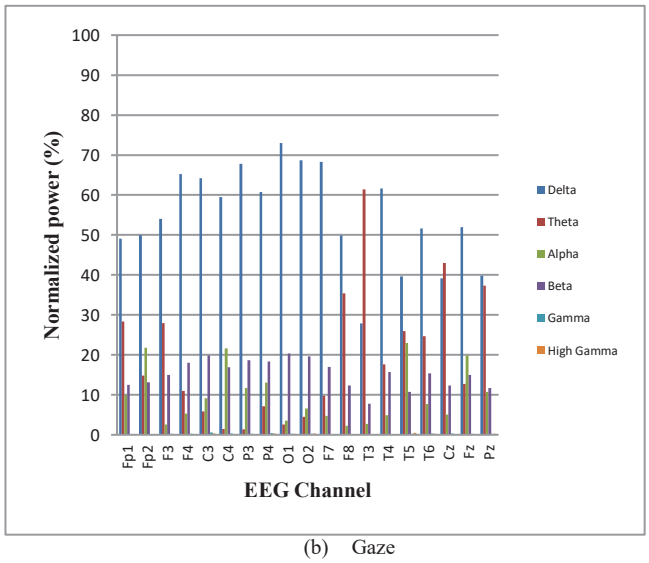

(b) Gaze

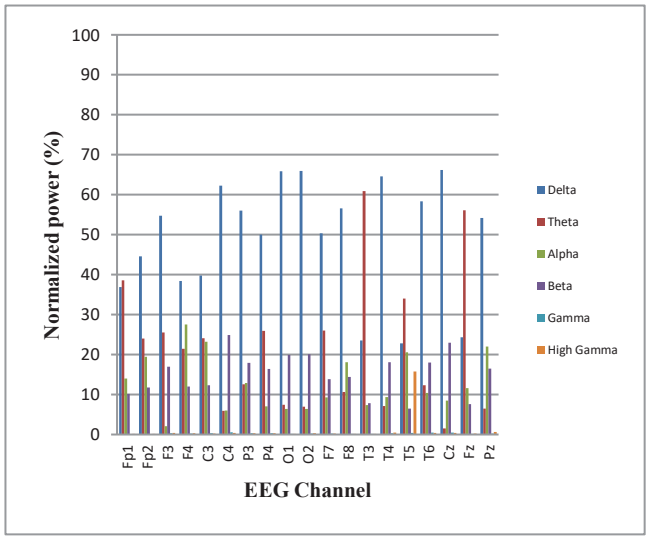

(c)Trace

Fig. 2 Preferred graphic rule during (a) control,(b) gaze and (c) trace task

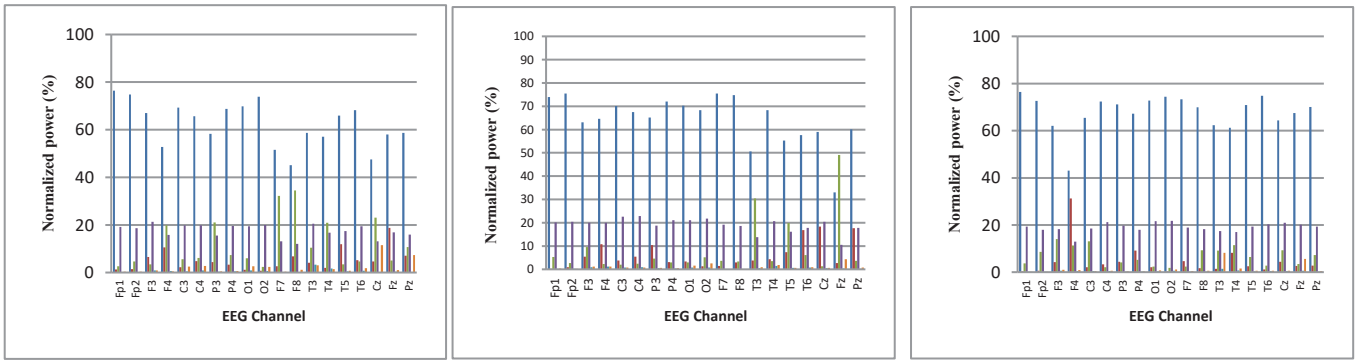

(a) Control (b) Gaze (c) Trace

Fig. 3 Non-Preferred graphic rule during (a) control, (b) gaze and (c) trace task

The significant differences of EEG frequency bands were varied between control task with gaze and trace tasks based on graphic rule as shown in Fig. 4 and Fig. 5.

The control task (preferred graphic rule) showed better performance in tracing task compared to the control task (non-preferred graphic rule) as it shows higher high gamma at T5 that corresponded to higher motor function where it can recognize shape before drawing. Meanwhile, it also shows higher alpha at C3 where it is responsible for motor control to plan shape.

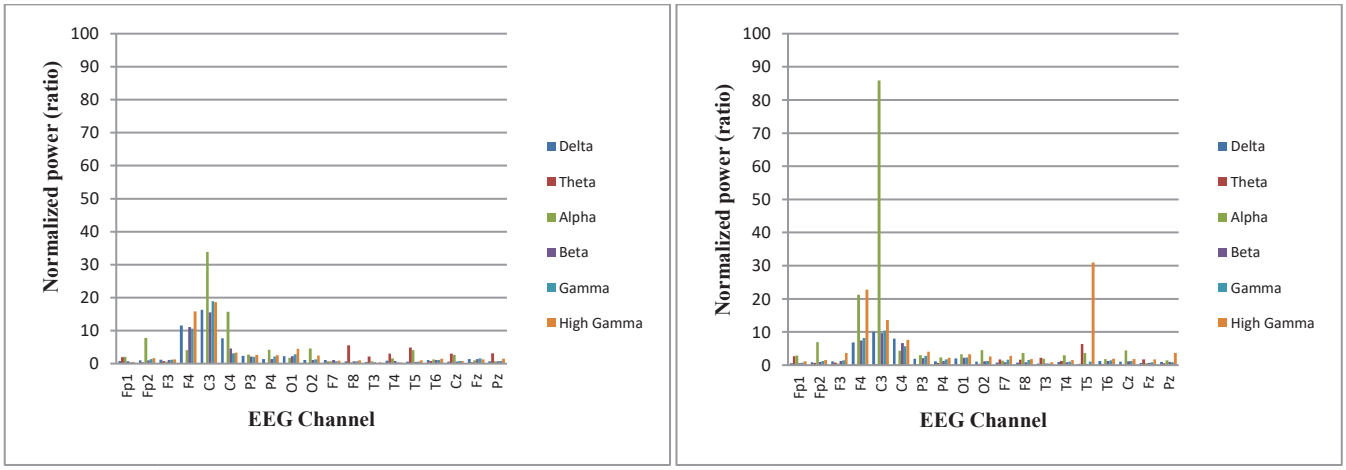

(a) Control-Gaze Tasks (b) Control- Trace Tasks

Fig. 4 Preferred graphic rule during (a) Control-Gaze Tasks and (b) Control- Trace Tasks

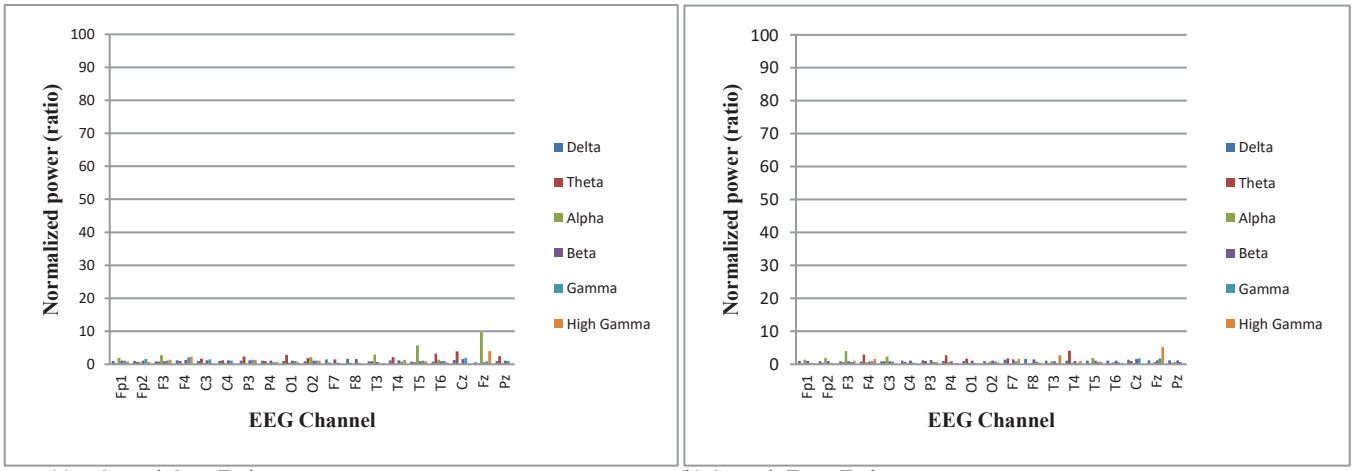

(a) Control-Gaze Tasks (b) Control- Trace Tasks

Fig. 5 Non- Preferred graphic rule during (a) Control-Gaze Tasks and (b) Control- Trace Tasks

V. CONCLUSION

In conclusion, the first objective of sub-band frequency analysis of brain electrical activity based on preferred and non-preferred graphic rule was successfully implemented. Filter based on each sub-band frequency was successfully designed using MATLAB. From the design filter, transfer function for each sub-band frequency were determined. The second objective to analysis significant differences of power spectral sub-band frequency using FFT were determined. The most significant parameter in differentiating both groups was founded during tracing task and the parameter involved was at central area C3 and temporal area T5. Therefore, preferred subject were better in recognize and plan shape before drawing during performing tracing and gazing tasks compared to non-preferred subject.

REFERENCES

[1] P. I. Khalid, J. Yunus and R.Adnan 2010. Extraction of Dynamic Features from Hand Drawn Data for the identification of children with Handwriting Difficulty, Research in Development Disabilities. 31:256-262.

[2] Berninger, V. (2012). Evidence-Based, Developmentally Appropriate Writing Skills K–5: Teaching the Orthographic Loop of Working Memory to Write Letters So Developing Writers Can Spell Words and Express Ideas. In Handwriting in the 21st century : An Educational Summit. Washington, D.C.

[3] Case-Smith, J. (2012). Benefits of an OT/Teacher Model for First Grade Handwriting Instruction. In Summit, A. E. (Ed.). Handwriting in the 21st century. Washington, D.C.

[4] Peverly, S. (2012). The Relationship of Transcription Speed and Other Cognitive Variables to Note-Taking and Test Performance. In A. E. Summit ((Ed.). Handwriting in the 21st century. Washington, D.C

[5] S. Hashim, N. M. Safri, P. I. Khalid, M. A. Othman and J. Yunus, "Differences in Cortico-cortical functional connections between children with good and poor handwriting: A case study," IEEE Region 10 Symposium, pp 34-38,2014.

[6] Khalid, P. I., Yunus, J., and Adnan, R. (2010). Extraction of Dynamic Features from Hand Drawn Data for the Identification of Children with Handwriting Difficulty. Research in Development Disabilities, 31(1), 256–262.

[7] H. Z. Kosnan et al. Characterization of young children with preferred and non-preferred graphic rule during drawing, Jurnal Teknologi (Sciences & Engineering) 78:7-5(2016) 89-96.

[8] M. M. Shaker. 2007. EEG waves classifier using wavelet transform and Fourier Transform. International Journal of Medical, Health, Biomedical, Bioengineering and Pharmaceutical Engineering Vol:1. No:3,2007.

[9] R. M. Rangayyan (2015). Biomedical Signal Analysis, 2nd Edition ; John Wiley & Sons, Inc. chapter 1.

[10] Ross and Wilson (2011). Anatomy and Physiology in Health and Illness, 11th Edition; Churchill Livingstone Elsevier. 148-151.

[11] Brain Injury Association of America.(2013). Living with brain injury. Retrieved from Brain Injury Association of America website: http://www.biausa.org/living-with-brain-injury.htm, [Accessed October 19, 2016]

[12] K. J. Blinowska; J. Zygierewicz, Practical Biomedical Signal Analysis Using Matlab, 1st ed; CRC Press Taylor & Francis Group: Broken Sound Parkway NW, Suite 300 Boca Raton,2012; pp. 25-27, 95-97

[13] Majumdar, K. (2009). Fourier Uniformity : An Useful Tool for Analyzing EEG Signals with An Application to Source Localization. Proceedingd of the 2009 International Joint Conference on Neural Networks (IJCNN), 14-19 Jun. Atlanta, Georgia, USA: IEEE, 1-5

[14] Adeli, H., Zhou, Z., and Dadmehr, N. (2003). Analysis of EEG Records in an Epileptic Patient Using Wavelet Transform. Journal Neuroscience Methods, 123(1), 69–87.

[15] Subasi, A., and Gursoy, M. I. (2010). Expert Systems with Applications EEG Signal Classification Using PCA, ICA, LDA and Support Vector Machines. Expert Systems With Applications, 37(12), 8659–8666.

[16] P. Bourke (1993). "Discrete Fourier Transform & Fast Fourier Transform." Retrieved from Paul Bourke website: http://paulbourke.net/miscellaneous/dft/, [Accessed May 9, 2017]

[17] Butterworth Filter.(2015, January 6). Retrieved from Electronic Hub website:http://www.electronicshub.org/butterworth-filter/#Butterworth_Filter, [Accessed October 10, 2016]

[18] Electronic Tutorials. Second order filter. Retrieved from Electronic Tutorials website: http://www.electronics-tutorials.ws/filter/second-order-filters.html, [Accessed October 5, 2016]

[19] Smith, E.J. Introduction to EEG. Retrieved from ebme Biomedical and Clinical Engineering Websites: http://www.ebme.co.uk/articles/clinical-engineering/56-introduction-to-eeg , [Accessed May 5, 2017]

[20] Amjed S. Al-Fahoum and Ausilah A. Al-Fraihat, "Methods of EEG Signal Features Extraction Using Linear Analysis in Frequency and Time-Frequency Domains," ISRN Neuroscience, vol. 2014, Article ID 730218, 7 pages, 2014. doi:10.1155/2014/730218

Rehabilitation Monitoring Device for Knee Osteoathritis

Nur Amirah binti Ishak
Faculty of Electrical Engineering
Universiti Teknologi Malaysia
Johor Bahru, Malaysia.
amirahishak94@yahoo.com

Dr. Mitra binti Mohd Addi
Department of Electronics and Computer Engineering
Faculty of Electrical Engineering
Universiti Teknologi Malaysia
Johor Bahru, Malaysia.
mitra@fke.utm.my

Abstract— **Osteoarthritis is a diseases that happen when joints is damaged. The treatment to reduce the pain is by having the rehabilitation exercises. By having the monitoring system of rehabilitation exercises at home, it will help patient to do the correct posture of exercises and give feedback immediately if they do a wrong posture. In this project, MPU6050 is used to get the raw data of motion from body. This sensor will be put on two different location which are on thigh and ankle in order to get the raw data by doing two types of rehabilitation exercises recommended by physician. Then, these raw data will be translate into degree and process it by using the Arduino to make classification of exercise and detection of improper movement of exercises. The accuracy for classification of exercises for SAE is 100% while for SLR is 60%. For improper identification accuracy for SAE is 87% and for SLR , the raising angle not approximately 45^{o} shows highest accuracy while the hip joint external rotation shows lowest accuracy. The algorithm used can be implemented for classification of exercises and detection of improper movement of exercises.**

Keywords— Osteoarthritis; Arduino; MPU6050; Straight Leg Exercises; Short Arc Exercise

I. INTRODUCTION

Osteoarthritis (OA) or known as degenerative arthritis is a joint disease due to the loss of cartilage that causes pain and movement disability. It is a long term disease that usually happens to adult from the age of 30 to 65 years old and above. In Malaysia, 9.3% of adults complained to have knee pain where 23% were those 55 years and above and 39% were adults at 65 years and above[1, 2]. Based on a study that involves random body x-ray samples of adults, 50% were found to be between the age of 55-64 years old and 83% were males while 87% are females[3]. Although there is no proven cure for OA, several treatments are available to reduce pain in OA patients [4] such as cortisone injection, hot and cold therapies and joint replacement surgery. The safest and efficient treatment for knee OA patients is the appropriate physical activities prescribed by specialist and conducted regularly. It is found that low impact exercises have several benefits which include reduce pain reduction, improvement of knee function and increase in strength and mobility of joints[4-7]. If the physical exercises are conducted regularly and correctly, it will help in reducing pain and may avoid patients to undergo knee replacement surgery[4]. A research by Thomas K. *et al.* reported that 76% of patients who completed a home-exercise program has shown significant decrease in pain and increase function of joint mobility[8]. The Joint Mobility Centre, Hospital for surgery, Arthritis Foundation, suggested several exercises which are prescribed by specialists for knee OA patients. These include Short Arc Exercise (SAE) and Straight Leg Raise (SLR) .These exercises were found to be able to help knee OA patients in strengthening the affected knee, quadriceps muscle, hamstring and buttocks. Although exercise is essential for OA patients, generally the awareness among patients is low. Rehabilitation exercises are normally conducted in the hospital and monitored by specialists. Each patient will be prescribed with several appropriate sets of exercises and may use different equipment which are readily at the hospitals. However, most of the equipment for the rehabilitation exercise are sophisticated, expensive and are suitable for general types of exercise. Thus, the utilization of these equipment are only limited to a group of patients as it is not customize for different levels of OA severity [6, 9]. An alternative to that is the introduction of conducting rehabilitation exercises at home. However, the issue is that they are not able to get immediate feedback on the right exercise postures since they are not monitored by specialist [10]. Incorrect exercise postures may increase stress to injured part of the knee and slow down the recovery progress[4]. At the same time, the monitoring system that available are costly and using the complicated algorithm. To address the issues mentioned about home rehabilitation exercise for OA patients, a low cost monitoring system for rehabilitation exercises of knee OA is proposed using our own algorithm and process it by using the Arduino. For the system, we will analyze the accuracy of the algorithm to make classification of exercises and to detect the improper step of exercises. The proposed monitoring system is designed to ensure patients are conducting the correct exercise posture and to avoid further injuries.

II. LITERATURE REVIEW

A. Recommendation of Self Management of Knee OA

Generally, physical activity recognition is important to help patients manage the proper exercises and triggered the recovery process [11, 12]. A good recognition method will help increase the accuracy of the physical activity movements and enable the

access the performance of the severity of OA. There have several recommendations that can be used to improve quality of life for knee OA patients since this diseases have not cure but it can be reduced by designed a good management.

B. Wearable Sensor and Wireless Communication

Usually, the accelerometer used will be built in one nodes sensor consist of accelerometer, wireless communication to communicate with other node sensor and microcontroller to process the data and make classify. Taylor et al.[13] used wireless body sensor that includes tri-axial accelerometer and microelectromechanical. Karantonis et al. [10] used Wireless TA unit that consist of dual axis accelerometer, microcontroller Texas Instrument (2KB of RAM) and the wireless communication use Zigbee compliant transceiver modules. These system have problem with microcontroller which is the memory is only 2KB where it is unable to process the data more 3 s. This paper has suggest the improvement that the system need high memory to process the data. Figure 2.1 shows that how the system illustrated. The microcontroller is used to perform the processing data from triaxial accelerometer and information is transfer to receiver unit then forwarded to computer for display and analysis.

C. Sensor Location

Karantonis et al.[10] used the data extract from a tri-axial accelerometer located on hip to classify the type of human movement in real time. Their system are able to differentiate between periods and rest of activity, detecting the events of walking and fall to an appropriate degree of angle, recognizing the orientation of body posture and measure the metabolic energy expenditure. Taylor et al. [13] used tri-axis accelerometer at five different location on the body which are both thigh and shank of leg and on the waist. This system is to classify the quality of exercises by included the algorithm to differentiate the type of exercises and incorrect exercises. They perform three kinds of exercise which are standing hamstring curl (SHC) , reverse hip abduction (RHA) and lying straight leg raise (SLR).

D. Algorithm for Feature Extraction and Classifier

For classifier, based on Fahrenberg J. et al.[14], to classify the activities, they used Hierarchical method. Hierarchical method is the decisions made at each node based on constructed manually by user. It is made at each node based on input, manual assessment and analysis of the training numbers. At each node, it is generates a final result or move to another node where further decision is made. They extract the data from accelerometers that put on the thigh, chest, shank and wrist to get time domain features but they found that the method unable to differentiate between stair walking and level walking. The Bayesian method is one of the algorithm to classify the activity. It is approach based on the probabilities of signal features available from each class. It can measure the probability of new pattern of activity come from specific activity. Foerster et al.[15] used K-nearest neighbor for recognize the activities. K-nearest neighbor is a multi-dimensional feature space. Each dimension have different feature. Firstly, each point represents a specific activity and testing data point will be classified by identified training data which correspond to a given activity. The value of K typically ranges from 1 to a small percentage of the training data and is selected using trial and error. The data will be extracted to get time domain features from accelerometer and classify the activity using K-nearest neighbor. They proposed also to make combination of K-neighbor method and Hierarchical method to make differentiate wider range of physical activities. The decision tree method is similar to Hierarchical method but it is method to process and create a complex of rules

III. PROJECT METHODOLGY

In this project , it consists of two parts to be implemented which are hardware part which is consist of two sensors of MPU6050, Arduino Uno as microcontroller and LED as indicator of improper movement of exercises. While another part is software implementation where the algorithm of classification of type of exercise and incorrect movement of exercise are programmed inside the microcontroller.

A. Hardware Setup

The hardware setup (see Figure 3.1) consists of two sensors of MPU6050, Arduino UNO as a microcontroller and LED is used as indicator to show the improper movement of two exercises. The sensor module are includes an accelerometer and a gyroscope to acquire motion data from the body's movement. The accelerometer is used to measure the inclination of human body, acceleration, gravity as well as angle of flexion of bending motion. Whereas the gyroscope is used to extract the information about body orientation. The combination of these sensors is to increase the accuracy of the data collection. Two (2) sensors will be placed at two different location on the body which are thigh and shank (see Figure 3.2). The subject will do two types of exercises which are Short Arc Exercise (SAE) and Straight Leg Exercise(SLR).

Fig. 1. Hardware setup for the system.

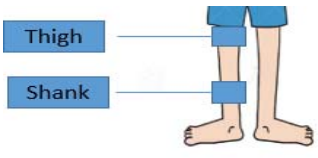

Fig. 2. Sensor's Location

B. Software System

Arduino UNO is used as a microcontroller to process the raw data from MPU6050 for classification of exercises and detection of improper movement of exercises. We used software Arduino IDE to implement the C language programming

C. Equations

MPU6050 consists of three axes which are x , y and z axis for accelerometer and gyroscope and the output of the sensor are acceleration and rotation distance per time . To translate these information into degree, we will calculate the tilt angles for both accelerometer by using equation (1-3) . After that the data was filtered by using Complementary filter. To get the filtered angled the equation (4) is used.

$$p = \tan^{-1}\left(\frac{Ax}{\sqrt{(Ay^2+Az^2)}}\right) \quad (1)$$

$$\Psi = \tan^{-1}\left(\frac{Ay}{\sqrt{(Ax^2+Az^2)}}\right) \quad (2)$$

$$\Theta = \tan^{-1}\left(\frac{Az}{\sqrt{(Ax^2+Ay^2)}}\right) \quad (3)$$

where p is the tilt angle of x-axis and the ground, Ψ is the tilt angle between y-axis and the ground while Θ is the tilt angles x ,y and z axis and the ground.

Filtered Angle (4)
$=\alpha*(\text{Gyroscope angle}) + (1- \alpha)* (\text{Accelerometer tilt angle})$

Where $\alpha = T/(T+\Delta t)$ and Gyroscope angle = Last Measured Filtered Angle + $\omega*\Delta t$
Δt is sampling rate which is about 0.04 s, T is time constant greater than timescale of typical accelerometer noise about 1 s and giving $\alpha \approx 0.96$

D. Algorithm.

For this system, we create the algorithm by using the flow chart (see figure 3) which are for the classification and the detection for improper exercises. For sensor 1 that put on the shank is labelled as S1 while for sensor 2 that located on thigh is labelled as S2. For each exercise, we labeled the incorrect posture as recommended by physician (see table 1). We programmed the system to detect the improper movement of exercise.

TABLE I. LABELING FOR IMPROPER MOVEMENT OF EXERCISE.

Exercises	Label	Threshold °
SAE	Initial knee flexion > 25 °	7
	Knee not fully extended	7
SLR	Knee not fully extended	20
	Hip joint external rotation	20
	Raise angle not approximately 45 °	10

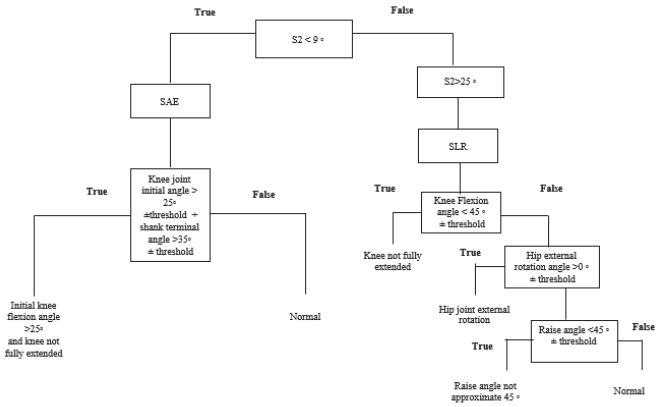

Fig. 3. Flow chart of system

IV. RESULT AND ANALYSIS

For this project, the accuracy of classification of exercises, the labeling for improper movement exercises and the average angle for each labeling was determined. Excel 2013 is used to plot the graph acquired from the serial monitor of Arduino for further analysis.

A. Accuracy of classification of exercises and improper movement of exercises

LED is used as indicator for classification of exercises and detection of improper movement. To determine the accuracy of the classification of exercises, the subject will perform the exercise for one set for ten times. We set the table (see table 2) to determine the classification of exercise based on LED. LED 1 as indicator for exercise SAE while LED 3 as indicator for exercise SLR.

TABLE II. CLASSIFICATION OF EXERCISE BASED ON LED.

LED	REPETITION									
	1	2	3	4	5	6	7	8	9	10
1	/	/	/	/	/	/	/	/	/	/
3	/	/	/	/	X	X	X	X	/	/

As we can conclude, for classification of exercises, for SAE , the accuracy is 100% while for SLR, the accuracy is 60%. We can compared with decision three method [16] for SAE is 96.58% which is low than the algorithm used for this project. While decision three method for SLR is 95.94% which is quite high than the algorithm used. This is because for SLR exercise, it is difficult to differentiate the sensor put in the thigh by using the Arduino.

For accuracy of improper movement of exercises, each subject need to perform three set for each exercises and need to repeat it about ten times. Table 3 shows the marking for LED. If the LED is ON, the graph (see figure 4) should be out of the range so we can consider it as accuracy. For labeling , LED 2 as initial knee flexion angle and knee not fully extended in SAE, LED 4 as knee not fully extended, LED 5 as hip joint external rotation and LED 6 as raise angle not approximately 45° in SLR.

TABLE III. MARKING LED FOR SLR

LED	REPETITION									
	1	2	3	4	5	6	7	8	9	10
4		/	/				/			
5							/	/	/	/
6	/	/	/	/	/	/	/	/	/	/

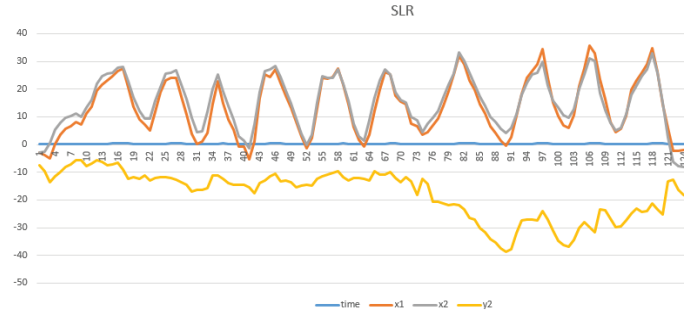

Fig. 4. Graph for SLR to detect the improper movement of exercises

As we can see for cycle 3, the LED 4 is ON but the graph is not approach 25° yet. So we need reject the marking because they are not tally. Same as in cycle 7, LED 4 is off but the graph shows that, it should be ON since it in the allowable range which is 25° to 65°. For the first set, the accuracy of knee flexion angle not fully extended is 33.3%, for second set is 100% and last set is 100%. For improper labeling of hip joint external rotation, the accuracy for the first set is 75%, second set is 0% and last set is 16.7%. For labeling of raise angle not approximate 45°, for first set is 90%, second set is 100% and last set is 88.9%. For SAE exercise, the accuracy of initial knee flexion angle and not fully extended is 100% .We can compare for hierarchical method [16] for the improper identification accuracy for SAE is 87%. For our project, the algorithm used for SAE is quite good as we used one sensor to detect the angle for this exercise. But for SLR, we can see the variation of the accuracy. In table 3 for labeling of raising angle not approximately 45° , the subject is tend to do this improper movement because it depends on their effort to achieve the allowable range which is 35° to 55°. Their accuracy mostly high. But for second labeling in SLR which is hip joint external rotation, the accuracy is low. This is because, the sensor used which is MPU6050 is sensitive and it is hard to handle. At the same time, this is wired system that might disturb the movement and also the result.

B. *Average angle for each labeling of improper movement of exercise.*

To get the average angle of improper movement of exercises from the graph shows in figure 5, the maximum peak for each cycle is subtracted to minimum peak for each cycle and these will be divided by 10. The summation for each result is the average angle for each improper movement of exercises.

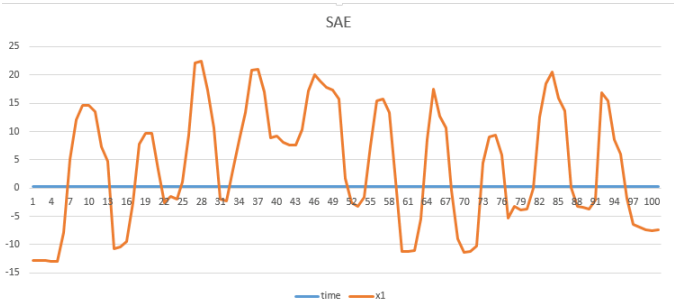

Fig. 5. Graph for SAE to detect the improper movement of exercises

For SAE, the average angle for initial knee flexion angle and knee not fully extended is 21.9° which is in the allowable range of 18° to 67°. For SLR, the average angle for knee flexion angle is 27.2° , hip joint rotational angle is 8.8° and the raise angle not approximately 45° is 25.6°.

V. CONCLUSION

From the paper that we have read, the method for classification of exercise and the detection of improper movement of exercises is complicated. At the same time, the tools used are quite expensive. So by having this system with this algorithm, it is easy to be implemented. The accuracy is acceptable when compared to other method. For recommendation in the future, we can add the wireless system to replace the wired.

REFERENCES

[1] K., V., Osteoarthritis – Asian Perspective. In Howe HS, Feng PH eds. Textbook of Clinical Rheumatology. Singapore National Arthritis Foundation, 1997: p. pp 294-95.

[2] K., V., Epidemiology of Rheumatic Diseases in Malaysia. In Nasution AR, Darwawan J, Isbagio H eds. Proceedings of the 7th APLAR Congress of Rheumatology, 1992: p. pp 397-399.

[3] Keefe, F.J., et al., Osteoarthritic knee pain: a behavioral analysis. Pain, 1987. 28(3): p. 309-321.

[4] O'Reilly, S.C., K.R. Muir, and M. Doherty, Effectiveness of home exercise on pain and disability from osteoarthritis of the knee: a randomised controlled trial. Annals of the Rheumatic Diseases, 1999. 58(1): p. 15-19.

[5] Talbot, L.A., et al., A Home-Based Pedometer-Driven Walking Program to Increase Physical Activity in Older Adults with Osteoarthritis of the Knee: A Preliminary Study. Journal of the American Geriatrics Society, 2003. 51(3): p. 387-392.

[6] Deyle, G.D., et al., Effectiveness of manual physical therapy and exercise in osteoarthritis of the knee: a randomized, controlled trial. Annals of internal medicine, 2000. 132(3): p. 173-181.

[7] McAlindon, T., et al., Determinants of disability in osteoarthritis of the knee. Annals of the rheumatic diseases, 1993. 52(4): p. 258-262.

[8] Thomas, K., et al., Home based exercise programme for knee pain and knee osteoarthritis: randomised controlled trial. Bmj, 2002. 325(7367): p.752.

[9] Fisher, N.M., et al., Muscle rehabilitation: its effect on muscular and functional performance of patients with knee osteoarthritis. Arch Phys Med Rehabil, 1991. 72(6): p. 367-374.

[10] Karantonis, D.M., et al., Implementation of a real-time human movement classifier using a triaxial accelerometer for ambulatory monitoring. IEEE transactions on information technology in biomedicine, 2006. 10(1): p. 156-167.

[11] Mathie, M.J., et al., Accelerometry: providing an integrated, practical method for long-term, ambulatory monitoring of human movement. Physiological measurement, 2004. 25(2): p. R1.

[12] Preece, S.J., et al., Activity identification using body-mounted sensors—a review of classification techniques. Physiological measurement, 2009. 30(4): p. R1.

[13] Taylor, P.E., et al. Classifying human motion quality for knee osteoarthritis using accelerometers. in 2010 Annual International Conference of the IEEE Engineering in Medicine and Biology. 2010. IEEE.

[14] Fahrenberg, J., et al., Assessment of posture and motion by multichannel piezoresistive accelerometer recordings. Psychophysiology, 1997. 34(5): p. 607-612.

[15] Foerster, F., M. Smeja, and J. Fahrenberg, Detection of posture and motion by accelerometry: a validation study in ambulatory monitoring. Computers in Human Behavior, 1999. 15(5): p. 571-583.

[16] Chen, K.-H., et al., *Wearable sensor-based rehabilitation exercise assessment for knee osteoarthritis.* Sensors, 2015. **15**(2): p. 4193-4211.

Network Processing Multi-Processor System-on-Chip on Field Programmable Gate Array

Yiew Kah Yee, Alireza Monemi and Muhammad Nadzir Marsono
Faculty of Electrical Engineering,
Universiti Teknologi Malaysia,
81310 UTM Johor Bahru,
Johor Darul Takzim,
Malaysia.

***Abstract*—Growing network speed and the emergence of more network applications have created greater demand for more flexible and faster network processing system. Programmable multi-processor system-on-chip (MPSoC) based network processing platform is a viable solution. In this paper, an MPSoC based network processors is developed using ProNoC MPSoC platform and implemented on Altera De2-115 FPGA board. Case studies of network intrusion detection system will then be carried out on the network processing platform to evaluate its performance. The network processing platform implementation on FPGA shows that the platform is able to handle network application from Open System Interconnection level 2 and above. Firewall and malware signature matching applications implemented on the network processors show that signature matching is very processing intensive and become bottleneck to the system.**

Keywords—network processing; MPSoC; ProNoC; FPGA; network intrusion detection.

I. INTRODUCTION

Network traffic is expected to increase in both volume and velocity as more new network applications emerge [1,2,3]. Hence, networking system need to forward packets at high speed among large number of networks as well as providing and maintaining huge amount of network services. Thus, there are needs for faster and flexible network system to address fast changing technology, increasing customer needs and faster time-to-market [3]. Flexible network system imply that the system configuration can be done in short amount of time, thus ease the system design process and reduce time-to-market.

It became extremely difficult to develop Application Specific Integrated Circuit (ASIC) solutions as the networking tasks involved processing of thousands of packets for different tasks [6]. Thus, ASIC solutions become less viable. Therefore, network processors emerged as new technology to provide a better solution [3,4]. Network processors is an Application-Specific Instruction Processor (ASIP) designed for networking application [3,4]. Most current network processors are built as programmable MPSoC to exploit parallelism and multi-processing in handling data packets [5,11]. As network processors is not faster than ASIC and is harder to be programmed, developing network processing system on reconfigurable platform could provide correct trade off in between performance, flexibility, time-to-market and development time [6,7].

This paper proposes implementation of MPSoC based network processors on Altera DE2-115 FPGA board using ProNoC MPSoC platform [23]. ProNoC MPSoC platform plays a very important role in developing the hardware and software for this implementation. It provides complete and modular MPSoC design environment that have high level of abstraction to the underlying components interconnection. This platform is able to handle Open System Interconnection (OSI) Layer 2 and above. Case studies consist of firewall and Network Intrusion Detection System (NIDS) are then implemented on the MPSoC network processing platform.

The rest of the paper is organized as follow. Section Ⅱ reviews several criteria of network processing tasks. Section Ⅲ discusses about FPGA based network processing platform and related works. Section Ⅳ presents the ProNoC MPSoC platform and the proposed design of network processors. The experiment results are provided in section Ⅴ and the paper is concluded in section Ⅵ.

II. NETWORK PROCESSING TASKS

Network processing is the key technology that enable data communication and networking at higher speed and higher bandwidth. While travelling from node to node, network packets undergo both packet-based processing or flow-based processing. Packet-based processing is mainly used to retrieve and extract useful content in a packet. Flow-based processing is used to control and reorder the sequences of packets that flow through data stream [8,9,11].

Network processing task can be further divided into three categories which are basic, byte manipulation and control-flow intensive [5]. Basic processing tasks involve common packets processing that is necessary for a network to function properly such as medium access control (MAC) addressing, switching and routing of packets. On the other hand, byte-manipulation processing tasks involve transformation of bytes in network packets for certain network applications such as cryptography and compression. Control-flow intensive processing tasks are the most computational intensive tasks. These inspect and analyze packets for intensive classification and searching. This

task typically involves operations such as NIDS, firewall and control-based networking [5,10].

For effective network processing, several network processing tasks are required to run independently, which can be made as task-parallel. Task-level parallelism can be achieved by running several tasks simultaneously. In network application that consist of three-phase network processing task such as NIDS, coarse-grain synchronization is preferred due to its simplicity [56]. The network packets are processed in parallel, and have to go through three phases of capturing, reassembling and detecting.

III. FPGA IN NETWORK PROCESSING

FPGA implementations provide scalable and flexible computational solution suitable for network processing application tasks that have inconsistent data access and control flow [12]. The flexibility of FPGA enables rapid prototype of parallelism into network processing system to harness the parallelism available in network packets processing tasks. This enables increases in the throughput and processing capability of network processors with short development time [12]. In addition, the freedom of partitioning and allocating FPGA resources enable hardware accelerators or softcore processor to be incorporated into any design. In fact, 40% of FPGA sales are from communication industry [12].

A. Reconfigurable MPSoC for Network Processing

Most network processors available on market currently are MPSoC [4]. Reconfigurable MPSoC consist of multiple softcore processors, memories and peripheral components connected together with bus network on FPGA [14,15,16,17]. Each of these softcore processors are general-purpose processors that are programmable using high level language. Therefore, this reduces the complexity in adjusting network processing functions. Besides, different number of softcore processors can be plugged into reconfigurable MPSoC to provide greater assistance in exploiting system parallelism. Without considering the effect of inter-processor communication, MPSoC design on FPGA is constrained only by logic element sizes and memory.

Reconfigurability of FPGA provides scalability and flexibility when designing MPSoC hardware. Thus, the number of processing elements required for MPSoC design could be adjusted depending on the needs of task-level parallelism for an application. By having more than one processing unit, MPSoC is able to carry out multiple tasks at any time to achieve better performance. This makes MPSoC as an ideal candidate to execute loop-intensive embedded application and bandwidth-demanding applications.

There are actually various tools available to transform high level language into hardware description language [20,21,31,42]. This enables fast hardware realization of network processing algorithm. However, this usually lead to creation of huge amount of states and produce bulky circuit; hence making it not suitable for high speed network processing application [5,42].

B. Related Works

Various researches have been carried out to improve network processing using FPGA. The research consists of developments of network processing hardware accelerators and also development of software-based network processing approaches on FPGA. Table 1 shows the list of previous works of hardware implementation on network processing.

TABLE I. PREVIOUS WORKS OF HARDWARE IMPLEMENTATIONS FOR NETWORK PROCESSING

Author	FPGA Platform	Network Processing Applications
Singaraju and Chandy [34]	Xilinx Virtex-II Pro	String matching hardware accelerator for network processing.
Muhlbach and Koch [35]	Xilinx Virtex 5	NetStage, self-adaptable FPGA Platform for application-level network security.
Muhlbach and Koch [36]	NetFPGA 10G	NetStage demonstrated as hardware honeypot
Rajan and Harish [37]	Xilinx Virtex-7	FPGA based hardware Honeypot for malware collection with stateful TCP implementation.
Proudfoot et al. [39]	Amirix AP1100 FPGA	Network intrusion detection system with string matching hardware accelerator.
Clark et al. [40]	Xilinx Virtex-1000	Pattern-matching hardware accelerator with rule mapped from Snort.

Software-based network processing approaches involve the development of programmable network processors by using softcore processors on FPGA. This enables the implementation of software packet processing using high level language (5,11,28). Among the prior researches, a similar open source network processing MPSoC platform known as NetThread is available to develop FPGA based MPSoC network processors [11,12,26,28]. Table Ⅱ shows a list of previous implementations of network processors with softcore processors on FPGA.

TABLE II. PREVIOUS WORK OF NETWORK PROCESSORS ON FPGA

Author	FPGA Platform	Softcore Processor	Related Works
Labrecque et al. [11]	NetFPGA	MicroBlaze	NetThread, multicore network processors and parallel packet processing
Labrecque et al. [12]	Altera Stratix FPGA	MicroBlaze	NetThread, Design and evaluate real FPGA multiprocessor systems.
Kekai [23]	Altera DE4 board	Plasma	Multicore network processors security platform,
Byma et al. [28]	NetFPGA-10G	MicroBlaze	NetThread, multicore network processors and deep packet inspection
Kachris et al. [29]	Xilinx Virtex II Pro	MicroBlaze	Dual core network processors, multi-services router
Herkersdorf et al. [30]	Xilinx Virtex-II Pro	PowerPC	Multicore network processors
Sadoun [32]	Xilinx Virtex 5	MicroBlaze	Multicore network processors for DNS/DNSSEC authoritative server

Besides, implementation of NIDS such as firewall, malware signature matching and honeypot have been carried out to evaluate the functionality and performance of network processing function on FPGA [11,28,36,39]. String matching function in NIDS is very computationally intensive and various algorithm has also been developed to reduce the processing time of string matching. These include Brute Force algorithm, Boyer-Moore algorithm, Rabin-Karp algorithm [43,44,45,46,47].

IV. Network Processing on ProNoC MPSoC Platform

Prototype-NoC (ProNoC) is an electronic design automation (EDA) tool used for building custom heterogenous NoC-based MPSoC [23]. It provides plug-and-play and modular interface in generating complete MPSoC RTL code. The MPSoC is created using customizable processing elements and peripheral components [23]. This helps to greatly reduce development time of MPSoC.

A. ProNoC MPSoC System

ProNoC MPSoC system are built by connecting processing tiles (PTs) that consist of customizable set of intellectual properties (IPs). These processing tiles are connected with network-on-chip (NoC) as shown in Figure 1. The NoC in ProNoC is a two-clock cycle wormhole VC-based NoC router [23]. This enable parallelism in communication between processing element which does not exist in conventional bus interface and thus, improves intercommunication bandwidth [23,24,25].

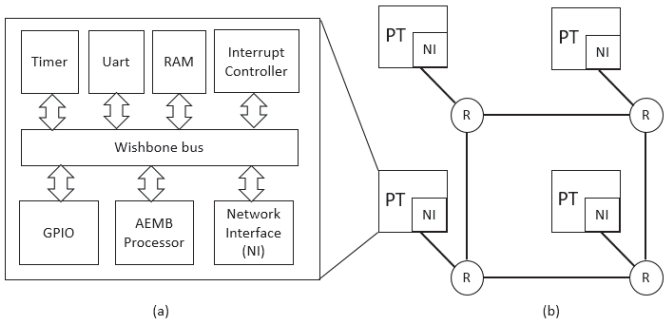

Fig. 1. ProNoC functional block diagram(a) Processing Tile (PT) , (b) MPSoC [23]

B. Network Processing MPSoC

On top of the PTs, network intrusion detection applications for simple firewall and malware signature detection are implemented in software to test the functionality and performance of the network processing system.

1) *Hardware Design:* Network processors hardware design are based on heterogenous MPSoC architecture. Two different PTs (master tile and slave tile) are built with a combination of IP components that are available in ProNoC. The IP components consist of AEMB softcore processor [48], Ethernet MAC 10/100 Mbps controller [49], Altera JTAG UART, timer, interrupt controller, Wishbone bus and network interface. As shown in Figure 2, master tile has the additional Ethernet MAC 10/100 Mbps controller.

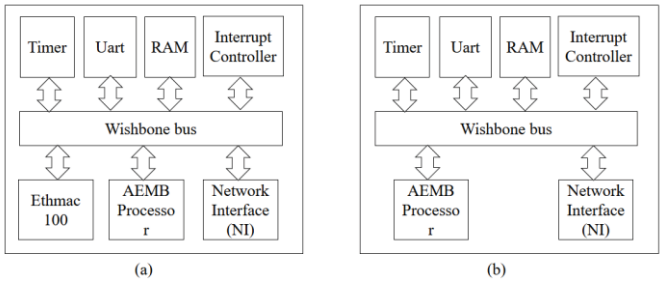

Fig. 2. Processing tile block diagram (a) Master tile, (b) Slave tile

As shown in Figure 3,a combination of one master tile and three slave tiles are connected with NoC routers through network interface to form a quad-core MPSoC. This arrangement is based on consideration of the network processing tasks to be carried out by the MPSoC as shown in Figure 4.

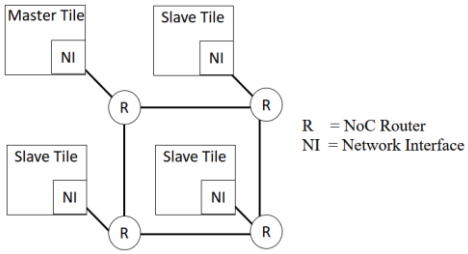

Fig. 3. Heterogenous MPSoC block diagram

C. Task Distribution and Data Flow

On top of MPSoC network processors hardware, basic NIDS is implemented. The task for each tile and the data flow of Ethernet packets are shown in Figure 4. The master tile receives ethernet packets and pre-process the packets into header and payload sub-packets. Ethernet packet header is transferred to tile 0 and packet payload will be transferred to tile 1 and tile2 alternately.

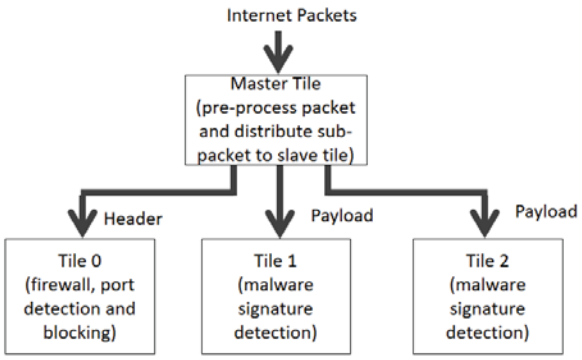

Fig. 4. MPSoC task distribution and data flow

D. Software Design

The master tile is programmed to service Ethernet MAC interrupt service routine (ISR) when an ethernet packet is received. As shown in Figure 5, the ISR will pre-process and distribute packets to slave tiles.

In contrary, tile 0 perform port detection function as a firewall as shown in Figure 6. On the other hand, tile 1 and tile 2 receive payload alternately and carry out malware signature detection function. Malware signature involves implementation of string matching over a series of malware signature. The list of blocked port and malware signatures are obtained from open source Snort community rules [51] and also malware signature extracted from Snort [52].

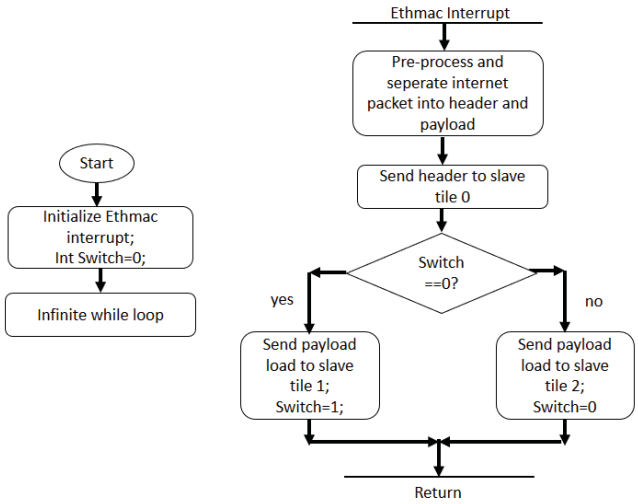

Fig. 5. Program flow chart of master tile

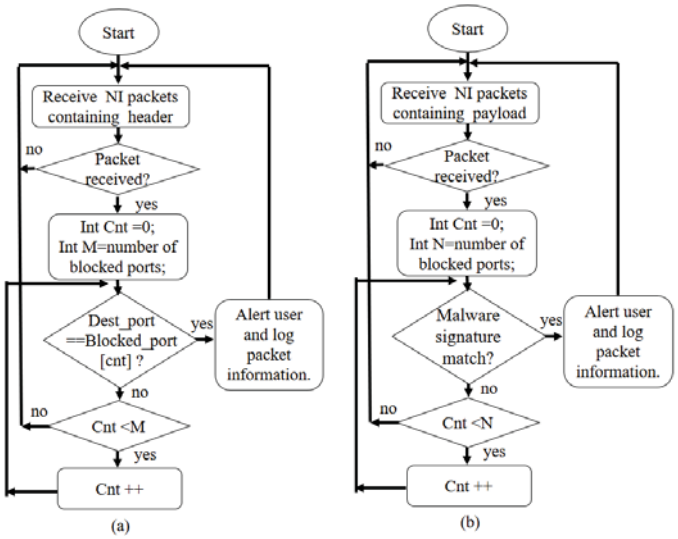

Fig. 6. Programming flow chart of (a) tile 0 with firewall function , (b) tile 1 and tile 2 with malware signature matching function.

E. *Methodology for Functionality and Performance Evaluation*

To test the functionality of the system, a PCAP (packet capture) file that consists of a series of malware packets is injected into the system using TCPreplay tool [53]. The malware exploits Windows Local Security Authority Subsystem Service (LSASS) on several ports and try to download ssms.exe file from an ftp [54]. The network processing system would alert server on this exploit based on the port and signature of the malware.

The performance of the system is characterized over increasing number of ports and malware signatures. Two string matching algorithms which are Boyer-Moore algorithm, Rabin-Karp algorithm are also investigated.

Random packets loss of different size and sequences will cause discrepancy in the performance throughput measurement. Hence, to improve result accuracy, the PCAP file used in evaluating system performance consist of only one TCP packet with constant size of 1514 bytes. The injection rate is fixed at constant rate of 1000 packet per second (pps). Improved accuracy is also observed in our simulation by taking an average of five result repetition. In addition, the processing speed of the system is calculated by dividing accumulated packet bytes and time recorded by timer hardware as shown in Figure 7.

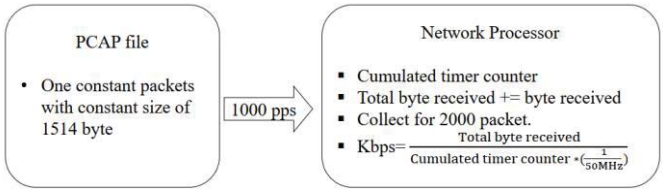

Fig. 7. Performance evaluation of system

V. RESULT AND DISCUSSION

A. *Hardware Implementation and Functionality Analysis*

TABLE III. HARDWARD IMPLEMENTATION ANALYSIS

Development board	Altera DE2-115
Device	Cyclone IV E EP4CE115F29C8
Total logic element	18,280/114,480 (16%)
Total combination functions	17513/114,480 (15%)
Dedicated logic registers	9462 /114,480 (8%)
Total registers	9501
Total memory bits	636,800/3,981,312 (16%)
Operating frequency	50Mhz
Maximum operating frequency	111.73Mhz

With malware PCAP injected for functionality test, the system is able to recognize the LSASS attack at port 455 with signature 0x90909090.

B. *Performance Characterizition with Increasing Number of Malware Signatures (Boyer-Moore Algorithm)*

The performance of Boyer-Moore signature matching drop exponentially from 16.3 pps to 2.7 pps as number of signatures increase.

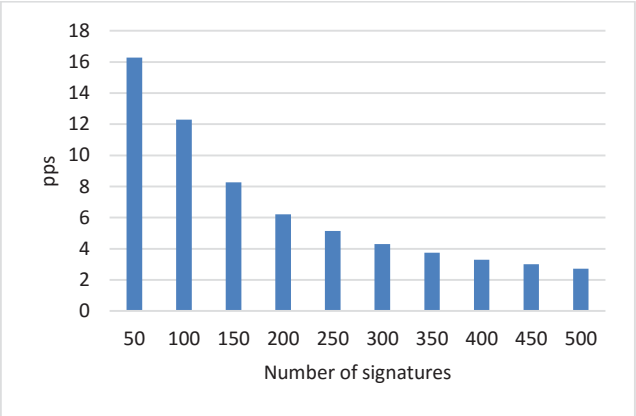

Fig. 8. Graph of packet per second (pps) against number of signatures detection

C. *Performance Characterizition with Increasing Number of Malware Signatures (Rabin-Karp Algorithm)*

Rabin-Karp signature matching performance is slower compare to Boyer-Moore signature matching. The performance drop exponentially from 2.7 pps to 0.3 pps as number of signatures increase. This is because Rabin-Karp hashing of character array into integer array before carrying out pattern searching of integer array. Additional hashing function and larger data comparison of 32-bit integer array instead of 8-bit character array incur heavy overhead in network processing.

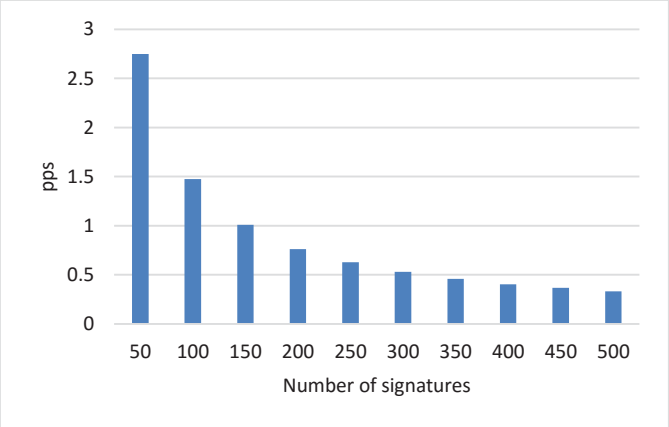

Fig. 9. Graph of packet per second(pps) against number of signature detection

D. *Performance Characterizition with Increasing Number of Port Blocked*

The performance shows minor changes as number of ports detection increases. Port detection involves only matching of 2 bytes per port as compared to signature matching that involve searching hundred of bytes. Thus, processing time of port detection is insignificant as compare to signature matching. Hence, signature matching is the bottleneck of this NIDS system.

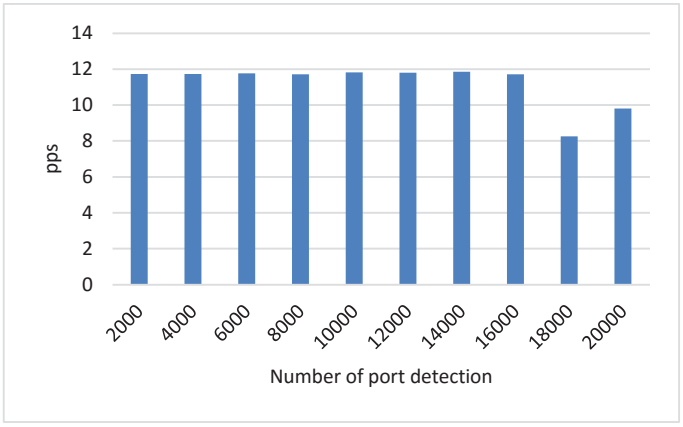

Fig. 10. Graph of packet per second(pps) against number of port detection

VI. Conclusion

Networks processing platform developed is able to handle application from OSI level 2 and beyond. The development time of the system is greatly reduced by utilising ProNoC EDA tool. On top of the network processors, a firewall and malware signature detection are implemented. The results show that ProNoC MPSoC platform is suitable in developing FPGA based MPSoC network processors. Malware signature matching is found to be very processing intensive and become bottleneck to the system.

In future works, shared memory between processing tiles will be incorporated into the network processing platform to reduce intercommunication overhead. Besides, implementation of this platform on NetFPGA development board which has larger logic size, memories and supports will also be attempted.

References

[1] Cisco Visual Networking Index (2016). The Zettabyte Era: Trends and Analysis. Retrieved from http://www.cisco.com.

[2] Q. Li, H. Niu, A. Papathanassiou and G. Wu (2014). 5G Network Capacity: Key Elements and Technologies. Vehicular Technology Magazine, IEEE, vol. 9, no. 1, pp. 71–78, March 2014.

[3] M. Ahmadi& S. Wong. (2017). Network Processors: Challenges and Trends.Electrical Engineering,Mathematics and Computer Science Department, Delft University of Technology.

[4] R. Giladi. (2008). Network Processors: Architecture, Programming, and Implementation. Morgan Kautmann.

[5] M. Labrecque (2011). Overlay Architectures for FPGA-Based Software Packet Processing (Published Thesis).

[6] D. Comer (2004). Network Processors: Programmable Technology for Building Network Systems. The Internet Protocol Journal - Volume 7, Number 4, December 2004 pages 2-12.

[7] X. Nie, U. Norvviqst, L. Gazsi, and D. Liu (2004) Network Processors for Access Network Trends and Chalenges. Proceeding IEEE, 2004.

[8] Jupiter Network (2016). Flow-Based and Packet-BasedProcessing Library for Security Devices. Retrieve from http://www.juniper.net.

[9] D. H. Cuong et al. (2006). Flow-based forwarding scheme and performance analysis in mobile IPv6 networks.2006 8th International Conference Advanced Communication Technology, Phoenix Park, pp. 6.

[10] Carzaniga and A. L. Wolf (2001). Content-based networking: A new communication infrastructure," in NSF Workshop on an Infrastructure for Mobile and Wireless Systems, pp. 59–68.

[11] H. Kristian (2016). Performance Analysis of Packet Processing Systems. (Published Master Thesis).

[12] M. Labrecque et al. (2009). NetThreads: Programming NetFPGA with threaded software. In: NetFPGA Developers Workshop.

[13] M. Labrecque, P. Yiannacouras and J. G. Steffan (2008).Scaling Soft Processor Systems. 2008 16th International Symposium on Field-Programmable Custom Computing Machines, Palo Alto, CA,pp. 195-205.

[14] Taho Dorta et al. (2010). Reconfigurable Multiprocessor Systems: A Review. International Journal of Reconfigurable Computing.

[15] S. Ben Othman et Al. (2012). MPSoC design approach of FPGA-based controller for induction motor drive. 2012 IEEE International Conference on Industrial Technology, Athens, pp. 134-139.

[16] W. M. José (2009). Multiprocessor system in an FPGA. International Conference on Reconfigurable Computing and FPGA's, pp.273-278.

[17] B. G. Shivaraja et al. (2015). A Survey Approach - Multiprocessing on FPGA using Light Weight Processor. International Journal of Innovative Research in Electrical, Electrical, Electronics, Instrumentation and Control Engineering, Vol 3, Issue 3.

[18] A. Bouajila (2012)A low-overhead monitoring ring interconnect for MPSoC parameter optimization," 2012 IEEE 15th International Symposium on Design and Diagnostics of .Electronic Circuits & Systems (DDECS), Tallinn, 2012, pp. 46-49.

[19] S. V. Tota (2009). A Case Study for NoC-Based Homogeneous MPSoC Architectures. IEEE TRANSACTIONS ON VERY LARGE SCALE INTEGRATION (VLSI) SYSTEMS, VOL. 17.

[20] P. Cotret et al. (2012). Self-configuration of latency-efficient security enhancements for MPSoC communications monitoring. Retrieved from https://pascalcotret.files.wordpress.com

[21] A. Rashed (2016). Review of FPD'S Languages, Compilers, Interpreters and Tools.International Journal of Novel Research in Computer Science and Software Engineering.

[22] D. Luke (2014). A Survey of High Level Synthesis Languages, Tools, and Compilers for Reconfigurable High Performance Computing. Springer International Publishing Switzerland.

[23] Alireza Monemi (2016) Low latency Network-On-Chip for Many-Core System-On-Chip Prototyping on Field Programmable Gate Array (Published Thesis).

[24] H. Kekai (2015). Securing Network Processors with Hardware Monitors. (Publish Thesis).

[25] A. Ehliar and D. Liu (2007). An FPGA Based Open Source Network-on-Chip Architecture.2007 International Conference on Field Programmable Logic and Applications, Amsterdam, pp. 800-803.

[26] V. Veeraprathap, M. Nagaraja and M. Z. Kurian (2013). Network on chip design and implementation on FPGA with advanced hardware and networking functionalities. Fourth International Conference on Computing, Communications and Networking Technologies, pp. 1-6.

[27] M. Labrecque (2013) NetThreads. Retrieve from https://github.com/NetFPGA/

[28] J. Fu (2006). Design and Evaluation of Network Processor Systems and Forwarding Applications (Publish Thesis).

[29] S. Byma et al. (2013). Netthreads-10g: Software packet processing on netfpga-10g in a virtualized networking environment demonstration abstract. In Field Programmable Logic and Applications (FPL), 2013 23rd International Conference.

[30] C. Kachris et al. (2007). Design and performance evaluation of an adaptive FPGA for network applications.Microelectronics Journal.

[31] A. Herkersdorf et al. (2005). FlexPath NP: a network processor concept with application-driven flexible processing paths. 2005 Third IEEE/ACM/IFIP International Conference on Hardware/Software Codesign and System Synthesis (CODES+ISSS'05), Jersey City, NJ, USA, 2005, pp. 279-284.

[32] R. K. Eric (2005). Programming Model for Network Processing on FPGA (publish thesis).

[33] M. Labrecque (2006). Towards a Compilation Infrastructure for Network Processors (Publish Thesis).

[34] R. Sadoun (2011). An FPGA based soft multiprocessor for dns/dnssec authoritative server. Microprocess. Microsyst., vol. 35, no. 5, pp. 473–483,Jul. 2011.

[35] J. Singaraju and J.A. Chandy (2008). FPGA based string matching for network processing applications. Microprocess. Microsyst page 210–222.

[36] S. Muhlbach and A. Koch (2011). NetStage/DPR: A Self-adaptable FPGA Platform for Application-Level Network Security.Proceedings of the 7th International Symposium on Applied Reconfigurable Computing. Springer, LNCS,2011.

[37] S. Mühlbach and A. Koch (2014). A Reconfigurable Platform and Programming Tools for High-Level Network Applications Demonstrated as a Hardware Honeypot. IEEE Journal on Selected Areas in Communications, vol. 32, no. 10, pp. 1919-1932, Oct. 2014.

[38] S. Rajan and R. D. S. Harish (2016). FPGA Based Honeypot with Stateful TCP Emulation for SMTP Malware Collection.

[39] H. C. Young et al. (2002). Specialized Hardware for Deep Network Packet Filtering.12th Conference on Field Programmable Logic and Applications.

[40] R. Proudfoot et al. (2008). Flexible Software-Hardware Network Intrusion Detection System. 2008 The 19th IEEE/IFIP International Symposium on Rapid System Prototyping, Monterey, CA, pp. 182-188.

[41] C. Clark et al. (2004). A hardware platform for network intrusion detection and prevention. In: Proceedings of the 3rd Workshop on Network Processors and Applications .

[42] S. Ioannis (2004). Efficient and High-Speed FPGA-based String Matching for Packet Inspection (Published Thesis).

[43] E. Casseau et al. (2005) .C-based rapid prototyping for digital signal processing. in Proc. of the 13th European Signal Processing Conference (EUSIPCO), Antalya,Turkey.

[44] Y. Weinsberg (2006) High performance string matching algorithm for a network intrusion prevention system (nips). High Performance Switching and Routing (HPSR06)

[45] J. Harbola. (2014). An Examination of Network Intrusion Detection System Tools and Algorithms: A Review. International Journal of Computer Applications.

[46] L. D. Nguyen (2016). A New Multiple-Pattern Matching Algorithm for the Network Intrusion Detection System. IACSIT International Journal of Engineering and Technology, Vol. 8, No. 2.

[47] V. K. Pachghare and P. Kulkarni (2008). Network Security Based On Pattern Matching: An Overview. IJCSNS International Journal of Computer Science and Network Security, VOL.8 No.10.

[48] B. Raju and B. Srinivas (2012). Network Intrusion Detection System Using KMP Pattern Matching Algorithm. International Journal of Computer Science and Telecommunications Volume 3, Issue 1.

[49] S. Tan (2009). AEMB Softcore. Retrieved from https://opencores.org/project,aemb.

[50] M. Igor et al. (2012). Ethermac MAC 10/100Mbps. Retrieved from https://opencores.org/project,ethmac.

[51] R. Friend (2004). Making the gigabit IPSec VPN architecture secure. Computer, 2004. 37(6): 54–60.

[52] Snort community rules. Retrieve from https://www.snort.org/downloads.

[53] I. Ismahani , M. N. Marsono and M. N. Sulaiman (2014). Malware detection using augmented naive Bayes with domain knowledge and under presence of class noise.International Journal of Information and Computer Security, pp 179-197.

[54] D. Angelo (2010). Forensic Challenge 2010 – pcap attack trace. Retrieve from https://www.honeynet.org/node/504.

[55] W. Jonathan (2004). Exploiting the LSASS Buffer Overflow. SANS Institute.

[56] C. C. Minh et al. (2008). STAMP: Stanford transactional applications for multi-processing. IISWC '08: Proceedings of The IEEE International Symposium on Workload Characterization, September 2008.

Energy Harvesting of Vibrational Input using Piezo Generator to Sustain Electricity

Farah Amira Binti Hamdan, Suhana Mohamed Sultan
Faculty of Electrical Engineering
Universiti Teknologi Malaysia, Skudai.
farahamirahamdan@gmail.com

***Abstract* – Daily energy created or consumed either direct or indirectly is actually can be extracted to create another form of energy. The process was called as energy harvesting or energy scavenging. Advantages of energy harvesting is the sustainability and low cost instalment. In this study, vibrational input from piezo-generator plates was harvested through a simple rectifying circuit. The output from the circuit was fed into a DC-DC booster which require 3.5V minimum and 1A minimum. Multisim simulation was conducted to simulate the working mechanism of the intermediate circuit. Results show high potential in harvesting the vibrational inputs to a useful energy.**

Keywords—energy harvesting, storage, circuit interface, vibration, piezo generator.

I. INTRODUCTION

Energy sources such as mechanical vibrations, temperature vibrations and wind vibrations can be converted and stored for energy harvesting [1]. These sources are non-renewable potential for energy generation. However energy harvesting using piezo analogous signal produces small signals in the range of 1 to 4 volt only in 4 minutes time. Input generated. Therefore, it is essential to design a suitable technique to harvest energy from piezo plates. Extended life of electronic devices is very important, In this work, a simple circuit is proposed to connect the input from the piezo plate to the basic small signal circuit rectifier which will undergo an AC to DC conversion. The idea is to make the project independent from any external power supply.

The target is to create a rechargeable energy storage in an enclosed product. Since the input can only generate small signal input in range of 4V minimum and 6V maximum, therefore an energy booster of DC-DC converter using LM2596 will be part of the project. This booster will upgrade value of the current and the voltage parameters suitable with required demand of the appliances with the potential switch provided.

II. PIEZO GENERATOR

Piezo can be classified as two types; one is piezoelectric, and another one is piezoresistive. This project using the piezoelectric effect because the piezoelectric material generates voltage under pressure or vibration. Unlike the piezoresistive, the component effects involves pressure or stress, however it produces changes in resistance across the piezo material, not charge or voltage. According to Chasalani S. (2008) [5] piezoelectric materials has a wide variety usage either for actuating, sensing or harvesting In this work, 4 units of piezo generator were used to scavenging the sources. The piezo plates were soldered in series in order to accumulate the energy collected.

Details study for the piezoelectric materials were not included in the scope work, because the main intention is to convert the vibrational energy on the piezo surface to an electrical energy.

III. METHODOLOGY

A. Capacitor

Capacitors are generally known as a component that stored electricity much like a small rechargeable battery [3]. Energy stored in a capacitor is basically the electric field produced between the plates with certain distance.

$$E = \frac{V}{d} \qquad (1)$$

Eq. (1) state that V is the voltage, E is the electric field and d is the distance. By this relationship, if the distance is narrower, electric field obtained will be greater. Hence, to create a greater the electric field, the two capacitor plates need to be closer to one another.

The structure of a capacitor consist of two metal plate with parallel separate and air, vacuum or any other dielectric materials in the middle of the two plates. The energy was delivered from a battery or some other power sources to move

electrons to one of the plate and away from one another. This phenomenon makes one plate positively charged and the other negatively charged. The capacitor will be fully charged when the voltage across both plates is equal to the applied voltage [2]. According to Eq. (2), C is directly proportional to Q which make, as capacitance increase, the amount of charge in the capacitor will also increase.

$$C = \frac{Q}{V} \qquad (2)$$

Capacitors also can eliminate ripples to perform DC voltage. For energy storage, capacitor of 100 µF was used to store the electricity collected. After the input has been rectified by the diode 1N4007, the energy will directly store in the capacitor.

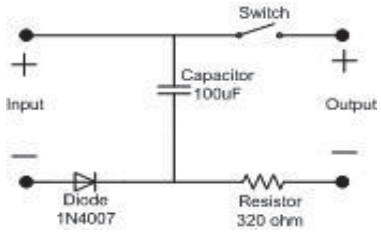

Figure 1: Circuit to deliver the AC input from piezo to DC DC Boost Converter

In Figure 1, diode acts as the rectifier to stable the AC signal input. Hence, energy will be stored in the capacitor. Once the switch had been pushed, the circuit will give an output as it will be fed to the DC DC Boost converter, which is not shown in the circuit diagram.

B. DC DC Booster Converter

After generating some energy and store it in a capacitor, all energy stored will be fed in to the DC DC booster as it will burst the current and voltage until it is sufficient to be used for next appliances. Specifications of the booster are in Table 1.

Table 1 DC DC Booster specifications

Rated Parameters	
Input Voltage	3.5V-28V
Input Current	1A
Output Voltage	1.25V-26V
Output Current	1A
Absolute Maximum Rating	
Input Voltage	32V
Input Current	3A
Output Voltage	32V
Output Current	3A

Figure 2: Adjustable DC-DC converter automatic step up step down

This is a small size device with high efficiency. This module can realize automatic lifting pressure within a certain range of input voltage and then automatically adjust the output voltage as it will not affects the input voltage [4].

IV. RESULT

After attempting numerous of test and experiment on the piezo generator plate, consideration on cumulative data collection shall base on the configuration of the piezo generator plate. For this project, the plates were connected in series to accumulate the amount of the voltage or current desired. The arrangement of the piezo plate are shown in Figure 3

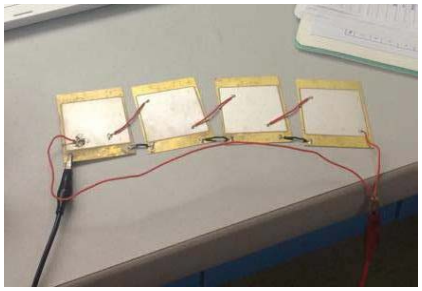

Figure 3: The piezo generator arrangement

Since piezo can only generate a small signal, therefore any experiment that had been run onto this plate will only result a very limited voltage. Method used to characterize the piezo was apply a pressure on the plate then observe the signal generated through digital oscilloscope.

Number of piezo plates units also can affect the amount electricity generated. As if, more piezo plates been used, higher voltage can be generated. In this work, four pieces of piezo were used. The effect of number of active piezo with the voltage generated is tabulated in Table 2. Figure 4 shows a plot to observe the relationship between the voltage

generated with the number of active piezo plates used. Results show there is linear relationship between the two parameters.

Table 2: The relationship is number of piezo is proportionally to value of voltage generate

Number of piezo	Voltage generated
One	1.2V
Two	2.2V
Three	2.9V
Four	4.0V

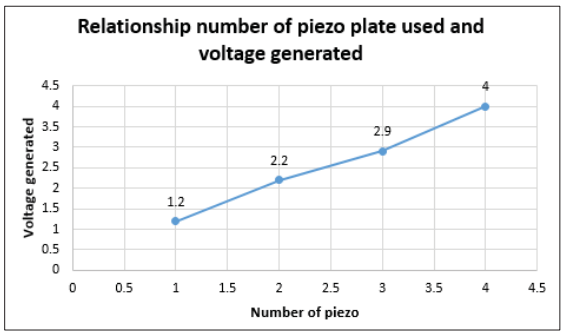

Figure 4: Linearity of number of piezo plate used to generate electricity

A. Hardware Implementation

1. Slightly Pressed

Further characterizations were executed on the piezo plates. Figure 5 shows the voltage response when the plates were pressed slightly on all the four plates simultaneously. The average peak-to-peak voltage reach to ±300 mV. This voltage is very low and barely can supply any electronic applications.

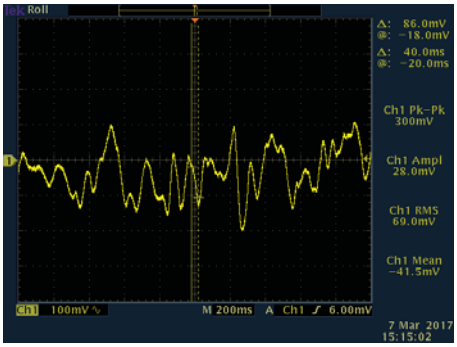

Figure 5 Voltage response when piezo plates are slightly pressed gives 300 mV

Therefore another approach will be used to increase the voltage value.

2. A tapping method on the piezo plates

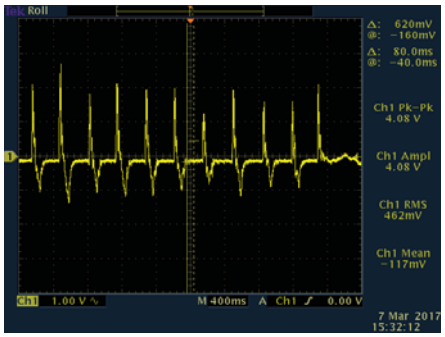

Figure 6 Tapping method on the piezo plates gives a maximum voltage of 4.08 V

This method is tapping using fingers on the four plates simultaneously. Using this method, voltage generated increased drastically from the slight press method. Figure 6 shows the voltage response during the tapping method. The waveform can be seen as pulse generated on each time of tapping. Besides, the voltage generated is quite high and already sufficient to supply to any controllers that require 3 V as input such as Arduino board.

The whole system invented for this project uses AC source as input signal. The AC signal collected from the piezo plates will be converted to DC signal through the processes of rectifying and filtering the signal until it reach a smooth and constant DC value. The desired system is illustrated in Figure 7. The collected input has to undergo rectifying process which is to convert an AC signal to a DC signal. The expected outcome appear as a constant DC line on the oscilloscope with amplified output due to LM 2596 which is role as a DC DC converter to step up the input. LM 2596 is a switching power module combine with buck and booster switching IC and able to supply up to 3A of current.

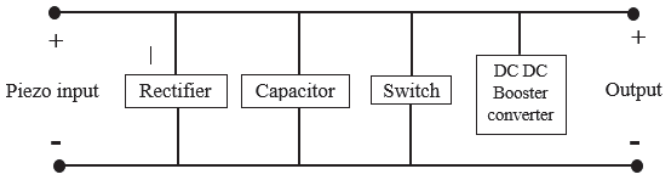

Figure 7: Circuit development design

B. Simulation

Using MultiSim, the simulation of final circuit before the DC DC Booster Converter can be predicted. Figure 8 shows the schematic circuit in MultiSim simulation.

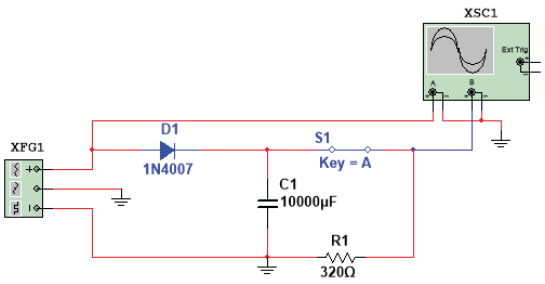

Figure 8: Circuit interface from piezo generator

In simulation, function generator were used to replace piezo as input for the circuit. Vp value was 2V approximately as can be seen in Figure 9. The diode was used to rectify the input signal and this rectifying method used was half wave rectifier. Reason of using half wave rectifier instead of full wave rectifier is, full wave rectifier were using 4 units of diodes and this will cause a huge current loss from the components and resulting zero output at the end of the circuit. Since this circuit only used one unit of diode thus it will cause a ripple. Increasing the capacitance value will smoothens the output signal as can be seen in Figure 9. Thus capacitor value used was 10mF. Then to complete the circuit interface, a resistor of 320Ω was used. Low resistance used due to low current throughout the circuit.

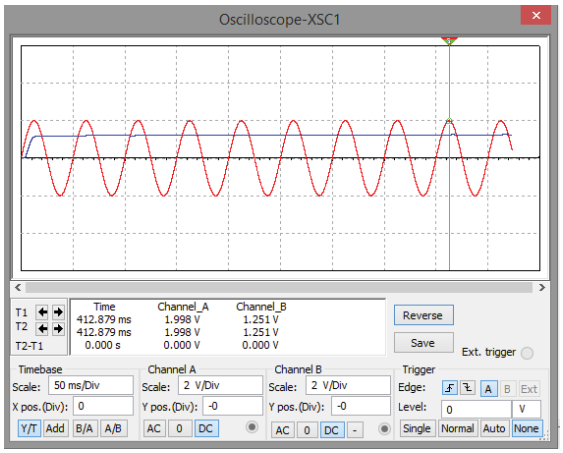

Figure 9: Waveform of the circuit simulation to convert the AC input to a DC output

: Input

: Output

According to this simulation, DC signal has successfully obtained.

V. DISCUSSION

Since this project is a small signal generated work, and no external supply shall be used to power up any component in this system. For example, components like transistors or operational amplifier (Op Amp) are active component which needs an extra supply to turn on. Therefore, concerns of this project will only focus on passive elements such as diodes, capacitor, and resistor as those mentioned elements are not capable of generating electrical energy. This issue will be a challenge for this work striving its goals because using an active elements will be a shortcut to generate energy from any input and the output can by increased using any application that available in the market.

However, since the objective is to create a portable energy supply as well as to derive energy from the ambient to be converted to a usable power supply by using a piezo generator, thus only passive element shall be use to avoid any malfunction in the system.

1) Piezo

From the piezo stage, according to the experimental result, the output goes dramatically increased when a pressure applied on the plate one at time but at frequent rate. For example, one tap per one second or more taps applied per one second. This approach can generate higher voltage compared to continuous pressure on the plate.

2) Current

The biggest problem face by this project was current lost in the circuit development. From the input, current generated maximum was 0.6mA. However, along the travel of current in the circuit interface, a lot amount of current has loss which resulted at the output to be measured only pico Amperes or nano Amperes left for the next stage which is the LM 2596. Unfortunately, the DC DC converter require a lot of minimum current input to turn on which is 1000mA or 1A. To identify which process that consume highest current, troubleshooting every part of the circuit interface need to be done. After some times of troubleshooting, rectifier was identified as black hole for the current. Therefore to overcome such things to be happen, from the original design, full bridge rectifier were used then replaced with half bridge rectifier to reduce great current losses. Thus by applying this approach, the DC DC converter can turn on.

3) Voltage

Desired voltage generated for this project shall be 3V up to 5V. Regarding to Figure 3 in chapter Result, the voltage generated shown was 4V. This result shows that the output voltage created was already adequate to be use for the end product applications.

4) Portability

One of the main objective of this project is to sustain the electricity power. Therefore this work is to aim portability so it can be use at any locations as long as vibrational input on the piezo generator plate can be applied. Idea of this proposal was to overcome the limitation in propagation of electrical current through the grid, electrical losses are especially significant when power supplies are located far from their uses. In addition, hope of this work is the device created is deploy-able in rural area to benefits the needed.

VI. CONCLUSION

This project can be furthered in future work such as a free charging center because the input of the piezo only need ambient supply which is vibrations. Vibrations from the ambient can be generated everywhere such as, step from the pedestrian walk, wheel rolls from the broadways and more. This project could save costs and sustains a lot of source in many perspective.

ACKNOWLEDGMENTS

Authors would like to acknowledge the support from UTM Research Management Centre and financial support from GUP Tier 1 vot 14H63.

REFERENCES

.

[1] Yusuf, S.T. & M Yatim, A. H. (2013) Mechanical Energy Harvesting Devices for Low Frequency Applications: Revisited, ARPN Journal of Engineering and Applied Science, Vol 8 no 7, 504-512.

[2] Brain. M., Bryant W. C. (2002). How Capacitors Work. Retrieved from URL: http://electronics.howstuffworks.com/capacitor1.htm

[3] Introduction to Capacitors. (2016). Retrieved from URL: http://www.electronics-tutorials.ws/capacitor/cap_1.html

[4] Product description: DC-DC Converter Automatic Step Up Step Down Module. Retrieved from URL: https://www.lelong.com.my/dc-dc-converter-automatic-step-step-module-3-5v-28v-to-1-25v-beaulife-I5501023-2007-01-Sale-I.htm

[5] S. Chasalani & J. M. Conrad "A surveys of Energy Harvesting Source for Embedded System." 2008, pp 442-447

Portable Heart Rate Monitoring System

Muhammad Amirul Amin Ahmad
Faculty of Electrical Engineering
Universiti Teknologi Malaysia (UTM)
Johor, Malaysia.
amirulamin824@gmail.com

Dr Zaid Omar
Electronic & Computer Eng. Department
Faculty of Electrical Engineering
Universiti Teknologi Malaysia (UTM)
zaid@fke.utm.my

***Abstract*— Advancement in technologies encourage people to develop more reliable devices or gadgets to improve their lifestyle. These are also happened in electronic biomedical scope, in which people keeps innovating technology to improve current available devices and reduce statistics of patients or even number of deaths caused by it. Some certain diseases such as cardiac diseases need real-time and constant monitoring procedure after diagnosis to prevent probability of further damage. Usually, the process of monitoring can only be done at hospitals or any healthcare centers. Specifically, heart arrhythmias need continual long-term monitoring in many cases and it will involve the man-power and times consuming for these institutions. Other than that, other well-known issues for both the healthcare institutions and the patients is longer period for patient hospitalization procedures. In this research project, a portable and wearable heartrate monitoring system device is designed. It will enable users to monitor his/her heart rate precisely in real time and a warning notification will appear if unusual heart rate encountered. We have determined our target users for this project which including patients undergoing cardiac rehabilitation, professional players during training or person who tend to do extreme exercises in their daily life. The project basically will consist of pulse sensor, Arduino Nano, OLED display, battery and Bluetooth module. Other than that, Arduino and MATLAB software have also been used for irregularity of heart rhythm detection. With the introduction of this system, it will surely help to improve on maintaining currently available quality of the system and perhaps develop it to another level.**

Keywords—real-time; heart rate; monitoring; rehabilitation; irregularity

I. INTRODUCTION

In 1950, a medical specialized doctor in cardiology and electrophysiology named Herman Hellerstein build his own clinic in Cleveland, Ohio. He has been honored for his focus to cardiovascular disease patients. He intended to develop the clinical way for physiology exercise, and more specifically, cardiac rehabilitation by proving that exercise was healthy and suitable way to rehabilitate from cardiac diseases. [4] However, most early 20th century cardiac disease prescriptions recovery included bed rest, in which contradicted to cardiac rehab concept in the 1950s after medical community advocates, such as Hellerstein, advised that a "graded step" program be implemented for patients.

In 1963, Hellerstein published a study on the benefits of aerobic training for cardiac disease (myocardial infarction, angina, or both) patients to be specific, the study show that heart rate, oxygen uptake, and blood pressure of the cardiac patients able to improve responses to exercise.it demonstrated that patients participating in aerobic training program had more efficient heart rhythm and the tendency for the heart to become stronger, thereby delivering more oxygen-rich blood to tissues.[1]

Moreover, improved exercise workload capacity and blood pressure allowed the cardiac patients to increase their heart's efficiency gradually over time. Hellerstein published a famous book for medical titled, "Healing Your Heart" in 1993. He passed away just three years later due to complication of cancer. Exercise physiology clinically has come a long way since the pioneering cardiac rehab studies back in 1950s. Over the last 65 years, clinical exercise physiology has growth and expended to take care of cardiac patients. [3]

Sinus rhythm is the normal regular rhythm of the heart set by the natural pacemaker of the heart called the sinoatrial (or sinus) node. [7] Normal heart impulses start in the wall of right atrium and are transmitted to the atria and down to the ventricle. Basically, there are four categories of rhythms that originate in sinus node which includes Normal Sinus Rhythm (NSR), Sinus Bradycardia, Sinus Tachycardia and Sinus Arrhythmia. Each group has its own information and rules necessary to be able to identify the arrhythmia.

Firstly, Normal Sinus Rhythm (NSR) which is not an arrhythmia because it is a normal, rhythmic pattern technically. In NSR, the pacemaker of the impulse originates in the sinus node and travels through the normal conduction pathways within normal time frames. The P waves will be uniform, and since conduction is normal, one P wave will be in front of every QRS complex due to the pacemaker which originates in the sinus node.

NSR is defined as being a regular rhythm, thus the R-R interval must be regular across the entire strip. It must be a regular pattern, at a rate between 60 and 100, with an upright P wave in front of every QRS complex. The measurement of PR interval must fall between 0.12 and 0.20 second, and it must be the same duration across the entire strip. If the PRI changes from one complex to another, even if it stays within the normal range, it would not be considered as Normal Sinus Rhythm. It must follow those rules as stated in ***Figure 1.1*** to maintain as NSR or normal heart rhythm.

Cardiac rehabilitation program required patients to optimize their exercises as part of the process for them to get back to a healthy heart. Normally, this process is being held in hospital or

any clinic after patient's operation with the guidance of doctors and staffs. But, after being treat for some period the doctor will suggest patient to continue it themselves at home. But, the problem is most of them were frightened that excessive exercises or workload will damage their current heart conditions or the cardiac will reoccurred. Based on the problem faced by the cardiac patients and the requirement of maintaining healthy lifestyle, we determine to design this portable heart rate monitoring system device which will helps them to monitor real-time heart rate and notified them if any irregular heart rhythm start to occur right away. They can now optimize physical activities in their own to get a healthy heart back.

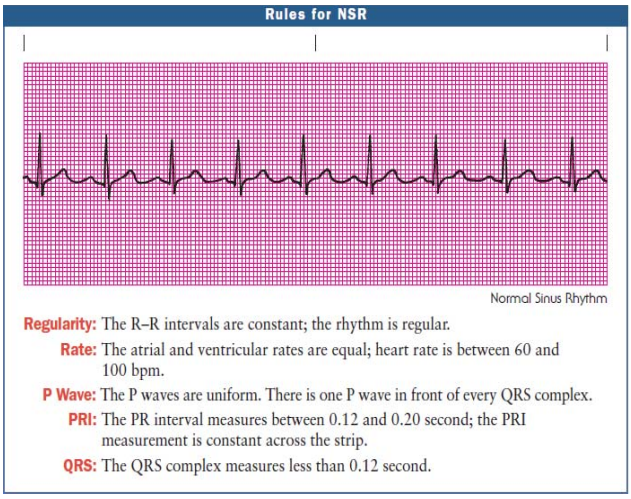

Figure 1.1 *Rules for NSR*

II. LITERATURE REVIEW

In 2010, a system of heartbeat monitoring has been developed as part of patient monitoring process. The system also can measure temperature of patient and the wireless system make it capable to send the data collected to doctors or examiners at distant location. This encourage patient to do physical activities without being monitored or need to go to same clinical institution which can cost their time and money.

Heartbeat sensor as sown in **Figure 2.1** is designed to give digital output of heartbeat when finger is placed on it. The digital output is connected directly to microcontroller to measure the Beats Per Minute (BPM) rate. It also works on the light modulation principle by blood flow through finger at each pulse.

It is however only can display number of heartbeat per minute of the patient which is not very efficient cause it took a minute of time for the data to be process and displayed. It is not specifically a real-time processing display and is not suitable for cardiac patient usage in which irregular heart rhythm may occur in seconds. [2]

In 2015, a group of researches in Mexico have developed a simple portable biomedical electronic device to detect cardiac arrhythmias in humans. They used the simplest configuration of Einthoven's triangle, named to remember pioneer of electrocardiography Willem Einthoven as shown in **Figure 2.2**. It shows that three surface electrodes placed to detect pulse rate.

The data obtained by the surface electrodes will be send to the recording instrument, named electrocardiograph for plotting the PQRST complex wave or well known as heart rhythm. [5] The device is successfully done and achieved the objective to detects cardiac arrhythmias, portable, reliable and user-friendly. It has been tested in Cardiology Department at University Hospital of Puebla, Mexico and the diagnosis are successfully done.

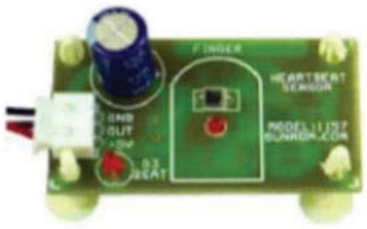

Figure 2.1 *Heartbeat Sensor*

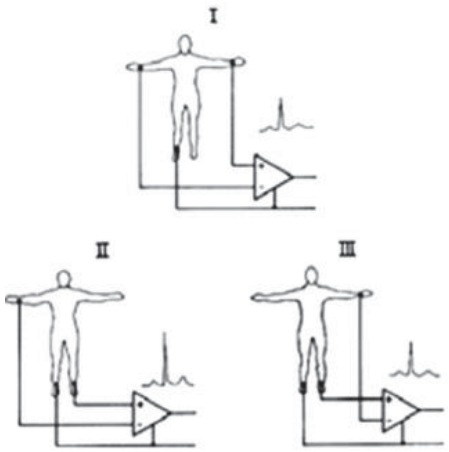

Figure 2.2 *Electrodes of Einthoven's connection*

III. PROJECT METHODOLOGY

The objectives of this project are to design a portable heart rate monitoring system device, determine and give warning if irregularity of heart rhythm start to occur, and improve cardiac rehabilitation process. To achieve that, the Arduino and MATLAB software are used to produce and analyzed the data produce by the sensor. The general block diagram of the project is shown in **Figure 3.1**.

At first, input generated by pulse sensor that being attached to finger of the user or patient. The data then will be send to Arduino microcontroller which is being power supplied by battery. The heart rhythm (output data) produced will be displayed to OLED display and analysis of regular or irregularity of heart rhythm is conducted by Arduino and give warning to user through OLED display.

Figure 3.2 shows the flowchart of this project. In completing the project, there must be standard steps that need to obey. Firstly, the input data is being read by pulse sensor which connected to Arduino microcontroller. [6] The microcontroller will process the data and display the heart rhythm on the OLED

Display. In the meantime, the data also been analyses to configure if any sort of irregular heart rhythm start to occur.

If the heart rhythm is normal, then the process will just return to the input sensor to sense next pulse and redo the processes. However, if there any irregular heart rhythm start to occur then the system will give a notification for patients or users as warning for them to stop the physical activities that they are currently doing. They also can take further actions by calling for clinical references by the doctors or specialist. Further development and precise measurement may be required otherwise.

The circuit for the project is implemented and the 3D casing is printed and designed by using SolidWork software as shown in **Figure 3.3** below.

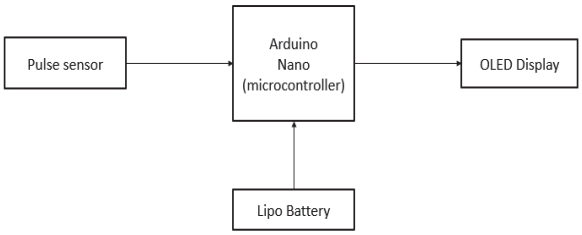

Figure 3.1 *General Block Diagram of the Project*

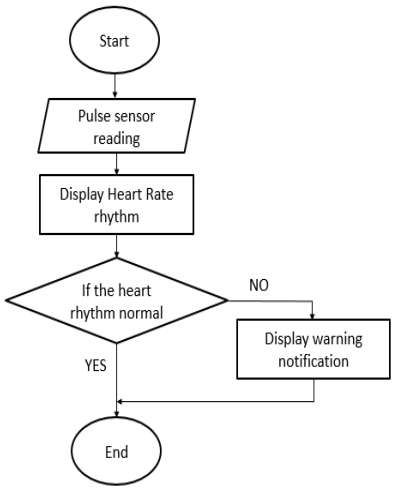

Figure 3.2 *Flowchart of the Project*

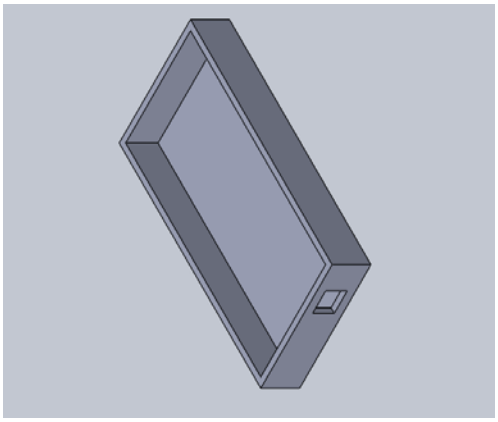

Figure 3.3 *3D Casing Design*

IV. RESULT AND ANALYSIS

A. Pre-processing PC monitor

At first part of the project, the result of data obtained by the pulse sensor is projected trough PC monitor by using Arduino application, Serial Plotter. It will produce the real-time heart rhythm when a finger is placed to the sensor. The reading is taken by 115 200 baud rate, which is fast enough to capture the heart rate of every 2ms. **Figure 4.1** shows the Serial Plotter result of real-time heart rhythm in normal state condition.

As this project is designed for rehabilitation process of arrhythmia patients, the sensor is tested in exercise condition to see the difference of heart rhythm produced. **Figure 4.2** below shows the heart rhythm produced by pulse sensor when exercising.

Figure 4.1 *Serial Plotter of Normal Heart Rhythm*

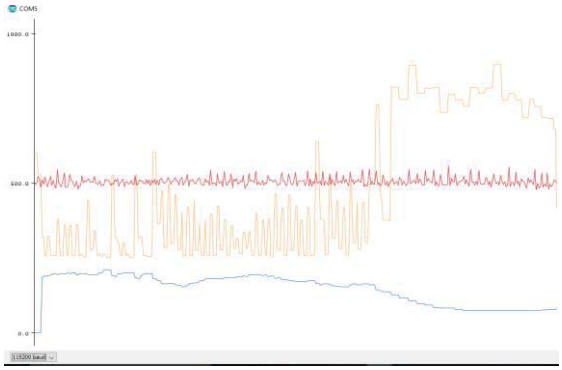

Figure 4.2 *Heart Rhythm when Exercising*

B. Portable version and OLED Display

The circuit then is being transferred from a breadboard and PC monitor to a doughnut board and soldered. The display also has been replaced to an OLED Display to make the project portable as shown in **Figure 4.3**.

As for the result that being displayed on the OLED Display, the heart rhythm and the reading of Beats Per Minute (BPM) can be seen in **Figure 4.4** and **Figure 4.5** respectively. The display also give user alert if the heart rhythm is considered high to make them aware and reduce the amount of exercises that being held.

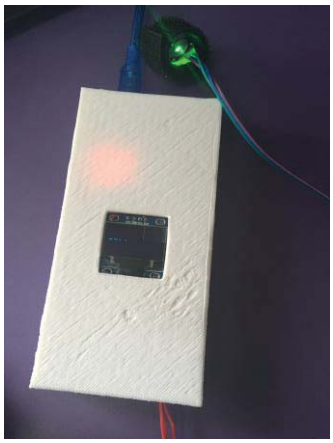

Figure 4.3 *Portable Heart Rate Monitor*

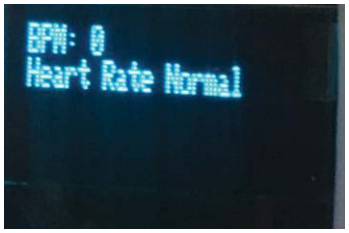

Figure 4.4 *BPM reading on OLED Display*

Figure 4.5 *Heart rhythm on OLED Display*

V. CONCLUSION

As conclusion, literature review of previous related projects has been studied. Other than that, the basic structure and irregularity of heart rhythm have also been investigated. The device properties such as pulse sensor, Arduino microcontroller and Arduino software have been explored too.

There are many benefits that can be obtained if this project is successfully done. Firstly, it will allow a subject to monitor their heart rhythm in real-time anywhere. Secondly, it will help cardiac patients to undergo better cardiac rehabilitation process without any monitoring of doctors or specialists. They will be encouraged not to be afraid to enjoy their daily life, keep exercising and do physical activities and improving it to get a healthy heart back. Lastly, this device can also improve quality of healthy lifestyle since it can also be use by anyone not specifically cardiac patients.

REFERENCES

[1] *Certo, CM*. History of Cardiac Rehabilitation. Phys Ther, 1985.

[2] *H. Azucena, E. Rios, R.D. Pena, J. Diaz,* Design and Implementation of A Simple Portable Device to Diagnose Cardiac Arrhythmias, 2015.

[3] *Hellerstein*, HK. Exercise Therapy In Coronary Disease. Bull N Y Acad Med, 1968.

[4] *Weinberg, SL.* Herman Hellerstein Remembered. Clin Cardiol, 1996.

[5] *Bandana Mallick, Ajit Kumar Patro*, Heart Rate Monitoring System Using Fingertip Through Arduino and Processing Software, IJSETR, 2016.

[6] *Kenneth.J.Ayala*, The 8051 Microcontroller Architechture, Programming and Applications, 2001.

[7] *Gail Wavren*, Basic Arrhythmias, Pearson, Seventh Edition, 2011.

[8] *Azil Azrin Mohd Nor,* Sport Centre Resevation System via Arduino, UTM, 2015.

[9] *Nuruddin Rusli,* Photovoltaic Cleaning System Using Robotic Arduino Approach, UTM, 2016.

C-V Characterization of N-Channel and P-Channel Twin Silicon Nanowire Field Effect Transistor

Alia Noor Fiswani Agussalim, Nurul Ezaila Alias, Zaharah Johari, Yusmeeraz Yusof, Mohd Rashidi Salim, Mohd Amri Md. Yunus and Mohd Hafizi Ahmad
Faculty of Electrical Engineering
Universiti Teknologi Malaysia
81310 Skudai, Johor, Malaysia
ezaila@fke.utm.my

Abstract – Twin Silicon Nanowire FET is one of the good applicants and grows into among of new idea transistor for upcoming development of transistors. In this paper, simulation on C-V characteristics were performed directly by measuring capacitances from an optimized structure of n-channel and p-channel of Twin Silicon Nanowire FET (TSNWFET), which have been designed in 3-Dimensional (3D) TCAD Simulation Tools. The parasitic capacitances can be analyzed through C-V curves based on high frequency applications. Additionally, the overall parasitic capacitances of TSNWFET device for both polysilicon gate and nickel gate are extracted and their performances were compared. The parasitic capacitances are also compared between n-channel and p-channel of TSNWFET and the performances at high frequency were investigated. C-V measurements proved that the total parasitic capacitance versus gate voltage of p-channel TSNWFET is~ 15% greater than n-TSNWFET. In addition, the parasitic capacitances of TSNWFET with polysilicon gate have shown greater than that with nickel gate.

Keywords—nanowires, c-v curve, parasitic capacitances

I. INTRODUCTION

Twin Silicon Nanowire FET (TSNWFET) with gate length of 30 nm exhibits high drive current of 2.37 mA/um and 1.3 mA/um at saturation region for n-channel and p-channel, respectively with TiN metal gate [1]. Due to gate-all-around structure and nanowires channel, it reveals good short channel effects (SCEs) immunity for 30nm gate length. Despite the fact that TSNWFET is fabricated on bulk silicon wafer, bottom parasitic capacitance does not much influence whole implementation [1]. However, substituting a polysilicon gate with a metal gate significantly lessens the gate leakage as a result of removal of polysilicon gate depletion, where the identical capacitance is equivalent to the oxide thickness in inversion [2]. The work function of metal gate also can be influence to the tunneling performances in transistor and it is importance in the accumulation region. Details analysis state that the metal gate with mid-gap work function decrease the tunneling between gate and source-drain extension (SDE) in both channel of transistor [2].

Previous study has investigated the effects of parasitic capacitances are important in silicon nanowire transistors due to very small transistor size. Parasitic resistances caused by the ultranarrow SDE area has become a major contributor to the total capacitances, where it was greatly affected the RF performance of silicon nanowire transistors while for contact resistance, it has quite low impact as compared to that of the SDE area [3]. Nowadays, there are many research have been done on capacitance-voltage (C-V) characteristics of planar metal-oxide-semiconductor field effect transistor (MOSFET) to analyze the effects of dielectric layers and interfaces with different type of semiconductors. Further investigations need to be performed for semiconductor nanowires but it is still elusive to predict so far because of difficulties in measuring very small intrinsic capacitance [4].

The capacitance between gate and channel contribute the basis information of the device such as equivalent oxide thickness, inversion charge, mobility, flat-band voltage and may more [5]. However, the capacitance of dual nanowire device such as TSNWFET is hard to measured, because the channel active area has become ultranarrow [5]. The impact of gate tunneling current with thin oxide also deformed the C-V curve. Opportunely, the nanowire FET operates with small gate leakage because of gate-all-around structure. However, it is still complicated with its ultranarrow active region issues. The parasitic capacitances reduce the execution of the device because of 3-Dimensional (3-D) device. Very few experimental on C-V studies have been published for nanowires capacitances with 3-D design.

In this project, simulations on C-V characteristics of TSNWFET with polysilicon gate and metal gate for both n-channel and p-channel are presented. There are two parts which are design optimization of the TSNWFET device structures and its C-V simulation. The design optimization of the device structures was a continuation work from other's [6]. Then, the effects of parasitic capacitances are compared between n-channel and p-channel for both polysilicon gate and metal gate respectively. Finally, analyses are performed based on high frequency applications.

II. SIMULATION SETUP

In this project, the simulations are conducted by Sentaurus TCAD Tools software in 3D. The physical structure of TSNWFET for both n-channel and p-channel has been designed and optimized by previous study [6]. Sentaurus software

contains four primary tools that require to be run under Sentaurus Workbench in order to do the characterization of the devices. These four primary tools are Sentaurus Structure Editor (SDE), Sentaurus Process (SProcess), Sentaurus Device (SDevice) and Inspect Tool.

Both of n-channel and p-channel of TSNWFET are designed for two different types of gates. Those are polysilicon gate and metal gate which is nickel. Also, the frequency used for C-V simulation is 1MHz. Table 1 shows the device parameters and their dimensions.

Device Parameter	Dimension
Gate length, L_g	15 nm
Oxide Thickness, t_{ox}	2.5 nm
Nanowires radius, r_{nw}	5.0 nm
Width/Length, W/L	200nm/150nm
Channel Concentration, N_D	$2 \times 10^{13}\ cm^{-3}$
S/D Concentration, $N_{S/D}$	$2.3 \times 10^{14}\ cm^{-3}$ (n-TSNWFET) $1.3 \times 10^{15}\ cm^{-3}$ (p-TSNWFET)

Table 1: The device parameters and dimensions of TSNWFET

The device dimensions of TSNWFET are similar for both n-channel and p-channel. The electrical characteristics such as threshold voltage (V_{th}), subthreshold swing (SS) and the on-off current ratio (I_{on}/I_{off}) have been extracted from current-voltage (I-V) curves while the parasitic capacitances are analyzed from capacitance-voltage (C-V) curves. Based on the investigation, the first direct measurements of gate capacitances in silicon nanowire transistors to both polysilicon gate and metal gate geometries have been performed with specific range of the nanowire channel lengths [4]. This allows the assessment of holes mobility in silicon nanowires using capacitance data.

Figure 1 shows the 3-D structure of TSNWFET with various main parasitic capacitances. The capacitances such as gate-to-source/drain/bulk capacitance (C_{gsdb}), gate-to-bulk capacitance (C_{gb}) and gate-to-source/drain capacitance (C_{gsd}) have been measured from nanowires capacitor with V_g in the range of -2V to 2V for both polysilicon gate and metal. The values of each capacitance are also extracted for exact comparison.

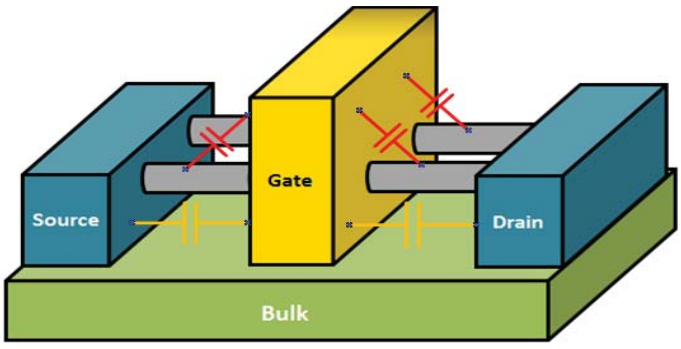

Figure 1: The structure of TSNWFET with the capacitances

III. Result and Discussion

A. I-V Characterization of TSNWFET

Figure 2 (a) and (b) depict the TSNWFET device structure simulated in 3D with the doping concentration for both of n-channel and p-channel.

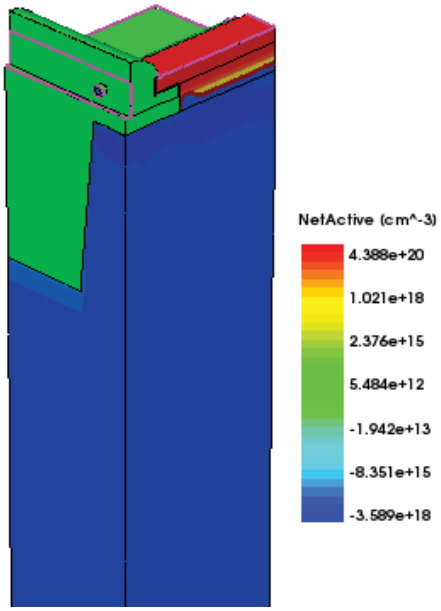

(a) n-channel

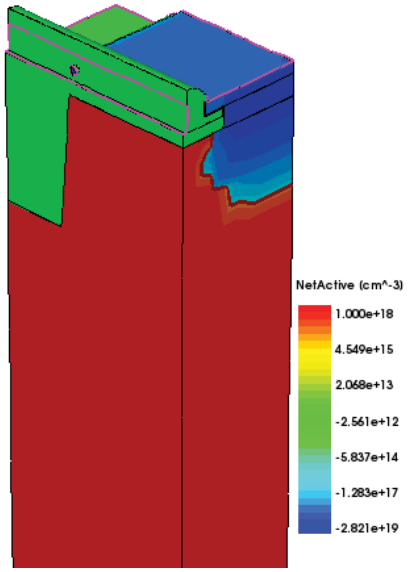

(b) p-channel

Figure 2: The TSNWFET device structure in 3D with doping concentration

In order to obtain symmetrical $I_D - V_g$ graph of the n-TSNWFET, the doping concentration of p-TSNWFET were adjusted. The metal gate desires higher doping concentration due to its fixed work function different and needs higher concentration so that the current can drift from source to drain.

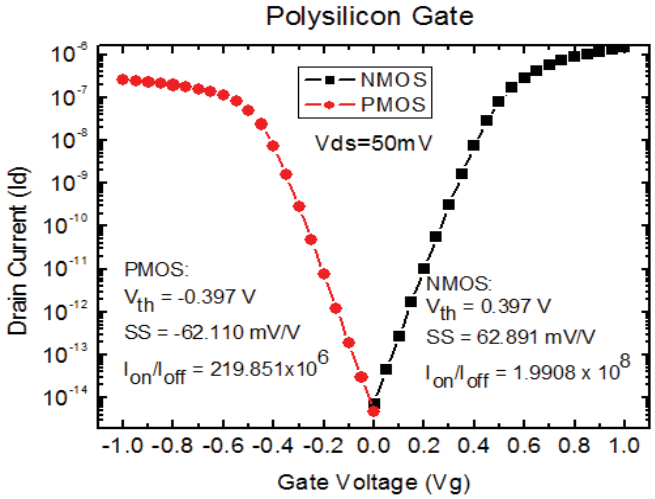

Figure 3: $I_D - V_G$ curves of TSNWFET for polysilicon gate

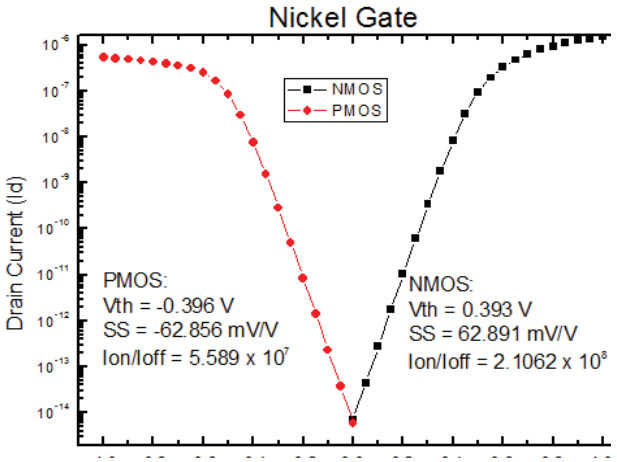

Figure 4: $I_D - V_G$ curves of TSNWFET for metal gate

Both $I_D - V_g$ curves of TSNWFET for polysilicon gate and metal gate are in linear mode ($V_{ds} = 0.1\ V$). From the I-V curve, it also indicates the optimized electrical characteristics; threshold voltage, V_{th} of ~0.39 V, subthreshold swing, SS of ~60 mV and the on-off current ratio, I_{ON}/I_{OFF} of exponential of 10^8 [6]. Although both I-V curves are almost identical but their leakage current (I_{OFF}) are different due to its dissimilar work function's value.

B. C-V Characterization of TSNWFET

The C-V characteristics have been observed between polysilicon gate and metal gate for both of n-channel and p-channel of TSNWFET. Figure 5 and 6 indicate the performance of various capacitances (C_{gsdb},C_{gsd}, C_{gb}) for both channels of TSNWFET varies with V_g at frequency of 1 MHz for polysilicon gate and nickel gate. The small signal analyses are obviously discussed based on the simulation data with the use of the descriptive representation as shown in Figure 7.

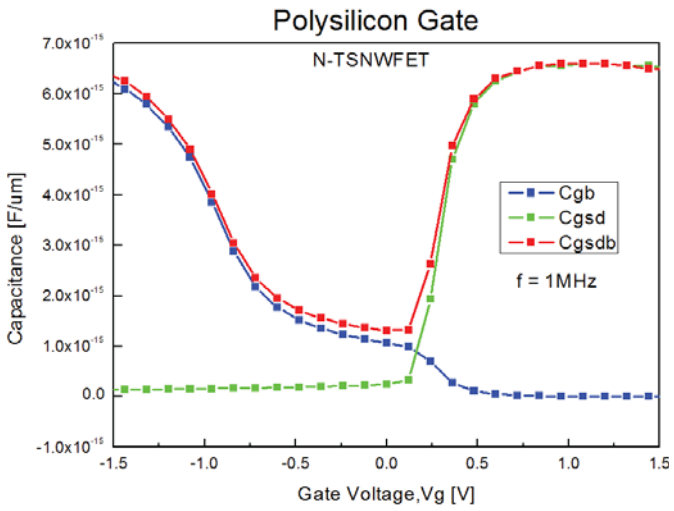

(a)

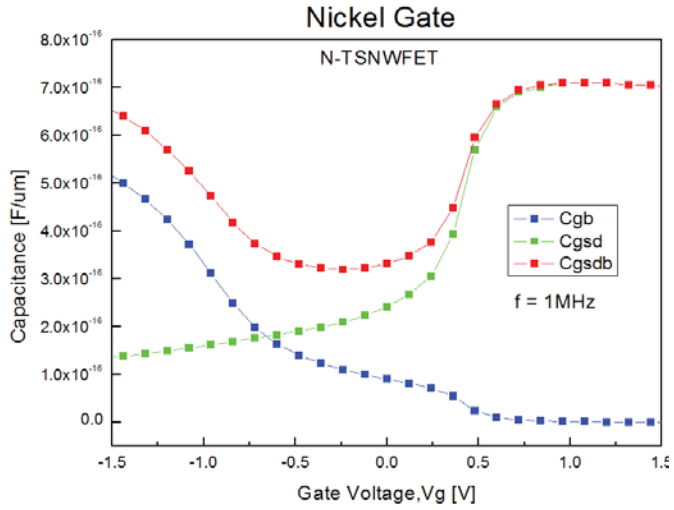

(b)

Figure 5: C-V curves of n-TSNWFET for (a) polysilicon and (b) nickel gate

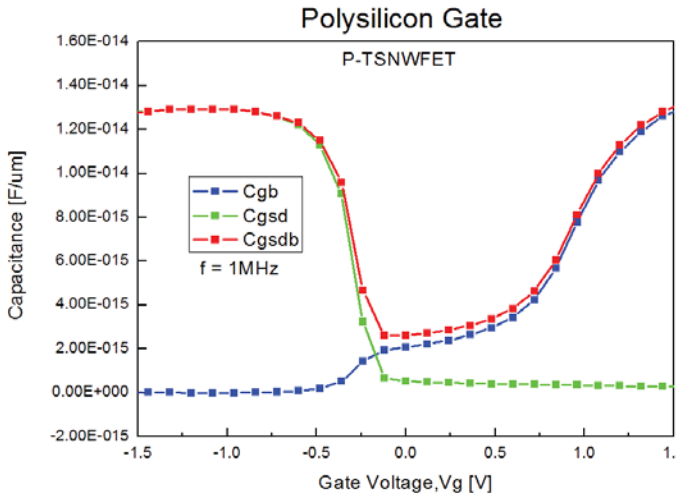

(a)

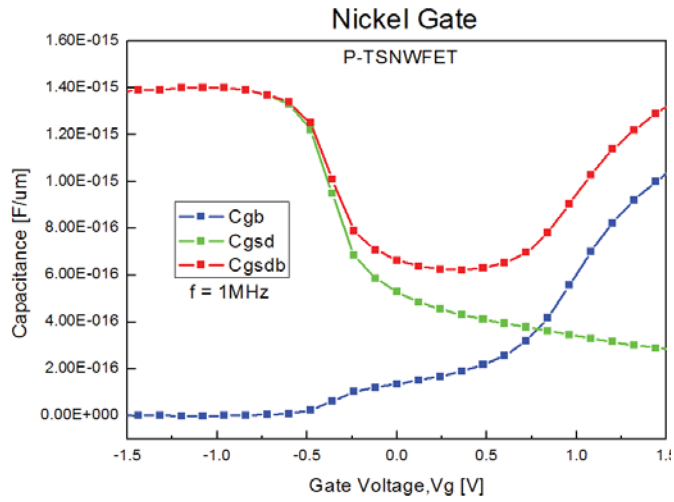

(b)

Figure 6: C-V curves of p-TSNWFET for (a) polysilicon and (b) nickel gate

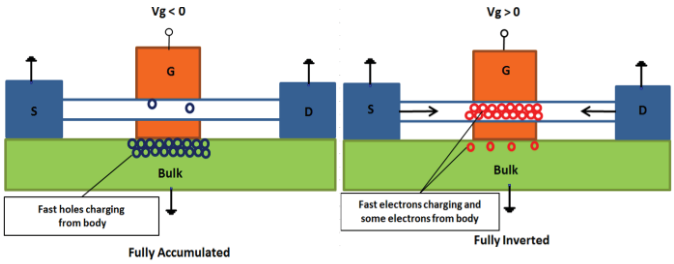

Figure 7: Illustration of the carrier mobility in n-TSNWFET of polysilicon gate under positive and negative V_g for C_{gsd}

C_{gsdb} is the total capacitances of C_{gsd} and C_{gb}. From Figure 7, it illustrates the curve of capacitance (see Figure 5(a)) where C_{gsdb} is similar with C_{gsd} during the accumulation regime. It indicates that the C_{gb} affected by fast hole charging or discharging from bottom silicon creates the main factor of C_{gsdb}. Mostly C_{gsdb} contains of fast electron charging or discharging between source-drain and the channel in inversion regime and there is some steadily formed electrons in the bottom silicon bulk.

In other hand, it has also been observed that the total capacitance in polysilicon gate is higher than the metal gate for both n-channel and p-channel of TSNWFET. Conventionally, polysilicon gate has been commonly used as the gate electrode of nanowire transistor. In TSNWFET, when voltage is applied to the gate, a depletion region will be formed because of doped polysilicon is a semiconductor material. In this manner, the depletion region operates extremely same as a thicker oxide which minimizes the inversion charge, thereby decreasing the inversion capacitance that caused a degeneration in the on-state current as shown in Figure 4 and 5 where the I_{ON}/I_{OFF} of n-channel and p-channel are $1.9908 \times 10^8$and 3.283×10^7, respectively. Substituting the polysilicon gate with a metal gate which is nickel removes poly-depletion. Additionally, the higher gate work function also refines the DIBL, SS, on-off current ratio nevertheless owing to degradation in device drive current [7]. TSNWFET reacts as similar as a thinner oxide in inversion with connected capacitance and drift current enhancement as shown in Figure 4 and 5 where the I_{ON}/I_{OFF} of n-channel and p-channel are 2.1062×10^8 and 5.589×10^7, respectively.

$C-V$ measurements proved that the total capacitances versus gate voltage for p-channel TSNWFET was ~ 15% greater than n-TSNWFET. It is given that the evidence of superior electrostatic control of channel for n-TSNWFET. Moreover, n-TSNWFET is faster than p-TSNWFET by way of mobility of carriers in n-channel which are electrons higher than holes which are carriers in p-channel. The higher the mobility of electrons, the larger the conductivity owing to the fact that conductivity is proportional to the mobility as the equation below [3]:

$$\mu = \frac{g_m L}{W C_{ox} V_{DS}} \quad (1)$$

Consequently, n-channel contributes lower capacitance than p-channel with equivalent device dimension in TSNWFET. Meanwhile the mobility of the carriers in n-channel are nearly two times higher than that of a p-channel, hence an n-channel device is faster than a p-channel device. Also, the size of p-channel device of any transistor logic is usually bigger two or three times than n-channel device so it has higher gate capacitances. However, p-channel devices also have their own benefits of greatly manageable, low cost in procedure, a worthy profit and high noise freedom. In high frequency applications a p-TSNWFET causes into advanced switching losses as a result of higher gate charge necessity than an n-TSNWFET for the equal current carrying capacity.

IV. Conclusion

In this project, the C-V simulations of TSNWFET were presented and their characteristics have been discussed based on the simulated data. There are several advantages in gaining information about device characteristics in terms of capacitances when the C-V characterization of TSNWFET between n-channel and p-channel were compared. Since the parasitic capacitance is the main contributors which can severe affect the performance of semiconductor device, therefore need to be reduced so that the overall performance of the device can be improved. The total capacitance of polysilicon gate is higher than the metal gate for both channel of TSNWFET due to the fact that nickel has higher work function. In addition, the n-channel exhibits better characteristic in term of capacitance compared to p-channel because it contributes lower capacitances in TSNWFET. Finally, it can be concluded that the parasitic capacitances need to be as minimize as possible specifically for high frequency applications.

References

[1] S. D. Suk, *et al*., "High performance twin silicon nanowire MOSFET (TSNWFET) on bulk Si wafer," IEEE Transactions on Nanotechnology, Vol. 7, No. 2, March 2008.

[2] Y-T Huo *et al*., "Metal Gate Work Function Engineering on Gate Leakage of MOSFETs," IEEE Transactions on Electron Devices, Vol.51, No.11, November 2004.

[3] J. Zhuge *et al*., "Investigation of Parasitic Effects and Design Optimization in Silicon Nanowire MOSFETs for RF Applications," IEEE Transactions on Electron Devices, Vol. 55, No. 8, August 2008.

[4] R. Tu, L. Zhang, Y. Nishi and H. Dai, "Measuring the capacitance of individual semiconductor nanowires for carrier mobility assessment," Nano Letters, 2007, Vol. 7, No. 6, pp. 1561-1565.

[5] Y-H Jeong *et al*., "Comparative study of C-V characteristics in Si-NWFET and MOSFET," IEEE Nanotechnology Materials and Devices, pp. 12-15, 2010.

[6] Muhammad Nurhaziq bin Haridan, "Performance evaluation of 3-D n-channel and p-channel twin silicon nanowire MOSFET (TSNWFET)," Faculty of Electrical Engineering, University of Technology Malaysia, December 2016.

[7] M. Mustafa *et al*., " Threshold voltage sensitivity to metal gate work-function based performance evaluation of double-gate n-FinFET structures for LSTP technology," World Journal of Nano Science and Engineering, 2013, 3, 17-22.

Iot Based Flood Monitoring System

Mohamad Harith Bin Harun @ Hassan
Faculty of Electrical Engineering
Universiti Teknologi Malaysia
Johor Bahru, Malaysia.
mohamadharith93@gmail.com

Dr. Muhammad Ariff Bin Baharudin
Department of Communication
Faculty of Electrical Engineering
Universiti Teknologi Malaysia
Johor Bahru, Malaysia.
mariff@utm.my

***Abstract*—Flash flood is a critical problem faced in many cities in the world. This is more apparent since it can happen suddenly without people noticing, and may cause serious road congestions and vehicle damages. Therefore, this project was developed to detect the possibilities of flash flood happening and to give an early warning to users via developed website and alert users with Telegram application. The system was developed using Wireless Sensor Network (WSN)-where data collected by the sensor nodes are transmitted to the base station. Both sensor nodes and base station are constructed using embedded circuit boards and equipped with radio frequency module. Then, the Internet of Things (IoT) concept was implemented by extracting real time data from the base station and sending the data to an online database (Ubidots) before being transmitted to the developed webpage for users' reference. As a result, the users able to have real-time water level and get a notification from this project. This system is a more effective solution to provide a fast and reliable communication system.**

Keywords—Wireless Sensor Network(WSN); Internet of Thing(IoT); Ultrasonic Sensor

I. INTRODUCTION

Flash flood is a sudden local flood which is typically due to heavy rain. In cities, this disaster is usually influenced by the overflow of water from water bodies such as lake or drainage system which have not been maintenance properly. If this occurs, it may contribute to the loss of precious lives and a lot of destruction of properties. Normal flood usually occur gradually but flash floods, on the other hand, can develop in just a few minutes. Usually, flash flood happens in low-lying areas or flat areas that can be submerged very quickly before it begins to move to higher ground, especially when water is drastically supplied by rainfall. Flash flood usually occurs especially during heavy rain and thunder storms. Drainage system management by the authorities must be in the best and leads to good water flow without stuck by rubbish. In conclusion, flash flood may occur suddenly and driver could trapped into it if does not receive early notification.

The objective of this project is to create a system utilizing the Internet of Thing (IoT) platform with real time water level monitoring to give an early warning to users via the developed webpage and via Telegram application. Users may know the current water level and flood warning with the developed webpage. Besides that, users may get a notification via Telegram application if the current water level have reached the warning water level and get prediction if flash flood occurs.

In recent years, Wireless Sensor Network (WSN) has been developed for fast data dissemination without using cables. Without WSN, the data transmission process is very limited due to cabling and the medium for data transmission. Furthermore, non-WSN based telematics system fail to ensure fast nor reliable warning system [3]. The WSN is divided into two categories which are long-range communication and short-range communication. Modern wireless sensor network has bi-directional communication capabilities that enable the users to control of sensor network and transferring data. This technology has been utilized in many applications such as industrial process monitoring and control, machine health monitoring and disaster monitoring [2]. Hence, this technology will be applied for this project for data transmission between two nodes.

Internet of Things (IoT) is the internetworking of physical devices that connected between smart devices and other items. The nodes have the capability to send their data to an online server via the Internet, and users are able to control and monitor the nodes remotely across existing network infrastructure through their smartphones or other mobile devices [11]. In IoT, everything is connected to the internet and each thing is uniquely identifiable through its embedded computing system but is able to interoperate within the existing Internet infrastructure. Experts estimate that the IoT will consist of almost 50 billion objects and devices by 2020 [9]. The structure of IoT is based on three main components which sensor nodes, server and applications.

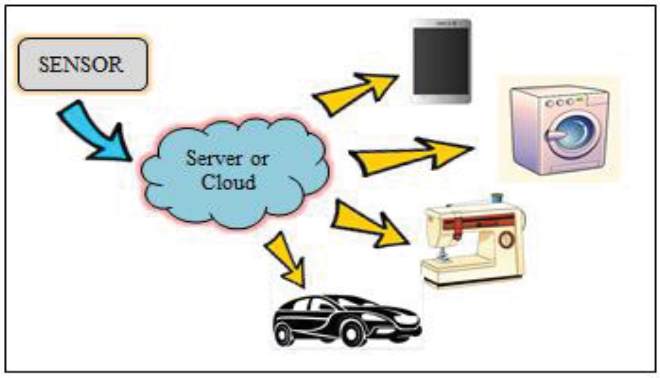

Fig. 1. Main components of IoT

Currently, there are several existing technologies on flood monitoring that have been developed. The technology related to

flood disaster nowadays is not fully applicable and not user friendly. These technologies does not have automated early warning system that will alert the users about flood occurrence or possible flood occurrence. Therefore, this project proposes to introduce a flood monitoring system that can give an early warning to users via Telegram application and the developed webpage.

II. Related Work

Research paper author	System network	Wireless data transferring	Sensor
Md. Asraful Islam, Taoufikul Islam, Minhaz Ahmed Syrus, Nova Ahmed [3]	Mesh Network	Zigbee module	Honeywell water sensor LL103101
Abhijeet A Pasi and UdayBhave [1]	Mesh and grid network	Radio Frequency	Under water Sensor
Ka-Heng Chan, Chi-SengCheang and Wai-Wa Choi [5]	Mesh network	Zigbee module	Ultrasonic Sensor
HarminderKaur, Ravinder Singh Sawhney and NavitaKomal[2]	Need strong network to Base station	WSN	Water Level,

Table 1. Main components of IoT

III. Methodology

A. System Architecture

The concept design of the project is based on Internet of Things (IoT) approach. The WSN is used to transmit data from sensor node to the base station. The sensor nodes, which are located at suspected flood prone areas (e.g. drainage system and sewers), act as the platform to collect data and measure the current water level. This system will help user by giving early warning for flood or flash flood could occur in certain places so that they could avoid those places in advance.

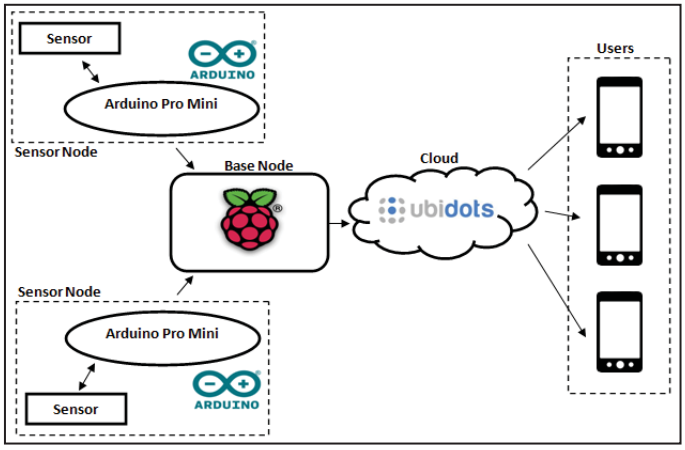

Fig. 2. Project architecture

Fig 2 shows the project architecture for flood monitoring system and the flow of this system from sensor nodes to users. The sensor node is constructed using Arduino Pro Mini equipped with a distance sensor to detect the water level. The collected data from the sensor will be transmitted to the base node which is a Raspberry Pi 3-Model B.

The interface to transmit between the sensor node and the base node is using radio frequency transceiver and able to transmit data up to 2 Mbps. The Wireless Sensor Network (WSN) has been used for transmitting data from sensor node station to base node station. Radio frequency (RF) transceiver module which is NRF24L01+ was used to transmit data. For the communication range of this RF module, it is able to transmit the data up to 250 meters in open area.

The purpose of the base node is to collecting the data from the sensor nodes before transmitting the data to “Ubidots.com”, an online database server. The base node is used to calculate and generate prediction to users and display on the developed webpage. “Ubidots.com” is the platform to collect data via the internet from base node which is Raspberry Pi 3-Model B and embedded into the developed webpage in term of data and chart for users. Furthermore, early warnings are sent to the users via Telegram application from “Ubidots.com”.

B. *Hardware Design*

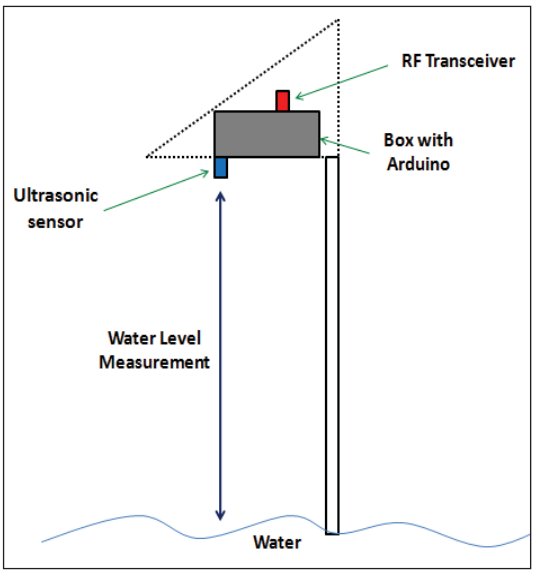

Fig. 3. Sensor Node

This section explains the overall hardware and the devices used in this project development based on the architecture design. An Ultrasonic sensor is used to measure and monitor the rate of change of water level. The water level is measured using ultrasonic sensor to obtain the distance between sensor and the surface of water as shown in Fig 3. This module was designed as a sensor node to collect instantaneous water level and transmit the information to the base node. The data collected at the sensor nodes will be transmitted to the base node using radio frequency transceiver module (NRF24L01+). Both base node and sensor node is connected via radio frequency transceiver module.

Base node which is implemented using by Raspberry Pi 3 functions as the device that collects and process the data. The base node is used to calculate the received data from sensor nodes for the flash flood prediction. Next, the architecture of Internet of Things (IoT) is implemented in the hardware development. Raspberry Pi 3 has a built-in with Wi-Fi Module which enables the base node to connect to the Internet without any external circuit. The data will be transmitted to online database server via Internet.

IV. RESULTS

A. *Sensor Node Station*

To collect data for measuring water level on sensor node, the ultrasonic sensor is used to measure the distance between sensor and the surface of the water. The distance from sensor to the surface of water is measure as current water level.

On the Arduino Software, there are two values displayed on the serial COM monitor as shown in Fig 4. The left side is displays the real distance between the Ultrasonic sensor and the surface of the water while, the right side shows the water level increase as distance decrease. The calculation to obtain water level reading is shown in Equation (1). This sensor is able to measure the distance up to 250 centimeters in open area but for this project, the distance was set up to 200 centimeters only.

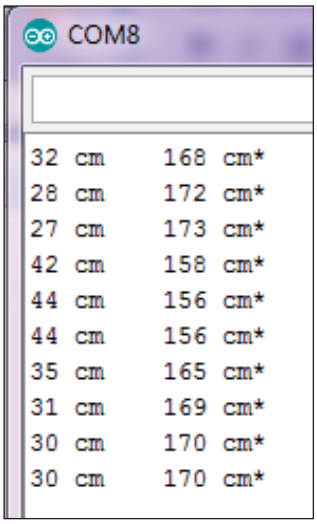

Fig. 4. The ultrasonic sensor data

$$Water\ level(cm) = 200cm\ - Sensor\ reading(cm) \tag{1}$$

B. *Received Data from Sensor Node*

Base node station is also required to implement RF transceiver with NRF24L01+ module to receive data from sensor node. This project was used 2.4GHz as transmitting and receiving frequency because RF transceiver module is operating in the range of frequency from 2.4GHz to 2.525GHz.

Based on Fig 5, it shows the RF transceiver is working well and ready to receive data from sensor node station. The Fig 5 also shows the transfer data rate from sensor node to base node up to 1 Mbps.

```
STATUS    = 0x0e RX_DR=0 TX_DS=0 MAX_RT=0 RX_P_NO=7 TX_FULL=0
RX_ADDR_P0-1     = 0xe7e7e7e7e7 0xf0f0f0f0e1
RX_ADDR_P2-5     = 0xc3 0xc4 0xc5 0xc6
TX_ADDR           = 0xe7e7e7e7e7
RX_PW_P0-6       = 0x00 0x20 0x00 0x00 0x00 0x00
EN_AA             = 0x3f
EN_RXADDR        = 0x03
RF_CH             = 0x76
RF_SETUP         = 0x01
CONFIG            = 0x0c
DYNPD/FEATURE    = 0x3f 0x06
Data Rate         = 1MBPS
Model             = nRF24l01+
CRC Length        = 16 bits
PA Power          = PA_MIN
RECEIVED: [149]
```

Fig. 5. Received data from sensor node

C. Proposed Algorithm

Base node was developed to manipulate received data from sensor node. The received data from sensor node basically is used to predict flash flood occurrence and to set up the threshold level either the water level in normal level or warning level.

The possibility of flash flood is predicted via mathematical method based on the current water level data and the rate of water level increment/decrement. The rate of water level increment/decrement is obtained by calculating the difference between the current water level reading and the previous reading and dividing this difference with the time difference between to reading as shown in Equation (2).

$$water\ level\ change\ rate = \frac{(current\ data - previous\ data)}{t} \quad (2)$$

$$prediction = T(water\ level\ change\ rate) \quad (3)$$

The prediction of flash flood to occur is based on the Equation (3), where the value of T can be change according how often data was collected on sensor nodes. For this project, the data was taken every 10 minutes. The value of T will be used to obtain the prediction for flash flood occurrence.

These formula are being use to calculate the increment of water level based on time. This is the flow to calculate the estimated water level, and flood occurrence prediction.

1) Specify the flash flood prone area.

2) Take a sample data for normal water level.

3) During rainfall, record the increment of water level for specific time.

4) Set the reference water level and the maximum water level at that area in the calculation for Raspberry Pi.

5) Send to online server for users references.

The prediction of flash flood will alert users by giving a notification to prevent users from going to the flood prone places. This alert will activate when there are drastic increments of water level within the time that has been set. Fig 6 shows the example of the prediction.

Based on the sample data in Fig 6, the a "warning level" alert will be given when the water level reaches 140cm or higher. This means the current water level is exceeding the normal water level as labelled with the green box in Fig 6. The data was taken every 10 minutes. If the base node receives three consecutive "warning level" readings (including the first reading), the users will receive second alert as shown in black-dash box. The prediction notification will send to users when consecutive data occur.

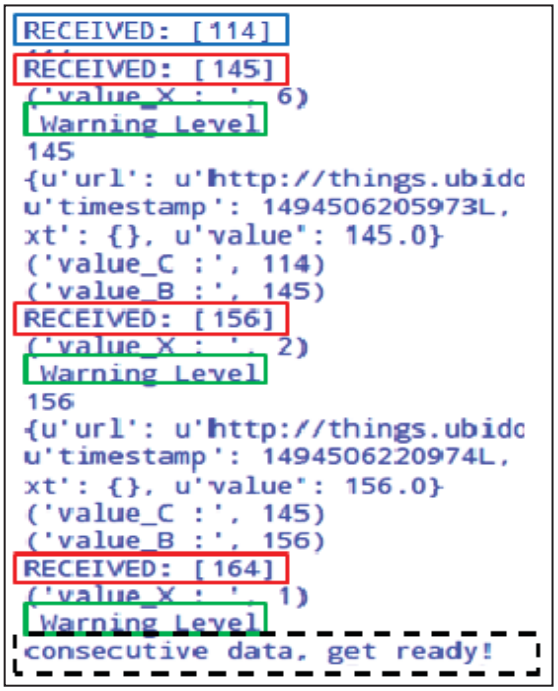

Fig. 6. Example data taken

The water level is divided into three categories of water level which are normal water level, warning water level and the level if the area already flooded as shown in Fig 7. Based on the data that was collected as shown in Fig 6, the received consecutive data have the average increment of 10cm. The investigated area is being set to be flooded when the water level exceeds or equal to 190cm.The prediction of flash flood is calculated using the increment rate of water level and the average time for every data received from sensor nodes. From this example, the average increment of water level is 10 cm and the data is collected at sensor nodes at the interval of 10 minutes. Thus, the water level at the investigated area will reach 190cm approximately in 25 minutes. Users will get a notification of the flood occurance, so that it could prevent them from going to the flooded location.

D. Internet of Things(IoT)

All data are sent to online database server, Ubidots before being displayed on the developed webpage. The webpage functions as a medium to deliver the real-time water level collected by the sensor nodes. Besides that, users are able to receive notification and early warning if flood may occurs via Telegram application. Fig 8 shows the developed webpage displayed real-time water level from sensor nodes.

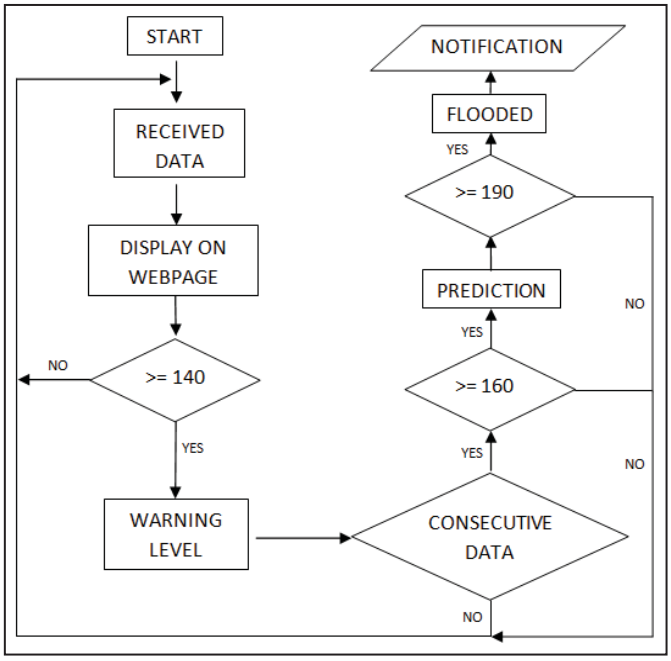

Fig. 7. Flowchart of flash flood

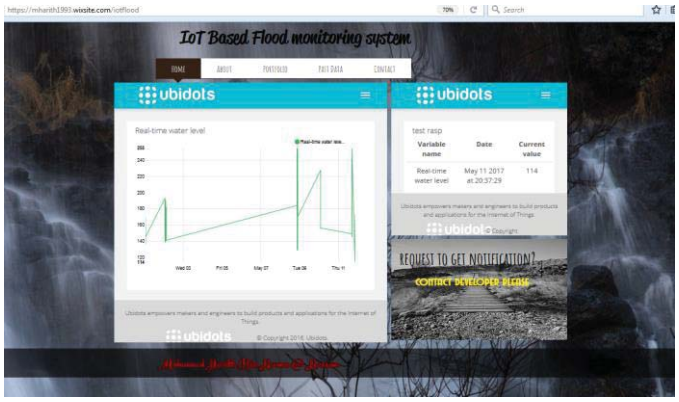

Fig. 8. Developed webpage

E. Communication

This project was developed based on Wireless Sensor Network (WSN) and Internet of Things (IoT). The speed of internet connection for IoT and distance between RF transceiver (sensor node to base node) in WSN due to the packet loss must be highlight. The internet connection and the distance between transceiver will influence data transmission. It will contribute to packets losses due the slower internet connection and longer distance between transceiver. TABLE I shows the comparison between internet connection either 2G, 3G or 4G connections. The slower internet connection will contribute to data packet loss. 2G internet connection is not able to transmit packet data due to limitation of transfer data rate.

TABLE II shows the comparison of packet data transmission of radio frequency module from sensor node to base node due to the distance between two nodes. For NRF24L01+ module, the maximum range for transferring data is up to 250 meter. From TABLE II, if the distance exceeds the maximum range, the packet data start to loss.

TABLE I. COMPARISON BETWEEN INTERNET CONNECTION

Number of packet data transmit	Internet Connection(delivered data)		
	2G	*3G*	*4G*
10 packets data	Not delivered	10 packets	10 packets
20 packets data	Not delivered	20 packets	20 packets

TABLE II. COMPARISON DISTANCE BETWEEN RF

Number of packet data transmit	Distance Between Transceiver (m)		
	90	*180*	*270*
10 packets data	10 packets	10 packets	8 packets
20 packets data	20 packets	20 packets	17 packets

V. CONCLUSION AND FUTURE WORK

Flash flood may occur in less than hour. Therefore, Internet of Things and WSN system may help the users to get quick information for flood disaster and flash flood. A real time flood monitoring has been developed in this project to reduce the possibilities of injuries and get an early warning on flash flood possible occurrence. For this project, the objective to provide real-time flood monitoring system to users was achieved. The water level is collected from sensor nodes and transmits to base node. The received data is used to calculate and do prediction for flash flood occurrence. Then it will display on developed webpage. In overall, this project is correspond with low budget, reliable system and can be implemented to have an early warning for flash flood.

Future works that can be implemented in this project is to use mesh network connection between transceiver. The advantage of using mesh network connection like Zigbee module is the possibility of the sensor nodes to communicate with each other. The maximum range of data transmission is much longer. Other than that, power source need to be considered in future work because this project using batteries which may have limitation. In future work, solar panel may be use as power source in this project.

REFERENCES

[1] Abhijeet A Pasi, UdayBhave. Flood Detection System Using Wireless Sensor Network.2015,IJARCSSE.February 2015.

[2] HarminderKaur, Ravinder Singh Sawhney, NavitaKomal. Wireless Sensor Networks For Disaster Management. 2012, IJARCET. July 2012

[3] Md. Asraful Islam, Taoufikul Islam, Minhaz Ahmed Syrus, Nova Ahmed. Implementation of Flash Flood Monitoring System Based on Wireless Sensor Network in Bangladesh. 2014, IEEE. 2014.

[4] Felan Carlo C. Garcia, Alvin E. Retamar, Joven C. Javier. A real Time Urban Flood Monitoring System For Metro Manilla. 2015, IEEE. 2015.

[5] Ka-Heng Chan, Chi-SengCheang, Wai-Wa Choi. Zigbee Wireless Sensor Network for Surface Drainage Monitoring and Flood Prediction. Dec 2014.

[6] Center for Neighbourhood Technology, Chicago IL, “The prevalence and cost of Urban Flooding”. May 2013.

[7] Evans, Dave. The Internet of Things; How the Next Evolution of the Internet changing Everything. April 2011.

[8] TIOBE software index. TIOBE Programming Community Index Python. 10 September 2015.

[9] A. Yusoff, N. M. Din, S. Yussof and S. U. Khan, "Big data analytics for Flood Information Management in Kelantan, Malaysia," *2015 IEEE Student Conference on Research and Development (SCOReD)*, Kuala Lumpur, 2015, pp. 311-316.

[10] Department of Irrigation and Drainage, Malaysia. "Water level data and Rainfall data Sungai Segamat", 2015-2016.

[11] Brown, Eric (13 September 2016). *"Who Needs the Internet of Things?"*. Linux.com. *Retrieved 23 October 2016*.

EEG Analysis for Chess Player with Different Chess Puzzles

Mohamad Saiful Amri Bin Rahmat
Faculty of Electrical Engineering
Universiti Teknologi Malaysia,
Johor Bahru, Malaysia
saifulamri106@gmail.com

Nasrul Humaimi Bin Mahmood and Norlaili Mat Safri
Faculty of Electrical Engineering
Universiti Teknologi Malaysia,
Johor Bahru, Malaysia
nasrulhumaimi@utm.my

***Abstract*— Chess is one of the examples of the task that need a lot of training and experience. The main aims of this work is comparing between baseline data with different chess puzzles among the subject. However, there are two classification of the subjects, master and novices. While there are consists of 3 types of chess puzzles which are mate in one, mate in two and mate in three or four. The data of the subjects collected by using electroencephalogram (EEG). The method that have been use in this work is Fast Fourier Transform (FFT) method. This method by converting the raw EEG data from time domain into frequency domain which is has been done in Mitsar data processing, EEG device. Then, T-test perform in comparing the overall changes of potential difference of resting state or baseline data with different chess levels. Significant value make sure whether that region has difference or not. The second analysis called frequency band analysis, this part focusing on the individual subject analysis by comparing the range of frequency band. This is due to the different activations of frequency band such as theta, delta, alpha, beta and gamma on human brain region of chess player between master and novices. At the end of the research, result showed there are difference significance value between baseline and different types of chess level and difference of frequency band for every position of subject's brain in different chess puzzle for second analysis.**

Keywords—chess; EEG; Fast Fourier Transform; frequency band

I. INTRODUCTION

Chess games is the games where need two players that played on a chess board with different strategies but main objective is to checkmates the opponent [1]. Most of people all around the world make the chess as their hobby and sometimes as a career. Therefore, the theory always focusing on the chess games and human brain where someone who expert in chess has good thinking style including problem solving and decision making compared to the novices. Then, there are some findings about chess games possibly influence of intelligence.

Firstly, the latest research found that the advance chess player not only score more on intelligent tests than the composed group by novices, but also such performance in correlated with their level of intelligence [2]. In the other research, they focusing about the relationship between intelligence, practice and experience of the playing the chess games. At last, they find out that practice is actually the factor that most influence chess player performance [3].

There are also the study about the effect of chess learning on development of metacognitive ability and the ability to solve problem situations in mathematics [4]. The conduct the group of students took chess lesson for 6 months. Then after 6 months, they try to compare to a control group, presented superior performance both in solving mathematical problem and in metacognitive activities. So, clearly the duration of 6 months of practice chess gives effect to human intelligence.

II. LITERATURE REVIEW

A. Relationship of chess games and brain activity

Chess games is classified as the task that needs a lot of training and experience. A few years ago, there are many researchers had done a research about chess problem. In addition, researchers found that there are some relationship between chess games and human intelligent. For example, there are differences in amplitudes of N2 and P3 components in event-related potential (ERP) signals between professionals and beginners chess player [5].

Then, the other imaging technique which is functional magnetic resonance imaging (fMRI), the different psychological functions and activate different brain areas during chess-related tasks is given as the final results. While comparing between chess players and control subjects obtained grey matter volume and cortical thickness were decreased in chess players compared to control subjects in the OTJ and precunei [6].

The other investigation is on the 4 simple chess problem. For example, "pattern recognition" 'pattern recognition" (if the king was not or on the board); if the king was in check, if the king was checkmated; checkmate in one move. There are noticing the type of given task gives impact to the theta and beta coherences [7].

B. Electroencephalogram (EEG)

Electroencephalography is the imaging technique that use to records and reads the electrical activity that generate by human brain. Then, electroencephalogram (EEG) is defined as electrical activity that recorded from the human scalp by using

metal plate electrodes and conductive media [8]. Thus electroencephalography can be classified as non-invasive method procedure that can be applied repeatedly to human. The metal electrodes that had been place on the subject's scalp will measure the potential difference that was produced during synaptic excitations of the dendrites of many pyramidal neurons in the cerebral cortex. A large number of population of active neurons will generate recordable electrical activity. The potential difference that was produced by the brain is measured from peak to peak and normally range between 0.5 to 100 μV in amplitude. This value is 100 times lower that the ECG signal. A weak signal detected from the metal electrodes are massively amplified, and then stored to the computer memory [9].

Brain waves have been classified into five basic group. Table 1 shows the classification of brain waves in human brain.

TABLE I. CLASSIFICATION OF BRAIN WAVES

Frequency Band	***Frequency***	***Brain State***
Delta	0.5-4 Hz	Sleep stages, especially "deep sleep"
Theta	4-7 Hz	Sleep Stages
Alpha	7.5-14 Hz	Quiet waking
Beta 1	14-20 Hz	Activated cortex
Beta 2	20-30 Hz	Activated cortex
Gamma	30-40 Hz	"cognitive" frequency band

The electrode that will be used in this analysis known as 10-20 electrode placement system or International 10-20 system shown in figure [1].

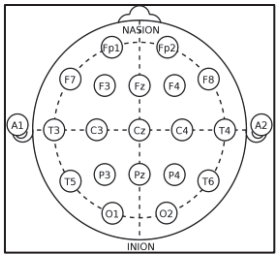

Figure 1: 10-20 electrode system

Then, the area of the brain was covered by this type of electrodes are F(frontal), C(central), P(posterior), and O(occipital). There are a specific labelling of human brain. The label of the 10-20 electrode system are Fp1, Fp2, Fpz, F7, F3, F3, F4, F8, C3, Cz, C4, T5, P3, Pz, P4, T6, O1, O2 and A1, A2 as reference electrodes. The odd number letter will be located at the left side of the head while the even number letter on the right side. Electrode cap is the type of electrode will be used in this project. Electrode caps consist of Ag-AgCl disks, with long flexible leads that can be directly plugged into an amplifier [10].

C. Human brain and its function

Human brain is the central organ of human nervous system. In addition, most of the activities of the body control by brain. There are several function of the brain such as processes, integrates, and coordinates all of the information it receives from the sense organs. Then, any changes of surrounding like temperature, humidity, feel and many more results in changes of brain activity. Human brain consists three parts: the brainstem, cerebellum and cerebrum. However, cerebrum is divided into four lobes named frontal, temporal, parietal and occipital. Different lobes played different roles.

Firstly, frontal lobes consist of two part which are right and left frontal lobes. The location of the lobes is at the forehead or front of human brain. The main function of this lobes are including response maintenance, problem solving, and cognitive flexibility in the body [11]. Secondly, temporal lobes is located at the beneath of lateral fissure on both cerebral hemisphere on human brain. It is same with frontal lobes which consist two part which are right temporal lobes and left temporal lobes. The function of temporal lobes are processing sensory input into the visual memories, emotions and language comprehension. Thirdly, parietal lobes also consist two parts. The main function of this lobes is integrating sensory information to form a single perception or cognition. Finally, the function of the occipital lobes is action as visual processing center.

III. METHODOLOGY

This section presents the applied method to the chess player and some analysis involved. There are 6 chess players as the subject were tested. Three of them is master in chess and the other remaining three is novices in chess games. Players took the chess matches with the computer with the help of chess application. There are three different chess puzzles need to be settled up by chess player which is mate in one (easy level), mate in two (intermediate level) and mate in three or four (difficult level). The chess application was displayed in the tablet. All subjects need to play the chess puzzles for 3 minutes each puzzle. Before that, it is important to ask all subjects to close their eyes for 2 minutes for their baseline data. During (and before) each puzzle the EEG signal from each player was recorded in 10-20 system. Then, the following electrodes were used:Fp1, Fp2, F7, F3, Fz, F4, F8, T3, C3, Cz, C4,T4, T5, Pz, P4, T6, O1, Oz, O2 and A1, A2 as reference electrodes; sampling frequency was 500 Hz. In the other hand, EEG signal was filtered with band pass 0.53-150 Hz and notch filter 45-55 Hz filter.

A. Data processing

Ordinary data known as raw data contain desired data and noises. There are several methods to get clean data. Firstly, using the Butterworth filter to filter noise in raw data. Next, the raw data in the form of time domain need to convert to frequency domain by using Fast Fourier Transform (FFT).

Fast Fourier Transform (FFT) given by (1) is the method to reduce the complexity of the Discrete Fourier Transform (DFT) [12] analysis. The amplitude of each frequency component is different for each electrode region, and was used to identify and classify into specific frequency.

$$x(n)=\frac{1}{N}\sum_{n=0}^{N-1} X(k)\, W_N^{-nk} \qquad (1)$$

After the FFT analysis was finished, all data were classified in the group of frequency band with the unit power/ frequency, μV^2.

B. Data Analysis

In this part, data of all subjects need to be analyze as the final result. In data analysis, t-test used as method. T-test given by (2), is an analysis of two or more population of means through the use of statistical examination. T-test was done by using Excel. There are several characteristics T-test. In this situation, we used 1-tailed distribution and type 1 which is paired.

$$t = \frac{\bar{x}_1 - \bar{x}_2}{\sqrt{\frac{s_1^2}{n_1} + \frac{s_2^2}{n_2}}} \qquad (2)$$

There are 3 different categories of test that need to be done like comparison between baseline data and mate in one puzzle (Easy), baseline data and mate in two (Middle) and baseline data and mate in three or four (Difficult). In addition, every test need to be compared with the same frequency band and need to be applied for every single part of electrode system. For instance, alpha band need to be compared with alpha band in order to gain significance difference in Fp1 region and followed with the other parts. The result from t-test are classified based on the significant value.

Other data analysis is frequency band comparison, in this part, list out of the frequency value divided into specific frequency range. As mentioned before, 6 types of frequency band such as delta, theta, alpha, beta 1, beta 2 and gamma refer table 1. The final data will be display in the form of brain mapping in order to make it easy to understand.

IV. RESULT AND DISCUSSION

This part discussed about result of all the subjects. Before than that, baseline signal framed out from 0.05 minutes to 2.05 minutes. Then, time frame for chess puzzle taken from 0.05 minutes to 3.05 minutes. Result divided into 2 types, T-test result and frequency band comparison.

A. T-test Result

Data of 6 subjects examined by using T-test. Bar chart represented the data of the subject based on significant values. Firstly, when significant difference, $p < 0.05$ the value of y-axis represented as "1", while when significant difference, $p < 0.001$ the value of y-axis represented as "2". There are 3 data of T-test which are Baseline data – Mate in One, Baseline data – Mate in Two and Baseline – Mate in Three or Four.

From the result above, clearly the number of significance difference of baseline-mate in one is the lowest. This is due to the mate in one chess puzzle is the simplest chess puzzle compared to the other two puzzle. The subject just use their ordinary skill to complete the task without thinking a lot about the strategies. The regions that have significant difference for baseline-mate in one chess puzzle are C3, T5, P3, PZ, P4, T6, O1 and O2. The highest significant value is at T5, P3 and T6. The highest value of significant difference are T5 and T6. Besides, the activation frequency band for this chess level are alpha and theta.

Secondly, from figure (2), the number of significant difference at baseline-mate in two chess puzzle is the highest. All regions of electrode consists of significant value except region Fz and F4. The region that have significant value of "2" are C3, CZ, C4, T4, T5, P3, PZ, P4, T6, O1 and O2. The activation of frequency band include delta, theta, alpha, beta 1 and gamma. From figure (4), baseline-mate in three or four puzzle are classified as a difficult task. So the significant difference value are different from the others two puzzle. The region that have difference of significant value are F4, T3, C3, CZ, C4, T4, T5, P3, PZ, P4, T6, O1 and O2. For the region that have "2" difference in significant value are T5, P3, P4, T6, 01 and O2. The activation of frequency band include delta, theta and alpha.

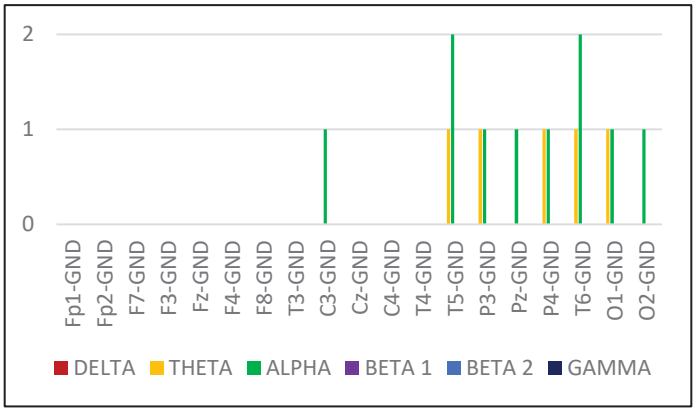

Figure 2: Baseline-Mate in one

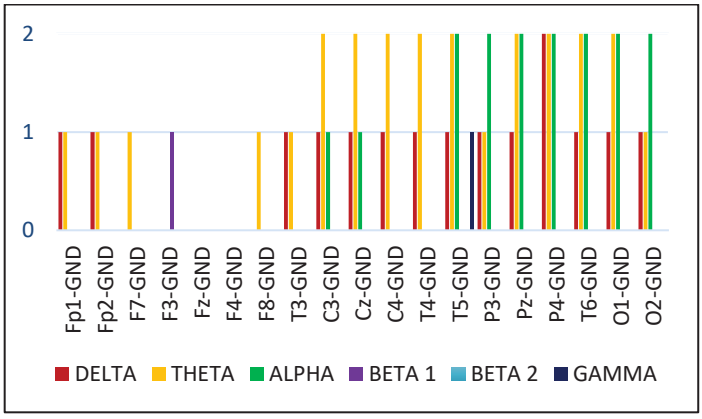

Figure 3: Baseline-Mate in two

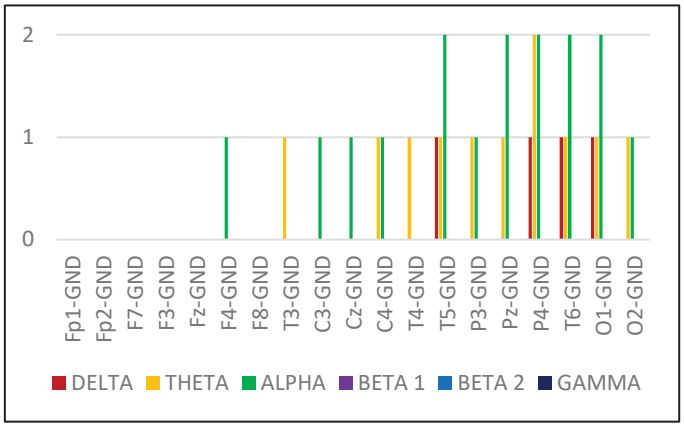

Figure 4 Baseline-Mate in three or four

The brain region that have significant difference which is the similar for all subjects in each chess puzzle are C3, T5, P3, PZ, P4, T6, O1 and O2. Next, the delta frequency is lower in baseline-mate in one compared to baseline-mate in three or four. In difficult task which is baseline-mate in three or four the region that have significant value are F4, T3 and C4. These 3 region of brain part does not consist in the other puzzles.

B. Frequency Band Result

This part is the comparison between player A, player B and player C where data displayed on brain mapping. All these player are classified based on national rating. Firstly, player A national rating is 1485. Then, player B national rating is 1697 and player C classified as unrated chess player. The detail about puzzle solved and success for every task competed by both subjects are shown in Table 2.

TABLE II. CHESS TASK COMPLETED BY SUBJECT

Player / Puzzle	A		B		C	
	Solved	Success	Solved	Success	Solved	Success
Mate in one	$^{68}/_{72}$	98%	$^{68}/_{72}$	96%	$^{50}/_{72}$	45%
Mate in two	$^{20}/_{40}$	94%	$^{18}/_{40}$	93%	$^{10}/_{40}$	46%
Mate in three or four	$^{8}/_{13}$	83%	$^{7}/_{13}$	86%	$^{2}/_{13}$	35%

This part, calculation of average for the overall time frame is needed in order to get mean of frequency of brain location. Therefore, it is easy to classify data based on frequency band. Brain activity affected by chess puzzle and cause the different of frequency band for every region. . The different types of colour represent the frequency band like delta(maroon), theta(yellow), beta 1(purple), beta 2(blue tiffany) and gamma(blue). Firstly, baseline data for player A, subject 1 the frequency band for region F3 is gamma. Then, region T3 and C4 is beta 1. Region T4 is beta 2 and the remaining regions are alpha. While mate in two puzzle, only 2 frequency band are activate which are beta 1 for the region Fp2 and F4, for the others region is alpha band. The middle puzzle level which is mate in two, the frequency band for Fz is theta and T6 is beta 1. For mate in three or four level the only one region consist beta 1 band was Fp1 and the remaining is alpha band.

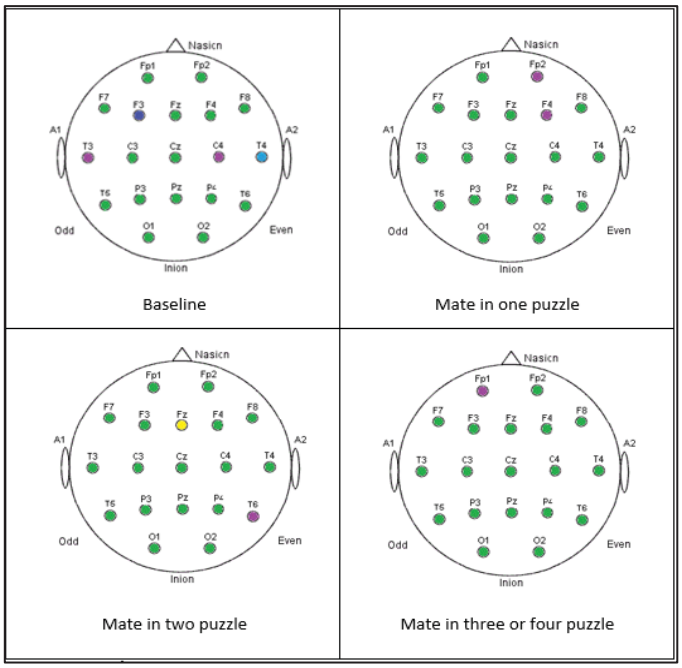

Figure 5: Frequency band for player A

Figure 6 is the result from player B show different region of brain activation compared to subject 1. Firstly, baseline showed Fp1, Fp2, F3, Fz, F4 and T3 are beta 2 frequency band. While, for the region F7, C3, Cz, C4, T4 and F4 are beta 1 band. The other remaining regions are alpha band. Next, mate in one consist 4 different frequencies band. Region Fp1, Fp2, F3, T3, C3, Cz, C4, T4 and P4 are beta 1 band. Then, F2 region is beta 1 and F8 region is delta. The number of beta 2 band decreases and beta band increases in easy puzzle of chess puzzle compared to baseline data.

Thirdly, mate in two puzzle consist of 3 types of frequency band like beta 1, delta and alpha. Beta 1 band in this chess level are Fp1, F3, Fz, T3 and C4. Surprisingly, F8 region remain same band with first puzzle which is delta band. Finally, there are increment of delta band in mate in three and four. The region that consist delta band are Fz, F4, F8, Cz, and C3. In this puzzle, there are 4 theta band which is in the region of Fp1, P3, Pz and P4.

Result of player C are shown in figure 7. He is novice in chess games. The final result showed there are consists two frequency band which is alpha and beta 1. In baseline stage, all the electrode result in alpha band due to resting stage of subject.

Figure 6: Brain mapping of player B

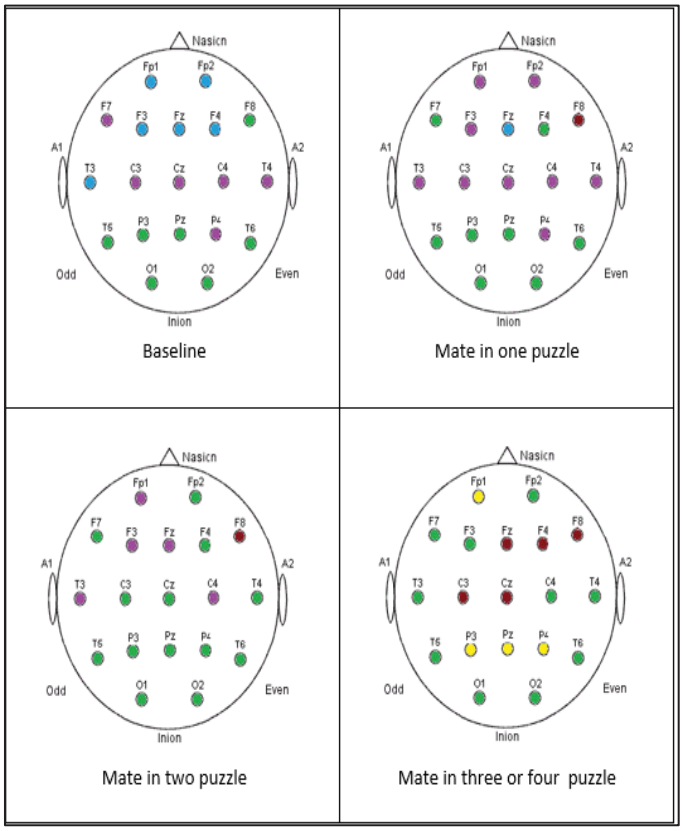

Figure 6: Brain mapping of player B

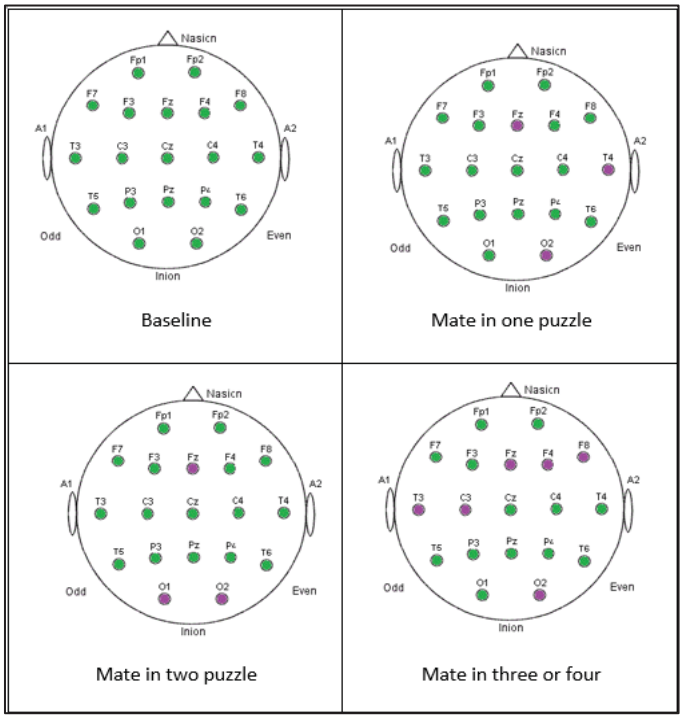

Figure7: Brain mapping of player C

Then, in easy stage the region that have change the frequency band to beta 1 are Fz, T4 and O2 whereas the other region remain the same frequency band. Next, the region of Fz, O1 and O2 are beta 1 while in middle chess puzzle. Last but not least, the number of electrode region change from alpha to beta 1 increase in Mate in three or four. All these regions are Fz, F4, F8, T3, C3 and O2

After comparing between novice and master in chess, the observation that can make is the changes of the frequency band from alpha to another frequencies band is from lower level to higher of chess level is novice chess player. While master in chess shown the same distribution of the frequency band form lower chess level to the higher. The reason why, the mater in chess have a lot of experience and training compared to the novices.

V. CONCLUSION

In T-test, the value of significance difference are different for different chess puzzle whereas the number of significant difference is lowest in baseline-mate in one and highest in baseline-mate in two. In addition, there are 3 regions that only have significant difference in baseline-mate in one but not consist in other chess level which are F4, T3 and C4 region. Next, the comparison between master and novice player showed different region of activation of frequency band for different chess puzzle. There are different between novices and master in chess whereas master in chess does not show to too much changes from baseline to difficult puzzle. Besides, the novice showed the increment of the beta 1 band form baseline to difficult chess level. For improvement, the need of gathering more data from more chess experts and comparing them with data from novice chess players.

REFERENCES

[1] Chisholm, Hugh, ed. (1911). "Chess". Encyclopædia Britannica. 6 (11th ed.). Cambridge University Press. pp. 93–106.

[2] R .H. Grabner. The role of intelligence for performance in the prototypical expertise domain of chess. Intelligence, 45: 26-33, 2014

[3] M. Bilalić, P. McLeod, F. Gobet. Does chess need intelligence? A study with young chess players. Intelligence, 35:457–470, 2007.

[4] F. Kazemi, M. Yektayar, A.M.B Abad. Investigation the impact of chess play on developing metacognitive ability and math problem-solving power of students at different levels of education. Procedia - Social and Behavioral Sciences, 32:372 – 379, 2012.

[5] Wright MJ, Gobet F, Chassy P, Ramchandani PN. Erp to chess stimuli reveal expert-novice differences in the amplitudes of n2 and p3 components. Psychophysiology. 2013; 50(10):1023–33.

[6] Hänggi J, Brütsch K, Siegel AM, Jäncke L. The architecture of the chess player's brain. Neuropsychologia. 2014; 62(0):152–62.

[7] Volke H-J, Dettmar P, Richter P, Rudolf M. Evoked coherences of eeg in chess playing. Int J Psychophysiol. 1998; 30(1-2):225–6.

[8] E. Niedermeyer, F. H. Lopes da Silva. 1993. Electroencephalography: Basic principles, clinical applications and related fields, 3rd edition, Lippincott, Williams & Wilkins, Philadelphia.

[9] F. S. Tyner, J. R.Knott. 1989. Fundamentals of EEG technology, Volume 1: Basic concepts and methods, Raven press, New York.

[10] J. D. Bronzino. 1995. Principles of Electroencephalography. In: J.D. Bronzino ed. The Biomedical Engineering Handbook, pp. 201-212, CRC Press, Florida.

[11] Julie A. Alvarez and Eugene Emory, 2006, Executive Function and the Frontal Lobes: Meta-Analytical review, vol 16. No.1

[12] A. V. Oppenheim and A. S. Willsky. Signals & Systems. Prentice Hall: Massachusetts Institute of Technology. 1997. p. 957.

.

Development of ROV Control System

Yeang Meng Hern
Faculty of Electrical Engineering
Universiti Teknologi Malaysia
Skudai, Johor Bahru, Malaysia.
yeang93@gmail.com

Prof. Madya Dr. Azli Bin Yahya
Faculty of Electrical Engineering
Universiti Teknologi Malaysia
Skudai, Johor Bahru, Malaysia.
azliyahya@utm.my

***Abstract*— Remotely Operated Vehicles (ROV) is a vehicle that is designed for the aquatic work environments such as underwater inspections, searching purpose and so all. There were many industries such as oil and gas industries are relying on this vehicle for their works and researches. There are many considerations and specifications of the development of the ROV such as the mechanical structurers, power system, communication system and the control system to operate the motions and functions of the ROV. Thus, the aim for this project is to develop a small scaled ROV with an advanced control system using high level programming. The platform to perform the control system is through MATLAB GUIDE software in order to support and program the Arduino microcontroller of the ROV. The software can support real time monitoring through the web camera installed in the ROV. Few image processing tools such as edges detections, contrast and so all will be performed for measuring the crack of the building. MATLAB GUIDE also provides a simple graphical user interface to control the motion of the ROV. Thus, the development of the ROV control system can be enhanced by using MATLAB GUIDE.**

Keywords—ROV; control system; MATLAB GUIDE ; arduino; real time monitoring

I. INTRODUCTION

A. Background of study

Unmanned underwater vehicle (UUV) is a vehicle that helps the human to work under the aquatic environment without a human inside the vehicles. Basically, these vehicles can be classified to two types, which is autonomous underwater vehicle (AUV) and remotely operated vehicle (ROV). [1] The operation of the AUV does not dependent to the user. It is based on the designed control system on it. While, ROV is a controlled vessel that requires full operation by the user. [2]. From the definition, the ROV can be classified as the simplest underwater robotic to design compared to the AUV. [3]

The operation of the ROV basically is controlled by using a remote control and a window controller is used for the monitoring purpose. In this project, the ROV's control system and the Graphical User Interface (GUI) are designed by using the MATLAB GUIDE. This project is more focusing on designing a serial interface system that is used to control the microcontroller of the ROV for the operation of ROV. Arduino board is used as the microcontroller to control all the servo motors and the web camera of the ROV. Besides, the project is also focus on the specification and the consideration in designing the mechanical part of the ROV to support the control system.

B. Statement of problem

Remotely Operated Vehicles is a very important vehicle that helps human to explore the underwater world for several purposes such as researches, search and rescues, industrial commercial purpose and so all. Human's ability is limited in the water therefore this vehicle can help in doing any underwater works. Thus, ROV has becoming more important over a wide range of application. However, most of the ROV are from overseas country and none of them is made in Malaysia. The price for the ROV is very high in the market and the scale of the ROV is very huge in size. Besides, some of the ROV's control system are not friendly to all users.

C. Objectives of the Study

Based on the problem statement and design specification, there are a few objectives needed to be achieved in this project:

- To design and develop a complete ROV.
- To implement the control system and the Graphical User Interface (GUI) of the ROV using MATLAB GUIDE and Arduino microcontroller.
- To simplify the control and system design of the ROV and friendly to all users.
- To develop a low cost and small scale ROV for underwater building inspection.

D. Scope of the Study

In this project, the ROV will be developed and designed according to the consideration and specification by fulfilling all the objectives of the project. Basically, the development of the ROV consist of two section, which is hardware design and software development. The hardware design of the ROV should consider about the buoyancy system, the hydrodynamic structure, and the waterproofing. The structure of the ROV is a cylindrical PVC pipe with a clear hemisphere dome at the front for camera viewing which is based on the hydrodynamic design. This design is used to reduce the drag and the friction exerted on the ROV when it is moving in the water. There are two thrusters mounted on the middle and the back of the ROV's body respectively for vertical and horizontal motion

purpose. A rudder is attached at the back of the ROV for changing the direction. The ROV is equipped with O-rings in between the joints of the PVC for the waterproofing system.
For the software development, there are two parts need to be considered which are the control system and the GUI for the ROV. MATLAB GUIDE is used to design the control system of the ROV where by the motion and the direction of the ROV can be controlled through the laptop by interfacing it with mouse. Arduino is used as the microcontroller of the ROV to control servo and the thrusters. Besides, MATLAB GUIDE also helps to implement the real-time inspection from the web camera. A GUI will be created to control the speed of the motors, the direction of ROV and the view of the camera. A USB serial port cable is used in the communication between the microcontroller and the computer.

II. LITERITURE REVIEW

ROV is a device that is designed for the aquatic work environments. We are required to have an insightful understanding on the control system in the ROV as well as the mechatronics parts for the movement of the ROV in order to design and develop a ROV. It is important to research and review on other ROV model in term of the design, function, and the control system so that we can gather more information and the data to improve the purposed design.

A. Buoyancy System

Buoyancy system design is a very important criterion to develop a ROV. Positive Buoyancy is needed to make the ROV float in the water and, also to improve the payload capacity of the ROV. Light weight structure such as syntactic foam is one of the method to achieve positive buoyancy of the ROV. This syntactic foam is a type of low density and high durability material that are widely used in subsea buoyancy applications such as ROV. Besides, there are many researches on building the buoyancy system of the ROV by using flexible ballast tank system. The ballast tank helps to control the buoyancy of the ROV by controlling the volume of water inside the tank. A research from Universiti Teknologi Malaysia Melaka had developed an auto depth control for ROV using flexible ballast tank system. In this ROV project, the flexible ballast tank is implemented by adding a pressure sensor to activate as a feedback for ballast tank system in controlling the flow of water in the tank itself to a certain control depth. [4]

B. Waterproofing

Waterproofing is also a significant issue in developing a ROV. The ROV must be waterproofed to prevent the damage of its circuit system. All the important parts must be sealed. O-rings are normally used for waterproofing the homebuilt ROV. The O-rings is usually located in between the connectors. The O-rings will be compressed and filled the gap between the connectors. Therefore, water cannot leak into the ROV. Moreover, the waterproof components also needed to be considered such as waterproofed servo motor, wiring and the connectors. A ROV technical report from Linn-Benton Community College stated that they used a flexible sleeve custom-made to stretch around existing connectors to solve the problem. The inner diameter of the connector sleeves is significantly smaller than the connector it is designed to fit over to keep the connectors dry by making a tight seal around the connector. Also, the soft silicone material compresses as the water pressure increases, forming a tighter seal at higher pressures. [5]

C. Hydrodynamic design

Dynamic motion inside the water basically is related to the hydrodynamic principle. The friction and drag of a moving object in a liquid is much higher than in the air. A hydrodynamic shape or design eventually can help to decrease the drag and friction in the water. Based on the research done by Roslan, he showed two different ROV designs for the hydrodynamic effect on the ROVs. One of the ROV with the smooth curve and another with the sharp edges. This two ROV models are tested using computational fluid dynamic (CFD) code of Flow Simulation module to observe and analyze the flow of resistance pattern in the water. The result shows the pressure exerted on the hydrodynamic shaped ROV is less than the other.

D. ROV Control Architecture

The control architecture of the ROV is varied depending on its specific functions. There are some reviews on some types control architecture with different model of ROV.

a) SY-II ROV Control Architecture

The control architecture of the SY-II ROV is divided into two part, surface platform and underwater vehicle. The control architecture on the surface platform consists of a wireless hand control unit which is used to control the motion of ROV. The LCD TV is used for the real-time inspection of water images shot by the ROV's video camera, an optical transmitter and receiver, which is responsible for digital data transmission and reception, hand control unit and so on. [6]

b) DENA ROV Control Architecture

The architecture consists of five electronic boards such as Board of Control, Power Board, Arm-Sensor Board and two identical Thrusters Boards. [7] The control board contains two microcontrollers which are equipment microcontroller and main microcontroller. AVR ATmega microcontroller series is the selected as both controllers because AVR ATmega microcontroller help to enhance the ROV control system such as watchdog timer which can help to reduce noises in the system, the ability to generate PWM pulses and others. [7] The programming parts are designed by using Visual Basic.NET. There are 3 layers in the programming part, which are Graphical User Interface, Software, and Interface layers.

III. METHODOLOGY

In this section, the project flow of designing and developing a ROV was explained from the starting until the end. The process of each stage was also discussed in detail from the material used and the steps to test and analyzing the performance of the ROV.

A. Project Flow

Figure 1. shows the flow chart of the whole project flow and steps. The project started with the hardware and software conceptual design. After the design concepts are determined, an engineering drawings is drawn out as the reference during the hardware development and assembly. Next, the materials were listed and purchased for the hardware development. At the same time, the circuitry and software development were started. When both hardware and software were done, the assembling process was taken place. During the assembling process, all the commands of the software were programmed into the microcontroller and ready for the next stage which is the testing and the tuning of the ROV. After the testing and tuning were done, the data collected was analyzed and visualized using graphs for documentation.

Fig. 1. Project Flow Chart

B. Hardware development

There are 3 major considerations for designing a workable ROV which are waterproofing, buoyancy system and the hydrodynamic design of the ROV. These concerns are important for the ROV to have the dynamics movements in the water without affecting the controlling circuit system inside the ROV. First, the basic structure of the ROV is designed based on the hydrodynamic structure. Therefore, the ROV's structure is made of the cylindrical shape with an acrylic hemisphere dome. This can help to reduce the friction force exerted on the ROV. An engineering drawing is drawn using Solidwork and is shown in Figure 2. Besides, the material for ROV's body structures is the 4 inch's PVC pipe because the hollow PVC pipe has the buoyancy force which allow the ROV to float just under the water. Besides, the waterproofing of the ROV is done by using the O-rings. The PVC pipe is closed by the end cap with an O-rings at the inner part of the end cap.

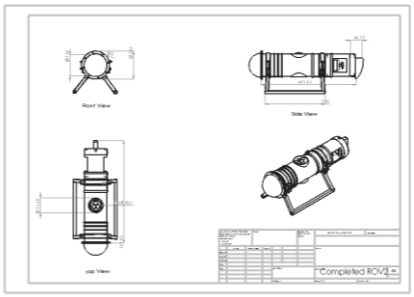

Fig. 2. Engineering Drawing with 2D dimension

C. Propulsion System

The propulsion system is very important in developing a ROV. Two thrusters will be used for the propulsion system in this project. One is attached on the middle of the ROV's body for vertical motion and another one will be attached on the back of the ROV for horizontal movement. The bilge pumps are used as the motor and the propeller used is the 2-bladed rake type propeller. A rudder is installed at the back of the ROV for direction changing purpose. A waterproof servo motor is used to move the rudder to change the direction of the ROV's motion.

D. Control Architecture

In the control architecture of the ROV, Arduino Uno is used as the microcontroller to control the motion of the ROV. The software used to program the microcontroller is MATLAB GUIDE. The purpose of choosing MATLAB GUIDE as the platform to program the ROV's control system is because MATLAB GUIDE can create a GUI for the ROV's control system and can program the web camera at the same time. Besides, thousands of prebuilt functions for image processing can be used to enhance the captured image. A mouse and a computer are needed for the users to control the motion of the ROV through the communication system via USB serial cable. The user uses mouse to click on the GUI on the computer screen to send the signal to the microcontroller for controlling the servo motors and the thrusters. A real-time inspection window is also created on the GUI for the web camera to inspect under the water. Figure 3 illustrates the flow chart of the control architecture of the ROV.

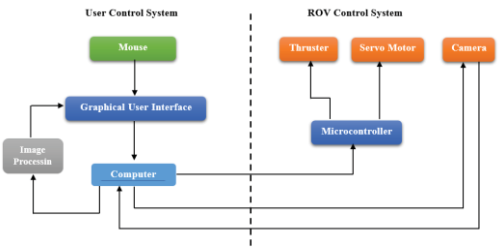

Fig. 3. Flow Chart of ROV's control architecture

E. Circuit design

In designing the circuitry of the system, the power consumption is always the main concern. There are two 12 V, 1.2 Ah battery to supply to the two thrusters which means each thruster uses one battery. Through this configuration, the operation hour of the ROV will increase. Furthermore, there are one 9 V battery used to supply the microcontroller because the supply from the USB serial cable is not enough to control the servo motors. Two motor shield driver, L298N are used in the system to control the direction and speed of the thrusters.

F. Testing and Tuning

After the ROV is fully assembled, the ROV will undergo the process of testing and tuning. The test will be tested in the pool. The process of testing involves the waterproofing test, control system test, communication test, and video test. Each of the process will be recorded for documentation. Calibration and tuning are needed for the system to achieve better performance.

IV. Result and Discussion

A. Hardware Implementation

The hardware implementation of the ROV in this project has been successfully built by following the specification and, also the engineering drawing design. The implementation works are mainly done in the laboratory with basic equipment. The development of hardware can be divided into few parts:

a) Support frame

The mild steel and aluminum plate are used to make the support. It requires welding technique to join them together. L-bar, bolt and nuts are used to assembly the parts to become the supports. The support is light and durable and can withstand the weight of the ROV.

Fig. 4. ROV support frame

b) Rudder

Another important part in implementing the hardware of ROV is the rudder part. The rudder is made of acrylic sheet and the design is as shown in figure. The parts are assembled by using bolt and nuts. The design of the rudder enable the servo motor to move the rudder by pulling and pushing.

Fig. 5. ROV rudder part

c) Front viewing deck

The hemisphere of the front deck is made from CCTV covers and the acrylic sheets. This hemisphere shape is the hydrodynamic design where it can reduce the friction during the motion in the water. The web camera will be placed in the front deck and is clear to capture the image.

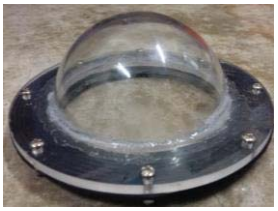

Fig. 6. ROV front viewing deck

B. Control Architecture

There are a few parts needed to be considered in developing the control architecture of the ROV which are GUI, MATLAB programming and the circuitry of the ROV control system.

a) MATLAB programming

In this project, MATLAB is used to program the Arduino, the microcontroller of the ROV. Thus, we need to install the supported package to access the permission of programming the Arduino. Figure 7 illustrates communication between the Arduino and computer using MATLAB language. The coding shows one of the callback function of the slider in the MATLAB GUI. The slider value is varied by the users and the value is then convert to the pulse width modulation (PWM) signal to control the speed of the ROV.

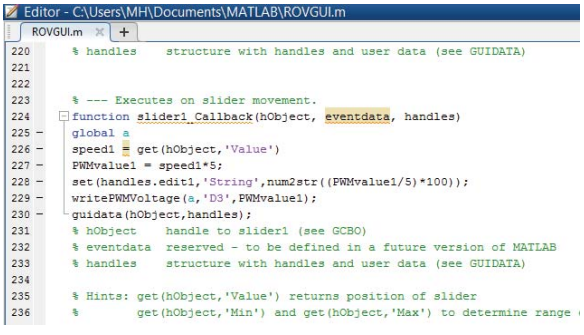

Fig. 7. Programming of ROV's control system in MATLAB

b) Graphical User Interface

A graphical user interface is created through MATLAB GUIDE for the users. Users can control the ROV by clicking

the buttons and slides bar using mouse. Besides, there will be a camera view in the GUI as well for the real-time inspection. The buttons for controlling the ROV are divided into 4 sections which are forward thruster, vertical thruster, direction motor and camera motor. Each section performs their function simultaneously. Figure 8. shows the design of the GUI for the ROV.

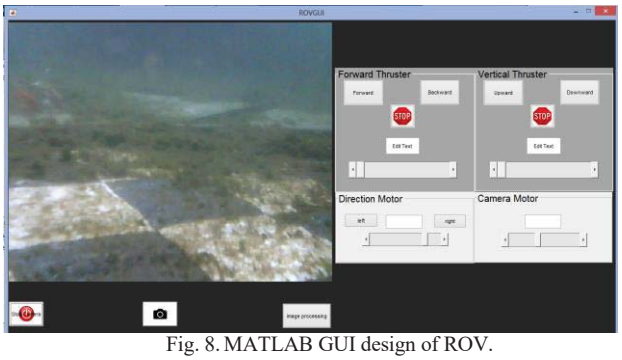

Fig. 8. MATLAB GUI design of ROV.

c) Circuitry

The circuit of the control system of the ROV is mainly located inside the body of the ROV. There are few components in the control system such as batteries, Arduino Uno board, bilge pump, servo motor, motor driver and the web camera. The wiring of the components is mainly wrapped by using the tape to prevent the leakage cases happen. Besides, the components are fixed inside the body of ROV using the duct tape.

C. Full design

The structure of the ROV is basically done if both hardware and software are assembled. The completed ROV is then tested on ground and under the water for data analyzing. Figure 9 shows the full structure of the ROV with all the parts assembled.

Fig. 9. Full ROV design

Based on Figure 10, the ROV is tested under the water and the results shows that the ROV is waterproofed and the buoyancy force is enough for floating. Thus, the ROV has passed the minimum requirement of the underwater ROV through the test. The ROV is then tested under the water for functionality test and also motion test.

Fig. 10. ROV is under the water for testing

D. CFD Simulation

A simple CFD simulation is done using Autodesk to verify the design of the ROV. The velocity of the water flow is 60 km/h Two model are compared with 1 flat surface and another with hydrodynamic shape. From the result, we can observe that the red region on the hydrodynamic design is smaller than the flat surface design. The red region represents the pressure exerted on the surface. The pressure exerted on the hydrodynamic design is 10kPa while the pressure exerted on the flat surface design is 15kPa. Thus, the design of the ROV in this project reduced the friction and pressure exerted on the project.

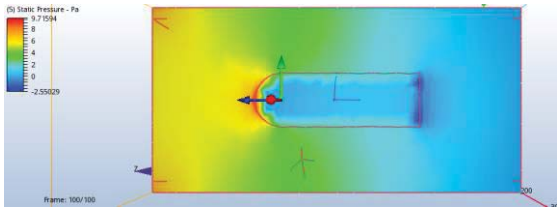

Fig. 11. CFD simulation with hydrodynamic shape module.

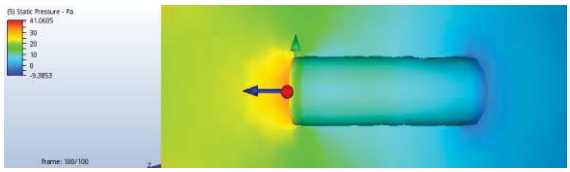

Fig. 12. CFD simulation with non-hydrodynamic shape module.

E. Camera View with Image Processing

The web camera is installed in the ROV and is attached to the servo motor where it can change the vertical direction to see different view. There is a capture function for the camera in the GUI to capture the image when having real-time inspection. The captured image will be saved in a folder and can apply image processing on it such as edges detections, contrast to make the captured image clearer. Figure 13 shows the different view of the camera with different angle.

Fig. 13. Camera View of ROV in 45 degree(left), 90 degree(middle) and 135 degree (right).

Figure 14 illustrate the image processing functions of the ROV. The figure on the left is the image captured under the water. The image is then undergoing image enhancement by increasing the contrast, we can see the image is clearer.

Therefore, the function is the same to apply the underwater building inspection. The main function of the ROV in this project is building inspection. Thus, this can enhance the process of the building inspection by having the clearer image.

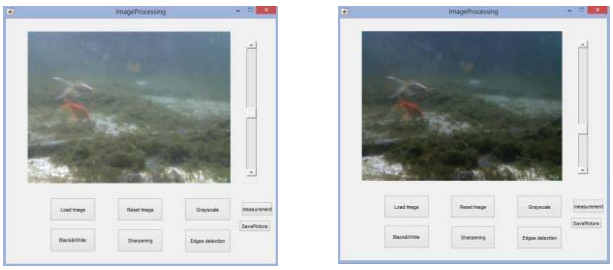

Fig. 14. The image processing on the captured image.

V. CONCLUSION

A. Conclusion

In conclusion, the project is describing about the process of development of ROV control system. A complete ROV including the hardware development of the ROV is constructed in order to test the development control system of the ROV. The project started with the conceptual hardware design of the ROV by using SolidWork 2014. All the specification such as the waterproof, buoyancy forces are considered in the process of designing the hardware structure of the ROV. The materials used for constructing the hardware part of the ROV are PVC pipes and the acrylic sheets. On the other hand, the software development, it divided into two parts which is the control system and the GUI. MATLAB GUIDE will be used to develop the control system of the ROV and an Arduino microcontroller is used as the interconnection between the user control surface and the ROV control surface. The hardware and software of the ROV are assembled after both of them are completed. The assembled ROV is then tested under the water for data analyzing. The results show that the ROV passed the minimum requirement of a ROV which is waterproofed and can float on the water. The functionality of the servo motors and thrusters are good in the water. However, there are some limitation where the ROV cannot move in the expected speed even the motors are in full speed. The real-time inspection is achieved and the image capture and the image processing functions are function well.

Based on the results, most of the function of the ROV are function well. The project has achieved the objectives where the ROV is developed in small and low cost by using MATLAB GUIDE. It is suitable for the underwater building inspection

B. Future Recommendation

There is limitation of the developed ROV where the ROV is designed for a maximum depth of 5meter only due to the limitation of the communication cable. Thus, in the future, the communication structure needed to be designed again to break the limitation. Besides, the power system of the ROV is not capable for this design. The power of the battery is not enough to supply the thrusters to push the ROV harder. Therefore, the ROV cannot move in fast speed. Thus, the power system of the ROV should be wired to the surface with a high cost thick cable to supply power on surface so that the power is enough to push the ROV.

REFERENCES

[1] I. S. Roslan, M. F. M Said, S. A. A. Bakar, "Conceptual Design of Remotely Operated Underwater Vehicle," *Journal of Transport System Engineering* vol. 1, no. 2, 2015, pp. 15-19.

[2] Luqman Al Hakim Bin Mohd Nor. "Design and Development of ROV for Underwater Surveillance," in *Faculty of Electrical Engineering Universiti Teknologi Malaysia*, 2016.

[3] A. Martins, J. B. Sousa, F. L. Pereira "A New ROV Design: Issues on Low Drag and Mechanical Symmetry," *Journal of Oceans*, vol. 3, no. 19, 2005, pp. 957– 962.

[4] M. S. M. Aras[1], S. S. Abdullah[2], "Auto Depth Control for Underwater Remotely Operated Vehicles using a Flexible Ballast Tank System," in *Universiti Teknikal Malaysia Melaka, Malaysia,* January - June 2015.

[5] Karelia Stetz-Walters, "Linn-Benton Community College ROV Technical Report" in *Linn-Benton Community College,* 2014.

[6] Hai, H., et al. Control Architecture of SY-II Ship Inspection Remote Operated Vehicle. in Computer Science & Service System (CSSS), 2012 International Conference on. 2012.

[7] Harsamizadeh Tehrani, N., et al. Development, depth control and stability analysis of an underwater Remotely Operated Vehicle (ROV). in Control and Automation (ICCA), 2010 8th IEEE International Conference on. 2010.

[8] Omerdic, E., et al. Smart ROV<inf>LATIS</inf>: Control architecture. in Control 2010, UKACC International Conference on. 2010.

[9] Hyeung-Sik, C., et al. Design and control of a convertible ROV. in OCEANS, 2012 - Yeosu. 2012.

[10] Jun, B.H., et al. Workspace control system of underwater tele-operated manipulators on ROVs. in OCEANS 2009 - EUROPE. 2009.

[11] Shim, H., "Dynamic Workspace Control Method of Underwater Manipulator based on Motion Compensation of an ROV". in OCEANS.2011.

[12] P. E. Stachiw, "Acrylic Plastic as Structural Material for Underwater Vehicles," *IEEE Trans.* vol. 1, no. 4, pp. 289-296, 2004.

[13] S. Webster, "The development of excavation technology for remotely operated vehicles," *Archaeological Oceanography*, pp. 41-64, 2008.

[14] T. Koh, M. Lau, E. Low, G. Seet, S. Swei, and P. Cheng, "Development and improvement of an under actuated underwater robotic vehicle," *in Proc. Oceans '02 MTS/IEEE*, vol. 4, pp. 2039–2044, 2002.

[15] D. A. Smallwood and L. L. Whitcomb, "Model-based dynamic positioning of underwater robotic vehicles: Theory and experiment," *IEEE Journal of Oceanic Engineering*, vol. 29, no. 1, pp. 169–186, January 2004.

Finger Spelling Using Flexible Sensors, Touch Sensor and Accelerometer

Muhammad Ridhzuan Bin Ab Rahman
Faculty of Electrical Engineering
Universiti Teknologi Malaysia
Johor Bahru, Malaysia.
ridhzuan1294@yahoo.com

Kamal Khalil
Department of Electronic and Computer Engineering
Faculty of Electrical Engineering
Universiti Teknologi Malaysia
Johor Bahru, Malaysia.
kamal@fke.utm.my

***Abstract*—Generally, hearing impaired and deaf people used sign language as the tool of communication to deliver information. The sign language consists of hand gesture with specific motion. However, not all the people in this world master the sign language and this makes the hearing impaired and deaf people difficult to interact with them. The aim of this project is to design a device that able to translate sign language finger spelling into text that can be understood by normal people. This scope of the project focuses on the sign language which is commonly used in this world which is American Sign Language. This device will translate all the alphabets and combine it into a sentence in the English language. The project started by study the theories about flexible bend sensor, accelerometer and pressure sensor. A flexible sensor is used to measure the gesture movement depends on the fingers' bending. The more the fingers bend, the value of the resistor will increase. The accelerometer is used to detect the dynamic acceleration resulting from the motion. This sensor is to detect the alphabet that consists of motion which are alphabets J and Z. The touch sensor is used to measure the sensor between the index and middle finger in order to difference between the alphabet U and V. All of the sensors values processed into the microcontroller will be program by using Arduino IDE's software. The data will be sending to the smart phone device using the Bluetooth module. An android application was developed to display the text that has been translated. This developed project will reduce the gap between the hearing impaired or deaf people with normal people.**

Keywords—Sign Language; Accelerometer; Touch Sensor; Flexible Bend Sensor

I. INTRODUCTION

Communication is one of the important things in daily life as a human being. It is because communicate can help peoples to share and receive information, ideas, and feelings. Peoples exchange the information by speaking but there are some peoples in this world are lack of hearing and speaking. There are called as deaf or hearing impaired people. Therefore, another language was created to help those people to communicate which is called as sign language. Sign language is a very important tool of communication for hearing impaired and deaf people [1]. Without this language, those people will unable to deliver desired information, ideas, and feelings to another people. Sign language is a system of communication that involves visual sign and gesture. There are many types of different sign language in this world such as American Sign Language, British Sign Language, Thai Sign Language and many more [2]. Sign language finger spelling is a basic that can sign all the alphabets. The alphabets will be combined and produce a sentence. This sign language has developed spontaneously and independently within all the hearing impaired and deaf user around the world [3]. The American Sign Language finger spelling gestures are shown in Fig. 1.

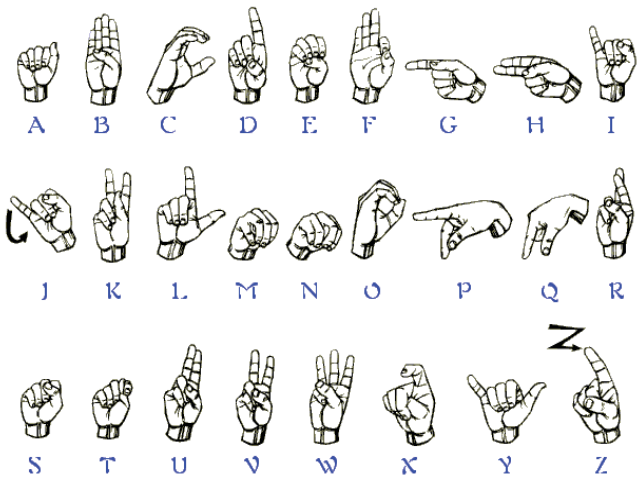

Fig. 1. Alphabets of American Sign Language

Hearing impaired and deaf people have a problem to deliver information, ideas, and feelings to public due to the limitations of sign language. It is impossible that all the people around the world will master the sign language. Therefore, there will be a barrier between those peoples and normal peoples. Based on the World Health Organizations (WHO), there are about 360 million in this world had hearing loss. Nowadays, it is getting hard to get a job. Many of the companies did not want to hire the hearing impaired and deaf people as a worker in their companies due to lack of communication. It is really hard to communicate with those peoples if another normal worker did not know sign language. Hence, a system need to be developed in order to solve the problem occur among the hearing impaired and deaf peoples.

This project focuses on develop and design a glove that able to translate sign language into text by using flexible bend sensors, accelerometer, touch sensor, Bluetooth module and microcontroller.

II. Literature Review

Many of projects that have been done by other researchers around the world are related to this project. Some of the projects are similar but the researchers did not success to complete the main goal which to detect all the alphabets. The background of these projects related to techniques, theories, software and hardware which give an idea to complete this project.

Flexible sensor is suitable for use that has the movement of the fingers. For example, a glove device that able to do several tasks such as picking and placing. The robots' hand was controlled by the glove that equips with flexible sensors and the servomotors are used to control the movement of the robots' hand. The flexible sensor on the glove acts as an input and the data will send to Analog to Digital (ADC) in a microcontroller. After that, the data collected will be used to control the robots' hand [4].

There is a low-cost interactive glove developed for hearing and speech impaired person. The glove is consists of seven bend sensors, an accelerometer, five Hall sensors and strong magnet. The glove was interfaced with MATLAB software [5]. The bend sensors enable to map the orientation of finger and hand. A bend sensor consists of photo diode, infrared diode, and flexible pipe tube. An accelerometer was placed on the hand to detect the dynamic acceleration resulting from motion [5] and the Hall sensors function to generate voltage output when the sensors near the magnet [5]. Although the cost of the bend sensors and Hall sensors that used are cheap but still have limitation such as the bend sensor only working if the finger bend and the Hall sensors unable to generate voltage if the sensors far away from the magnet [5].

There is also project to translate the Malaysian Sign Language (MSI) into text. Five flexible sensors are used to measure and capture the gesture of movement of hand but there are some alphabets that unable to be displayed because have similar gesture with another alphabet and consist of motion. Alphabets P have the same gesture with alphabet K, alphabet Q has the same gesture with alphabet G and alphabet V has the same gesture with alphabet U [6]. Alphabets J and Z unable to be displayed because consists of the movement of motion.

It is shown flexible bend sensor are suitable to be as the main sensor to translate sign language finger spelling into text. It is because most of the alphabets consist bending of fingers and the sensor is to detect the bend of the fingers. This project is to improve the previous project that had been done by another student. Some of the alphabets such as P, Q, V, J and Z unable to detect because of consists of same gesture with another alphabet and motion. Alphabets P and Q can be different from K and G by placing another flexible bend sensor on the wrist. Based on American Sign Language finger spelling, the different between those alphabets was wrist bending. Alphabet J and Z consists of motion, so it can be detected by placing an accelerometer on the glove. To different the alphabet V and U, a touch sensor is placing between the index finger and middle finger of the glove.

III. Project Methodology

The main components of development process divided into three parts which are the hardware and electronic circuit, software development, and integration between the hardware and software part. The hardware consists of accelerometer, flexible bend sensor, pressure sensor, and Bluetooth Module. For the software development part, Arduino IDE's software is used to program the microcontroller and MIT App Inventor 2 is used to create the app on smart phone. Finally, the integration between the hardware and software which combined both of the part will form a complete device. This device able to translate all the alphabets in American Sign Language and display on the phone display through Bluetooth module. Flowchart of the operation is shown in Fig. 2.

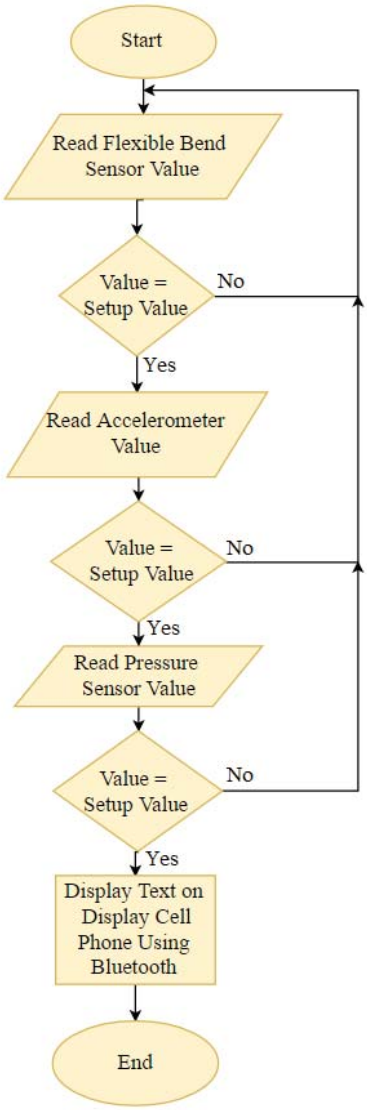

Fig. 2. Flowchart of Operation

A. Construction of Hardware

Genuino Micro is the smallest board of the Arduino family and it is easier to integrate into every component to make it interactive. It is based on the ATmega32U4 microcontroller with a built-in USB that will be recognizing as keyboard or mouse. The Micro has 20 digital inputs/outputs pins which 7 can be as PWM outputs and 12 as analog inputs. In this project used 10 analog inputs, so Genuino was the suitable to be selected [7].

The flexible bend sensor is used to measure the gesture movement of fingers. The value of resistance of the flexible bend sensor depends on the bending of the fingers as shown in Fig. 3. and the range of resistance for flexible bend sensor is between 10kΩ to 20 kΩ [8].

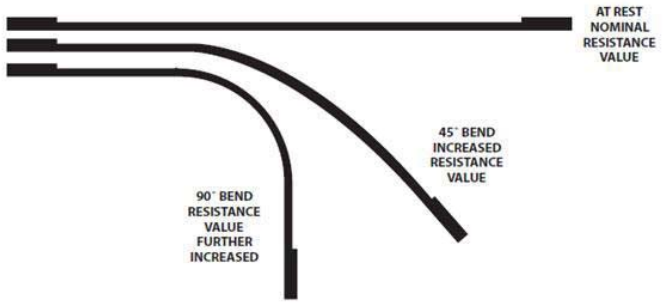

Fig. 3. Specification of Flexible Bend Sensor

Fig. 4. shows the basic circuit for the flexible bend sensor. The voltage divider circuit is implementing to interface the flex sensor. The impedance buffer in the flexible sensor is a single sided operational because the low bias current of the op amp reduces the error due to the source impedance of the flexible bend sensor as voltage regulator [9].

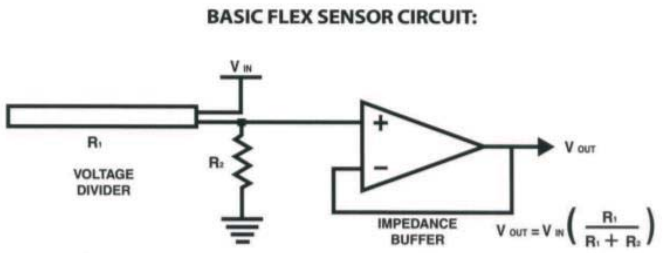

Fig. 4. Basic Flexible Bend Sensor Circuit

The accelerometer is to measure the dynamic acceleration resulting from the motion or shock depended on gravity. Therefore, orientation hand movement can be determining by using this sensor. The accelerometer will be attached to the index finger to measure the angle of tilted and can sensing the x, y, and z-axis.

The touch sensor creates by using a copper plate and two copper wires. One of copper wire is connected to 5V and another one connected to the ground. When the copper wire in contact with the copper plate, it will be active low. It is active high when there is no contact and active low if there is contact.

Bluetooth is the device that able to a form small local network with other similarity enabled devices within the immediate area [10]. Data can be transfer to other devices that shared the same network once the network established without any interrupt. In this project, HC-05 Bluetooth Module is used as a module to transfer the data from Arduino Micro to a smart phone. This module comes with an on board antenna that provides better signal quality and SSP where it will become serial COM port when the connection with the master Bluetooth is established [11].

B. Software Development

There are two software are used in this project which are are Arduino IDE and MIT App Inventor 2. Arduino IDE is easy-to-use software that runs on several platforms such as Windows, Macintosh OSX and LINUX operating systems. It can be sketched in normal Arduino files, C files, C++ files or header files. It contains a text editor for writing code, a message area, a text console, a toolbar and series of menus. After the program was writing, it will be compiled and upload into Arduino hardware [12].

MIT App Inventor 2 is software to create mobile applications for the smart phone using a web browser. Originally, this software provided by Google and now been maintained by the Massachusetts Institute of Technology (MIT). This software only supports Android application design and it uses graphical interface that allows the user to drag and drop visual object to create an application that can run on Android System [11].

IV. Result and Analysis

The function of the flexible sensor is to measure the degree of the bending finger which will change in resistance depends on the bending. The accelerometer will measure the dynamic acceleration resulting from the motion or shock depended on gravity while touch sensor will act as push button which is active low when the copper plate and copper wires in contact. All those sensors make the data collection become more accurate in order to convert it into alphabets.

A. Flexible Sensor Analysis

The flexible sensor was tested on four different angle by using the multimeter. The angle that had been test are 0°, 45°, 90° and 180°. The difference value of resistance been recorded on the Table 1 below.

B. Result

The finger spelling device was able to display all the alphabets from A until Z. Accelerometer was used when to different the alphabets K, P, Q, and G while touch sensor used when to different the alphabet U and alphabet V.

TABLE I. VALUE OF RESISTANCE AT DIFFERENT RESISTANCE

Degree(°)	Value of Resistance (kΩ)
0°	5.74
45°	5.97
90°	6.02
180°	6.32

TABLE II. RESULT OF EACH ALPHABET

Finger Spelling	Voltage (V)	Apps Display
	610 <V1< 670 655 <V2< 695 834 <V3< 867 690 <V4< 740 694 <V5< 726 V6< 815	
	V1> 733 461 <V2< 509 683 <V3< 711 523 <V4< 576 502 <V5< 563	
	620 <V1< 680 500 <V2< 600 820 <V3< 850 630 <V4< 675 590 <V5< 650	
	660 <V1< 750 475 <V2< 509 813 <V3< 853 673 <V4< 722 640 <V5< 682	
	740 <V1< 775 V2> 680 V3> 850 V4> 735 V5> 705	
	663 <V1< 719 528 <V2< 665 678 <V3< 755 537 <V4< 577 523 <V5< 566	
	634 <V1< 700 473 <V2< 518 V3> 855 V4> 686 V5> 596 V6< 800	
	670 <V1< 711 470 <V2< 521 690 <V3< 765 635 <V4< 670 650 <V5< 723	
	V1> 710 V2> 605 V3> 821 V4> 675 550 <V5< 605 80 <y< 200	
	V1> 710 V2> 605 V3> 821 V4> 675 550 <V5< 605 y < 80 and y >200	
	620 <V1< 695 475 <V2< 512 776 <V3< 835 672 <V4< 725 669 <V5< 718 V6< 800	
	537 <V1< 592 481 <V2< 523 V3> 824 V4> 694 V5> 686	
	735 <V1< 780 638 <V2< 673 820 <V3< 855 704 <V4< 720 680 <V5< 710 V6 < 815	
	726 <V1< 746 622 <V2< 680 830 <V3< 869 669 <V4< 705 688 <V5< 720 V6 < 815	
	675 <V1< 740 600 <V2< 670 835 <V3< 865 670 <V4< 720 660 <V5< 690	

Finger Spelling	Voltage (V)	Apps Display
	620 <V1< 695 475 <V2< 512 776 <V3< 835 672 <V4< 725 669 <V5< 718 V6> 800	
	634 <V1< 700 473 <V2< 518 V3> 855 V4> 686 V5> 596 V6> 800	
	V1> 720 490 <V2< 524 770 <V3< 820 V4> 690 V5> 674 D = 1	
	V1> 720 460 <V2< 500 679 <V3< 750 V4> 676 V5> 673 D = 0	
	V1> 720 460 <V2< 500 679 <V3< 750 V4> 676 V5> 673 D = 1	
	720 <V1< 765 463 <V2< 520 690 <V3< 768 530 <V4< 584 664 <V5< 720	
	V1> 672 580 <V2< 635 815 <V3< 867 690 <V4< 730 674 <V5< 726	
	544 <V1< 650 647 <V2< 690 813 <V3< 871 680 <V4< 740 550 <V5< 650	
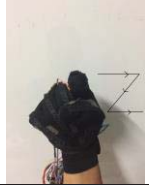	V1> 728 475 <V2< 513 814 <V3< 860 688 <V4< 730 686 <V5< 724 y < 110	

Finger Spelling	Voltage (V)	Apps Display
	705 <V1< 760 635 <V2< 690 830 <V3< 865 690 <V4< 740 690 <V5< 725 V6> 815	
	685 <V1< 710 655 <V2< 675 835 <V3< 855 690 <V4< 730 690 <V5< 719 V6< 815	

V. CONCLUSION

Finger Spelling Translator device was developed to help mute or deaf people to communicate with normal people. Generally, all the objectives are successfully achieved. The combination of six flexible bend sensor, accelerometer and touch sensor will recognize all the movement of fingers and hand gesture that will convert into text on the smart phone trough Bluetooth.

REFERENCES

[1] Parton, B. S. (2005). Sign Language Recognition and Translation: AMultidisciplined Approach From the Field of Artificial Intelligence. Journal of Deaf Studies and Deaf Education, 11(1), 94-101. Doi : 10.1093/deafed/enj003.

[2] Linguistic Society of America. (n.d.). Retrieved December 19, 2016, from http://www.linguisticsociety.org/content/what-sign-language.

[3] Liddell, S.K. (2003). Grammar, Gesture, and Meaning in American Sign Language. Cambridge University Press.

[4] Tee Heng Siang. “Universal Robot Hand With Glove Control”. Universiti Teknologi Malaysia. Bachelor’s Degree Thesis,2011.

[5] Chouhan,Tushar ; Panse, Ankit ; Voona, Anvesh Kumar ; Sameer, S.M., “Smart Glove with Gesture Recognition Ability fot the Hearing and Speech Impaired”, Global Humanitarian Technology Conference – South Asia Satellite (GHTC-SAS), 2014 IEEE, vol., no., pp. 105,110, 26-27 September 2014.

[6] Amir Syafiq Bin Ahmad Azam. “Translator Glove for Mutism and Hearing Impaired People”. Universiti Teknologi Malaysia. Bachelor’s Degree Thesis, 2015.

[7] Arduino - ArduinoBoardMicro. (n.d.). Retrieved December 19, 2016, from https://www.arduino.cc/en/Main/ArduinoBoardMicro

[8] Ahmed, S.F.; Ali, S.M.B.; Qureshi, S.S.M., "Electronic Speaking Glove for speechless patients, a tongue to a dumb," Sustainable Utilization and Development in Engineering and Technology (STUDENT), 2010 IEEE Conference on, vol., no., pp.56,60, 20-21 Nov. 2010.

[9] Flex Sensor Datasheet - SparkFun Electronics. (n.d.). Retrieved December19,2016,from https://cdn.sparkfun.com/datasheets/Sensors/ForceFlex/FLEX%20SENSOR%20DATA%20SHEET%202014.pdf

[10] Terrell, D.L , Electronics for Computer Technology. Clinton Park ; NY ; Thomas Delmas Learning, 2002 ; pg647

[11] Muhammad Hisyam Bin Idris. "Smart Glove for Hearing Impaired People." Universiti Teknologi Malaysia. Bachelor's Degree Thesis, 2013.

[12] Arduino.cc Inc. USA. “Arduino Software (IDE)”. Retrieved from: https://www.arduino.cc/en/Guide/Environment. Last Accessed on December 19, 2016.

ISBN 978-967-0194-95-0

UTM
UNIVERSITI TEKNOLOGI MALAYSIA

Faculty of
Electrical Engineering